Acta GEODAETICA, GEOPHYSICA et MONTANISTICA

ACADEMIAE SCIENTIARUM HUNGARICAE

AKADÉMIAI KIADÓ, BUDAPEST

TOMUS 16
FASCICULI 1
1981

ACTA GEODAETICA, GEOPHYSICA et MONTANISTICA

Academiae Scientiarum Hungaricae

A Magyar Tudományos Akadémia Föld- és Bányászati Tudományok Osztályának folyóirata

Szerkesztőség: H-9400 Sopron, Múzeum u. 6.
Kiadja az Akadémiai Kiadó, 1054 Budapest, Alkotmány utca 21.

Az *Acta Geodaetica, Geophysica et Montanistica* eredeti tanulmányokat közöl a geodézia, geofizika és a bányászati tudományok tárgyköréből, angol, német, francia vagy orosz nyelven. Félévenként jelenik meg, évi egy, kb. 400—500 oldalas kötetet alkotva.

Megrendelhető az Akadémiai Kiadónál (1363 Budapest Pf. 24.), a külföld részére pedig a „Kultura" Külkereskedelmi Vállalatnál (1389 Budapest 62, P.O.B. 149).

Acta Geodaetica, Geophysica et Montanistica is a semiannual review of the Hungarian Academy of Sciences, publishing papers on geodesy, geophysics and minings in English, German, French or Russian.

Editorial Office: H-9400 Sopron. Múzeum u. 6.

Orders may be placed with "Kultura" Foreign Trading Company (1389 Budapest 62, P.O.B. 149) or its representatives abroad.

ACTA GEODAETICA, GEOPHYSICA et MONTANISTICA

ACADEMIAE SCIENTIARUM HUNGARICAE

TOMUS 16

AKADÉMIAI KIADÓ, BUDAPEST
1981

INDEX

ACTA GEODAETICA, GEOPHYSICA et MONTANISTICA

ACADEMIAE SCIENTIARUM HUNGARICAE

TOMUS 16

AKADÉMIAI KIADÓ, BUDAPEST
1981

Acta Geodaet., Geophys. et Montanist. Acad. Sci. Hung. Tomus 16 (1), pp. 3—5 (1981)

PROFESSOR DR. H. C. ISTVÁN HAZAY OCTOGENARIO

The Hungarian geoscientists congratulate Professor Hazay with distinguished respect of his deep knowledge and outstanding human character at his 80th birthday occurring on April 15, 1981.

Professor Hazay was born in Budapest in 1901. He finished his schools there, and graduated in civil engineering at the Technical University of Budapest in 1922.

He entered state service as land surveyor in 1923 and gained a lot of experiences in all phases of geodetic and land surveying works for about 30 years. He was especially active in national geodetic control works (triangulation, precise leveling, geodetic astronomy etc.). His outstanding abilities manifested themselves already in his youth, thus he received soon managing tasks, at first in the geodetic control net and survey of Budapest, later in the national land survey of Hungary. From 1942 on, he became the head of the National Land Survey.

Together with this practical activity, he turned successfully towards scientific researches and professional education. His first papers appeared in 1930. He taught Adjustment and Geodetic Astronomy at special courses from 1929 on. After the successful solution of an astro-geodetic problem of the Hungarian national control net, he was awarded the doctor degree by the Technical University of Budapest in 1934. His first book appeared in 1938

entitled "Adjustment in civil engineering practice", which was honoured by the golden medal of the Hungarian Society of Civil Engineers and Architects. Already at that time he had several new ideas and scientific results — unfortunately in Hungarian language — which have became topics of the international interest quite recently and which have been generally accepted. On the basis of his educational and scientific activity, he was awarded the Professor title at the Technical University of Budapest in 1941.

In Hungary, the education of civil engineers specialized in geodesy, surveying and mapping was started in 1949. Professor Hazay has put all his force into the service of professional education from 1951, and obtained eminent merits in its organization and scientific guidance. As Professor for National Survey, Mathematical Cartography etc. and Head of the Department of Geodesy, he founded the knowledge in, the attitude towards and the affection for the profession of many generations of geodesists. Several of his students and assistents have became professors, outstanding engineers or scientists.

As professor, he wrote lecture notes and 4 textbooks which were published in several editions. His excellent educational and manage abilities appeared on the highest level when he was Dean of the Faculty for Civil Engineering in 1960—1964 and subsequently rector of the University till 1967.

In the meantime he continued his scientific activity. He published more than 100 papers and books presenting new scientific results. In addition to the 4 textbooks, he published 6 other scientific books, among them the "Adjusting Calculations in Surveying" which has been published also in English.

His most important scientific results are the following: a new theory of the mechanical principles of adjusting, static principles of the method of variation of co-ordinates, a method used in the adjustment of the new national control net: the so-called "method of dominant stations"; the adaptation of the Gauss-Krüger projection for Hungarian conditions with the necessary formulas and tables; representation of extended areas in a uniform projection coordinate system; solution of a number of other problems in connection with projections; application of the fictitious observations; special method of development and calculation of traverse nets; the transformation of weights in adjustment and its application in adjustment of geodetic control nets; adjustment of leveling nets for the detection or recent crustal movements by taking into account the velocity changes; theoretical investigations about the datum-problems of different reference ellipsoids etc.

The Hungarian Academy of Sciences acknowledged his scientific merits by electing him its corresponding and ordinary member in 1967 and in 1976, respectively. For a long time he had a leading role in the Hungarian geodetic science as president of the Geodetic Commission of the Hungarian Academy of Sciences. His bright knowledge, zeal and working capacity have been stimulus for all of us.

As appreciation of his merits in technical education and in scientific research, Professor Hazay was awarded several honours. He is holder of the State Kossuth-prize, of three governmental and two ministerial medals, and of the two Honorary Medals of Hungarian geodesists. The Technical University of Budapest awarded him the title doctor honoris causa and the Honorary Medal of the University.

At his 80th birthday we express our sincere wishes in the hope that Professor Hazay with his amiable, commonly respected personality and deep knowledge can further be active for a long time in good health for the development of his beloved science, the geodesy and in the education of new generations of engineers and scientists.

P. Biró

Acta Geodaet., Geophys. et Montanist. Acad. Sci. Hung. Tomus 16 (1), pp. 7—10 (1981)

PUBLICATIONS OF PROFESSOR ISTVÁN HAZAY

A) Books

1. Adjustment in Civil Engineering Practice (Kiegyenlítő számítás a geodéziai gyakorlatban). Own edition, Budapest, 1938. 380 p.
2. Computation of Gauss-Krüger Co-Ordinates (with A. Tárczy-Hornoch) (Gauss-Krüger koordináták számítása). Akadémiai Kiadó, Budapest, 1951. 357 p.
3. Terrestrial Projections (Földi vetületek). Akadémiai Kiadó, Budapest, 1954. 508 p.
4. Manual of Geodesy, Vol. I—III (Editor and author of about one quarter) (Geodéziai Kézikönyv I—III). Közgazdasági és Jogi Könyvkiadó, Budapest, 1956—1960. 2180 p.
5. National Survey (Országos felmérés). Tankönyvkiadó, Budapest, 1959. 360 p.
6. Geodesy (for "Manual of Mining") (Geodézia (Bányászati Kézikönyv számára)). Műszaki Könyvkiadó, Budapest, 1965. 130 p.
7. Projections (Vetülettan). Tankönyvkiadó, Budapest, 1965. 360 p.
8. Adjusting Calculations (Kiegyenlítő számítások). Tankönyvkiadó, Budapest, 1966. 630 p.
9. National Survey and Land Consolidation (with L. Szalontai) (Országos felmérés és műszaki földrendezés). Tankönyvkiadó, Budapest, 1967. 595 p.
   2nd edition in 1973.
10. Adjusting Calculations in Surveying. Akadémiai Kiadó, 1970. 630 p.
11. High-Scale Surveying (textbook) (Nagyméretarányú felmérések). Tankönyvkiadó, 1979. 280 p.
12. Geodesy (Engineering Manual) (Geodézia (Mérnöki Kézikönyv)) Edited by L. Palotás (in press). 120 p.

B) Papers in journals

1. Kino-theodolite (Kinó-teodolit). Geodéziai Közlöny, 1930.
2. Adjustment of the Orosháza network with Boltz's method (Orosháza belsőségi hálózatának kiegyenlítése Boltz módszere szerint). *Geodéziai Közlöny*, 1930.
3. Computations of lower order triangulation points (Alsóbbrendű háromszögelési pontok számítása). *Geodéziai Közlöny*, 1931.
4. Studies for the determination of the dimensions and position of the reference ellipsoid best approaching the Earth's surface in Hungary (Vizsgálatok Magyarország felületéhez legjobban simuló referencia ellipszoid méreteinek és elhelyezésének meghatározására). Dr. thesis, 1932.
5. Static adjustment of co-ordinates. For the use of the *National Survey*, lithography (Statikai koordináta-kiegyenlítés). 1936.
6. Statische Koordinatenausgleichung. *Műszaki és Gazdaságtudományi Egyetem Soproni Bánya- és Kohómérnöki Osztályának Közleményei, 1939.*
7. Die Lösung zusammengesetzter Aufgaben mittels statischer Ausgleichung. *Műszaki és Gazdaságtudományi Egyetem Soproni Bánya- és Kohómérnöki Osztályának Közleményei*, 1942.
8. Projections, with special respect to Hungarian surveying (Vetületek, különös tekintettel a hazai felmérésekre). Mérnöki Továbbképző Intézet kiadványa, 1942.
9. Activity of the National Land Survey (Az Állami Földmérés munkaköre). *Geodéziai Közlöny*, 1947.
10. Mathematic and mechanical principles of the adjustment of co-ordinates (A koordinátakiegyenlítés matematikai és mechanikai fogalmazása). *Állami Földmérés Közleményei*, 1949.

11. Transformation of Gauss-Krüger co-ordinates from one projectional stripe to the neighborous one (Átszámítás a Gauss-Krüger vetületnél az egyik vetületi sávról a szomszédos vetületi sávra). *Földméréstani Közlemények*, 1950.
12. Studies in connection with the use of the Gauss-Krüger co-ordinates in Hungary (Vizsgálatok a Gauss-Krüger ábrázolási mód magyarországi alkalmazásával kapcsolatban). *MTA Műsz. Oszt. Közl.*, 1951.
13. Zur Umrechnung der Gauss-Krügerschen Koordinaten von einem Projektionsstreifen in den benachbarten. *Acta Technica*, 1951.
14. Transformation of Gauss-Krüger co-ordinates from a narrower stripe to a broader one (Gauss-Krüger koordináták átszámítása keskeny sávról szélesebb sávra). *Földméréstani Közlemények*, 1951.
15. Transformation of Gauss-Krüger co-ordinates between different ellipsoids (Átszámítás különböző ellipszoidokhoz tartozó Gauss-Krüger koordináták között). *MTA Műsz. Tud. Oszt. Közl.*, 1952.
16. On the adjustment of national and continental networks (Az országos és kontinentális hálózatok kiegyenlítéséről). *MTA Műsz. Tud. Oszt. Közl.*, 1952.
17. The Congress on Geodesy and Geophysics in Budapest (A budapesti Geodéziai és Geofizikai Kongresszus). *Földméréstani Közlemények*, 1959.
18. Die Transformation Gauss-Krügerscher Koordinaten zwecks Darstellung in kleinem Maßstabverhältnis. *Acta Technica*, 1952.
19. Umrechnung zwischen Gauss-Krügerschen Koordinaten, die verschiedenen Ellipsoiden angehören. *Acta Technica*, 1952.
20. Über Ausgleichung von Landestriangulierungsnetzen und kontinentalen Triangulierungsnetzen. *Acta Technica*, 1953.
21. Mathematical principles of a uniform table of conformal maps in different positions. (Különböző elhelyezésű szögtartó hengervetületek egységes táblázatának matematikai alapja). *Földméréstani Közlöny*, 1953.
22. Some words on the scale of maps (Néhány szó a térképi méretarányról). *Földméréstani Közlemények*, 1954.
23. Mathematische Grundlage zur einheitlichen Tabelle verschiedener angeordneten winkeltreuer Zylinderprojektionen. *Acta Technica*, 1954.
24. Zeitgemäße Formeln für Reduktionen von winkeltreuen Zylinderprojektionen. *Acta Technica*, 1955.
25. Studies in connection with the projection between different ellipsoids I—XII (Vizsgálatok a különböző ellipszoidok közötti vetítés köréből I—XII). *Geodézia és Kartográfia*, 1955.
26. Die Umrechnung von der stereographischen Projektion und der konformen Zylinderprojektion auf die Gauss-Krügersche Projektion. *Acta Technica*, 1955.
27. Genauigkeitsuntersuchung der Triangulierungspunkte bei Richtungslinien verschiedenen Gewichtes. *A Bányamérnöki és Földmérőmérnöki Karok Közleményei*, 1955.
28. Untersuchungen über die Projektion zwischen Ellipsoiden und über die Bestimmung der relativen Lage der Ellipsoide durch Projektion. *Acta Technica*, 1956.
29. Beiträge zur Bestimmung der Konstanten bei der Projektion zwischen Ellipsoiden und der Lage des Ellipsoids. *Acta Technica*, 1956.
30. Die Lösung der Koordinatenausgleichung mit einem Punkt unter Berücksichtigung von Richtungsgewichten. *Bányamérnöki és Földmérőmérnöki Karok Közleményei*, 1956.
31. Azimutreduktion zwischen zwei Erdellipsoiden. *Acta Technica*, 1957.
32. Computation of a nodal point of traverses with fictitious direction measurements (Sokszögelési csomópont számítása fiktív iránymérési eredményekkel). *Geodézia és Kartográfia*, 1957.
33. A uniform interpretation of the break points of traverses oriented at its endpoints by several directions (A végpontjain többiránnyal tájékozott sokszögvonal törésszögeinek egységes értelmezése). *Geodézia és Kartográfia*, 1958.
34. Mechanical principles of the adjustment (A kiegyenlítés mechanikai elvei). *Geodézia és Kartográfia*, 1959.
35. Realization of the static adjustment. I. Adjustment of single points (A statikai koordinátakiegyenlítés végrehajtása I. Egypontos kiegyenlítés). *MTA Műsz. Tud. Oszt. Közl.*, 1959.
36. Realization of the static adjustment. II. Adjustment of several points together (A statikai koordinátakiegyenlítés végrehajtása II. Többpontos kiegyenlítés). *MTA Műsz. Tud. Oszt. Közl.*, 1959.
37. Über die Probleme der Projektion zwischen zwei Ellipsoiden. *Acta Technica*, 1959.
38. Berechnung des polygonalen Knotenpunktes aus Ergebnissen der fiktiven Richtungsmessungen. *Bányamérnöki és Földmérőmérnöki Karok Közleményei*, 1959.

39. Ausführung der statischen Koordinatenausgleichung I. Ausgleichung eines Punktes. *Acta Technica*, 1959.
40. Ausführung der statischen Koordinatenausgleichung II. Gemeinsame Ausgleichung mehrerer Punkte. *Acta Technica*, 1959.
41. Die mechanischen Prinzipien der Ausgleichung. *Acta Technica*, 1960.
42. Statische Koordinatenausgleichung mit Richtungsmessungen ohne Orientierungsrichtungen. *Acta Technica*, 1960.
43. Some words on certain formulas of error limits (Néhány szó egy-két hibahatárképletről). *Geodézia és Kartográfia*, 1961.
44. Studies on the use of Gauss-Krüger co-ordinates in Hungary (Vizsgálatok a Gauss-Krügerféle ábrázolási mód magyarországi alkalmazásához). *ÉKME Tud. Közl.*, 1961.
45. Die mechanischen Prinzipien der Ausgleichung. (Travaux du Groupe Spécial d'Études No 21 L'Association Internationale de Géodésie, Académie Polonaise des Sciences Kraków, 1961.)
46. Untersuchung zur Anwendung der Gauss-Krügerschen Abbildung in Ungarn. *Acta Technica*, 1961.
47. Polygonale Knotenpunktsysteme. *Acta Technica*, 1961.
48. Summer practice for surveying and mapping students (Termelési gyakorlatok a földmérőmérnökképzésben). *Geodézia és Kartográfia*, 1962.
49. The use of dimensional weights in the adjustment (Dimenziós súlyok alkalmazása a kiegyenlítő számításban). *Geodézia és Kartográfia*, 1962.
50. Dimensions for the subsidiary quantities of the adjustment (A kiegyenlítés segédmennyiségeinek dimenziója). *Geodézia és Kartográfia*, 1962.
51. Discussion on the paper by Z. Heinemann "Some remarks on the principle of the static adjustment" (Hozzászólás Heinemann Zoltán „Megjegyzések a statikai kiegyenlítési elvhez" c. tanulmányhoz). *MTA Műsz. Tud. Oszt. Közl.*, 1962.
52. Determination of the reliability of functional values directly from the normal equations of the co-ordinate adjustment (Függvényértékek megbízhatóságának meghatározása közvetlenül a koordináta-kiegyenlítés normálegyenleteiből). *Geodézia és Kartográfia*, 1963.
53. Computation of the mean square errors in connection with fictitious measurement results (A középhibák számítása a fiktív mérési eredményekkel kapcsolatban). *Geodézia és Kartográfia*, 1963.
54. The Use of Dimensional Weights in Adjusting Calculations. *Acta Technica*, 1963.
55. Systems of nodes in traverses (Sokszögelési csomópontrendszerek). *ÉKME Tud. Közl.*, 1963.
56. On the determination of the characteristic function of conformal projections with the basic equation of conformity (Szögtartó vetületek jellemző függvényének meghatározása a szögtartóság alapegyenletével). *Geodézia és Kartográfia*, 1963.
57. On the orthodrome and loxodrome (A loxodrómáról és az ortodromáról). *Geodézia és Kartográfia*, 1964.
58. О средней погрешности фиктивных наблюдений. Маркшейдерское дело в социалистических странах. Москва, 1964.
59. Bestimmung der charakteristischen Funktion der winkeltreuen Projektionen mit Hilfe der Grundgleichung der konformen Abbildung. *Acta Technica*, 1964.
60. Dimension of the Subsidiary Quantities of Adjustment. *Acta Technica*, 1964.
61. The picture of the degree-grid on a cylindric projection with oblique axis (A fokhálózat képe ferdetengelyű hengervetületen). *Geodézia és Kartográfia*, 1965.
62. The significance of Tissot's indicatrix (A Tissot-indikatrixok jelentősége.) *ÉKME Tud. Közl.*, 1965.
63. Die Bedeutung der Tissot-Indikatrix. *Acta Technica*, 1965.
64. On the problem of independence of the fictitious measurement results used in the adjustment of triangulation networks (Háromszögelési hálózatok kiegyenlítéséhez felhasznált fiktív mérési eredmények függetlenségének kérdése). *ÉKME Tud. Közl.*, 1966.
65. Über die Frage der Unabhängigkeit der aus Winkelmessungen in allen Kombinationen herrührenden fingierten Meßergebnisse. (Das Markscheidewesen in den sozialistischen Ländern) VEB Deutscher Verl. für Grundstoffindustrie, Leipzig, 1966.
66. Über die Loxodromen und die Orthodromen. *Acta Geod., Geoph. Mont. Hung.*, 1966.
67. Hungarian geodetic projections and their future problems (A magyar geodéziai vetületek és jövő kérdéseik). *MTA X. Oszt. Közl.*, 1967.
68. Illustration of extended areas in a uniform projection system of co-ordinates (Nagyobb területek ábrázolása egységes vetületi koordinátarendszerben.) *Geodézia és Kartográfia*, 1967.
69. On the adjustment of vertical crustal movement networks (A vertikális kéregmozgási hálózatok kiegyenlítése). *Geodézia és Kartográfia*, 1967.

70. Die Ausgleichung von Nivellementsnetzen für die Beobachtung der vertikalen Erdkrustenbewegungen. (Das Markscheidewesen in den sozialistischen Ländern) Miskolc, 1967.
71. The use of projections for ellipsoidic computations (Vetületek alkalmazása ellipszoid számításokhoz). *MTA X. Oszt. Közl.*, 1968. (Inaugural paper at the Hungarian Academy.)
72. К вопросу об ориентировании ходов полигонометрии. Маркшейдерское дело в социалистических странах. Том 4. Москва, 1969.
73. Anwendung von Projektionen bei ellipsoidischen Berechnungen. *Acta Geod., Geoph. Mont. Hung.*, 1969.
74. Weight transformations (Súlytranszformáció). *Geodézia és Kartográfia*, 1969.
75. The use of weight transformations for the adjustment of trilateration networks (A súlytranszformáció alkalmazása a tiszta hosszméréses hálózatok kiegyenlítésében). *Geodézia és Kartográfia*, 1970.
76. Gewichtstransformation. *Acta Geod. Geoph. Mont. Hung.*, 1970.
77. Anwendung der Gewichtstransformation bei der Ausgleichung der nur mit Streckenmessung hergeleiteten Netze. *Acta Geod., Geoph. Mont. Hung.*, 1970.
78. On the adjustment of triangulation networks with all lengths and angles measured (Valamennyi szögének és oldalának megmérésével meghatározott háromszögelési hálózat kiegyenlítése). *Geodézia és Kartográfia*, 1971.
79. Die methodische Auswahl unabhängiger Bedingungsgleichungen komplizierter Triangulationsnetze. Festschrift Karl Ledersteger, Wien, 1971.
80. Ausgleichung eines Triangulationsnetzes durch Messung sämtlicher Winkel und Seiten. *Acta Geod., Geoph. Mont. Hung.*, 1971.
81. Two length-conserving cylindric projections with parallel circles (Két hossztartó paralelkörű szögtartó hengervetület geodéziai alkalmazása). *Geodézia és Kartográfia*, 1972.
82. Some projectional aspects and practical problems of the uniform projection system of Hungary (Néhány vetületi szempont és az egységes országos vetületi koordináta-rendszer gyakorlati kérdései). *Geodézia és Kartográfia*, 1972.
83. 25 years of the education of survey engineers (25 éves a magyar földmérőmérnök-képzés). *Geodézia és Kartográfia*, 1974.
84. Transformation between conformal cylindrical projections with the transformation of directional angles (Átszámítás szögtartó hengervetületi rendszerek között az irányszögek transzformálásával). *Geodézia és Kartográfia*, 1974.
85. Construction of length- and area-preserving maps on the Gauss-Krüger projection (Hossz- és területtartó térképek készítése a Gauss-Krüger vetületen). *Geonómia és Bányászat*, 1974.
86. Constructing length- and area-preserving maps on the Gauss-Krüger projection. *Acta Geod., Geoph. Mont. Hung.*, 1974.
87. Eine längen- und flächentreue, großmaßstäbige Kartendarstellung in winkeltreuen Rahmen (Das Markscheidewesen in den sozialistischen Ländern). Warschau, 1975.
88. 25 years of education of civil engineers for geodesy and surveying in Hungary. *Periodica Polytechnica*, 1975.
89. Umrechnung zwischen den Gauss-Krüger Projektionsstreifen durch Transformation der Richtungswinkel. *Periodica Polytechnica*, 1975.
90. Talk with András Székely and Klára Füry (Beszélgetés Székely Andrással és Füry Klárával). *Geodézia és Kartográfia*, 1976.
91. Zur Arbeit »Über die Ableitung der Vertikalgeschwindigkeiten der Erdkruste aus zwei Nivellierungen nach Bedingungsgleichungen« von W. K. Hristow. *Acta Geod. Geoph. Mont. Hung.*, 1976.
92. Adjustment of leveling networks and computation of the velocity of vertical surface movements with consideration of the acceleration (A szintezési hálózatok kiegyenlítése és a földfelszín vertikális mozgássebességének számítása a gyorsulások figyelembevételével). *Geodézia és Kartográfia*, 1977.
93. Some ideas about the galery of Hungarian Surveyors (Gondolatok a Magyar Földmérők arcképcsarnokához). *Geodézia és Kartográfia*, 1977.
94. The adjustment of levelings for the determination of the vertical movements of the Earth's surface (A földfelszín vertikális mozgásának vizsgálatát szolgáló szintezések kiegyenlítése.) *MTA X. Oszt. Közleményei*, 1977.
95. Adjustment of levelings for the determination of the vertical movements of the earth's surface. *Acta Geod., Geoph. Mont. Hung.*, 1978.
96. Some variants of the adjusting straight line (A kiegyenlítő egyenes változatai). *Geodézia és Kartográfia*, 1980.

Acta Geodaet., Geophys. et Montanist. Acad. Sci. Hung. Tomus 16 (1), pp. 11—13 (1981)

PROFESSOR DR. LAJOS HOMORÓDI SEPTUAGENARIO

The rapid development of the last half century, the new tasks, the change in measurement and computation technics produced an increasing specialization in every field of science including geodesy. At present those dealing with theoretical geodesy are not familiar with the problems of photogrammetry, surveyors know only superficially about the problems of adjustment. Practical experts work quite independently from theoreticians and research workers. The number of scientists or engineers who produced significant results in several areas of geodesy, both in theoretical and practical problems is even internationally very low. It is the great luck of Hungarian geodesists that one of these exceptional personalities Dr. Lajos Homoródi lives and works among us.

Professor Homoródi was born in Arad in 1911. After completing the Technical University in Budapest, he graduated in 1934. In 1944, he was awarded the doctor degree with his work on "Error sources of high precision distances measurements with rods". In 1952, he obtained the title Candidate of Technical Sciences on the basis of his earlier scientific activity. In 1962, a work entitled "Solution of coordinate transformations necessary for the application of the new national triangulation net" brought him the title Doctor of Technical

Sciences. The Hungarian Academy of Sciences elected him corresponding and ordinary member in 1973 and 1979, respectively.

Between 1934 and 1959, he occupied different positions at the National Land Survey, thus he was for a time Director of the Surveying and Mapping Enterprise in Budapest. Since 1959, he has been working at the university, at first in the Institute of Theoretical Geodesy, later in the Institute of Photogrammetry. In 1962 he was nominated to Professor at the Technical University for Civil Engineering and Traffic, where he was Deputy Rector between 1962 and 1964 and Dean of the Faculty for Civil Engineering between 1964 and 1967. He was Director of the Institute for Geodesy at the Technical University Budapest between 1971 and 1978.

He acquired the knowledge necessary for a fruitful work in practical geodesy in the triangulation and polygon works of Budapest, further in the surveying made by the National Land Survey. From 1942 on, he took part in the high precision triangulation of the country. After the war his experiments were utilized in planning and organizing the newly started geodetic works. In the development of the first order chain-system he had taken an important role both by personal contributions and by the formulation of measurements and computation prescriptions.

Besides his practical activity he found always time to write papers which reflect the high theoretical level used in the solution of practical problems. He dealt in them with the accuracy of the angular and distance measurements of polygons in urban areas as well as with the testing of the instruments used. In several of his papers he discussed the basic problems of first order national triangulation like position and orientation of the network, influence of the dimension of the ellipsoid used, determination of the deflections of the vertical, reduction of measurement results, adjustment of the network. He treated the introduction of the new projection system and problems in connection with the development of the fourth order network. In connection with the application of the national network, he early recognized the necessity to establish precise leveling networks for engineering purposes, and also published the results of his investigations in this connection.

His wide theoretical and practical knowledge has been used since 1940 in teaching, too. He lectured geodesy and theoretical geodesy at corresponding courses. Since 1954, he has been taking part in university education with lectures on theoretical geodesy. Lecture notes for these were predecessors of the textbook published in 1966, being the first Hungarian textbook on Theoretical Geodesy. Since 1959, most of his time has been spent for university education. He lectured in Theoretical Geodesy between 1959 and 1978, in Photogrammetry since 1963. For shorter time, he also lectured Geophysics and Basic Networks in Geodesy. Most of these were accompanied by lecture notes, too. He takes also part in postgraduate education. He published not only papers on education

in geodesy, but led the compilation of the program for students in geodesy in the framework of the university reform.

As Professor at the Institute of Photogrammetry, he took an active part in researches and solutions of practical problems. He analyzed theoretical questions in analytic aerotriangulation, and published several papers on the non-cartographic use of photogrammetry.

Professor HOMORÓDI published more than hundred papers and nearly 150 recensions and reviews. A part of these publications has already been mentioned. His scientific portrait, however, would not be complete without mentioning the technical news from abroad which he introduced in Hungary, such as e.g. quartz clocks in 1937, atomic clocks in 1950, geodetic use of high capacity computers in 1954, and of satellites in 1964.

He promoted geodesy at home and abroad by a wide-ranging public activity. He is founder-member of the Society of Geodesy and Cartography, and was chairman of this Society between 1962 and 1980. At present, he is associate chairman of the Society. He has taken part from the beginning in the activity of the Comission of Geodesy of the Hungarian Academy of Sciences, where he has presided since 1975. Ha takes and took part in the activity of other comissions, too.

Professor HOMORÓDI is also well known outside of Hungary. He has participated for nearly three decades in the activity of the Fédération Internationale des Géomètres (FIG), where he was between 1972 and 1974 vice-chairman, between 1975 and 1976 chairman of Commission 2 (Education). He is also active in ISP and UGGI, thus promoting the reputation of Hungarian geodesy.

As an appreciation of Professor HOMORÓDI's merits, he was awarded several times, from which two governmental medals, the Lázár Deák and Fasching Antal medals of Hungarian geodesists, the price of the Association of Hungarian Technical Societies and a honorary diplom of FIG should be mentioned here.

We wish Professor HOMORÓDI at his seventieth birthday good health for many years coming, that his activity should not cease, that we could read his papers, hear his lectures and his opinion about the problems arising on the different fields of geodesy.

Acta Geodaet., Geophys. et Montanist. Acad. Sci. Hung. Tomus 16 (1), pp. 15—26 (1981)

GEODYNAMIC ASPECTS OF REPEATED GEODETIC LEVELINGS AND GRAVITY OBSERVATIONS

P. BIRÓ

TECHNICAL UNIVERSITY OF BUDAPEST

[Manuscript received September 23, 1980]

Theoretical investigations show that time changes of geopotential or elevation differences of bench marks characterize true vertical movements of Earth's surface (or crust) only in exceptional cases, which do not exist in the case of our real Earth. As far as true vertical displacements of gravity stations cannot be determined, observed changes of gravity are insufficient information to conclude to the non-tidal variations of Earth's gravity field. Theoretical and practical experiences show that the changes of gravity differences and of height differences are in linear correlation. Thereby repeated precise gravity measurements may be in principle substituted for repeated geodetic levelings as a more economical and rapid method especially for long distances. A new continental network scheme has been suggested for studying recent vertical movements. Attention is called to possible considerable irregular local changes of Earth's gravity field within restricted ranges. It is recommended to carry out repeated simultaneous precise gravity measurements and geodetic levelings completed by the observations of the vertical gradient of gravity along several test lines and areas.

Introduction

Geodetic levelings and precise observations of gravity as well are carried out in the gravity field and on the topographic surface of the Earth. The up to date dynamic view of geodesy requires to assume the secular and long periodic time variations both of the physical figure and of the gravity field of the Earth [e.g. BARTA 1979, BOULANGER 1979, TORGE 1979 etc.]. The mentioned time variation of the former is usually termed as "*recent crustal movement*" while that of the latter as "*non-tidal variations of gravity*". (Because of displacements of the topographic surface can be observed and we are not convinced that these are really followed by the entire crust, the term "*surface displacement (or movement)*" will be preferred instead of "crustal movement".)

There is no doubt that both geodetic levelings and gravity observations (either absolute or relative) are influenced by the mentioned time variations. Therefore the investigation of the *true physical interpretation* of the results of the mentioned geodetic observations is needed.

Repeated geodetic levelings

Geodetic leveling is the usual method of determining height differences between neighbouring bench marks. Repeated geodetic levelings are the common method of determining vertical surface displacements (so-called "recent crustal movements"). In both cases the equipotential surfaces of Earth's

gravity field serve as the reference system of heights. Basic assumption in determining heights, in particular, vertical surface displacements is the stability of our reference system, that is, the location of all level surfaces in space are supposed to be unchangeable (i.e. they do not vary with time).

Having nowadays more and more theoretical and practical information about variations of Earth's gravity field we have to check

— the influence of variation with time of Earth's gravity field on the heights of bench marks,

— the interpretation of the observed temporal changes of heights and of gravity i.e. to explain their true physical meaning.

Theoretic investigations led to the following basic relationships for two models of different complexities and for the real Earth [BIRÓ 1971—1979].

In the simple case of an earth model with perfectly *rigid* crust unable to any deformation, no vertical surface movement could arise. Any change of the potential of our bench marks would unambiguously show the variation with time of the gravity field, or vice versa, changes of the surface gravity would lead to unambiguous conclusions on the change of the potential. The displacement of the equipotential surfaces of the gravity field is expressed by

$$\delta N^r = \frac{\delta W}{g} \tag{1}$$

where δN^r is the displacement of the equipotential surface of the model earth of potential W, δW being the time variation of the potential at the tested point (i.e. bench mark), g the gravity at the same point.

Let the second model be a model earth with *elastic* crust, deformable upon gravity field changes. Consequently, field changes not only cause the displacement of the equipotential surfaces, but this displacement will be followed by the elastic deformation of the topographic surface (Fig. 1). Accordingly, the position of our bench mark P referring to the equipotential surfaces of the gravity field, i.e. its height above the sea level H_P will change by

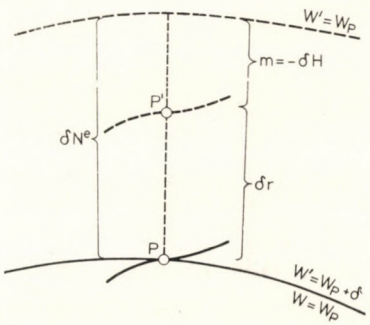

Fig. 1

$$\delta H_P = -m_P = -\frac{W'_{P'} - W_P}{g} = -\frac{\delta W_{P'}}{g} . \tag{2}$$

In general, it has to be assumed that the time variations of the gravity field are different in different stations at the model surface. Let $\delta W_{P'}$ and $\delta W_{Q'}$ be the variation of the geopotential at points P' and Q' resp., the height difference H_{QP} between points P and Q will change by

$$\delta H_{QP} = H_{Q'P'} - H_{QP} = -\frac{1}{g}(\delta W_{P'} - \delta W_{Q'}) . \tag{3}$$

It should be noticed that this is the difference of displacements of the tested bench marks referred to the equipotential surfaces of the gravity field. Since, however, the equipotential surfaces themselves are shifted in the space, (3) fails to indicate the true vertical movements of the points. In our simple model, beside elastic deformations following gravity field variations, no other, e.g. geological surface movements have been assumed to occur.

Using for qualitative discussions Love's theory of Earth's elasticity (instead of a visco-elastic model), the true vertical displacements of points P and Q on elastic model surface can be estimated by

$$\delta r = h^* \delta N^r = -\frac{h^*}{D}\delta H \tag{4}$$

being

$$\delta N^r = \frac{\delta W}{g} = \frac{1}{g}\frac{W'_{P'} - W_P}{D} = -\frac{\delta H}{D}$$

where $D = 1 - h^* + k^*$; h^* and k^* being special values of Love's numbers.

The difference between the true vertical displacements of points P and Q will be

$$\delta r_P - \delta r_Q = -\frac{h}{D}\delta H_{QP} . \tag{5}$$

As the difference of Eqs (3) and (5) expressing the difference between the true and the relative displacement of model surface points, we obtain

$$d = \delta H_{QP} - (\delta r_P - \delta r_Q) = \left(1 + \frac{h^*}{D}\right)\delta H_{QP} = -\left(1 + \frac{h^*}{D}\right)\frac{\delta W_{P'} - \delta W_{Q'}}{g} \tag{6}$$

that would be zero only for quite exceptional values of h^* and k^*; in general, however, it is significantly non-zero. The difference depends on the real values of the Love's numbers. Their empirical values being known only from observa-

tions of relatively short-period phenomena, determination of special values of Love's numbers for long period or secular variations of the gravity field needs further investigations.

Anyhow, from the available data it can be stated that both the relative height difference and the true location in space of surface points in a gravity field varying with time are in general time-dependent, even if no kind of geological movement intervened. Thus, a due circumspection is needed when interpreting observed changes of height differences.

In the *general* case of our *real Earth*, vertical displacements of Earth's surface are caused, — in addition to elastic deformations *e* following time variations of the gravity field, — also by other unknown movements *b*, e.g. those of geological origin (Fig. 2). The complete Earth surface displacement is thus a resultant of different effects, hence also the observed variations of the surface gravity are composed both of the effect of surface displacements and of field changes.

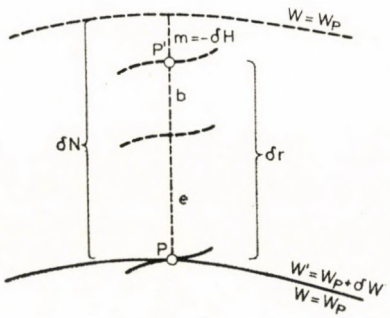

Fig. 2

In this general case, too, geodetic levelings lead only to relative displacements of Earth's surface referred to the equipotential surfaces of the gravity field which can be expressed by (2) where $\delta W_{P'}$ is the variation of geopotential on Earth's surface displaced by several causes.

In calculating the true vertical displacement of Earth's surface δr the relative displacement m ought to be reduced by the displacement of the equipotential surfaces of the gravity field (Fig. 2):

$$\delta r_P = \delta N_P - m_P = \delta N_P + \delta H_P . \tag{7}$$

Unfortunately, however, in the time being no exact method can be suggested for calculating δN from the temporal gravity variations like in case of a rigid Earth body or of purely elastic deformations, namely now it contains various unknown effects. This is why researches to determine the absolute displacement of equipotential surfaces by other means, or to determine the

secular variation of the gravity field from the observation of that of some other physical field (e.g. the Earth's magnetic field) are of great importance. There have been published some model investigations for different specific models esp. for earthquakes giving formulae for the estimation of the real vertical displacement of the ground surface, but they can not be accepted as exact solution for our general case [WHITCOMB 1976, WALSH and RICE 1979].

Until no relevant research result is available, one must be aware that the vertical surface movements observed by usual repeated geodetic levelings are but relative values referred to the equipotential surface which may significantly differ from the true surface displacements.

Repeated gravity observations

It is known that observed gravity at the Earth's surface is a function of the location of the station on one side and that of the distribution of Earth's masses on the other side. Assuming a time variation of both variables, the variation of gravity will be

$$\delta g = \frac{\partial g}{\partial v}\bar{v} + \frac{\partial g}{\partial W}\delta W \tag{8}$$

being g the gravity vector, δW the time variation of the potential of Earth's gravity field — as before — caused by a redistribution of Earth's masses and v the displacement vector of the station.

Temporarily neglecting the effect of the horizontal components of v, for the vertical component of the variation of gravity can be written

$$\delta g \doteq \frac{\partial g}{\partial H}\delta r + \frac{\partial g}{\partial W}\delta W \tag{9}$$

being δr the vertical component of v, i.e. the true vertical displacement of the Earth's surface.

Formula (9) with observed changes of surface gravity on the left side is one equation with two unknowns δr and δW. It could be solved for δW only in that case if the determination of the real vertical displacement δr of the station were possible.

In the simple case of the model with rigid crust there is no surface movement, i.e. $\delta r = 0$ and (9) leads to a unique solution for δW the time variation of the gravity field being

$$\delta g = \frac{\partial g}{\partial W}\delta W = C^{-1}\delta W \tag{10}$$

with

$$C^{-1} = \frac{\partial g}{\partial H}\frac{\partial H}{\partial W} = -\frac{1}{g}\frac{\partial g}{\partial H}. \tag{11}$$

Equation (10) is a basic relation between variation of gravity and that of the potential in the same point of the space.

If Earth's crust showed pure *elastic* deformation it could be determined by using Love's theory of Earth's elasticity being δr the single component of the true vertical displacement of Earth's surface. It could be calculated in the terms of the observed change of elevation and Love's numbers by formula (4) (see Fig. 1), or more exactly by a visco-elastic model.

Unfortunately in the *general case* (Fig. 2) the vertical displacement of Earth's surface

$$\delta r = b + e \tag{12}$$

is the resultant of more components (elastic and other deformations) and we do not know any exact function either for $\delta r = \delta r(\delta H)$ or for $\delta r = \delta r(\delta g)$ determining uniquely the complete true vertical displacement in the term of the variation of height or that of the gravity. (Some authors suggested the application of Stoke's integral formula for $\delta r = \delta r(\delta g)$ but we did not succeed in proving the correctness of this application by the theory of potential.)

It should be noticed that repeated determination of geocentric coordinates of the station by satellite geodesy would result in the needed true surface displacement δr only in the case if the displacement of the geocentre could be simultaneously determined.

As we do not see any other possibility for the determination of the true vertical displacement of Earth's surface at the time being, we came to the conclusion that *it seems not to be possible without further information to conclude from observed changes of surface gravity to the non-tidal variations of Earth's gravity field.* It seems that neither geodetic leveling nor satellite geodesy itself leads to the needed further information.

Geodynamic use of repeated geodetic levelings and gravity observations

Let the variation of gravity on the real Earth's surface (Fig. 2) expressed by (9)

$$\delta g = g'_{P'} - g_P = \frac{\partial g}{\partial H}\delta r + \frac{\partial g}{\partial W}\delta W. \tag{13}$$

Replacing (7) for δr, (2) for δH_P, (10) and (11) for $\partial g/\partial W$ and

$$\delta N_P = \frac{\delta W}{g}$$

in (13) we get

$$\delta g = g'_{P'} - g_P = -\frac{1}{g}\frac{\partial g}{\partial H}(W'_{P'} - W_P) = C^{-1}(W'_{P'} - W_P) \tag{14}$$

which is the generalization of (10) for the conversion of the variation of potential to that of the gravity on the displacing Earth's surface.

By dividing both sides of (14) by g we get with

$$B = -\frac{C}{g} = \left(\frac{\partial g}{\partial H}\right)^{-1}$$

the relation

$$B(g'_{P'} - g_P) = -\frac{W'_{P'} - W_P}{g} = \delta H_P \tag{15}$$

which leads to the conclusion that changes of geopotential (or that of the height) can be determined either by repeated leveling or in principle by repeated gravity observations with a known vertical gradient of gravity.

The same relation is valid for the case of measurements between neighbouring bench marks as follows:

$$B_P\,\delta g_{P'} - B_Q\,\delta g_{Q'} = -\frac{\delta W_{P'} - \delta W_{Q'}}{g} = \delta H_{QP} = \delta(H_P - H_Q) \tag{16}$$

being

$$\delta g_{P'} - \delta g_{Q'} = (g'_{P'} - g_P) - (g'_{Q'} - g_Q)$$

and

$$\delta W_{P'} - \delta W_{Q'} = (W'_{P'} - W_P) - (W'_{Q'} - W_Q).$$

Equations (15) and (16) show that repeated gravity observations can in principle be substituted for repeated geodetic levelings if the vertical gradient (i.e. factor B) is known [Biró 1973]. Both kinds of observations yield the change of the potential difference of the bench marks. The experiences by Nakagawa and Satomura (1977), Jachens (1978), Torge (1979) and some other authors do coincide with this theoretical conclusion.

This conclusion has led to the suggestion that extended leveling lines for determining the relative crustal movements can be replaced or controlled by repeated precise gravity measurements [Biró 1975, Nakagawa and Satomura 1977]. Considering the accuracy of modern absolute or relative precise gravity observations they are safely comparable to the reliability of a leveling of several hundred or 1000 to 1500 km length.

Therefore a new possible scheme of vertical crustal movement control net presented in Fig. 3 has been suggested [Biró 1975, 1979].

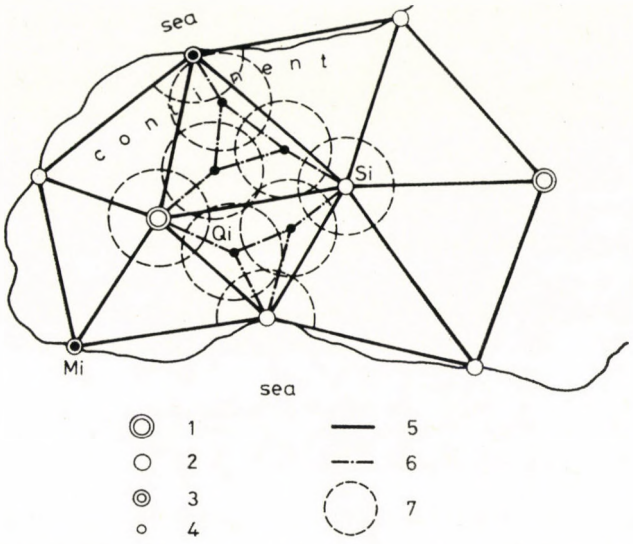

Fig. 3. Suggested scheme of a continental control network for studying recent vertical surface movements. Legenda: 1 — super control point (with absolute gravity measurement), 2 — regional control point, 3 — regional control point with tide gauge, 4 — local reference station, 5 — gravimetric connections, 6 — regional leveling lines, 7 — local systems for studies of crustal movements

Relative surface (crustal) movements can be determined by usual repeated geodetic levelings in local systems related to the level surface of local reference stations Q_i. These reference stations can be connected to each other and to regional control points S_i by regional geodetic leveling lines. Some of these on the shore should be connected to tide gauges (i.e. to the current mean sea level). Regional control points should be connected to each other and to some super control points with known absolute gravity by relative precise gravity measurements. Absolute gravity observations should be completed within the possible shortest time interval (quasi simultaneously) in the entire net.

National vertical control nets could serve for local systems. Average distance of local reference stations (reference bench marks) can be about some hundred kilometers, average distance of regional control points could be suggested as 1000 to 2000 km. On this way the reliability of relative crustal movements could be increased very economically. The only one question is the knowledge of the actual values of factor B in (15) and (16), therefore it should be empirically determined at the gravity stations.

Formula (16) can be checked empirically with the conclusions deduced therefrom by simultaneously observing both quantities. Special precise gravity lines (as for example the Fennoscandian land uplift gravity line [KIVINIEMI 1977], or the E—W gravity line in the GDR [ELSTNER et al. 1978] and similar others) will give very important information also for this purpose if also varia-

tions of height differences will be simultaneously observed directly by repeated geodetic leveling between the stations.

NAKAGAWA and SATOMURA (1977) succeeded in making repeated simultaneous gravity observations and precise levelings around Lake Biwa (Japan) between 1971 and 1976. They have 15 bench marks on a line of about 90 km and made observations every year by LaCoste-Romberg G gravimeters. In their paper they have graphically shown the gravity change and the changes of elevations of bench marks and stated the obvious correlation of both measurements.

With kind allowance of the authors we checked numerically this correlation and got a correlation factor of -0.63 which is not too low, but also not very high. But gravity change and changes of elevations above the sea level are loaded by many uncertainties (i.e. unknown changes of gravity and that of the elevation of the reference station, inhomogeneous reliability of data etc.). Therefore it is more useful to check the correlation of *changes* of gravity differences and of height differences between neighbouring bench marks by formula (16) assuming approximately being $B_P \doteq B_Q = B$. Observations (gravity measurement and geodetic leveling) directly result in these changes without making any assumption, and most probably with nearly the same accuracy for any couple of stations. Between 15 bench marks one gets 14 differences. Gravity observations were available from 4 or 5 years and levelings from 1971 and 1975/1976. According to this fact we had a set of data for the change of height differences $\delta(H_P - H_Q)$ between 1971 and 1975/1976 and another set of data for the change of gravity differences of neighbouring bench marks for the same time interval (Fig. 4). This latter has been calculated according to two alternatives:

a) as the difference of the observed gravity difference of 1971 and 1975/1976, when also levelings were completed *(observed* changes of gravity differences);

b) for the time interval of the levelings, fitting a straight line by the least squares method to the observed gravity differences of each couple of neighbouring bench marks in each of the years between 1971 and 1975/1976 (*predicted* changes of gravity differences).

Applying both sets of changes of gravity differences $\delta(g_P - g_Q)$ the correlation of them with the changes of height differences has been tested, yielding the correlation factors of $r = -0.84$ and $r = -0.70$ for observed and for predicted changes of gravity differences respectively, showing a significant correlation of the analyzed quantities.

Correlation factor for the predicted gravity changes is less significant than that for the observed ones. This may be attributed to the fact that gravity changes of all the bench marks are not really linear. The deviations of observations from the "least squares" straight line are only partly due to errors

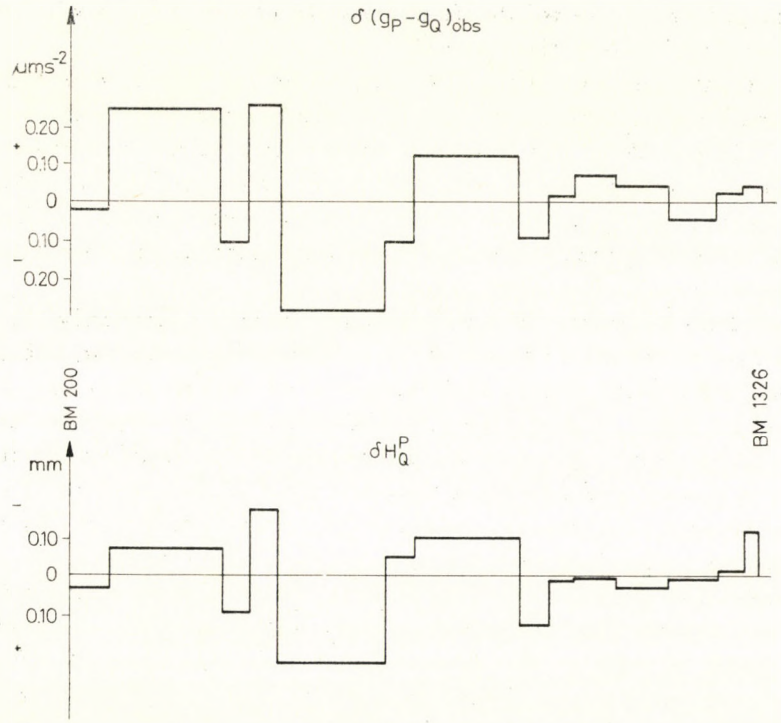

Fig. 4

of observations, partly they show real differences of gravity changes between the different years. It means that gravity changes are most probably "rapid" (irregular), local variations and in most part not regional, secular ones (trends have different signs).

Checking the correlation of the both complete sets of observations by fitting a mean adjusting straight line respecting also the different weights of the different kinds of observations we got as results

$$B = -85 \cdot 10^9 \text{ s}^2 (= -0.85 \text{ m/mgal}) \text{ and}$$

$$B^{-1} = -11.8 \cdot 10^{-6} \text{ s}^{-2} (= -1.18 \text{ mgal/m}) \text{ resp.}$$

It must be mentioned that only a few of the pairs of observations do exceed the amount of their mean square error. Selecting only this three pairs of observations which can be regarded significant, the direct determination of the factor B and its reciprocal results in

$$-78 < B < -32 \cdot 10^{-9} \text{ s}^2 \quad \text{resp.} \quad -30.9 < B^{-1} < -12.8 \cdot 10^{-6} \text{ s}^{-2}$$

$$(-0.78 < B < -0.32 \text{ m/mgal resp.} \quad -3.09 < B^{-1} < -1.28 \text{ mgal/m})$$

or in average

$$B = -60 \cdot 10^{-9} \text{ s}^2 (= -0.60 \text{ m/mgal}) \text{ and}$$

$$B^{-1} = -16.7 \cdot 10^{-6} \text{ s}^{-2} (= -1.67 \text{ mgal/m}).$$

TORGE (1979) reported the analysis of gravity and height variations in Northern Iceland. He got for the gravity-height-variation ratio (i.e. reciprocal factor B^{-1}) figures between $-1.2 \cdot 10^{-6}\,\text{s}^{-2}$ and $-4.3 \cdot 10^{-6}\,\text{s}^{-2}$ (-0.12 and -0.43 mgal/m) and reported an anomalous value of $+13 \cdot 10^{-6}\,\text{s}^{-2}$ ($+1.3$ mgal/m)! Further theoretical and empiric figures are referred by JACHENS (1978).

All these experiences call the attention to that the gravity-height-variation ratio (the reciprocal factor B^{-1}) can vary between very extreme values being some times more or less than the theoretical (free air type) one and show considerable irregular local changes within restricted ranges (few kilometers especially in active regions). Deduction of any mean value for the factor B^{-1} even for very restricted areas can be very misleading. Therefore further investigations by repeated simultaneous precise gravity observations, geodetic levelings and direct observations of the vertical gravity gradient along different test lines in different areas of the world are of outstanding interest in the future.

Acknowledgements

Thanks are due to Professor NAKAGAWA and to Mr. SATOMURA for making available their observations.

REFERENCES

BARTA, G. 1979: Mass distribution of the Earth on the surface and at depth and the global secular variation of the gravity field. Bulletin d'Information, Bureau Gravimetrique International N° 44, pp. I-D-24-29, Paris.

BIRÓ, P. 1971.: Vertical Earth's Crust Movements and Secular Variations of the Earth's Gravity Field. Report presented at the XVth General Assembly of IUGG, Moscow.

BIRÓ, P. 1973.: Der Einfluß von zeitlichen Änderungen des Erdschwerefeldes auf die Höhe von Nivellementsfestpunkten. *Wiss. Mitteilungen aus dem Inst. für theor. Geod. der Univ. Bonn*, No. 12, pp. 1—12, Bonn.

BIRÓ, P. 1974.: Theory of heights in gravity field varying in time. Thesis, pp. 1—162, Hungarian Academy of Sciences, Budapest.

BIRÓ, P. 1975.: Vertical Crustal Movements and Time Changes of the Gravity Field. Report presented at the Symposium on Recent Crustal Movements of the XVIth General Assembly of IUGG, pp. 1—8, Grenoble.

BIRÓ, P. 1979.: Dynamic Aspects of Repeated Geodetic Leveling. Report presented at the XVIIth General Assembly of IUGG, pp. 1—23. Canberra.

BIRÓ, P.: Zur Anwendung der Stokes'schen Formel für zeitliche Schwereänderungen. *Zeitschrift für Vermessungswesen* (in press).

BIRÓ, P.: Wiederholte Schweremessungen und zeitliche Änderungen des Erdschwerefeldes. *Allgemeine Vermessungsnachrichten* (in press).

BOULANGER, Y. D. 1979.: Brief Review of Research on Non-tidal Gravity Variations 1974—1978. Report of the Special Study Group 3.40 IAG, Bulletin d'Information, Bureau Gravimetrique International N° 44, pp. I-D-1-14, Paris.

ELSTNER, CL.—HARNISCH, G.—ALTMANN, W. 1978.: Ergebnisse präzisionsgravimetrischer Messungen auf der W-E-Linie der DDR 1970—76. *Vermessungstechnik*, pp. 12—14.
JACHENS, R. C. 1978.: The gravity method and interpretative techniques for detecting vertical crustal movements. Geop.-9 Conference Proceedings, Columbus, Ohio, October.
KIVINIEMI, A. 1977.: The Finnish measurements at the Fennoscandian land uplift gravity lines. Report presented at the Symposium on Non-tidal Gravity Variations and Methods for their Study, pp. 1—6. Trieste, Italy.
NAKAGAWA, I.—SATOMURA, M. 1977.: Gravity change observed near Lake Biwa, Japan. *Bulletin Geodésique*, Vol. 51, pp. 213—217.
TORGE, W. 1979.: Gravity and Height Variations Connected with the Current Rifting Episode in Northern Iceland. Report presented to the Symposium on Recent Crustal Movements, XVII. General Assembly of the International Union of Geodesy and Geophysics, pp. 1—12. Canberra.
WALSH, J. B.—RICE, J. R. 1979.: Local changes in gravity resulting from deformation. *J. Geoph. Res.*, 84, pp. 165—170.
WHITECOMB, J. H.: New vertical geodesy. *J. Geoph. Res.*, 81, pp. 4937—4944. 1976.

ГЕОДИНАМИЧЕСКИЕ ОТНОШЕНИЯ ПОВТОРНЫХ ТОЧНЫХ НИВЕЛИРОВАНИЙ И ИЗМЕРЕНИЯ ГРАВИТАЦИОННОГО УСКОРЕНИЯ

П. БИРО

РЕЗЮМЕ

Проведенные теоретические изучения показывают, что изменение разности высот точек на поверхности Земли или высоты точек над уровнем моря по времени характеризует реальную вертикальную дислокацию поверхности только в идеальных случаях, не сутществующих в случае нашей Земли. До тех пор, пока геодезическими методами невозможно определить реальные вертикальные дислокации наших гравитационных основных точек, нельзя вывести однозначное заключение из наблюденных гравитационных изменений этих точек на те изменения поля силы земного притяжения по времени, которые происходят не из явления приливы-отливы. Доказано, что изменение высоты поверхностных точек и гравитационного ускорения пропорционально друг другу. Фактор пропорциональности пропорционален вертикальному градиенту гравитационного ускорения и в зависимости геологической структуры изменяется даже и на тесной территории в широких пределах. На основание японских измерений автор показывает пример для эмпирического определения этого фактора. В завершение он обращает внимание не важность установления таких испытательных линий (территорий), где по систематическим временам производятся повторянное симултаническое точное нивелирование, абсолютные и релятивные измерения гравитационного ускорения и определение вертикального градиента гравитационного ускорения в каждых наблюденных точках.

Acta Geodaet., Geophys. et Montanist. Acad. Sci. Hung. Tomus 16 (1), pp. 27—39 (1981)

EVALUATION OF AUTOMATIZED GYROTHEODOLITE MEASUREMENTS WITH SPECIAL RESPECT TO MOM GYROTHEODOLITES

F. HALMOS†
DR. TECHN. SCI.

GEODETIC AND GEOPHYSICAL RESEARCH INSTITUTE OF THE HUNGARIAN ACADEMY OF SCIENCES, SOPRON

[Manuscript received June 25, 1979]

Precise azimuths are determined by gyrotheodolites in different measurement cases at the surface or in subsurface measurements. After a short instrumental description, the theoretical problems of the analysis of the measurement results are presented. Based on the mathematical theory of the evaluation, a quick and simple method is proposed for the determination of the instrumental constant and of azimuths. Technical solution, theoretical investigations and some results of practical examples are given. The mean square error of a double azimuth determination will be $\pm 2-3''$ by using the measurement method proposed in the paper.

1. Introduction

The increase of the accuracy of gyrotheodolites, the development of an automatized observation and evaluation system led to high accuracy azimuth determinations by gyrotheodolites [1—7]. From the instrument types, MOM Gi-B21 (1972—73) should be mentioned which has a mean square error in azimuth of $\pm 2-3''$ for a single measurement, further GYMO Gi-BlA (1974) which is a common construction of the Hungarian firm MOM and the Canadian firms Tellurometer and Plessy [8].

The determination of the equilibrium position (rest position) of the pendulum system in both the gyroscopic and the free swinging case is carried out by the automatic measurement of transit times and their numerical evaluation. Digital, objective transit time measurements have several advantages:

a) no vibration errors due to manipulations with the instrument;

b) no subjective errors in the observations of the following of the swingings, which means an increase of the accuracy by at least one order of magnitude;

c) transit times can be accurately observed in case of medium sized amplitudes ($\pm 40'$) and the irregular torsional resistance of the suspension band, as well as small disturbances of the pendulum momentum are eliminated [2];

d) in case of medium sized amplitudes, the reversion points can be observed on the scale of the autocollimators, which enables the use of combined measurement methods [9];

e) using measurements with and without following in turn at a single station, the torsional coefficient most characteristic for the measurement conditions can be deduced [2, 7, 9];

f) by measuring the transit times at three positions with photodiodes, the differences of the transit times can be obtained, too, which enables the use of the transit time difference-method [1, 9, 10];

g) using lighter material for the pendulum housing, the weight and the torsional disturbing effect during the precessional movement can be decreased, thus the accuracy can be increased;

h) the continuous measurement of transit times enables a significant decrease of the computation and the introduction of simplified evaluation methods [8], or even a rigorous evaluation program can be set up [11];

i) in addition to the digital display of the time values, an audio signal reminds to the continuous readout of digital time values, if the instrument is not a recording one.

2. The automatized transit-time measurement

2.1 *Technical description*

In case of automatized transit-time measurements the light reflected from the mirror of the swinging system, consisting of the gyroscope and of the suspension band must not be read out through the autocollimator as in case of gyrotheodolites MOM Gi-B1 and Gi-B2, but it arrives through a slit to photodiodes. The light signals result in electric impulses which drive a quartz-stabilized impulse-counter, thus transit-times can be measured and recorded theoretically with an accuracy of hundredth of seconds. The instrument includes generally one slit and 2—3 photodiodes (phototransistors). In case of the instrument MOM Gi-B1 two photodiodes are used recently, one of them being near to the scale division $+10$, the other near to -10, that means the angle $\Delta\alpha$ between them is approximately $600''$.

The symmetry axis of the two photodiodes is the limb division corresponding to the preliminarily determined North direction (α_H), theoretically coinciding with the zero division of the autocollimator scale. The transit times follow each other in a logical sequence. So e.g. in case of two-sided swingings, the time measuring device is set to zero when the light crosses the first (L) photodiode, then the first transit time is measured on the right-hand side photodiode (R) as $t_{10} = 0$. Reaching the right extreme position of the swing, the reversion point n_1 can even be read out in scale divisions on the autocollimator (Fig. 1). As next the light slit is crossing again the photodiode R and the transit time t_{11} is measured which must be already recorded in the protocol. Now

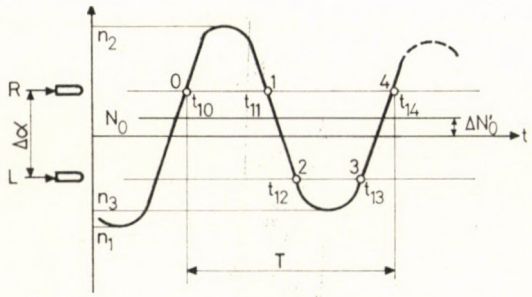

Fig. 1

come in turn the transit times t_{12}, t_{13} on the left-hand side photodiodes which are also remarked in the protocol. If necessary, the position of the reversion point n_2 can also be read out between them in scale divisions. In case of gyrotheodolites MOM Gi-B the condition for this possibility is that the amplitude of the swinging should not be greater than $\pm 40'$, due to the extension of the scale divisions. At last the transit time t_{14} is read out at the transit on the photodiode R. The time value of t_{14} is simultaneously the first measured value of the next full swinging, i.e. $t_{21} = 0$. Afterwards the measurement is carried on automatically. The data of the impulse counter are displayed till the next time value appears. This is accompanied by an audio signal as warning. The serial number of the value is also displayed. Displayed values can also be printed out or recorded on punched or magnetic tape in order to enable further processing in on-line system.

2.2 *Problems of observation technics*

In order to eliminate hysteresis-like drifts resulting from warming up of the suspension bands, it is advisaeable to run the motor before the first measurement some 5—15 minutes depending on the outside temperature, further to let the pendulum freely swing by arresting it in a position significantly differring from the torsionfree position for a significantly long time.

The high-accuracy azimuth determination requires a preliminary orientation of the instrument in the North direction with the possible highest accuracy ($\pm 20-30''$). The torsion-free position of the suspension band can be best regulated into the zero division of the autocollimator scale (with an accuracy of ± 1 scale divisions). The centripetal force due to the rotation of the Earth and the gyroscopic momentum due to the rotation of the gyroscope (M_G) together with the torsion momentum of the suspension band (M_{free}) give as vectorial resultant the rest position with torsion (Fig. 2) (N_0'). In case of a well approximated preliminary North the gyroscopic swingings are nearly symmetrical in respect of the zero division of the autocollimator scale. If the torsion-free position of the band has also a value near to zero, the swinging is also symmetri-

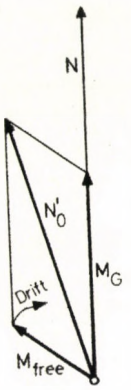

Fig. 2

cal in respect to it. If this is not the case, a slow change of the torsion-free position will be found during the whole time of the measurement due to the counteraction between the gyroscopic momentum and the torsional momentum of the band, i.e. a slow drift of the torsion-free position towards the rest position will be found. Since the gyroscopic momentum is about four-five times greater than the torsional momentum of the band, only a slight change of the torsional constant is to be expected in consequence of the effects of forces.

As it is known, the coefficient of the torsional momentum c is:

$$c = \frac{M_b}{M_G} = \left(\frac{T_{\text{fol}}}{T_{\text{wf}}}\right)^2 - 1 \tag{1}$$

where T_{fol} is the swinging time with following, T_{wf} is the swinging time without following. According to experiences it can be stated that the temperature effects due to running and current input, further the effects of mechanical stresses result in changes of the swinging time in the order of 1 s (Table I). This means a change already in the third digit of c, and this causes an error of about one second of arc in the determination of the rest position. To these, the effect of the change of geographical latitude is added. Therefore it is adviseable to determine the c value corresponding to the environment of the measurements directly from the results of the measurements. For this purpose, exact swinging times with and without following are needed at each station. In case of instruments, which enable automatic following but the automatics can be switched off, this possibility is ensured. The swinging times T can be determined in case of instruments with automatic determination of transit times with a very high accuracy ($T = t_{14}$). It is therefore concluded that observations are necessary at each station with and without following. A more accurate North determination necessitates anyway a several times repeated determination of the North direction with the gyroscope.

Table I

Changes of the torsional constant c

No.	Value of c	Temperature, °C	Place of the measurement
1	0.111 19		
2	0.109 30	22	laboratory
3	0.110 70		
4	0.110 82	14	subsurface measurement
5	0.109 39		
6	0.108 33		
7	0.109 52	20—25	field measurement
8	0.108 97		
9	0.111 02		
mean value	0.109 77		

2.3 *Computational problems of the automatic gyroscopic North determination*

The present paper discusses mainly the solution with two photodiodes as that with three photodiodes has already been discussed earlier [2, 4]. According to Fig. 3 let us denote these two photodiodes (phototransistors) by L and R. Let the angle between them be $\Delta\alpha$ (in case of MOM Gi-B21 600″). The rest position with torsion to be determined should be N_0. The measured time values are $t_{10} = 0$, t_{11}, t_{12}, t_{13}, $t_{14} = t_{20}$, $t_{21} \ldots t_{24}$, $t_{31} \ldots t_{34}$, (t_{ij}). If more full swingings are observed, the algebraic average of the corresponding time values can be used. Let α_M be the limb read out corresponding to the geometric central line of the two photodiodes and A the amplitude of the swinging. The position of the pendulum in the moment t_i can be given on the limb circle in case of measurements with following in the form [2]:

$$N_{t_i} = \alpha_M + A \sin\left(\frac{2\pi}{T_{\text{foll}}} t_i\right) \cdot \exp\left(-\frac{f_a t_i}{2}\right) + \text{const} \qquad (2)$$

where f_a is the damping coefficient of the pendulum, and the constant means the deviation of the gyroscopic axis from the North (due to e.g. band torsion or other disturbing factors). By substituting the time values t_{ij} for t_i the rest position N_0' is obtained by taking the exponential term equal one, what is here anyway an allowed neglection:

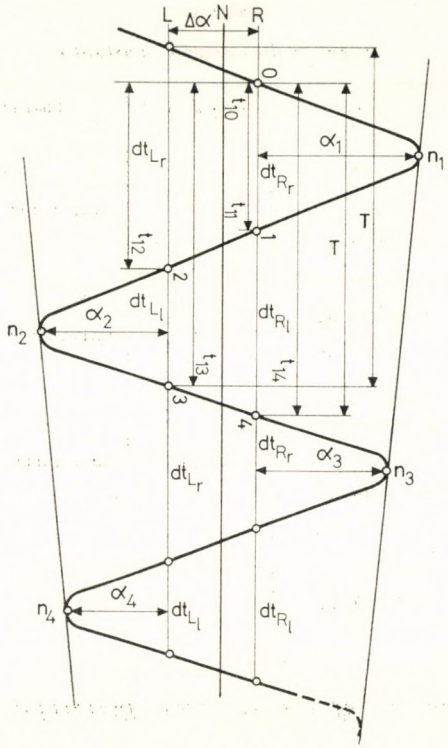

Fig. 3

$$N_0' = \alpha_M + A \sin \frac{\pi}{2} \left(\frac{2\, t_{ij} - T_{\text{foll}}}{T_{\text{foll}}} \right) = \alpha_M + A \cos \pi \left(\frac{i_{ij}}{T_{\text{foll}}} \right). \tag{3}$$

Be α_R the distance of the phototransistor R from the reversion n_1, and α_L the distance of the phototransistor L from the reversion n_2. In this case it can be written [2]:

$$\frac{\alpha_R}{\alpha_R + \Delta\alpha} = \frac{A \cos \dfrac{2\pi}{T_{\text{foll}}} \left(\dfrac{t_{11}}{2} \right)}{A \cos \dfrac{2\pi}{T_{\text{foll}}} \left(\dfrac{T_{\text{foll}} - (t_{13} - t_{12})}{2} \right)} = \tag{4}$$

$$= \frac{\cos \left(\pi \dfrac{t_{11}}{T_{\text{foll}}} \right)}{\cos \left[\pi - \pi \dfrac{t_{13} - t_{12}}{T_{\text{foll}}} \right]} = \frac{\cos \left(\pi \dfrac{t_{11}}{T_{\text{foll}}} \right)}{\cos \left[\pi \dfrac{(t_{13} - t_{12})}{T_{\text{foll}}} \right]}.$$

Similarly it can be written:

$$\frac{\alpha_L}{\alpha_L + \Delta\alpha} = \frac{A \cos\left[\frac{2\pi}{T_{\text{foll}}}\left(\frac{t_{13} - t_{12}}{2}\right)\right]}{A \cos\left[\frac{2\pi}{T_{\text{foll}}}\left(\frac{T_{\text{foll}} - t_{11}}{2}\right)\right]} = \tag{5}$$

$$= \frac{\cos\left[\pi \frac{(t_{13} - t_{12})}{T_{\text{foll}}}\right]}{\cos\left[\pi - \pi \frac{t_{11}}{T_{\text{foll}}}\right]} = \frac{\cos\left(\pi \frac{t_{13} - t_{12}}{T_{\text{foll}}}\right)}{\cos\left(\pi \frac{t_{11}}{T_{\text{foll}}}\right)} .$$

Let us introduce the notations:

$$t_{11} = d_1,\ t_{13} - t_{12} = d_2,\ t_{14} = T_{\text{foll}} = s. \tag{6}$$

Now Eqs 4 and 5 can be written as follows:

$$\frac{\alpha_R}{\alpha_R + \Delta\alpha} = -\frac{\cos \pi \frac{d_1}{s}}{\cos \pi \frac{d_2}{s}} = -\frac{\cos\left(180 \frac{d_1}{s}\right)}{\cos\left(180 \frac{d_2}{s}\right)} = -\frac{e}{f} \tag{7}$$

and

$$\frac{\alpha_L}{\alpha_L + \Delta\alpha} = -\frac{\cos\left(180 \frac{d_2}{s}\right)}{\cos\left(180 \frac{d_1}{s}\right)} = -\frac{f}{e} \tag{8}$$

where

$$\cos\left(180 \frac{d_1}{s}\right) = e \tag{9}$$

$$\cos\left(180 \frac{d_2}{s}\right) = f. \tag{10}$$

For the rest position (N_0') the following connection holds:

$$N_0' = \alpha_M - \frac{\alpha_R - \alpha_L}{2} . \tag{11}$$

According to Eqs 7 and 8. the values of α_R and α_L are obtained as:

$$\alpha_R = -\frac{\Delta\alpha \cdot e}{e + f}, \tag{12}$$

$$\alpha_L = \frac{\Delta\alpha \cdot f}{e+f}. \tag{13}$$

By substituting the Eqs 12 and 13 into 11 one gets:

$$N_0' = \alpha_M - \frac{\Delta\alpha}{2}\frac{e-f}{e+f} \tag{14}$$

where $\Delta\alpha = 600''$, is the angular distance between the two photodiodes expressed in angle. Eq. 14 holds for measurements with following. If a measurement without following is made, these formulas will be somewhat modified due to the lack of following, thus e.g. instead of Eq. 14, the following equation is to be used:

$$N_0' = \alpha_M - \frac{\Delta\alpha}{2}(1+c)\frac{e-f}{e+f} \tag{15}$$

where c is obtained from the swinging time deduced from momentaneous exact transit time measurements ($t_{14} = T$).

For the determination of the zero point correction of the band torsion observations similar to those described in the preceedings are to be carried out with non rotating gyroscope, i.e. free swingings are to be observed. Since the computational formulas are identical with those for gyroscopic swingings, for the sake of distinction the values measured here are denoted by an upper line. The torsional correction denoted by ΔN can be written as follows:

$$N = \frac{\Delta\alpha \cdot c}{2}\frac{e'-f'}{e'+f'}. \tag{16}$$

Let us introduce for the term containing $\Delta\alpha$ in Eqs 14 and 15 the notation g, for the remaining factor the notation L, then one gets:

$$N_0' = \alpha_M - gL. \tag{17}$$

Carrying out the same for the terms in Eq. 16 one gets:

$$\Delta N = hM \tag{18}$$

where:

$$h = \frac{\Delta\alpha\, c}{2} \tag{19}$$

$$M = \frac{e'-f'}{e'+f'}. \tag{20}$$

The corrected rest position (N_0) is computed from the following formula:

$$N_0 = \alpha_M - gL + hM = \alpha_M + \delta N_0. \tag{21}$$

Thus we reached the equation which is used in the factory MOM for the schematized determination of the rest position in case of the gyrotheodolites MOM Gi-B21. If not only one, but several full swingings are observed — what is generally the case —, one gets e.g. for two full swingings:

$$t_{11} + t_{21} = d_1\,;\; t_{13} + t_{23} - t_{12} - t_{22} = d_2\,;\; t_{14} + t_{24} = s. \tag{22}$$

In case of three full swinging periods:

$$t_{11} + t_{21} + t_{31} = d_1;\; t_{13} + t_{23} + t_{33} - t_{12} - t_{22} - t_{32} = d_2;\; t_{14} + t_{24} + t_{34} = s. \tag{23}$$

After finishing the measurements one needs about 10—12 minutes for the computations, when using a simple calculator with trigonometric functions. In case of a programable pocket calculator it takes 2—3 minutes of computation.

It follows from Eq. 11 that if one takes the algebraic average of the time value differences measured at the phototransistors L and R $\left(\frac{1}{2}[dt_{R_l} + dt_{L_l}] = dt_{M_l}\right)$ one gets a time value corresponding to the theoretical geometric central line (M). The necessary amplitude values can be obtained by using the reversion points $n_1, n_2, n_3 \ldots$ from the Fox—Schuler formula. In case of a pure transit time measurement, there is no need to know the amplitudes as shown by formulas presented. In case of a combination of transit times and reversions, an independent North determination can also be carried out by means of these values. If one takes into account the formula

$$\Delta t = \frac{1}{2}[(dt_{Rl} - dt_{R_r}) + (dt_{L_l} - dt_{L_r})] \tag{24}$$

on the basis of the time differences dt, then by taking into account the linear term one gets:

$$N_0' = \alpha_M - \frac{\pi}{2\,T_{\text{foll}}} A \cdot \Delta t \tag{25}$$

where A means again the amplitude computed from the reversion. In Eq. 25, A is measured in seconds of arc and Δt and T_{foll} in seconds of time. Taking into

account that the reversions are read out in the scale divisions of the autocollimator, it is necessary to take into account the value of the scale divisions in seconds of arc (20—30″).

In case of measurement without following one has the following formula:

$$N_0' = \alpha_M = \frac{\pi}{2T_{\text{wf}}}(1 + c)\, A\, \Delta t \tag{26}$$

where T_{wf} is the full swinging time without following.

2.4 *Measurement and observational program and the evaluation of the results*

The observational program for the automatized transit time measurements consists of the following steps:

1. Short free swinging and running of the motor in order to eliminate disturbing torsions and to ensure constant inner temperature. Measurement of the outer directions (3—5 minutes).

2. Determination of the zero position of the suspension band during a full free swinging (2—2.5 minutes).

3. Speeding up the motor, then desarretation, then the measurement of the transit time of a full or of a half swinging in order to obtain an acceptable approximative North direction (10—15 minutes).

4. After a repeated start the determination of the transit times and reversion points of three full swingings with following for the determination of the exact North direction. The reading on the limb must be set to the preliminary approximative North.

5. After breaking the motor the observation of a full free swinging (transit times and reversions) for the determination of the zero point position of the suspension band to be used in the final computation of the torsional correction.

6. The measurements of the directions of outer points.

7. With repeated speeding up of the motor the observation of transit times and reversions during three full swingings without following. Before the measurements the reading on the limb must be set to the value determined earlier.

8. Repetition of the manipulations described in 5. and 6. in order to determine the corrections.

9. In case of high precision azimuth determinations, it is adviseable to repeat the steps 4 and 8 once or twice.

10. Evaluation of the measurement data, determination of the most probable values and their mean square errors.

The instrumental constant (Δ) is determined from calibration measurements on a station with known azimuths. The observation and computation program is identical with that described.

For illustration we present the scheme used in the firm MOM for the instrument MOM Gi-B21 (Table II). The first block contains data on the station and the measurement.

Table II

P r o t o c o l	C_0=0.11355	$\Delta\alpha$=600" Page no.
Instrument: Gi-B 21	Time: 1974.06.17.	Surveyor: XY
No. of the instr.: 06 8266	Station: GM 5	Recorder: NN

Gyroscopic measurement:

	10	20	30	d	$180\frac{d}{S}$	cos	g
1	+229.83	+229.43	+	=459.26	76.0029	0.2419	334.07
2	−273.84	−273.53	−				
3	+499.97	+499.71	+	=452.31	74.8527	0.2613	
4	+543.97	+543.71	+	=1087.68		−0.0194	L
				S		+0.5032	−0.03861

gL
−12.9

Free swinging:

	10	20	30	d	$180\frac{d}{S}$	cos	h
1	+ 39.36	+39.21	+	=78.57	70.2110	0.3386	34.07
2	− 51.14	−51.16	−				
3	+ 88.87	+88.72	+	=75.29	69.2800	0.3862	
4	+ 100.71	+100.72	+	=201.43		−0.0476	M
				S		+0.7248	−0.06577

hM
−2.2

δN_o
+10.7

Δ	
	GM6
J_I	323-52-45
J_{II}	143-53-14
A	182-14-19.0
−J	323-52-59.0
	218-21-19.5
$+\alpha_M$	232-26-10.0
	90-47-29.5
$+N_o$	10.7
=Δ	90-47-40.2
$\Delta=A-J\alpha M+\delta N_o$	

Azimuth				
	GM6			
J_I	323-52-45			
J_{II}	143-53-14			
Δ	90-47-40.0			
$-\alpha_M$	232-26-10.0			
	218-21-30.2			
$-\delta N_o$	10.7			
	218-21-19.5			
+J	323-52-59.5			
=A	182-14-19.0			
$A=\Delta-\alpha M-\delta N_o+J$				

At the left hand side of block 2 one can find the time values of two full t_{ij} (gyroscopic measurement). The values 10, 20, 30 at the column's head are the numbers of the swingings (i) and the vertical columns contain the transit times (j). At the right hand side of the block there are deduced values which can be simply obtained from the formulas presented in the present paper. As a result one obtains the deviation (gL) of the rest position burdened by the torsion from the symmetry axis of the two phototransistors.

The third block consists observational and computational data on the free swingings. The result is the torsional correction hM. According to Eq. 21, a summation of the terms gL and hM yields δN_0. This added to the limb read out α_M, one gets the value N_0.

The fourth block contains the schemes both for the determination of the azimuth A and for the determination of the instrumental constant Δ. The direction values measured in both positions of the telescope are denoted by I_1, I_2. If the instrumental constant Δ is looked for, a direction with known azimuth A (or several such directions) are needed. Vice versa, if the azimuths A are unknown, the instrumental constant Δ is necessary. In form of equations:

$$\Delta = A - I + \alpha_M + \delta N_0 \tag{27}$$

and

$$A = \Delta - \alpha_M - \delta N_0 + I, \tag{28}$$

respectively. Here I denotes the average value of the two telescope positions. In case of measurements towards several targets, several azimuths, or several instrumental constants can be determined. In case of repeated measurements the algebraic average of the values is used.

This method ensures an azimuth determination with a mean square error of $\pm 2-3''$ depending on the momentaneous conditions. Some empiric data can be found in Table III. These are deduced from twice repeated measurements with and without following carried out within field conditions, at normal meteorological conditions.

Table III

No.	Azimuth determination as the average of two measurements with and without following			
	1	2	3	4
	measurement			
1	207°38′40.9″	90°47′44.8″	116°45′18.3″	35°07′27.8″
2	46.7″	51.6″	13.3″	28.9″
3	48.9″	45.2″	15.8″	32.5″
4	44.3″	48.3″	18.9″	26.2″
5	45.8″	44.5″	14.8″	29.9″
Average value	207°38′45.3″	90°47′46.9″	116°45′16.2″	35°07′29.1″
Mean square error of a single measurement	±2.8″	±2.7″	±2.1″	±2.2″

3. Summary

A schematizable, simple computation method is presented for the MOM gyrotheodolites, departing from the theoretical formulas of the azimuth determination using automatized gyroscopes with digital display. Experiments and practical azimuth determinations have shown that azimuths with mean square errors of $\pm 2-3''$ can be deduced from measurements at a single station with one repetition and with immediate determination of the torsional constant. Moreover, not only a quick and acceptably accurate evaluation method is given, but the possibility of the adjustment is also ensured.

REFERENCES

1. Grafarend, E.: Fehlertheoretische Untersuchungen und chronometrische Meßverfahren beim Einsatz von Aufsatzkreiseln in Kombination mit dem elektrooptischen Entfernungsmeßgerät AGA-Geodimeter 4 B. DGK Reihe C, No. 112, München, (1967) Beck'scher Verlag.
2. Halmos, F.: Giroteodolitok geodéziai alkalmazásának elméleti és gyakorlati kérdései (Theoretical and practical problems of the use of gyrotheodolites) Dissertation, Sopron, 1968—71.
3. Pusztai, F.—Beskó, D.: Vizsgálatok a giroteodolitok pontosságának fokozására (Investigations to increase the accuracy of gyrotheodolites), *Bányászati és Kohászati Lapok; Bányászat* (1970), 399—401.
4. Halmos, F.: Instrumentelle und methodische Fragen der geodätischen Anwendung von zeitgemäßen Kreiseltheodoliten. *Allg. Verm.-Nachrichten* (1971), 105—111.
5. Gregerson, L. F.—Vaníček, P.—Symonds, G. R.: Report experiments with a gyroscope equipped with electronic registration. Paper presented at the IAG Congress in Moscow, 1971.
6. Tarcsafalvi, A.: Neuer digitaler Gyrotheodolit der Fa. MOM. Geodetic Instruments, 1974 (MOM, Budapest).
7. Halmos, F.: Theoretical and practical problems of the use of gyrotheodolites in geodesy. Edited by Geod. Geoph. Res. Inst. of the Hung. Acad. of Sci. No. 6. 1977.
8. Halmos, F.: High precision measurements and evaluation method for azimuth determination with gyrotheodolites. Manuscripta Geodaetica, Vol. 2 (1977a), 213—231.
9. Halmos, F.: Giroteodolitos azimutmeghatározások módszertani és pontossági vizsgálata (Methodological and practical problems of the azimuth determinations using gyrotheodolites), *Geodézia és Kartográfia* (1968).
10. Grafarend, E.—Rymarczyk, H.: Neuartige chronometrische Meßverfahren zur Nordbestimmung mit Vermessungskreiseln. *Allg. Verm.-Nachrichten* (1971).
11. Halmos, F.—Závoti, J.: Ausgleichung kreiseltechnischer Schwingungsbeobachtungen. *Allg. Verm.-Nachrichten* (1979).

РАСЧЕТ АВТОМАТИЗИРОВАННЫХ ГИРОТЕОДОЛИТНЫХ ИЗМЕРЕНИЙ, УДЕЛЯЯ ОСОБОЕ ВНИМАНИЕ ГИРОТЕОДОЛИТАМ, ИЗГОТОВЛЕННЫХ В ОБЪЕДИНЕНИИ ЗАВОДОВ МОМ

Ф. ХАЛМОШ

РЕЗЮМЕ

Определены точные азимуты гиротеодолитами в разных измерительных ситуациях при наземных или подземных измерениях. После краткого описания инструмента представлены теоретические задачи исследований измерительных результатов. Основываясь на математической теории расчета предлагается быстрый и простой метод для определения постоянной инструмента и азимутов. Даются техническое решение, теоретические исследования и некоторые результаты практических примеров. Применяя предлагаемый метод — средние квадратические ошибки двойных измерений азимутов будут $\pm 2-3''$.

Acta Geodaet., Geophys. et Montanist. Acad. Sci. Hung. Tomus 16 (1), pp. 41—49 (1981)

APPLICATION OF LEAST SQUARES COLLOCATION FOR MINERAL RESERVE ESTIMATION

GY. ALPÁR

DOCTOR OF TECHNICAL SCIENCES
RESEARCH INSTITUTE OF ALUMINIUM INDUSTRY, BUDAPEST

[Manuscript received September 8, 1979]

The planning of investments in mining needs a more and more exact estimation of mineral reserves. For this purpose the so-called "kriging" method based on mathematical statistics is widely applied.

In case of similar estimation problems the least squares collocation method has been successfully applied in physical geodesy.

In the paper the congruence of the two methods is numerically and algebraically proved. The estimation of ore reserves by the least squares collocation method is not only equivalent to kriging, but also offers some remarkable advantages in computing technics.

The planning of mining investments needs among the present technical-economical circumstances a more and more exact estimation of mineral reserves. Thus, it is obvious that more and more attention is paid to the so-called geostatistical estimation methods. In this field of mineral estimation the best known method is "kriging" developed by G. MATHERON and his school and named after the South African researcher D. G. KRIGE [1]. This estimation method (of which more variants are used) secures more exact results because from the point of view of mathematical statistics, it takes correctly into account the variance-covariance relations of the input data and of the values interpolated by means of the input data. From that follows that with kriging the error of the mineral reserve estimation can also be determined applying the methods of mathematical statistics. Thus, the error estimation of the technical-economical calculations based on mineral reserve estimation can also be made without bias. In case of more simple mineral reserve estimation methods, the surplus information given by the determination of the variance-covariance relations are usually not taken into account.

On other fields of geosciences, first of all in the physical geodesy the least squares based on the collocation method has been developed almost simultaneously [2]. Here, again, the variance-covariance relations of the input data are correctly taken into account from the point of view of mathematical statistics and the interpolation is also made in correspondence with this. Consequently, a comparison of both methods is obvious in order to propose on this basis the application of collocation by least squares method (LSC) to mineral estimation.

The comparison would be very difficult if the methods based on different concepts would be confronted in accordance to their mathematical presentation. However, are the methods in question regarded as numerical methods in accordance with the requests of practice, a clear and simple comparison is possible.

For the sake of comprehension and mathematical proof the comparison will be shown both numerically and algebraically on the basis of a simple calculation example taken from [1]. The example is demonstrated on Fig. 1 [1].

The task is to determine the value l_p on the basis of the known values l_1, l_2, l_3 and l_4. In case of mineral reserve estimations the l values represent some date of analyses or thicknesses of penetrated layers from exploration borings situated e.g. according to Fig. 1.

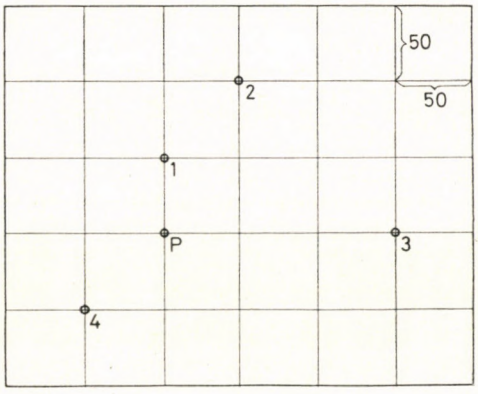

Fig. 1

Kriging presents the requested (interpolated) characteristics of the mineral reserve in the p point of the quadratic net covering the explored area by the linear formula

$$l_p = \sum_{i=1}^{n} a_i \, l_i, \tag{1}$$

where the main point of the method lies of course in the determination method of the "weight" numbers a_i. This most simple case of kriging is called point-kriging. If the characteristics of the mineral reserve are determined for each point of the quadratic net, the borders of the exploitable mineral reserve can be easily determined by taking into account the cut off values of the characteristics with respect to the actual economic situation.

For the determination of the weight-numbers in kriging, two conditions most be satisfied: the variance of the l_p-values to be interpolated must be minimized and the estimation of the l_p-values must be without bias. For the first condition the variance of the l_p-values will be

$$\mathrm{Var}(l_p) = \mathrm{Var}(l) - 2\sum_{i=1}^{n} a_i \mathrm{Cov}(l_p, l_i) - 2\sum_{i=1}^{n}\sum_{j=1}^{n} a_{i,j}\mathrm{Cov}(l_i, l_j) \tag{2}$$

where $\mathrm{Var}(l)$ is the variance of the uncorrelated l-values, $\mathrm{Cov}(l_p, l_i)$ the covariance between the l-values to be interpolated and those known, and $\mathrm{Cov}(l_i, l_j)$ the covariance between the l-values known.

In order to the second condition, the following simple equation follows from the requirement $E(\sum_{i=1}^{n} a_i l_i) = E(l_p)$ (the expected value of l_p should be equal to the expected value of l_i = unbiased estimation):

$$\sum_{i=1}^{n} a_i = 1. \tag{3}$$

The minimum after a_i of Eq. (2) at the simultaneous fulfilment of condition (3) can be calculated by the Lagrange method. In accordance with this the derivatives after a_i of the function

$$F = \mathrm{Var}(l_p) + 2\,k(\sum_{i=1}^{n} a_i - 1)$$

give the following linear equation system:

$$\begin{aligned}
c_{11}a_1 + c_{12}a_2 + c_{13}a_3 + \ldots + {}_{1n}a_n + k &= c_{p1}\\
c_{21}a_1 + c_{22}a_2 + c_{23}a_3 + \ldots + c_{2n}a_n + k &= c_{p2}\\
c_{31}a_1 + c_{32}a_2 + c_{33}a_3 + \ldots + c_{3n}a_n + k &= c_{p3}\\
&\vdots\\
c_{n1}a_1 + c_{n2}a_2 + c_{n3}a_3 + \ldots + c_{nn}\,a_n + k &= c_{pn}\\
a_1 + a_2 + a_3 + \ldots + a_n &= 1,
\end{aligned} \tag{4}$$

where $c_{i,j}$ means the values $\mathrm{Cov}(l_i, l_j)$, $c_{p,i}$ the values $\mathrm{Cov}(l_p, l_i)$ and k the so-called Lagrange factor.

When using matrix notation the equation system (4) can be written in the following form:

$$\begin{pmatrix} \underset{nn}{\mathbf{C}} & \underset{n1}{\mathbf{I}} \\ \underset{1n}{\mathbf{I}^T} & \underset{11}{\mathbf{0}} \end{pmatrix} \begin{pmatrix} \underset{n1}{\mathbf{a}} \\ \underset{11}{k} \end{pmatrix} = \begin{pmatrix} \underset{n1}{\mathbf{c}_p} \\ 1 \end{pmatrix} \tag{4a}$$

where $\mathbf{C}$ means the matrix which contains the covariance values $c_{i,j}$, $\mathbf{I}$ is a unit vector, the notation with capital letter aims to indicate the submatrix. Vectors

a and $\mathbf{c}_p$ in Eq. (4a) follow from the notations of equation system (4) and contain the elements a_i and $c_{p,i}$, respectively.

In case of kriging the solution of Eq, (4a) is calculated without respect to the possibility of matrix partitioning; it has here the form:

$$\begin{pmatrix} \mathbf{a} \\ k \end{pmatrix} = \begin{pmatrix} \mathbf{C} & \mathbf{I} \\ \mathbf{I}^T & \mathbf{0} \end{pmatrix}^{-1} \begin{pmatrix} \mathbf{c}_p \\ 1 \end{pmatrix} . \tag{5}$$

Returning to the example in Fig. 1, Fig. 2 presents the diagram of the $c_{i,j}$-values (given numerically in [1]) as well as the variogram γ from which the values $c_{i,j}$ have been derived and to whose short explanation will be returned later.

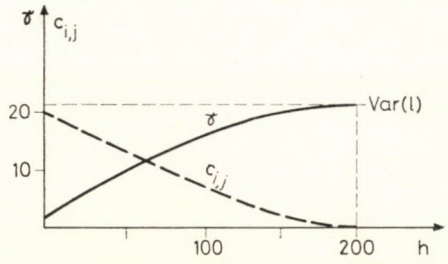

Fig. 2

With the covariance values $c_{i,j}$ and $c_{p,i}$, which can be easily determined as the function of the distance of the points taken from one to other by means of Figs. 1 and 2, Eq. (4a) will be in this case:

$$\begin{pmatrix} 22.00 & 9.84 & 1.23 & 4.98 & 1.00 \\ 9.84 & 22.00 & 2.33 & 0.29 & 1.00 \\ 1.23 & 2.33 & 22.00 & 0.00 & 1.00 \\ 4.98 & 0.29 & 0.00 & 22.00 & 1.00 \\ 1.00 & 1.00 & 1.00 & 1.00 & 0.00 \end{pmatrix} \begin{pmatrix} a_1 \\ a_2 \\ a_3 \\ a_4 \\ k \end{pmatrix} = \begin{pmatrix} 12.66 \\ 4.98 \\ 1.72 \\ 9.84 \\ 1.00 \end{pmatrix} .$$

The solution according to (5) will be (for sake of simplicity the symmetrical matrix elements will be denoted from here on only with dots):

$$\begin{pmatrix} a_1 \\ a_2 \\ a_3 \\ a_4 \\ k \end{pmatrix} = \begin{pmatrix} 0.057560996 & -0.031548091 & -0.006638002 & -0.019374904 & 0.148743063 \\ . & 0.050310101 & -0.014402322 & -0.004359688 & 0.238432705 \\ . & . & 0.033349440 & -0.012309116 & 0.308034474 \\ . & . & . & 0.036043708 & 0.304789758 \\ . & . & . & . & -7.515260605 \end{pmatrix} \begin{pmatrix} 12.66 \\ 4.98 \\ 1.72 \\ 9.84 \\ 1.00 \end{pmatrix} .$$

Finally, after the matrix multiplication one gets:

$$a_1 = 0.518289360$$
$$a_2 = 0.021906852$$
$$a_3 = 0.088513141$$
$$a_4 = 0.371290634$$
$$k = -0.915828042.$$

The here calculated a_i-values rounded off to three decimal places are completely identical with those given in [1]. The calculation for nine decimal places has no practical meaning and was adopted here only for the comparison following below.

Going over now to the LSC method, its interpolation strategy can be represented by the following equation:

$$l_i + v_i = u_0 + b_i u_1 + b_i^2 u_2 + b_i^3 u_3 + \ldots + b_i^m u_m + s_i , \tag{6}$$

where l_i has the same meaning as before; v_i is the random error of l_i; $\underset{nm\ m1}{\mathbf{B}\ \mathbf{u}}$ is the trend-function with the parameter u and s_i the so-called "signal" appearing at the place i, which is the part of l_i that cannot be taken into account by the trend-function. The expression "signal" comes from the information theory related with communication technics, but some authors, as e.g. KRAKIWSKY [3] have adopted it for the refinement of the mathematical model **Bu** describing the phenomenon l_i. These "signals" are regarded generally as correlated and in our case it should be supposed that the variance-covariance relations are described by the same matrix **C** as used in Eq. (4a). Further, it should be supposed that vector $\mathbf{c}_p$ contains the covariance elements between the s_p-values to be interpolated and the s_i-values.

The unknown parameters u of the trend-function are calculated in case of the LSC method as follows [2]:

$$\underset{m1}{u} = (\underset{mn}{\mathbf{B}^T}\ \underset{nn}{\mathbf{C}^{-1}}\ \underset{nm}{\mathbf{B}})^{-1}\ \underset{mn}{\mathbf{B}^T}\ \underset{nn}{\mathbf{C}^{-1}}\ \underset{n1}{\mathbf{l}} , \tag{7}$$

where besides the notation already known $\underset{nm}{\mathbf{B}}$ means the matrix composed from the trend coefficients b_i in Eq. (6). Thus, the trend-parameters u can be calculated from the linear combination of the l_i-values by taking into account the variance-covariance relations.

For the sake of comparison with the point-kriging method mentioned above the number of trend-parameters must be here reduced to one. In practice this means the weighted averaging of the values l_i (the average of the l_i-values is the most simple trend-function).

If this simplification would not be introduced, the LSC method should be compared with the so-called universal kriging [4], but this would be more difficult to follow and its result can be reached on the way of induction, too.

In case of point-kriging Eq. (6) becomes:

$$l_i + v_i = u + s_i \,, \tag{6a}$$

where

$$u = \underset{1n}{(\mathbf{I}^T} \underset{nn}{\mathbf{C}^{-1}} \underset{n1}{\mathbf{I})^{-1}} \underset{1n}{\mathbf{I}^T} \underset{nn}{\mathbf{C}^{-1}} \underset{n1}{\mathbf{l}} \tag{7a}$$

in correspondence with (7).

Matrix **I** has here the same meaning as in Eq. (4a), though it can be derived from the coefficient 1 of the trend-parameter u in Eq. (6a).

Finally, the l_p-values to be interpolated will be from the LSC method [2]:

$$l_p = u + s_p, \tag{8}$$

where the signal appearing in point p is [2]:

$$\underset{11}{s_p} = \underset{1n}{c_p} \underset{nn}{\mathbf{C}^{-1}} (\underset{n1}{\mathbf{l}} - \underset{n1}{\mathbf{I}} \underset{11}{u}). \tag{9}$$

Applying the LSC method to the example in Fig. 1, Eq. (7) will be the following:

$$u = \left[(1\,1\,1\,1) \begin{pmatrix} 22.00 & 9.84 & 1.23 & 4.98 \\ . & 22.00 & 2.33 & 0.29 \\ . & . & 22.00 & 0.00 \\ . & . & . & 22.00 \end{pmatrix}^{-1} \begin{pmatrix} 1 \\ 1 \\ 1 \\ 1 \end{pmatrix} \right]^{-1} (1\,1\,1\,1) \begin{pmatrix} 22.00 & 9.84 & 1.23 & 4.98 \\ . & 22.00 & 2.33 & 0.29 \\ . & . & 22.00 & 0.00 \\ . & . & . & 22.00 \end{pmatrix}^{-1} \begin{pmatrix} l_1 \\ l_2 \\ l_3 \\ l_4 \end{pmatrix}.$$

It can be seen that matrix **C** to be inverted has here the dimension 4×4, which will be given here with a similar accuracy for the sake of comparison to the matrix with dimension 5×5 inverted at the point-kriging:

$$\underset{44}{\mathbf{C}^{-1}} = \begin{pmatrix} 0.060504939 & -0.026828998 & -0.000541341 & -0.013342463 \\ . & 0.057874730 & -0.004629475 & 0.005310215 \\ . & . & 0.045975115 & 0.000183565 \\ . & . & . & 0.048404976 \end{pmatrix}.$$

Finally, for the values u and s_p, and from them for l_p one gets:

$$u = \begin{pmatrix} 0.148743066 \\ 0.238432703 \\ 0.308034476 \\ 0.304789755 \end{pmatrix}^T \begin{pmatrix} l_1 \\ l_2 \\ l_3 \\ l_4 \end{pmatrix} \quad s_p = \begin{pmatrix} 0.369546302 \\ -0.216525854 \\ -0.219521329 \\ 0.066500881 \end{pmatrix}^T \begin{pmatrix} l_1 \\ l_2 \\ l_3 \\ l_4 \end{pmatrix} \quad l_p = \begin{pmatrix} 0.518289368 \\ 0.021906849 \\ 0.088513147 \\ 0.371290636 \end{pmatrix}^T \begin{pmatrix} l_1 \\ l_2 \\ l_3 \\ l_4 \end{pmatrix}.$$

It can be seen that the coefficients of l_p are — not regarding the rounding-off error in the ninth place of decimal — identical with the a-values of kriging, i.e. in case of the numerical example shown here it has been proved that kriging and LSC lead to the same result.

The equivalence has general validity, to prove this algebraically one has to start from the inversion by Frobenian decomposition of the hypermatrix

$$\begin{pmatrix} \underset{nn}{\mathbf{C}} & \underset{n1}{\mathbf{I}} \\ \underset{1n}{\mathbf{I}^T} & \underset{11}{\mathbf{O}} \end{pmatrix} = K$$

to be found in Eq. (4a). (Notation K has been chosen with respect to kriging and in honour of D. G. KRIGE [4].)

Let be introduced the following substitutions:

$$\underset{n1}{\mathbf{q}} = \underset{nn}{\mathbf{C}^{-1}} \underset{n1}{\mathbf{I}} \; ; \quad \underset{11}{r} = -\left(\underset{1n}{\mathbf{I}^T} \underset{nn}{\mathbf{C}^{-1}} \underset{n1}{\mathbf{I}}\right) . \tag{10}$$

The requested inverse matrix will be then:

$$\mathbf{K}^{-1} = \begin{pmatrix} \underset{nn}{\mathbf{C}^{-1}} + \underset{n}{\mathbf{q}}\, r^{-1}\, \underset{n}{\mathbf{q}^T} & -\underset{n1}{\mathbf{q}} r^{-1} \\ -\underset{1}{r^{-1}}\, \underset{1}{q_1^T} & \underset{11}{r^{-1}} \end{pmatrix} .$$

Let be expressed now from Eq. (5) only the values a by using the decomposed form of $\mathbf{K}^{-1}$:

$$\underset{n1}{\mathbf{a}} = \left(\underset{nn}{\mathbf{C}^{-1}} + \underset{n}{\mathbf{q}} r^{-1}\, \underset{n}{\mathbf{q}^T} \quad -\underset{n1}{\mathbf{q}}\, r^{-1}\right) \begin{pmatrix} \underset{n1}{\mathbf{c}_p} \\ \mathbf{1} \end{pmatrix} = \underset{n}{\mathbf{C}^{-1}}\, \underset{1}{\mathbf{c}_p} + \underset{n}{\mathbf{q}}\, r^{-1}\, \underset{n}{\mathbf{q}^T}\, \underset{1}{\mathbf{c}_p} - \underset{n1}{\mathbf{q}}\, r^{-1} .$$

Substituting finally these values into Eq. (1) and resolving in the mean time the substitutions in (10), the l_p-value according to point-kriging will be:

$$l_p = \mathbf{c}_p^T \mathbf{C}^{-1} l - \mathbf{c}_p^T \mathbf{C}^{-1} \mathbf{I} (\mathbf{I}^T \mathbf{C}^{-1} \mathbf{I})^{-1} \mathbf{I}^T \mathbf{C}^{-1} l + (\mathbf{I}^T \mathbf{C}^{-1} \mathbf{I})^{-1} \mathbf{I}^T \mathbf{C}^{-1} l. \tag{8a}$$

Taking into consideration now Eqs (7a), (8) and (9) the identity of Eqs (8) and (8a) can be verified, and hence the identity between point-kriging and LSC method is proved, too.

In the general case of kriging — this is called universal kriging or kriging of k-th order [4] — the trend-function of Eq. (6) will be taken into account with further condition equations written in the sense of Eq. (3). In this case the matrix

K will be increased by a number of rows and columns that correspond to the parameters of the trend-function, whereby 0 elements come again into the main diagonal of the matrix ([4]; pp. 316—320).

Thus, in case of universal kriging as many Lagrange factors are to be determined together with the weight numbers a, as many parameters the trend-function has. The decomposition technics applied above, which is an inherent characteristic of the LSC method, ensures a possibility here, too, to prove the identity of the two methods discussed.

The fact that the size of matrix **K** increases together with the number of the parameters of the trend-function indicates unambiguously the practical advantage of the LSC method, because the size of the variance-covariance matrix **C** to be inverted directly is always smaller than that of matrix **K**. The apparent difference between the two numerical methods is that in the LSC method the interpolation is made with the s-values centered by the trend-function, while in case of kriging the complete input l-values are used. The decomposition of the l-values after Eq. (8) results in the clear structure of the LSC method which means an advantage from the point of view of programing, too.

It has been proved in detail [2] that the LSC method is a BLUE (Best Linear Unbiased Estimation) method. The same was proved from kriging [4] and this demonstrates that the error estimations of both methods are the same. Without going into further details it must be shortly mentioned that both methods can be traced back to older methods based on least squares and regarded nowadays as classical ones [5], as already has been proved of the LSC method [6]. Further interesting comparisons can be found in [3], where results achieved in the last years in this field can be studied, too.

Finally, some attention must be paid to the situation in connection with the determination of the covariance values $c_{i,j}$ and $c_{p,i}$, respectively. It is the central problem of the Matheronian geostatistics and the covariance values are reached by the practical determination (related to individual cases) of the variograms mentioned in Fig. 2 (see Chapter 4 in [1]).

The point of the determination of the variograms is the variance analysis of the differences of the input l-values and thus the elimination of the negative covariance values is automatically ensured. In connection with the LSC method the practical determination of the covariance functions is less emphasized, but attention must be paid to avoid negative covariance values resulting from convolution technics. The effect of the different covariance functions is very expressively demonstrated in [7], it is very instructive especially for those who apply the interpolation in practice. It is rather difficult yet to overlook the situation on this field. Here it should be only remarked that it would be very useful to compare the great experiences collected with both methods as soon as possible. This, however, could not have been done in the framework of this paper.

As conclusion it can be said that the LSC method can be used to the up-to-date mineral reserve estimation as it was proved numerically and algebraically. First calculations based on this methods are carried out for the determination of bauxite reserves in the Hungarian Research Institute of Aluminium Industry, whereby the numerical investigations shown here were needed to the construction of the mathematical model of calculation.

REFERENCES

1. David, M.: Geostatistical ore reserve estimation. Elsevier Sc. Pub., 1977.
2. Moritz, H.: Least-Squares Collocation. Deutsche Geodätische Komm. der Bayerischen Akademie d. Wissenschaften München. Reihe A, Nr. 75, 1973.
3. Krakiwsky, E. J.: A synthesis of recent advances in the method of least squares. Lecture Notes No 42. Department of Surveying Engineering, University of New Brunswick, Frederiction N. B. Canada, 1975.
4. Journel, A. G.—Huijbregts, Ch. J.: Mining Geostatistics Academy Press, London, 1978.
5. Helmert, F. R.: Die Ausgleichungsrechnung nach der Methode der kleinsten Quadrate, Leipzig/Berlin, 1924.
6. Wolf, H.: Zur Grundlegung der Kollokationsmethode. *Z. f. Vermessungswesen*, 102(1977), 237—239.
7. Assmus, E.—Kraus, K.: Die Interpolation nach kleinsten Quadraten, Prädiktionswerte simulierter Beispiele und ihre Genauigkeit. Deutsche Geodätische Kommission d. Bayerischen Akad. d. W., München, Reihe A, Nr. 76, 1974.

ПРИМЕНЕНИЕ КОЛЛОКАЦИИ ПО МЕТОДУ НАИМЕНЬШИХ КВАДРАТОВ ДЛЯ РАСЦЕНКИ МИНЕРАЛЬНЫХ РЕСУРСОВ

ДЬ. АЛПАР

РЕЗЮМЕ

Планирование инвестирований в горном деле все более и более требует точную расценку минеральных ресурсов. С этой целью широко применяется так называемый метод «кригинга», который основывается на математической статистике. В случае подобных задач расценки метод коллокации успешно применялся в физической геодезии. В статье доказывается численное и алгебраическое совпадение этих методов. Расценка рудных ресурсов с помощью коллокации по методу наименьших квадратов не только равносильна методу кригинга, но и представляет некоторые замечательные преимущества в вычислительной технике.

Acta Geodaet., Geophys. et Montanist. Acad. Sci. Hung. Tomus 16 (1), pp. 51—61 (1981)

FREIE AUSGLEICHUNG IM GAUSS-HELMERT MODELL

H. WOLF

O. UNIV.-PROF., BONN

[Eingegangen am 2. Februar 1980]

Für die Form der Ausgleichung nach bedingten Beobachtungen mit Unbekannten, neuerdings als das »Gauss-Helmert-Modell« bezeichnet, wird die Theorie der »freien Ausgleichung« entwickelt, worunter man Ausgleichungen mit singulärer Normalgleichungsmatrix versteht. Dabei gelangt man auf eine 1948 von Prof. Tárczy-Hornoch und H. Wolf angegebenen allgemeine Ausgleichungsform. Die Theorie kann gänzlich ohne Benützung der »verallgemeinerten Inversen« dargestellt werden. Zur Demonstration wird ein Zahlenbeispiel beigefügt.

Der von MITTERMAYER [6] eingeführte Begriff der »freien Ausgleichung«, womit Ausgleichungen bei singulärer Normalgleichungs-Koeffizientenmatrix gemeint sind, ist seither nur für den Fall der vermittelnden Beobachtungen behandelt worden. Er läßt sich aber auch für den Fall der bedingten Beobachtungen mit Unbekannten (dem sog. Gauss-Helmert-Modell) definieren. Man gelangt dann auf eine von TÁRCZY-HORNOCH [8] angegebene Ausgleichungsform. Im nachstehenden soll dieser Fall näher untersucht und an einem Zahlenbeispiel demonstriert werden.

1. Der Begriff der Überparametrisierung

Eine »Überparametrisierung« liegt dann vor, wenn bei einer Ausgleichungsaufgabe *mehr* Unbekannte (= »Parameter«) eingeführt werden, als zur eindeutigen Beschreibung des jeweiligen geometrischen oder physikalischen Sachverhalts erforderlich sind. Die Anzahl g der zuviel eingeführten Unbekannten sei als »Grad der Überparametrisierung« bezeichnet.

Beispiele:

a) Werden in eine Stationsausgleichung zur Darstellung des stationsausgeglichenen Richtungsbüschels nach s Zielen nicht $(s-1)$ Winkelunbekannte (wie bei BESSEL) eingeführt, sondern s Richtungsunbekannte (wie bei HANSEN), so ist $g = 1$.

b) Werden bei der Berechnung von Strichkorrektionen an linearen Skalen oder Libellenteilungen mit s Teilstrichen nicht $(s-1)$ Intervalle als Unbekannte eingeführt, sondern die Lage der s Teilstriche, vgl. TÁRCZY-HORNOCH and ALPÁR [9], so ist gleichfalls $g = 1$.

c) Wenn bei der Ausgleichung eines Nivellementsnetzes mit s Höhenpunkten alle s Höhen als Unbekannte benützt werden, ist ebenfalls $g = 1$.

d) Wenn bei der Ausgleichung von zwei- und dreidimensionalen geodätischen Netzen auch für die Anschlußpunkte variable Koordinaten eingeführt werden, liegt ebenfalls Überparametrisierung vor.

e) Desgleichen auch, wenn bei einseitigen Höhenwinkeln im Höhennetz außer den Höhenwerten auch noch die Refraktion als Unbekannte eingeführt wird, oder

f) wenn bei einer fast kreisförmigen Satelliten-Bahn neben der mittleren Anomalie M auch noch das Argument ω des Perigäums als Unbekannte benützt wird, vgl. WOLF [12].

2. Die Verfügung über die überflüssigen Freiheitsgrade

Jede Überparametrisierung hat zur Folge, daß man zur Herbeiführung einer eindeutigen Lösung ebensoviele Bedingungen zwischen den Unbekannten aufzustellen und in die Ausgleichung einzuführen hat, wie die Zahl g der Überparametrisierung angibt.

Diese Lösung des Problems der überparametrisierten Ausgleichung (heute »freie« Ausgleichung) mittels Bedingungsgleichungen zwischen den Unbekannten verdankt man HANSEN [1]. Sind dabei die u Unbekannten $x_1, x_2, \ldots, x_u$ im Lösungsvektor

$$\mathbf{x} = [x_1, x_2, \ldots, x_u]^T$$

zusammengefaßt, so seien diese g Bedingungen, in linearer oder linearisierter Form, zunächst durch

$$\underset{(g,u)(u,1)}{\mathbf{G}}\ \underset{(u,1)}{\mathbf{x}} + \underset{(g,1)}{\mathbf{c}_G} = \underset{(g,1)}{\mathbf{o}} \tag{1}$$

ausgedrückt, worin $\mathbf{c}_G$ ein Konstantenvektor ist.

3. Das Gauss-Helmert-Modell

Werden die n Messungen $L_1, L_2, \ldots, L_n$ im Vektor

$$\mathbf{l} = [L_1, L_2, \ldots, L_n]^T$$

untergebracht, und handele es sich dabei um korrelierte Beobachtungen mit der Kovarianzmatrix $\mathrm{cov}(\mathbf{l}) = \mathbf{Q}$, wobei $\mathrm{rang}\ \mathbf{Q} = n$, so ist das Gauss-Helmert-Modell gegeben durch

$$\underset{(r,n)}{\mathbf{A}} \cdot \underset{(n,1)}{E\{\mathbf{l}\}} + \underset{(r,u)}{\mathbf{B}}\ \underset{(u,1)}{\mathbf{x}} + \underset{(r,1)}{\mathbf{c}_A} = \underset{(r,1)}{\mathbf{o}}\,, \tag{2}$$

worin E den Erwartungswert, $\mathbf{c}_A$ einen Konstantenvektor, sowie $\mathbf{A}$ und $\mathbf{B}$ Koeffizientenmatrizen bedeuten. Dabei sei rang $\mathbf{A} = r < n$, während wegen der vorausgesetzten Überparametrisierung

$$\text{rang } \mathbf{B} = u - g \tag{3}$$

ist; g ist der »Defekt« von $\mathbf{B}$, der den Grad der Überparametrisierung angibt.

Geht man von den Erwartungswerten zu den gemessenen Werten $\mathbf{l}$ über, an denen man die Verbesserungen $\mathbf{v}$ anbringt, so erhält man aus (2) die Helmertschen »Bedingungsgleichungen mit Unbekannten«, vgl. HELMERT [4],: S. 286

$$\mathbf{Av} + \mathbf{B}\hat{\mathbf{x}} + \mathbf{w} = \mathbf{o}, \text{ womit } \mathbf{w} = \mathbf{Al} + \mathbf{c}_A \tag{4}$$

und wobei $\hat{\mathbf{x}}$ den ausgeglichenen Wert (Schätzwert) von $\mathbf{x}$ bezeichnet.

4. Das Gauss-Helmert-Modell mit Zusatzbedingungen

Zusammen mit den Hansenschen Bedingungsgleichungen (1) führt die Methode der kleinsten Quadrate auf Grund von (4) gemäß

$$\mathbf{v}^T \mathbf{Q}^{-1} \mathbf{v} = \min$$

bekanntlich auf das von TÁRCZY-HORNOCH [8] angegebene Normalgleichungssystem, vgl. auch WOLF [11, 13], worin $\mathbf{k}_1$ und $\mathbf{k}_2$ Korrelatenvektoren (Lagrangesche Multiplikatoren) bedeuten:

$$\begin{cases} \mathbf{N}_0 \mathbf{k}_1 + \mathbf{B}\hat{\mathbf{x}} + \mathbf{w} = \mathbf{o}, \text{ mit } \mathbf{N}_0 = \mathbf{AQA}^T \\ \mathbf{B}^T \mathbf{k}_1 - \mathbf{G}^T \mathbf{k}_2 = \mathbf{o} \\ -\mathbf{G}\hat{\mathbf{x}} - \mathbf{c}_G = \mathbf{o} \end{cases} \tag{5}$$

(aus Symmetriegründen ist dabei die Hansensche Zusatzbedingung mit dem Faktor —1 multipliziert worden).

Die Korrelaten bestimmen die Verbesserungen v, indem

$$\mathbf{v} = \mathbf{Q}\,\mathbf{A}^T \mathbf{k}_1. \tag{6}$$

Gl. (5) läßt sich auch ausdrücken durch

$$\begin{bmatrix} \mathbf{N}_0, & \mathbf{B}, & \mathbf{O} \\ \mathbf{B}^T, & \mathbf{O} & -\mathbf{G}^T \\ \mathbf{O}, & -\mathbf{G}, & \mathbf{O} \end{bmatrix} \begin{bmatrix} \mathbf{k}_1 \\ \hat{\mathbf{x}} \\ \mathbf{k}_2 \end{bmatrix} + \begin{bmatrix} \mathbf{w} \\ \mathbf{o} \\ -\mathbf{c}_G \end{bmatrix} = \mathbf{o}$$

oder

$$\mathbf{N}[\mathbf{k}_1^T, \hat{\mathbf{x}}^T, \mathbf{k}_2^T]^T + [\mathbf{w}^T, \mathbf{o}^T - \mathbf{c}_G^T]^T = \mathbf{o}\,.$$

Wegen rang $\mathbf{A} = r$ ist $\det \mathbf{N}_0 \neq 0$. Auch ist $\det \mathbf{N} \neq 0$, wenn nicht weniger als g linear unabhängige Bedingungen (1) aufgestellt worden sind. Da also $\det \mathbf{N}_0 \neq \neq 0$, so kann $\mathbf{k}_1$ aus (5) eliminiert werden. Wir multiplizieren hierfür die 1. Gleichung von (5) mit $-\mathbf{B}^T\mathbf{N}_0^{-1}$ und addieren diese zur 2. hinzu. Dies ergibt

$$-\mathbf{B}^T\,\mathbf{N}_0^{-1}\,\mathbf{B}\,\hat{\mathbf{x}} - \mathbf{G}^T\,\mathbf{k}_2 - \mathbf{B}^T\,\mathbf{N}_0^{-1}\,\mathbf{w} = \mathbf{o}$$

und mit

$$\mathbf{B}^T\,\mathbf{N}_0^{-1}\,\mathbf{B} = \mathbf{N}_{11}$$

$$\begin{cases} \mathbf{N}_{11}\,\hat{\mathbf{x}} + \mathbf{G}^T\,\mathbf{k}_2 + \mathbf{B}^T\,\mathbf{N}_0^{-1}\,\mathbf{w} = \mathbf{o} \\ \mathbf{G}\,\hat{\mathbf{x}} \qquad\qquad + \mathbf{c}_G \qquad\qquad = \mathbf{o}\,. \end{cases} \tag{7}$$

Wegen (3) ist $\mathbf{N}_{11}$ singulär, d. h.

$$\det \mathbf{N}_{11} = 0. \tag{8}$$

5. Die numerische Auflösung des Normalgleichungssystems

Die numerische Auflösung von (5) gelingt wegen (8) nur dann, wenn man die Reihenfolge der Elemente im Vektor $[\hat{\mathbf{x}}^T, \mathbf{k}_2^T]$ so ändert, d. h. Zeilen und Spalten symmetrisch so vertauscht, daß als letzte jeweils g Unbekannte $\hat{\mathbf{x}}$ bestimmt werden (nicht die g Korrelaten $\mathbf{k}_2$). Es ist dies eine Erkenntnis, die man HELMERT ([4], S. 282) verdankt. Das gilt für die »bestimmte« Auflösung (zur Ermittlung des Lösungsvektors) ebenso wie für die »unbestimmte« Auflösung (zur Inversion der Normalgleichungskoeffizientenmatrix).

Wieder zur ursprünglichen Reihenfolge zurückgebracht, sei

$$\begin{bmatrix} \mathbf{N}_{11}, & \mathbf{G}^T \\ \mathbf{G}, & \mathbf{0} \end{bmatrix}^{-1} = \begin{bmatrix} \mathbf{S}, & \mathbf{R} \\ \mathbf{R}^T, & \mathbf{M} \end{bmatrix}, \tag{9}$$

da die Kehrmatrix einer symmetrischen Matrix gleichfalls eine symmetrische Matrix ist.

6. Wahl der Bedingungs-Matrix G

Die Vielzahl der (möglichen) G-Matrizen in (1) werde durch gewisse Forderungen eingeschränkt:

a) Es soll sein:

$$\hat{\mathbf{x}}^T\,\hat{\mathbf{x}} = \min. \tag{10}$$

Seien $\bar{\mathbf{x}}$ alle jene Lösungsvektoren, die (10) nicht erfüllen, so soll zwischen $\hat{\mathbf{x}}$ und $\bar{\mathbf{x}}$ die folgende Transformationsgleichung bestehen:

$$\hat{\mathbf{x}} = \bar{\mathbf{x}} + \mathbf{C}\hat{\mathbf{t}}, \tag{11}$$

wobei in $\hat{\mathbf{t}}$ gewisse äußere Parameter enthalten seien, deren Anzahl mit der Defektzahl g übereinstimme, die den Grad der Überparametrisierung angibt.

Soll $\hat{\mathbf{x}}^T\hat{\mathbf{x}}$ minimiert werden, so folgt aus (11) — als Verbesserungsgleichungen genommen — das nachstehende Normalgleichungssystem zur Berechnung der Schätzwerte $\hat{\mathbf{t}}$ von $\mathbf{t}$:

$$\mathbf{C}^T\mathbf{C}\hat{\mathbf{t}} + \mathbf{C}^T\bar{\mathbf{x}} = \mathbf{o},$$

so daß

$$\hat{\mathbf{t}} = -(\mathbf{C}^T\mathbf{C})^{-1}\mathbf{C}^T\bar{\mathbf{x}},$$

womit nach (11):

$$\hat{\mathbf{x}} = \bar{\mathbf{x}} - \mathbf{C}(\mathbf{C}^T\mathbf{C})^{-1}\mathbf{C}^T\bar{\mathbf{x}},$$

und damit

$$\mathbf{C}^T\hat{\mathbf{x}} = \mathbf{C}^T\mathbf{x} - \mathbf{C}^T\mathbf{C}(\mathbf{C}^T\mathbf{C})^{-1}\mathbf{C}^T\bar{\mathbf{x}}, \tag{12}$$

so daß

$$\mathbf{C}^T\hat{\mathbf{x}} = \mathbf{o}.$$

Man erkennt: In Gl. (1) muß sein:

$$\mathbf{G} = \mathbf{C}^T \text{ und } \mathbf{c}_G = \mathbf{o}, \tag{13}$$

wenn das Minimum in (10) eintreten soll.

b) Eine weitere Forderung soll darin bestehen, daß die ausgeglichenen Beobachtungswerte $(\mathbf{l} + \mathbf{v})$ invariant gegenüber $\hat{\mathbf{t}}$ sein sollen. Zu diesem Zweck entnehmen wir $\mathbf{k}_1$ aus (5) zu

$$\mathbf{k}_1 = -\mathbf{N}_0^{-1}(\mathbf{B}\hat{\mathbf{x}} + \mathbf{w})$$

und setzen dies in (6) ein, so daß mit (4):

$$\mathbf{v} = -\mathbf{Q}\mathbf{A}^T\mathbf{N}_0^{-1}(\mathbf{B}\hat{\mathbf{x}} + \mathbf{A}\mathbf{l} + \mathbf{c}_A)$$

oder, wenn mit $\mathbf{I}$ die Einheitsmatrix bezeichnet wird:

$$\mathbf{l} + \mathbf{v} = (\mathbf{I} - \mathbf{Q}\mathbf{A}^T\mathbf{N}_0^{-1}\mathbf{A})\mathbf{l} - \mathbf{Q}\mathbf{A}^T\mathbf{N}_0^{-1}\mathbf{B}(\bar{\mathbf{x}} + \mathbf{C}\hat{\mathbf{t}}) - \mathbf{Q}\mathbf{A}^T\mathbf{N}_0^{-1}\mathbf{c}_A.$$

Dies soll dann — per definitionem — identisch sein mit

$$\mathbf{l} + \mathbf{v} = (\mathbf{I} - \mathbf{Q}\mathbf{A}^T\mathbf{N}_0^{-1}\mathbf{A})\mathbf{l} - \mathbf{Q}\mathbf{A}^T\mathbf{N}_0^{-1}\mathbf{B}\bar{\mathbf{x}} - \mathbf{Q}\mathbf{A}^T\mathbf{N}_0^{-1}\mathbf{c}_A.$$

Die Differenz der beiden letzten Ausdrücke liefert

$$\mathbf{o} = \mathbf{Q}\,\mathbf{A}^T\,\mathbf{N}_0^{-1}\,\mathbf{B}\,\mathbf{C}\,\hat{\mathbf{t}}.$$

Dieser Bedingung wird genügt, wenn

$$\mathbf{B}\,\mathbf{C} = \mathbf{O}, \quad \text{oder} \quad \mathbf{C}^T\,\mathbf{B}^T = \mathbf{O} \tag{14}$$

oder auch $$\mathbf{B}^T\,\mathbf{N}_0^{-1}\,\mathbf{B}\,\mathbf{C} = \mathbf{O} \quad \text{oder} \quad \mathbf{N}_{11}\,\mathbf{C} = \mathbf{O}, \tag{15}$$

bzw. $$\mathbf{C}^T\,\mathbf{N}_{11} = \mathbf{O}. \tag{16}$$

Man kann entweder durch Auflösung des homogenen Gleichungssystems $\mathbf{N}_{11}\mathbf{C} = \mathbf{O}$ die einzelnen Elemente der Matrix $\mathbf{C}$ bestimmen, was mit dem Algorithmus zur Berechnung von Eigenwerten durchgeführt werden kann, vgl. MITTERMAYER [7], WELSCH [10], HEIN [3]; oder aber man kennt von vornherein — aus der Geometrie der Aufgabenstellung — die Struktur der Transformationsmatrix, welche die Bedingung (13) von Haus aus erfüllt, zusammen mit den zugehörigen äußeren Parametern $\mathbf{t}$:

So ist bei Stationsausgleichungen im Vektor $\mathbf{t}$ nur eine Drehung (= Orientierungsunbekannte) enthalten, und $\mathbf{C}$ ist dann der Summationsvektor: $\mathbf{C}^T = [1, 1, 1, \ldots]$, während bei Skalenuntersuchungen in $\mathbf{t}$ nur eine Translationsunbekannte vorkommt, und bei Höhennetzen besteht $\mathbf{t}$ aus einer Höhenverschiebung. Bei ebenen Triangulationsnetzen enthält $\mathbf{t}$ zwei Translationen, eine Drehung und eine Maßstabsänderung, so daß $\mathbf{C}\hat{\mathbf{t}}$ die Ähnlichkeitstransformation beschreibt, während bei dreidimensionalen Triangulationen 3 Translationen, 3 Drehungen und eine Maßstabsänderung in $\mathbf{t}$ enthalten sind. (Bei Anwesenheit von Streckenmessungen entfällt die Maßstabsänderung als äußerer Parameter.)

7. Eigenschaften der Lösung

a) Bei der *bestimmten* Auflösung der Normalgleichungen erhält man aus der Multiplikation von (7) mit $\mathbf{C}^T$:

$$\mathbf{C}^T\,\mathbf{N}_{11}\,\hat{\mathbf{x}} + \mathbf{C}^T\,\mathbf{C}\,\mathbf{k}_2 + \mathbf{C}^T\,\mathbf{B}^T\,\mathbf{N}_0^{-1}\,\mathbf{w} = \mathbf{o},$$

oder wegen (16) und (14):

$$\mathbf{C}^T\mathbf{C}\mathbf{k}_2 = \mathbf{o}$$

woraus, vgl. MITTERMAYER [7]: $\mathbf{k}_2 = \mathbf{o}$ (17)

b) Bei der *unbestimmten* Auflösung ergeben sich der Reihe nach aus

$$\begin{bmatrix} \mathbf{N}_{11}, & \mathbf{C} \\ \mathbf{C}^T, & \mathbf{O} \end{bmatrix} \begin{bmatrix} \mathbf{S}, & \mathbf{R} \\ \mathbf{R}^T, & \mathbf{M} \end{bmatrix} = \begin{bmatrix} \mathbf{I}, & \mathbf{O} \\ \mathbf{O}, & \mathbf{I} \end{bmatrix}$$

aa) $\mathbf{N}_{11}\,\mathbf{R} + \mathbf{C}\,\mathbf{M} = \mathbf{O}$, bzw. $\mathbf{C}^T\,\mathbf{N}_{11}\,\mathbf{R} + \mathbf{C}^T\,\mathbf{C}\,\mathbf{M} = \mathbf{O}$,

was wegen (16) $\mathbf{C}^T\mathbf{C}\mathbf{M} = \mathbf{O}$ liefert, so daß, vgl. MEISSL [5]:

$$\mathbf{M} = \mathbf{O}. \tag{18}$$

bb) $$\mathbf{C}^T\mathbf{S} = \mathbf{O}, \quad \text{bzw.} \quad \mathbf{S}\mathbf{C} = \mathbf{O}. \tag{19}$$

cc) $$\mathbf{N}_{11}\,\mathbf{S} + \mathbf{C}\,\mathbf{R}^T = \mathbf{I}, \quad \text{oder}$$

$$\mathbf{S}\,\mathbf{N}_{11}\,\mathbf{S} + \mathbf{S}\,\mathbf{C}\,\mathbf{R}^T = \mathbf{S} \quad \text{woraus wegen (19):}$$

$$\mathbf{S}\,\mathbf{N}_{11}\,\mathbf{S} = \mathbf{S}. \tag{20}$$

dd) $$\mathbf{N}_{11}\,\mathbf{S}\,\mathbf{N}_{11} + \mathbf{C}\,\mathbf{R}^T\mathbf{N}_{11} = \mathbf{N}_{11}.$$

Da aber $\mathbf{N}_{11}\,\mathbf{R} + \mathbf{C}\mathbf{M} = \mathbf{O}$ oder mit (18): $\mathbf{N}_{11}\,\mathbf{R} = \mathbf{O}$ und $\mathbf{R}^T\,\mathbf{N}_{11} = \mathbf{O}$,

so wird

$$\mathbf{N}_{11}\,\mathbf{S}\,\mathbf{N}_{11} = \mathbf{N}_{11}. \tag{21}$$

8. Darstellung des Lösungsvektors

Wegen (13) und (17) wird aus (7):

$$\begin{bmatrix} \mathbf{N}_{11}, & \mathbf{C} \\ \mathbf{C}^T, & \mathbf{O} \end{bmatrix} \begin{bmatrix} \hat{\mathbf{x}} \\ \mathbf{o} \end{bmatrix} = -\begin{bmatrix} \mathbf{B}^T\,\mathbf{N}_0^{-1}\,\mathbf{w} \\ \mathbf{o} \end{bmatrix}, \quad \text{woraus}$$

$$\begin{bmatrix} \hat{\mathbf{x}} \\ \mathbf{o} \end{bmatrix} = -\begin{bmatrix} \mathbf{N}_{11}, & \mathbf{C} \\ \mathbf{C}^T & \mathbf{O} \end{bmatrix}^{-1} \begin{bmatrix} \mathbf{B}^T\mathbf{N}_0^{-1}\mathbf{w} \\ \mathbf{o} \end{bmatrix} = -\begin{bmatrix} \mathbf{S}, & \mathbf{R} \\ \mathbf{R}^T, & \mathbf{O} \end{bmatrix} \begin{bmatrix} \mathbf{B}^T\,\mathbf{N}_0^{-1}\,\mathbf{w} \\ \mathbf{o} \end{bmatrix},$$

so daß

$$\hat{\mathbf{x}} = -\,\mathbf{S}\,\mathbf{B}^T\,\mathbf{N}_0^{-1}\,\mathbf{w} = -\,\mathbf{S}\,\mathbf{B}^T\,\mathbf{N}_0^{-1}\,(\mathbf{A}\,\mathbf{l} + \mathbf{c}_A)\,. \tag{22}$$

9. Fehlerrechnung

In der Fehlerrechnung (= »Intervallschätzung«) ist der mittlere Fehler m_{x_i} des Elements $\hat{x}_i$ (aus $\hat{\mathbf{x}}$) zu berechnen gemäß

$$m_{x_i} = m_0 \sqrt{Q_{x_i x_i}} \tag{23}$$

worin

$$m_0 = \sqrt{\mathbf{v}^T \mathbf{Q}^{-1} \mathbf{v}/(r - u + g)}. \tag{24}$$

Dabei ist $Q_{x_i x_i}$ Diagonalelement der Matrix $\mathbf{Q}_{\hat{x}}$, die sich in einfachster Weise nach dem Fehlerfortpflanzungsgesetz, vgl. WOLF ([13] S. 72), ergibt: Ausgehend von (22) findet man:

$$\mathbf{Q}_{\hat{x}} = \mathbf{S}\mathbf{B}^T \mathbf{N}_0^{-1} \mathbf{A}\,\mathbf{Q}\,\mathbf{A}^T \mathbf{N}_0^{-1} \mathbf{B}\,\mathbf{S} = \mathbf{S}\mathbf{B}^T \mathbf{N}_0^{-1} \mathbf{N}_0 \mathbf{N}_0^{-1} \mathbf{B}\mathbf{S} =$$
$$= \mathbf{S}\,\mathbf{B}^T \mathbf{N}_0^{-1} \mathbf{B}\,\mathbf{S} = \mathbf{S}\,\mathbf{N}_{11}\,\mathbf{S} = \mathbf{S}.$$

Mithin

$$\mathbf{Q}_{\hat{x}} = \mathbf{S}. \tag{25}$$

10. Kleinste mittlere Fehler (minimale Varianz)

Da nach (14) die $(\mathbf{l} + \mathbf{v})$ und somit die $\mathbf{v}$ invariant gegenüber $\hat{\mathbf{t}}$ sind, ist $\mathbf{v}^T\mathbf{Q}^{-1}\mathbf{v}$ gleichfalls invariant bzgl. $\hat{\mathbf{t}}$. Dagegen ist von $\hat{\mathbf{t}}$ die quadratische Form $\hat{\mathbf{x}}^T\hat{\mathbf{x}}$, bzw. $\bar{\mathbf{x}}^T\bar{\mathbf{x}}$ voll abhängig, vgl. (11). Für einen konstanten Wert $\mathbf{v}^T\mathbf{Q}^{-1}\mathbf{v}$ existieren, je nach der Wahl von $\hat{\mathbf{t}}$, unendlich viele $\bar{\mathbf{x}}^T\bar{\mathbf{x}}$, von denen hier mit (12) ein spezieller Vektor $\hat{\mathbf{x}}$ nach der Methode der kleinsten Quadrate ausgewählt wurde. Nun weiß man von GAUSS und HELMERT ([4] S. 185f), daß die aus der Bedingung $\hat{\mathbf{x}}^T\hat{\mathbf{x}} = \min$ folgenden Unbekannten kleinste mittlere Fehler (gegenüber allen anderen Lösungen $\bar{\mathbf{x}}$) besitzen, so daß für konstante m_0, (bzw. konstante $\mathbf{v}$) gilt:

$$m_{t_i} = m_0 \sqrt{Q_{t_i t_i}} = \min. \tag{26}$$

Dabei ist $Q_{t_i t_i}$ Diagonalelement von $\mathbf{Q}_t = (\mathbf{C}^T\mathbf{C})^{-1}$. Außerdem ist, im Anschluß an (12), mit $\mathbf{C}(\mathbf{C}^T\mathbf{C})^{-1}\mathbf{C}^T = \mathbf{R}$ und $\mathbf{R}^T\mathbf{R} = \mathbf{R}\mathbf{R} = \mathbf{R}$

sodann $\hat{\mathbf{x}} = (\mathbf{I} - \mathbf{R})\bar{\mathbf{x}}$, woraus $\mathbf{Q}\hat{\mathbf{x}} = (\mathbf{I} - \mathbf{R})\mathbf{Q}_{\bar{x}}(\mathbf{I} - \mathbf{R})$, oder

$$\mathbf{Q}_{\hat{x}} = \mathbf{Q}_{\bar{x}} - \mathbf{R}\,\mathbf{Q}_{\bar{x}} - \mathbf{Q}_{\bar{x}}\,\mathbf{R} + \mathbf{R}\,\mathbf{Q}_{\bar{x}}\,\mathbf{R}, \text{ und mit}$$

$$\text{Spur}\,(\mathbf{R}\,\mathbf{Q}_{\bar{x}}\,\mathbf{R}) = \text{Spur}\,(\mathbf{Q}_{\bar{x}}\,\mathbf{R}\,\mathbf{R}) = \text{Spur}\,(\mathbf{Q}_{\bar{x}}\,\mathbf{R}) = \text{Spur}\,(\mathbf{R}\,\mathbf{Q}_{\bar{x}}) \text{ wird}$$

$$\text{Spur}\,\mathbf{Q}_{\hat{x}} = \text{Spur}\,\mathbf{Q}_{\bar{x}} - \text{Spur}\,(\mathbf{R}\,\mathbf{Q}_{\bar{x}}) - \text{Spur}\,(\mathbf{R}\,\mathbf{Q}_{\bar{x}}) + \text{Spur}\,(\mathbf{R}\,\mathbf{Q}_{\bar{x}}),$$

so daß

$$\text{Spur}\,\mathbf{Q}_{\hat{x}} < \text{Spur}\,\mathbf{Q}_{\bar{x}}, \text{ d. h.}$$

$$\text{Spur}\,\mathbf{S} = \text{Spur}\,\mathbf{Q}_{\hat{x}} = \min. \tag{27}$$

Bemerkung: Die Größen $\mathbf{S}$ mit den Eigenschaften (20, 21, 25, 27) heißen auch Pseudo-Inversen und werden mit $\mathbf{N}_{11}^{+}$ bezeichnet. Für sie gelten alle jene Rela-

tionen, die aus der Theorie der verallgemeinerten Inversen bekannt sind. — Man ersieht, daß die Theorie der freien Ausgleichungen, d. h. von singulären Systemen, auch *ohne* Benutzung der verallgemeinerten Inversen darstellbar ist.

11. Ein Zahlenbeispiel

In einem ebenen Dreieck seien die 3 Winkel α, β, γ je mit dem mittleren Fehler (a priori) von $\pm\mu$ gemessen sowie die beiden Seiten a und b mit den mittleren Fehlern μ_a bzw. μ_b.

Bei der Ausgleichung soll für die Seiten a und b je eine Maßstabsunbekannte δx_a bzw. δx_b in Ansatz gebracht werden.

Die Aufgabe ist überparametrisiert: Es kann nur eine Maßstabsunbekannte bestimmt werden; die Ermittlung von z.B. δx_a setzt voraus, daß der Maßstab der Seite b fest vorgegeben ist ($\delta x_b = 0$). Sollen — formal — aber beide Unbekanten mitgeführt werden, so ist der offene Freiheitsgrad nach HANSEN [2] durch eine Zusatzverfügung in Form einer Bedingungsgleichung der Art (12) auszufüllen. Dabei ist $g = 1$.

Wir stellen zunächst die Netzbedingungen auf, wobei an den Messungen α, β, γ, a, b die Verbesserungen v_α, v_β, v_γ, v_a, v_b angebracht werden sollen, und erhalten:

$$a)\quad (\alpha + v_\alpha) + (\beta + v_\beta) + (\gamma + v_\gamma) = 180^\circ$$

$$\text{oder}\quad v_\alpha + v_\beta + v_\gamma + w_1' = 0,\ \text{mit}\ w_1' = \alpha + \beta + \gamma - 180^\circ$$

$$b)\qquad \frac{\sin(\alpha + v_\alpha)}{\sin(\beta + v_\beta)} = \frac{(1 + \delta x_a)(a + v_a)}{(1 + \delta x_b)(b + v_b)}\,.$$

Durch Logarithmieren und Anwendung des Taylorsatzes erhält man die folgende linearisierte Bedingungsgleichung:

$$-v_\alpha \cot\alpha + v_\beta \cot\beta + \frac{v_a}{a} - \frac{v_b}{b} + \delta\hat{x}_a - \delta\hat{x}_b + w_1'' = 0, \tag{28}$$

wobei

$$w_1'' = \ln(a \sin\beta / b \sin\alpha).$$

Der besseren Übersicht wegen setzen wir $v_a/a = \bar{v}_a$, $v_b/b = \bar{v}_b$ und nehmen speziell $\alpha \approx \beta \approx 45^\circ$ an. Drückt man alle Winkelgrößen und ihre Änderungen im Bogenmaß aus (womit $\varrho = 1$), so ist

$$\mathbf{v}^T = [v_\alpha, v_\beta, v_\gamma, \bar{v}_a, \bar{v}_b]\,, \quad \mathbf{A} = \begin{bmatrix} 1, & 1, & 1, & 0, & 0 \\ -1, & 1, & 0, & 1, & -1 \end{bmatrix}.$$

Zur Aufstellung der Hansenschen Zusatzbedingung soll sein (um die Überparametrisierung aufzuheben):

$$\hat{\mathbf{x}}^T \hat{\mathbf{x}} = \delta \hat{\mathbf{x}}_a^2 + \delta \hat{\mathbf{x}}_b^2 = \min ,$$

was nach (12) erreicht wird durch die Bedingungsgleichung

$$\delta \hat{x}_a + \delta \hat{x}_b = 0 \tag{29}$$

womit

$$\mathbf{C}^T = [1, 1].$$

Verfügen wir außerdem noch, daß

$$\mu_a/a = \mu_{\bar{a}} = \mu_0\sqrt{2} \quad \text{und} \quad \mu_b/b = \mu_b = \mu_0\sqrt{2} ,$$

so wird

$$\mathbf{Q} = \mu_0^2 \operatorname{diag}[1, 1, 1, 2, 2] = \mathbf{p}^{-1}.$$

Da aber bekanntermaßen das Ergebnis einer Ausgleichung unabhängig ist von der Wahl der Gewichtskonstanten, so kann im folgenden unbedenklich $\mu_0 = 1$ gesetzt werden. Mit den Korrelaten k_1' und k_1'' für die beiden ersten Bedingungen erhält man die nachstehenden Normalgleichungen, in denen sogleich nach HELMERT (a.a.O. S. 282) die Reihenfolge der Unbekannten im Hinblick auf die numerische Auflösbarkeit festgelegt worden ist:

$$\begin{aligned}
3\,k_1' + 0\,k_1'' + 0\,\delta x_a + 0\,k_2 + 0\,\delta x_b + w_1' &= 0 \\
\ldots + 6\,k_1'' + 1\,\delta x_a + 0\,k_2 - 1\,\delta x_b + w_1'' &= 0 \\
\ldots + 0\,\delta x_a + 1\,k_2 + 0\,\delta x_b &= 0 \\
\ldots + 0\,k_2 + 1\,\delta x_b &= 0 \\
+ 0\,\delta x_b &= 0.
\end{aligned} \tag{30}$$

k_2 ist dabei die Korrelate für die Hansensche Zusatzbedingung (29). Die »bestimmte« Auflösung des Systems (30) ergibt:

$$k_1' = -w_1'/3,\ k_1'' = 0,\ \delta x_a = -w_1''/2,\ \ k_2 = 0,\ \delta x_b = w_1''/2.$$

Berechnet man hiermit nach (6) die Verbesserungen, so findet man:

$$v_\alpha = v_\beta = v_\gamma = -w_1'/3,\ \bar{v}_a = \bar{v}_b = 0, \text{ so daß } v_a = v_b = 0.$$

Diese Verbesserungen erfüllen nachweislich, zusammen mit den Unbekannten, die aufgestellten linearen Netzbedingungsgleichungen, ebenso wie die Hansensche Zusatzbedingung.

Außerdem ergibt sich: $\mathbf{v}^T\mathbf{Q}^{-1}\mathbf{v} = -\mathbf{w}^T\mathbf{k} = (w_1')^2/3$. Die »unbestimmte« Auflösung der Normalgleichungen (30) mit Hilfe des Gaußschen Algorithmus liefert:

$$\mathbf{R} = \mathbf{R}^T = \begin{bmatrix} -\frac{1}{2} \end{bmatrix} \quad \text{und} \quad \mathbf{S} = \mathbf{N}_{11}^{+} = \mathbf{Q}_x = \frac{1}{2}\begin{bmatrix} 3, & -3 \\ -3, & 3 \end{bmatrix}.$$

In der Fehlerrechnung ergibt sich:

$$m_0 = \sqrt{(w_1')^2/3\,(2 - 2\sqrt{+\,1})} = \pm\, w_1'/\sqrt{3}\,,$$

$$m_{x_a} = m_{x_b} = m_0\sqrt{3/2} = \pm\, w_1'/\sqrt{2}\,.$$

Bemerkung: Man hätte, in gewisser Weise, schon voraussehen können, daß $v_a = v_b = 0$ sich ergibt. Dann würde man in (28) lediglich $v_a/a = 0$ und $v_b/b = 0$ zu setzen haben und müßte die »freie« Ausgleichung in genau der gleichen Weise fortsetzen wie vorstehend gezeigt.

SCHRIFTTUM

1. Hansen, P. A.: Auflösung einer allgemeinen Aufgabe aus der Wahrscheinlichkeitsrechnung. *Astron. Nachr.*, 1839.
2. Hansen, P. A.: Von der Methode der kleinsten Quadrate. Abh. math.-phys. Cl., Kgl. Sächs. Ges. d. Wiss., VIII. Leipzig, 1867.
3. Hein, G.: Free Adjustment of a Torsion Balance. Net. Boll. Geodes. Sc. Aff., Florence, 1975.
4. Helmert, F. R.: Die Ausgleichungsrechnung nach der Methode der kleinsten Quadrate. 3. Aufl. Leipzig/Berlin, 1924.
5. Meissl, P.: Zusammenfassung und Ausbau der inneren Fehlertheorie eines Punkthaufens. Veröfftl. DGK, A61, München, 1969.
6. Mittermayer, E.: Eine Verallgemeinerung der Methode der kleinsten Quadrate zur Ausgleichung freier Netze. *ZfV*, 96 (1971), 401.
7. Mittermayer, E.: Zur Ausgleichung freier Netze. *ZfV*, 97 (1972), 481.
8. Tárczy-Hornoch, A.: Eine weitere Ausgleichungsgruppe. Mittlg. d. berg- u. hüttenm. Abt. d. Ung. Universität f. Techn. u. Wirtsch.-Wiss. Sopron. Bd. XVIII, 1948/49.
9. Tárczy-Hornoch, A.—Alpár, Gy.: Über eine rechnerische Methode zur Erhöhung der Genauigkeit der mit Sekundenlibellen gemessenen kleinen Winkel. In: »50 Jahre Wild«. Heerbrugg, 1971.
10. Welsch, W.: Insingma, — ein Algorithmus in Algol 60 zur Invertierung singulärer Normalgleichungsmatrizen. *ZfV*, 99 (1974), 35.
11. Wolf, H.: Über eine allgemeine Form der Ausgleichungsrechnung nach der Methode der kleinsten Quadrate. Naturforsch. Gesellsch. Bamberg, 1948.
12. Wolf, H.: Short-arc-Methode und räumliche Bahnglättung in der Satellitentriangulation. *ZfV*, 95 (1970), 37.
13. Wolf, H.: Ausgleichungsrechnung. Formeln zur praktischen Anwendung. Bonn, 1975.

СВОБОДНОЕ УРАВНИВАНИЕ В МОДЕЛИ ГАУССА-ГЕЛЬМЕРТА

Х. ВОЛЬФ

РЕЗЮМЕ

Для формы уравнивания по способу условных измерений с неизвестными, который в последнее время называется моделью Гаусса-Гельмерта, развивается теория свободного уравнивания, под которой подразумевается уравнивание с сингулярной матрицей нормального уравнения. При этом получается форма уравниваний, разработанная профессором Тарци-Хорнох и Вольфом в 1948 году. Эту теорию можно представить без использования «обобщённых инверсов». Для наглядности прилагается числовой пример.

Acta Geodaet., Geophys. et Montanist. Acad. Sci. Hung. Tomus 16 (1), pp. 63—72 (1981)

ORIENTATION-INDEPENDENT FILTERING IN GRAVITY ANALYSIS*

M. K. PAUL

GRAVITY AND GEODYNAMICS DIVISION, EARTH PHYSICS BRANCH, DEPARTMENT OF ENERGY, MINES AND RESOURCES, OTTAWA, CANADA

[Manuscript received November 10, 1978]

Some formulae for the coefficients for band-pass filtering of Bouguer gravity anomaly have been derived so that when they are used in the weighted summations of gridded gravity values, the results are independent of the orientation of the axes of rectangular grids. Such a derivation has been achieved by starting from a transfer function of circular symmetry that fulfils the requirements of a band-pass filter and then integrating its contribution over a rectangle with a grid point at its center. Computational checks applied to different sets of coefficients as evaluated by the proposed method confirm their accuracy to at least five significant digits.

Introduction

Orientation dependence of different filtering methods in the field of gravity analysis has recently been a subject of considerable discussion in a series of papers [7, 9, 10, 13, 14, 15].

Filtering of the Bouguer gravity anomaly is a pre-requisite for most of its standard interpretations. Numerous investigations have been carried out on this topic during the past three decades that have resulted in several methods of separation of residuals, evaluation of the first and second derivatives and analytical continuation of fields. Some of these different methods have been subjected to comparative studies. FAJKLEWICZ [3] applied the first derivative method of BARANOV [1] and second derivative methods of ELKINS [2] and PAUL [11] to some model gravity anomalies due to assumed spherical masses at some depth. While observing from his analysis that 'of the three formulas considered, the Paul formula is by a small margin the best', he obtained undesirable fictitious peaks in the contour maps of the derivatives by each of the above methods and interpreted them as due to the inherent defect of these methods. MESKÓ [8] and FULLER [4] examined these as well as other methods due to ROSENBACH [12], HAALCK [5], HENDERSON and ZEITZ [6] using Fourier transform technique and presented diagrams of their transfer functions or frequency response functions. These diagrams show a considerable lack of circular symmetry, or orientation independence, beyond some magnitudes of frequency and, as such, results of practical computations by these methods are subject to distortion through orientation dependence.

* Earth Physics Branch Contribution No. 926.

In the above filtering methods, the coefficients of the rectangularly gridded gravity data were always assumed to have circular symmetry being dependent on the radial distance only. This causes loss of circular symmetry for the transfer functions as it is mathematically impossible to maintain circular symmetry of both the coefficients and transfer functions simultaneously.

However, if the coefficients of the gridded data are not constrained with circular symmetry, we may obtain some transfer functions free from orientation dependence. Thus, starting from an orientation independent model for transfer functions, we should be able to find the coefficients of the grid gravity values which do not possess circular symmetry. The method described in the following section is approached from this standpoint.

Present method

At first, let us note that with (r, θ) and (σ, λ) as the polar coordinates in space and frequency domains respectively, the gravity anomaly $g(r, \theta)$ can be related reciprocally to a transform $G(\sigma, \lambda)$ as follows

$$\left.\begin{aligned} G(\sigma, \lambda) &= \int_0^\infty \int_{-\pi}^{\pi} g(r, \theta)\, K(r, \theta, \sigma, \lambda)\, r\, \mathrm{d}r\, \mathrm{d}\theta \\ g(r, \theta) &= \int_0^\infty \int_{-\pi}^{\pi} G(\sigma, \lambda)\, K(\sigma, \lambda, r, \theta)\, \sigma\, \mathrm{d}\sigma\, \mathrm{d}\lambda \end{aligned}\right\} \tag{1}$$

where, as one of many choices for the kernel,

$$K(r, \theta, \sigma, \lambda) = K(\sigma, \lambda, r, \theta) = \frac{1}{2\pi}\left[J_0(\sigma r) + 2 \sum_{m+1}^{\infty} \delta_m J_m(\sigma r) \cos\{m(\theta - \lambda)\}\right]$$

$$= \frac{1}{2\pi}[\cos\{\sigma r \sin(\theta - \lambda)\} + \sin\{\sigma r \cos(\theta - \lambda)\}] \tag{2}$$

with $\delta_m = 1$ or $(-1)^{(m-1)/2}$ according as m is even or odd respectively.

Now, without any loss of generality we can assume that the origin of the coordinate system in the space domain is at the point of computation; the relationship (assumed linear) between the filtered and non-filtered gravity anomalies can then be expressed as:

$$g_R(0, 0) = \int_0^\infty \int_{-\pi}^{\pi} g(r, \theta)\, w(r)\, r\, \mathrm{d}r\, \mathrm{d}\theta \tag{3}$$

where the weighting function w must be independent of θ so that $g_R(0, 0)$ remains invariant under rotation of the reference system.

Then, from the substitutions of (1) and (2) in (3) we have

$$g_R(0, 0) = \int_0^{\infty} \int_{-\pi}^{\pi} G(\sigma, \lambda)\ W(\sigma)\ \sigma\ \mathrm{d}\sigma\ \mathrm{d}\lambda \tag{4}$$

where

$$W(\sigma) = \int_0^{\infty} \int_{-\pi}^{\pi} w(r)\ K(r, \theta, \sigma, \lambda)\ r\ \mathrm{d}r\ \mathrm{d}\theta = \int_0^{\infty} w(r)\ J_0(\sigma r)\ r\ \mathrm{d}r \tag{5a}$$

and hence

$$w(r) = \int_0^{\infty} W(\sigma)\ J_0(\sigma r)\ \sigma\ \mathrm{d}\sigma\ . \tag{5b}$$

It should be noted here that only the first term of the series (2) for $K(r, \theta, \sigma, \lambda)$ has its contribution in (5a) as those of the other terms vanish when they are integrated over θ from $-\pi$ to π.

Now since $K(0, 0, \sigma, \lambda) = 1$, we find from comparison of (4) with (1) that

$$G_R(\sigma, \lambda) = G(\sigma, \lambda)\ W(\sigma) \tag{6}$$

where $G_R(\sigma, \lambda)$ represents the transform of the filtered gravity.

From (6) we note that $W(\sigma)$ is the transfer function or frequency response function of the present filtering method and this, being free from λ, is orientation independent.

Let us consider a model transfer function for band-pass filtering

$$W(\sigma) = \frac{1}{2\pi}\, e^{n(1-\sigma^2/\sigma_c^2)}\ (\sigma/\sigma_c)^{2n} \tag{7}$$

which has been constructed such that

(i) $W(\sigma)$ is maximum at $\sigma = \sigma_c$ i.e. gravity anomaly of frequency around σ_c has the maximum ratio of contribution in filtered anomaly,

(ii) $2\pi W(\sigma_c) = 1$, which ensures fully unattenuated filtering of anomaly of frequency σ_c, and

(iii) the width of the filter slot, being proportional to the radius of curvature of $W(\sigma)$ at σ_c, is related to the integral parameter n as

$$\text{width } \alpha \text{ (radius of curvature) } \sigma_c = \frac{-1}{\left(\dfrac{d^2 W}{d\sigma^2}\right)_{\sigma_c}} = \frac{\pi \sigma_c^2}{2n}$$

which indicates that the width can be reduced by increasing n and vice versa.

Substituting (7) in (5b) we obtain

$$w(r) = \frac{e^n (n!)^2}{4\pi n^{n+1}} \sigma_c^2 e^{-r^2 \sigma_c / 4n} \sum_{k=0}^{n} \frac{(-r^2 \sigma_c^2/4n)^k}{(k!)^2 (n-k)!} =$$

$$= \frac{e^n (n!)^2}{4\pi n^{n+1}} \sigma_c^2 \sum_{k=0}^{n} \frac{(-\sigma_c^2/4n)^k}{k!\,(n-k)!} \cdot$$

$$\cdot \sum_{l=0}^{k} \frac{(e^{-x^2 \sigma_c^2/4n} x^{2l})\ (e^{-y^2 \sigma_c^2/4n} y^{2(k-l)})}{l! \qquad (k-l)!}, \tag{8}$$

where $r^2 = x^2 + y^2$.

A few curves of $W(\sigma)$ and $w(r)$ for $\sigma_c = 1$ and $n = 2, 4, 8, 16$ and 32 have been shown in Figs 1 and 2, respectively. It can be clearly seen that widths of w-curves increase as those of W-curves decrease which implies that practical computations will require coverage of bigger areas with gravity data for narrower filters.

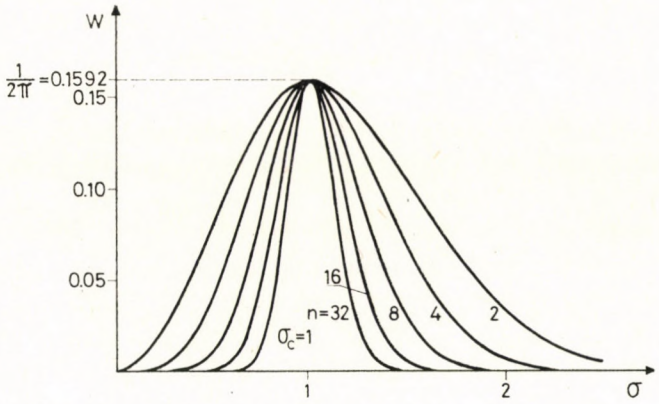

Fig. 1. Curves of $W(\sigma)$ for $\sigma_c = 1$ and $n = 2, 4, 8, 16$ and 32

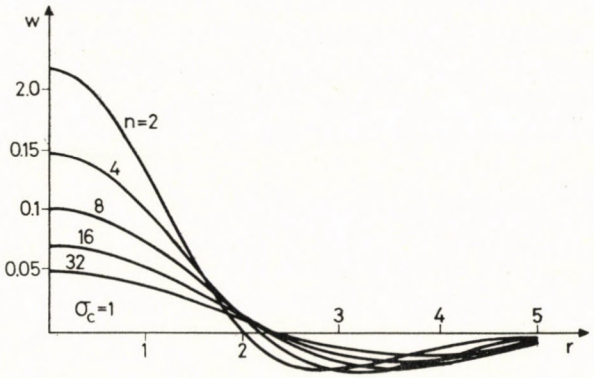

Fig. 2. Curves of $w(r)$ for $\sigma_c = 1$ and $n = 2, 4, 8, 16$ and 32

Now let us consider the application of (3) to rectangular grid values, $g(\mu s, \nu s)$, $\mu, \nu = 0, \pm 1, \pm 2, \ldots, s =$ grid separation. When s is sufficiently small, the gravity anomaly over an $s \times s$ rectangle around a grid point can be assumed constant and equal to the value at the grid point. Hence we have

$$g_R(0, 0) = \sum_{\mu=-\infty}^{\infty} \sum_{\nu=-\infty}^{\infty} w_{\mu\nu}\, g(\mu s, \nu s) \tag{9}$$

where

$$w_{\mu\nu} = \int_{(\mu-\frac{1}{2})s}^{(\mu+\frac{1}{2})s} \int_{(\nu-\frac{1}{2})s}^{(\nu+\frac{1}{2})s} w(r)\, dx\, dy, \tag{10}$$

$$\mu, \nu = 0, \pm 1, \pm 2, \ldots$$

The coefficients $w_{\mu\nu}$ can have circular symmetry i.e. $w_{\mu\nu} = f(\mu^2 + \nu^2)$ (e.g. $w_{43} = w_{50}$ and $w_{12.5} = w_{13.0}$) only when $w(r)$ is assumed constant and equal to $w(\sqrt{\mu^2 + \nu^2}\, s)$ over the rectangle of integration in (10) and such an assumption can hardly find any realistic basis. But all the filtering methods mentioned above end up with virtually the same assumption as their coefficients were found to possess circular symmetry which in turn introduced orientation dependence to the corresponding transfer functions. In the present method we substitute (8) for $w(r)$ in (10) and perform the integration formally when we obtain

$$w_{\mu\nu} = \frac{e^n (n!)^2}{\pi n^n} \sum_{k=0}^{n} \sum_{l=0}^{k} (-1)^k \frac{[\varepsilon_l(\overline{\mu + 1/2}\,\alpha) - \varepsilon_l(\overline{\mu - 1/2}\,\alpha)]}{k!\,(n-k)!\,l!\,(k-l)!} \cdot$$

$$\cdot [\varepsilon_{k-l}(\overline{\nu + 1/2}\,\alpha) - \varepsilon_{k-l}(\overline{\nu - 1/2}\,\alpha)] \tag{11}$$

where $\alpha = \dfrac{\sigma_c\, s}{2n}$ and $\varepsilon_m(x) = \int_0^x e^{-x^2} x^{2m}\, dx$. Evidently, these coefficients are not functions of $(\mu^2 + \nu^2)$.

Computations

Computation of the coefficient $w_{\mu\nu}$ from (11) has been carried out on a CDC CYBER 74 computer with our Fortran subroutine to evaluate $\varepsilon_m(x)$. Different values of $\sigma_c s$ and n have been considered with μ and ν varying from 0 to 34. For economy of space, only a few sets of these results for $\sigma_c\, s = 0.5$, 1.0, 2.0, $n = 2$, 8 and $\mu, \nu = 0, 1, \ldots, 5$ are given in Table I. Disagreements in the values of w_{43} and w_{50} confirm the expected departure of circular symmetry in these coefficients. Similar effects, although not as easily demonstrable, are found in the rest of the coefficients as well.

Table I

Different sets of coefficients $w_{\mu\nu}$

μ	ν	$\sigma_c s = 0.5$		$\sigma_c s = 1.0$		$\sigma_c s = 2.0$	
		$n = 2$	$n = 8$	$n = 2$	$n = 8$	$n = 2$	$n = 8$
0	0	.36180 E−01	.17608 E−01	.13808 E+00	.67982 E−01	.45691 E+00	.23534 E+00
1	0	.32909 E−01	.16395 E−01	.93181 E−01	.50386 E−01	.54175 E−01	.44669 E−01
1	1	.29837 E−01	.15229 E−01	.58418 E−01	.35427 E−01	−.75243 E−01	−.45194 E−01
2	0	.24251 E−01	.13033 E−01	.11900 E−01	.12274 E−01	−.72783 E−01	−.72538 E−01
2	1	.21718 E−01	.12001 E−01	−.27474 E−02	.35735 E−02	−.44170 E−01	−.53758 E−01
2	2	.15053 E−01	.91474 E−02	−.24836 E−01	−.13596 E−01	.47819 E−02	.10740 E−01
3	0	.13116 E−01	.82742 E−02	−.27387 E−01	−.16943 E−01	.96050 E−02	.23653 E−01
3	1	.11310 E−01	.74381 E−02	−.28387 E−01	−.19353 E−01	.11124 E−01	.31537 E−01
3	2	.66031 E−02	.51412 E−02	−.25773 E−01	−.22219 E−01	.80647 E−02	.30911 E−01
3	3	.77374 E−03	.19563 E−02	−.14932 E−01	−.18129 E−01	.21652 E−02	.19682 E−02
4	0	.28361 E−02	.31396 E−02	−.19477 E−01	−.20640 E−01	.39096 E−02	.13690 E−01
4	1	.17634 E−02	.25335 E−02	−.17188 E−01	−.19490 E−01	.29294 E−02	.75784 E−02
4	2	−.97545 E−03	.88513 E−03	−.10740 E−01	−.14990 E−01	.11399 E−02	−.65652 E−02
4	3	−.41971 E−02	−.13469 E−02	−.28328 E−02	−.63296 E−02	.19895 E−03	−.12857 E−01
4	4	−.66198 E−02	−.35534 E−02	.23039 E−02	.36675 E−02	.13935 E−04	−.36846 E−02
5	0	−.41974 E−02	−.13469 E−02	−.28358 E−02	−.63345 E−02	.19487 E−03	−.12866 E−01
5	1	−.46740 E−02	−.17233 E−02	−.17215 E−02	−.46699 E−02	.13498 E−03	−.12191 E−01
5	2	−.58263 E−02	−.27260 E−02	.80011 E−03	−.99477 E−04	.43734 E−04	−.83365 E−02
5	3	−.69823 E−02	−.40164 E−02	.28785 E−02	.56773 E−02	.62443 E−05	−.99636 E−03
5	4	−.74528 E−02	−.51533 E−02	.32488 E−02	.96418 E−02	.36829 E−06	.35777 E−02
5	5	−.68865 E−02	−.57326 E−02	.22726 E−02	.92657 E−02	.85216 E−08	.19849 E−02

These coefficients have been subjected to several checks based on the following relations

$$\left.\begin{aligned} \frac{1}{2\pi}\sum_{\mu=-M}^{M}\sum_{\nu=-M}^{M} w_{\mu\nu} J_0(\sigma s\sqrt{\mu^2+\nu^2}) &\approx W(\sigma) \\ \sum_{\mu=-M}^{M}\sum_{\nu=-M}^{M} w_{\mu\nu}(\mu^2+\nu^2)^k &\approx \frac{(-e)^n 4^k k!^2 n^{k-n}}{(\sigma_c s)^{2k}(k-n)!}, \quad k \geq n \\ &\approx 0, \quad k < n. \end{aligned}\right\} \quad (12)$$

The first one of these follows readily from (5a) and the other from the k^{th} derivative of $W(\sigma)$ at $\sigma = 0$ where the integrals have been approximated by the summations of function values at the center of $s \times s$ rectangle, weighted by $w_{\mu\nu}$, over $(2M+1)^2$ number of rectangles in place of an infinite number of them. Evaluations of the left hand sides of these relations have been carried out for specific values of $\sigma_c s$, σs, n, k and M and then compared with the computed values of the right hand sides. These results for the first and the second of the above equations may be found in Tables II and III, respectively. For higher M, the left hand sides approach closer to the right hand sides — as should be expected. Such agreements, however, can never be exact because of the error involved in replacing an integral over any of the rectangles by the corresponding product of the coefficient and the value of the function at the center of the block.

Table II

Comparison between two sides of the first equation in (12)

n	σs	$\sigma_c s$	Left hand sides computed for			Right hand side
			$M = 15$	$M = 25$	$M = 35$	
2	0	0.5	−.60378 E−02	−.17700 E−06	−.48374 E−14	0
		1.0	−.16254 E−09	.87714 E−16	.87714 E−16	
		2.0	.30783 E−14	.30783 E−14	.30783 E−14	
8		0.5	.32168 E−01	−.64797 E−02	−.35739 E−03	
		1.0	.33402 E−02	.52638 E−05	−.22468 E−09	
		2.0	−.26910 E−06	−.61705 E−13	−.61705 E−13	
2	0.5	0.5	.15689	.15750	.15750	.15915
	1.0	1.0	.15262	.15262	.15262	
	2.0	2.0	.13461	.13461	.13461	
8	0.5	0.5	.13460	.15421	.15740	
	1.0	1.0	.15186	.15262	.15262	
	2.0	2.0	.13413	.13413	.13413	

Table III

Comparison between two sides of the second equation in (12)

$\sigma_c s$	n	k	Left hand sides computed for			Right hand side
			$M = 15$	$M = 25$	$M = 35$	
0.5	2	1	−.10457 E+02	−.73247 E−03	−.31280 E−10	0
		2	.45953 E+04	.75659 E+04	.75664 E+04	.75664 E+04
	8	4	.56511 E+09	.63119 E+10	−.15265 E+11	0
		8	−.49582 E+19	.92584 E+21	.80553 E+22	.20814 E+23
1.0	2	1	−.23522 E−06	.62885 E−12	.62885 E−12	0
		2	.47290 E+03	.47290 E+03	.47290 E+03	.47290 E+03
	8	4	.42652 E+08	.23212 E+07	−.36353 E+03	0
		8	−.22765 E+18	−.15841 E+19	.30796 E+18	.31760 E+18
2.0	2	1	−.14234 E−04	−.14234 E−04	−.14234 E−04	0
		2	.29557 E+02	.29557 E+02	.29557 E+02	.29557 E+02
	8	4	−.53937 E+04	.17105 E−05	.17105 E−05	0
		8	−.13843 E+14	.48462 E+13	.48462 E+13	.48462 E+13

To serve as a further check, a few selected coefficients have also been evaluated by performing the integration in (10) numerically. For the same accuracy, the method takes several times more computer-time than that required by our method and, therefore, should be normally avoided. However, as can be seen in Table IV, these results agree more closely with our previous results as the number of ordinates used in numerical integration increases. Evidently, they confirm the accuracy of our proposed method to at least five significant digits which is sufficient for any practical purpose.

Table IV

Comparison of the coefficients $w_{\mu\nu}$ as computed by our method with the same obtained by numerical integration techniques

$\sigma_e s$	n	μ	ν	Our method	Numerical integrations using number of ordinates as:			
					20	40	60	80
0.5	2	0	0	.36180 E−01	.36182 E−01	.36180 E−01	.36180 E−01	.36180 E−01
		4	3	−.41971 E−02	−.41969 E−02	−.41971 E−02	−.41971 E−02	−.41971 E−02
		12	4	.85632 E−03	.85634 E−03	.85633 E−03	.85633 E−03	.85633 E−03
		14	14	.93864 E−05	.93865 E−05	.93865 E−05	.93864 E−05	.93864 E−05
	8	0	0	.17608 E−01	.17608 E−01	.17608 E−01	.17608 E−01	.17608 E−01
		4	3	−.13469 E−02	−.13467 E−02	−.13468 E−02	−.13469 E−02	−.13469 E−02
1.0	2	0	0	.13808 E+00	.13810 E+00	.13808 E+00	.13808 E+00	.13808 E+00
		4	3	−.28328 E−02	−.28333 E−02	−.28329 E−02	−.28329 E−02	−.28328 E−02
		12	4	.65116 E−07	.65099 E−07	.65112 E−07	.65114 E−07	.65115 E−07
		14	14	.19573 E−18	.19573 E−18	.19573 E−18	.19573 E−18	.19573 E−18
	8	0	0	.67982 E−01	.67990 E−01	.67984 E−01	.67983 E−01	.67982 E−01
		4	3	−.63296 E−02	−.63302 E−02	−.63297 E−02	−.63296 E−02	−.63296 E−02
2.0	2	0	0	.45691 E+00	.45717 E+00	.45698 E+00	.45694 E+00	.45693 E+00
		4	3	.19895 E−03	.19871 E−03	.19895 E−03	.19895 E−03	.19895 E−03
		12	4	.14718 E−29	.14439 E−29	.14506 E−29	.14518 E−29	.14522 E−29
		14	14	0*	.37398 E−77	.37500 E−77	.37505 E−77	.37505 E−77
	8	0	0	.23534 E+00	.23545 E+00	.23537 E+00	.23535 E+00	.23535 E+00
		4	3	−.12857 E−01	−.12857 E−01	−.12857 E−01	−.12857 E−01	−.12857 E−01

* Our method sets a coefficient less than 10^{-50} to zero.

REFERENCES

1. Baranov, V.: Calcul du gradient vertical de champ de gravite ou du champ magnetique mesure à la surface du sol. *Geophys. Prosp.*, 1 (1953), 171—191.
2. Elkins, T. A.: The second derivative method of gravity interpretation. *Geophysics*, 16 (1951), 29—50.
3. Fajklewicz, Z. J.: Fictitious anomalies of higher vertical derivatives of gravity. *Geophysics*, 30 (1965), 1094—1107.
4. Fuller, B. D.: Two-dimensional frequency analysis and design of grid operators. *Mining Geophys.*, 2 (1967), 658—708.
5. Haalck, F.: A torsion-magnetometer for measuring the vertical component of the earth's magnetic field. *Geophys. Prosp.*, 4 (1956), 424—441.
6. Henderson, R. G.—Zeitz, I.: Computation of second vertical derivatives of geomagnetic fields. *Geophysics*, 14 (1949), 508—516.
7. Kovács, F.—Meskó, A.: Some notes on the transfer properties of two-dimensional polynomial fitting. *Acta Geod. Geoph. Mont. Hung.*, 10 (1975), 375—387.
8. Meskó, A.: Gravity interpretation and information theory III. The method of second derivatives. *Ann. Univ. Sci. Budapestiensis*, 13 (1967), 37—60.
9. Meskó, A.: Gravity interpretation and information theory. Design and application of low-pass, high-pass and band-pass filters. *Ann. Univ. Sci. Budapestiensis*, 15 (1969), 67—80.
10. Meskó, A.—Kovács, F.: An unbiassed comparison of two methods suggested for the computation of residual gravity. *Acta Geod. Geoph. Mont. Hung.*, 10 (1975), 69—78.
11. Paul, M. K.: On computation of second derivatives from gravity data. *Geoph. Pura e Appl.*, 48 (1961), 3—11.
12. Rosenbach, O.: A contribution to the computation of the 'second derivative' from gravity data. *Geophysics*, 18 (1953), 894—909.
13. Steiner, F.: Characterization and derivation of map transformations on the basis of the anomalous body-map relationship. *Acta Geod. Geoph. Mont. Hung.*, 8 (1973), 71—84.
14. Steiner, F.: Derivation of fully-matrixed map transformations. *Acta Geod. Geoph. Mont. Hung.*, 8 (1973), 85—102.
15. Steiner, F.: The proper use of the gravitational filters. *Acta Geod. Geoph. Mont. Hung.*, 10 (1975), 189—197.

ФИЛЬТРАЦИЯ, НЕЗАВИСЯШАЯ ОТ ОРИЕНТАЦИИ В ГРАВИМЕТРИЧЕСКИХ ИССЛЕДОВАНИЯХ

М. К. ПАУЛ

РЕЗЮМЕ

Выводятся некоторые формулы для коэффициентов полосно-пропускающей фильтрации гравитационной аномалии Буге таким образом, что когда они используются в весовой сумме средних гравитационных значений в сетких, результаты не зависят от ориентации осей квадратных сеток. Такой вывод получили исходя из функции передачи с круговой симметрией — которая удовлетворяет требованиям полосно-пропускающего фильтра — интегрируя её вклад в области квадрата с сеточным пунктом в центре. Проверка вычислительным путем подтверждает точность коэффициентов различных последовательностей, полученных предлагаемым методом до пяти ценных знаков

Acta Geodaet., Geophys. et Montanist. Acad. Sci. Hung. Tomus 16 (1), pp. 73—90 (1981)

GENERAL VALIDITY OF THE LAW OF LARGE NUMBERS IN CASE OF ADJUSTMENTS ACCORDING TO THE MOST FREQUENT VALUE

L. CSERNYÁK—B. HAJAGOS—F. STEINER

TECHNICAL UNIVERSITY OF HEAVY INDUSTRY, MISKOLC

[Manuscript received July 16, 1979]

The technical practice tries to achieve higher accuracy by increasing the number of measurements (at a given technical level with given physical conditions). It is often found however, in the geophysical pratice that the increase of the number of measurements does not lead to the expected decrease of the error (in ratio with $1/\sqrt{n}$). Even the case is rather frequently met in the geophysical practice (e.g. see the frequency curves in [6]) when in spite of the increase of the number of measurements, the values adjusted according to the least squares hypothesis, or in the most simple case, the averages of the data do not have a normal distribution.

GNEDENKO and KOLMOGOROV call in [2] the idea a "biassed prejudice" that only the normal distribution can be a realistic limit distribution. Consequently even density functions with infinite scatter can be used for the approximation of the measurement results or of values deduced from them if the curve of the empirical cumulative frequencies necessitate either theoretically or practically their application. (It is namely well known that in cases with finite scatter, the normal distribution is necessarily the limit distribution.)

The distributions with infinite scatter can be manyfold. For some of them, no usual form of the law of large numbers is valid: the confidence intervals of the averages computed from n data do not decrease if n is increasing. A study of cases presented in this paper shows that *the accuracy of the most frequent value increases in each case with n*, i.e. from practical point of view even the distribution which does not fulfil the law of large numbers (in any usual form of it) is easy to process independently from the complete unapplicability of the adjustment according to the expected value (method of the least squares) to obtain reliably the information content of the data.

1.

Under the law of large numbers the following is understood in the technical practice: if a characteristic quantity being important from any technical point of view is determined from a greater block of data, this quantity can be the more accurately determined, the greater is the number of data n. The accuracy of the determination is on its turn greater if the confidence interval of the frequency curve for any level of probability (e.g. mid-value width) is smaller. The frequency curve is here determined from many (e.g. or at least 200) measurement data sets of n values each used for the determination of the characteristic quantity.

This characteristic quantity used to be in the overwhelming majority of cases the algebraic average (to which the result of the adjustment according to the least squares corresponds in case of a many-parameter adjustment). The theorems known as "the laws of large numbers" from the theory of probabilities (e.g. in [3]) refer also to this quantity.

According to Glivenko's basic theorem of mathematical statistics the empiric distribution functions converge uniformly with a probability of 1 to the corresponding theoretical distribution functions (in [3] p. 423). The latter is naturally completely determined by the phenomenon studied or by the set of phenomena being effective during the measurements independently from any subjective wishes. Therefore if no part of the measurement results will be arbitrarily omitted, then in the geophysical practice not rarely a theoretical distribution having infinite scatter is the best approximation of the empiric distribution function.

It is therefore possible that the law of the large numbers is not fulfilled if the algebraic average (the results of an adjustment according to the least squares method) is taken as characteristic quantity. As it has been mentioned the usual procedure in such cases is that certain values are arbitrarily omitted and thus the results are distorted to a mathematical model well-known in the technical practice. The authors of the present paper propose instead of this theoretically hardly acceptable practice the use of such a characteristic quantity which follows for every distribution the law of large numbers.

It can be easily seen according to the results in [5] that the most frequent value defined in [4] has such a property. It is namely shown there that the error of the most frequent value M determined from n data is

$$\frac{c \cdot \varepsilon_0}{\sqrt{n}} \tag{1}$$

where the finite constant c depends on the type of the distribution, ε_0 is the so-called reciprocal cohesion playing an important role in the computation and estimation of the accuracy of the most frequent value M. It is sufficient therefore to prove that the value of ε_0 is finite for each distribution function with the density function $f(x)$. According to [4] ε_0 is the greatest maximum place of the function

$$F(\varepsilon) \equiv \varepsilon^3 \left[\int_{-\infty}^{\infty} \frac{1}{x^2 + \varepsilon^2} f(x)\, dx \right]^2 . \tag{2}$$

Now it remains to prove that if ε increases infinitely, $F(\varepsilon)$ converges to zero. This is identical with:

$$F(\varepsilon) = \frac{1}{\varepsilon} \left[\int_{-\infty}^{\infty} \frac{\varepsilon^2}{x^2 + \varepsilon^2} f(x)\, d(x) \right]^2 < \frac{1}{\varepsilon} \to 0 \tag{3}$$

being true as $f(x)$ an integrand normed to unit is decreased by the factor $\frac{\varepsilon^2}{x^2 + \varepsilon^2}$ being always less than unit (with the exception of the place with the argument 0). (The finiteness of ε_0 follows else from the considerations published in [1], too).

It is naturally problematic how often distributions with infinite scatter are met. Namely, if empiric quadratic errors are determined from measurement results, this value is naturally *always* finite. The fact may lead to the idea that a theoretical distribution function which is approximated by the empiric distribution function has also a finite scatter.

Distributions with finite scatter belong to the attraction field of normal distributions; this is the sense of the central limit theorem. The attribute "central" refers to the role of the theorem, and it tells us that the theoretical distributions are supposed to be practically without exception distributions with finite scatter.

The theory of probabilities and the mathematical statistics based on it in their present form (quickly outgrowing the frames of gambles of hazard) can correctly handle first of all the cases with finite scatter according to the demands of mass production (the deviations of the dimensions of a product can be naturally well characterized by a theoretical distribution with finite scatter). In geophysics, however, it cannot be said from all distributions occurring in the praxis that they have finite scatter (see e.g. the frequency curves in [6]).

The classical representants of the probability theory have significantly better worked out the problematics of the limit distributions as it is at present known in the technical, specially in the geophysical practice (see e.g. the excellent summarizing work of GNEDENKO and KOLMOGOROV [2]). Let us refer from there only to one single theorem: it is true for all characteristic functions $\varphi(t)$ of all limit distributions that their logarithms can be written as:

$$\log \varphi(t) = i\gamma t - c|t|^{\alpha}\left[1 + i\beta\frac{t}{|t|}\omega(t,\alpha)\right] \tag{4}$$

where γ is an arbitrary real number, $-1 \leq \beta \leq 1$, $0 < \alpha \leq 2$, $c \geq 0$ and:

$$\omega(t,\alpha) = \begin{cases} tg\dfrac{\pi}{2}\alpha, & \text{if } \alpha \neq 1 \\ \dfrac{2}{\pi}\log|t| & \text{if } \alpha = 1\,. \end{cases} \tag{4a}$$

From the possible values of α being a set with a continuum cardinal number, there is only a single one, the case $\alpha = 2$ which the central limit theorem refers to; as the normal distribution is the limit distribution for all distributions with finite scatter, a non-estimable quantity of possibilities would be excluded without any reason, if empiric distribution functions would not be approximated by theoretical distribution functions with infinite scatter if they are necessitated by the data sets.

2.

It is clear on the basis of Chapter 1 that the examples cannot be taken from the small sample of probabilistic distributions with finite scatter which are referred to in overwhelming majority not only in handbooks, but also in special works dealing with probability theory and/or mathematical statistics.

The present investigations will be carried out on the following distributions defined by their probability density functions $f(x)$:

$$f(x) = \frac{3\sqrt{3}}{4\pi} \frac{1}{|x|^3 + 1}; \tag{5}$$

$$f(x) = \frac{3\sqrt{3}}{8\pi} \frac{1}{|x|^{3/2} + 1}; \tag{6}$$

$$f(x) = \frac{1}{2(|x| + 1)^2}; \tag{7}$$

$$f(x) = \begin{cases} 0.25 & |x| \leq 1 \\ \dfrac{0.25}{x^2} & |x| > 1 \end{cases} \tag{8}$$

$$f(x) = \begin{cases} \dfrac{2}{\pi} \dfrac{1}{x^2 + 1} & x \geq 0 \\ 0 & x < 0 \end{cases} \tag{9}$$

$$f(x) = \begin{cases} \dfrac{1}{\sqrt{2\pi}} \cdot e^{-\frac{1}{2x}} x^{-\frac{3}{2}} & x > 0 \\ 0 & x \leq 0\,. \end{cases} \tag{10}$$

It is clear at a first glance for all these distributions that their scatter is infinite, as the functions $x^2 \cdot f(x)$ cannot be integrated in the interval $(-\infty, \infty)$. (Further there are no expected values for the distributions 6—10, as there the function $x \cdot f(x)$ cannot be integrated either). If the curves $f(x)$ for the distributions being symmetrical to the origine are represented (left-hand side curves in Figs 1—4), it can hardly be understood why these distributions do not yield unambiguously their symmetry points more and more accurately with increasing n? In fact, the acceptance of the expected value as a characteristic quantity must rather be doubted than to loose the possibility of the accurate evaluation of such data systems under the pretext of the infiniteness of scatter.

According to the short theoretical considerations in Chapter 1, the acceptance of the most frequent value as a characteristic quantity reaches the aim,

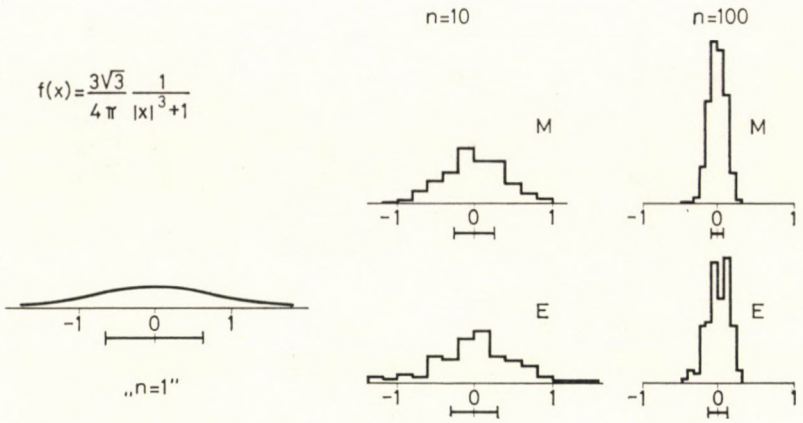

Fig. 1

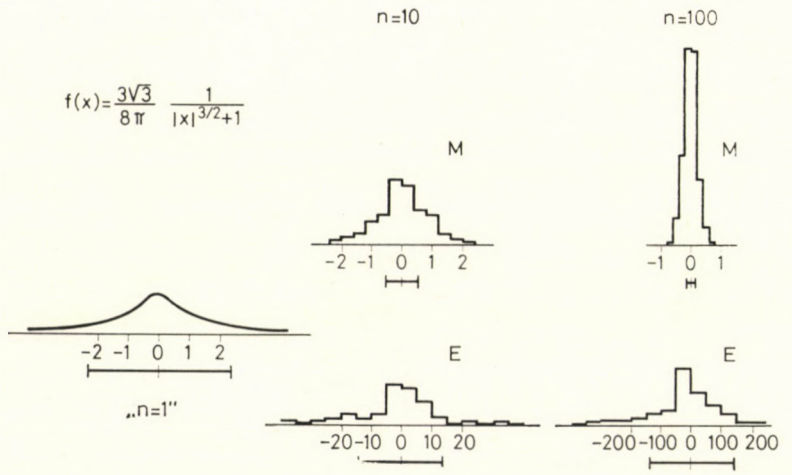

Fig. 2

as its error decreases for each distribution with increasing n according to Eq. 1. Let us consider in the following the validity of the law of large numbers in the previous examples, if the most frequent values are determined from data sets with n values of the random variable with the given probability distributions, instead of using the generally accepted method to use the averages (from the same sets with n data).

The density function of Eq. 5 is represented in the left-hand side of Fig. 1. The legend "$n = 1$" means that the density function here should be regarded as the frequency curve of one-element samples (i.e. belonging to $n = 1$). In case of $n = 1$ the average and the most frequent value are naturally identical.

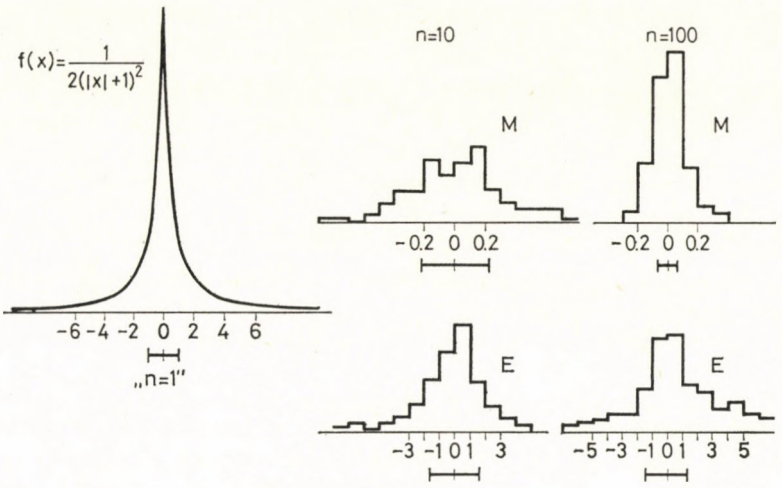

Fig. 3

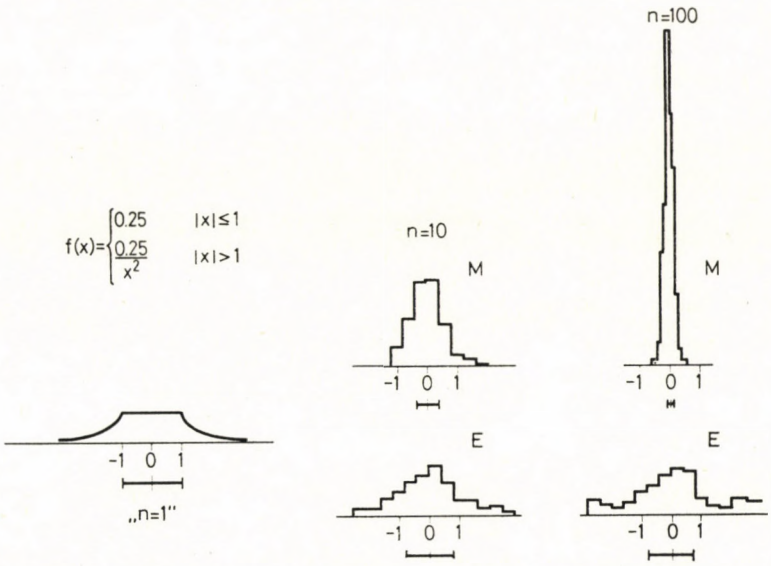

Fig. 4

The frequency diagrams of data sets with $n = 10$ and $n = 100$ data are identified in case of an adjustment according to the most frequent value by the letter M; the algebraic averages computed from the same data sets are denoted by E. In both cases of $n = 10$ and $n = 100$, the computations were carried out for 200 sets, and the frequency curves refer to these results.

The above said is also valid for Figs 2—6 without any change. Since all frequency diagrams refer to 200 data sets, the plotting of the ordinates seemed

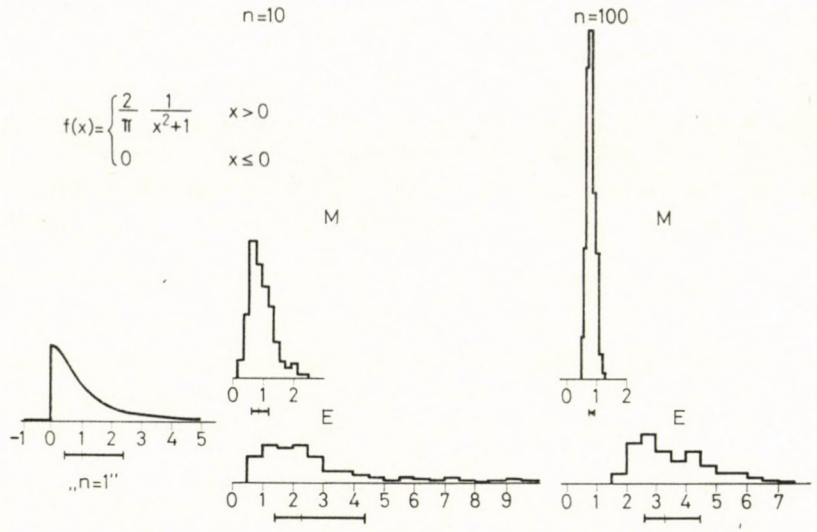

Fig. 5

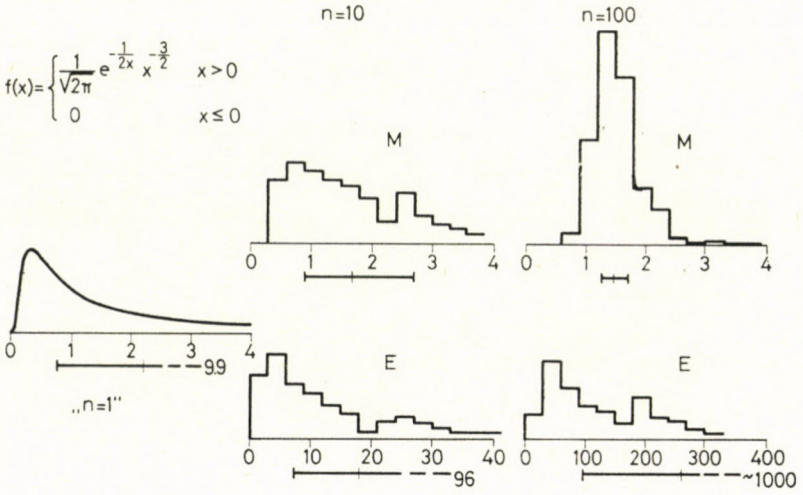

Fig. 6

us to be superfluous, and were omitted. At the same time, however, in all examples i.e. on all figures — in order to enable better comparisons — an ordinate scale is used due to which the identical areas below the curves of any two frequency diagrams out of the five define the intervals of the data occurring with identical probability (e.g. M_n or E_n values). On Figs 1—6 below the abscissae of the five frequency distributions the interval in which the probability of the occurrence is 50% is shown in a way that the smallest values at

left-hand side end and the greater values at the right hand side end have equally the occurrence probability of 25%. This interval is called in the following the interval of the semivalue width, its length is the semi-value width (the more usual name for it is interquartile semi-dimension). On the intervals of the semi-value width, the value of the median is always noted.

As it is known the values of a random variable with the density function $f(x)$ can be obtained by the following procedure: at first the distribution function $\Phi(x) = \int_{-\infty}^{x} f(x)\,dx$ is computed, the interval (0,1) is distributed into a great number (at least 500) intervals of identical lengths, the intersection points are projected through the $\Phi(x)$ curve to the abscissae-axis, and from this series of data that one is taken whose serial number coincides with the serial number chosen by the random number generator of the computer (the uniformly distributed random numbers can be easily converted into serial numbers). (It must be noticed that the finite representation of the probability distributions doesn't allow an arbitrary large n-value. The case of $n = 100$ is still correct for our

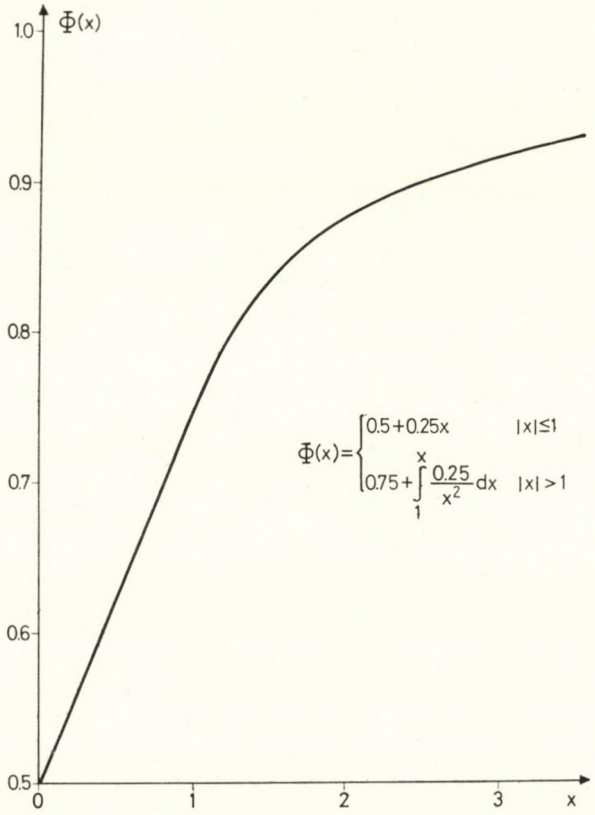

Fig. 7

probability models and for our purposes; if n would be too large the effect of finiteness would overwhelm the very behaviour of the original probability distribution.) Taking into account this procedure, further in order to get a better picture of the asymptotic properties of the distributions, the distribution functions of the random variables characterized in Figs 1—6 by their density functions $f(x)$ are also drawn (Figs 7—12).

Let us now return to the probability distribution shown in Fig. 1 (its definition is Eq. 5). The scatter is infinite in this case, too, but the law of great numbers is nearly exactly as valid for the simple algebraic averages (diagrams denoted by E) as for the most frequent values (diagrams denoted by M). The values can be compared by the semi-value widths.

In complete difference from this the distribution defined by Eq. 6 (Fig. 2) shows a drastic widening of the E-curves with increasing n. In case of $n = 10$ the abscissae must be reduced ten times, in case of $n = 100$, hundred times to enable a representation of the semi-widths, the left- and right-side ends of the E-diagrams had to be omitted even with this reduction. The M-diagrams having an unchanged abscissa-scale show also in this case a decrease of the semi-value width according to $1/\sqrt{n}$. This is the more remarkable since the algebraic averages show an inversed validity of the law of great numbers: the greater is the set (n), the worse estimates of the symmetry point of the distribution are given by the averages.

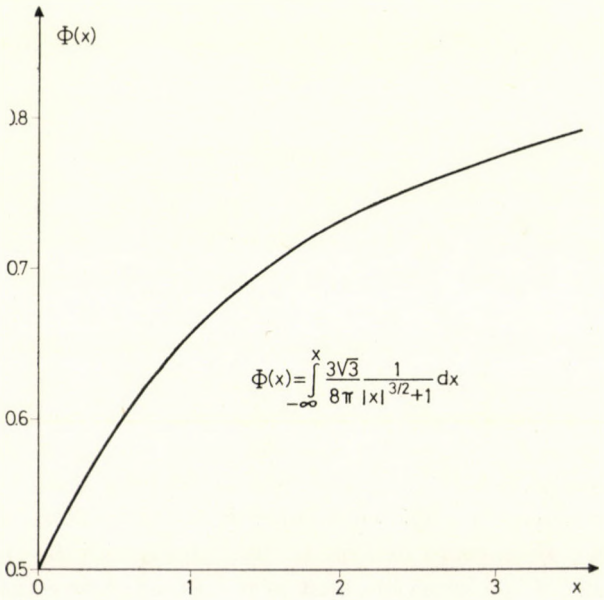

Fig. 8

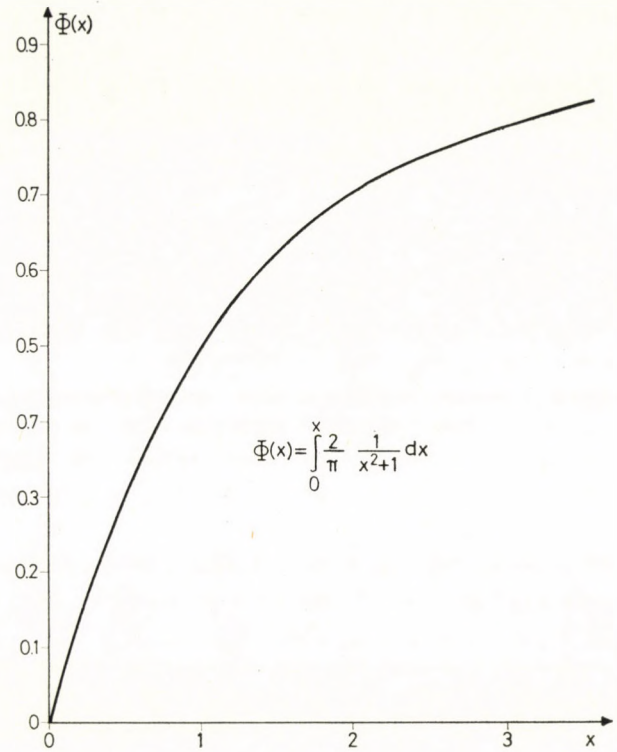

Fig. 9

Equations (7) and (8) are special cases of the distributions having the form:

$$f(x) = \text{const.}\ \frac{1}{|x|}\,\frac{1}{(|x|^m + |x|^{-m})^{1/m}} \tag{11}$$

(the constant is a norming factor which makes the integral of $f(x)$ equal to unit in the interval $(-\infty, \infty)$). The distributions (11) of the values of the random variable ξ and of its reciprocal, i.e. the values $1/\xi$ have the same distribuiton. Equation (7) means the case $m = 1/2$, Eq. 8 is received if $m \to \infty$. (The substitution $m = 1$ yields the well-known Cauchy-distribution.)

It follows from the self-reciprocal property that in Figs 3 and 4, corresponding to Eqs 7 and 8, the interval of the semi-value width is the interval $(-1, +1)$. On both Figs 3 and 4, the semi-value widths of the E-diagrams hardly change if n increases to 10 and then to 100: the law of great numbers is not valid for the averages. The shortening of the interval is, however, apparent in case of the M-diagram of Fig. 4, while in case of the strongly peaked distribution of Fig. 3 the abscissae had to be extended five times in order to illustrate them as the semi-value width decreases extremely rapidly. A similar

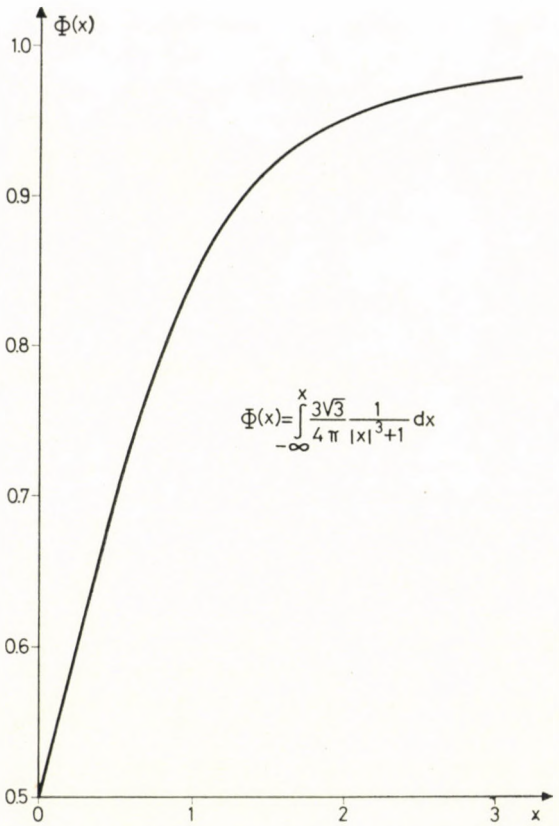

Fig. 10

conclusion can be obtained for the distribution of Eq. 9 which is essentially a Cauchy-distribution defined only for the positive values (compare Fig. 5): the semi-value width of the E-diagram is in case of $n = 100$ approximately equal to that of the original set $(f(x))$, corresponding to $n = 1$, while the semi-value width of the M-diagrams decrease quickly.

As a last example let us consider the Smirnov-distribution (p. 178 in [2]). The curve $f(x)$ of Fig. 6 shows the probability density function corresponding to Eq. 10. As it can be seen from the frequency curves of Fig. 6, the Smirnov-distribution is an asymmetric example of such distributions, where for the averages deduced from the elements the inverse of the law of the great numbers is valid: in case of $n = 10$ the abscissae had to be shortened ten times, in case of $n = 100$, hundred times in order to enable some kind of illustration. The right-hand side end-points of the semi-value widths could not be shown either, the numbers at the dotted line indicate for this case (and for $f(x)$, too) the position of the right hand side endpoint of the semi-value width interval.

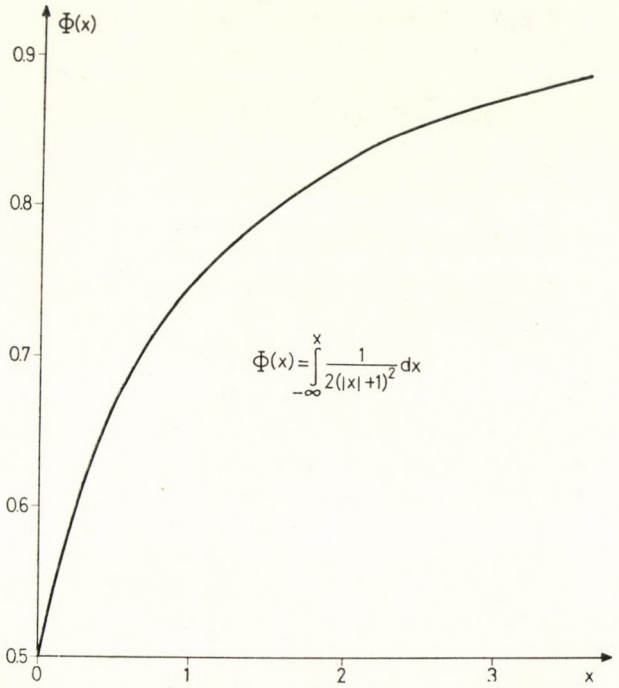
Φ(x)
0.9
0.8
0.7
0.6
0.5
0
1
2
3
x
$\Phi(x)=\int_{-\infty}^{x}\frac{1}{2(|x|+1)^2}dx$

Fig. 11

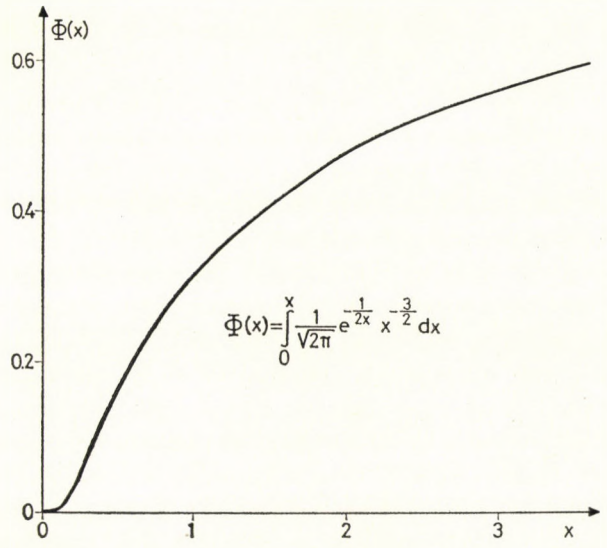
Φ(x)
0.6
0.4
0.2
0
0
1
2
3
x
$\Phi(x)=\int_{0}^{x}\frac{1}{\sqrt{2\pi}}e^{-\frac{1}{2x}}x^{-\frac{3}{2}}dx$

Fig. 12

The M-diagrams have an unchanged scale, and the law of great numbers is here fulfilled: the semi-value widths decrease quickly in case of the Smirnov-distribution, too. These examples strongly support the theoretical considerations presented in Chapter 1 on the general validity of the law of the great numbers, if the most frequent value is chosen as the characteristic quantity of the probability distribution. The fulfilment of this statement is independent from the advantageous or disadvantageous properties of the averages.

3.

The M-diagrams corresponding to $n = 100$ in Figs 1—6 approximate apparently a "regular" shape. It should be investigated therefore, if these frequency curves approximate a normal distribution.

The answer to this question can be looked for using the so-called Gaussian net (390 and following pp. in [3]). To each abscissa the respective cumulative frequency is plotted in percents (i.e. in how much percent of all cases is the value of the random variable less than the abscissa value). The scale on the ordinate corresponds to the inverse function of the standard normal distribution.

If normal distribution can be supposed, the points representing the values of the cumulative frequencies on the Gaussian net lie in the vicinity of a straight line. In Figs 13—18 representing the M-diagrams corresponding to the cases of

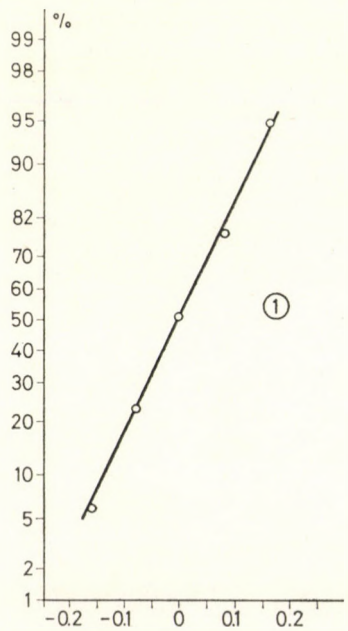

Fig. 13

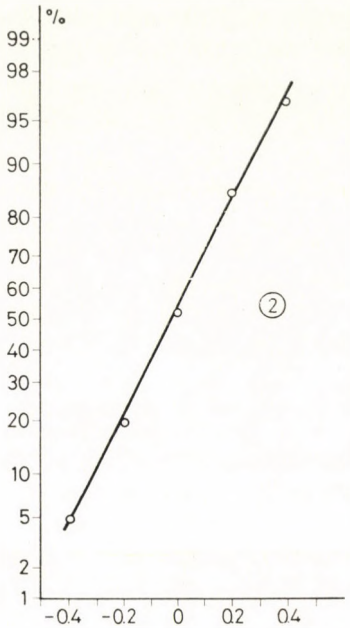
%
99
98
95
90
80
70
60
50
40
30
20
10
5
2
1
-0.4
-0.2
0
0.2
0.4
②

Fig. 14

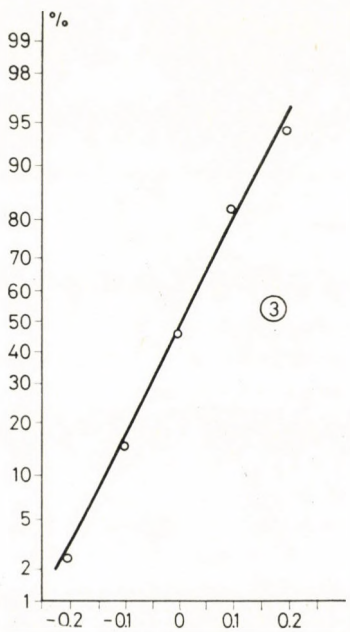
%
99
98
95
90
80
70
60
50
40
30
20
10
5
2
1
-0.2
-0.1
0
0.1
0.2
③

Fig. 15

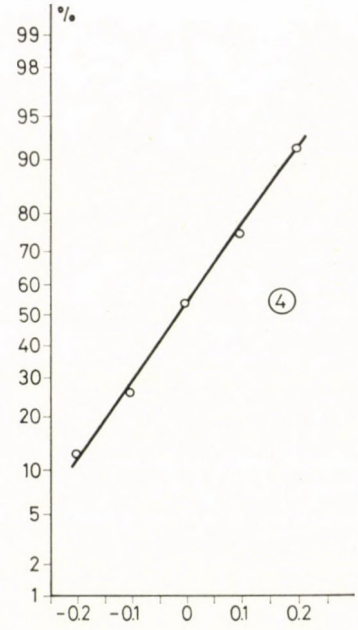
%
99
98
95
90
80
70
60
50
40
30
20
10
5
2
1
-0.2
-0.1
0
0.1
0.2
④

Fig. 16

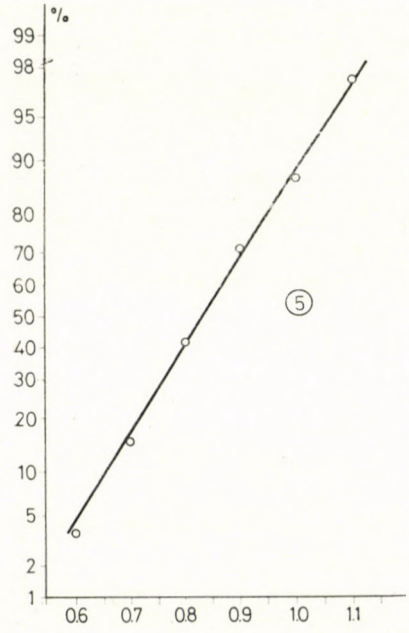
%
99
98
95
90
80
70
60
50
40
30
20
10
5
2
1
0.6
0.7
0.8
0.9
1.0
1.1
⑤

Fig. 17

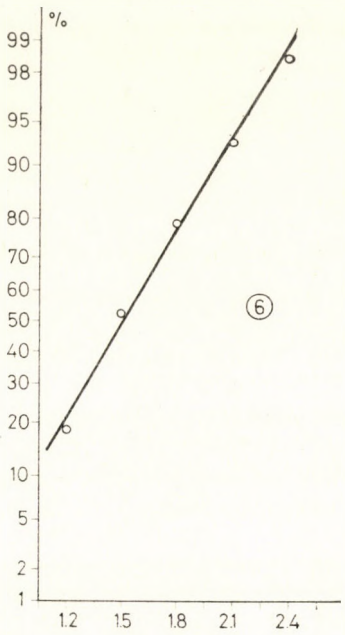

Fig. 18

Figs 1—6 with $n = 100$, the points well approximate a straight line, — consequently the frequency curves approximate the normal distribution. (The numbers in circles on these figures indicate the number of the figure to which they refer.) To obtain numerical values, khi-square tests were carried out; the data do not contradict on a level of significance 97.5% to the zero hypothesis.

The theoretical background of this interesting secondary result is the following. As it has been already shown in [5], the density function $f(x)$ can have any properties, the distribution

$$g(x) \equiv f(x) \cdot s(x) \tag{12a}$$

has in all cases an expected value and a scatter; here

$$s(x) = \frac{\text{const.}}{\varepsilon_0^2 + (M - x)^2} \tag{12b}$$

(for definitions of ε_0 and M see [4]). That means that if x_i follows a distribution $f(x)$, the expressions

$$\frac{\sum_{i=1}^{n} x_i \cdot s(x_i)}{n} \tag{12c}$$

as the averages from a sample with n elements of a distribution $g(x)$ with finite scatter, have to follow a normal distribution, if $n \to \infty$ (in the sense of the central limit theorem). Since the M-values can be computed with the help of the expression

$$\frac{\sum_{i=1}^{n} x_i \cdot s(x_i)}{\sum_{i=1}^{n} s(x_i)} \tag{12d}$$

(in the last step of an iterative program), and the sum $\Sigma s(x_i)$ is proportional to n (with the proportionality factor dependent on the type of the distribution), it follows from the distribution of the expressions in Eq. 12c being near to a normal distribution that the most frequent values have also a normal distribution in case of $n \to \infty$. The graphical method of the control of the normality and the numerical values obtained from the khi-square test are even in knowledge of the theoretical considerations surprising, as they show that already at not very great values of n ($n = 100$) the frequency curve of the M_n-values approximates rather closely the normal distribution.

REFERENCES

1. Csernyák, L.: On the most frequent value and cohesion of probability distributions. *Acta Geod. Geoph. Mont. Hung.*, 8 (1973), 397—402.
2. Gnedenko, B. V.—Kolmogorov, A. N.: Limiting distributions of the sums of independent random variables. Akadémiai Kiadó, Budapest, 1951.
3. Rényi, A.: Probability theory. Tankönyvkiadó, Budapest, 1954.
4. Steiner, F.: Most frequent value and cohesion of probability distributions. *Acta Geod. Geoph., Mont. Hung.*, 8 (1973), 381—396.
5. Steiner, F.: Estimated error of the most frequent value. *Acta Geod. Geoph. Mont. Hung.*, 15 (1980), 79—96.
6. Steiner, F.: Weighted M-adjustment. *A Nehézipari Műszaki Egyetem Idegennyelvű Közleményei*, Series I, Mining (in press).

ВСЕОБЩАЯ ДЕЙСТВИТЕЛЬНОСТЬ ЗАКОНА БОЛЬШИХ ЧИСЕЛ В МЕТОДЕ УРАВНИВАНИЯ ПО СПОСОБУ НАИМЕНЬШИХ ВЕЛИЧИН

Л. ЧЕРНЯК—Б. ХАЯГОШ—Ф. ШТЕЙНЕР

РЕЗЮМЕ

В инженерной практике (на данном техническом уровне и в рамках возможностей) стремятся достичь повышения точности увеличением числа измерений n. Однако, на основании геофизического опыта увеличение числа измерений не всегда сопровождается уменьшением ошибок в ожидаемой степени (по закону $1/\sqrt{n}$). Также нередкий случай в геофизической практике (см., например, кривые встречаемостей в [6]), когда напрасно увеличиваем число измерений все равно данные, уравненные по способу наименьших квадратов или в самом простом случае полученные усреднением, не проявляют нормальное распределение.

Гнеденко и Колмогоров в работе [2] называют «закоренелым предрассудком» то представление, по которому только нормальное распределение можем считать предельным распределением. Из этого сразу следует, что можем спокойно использовать и функции плотности с бесконечными разбросами для аппроксимирования кривых встречаемостей измеренных результатов величин, если использование этих кривых требуется либо принципиально либо формально. (Всеобщеизвестно, что в случаях конечного разброса обязательно получаем нормальное распределение как предельное распределение).

Распределения с бесконечным разбросом могут быть разнообразными. Для некоторых из них не выполняется обычная форма закона больших чисел: доверительные интервалы средних значений вычисленных из n данных не уменьшаются с ростом n. Исследование случаев, рассматриваемых в этой работе, показывает, *что точность наиболее частых величин в каждом случае увеличивается с ростом n*, т. е. и распределение удовлетворяющее обычному формированию закона больших чисел с практической точки зрения оказалось легко используемым, независимо современно от того, что для получения количества информации адэкватной точности уравнивание по математическому ожиданию (метод наименьших квадратов) у этих распределений, конечно, непригодно.

Acta Geodaet., Geophys. et Montanist. Acad. Sci. Hung. Tomus 16 (1), pp. 91–96 (1981)

RECENT RESULTS CONCERNING THE INVESTIGATION OF THE RELATION BETWEEN THE LEVEL OF ATMOSPHERIC RADIO NOISE AND FORBUSH-DECREASE

G. SÁTORI

GEODETIC AND GEOPHYSICAL RESEARCH INSTITUTE
OF THE HUNGARIAN ACADEMY OF SCIENCES, SOPRON

[Manuscript received March 28, 1980]

The effect of Forbush-decrease on the lower ionosphere has been quantitatively studied by means of the theory of VLF electromagnetic wave propagation and of atmospheric radio noise level recorded at 5 kHz in Panska Ves ($\lambda_m = 50.41°$ N, $\varphi_m = 97.59°$ E). The computed and measured effects of Forbush-decrease show a good agreement. The changes of computed attenuation and of atmospheric noise level are more characteristic at 5 kHz, than at 27 kHz.

1. Introduction

It has been shown in two previous papers that during Forbush-decreases the level of atmospheric radio noise decreases, if the shock wave, modulating the galactic cosmic ray particles, misses the Earth, and that it increases in case of geomagnetically active flares [1, 2]. It has been also found that the influence of Forbush-decreases increases gradually with decreasing frequency in the VLF band. The measured effects of Forbush-decreases have been compared with the results of theoretical computations [2]. At 5 kHz the theoretical computations preceded the investigation of atmospheric radio noise level connected with Forbush-decreases.

2. Method of analysis

The interpretation of the effect of Forbush-decreases in the lower ionosphere may be divided into three steps [2]:

a) Computation of ionization caused by galactic cosmic rays.

b) Calculation of electron density from ionization profiles.

c) Attenuation of VLF electromagnetic waves in the Earth-ionosphere waveguide.

At first the influence of the geomagnetic field was not considered in the computation of attenuation. In this study we used an inhomogeneous anisotropic ionosphere model. The calculations were made specially for the cases of

east-west, west-east propagation, as well as for north-south, south-north directions.

The attenuation may be obtained from the following expression [3, 4]:

$$L = -8.686 \cdot k \cdot \operatorname{Im} S_n \text{ [dB/Mm]}$$

where

$$\operatorname{Im} S_n = \alpha \frac{\left\{\frac{1}{2}(2h/a)^{-\frac{1}{2}}\left[(12n-5)\pi/6 - (2ka/3)(2h/a)^{\frac{3}{2}}\right] + 2kh\right\}}{2\left[2k^2 ha + (\alpha^2/4)(2h/a)^{-1}\right]}$$

k is the wave number, h is the height of the Earth-ionosphere waveguide, a is the radius of the Earth, n is the number of modes. α is also a complicated expression, which is the function of the plasma frequency, the effective collision frequency, the gyro frequency and naturally the frequency of the propagating electromagnetic wave. The geomagnetic field affects the propagation by the gyro frequency depending on the direction of propagation of the electromagnetic wave.

3. Results

The attenuation was computed for a given geomagnetic latitude ($\lambda_m = 54.36°$) in case of different directions (north-south, south-north and east-west, west-east) of propagation (Fig. 1). The similarity of the curves *A* (isotropical case) in *A1* (north-south, south-north propagation) indicates that in this case the attenuation of the dominant mode is not appreciably affected by the presence of a magnetic field. The attenuation in case of propagation from east-to-west (curve *A2*) is larger than in case of propagation from west-to-east (curve *A3*) and the influence of the geomagnetic field is more effective, than in

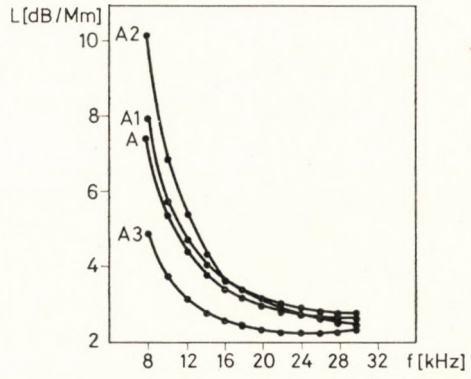

Fig. 1. Attenuation as a function of frequency at 54.36° geomagnetic latitude, in case of undisturbed, isotropical (curve *A)* and anisotropical (curves *A1*, *A2*, *A3*) ionosphere models, computed for the dominant ($n = 1$) mode

the *A1* case. Fig. 2 shows the change of the attenuation due to the influence of Forbush-decrease in different directions of propagation. It can be seen that the change of attenuation in case of the same Forbush-decrease is smallest for east-west propagation (curve $A2_{\Delta}$), altough the absolute value of attenuation is in this case largest (see Fig. 1). Generally, the attenuation decreases with increasing height of the Earth-ionosphere waveguide (Fig. 3).

The attenuation was computed in the 4—30 kHz VLF band for the geomagnetic latitude of Panska Ves for undisturbed condition and in case of Forbush-decreases in January and in July, assuming day-time, south-north waveguide propagation.

According to the theoretical computations the change of the attenuation at 5 kHz is 4—6 dB/Mm in case of a strong Forbush-decrease but no geomagnetic storm at the geomagnetic latitude of Panska Ves (Fig. 4). In case of both Forbush-decrease and geomagnetic storm, the computed attenuation differs only slightly from the undisturbed value. Namely the attenuation depends also on the decrease of the cut-off rigidity at the given geomagnetic latitude.

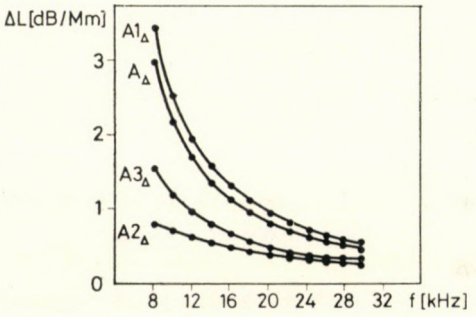

Fig. 2. Change of the attenuation in the dominant ($n = 1$) mode, as a function of frequency, at 54.36° geomagnetic latitude in case of Forbush-decrease, but no geomagnetic storm, determined for isotropical (curve A_{Δ}) and anisotropical (curves $A1_{\Delta}$, $A2_{\Delta}$, $A3_{\Delta}$) ionosphere models

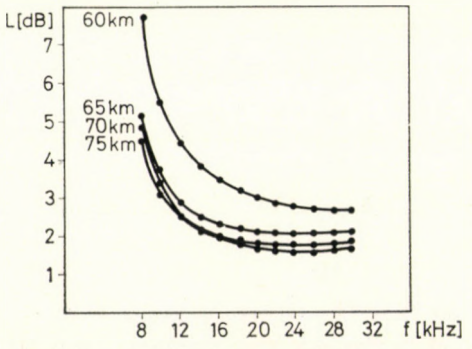

Fig. 3. Attenuation as a function of frequency at 54.36° geomagnetic latitude calculated for an undisturbed, anisotropical (south-north propagation) ionosphere, and different height of the waveguide

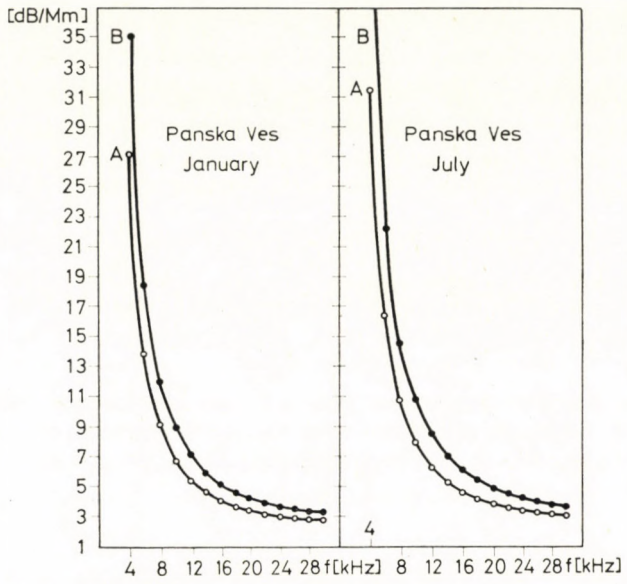

Fig. 4. Attenuation as a function of frequency in the dominant ($n = 1$) mode, in different seasons (January, July) at 50.41° geomagnetic latitude, referring to an undisturbed, anisotropical (south-north propagation) ionosphere model (curve *A*) and to a case of Forbush-decrease, but no geomagnetic storm (curve *B*)

4. The comparison of theoretical results with the level of atmospheric radio noise, measured at 5 kHz

Using the superposed epoch method with the days of occurrence of flares (3B, 2B) as key days, the following results were obtained at 5 kHz measured in Panska Ves.

If the flares were followed only by Forbush-decrease, the level of atmospheric radio noise decreased at 5 kHz, both day (08—12 h) and night (20—24 h), even more, than the simultaneously recorded level at 27 kHz (Fig. 5). (The mean error is ± 0.6—0.8 dB at the different days.) It may be supposed that the source-region of radio noise is situated day-time 1—2 Mm to the south-direction from the receiver site. The fall of the radio noise-level corresponds theoretically to the rise of the attenuation and inversely. Thus, it can be seen that the theoretically determined change of attenuation of VLF electromagnetic waves (4—6 dB/Mm) is in accordance with the measured variation of the atmospheric noise-level (≥ 4 dB).

It must be noted that the electromagnetic waves, producing the night-atmospheric noise-level in Panska Ves, originate from distances of 2—10 Mm and propagate in west and south-west directions depending on the season, partly from the day-side of the Earth. The height of the Earth-ionosphere

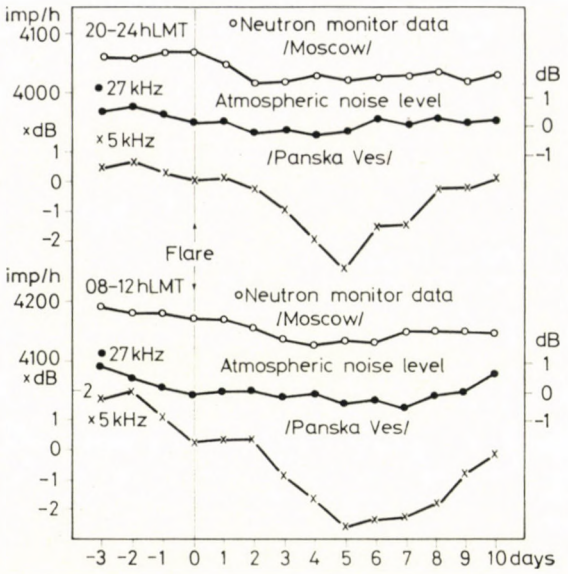

Fig. 5. Four hourly averages of neutron monitor data and that of the deviations from the monthly median of the noise level recorded in Panska Ves, at 27 kHz and 5 kHz before and after flares (Upper part night-time, lower part day-time, number of cases: 11)

waveguide changes during the propagation, therefore the theoretical interpretation becomes fairly complicated.

The reflection height (the height of the Earth-ionosphere waveguide) is lower, therefore the attenuation is larger theoretically too for 5 kHz, than at 27 kHz. Since the influence of Forbush-decrease is more effective below 70 km, the change of attenuation is also larger for 5 kHz, than at the higher frequencies of the VLF band. Consequently, the propagation parameters at the lower frequencies of electromagnetic waves of the VLF band are more sensitive both to geometrical and to physical properties of the Earth-ionosphere waveguide.

REFERENCES

1. SÁTORI, G.: Effect of the cosmic rays in the lower ionosphere as shown by the level of atmospheric radio noise. *Acta Geod. Geoph. Mont. Hung.*, 11 (1976), 229.
2. SÁTORI, G.: Interpretation of simultaneous variations of galactic cosmic rays and of the level of atmospheric radio noise. *Acta Geod. Geoph. Mont. Hung.*, 13 (1978), 475.
3. WAIT, J. R.: Electromagnetic Waves in Stratified Media. Pergamon Press Inc., New York, 1962.
4. SÁTORI, G.: Investigation of the D-region of ionosphere by means of the atmospheric radio noise. Thesis, Roland Eötvös University, Budapest, 1979.

НОВЫЕ РЕЗУЛЬТАТЫ ИССЛЕДОВАНИЯ СВЯЗИ МЕЖДУ ИНТЕНСИВНОСТЬЮ АТМОСФЕРНОГО РАДИОШУМА И ФОРБУШ-ПОНИЖЕНИЯ

Г. ШАТОРИ

РЕЗЮМЕ

Влияние Форбуш-понижения на нижней ионосфере количественно исследовалось при помощи распространения УНЧ электромагнитных волн и атмосферного радиошума, измеренного на частоте 5 кгц в Панска Вес ($\lambda_m = 50{,}41°$ N, $\varphi_m = 97{,}59°$ E). Вычисленные и измеренные эффекты Форбуш-понижения хорошо согласуются. Изменения вычисленного затухания и интенсивности атмосферного радиошума более характерны на 5 кгц, чем на 27 кгц.

Acta Geodaet., Geophys. et Montanist. Acad. Sci. Hung. Tomus 16 (1), pp. 97—113 (1981)

STATISTISCHE ZUSAMMENHÄNGE ZWISCHEN ELEKTRISCHER LEITFÄHIGKEITSVERTEILUNG UND BRUCHTEKTONIK IN TRANSDANUBIEN (WESTUNGARN)

A. ÁDÁM

GEODÄTISCHES UND GEOPHYSIKALISCHES FORSCHUNGSINSTITUT
DER UNGARISCHEN AKADEMIE DER WISSENSCHAFTEN, SOPRON

[Eingegangen am 5. April 1980]

Die Abhandlung geht auf die Verteilung der elektrischen Leitfähigkeit in Bereichen von Bruchzonen ein. Im besonderen wird die Leitfähigkeitsanomalie von Transdanubien behandelt.

Bei den äußerst veränderlichen geologischen und topographischen Verhältnissen werden vom Verfasser vorerst die die verzerrungsfreien Informationen liefernden magnetotellurischen Sondierungskurven (MTS) mit statistischen Methoden untersucht. Er stellt fest, daß die ϱ_{min} Kurven die wahrscheinlicheren Parameter für die gutleitenden Zonen liefern. Aus dieser Eigenschaft, sowie aus dem Zusammenhang der Anisotropie der Leitfähigkeitsverteilung mit der linearen Tektonik des Gebietes wurde die Folgerung gezogen, daß die transdanubische Leitfähigkeits-Anomalie mit den, während dem alpinen Gebirgsbildungs-Zyklus entstandenen Bruchsystemen verbunden ist.

Einleitung

Die tektonische Karte des NW-Teiles von Transdanubien (Abb. 1), sowie die Formations-Karte des Beckenuntergrundes von großer Dichte und großem spezifischen Widerstand (Abb. 2) weisen auf die starke tektonische Gliederung des Gebietes hin. Es können wichtige Lineamente (z. B. Rába-Linie, Balaton-Linie) riftartige Gräben (Mórer-Graben) und mosaikartige Blöcke (»basin and range« Struktur) unterschieden werden.

An Hand des geodynamischen Entwicklungs-Modells des Gebietes, nach STEGENA et al. [10] wurde das Gebiet in der letzten Phase der Entwicklung, im Pliozän einer starken Zug-Belastung ausgesetzt, ein Großteil der Brüche öffnete sich. Aufgrund der Zugspannung entstand im Pliozän und Pleistozän Basalt-Vulkanismus. Die Blockgrenzen sind zum größten Teil heute noch gelockert. In Zusammenhang mit der Tektonik des Gebietes weisen unter anderen Bauxitvorkommen auf die schwachen Zonen hin.

Die Haupt-Bruchrichtungen sind laut BALLA [5] die folgenden:

— Richtung der Alpen-Struktur O-NO
— Richtung der varistiden Brüche N-NW
— Richtung der prävaristiden Brüche O-SO
— Bruchrichtung des Rheines N-NO.

Ein Teil dieser trat im Laufe von mehreren tektonischen Zyklen wieder auf.

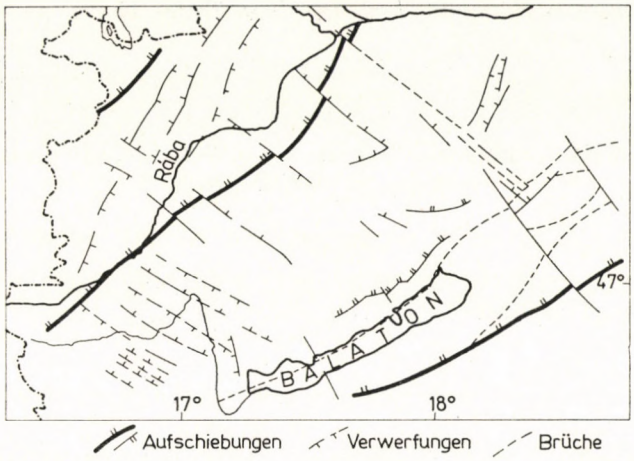

Abb. 1. Tektonische Karte des NW-Teiles von Transdanubien

Von den physikalischen Eigenschaften der Brüche von NW Transdanubien wurde in letzter Zeit die Verteilung der elektrischen Leitfähigkeit eingehend untersucht. Die Anregung hierfür kam teilweise aus der Literatur, welche über eine bedeutende Verstärkung der Leitfähigkeit entlang mehreren erstrangigen tektonischen Linien spricht. Solche Anomalien konnten an beinahe sämtlichen großtektonischen Einheiten beobachtet werden (z. B. die Karpaten-Anomalie, die Anomalie der Tafelgebiete (Bajkal Rift Zone) und des kristallinen Schildes (Kirovograd-Anomalie am Ukrainischen-Schild)). Die elektromagnetische Induktionsforschung in Ungarn konnte auch eine von den Längsbrüchen des Karpaten-Beckens herrührende regionale magnetotellurische Anisotropie feststellen [2]. Dies weist auf eine allgemeine Anwendbarkeit der Anisotropie-Untersuchungen auch in der spreading-Forschung zur Bestimmung der Plattenränder und transform-faults hin [9].

Über die Blockgrenzen (»schwachen Zonen«) schreibt Olszak [8]: »Eine Zone relativ hoher seismischer, magnetischer (basischer) und geothermischer Aktivität, die von tiefen Störungszonen begleitet und begrenzt wird, und in der sich intensivere vertikale Krustenbewegungen abspielen«. Diese Feststellung muß also damit ergänzt werden, daß die Bruchzonen auch durch eine große elektrische Leitfähigkeit charakterisiert werden können. Die Ursache ist einerseits im oberen Krustenbereich mit Elektrolyt-haltigem, zerklüftetem oder mit erzführendem, graphithaltigem Gestein zu suchen. Andererseits steht in den tieferen Krustenteilen das Erscheinen der Leitfähigkeitsanomalie mit der geothermischen Anomalie, u. zw. mit dem konvektiven Wärmefluß in Zusammenhang (ev. Schmelzung).

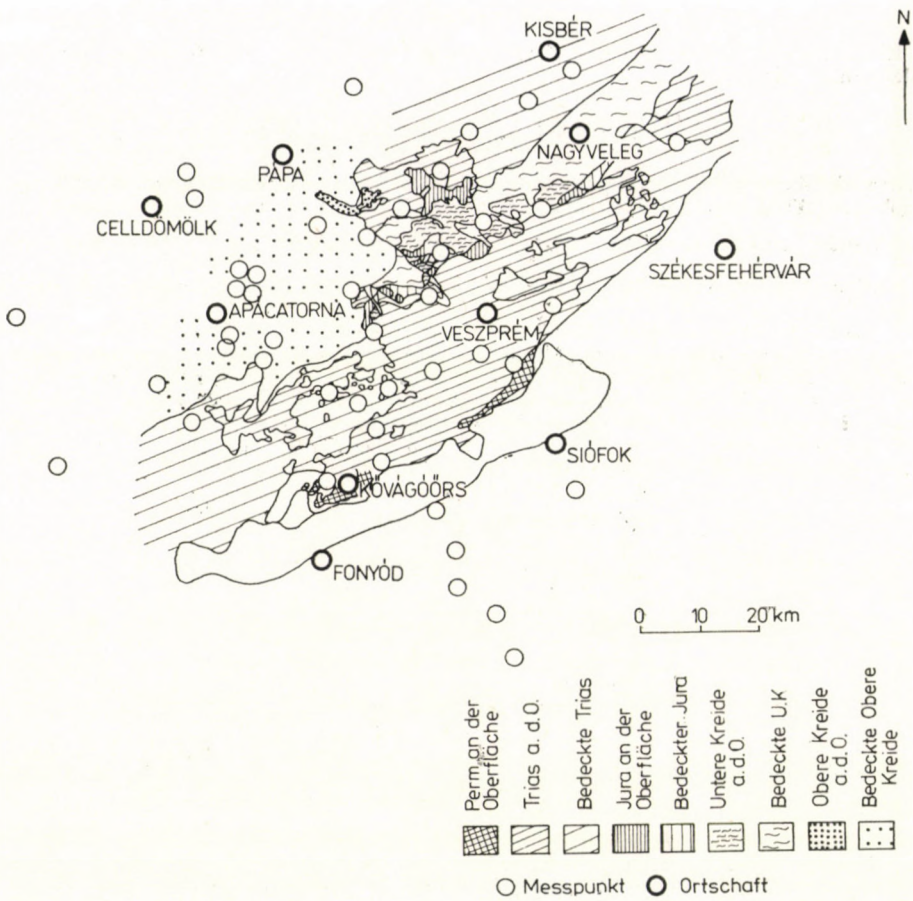

Abb. 2. Formationskarte des Beckenuntergrundes des geoelektrischen Anomalie-Gebietes

2. Forschungsmethoden

Zur Zeit wird die räumliche Verteilung der elektrischen spezifischen Leitfähigkeit (σ) bzw. des Widerstandes (ϱ) in der Erdkruste und im oberen Erdmantel, d.h. bis zu großen Tiefen am häufigsten mit magnetotellurischer (MTS) bzw. geomagnetischer Sondierung (GDS) untersucht. (Siehe in zahlreichen monographischen Arbeiten, z.B. [1].) Die Grundlage beider elektromagnetischer Induktionsmethoden ist der »Skin-Effekt«, wonach die Eindringungstiefe des elektromagnetischen Feldes in einem Medium von dessen spezifischem Widerstand und von der Periode der Feldänderung abhängt:

$$p^{[\mathrm{km}]} = \frac{1}{2\pi} \sqrt{10\, \varrho^{[\Omega\ \mathrm{m}]}\, T^{[s]}}. \tag{1}$$

So erhalten wir bis zur obigen Tiefe (p) Informationen über die ϱ-Verteilung bei einer elektromagnetischen Variation von Periode T. Das natürliche elektromagnetische Feld der Erde liefert in weiten Spektren die Feldänderungen zu diesen Untersuchungen.

Bei der magnetotellurischen Sondierung werden von dem Zusammenhang zwischen den geomagnetischen (H) und tellurischen Feldänderungen (E)

$$E = \{Z\} H \tag{2}$$

die Elemente des Impedanztensors Z und von diesen die extremen Werte des spezifischen Widerstandes berechnet:

$$\varrho(T)_{\substack{\max \\ \min}} = 0.2\, T \left(\frac{E}{H}\right)^2 = 0.2\, T\, Z_{xy\substack{\max \\ \min}}(T). \tag{3}$$

Werden die Werte ϱ im Koordinatensystem $\varrho - \sqrt{T}$ dargestellt, erhalten wir die MT Sondierungskurve (MTS). Das Polardiagram $Z_{xy}(\alpha)$ gibt die Richtung der Extremwerte des spezifischen Widerstandes, und der Koeffizient der horizontalen Anisotropie $\left(\lambda = \frac{\varrho_{\max}}{\varrho_{\min}}\right)$ kann auch berechnet werden. Die Tiefenänderung der Anisotropie kann auch in Funktion der Periode ermittelt werden.

Im Falle eines horizontal geschichteten Halbraumes hat der spezifische Widerstand keine Anisotropie. Bei zweidimensionalen, d. h. bei ausgedehnten zylindrischen Strukturen zeigen die Richtungen der Extremwerte von ϱ in Streich-, bzw. Fall-Richtung. Wird zur Berechnung von ϱ die mit der Streichrichtung parallele tellurische Komponente (E) angewendet, so handelt es sich um eine Polarisation E. Die den beiden Polarisationen entsprechenden Sondierungskurven geben spezielle Informationen, falls die in Abb. 3 dargestellte mit Ablagerungen bedeckte Beckensohle großen Widerstandes zweidimensionale Änderungen aufweist.

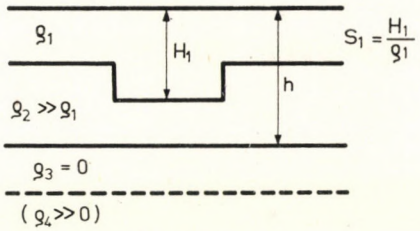

Abb. 3. Schichtenmodell mit veränderlicher Tiefe des hochohmigen Untergrundes zur Erklärung des S-Effektes

Die Kurve von Polarisation E charakterisiert die Parameter des gutleitenden Grundes ($\varrho_3 = 0$) (ev. Schicht) wesentlich genauer, als die der H-Polarisation. Die letztere gibt aber die horizontale Leitfähigkeit der obersten Schicht (z.B. der Ablagerung) $\left(S_1 = \frac{H_1}{\varrho_1}\right)$ meistens mit einer kleineren Verzerrung an, als die Sondierungskurve von Polarisation E. Die Sondierungskurve von Polarisation H verzerrt die Tiefe des gutleitenden Grundes (h) in Abhängigkeit von S_1 [6]. Werden also die von den Sondierungskurven von Polarisation H berechneten h-Werte in Funktion der horizontalen Leitfähigkeit der obersten Schicht (S_1) dargestellt, so erhalten wir irgendeinen linearen Zusammenhang. Dies ist mit der Feldverzerrung verbunden, und drückt keinen tatsächlichen geologischen Zusammenhang aus. Diese Verzerrung wird S-Effekt genannt.

Die charakteristischen, mit der Achse T einen Winkel von $\pm$ 63.5° einschließenden Asymptoten der MTS Kurven, die sog. S- und h-Linien können zur Bestimmung der horizontalen Leitfähigkeit der gutleitenden Schicht (S), bzw. der Tiefe (h) unmittelbar angewendet werden.

Die am häufigsten angewendete Methode der geomagnetischen Sondierung ist mit dem Namen eines deutschen Wissenschaftlers, WIESE verbunden. Der nach ihm benannte Wiese-Induktions-Pfeil, oder »Vektor« kann aus der Übertragungsfunktion $C_Z(T)$ des Zusammenhanges

$$Z(T) = C_Z(T)\, H_n(T) \tag{4}$$

mit einer einfachen graphischen Methode bestimmt werden. Der Wiese-Pfeil weist in Richtung der Formationen größeren Widerstandes hin (im Gegensatz zu dem, von einem ähnlichen Zusammenhang abgeleiteten sog. Parkinson-Vektor).

Die obigen Ausführungen sollen keine vollständige methodische Einleitung geben, sondern nur zum besseren Verständnis der Meßergebnisse beitragen.

3. Die Verzerrungen der magnetotellurischen Sondierungskurven und die Auswahl der Sondierungskurven der E-Polarisation

Die Mächtigkeit des oberflächennahen Sedimentes beträgt in Transdanubien und am Rande des Ungarischen Mittelgebirges von einigen *m* bis einige km (Abb. 4). Dementsprechend ist die Verzerrung der MTS Kurven groß (*S*-Effekt). BERDICHEVSKY und DMITRIEV [6] bewiesen für den gutleitenden Grund analytisch, TÁTRALLYAY gab aber [11] für selbständige, zweidimensionale gutleitende Körper mit paralleler Streichrichtung zur Beckensohle (z. B. Bruchzone) mit numerischen Berechnungen Beweise, daß die Sondierungskurven der Polarisation *E* die richtigen Parameter der gutleitenden Formation (Grund, Schicht, zweidimensionaler Körper) liefern. Im Falle von schmalen Zonen hat die ϱ_{min}-Kurve immer den Charakter der *E*-Polarisation. Die in den Bruchzonen vorhandenen gutleitenden Formationen erscheinen in den MT Sondierungen auch als Schichten, falls die Dichte der Bruchzonen in Verhältnis zur Eindringungstiefe des elektromagnetischen Feldes groß ist (Abb. 5).

Die Auswahl der Sondierungskurven der Polarisation *E* erfolgt in Kenntnis der Streichrichtung der Beckensohle. Obwohl die regionale Streichrichtung

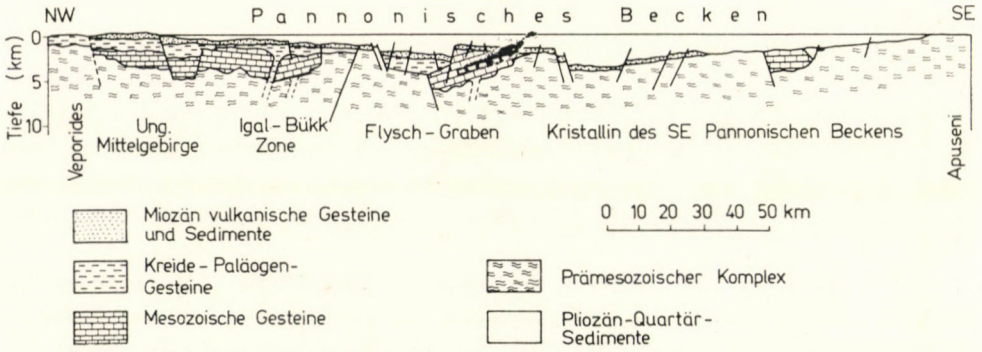

Abb. 4. Schematisches geologisches Profil des Pannonischen Beckens nach WEIN [13]. Es wurde vereinfacht von BOCCALETTI *et al.* [7]

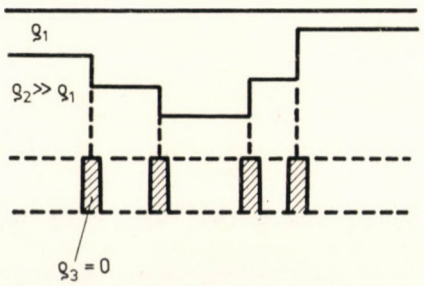

Abb. 5. Dicht nebeneinander liegende und mit gutleitendem Material erfüllte Bruchzonen

der geologischen Formationen in Transdanubien bekannt ist, kann die Streichrichtung der kleinen Teilbecken unter den Meßpunkten bedeutendere Abweichungen aufweisen (z. B. im Bakony Gebirge). Die Bestimmung der, der Streichrichtung entsprechenden Sondierungskurve erfordert daher eine nähere geologische Erkundung des Meßgebietes. Im Falle von gutleitenden Körpern (z. B. Bruchzonen) ist es auch fraglich, ob ihre Streichrichtung mit der des Beckengrundes übereinstimmt, und ob man diese als zweidimensionale betrachten kann. Es sei auch bemerkt, daß die sog. »epizentralen« Sondierungskurven bei den gutleitenden Körpern die richtige Tiefe angeben.

Die unmittelbare Lösung der Auswahl der Polarisation schien unmöglich zu sein. Aufgrund der Verzerrungstheorie des *S*-Effektes wurde eine indirekte statistische Lösung gesucht. Als Kriterium der Unterscheidung der Sondierungskurven von *E*- und *H*-Polarisation wurde der Zusammenhang zwischen den, von den Sondierungskurven abgeleiteten Parametern der gutleitenden Formationen (z. B. Tiefe, horizontale Leitfähigkeit) und den Parametern der, die Verzerrung verursachenden oberflächennahen Sedimenten betrachtet (z. B. S_1). Die Daten der Sondierungskurve der Polarisation *E* sind, wie bereits erwähnt, davon unabhängig.

Die folgenden statistischen Zusammenhänge beweisen eindeutig, daß die $\varrho_{\min}$ Kurven der Polarisation *E* entsprechen:

Die abnehmenden Äste der $\varrho_{\min}$ Kurven, die aus einem Meßprofil über das nördliche Vorgebiet des Bakonys, die mezozoischen Oberflächen-Karbonate des Bakonys und das Balaton-Gebiet gewonnen wurden, bilden mit den sog. »h« Tiefenlinien des $\varrho(\sqrt{T})$ Diagrammes ein annähernd paralleles und enges Bündel. Die Lage des abnehmenden Astes der $\varrho_{\max}$ Kurven ist aber von den Widerstandsverhältnissen der obersten Strukturen abhängig (Siehe Abb. 6 und 7).

Die aus den $\varrho_{\max}$ Kurven bestimmten Tiefenwerte der gutleitenden »Schicht« ($h\varrho_{\max}$) zeigen den verschiedenen geologischen Formationen entsprechende Häufigkeits-Spitzen. Im Falle der $\varrho_{\min}$ Kurven konnte dies nicht beobachtet werden (Siehe Abb. 8 und 9).

Die Werte $\varrho_{\max}$ zeigen mit der horizontalen Leitfähigkeit der Oberflächenschicht (S_1) folgenden, auf der Verzerrungstheorie beruhenden linearen Zusammenhang (Abb. 10):

$$h_{\varrho_{\max}}^{[\mathrm{km}]} = -0{,}04\, S_{1\varrho_{\max}}^{[\Omega^{-1}]} + 28{,}3\,. \tag{5}$$

Demgegenüber ist die Abhängigkeit der $h_{\varrho_{\min}}$ Werte von S_1 bedeutend kleiner (Abb. 11):

$$h_{\varrho_{\min}} = -8{,}6 \cdot 10^{-4} S_{1\varrho_{\min}} + 9{,}1\,. \tag{6}$$

Aufgrund der Gl. (5) und (6) sollte zwischen den aus den $\varrho_{\min}$ und $\varrho_{\max}$ Kurven berechneten Tiefenwerten ein Zusammenhang bestehen. Die Verbindung ist

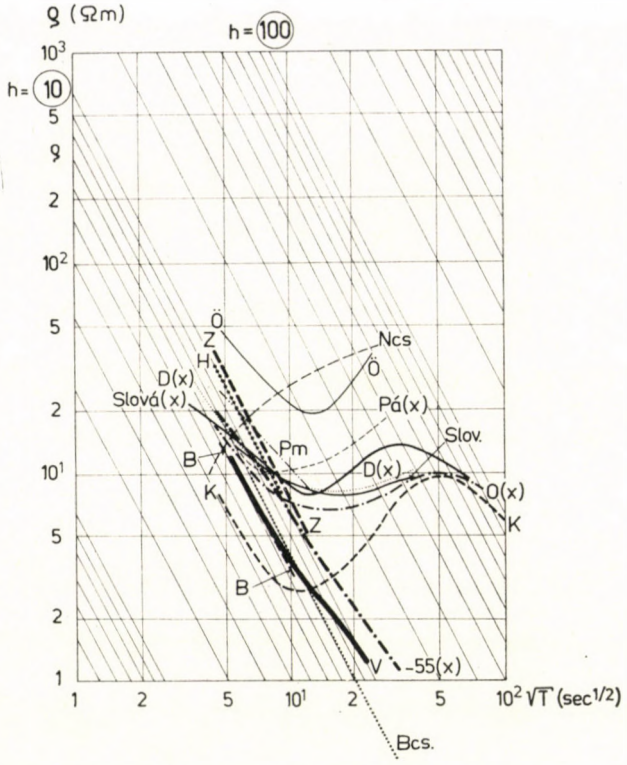

Abb. 6. $\varrho_{\min}$ Kurven aus dem Gebiet der Transdanubischen Leitfähigkeitsanomalie

durch die Regressions-Geraden der Abb. 12 bzw. deren Gleichungen gegeben, wonach $h_{\varrho_{\max}}$ nur in geringem Maße in die Berechnung von $h_{\varrho_{\min}}$ eingeht; z. B. im Falle von $S_1 = 0-20\ \Omega^{-1}$

$$h_{\varrho_{\min}} = 0{,}04\ h_{\varrho_{\max}} + 7{,}8\ . \tag{7}$$

Auch die Verteilung der horizontalen Leitfähigkeit der gutleitenden »Schicht« zeigt charakteristische Eigenschaften im Falle der Kurve $\varrho_{\min}$ bzw. $\varrho_{\max}$ in Abhängigkeit von der Tiefe. Während die von den $\varrho_{\min}$ Kurven berechneten $S_{\max}$ Werte ausgeprägte Maxima in beiden wichtigeren Tiefenbereichen haben, vermindern sich die von der Kurve $\varrho_{\max}$ berechneten Werte $S_{\min}$ mit der Tiefe exponentiell. In Abb. 13 wurden die S-Maxima mit der Wahrscheinlichkeits-Verteilungsfunktion der Form $S = a\, e^{-\frac{1}{2}Ah^2}$ angenähert. Laut Abb. 14 nimmt im Falle der Kurven $\varrho_{\max}$ der Zusammenhang $S(h)$ die folgende Form an:

$$S_{\min}^{[\Omega^{-1}]} = 914{,}8\ e^{-0{,}02h}\ .$$

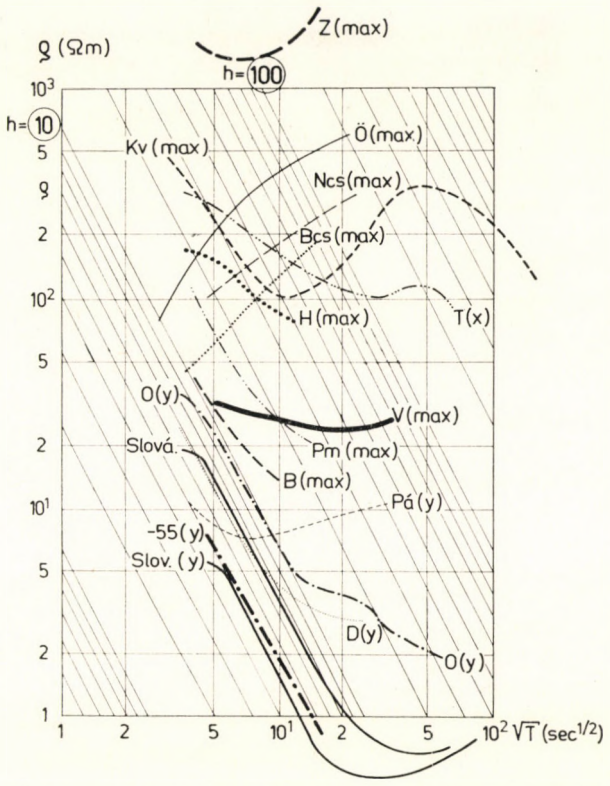

Abb. 7. ϱ_{max} Kurven aus dem Gebiet der Transdanubischen Leitfähigkeitsanomalie

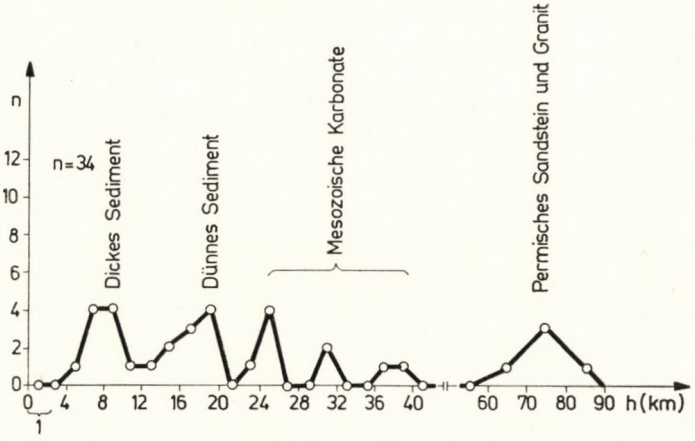

Abb. 8. Häufigkeitsverteilung der aus den ϱ_{max} Kurven bestimmten Tiefenwerte ($h_{\varrho_{max}}$) der gutleitenden Schicht

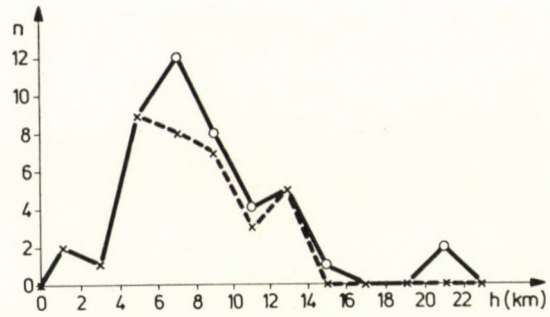

Abb. 9. Häufigkeitsverteilung der aus den ϱ_{min} Kurven bestimmten Tiefenwerte ($h_{\varrho_{min}}$) der gutleitenden Schicht

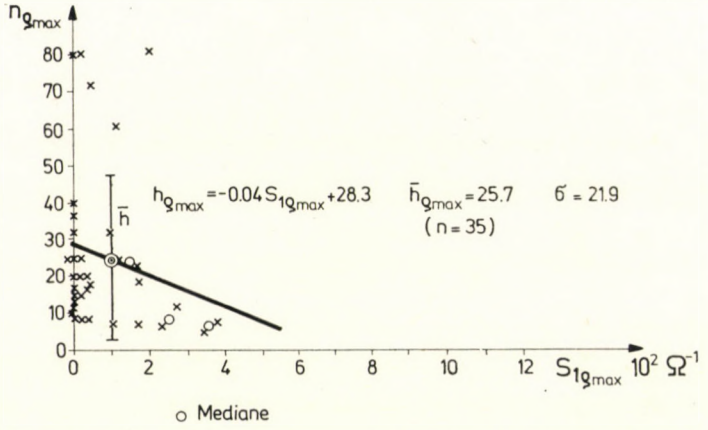

Abb. 10. Zusammenhang zwischen den $h_{\varrho_{max}}$ Werten und der horizontalen Leitfähigkeit (S_1) des oberflächlichen Sedimentes

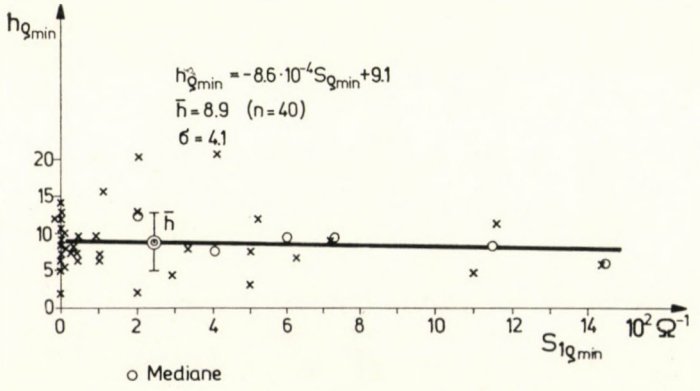

Abb. 11. Zusammenhang zwischen den $h_{\varrho_{min}}$ Werten und der horizontalen Leitfähigkeit (S_1) des oberflächlichen Sedimentes

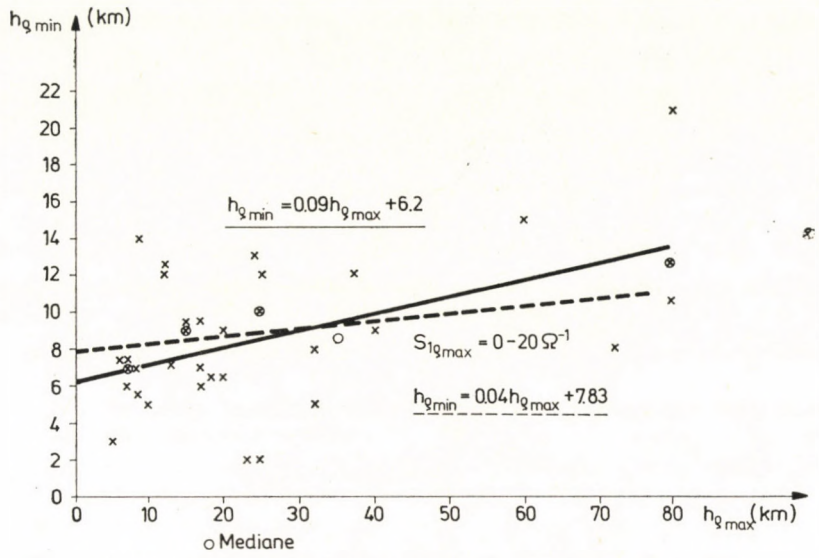

Abb. 12. Zusammenhang zwischen $h_{\varrho_{\min}}$ und $h_{\varrho_{\max}}$ Werten

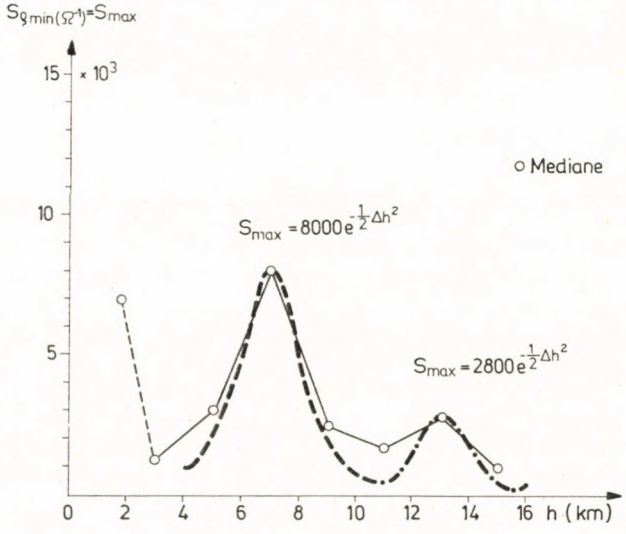

Abb. 13. Die Verteilung der aufgrund der $\varrho_{\min}$ Kurven bestimmten horizontalen Leitfähigkeit $S_{\max}$ in Abhängigkeit von der Tiefe $h_{\varrho_{\min}}$

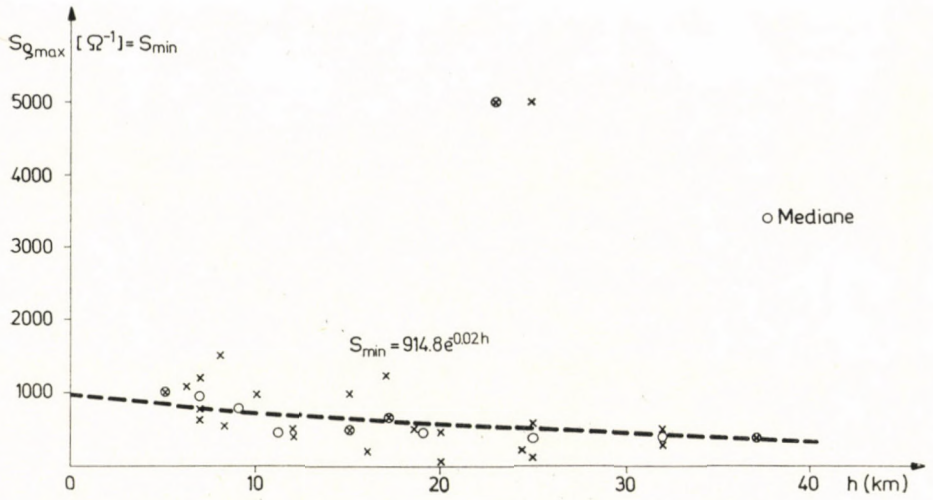

Abb. 14. Die Verteilung der aufgrund der ϱ_{max} Kurven bestimmten horizontalen Leitfähigkeit S_{min} in Abhängigkeit von der Tiefe $h_{\varrho max}$

4. Die Wirkung der Bruchtektonik auf die Leitfähigkeitsverteilung

Das unterschiedliche Verhalten der ϱ_{max} und ϱ_{min} Kurven beweist — unserer Meinung nach —, daß

1. die gutleitenden Zonen an die linearen Bruchzonen gebunden sind, deren Streichen die Richtung der ϱ_{min} bestimmt,

2. die gutleitenden Formationen jenen Brüchen angehören, welche in der Ausgestaltung der Beckenstruktur eine bedeutende Rolle spielen, d. h. von diesen Brüchen werden auch die Blöcke begrenzt.

Nur wenn dies gilt, repräsentieren die ϱ_{min} Kurven in statistisch überwiegender Mehrzahl die *E*-Polarisation, d. h. wenn die Streichlinien der Brüche, sowie Blöcke und der Becken parallel sind.

Zur weiteren Untersuchung dieser linearen Tektonik kann eine Variante der elektrischen Anisotropie als charakteristische Größe gewählt werden, nämlich der aufgrund der Kurven ϱ_{min} und ϱ_{max} berechnete Quotient der horizontalen Leitfähigkeit (S) der gutleitenden Formation ($:S_{max}/S_{min}$ Wert = S-Anisotropie).

Abb. 15 zeigt unsere S_{max} [$10^3\ \Omega^{-1}$] Karte. In Abb. 16 ist die Karte der Werte S_{max}/S_{min} und der Richtung der Impedanz Z_{xymax} dargestellt. Aus dem Vergleich der beiden Karten kann festgestellt werden — siehe die unterstrichenen Werte —, daß im Zweidrittel der Fälle die größten S_{max} Werte mit den größten S-Anisotropie-Werten verbunden sind.

Die Gültigkeit dieses Zusammenhanges wurde auch an der gesamten Datenmenge untersucht. Die S-Werte wurden als Funktion der S-Anisotropie

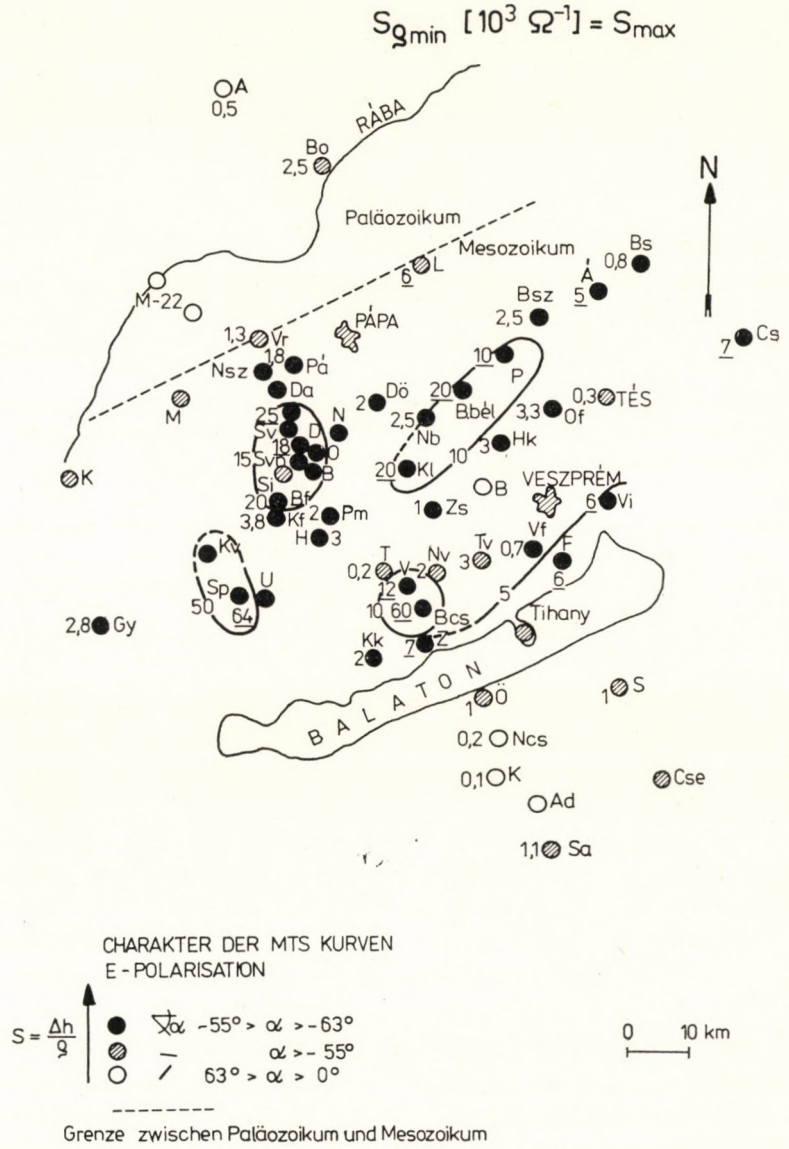

Abb. 15. Die Verteilung der S ($10^3\Omega^{-1}$) Werte auf dem Gebiet der Anomalie

in Abb. 17 dargestellt und durch eine Regressions-Gerade angenähert. (Für kleinere S-Anisotropie-Werte wurde eine etwas abweichende Beziehung gefunden. Die Abweichung der beiden Regressions-Geraden kann durch die große Streuung der größeren S-Anisotropie-Werte erklärt werden.)

Die Größe der horizontalen Leitfähigkeit in Streichrichtung S_{max} hängt also im wesentlichen vom Charakter der linearen Tektonik ab.

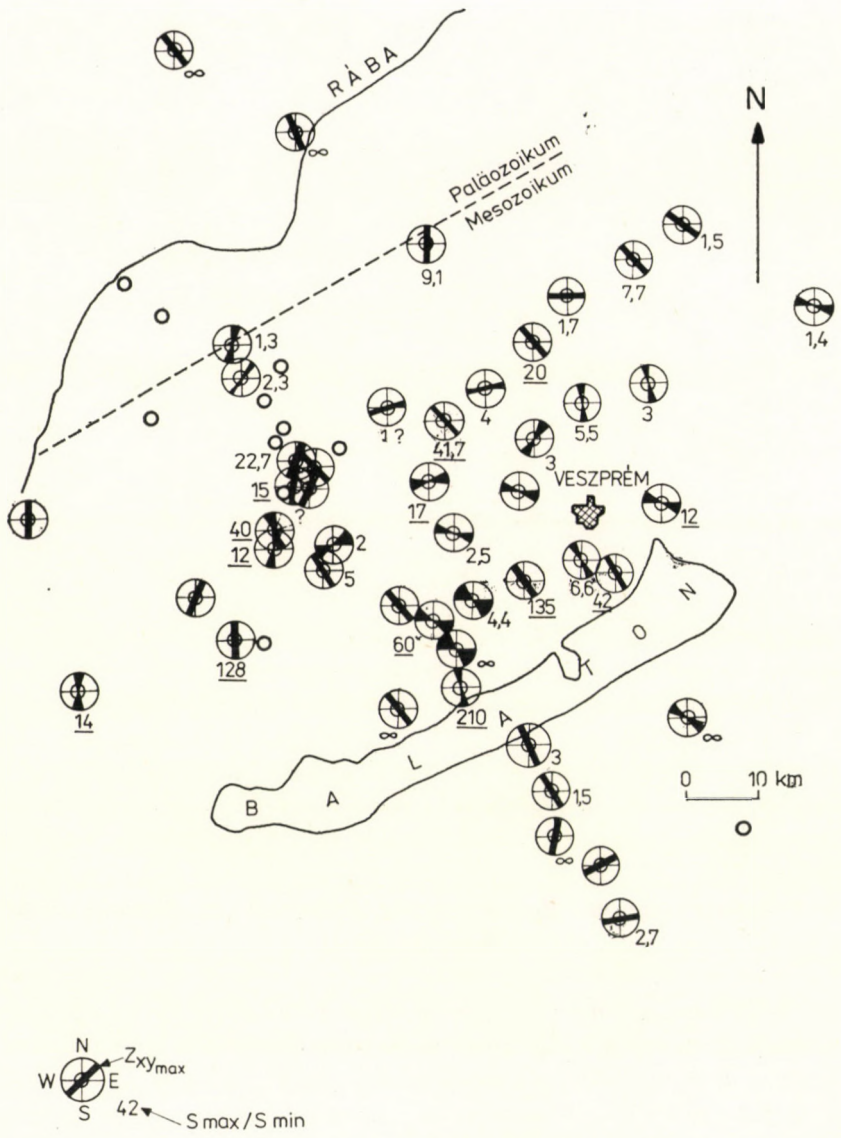

Abb. 16. Karte der Richtungen von Z_{xymax} Impedanz mit den S_{max}/S_{min} Anisotropie-Werten

Die gemeinsame Karte der Richtung der Impedanz Z_{xymax} und der S-Anisotropie geben Möglichkeit zur Untersuchung, in welchen Z_{xymax} Richtungen die maximale S-Anisotropie der gutleitenden Zone erscheint. Es kann festgestellt werden, daß bei 70% der unterstrichenen $S_{max}/S_{min} > 10$ Werte die Richtung von Z_{xymax} zwischen N und NW Richtung, d. h. rechtwinkelig zu den Längsbrüchen des Pannonischen Beckens liegt (siehe bei BALLA [5] die Rich-

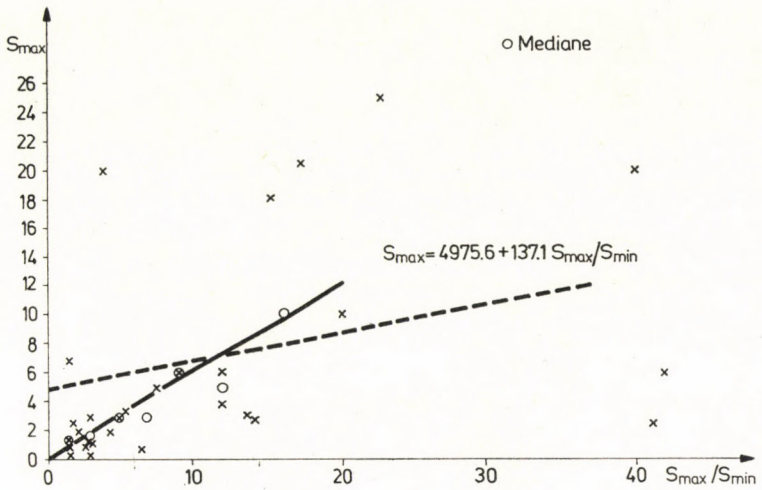

Abb. 17. Zusammenhang zwischen S_{max}/S_{min} Anisotropie-Werten und S_{max}-Werten

tung der Alpen-Struktur). Die gutleitende Formation ist also in diesen Brüchen stark ausgeprägt. Dies steht in Einklang mit der für das Pannonische Becken abgeleiteten regionalen magnetotellurischen Anisotropie [2].

Der Zusammenhang zwischen transdanubischer Leitfähigkeitsanomalie und der Tektonik wird auch durch den festgestellten Zusammenhang zwischen der Seismizität der Bruchzonen und den Tiefen der gutleitenden Zonen unterstrichen. Mit diesem Problemkreis befaßten wir uns in einer eigenen Studie [4].

5. Geographische und geologische Lage der Leitfähigkeitsanomalie in Transdanubien

Es folgt zwar aus der »regionalen magnetotellurischen Anisotropie«, daß die Tektonik des ganzen Pannonischen Beckens durch eine eigenartige elektrische Leitfähigkeitsverteilung charakterisiert wird; im NW-Teil von Transdanubien, hauptsächlich im Gebiete des Bakony Gebirges, wurde eine wesentliche Verstärkung dieses Effektes festgestellt. Der Grund hierfür scheint — wie bereits erwähnt — in geologischen, geochemischen und auch in geothermischen Faktoren zu liegen. Abb. 18 zeigt deutlich die NW-Grenze der Anomalie an der Grenze der mesozoischen und paläozoischen Beckensohle. Am N-Rand des Balatons liegt die Grenze der Anomalie ebenfalls beim Ausbiß der paläozoischen Formation. In NW kann die Auskeilung mit der tektonischen Hauptlinie des Flusses Rába in Zusammenhang gebracht werden.

In Abb. 18 sind außer den Meßpunkten noch die aufgrund der ϱ_{min} Kurven berechneten Tiefenwerte zu sehen. Die Isolinie von 10 km teilt das Gebiet

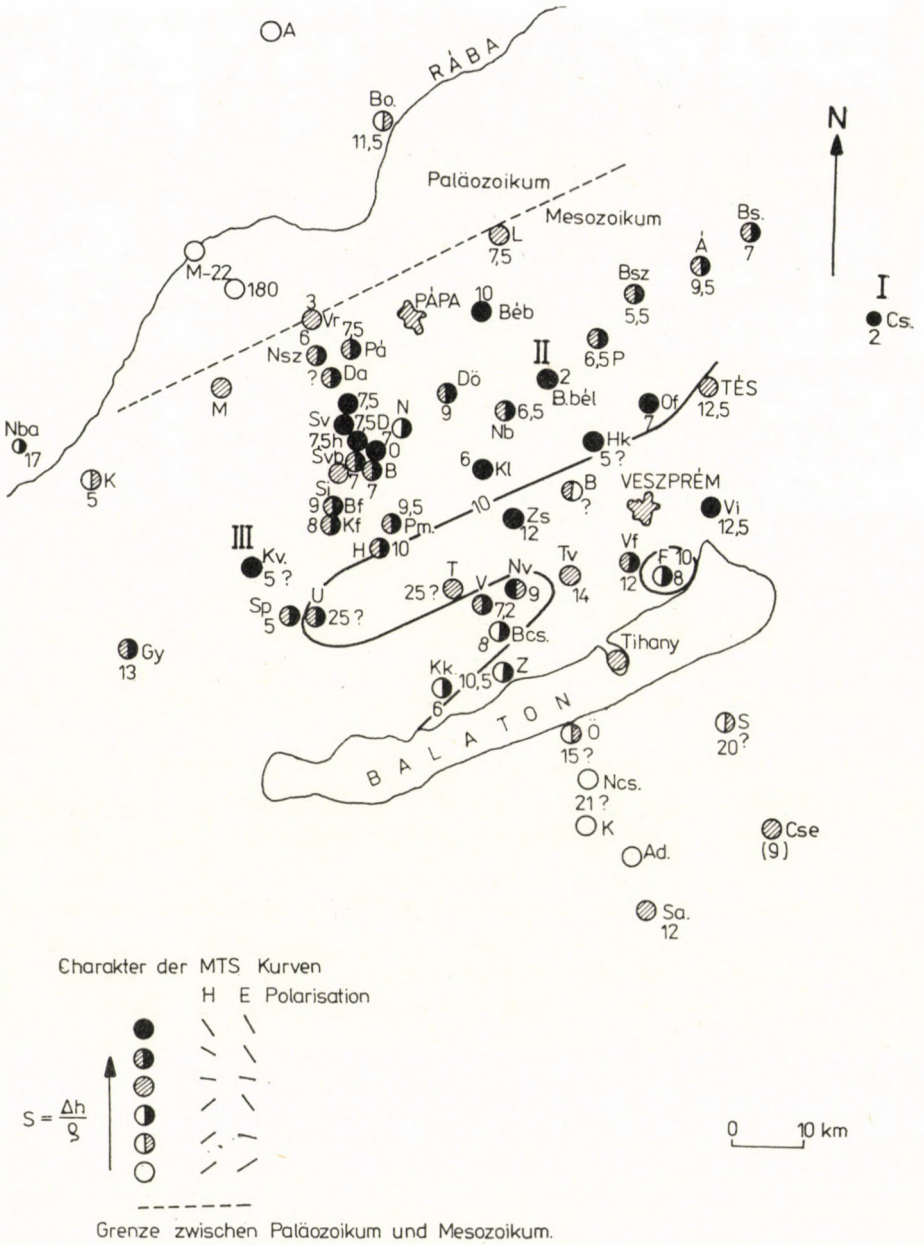

Abb. 18. Tiefenstruktur der gutleitenden »Schicht«

grob in einen NW- bzw. SO-Teil. Man kann etwa dieselben Anomaliestreifen in der Karte der Wiese-schen Induktions-Pfeile beobachten, die aus Variationen mit $T > 20$ sec bestimmt wurden [4, 12] (Abb. 19). Verzerrt die S-Wirkung

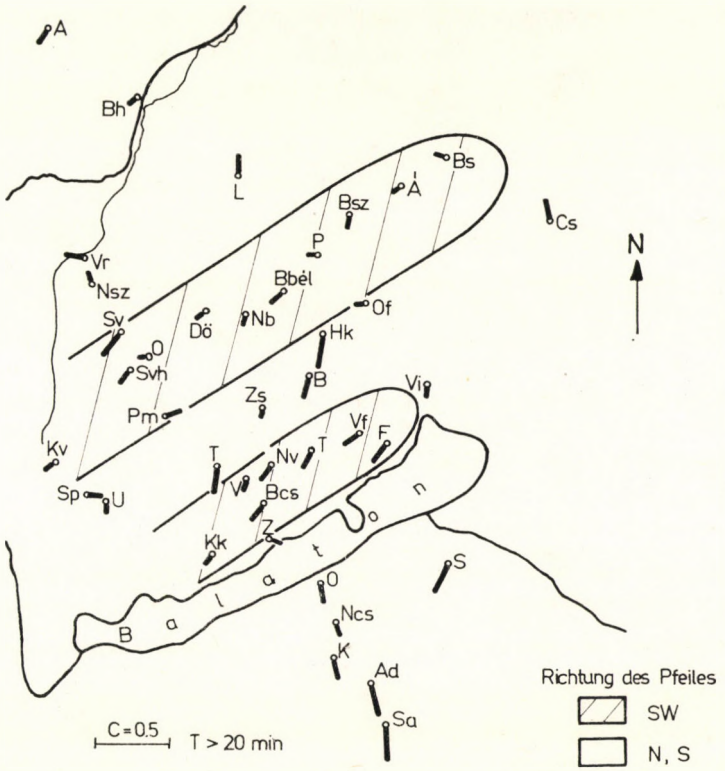

Abb. 19. Induktionspfeile nach Wiese auf dem Anomalie-Gebiet bestimmt von den Variationen mit der Periode von $T \geq 20$ Min

sogar die aus den ϱ_{min} Werten berechneten Tiefen (siehe Zusammenhang 6), so muß aufgrund der gemeinsamen Interpretation der MT Sondierung und der GDS trotzdem eine Vertiefung von einigen km im SO-Teil der Anomalie angenommen werden. Die Ursache dieser Erscheinung wird im späteren näher untersucht.

6. Schlußfolgerung

In den offenen Brüchen von Transdanubien ist in einer Tiefe von einigen km eine bedeutende Zunahme der Leitfähigkeit feststellbar, wie dies auch durch die statistische Aufarbeitung der elektromagnetischen Sondierungen bewiesen wurde. Das Auftreten der Leitfähigkeitsanomalie ist mit dem Vorkommen von mesozoischen Oberflächen-Karbonaten (Trias Kalkstein, Hauptdolomit) verbunden, sie entsteht aber nicht in diesen, sondern darunter, vermutlich in den paläozoischen Schichten. Zur Zeit sind bezüglich der Materie der gutleitenden Zone nur Annahmen möglich. Es gibt zweierlei Vorstellungen: Die Leiter sind

Graphit-Flöze, oder es liegt eine Anreicherung von Elektrolyten vor. Diese Teilfragen erfordern weitere Untersuchungen (Bohrungen).

Die Folgerung aus den besprochenen Ergebnissen ist, daß für die Beschreibung und Charakterisierung der tektonischen Linien eine Prüfung der elektrischen Eigenschaften von großem Vorteil ist.

SCHRIFTTUM

1. Ádám, A. (Ed.): Geoelectric and Geothermal Studies. Akadémiai Kiadó, Budapest, 1976
2. Ádám, A.: Appearance of the electrical inhomogeneity and anisotropy in the results of the complex electrical exploration of the Carpathian Basin. *Acta Geod. Geoph. Mont. Hung.*, 4 (1969), 187—197.
3. Ádám, A.: Distribution of the electrical conductivity in seismic (deep) fractures in Transdanubia. *Acta Geod. Geoph. Mont. Hung.*, 11 (1976), 277—285.
4. Ádám, A.—Wallner, Á.: Influence of tectonics on the direction of induction arrows in the Carpathian Basin. *Acta Geod. Geoph. Mont. Hung.*, 10 (1975), 199—205.
5. Balla, Z.: A Magyar Középhegység szerkezeti főirányai (Die wichtigsten Strukturlinien des Ungarischen Mittelgebirges). *Földtani Közlöny*, 97 (1967), 265—277.
6. Berdichevsky, M. N.—Dmitriev, V. I.: Distortion of magnetic and electric fields by near-surface lateral inhomogeneities. *Acta Geod. Geoph. Mont. Hung.*, 11 (1976), 447—483.
7. Boccaletti, M.—Horváth, F.—Loddo, M.—Mongelli, F.—Stegena, L.: The Tyrrhenian and Pannonian Basins: a comparison of two Mediterranean interarc basins. *Tectonophysics*, 35 (1976), 45—69.
8. Olszak, G.: Zu einigen Beziehungen zwischen Magmatismus-Tektonik und geologisch-geophysikalischer Tiefenstruktur. Tektonik und Magma, Teil 1, Freiberger Forschungshefte, R. C. S. 215, Leipzig, 1967.
9. Stegena, L.—Horváth, F.—Ádám, A.: Spreading tectonics investigated by magnetotelluric anisotropy. *Nature*, 231 (1971), 442—443.
10. Stegena, L.—Géczy, B.—Horváth, F.: Late Cenozoic evolution of the Pannonian Basin. *Tectonophysics*, 26 (1975), 71—90.
11. Tátrallyay, M.: On the interpretation of EM sounding curves by numerical modelling using the S. O. R. method. *Acta Geod. Geoph. Mont. Hung.*, 12 (1977), 279—285.
12. Wallner, Á.: The main features of the induction arrows on the area of the Transdanubian conductivity anomaly. *Acta Geod. Geoph. Mont. Hung.*, 12 (1977), 145—150.
13. Wein, G.: Zur Kenntnis der tektonischen Struktur im Untergrund des Neogens von Ungarn. *Jahrbuch Geol. Bundesamt*, 116 (1973), 85—101.

СТАТИСТИЧЕСКИЕ ЗАВИСИМОСТИ МЕЖДУ РАСПРЕДЕЛЕНИЕМ ЭЛЕКТРИЧЕСКОЙ ПРОВОДИМОСТИ И ТЕКТОНИКОЙ РАЗЛОМОВ НА ЗАДУНАЙСКОМ КРАЕ

А. АДАМ

РЕЗЮМЕ

Автор исследует распределение электрической проводимости в Задунайских разломах (Венгрия), на территориях которых в последние годы магнитотеллурическими зондированиями обнаружили большую геоэлектрическую аномалию.

В первую очередь автор поясняет проблемы магнитотеллурического метода. После этого, на основании связи направления разломов и анизотропии электрической проводимости, приходит к выводу, что геоэлектрическая аномалия находится в сильной связи с разломами, образованными вследствии альпийского орогенного цикла.

Acta Geodaet., Geophys. et Montanist. Acad. Sci. Hung. Tomus 16 (1), pp. 115—130 (1981)

CONNECTION BETWEEN THE GAS CONTENT AND STRENGTH OF ROCKS EXPOSED TO GAS OUTBURST DANGER

F. KOVÁCS

TECHNICAL UNIVERSITY OF HEAVY INDUSTRY, MISKOLC

[Manuscript received October 26, 1978]

The study analyses data from gas outbursts in the Mecsek Region (Hungary) and from the technical literature. Based upon this analysis the influence of porosity, gas content, gas pressure and rock strength upon the gas outburst danger is investigated. It is proved that these natural parameters have a decisive role in provoking outbursts.

An active tectonical structure and metamorphosis promote the comminution of coal, increase gas evaporation and produce greater gas content. The increase of pore volume and pore pressure reduces the strength of the coal layer and encourages deterioration. With increasing depth and rock stress, respectively, the pore volume and permeability decrease, thus increasing the danger of gas outburst.

Investigation of the properties of sandstones, being particularly susceptible to outbursts, shows that in the dangerous areas porosity is twice as great while rock strength only half that found in the nondangerous areas. Gas content and gas pressure decrease the strength of sandstones, encourage deterioration and hence increase the gas outburst danger.

As the strength of the coal layer increases, the average gas content decreases, thus reducing the risk of deterioration. A manifold of the average gas content is needed to produce outbursts.

Development of methods of protection against gas outbursts has relied upon experience of outbursts and statistical analysis of the data. The increasing danger of working at greater depths and the need for further development of protection methods demand a thorough investigation of outburst phenomena based on theoretical principles. It is necessary to determine the cause of unexpected rock and gas outbursts and the physical, mechanical and geological conditions leading to them.

A complex investigation of these problems requires an analysis of the load assumption and interaction of the rock-gas dual system. Results of such theoretical studies are reported in [1] and [2], where the load assumption of the rock-gas system, problems of the pillar effect and deterioration and the influence of various rock parameters (porosity, strength) are all investigated in order to determine the cause of gas outbursts.

The author of [1] and [2] took into account the fact that with increasing depth the gas content of the layers and the rock temperature increase while pore volume and gas permeability decrease. Eventually, the pore gas pressure increases. The mechanical consequences of the pillar effect and the protection seam working method and their controversial effects on the rock-gas system have also been studies in great details. Important discoveries have been made

concerning the conditions leading to gas outbursts derived from a thorough analysis of stress, deformation and deterioration. The role of pore gas pressure and strength, and, similarly, the effect of pore volume on the outburst danger have been emphasized.

The most important conclusions of SOMOSVÁRI's studies [1, 2] concerning the latter parameters are as follows. Pore gas pressure and coal strength have a basic role in the outbursts. Gas content of the layer and the pore pressure reduce strength to a major extent. If this effect exceeds that of the load relief by gas pressure, the state of stress comes closer to deterioration. Following a specific decrease in volume, the process of deterioration is accelerated or, in certain cases, it proceeds as an explosion. In creating the conditions of deterioration, the initial void ratio (porosity), pore gas pressure, the uniaxial compressive strength and YOUNG's modulus play a determinant role. The initial void ratio has an essential influence on the rate of change of the gas pressure and the effective stress due to loading and compression. A smaller void ratio brings about a greater increase in gas pressure when the load is increased. Thus there is a greater difference between the effective stress and the total stress, and the danger of gas outburst is increased. A decrease in void ratio or an increase in pore pressure enlarges the outburst danger.

In connection with the above statements, another question shall now be investigated, in particular, to what extent the results derived from theoretical mechanical equations can be proved by data taken from the literature and statistical analysis. It should be noted that the statements of studies [1] and [2] referring to coal, can be applied to sandstones affected by gas outburst danger.

The statistical analysis of gas outbursts in the lias region of Pécs is dealt with in [3]. Using the data from this paper, first, the specific gas output produced by the working and the value of gas content and pore gas pressure needed to cause deterioration or to create gas outbursts will be investigated, as a function of depth and rock pressure. According to our hypothesis, with a constant rock (coal) strength, an increase in the gas content or pore pressure (partly because of its strength-reducing effect) readily creates the conditions of deterioration. The initiation of the process only requires a slight excess load, excess gas content or excess gas evaporation.

The result of the statistical analysis carried out for three mines of the Pécs district are illustrated in Figs. 1 to 6. According to experience, the average gas output c produced by the mining operations, linearly varies with the working depth H. The specific gas outputs c^x experienced in various gas outbursts are plotted against the working depth and the average gas output in Figures. Average values of the specific output have been calculated for each level. The variation of the average is indicated by the line c^x. Further, the ratio of the specific gas output c^x of the outbursts to the average gas output c of the mining operations has been determined for each level. The variation of the ratio

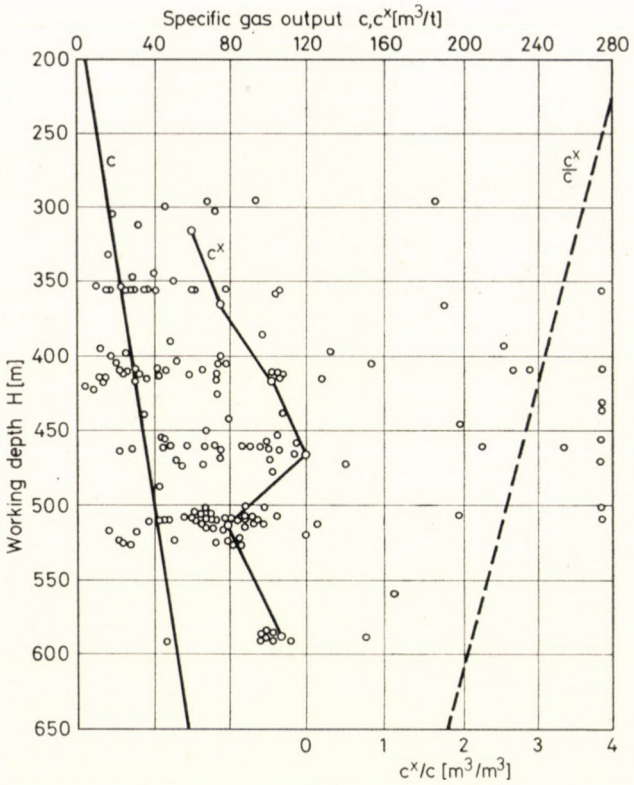

Fig. 1. The specific gas output and the ratio c^x/c as function of the working depth at Pécsbánya

c^x/c as a function of the working depth and the average gas output has been established using the regression method from the data of the levels. A similar tendency can be observed in all six Figures. If the working depth, the average gas output and the primary pore gas pressure increase or the porosity decreases, a smaller amount of excess gas content, excess gas pressure or excess stress is required to initiate the deterioration of the coal seem and to bring about the conditions of gas outbursts.

Some comments should be made regarding the determination and accuracy of the values c and c^x. Current measurements of ventilation do not yet enable us to determine precisely the original gas content of the seems or to separate the amount of the primary gas evaporating from the worked layer and that of the secondary gas coming from other seams and the side rock. Consequently, the value c is not the gas content of any single seam but rather an average specific gas output characteristic of the total of seams in a given production unit. The value of c also depends on the ratio of the worked seam thickness to the total thickness of the productive series. This distorting effect is evident in the data for Vasas, where the worked seam thickness is small com-

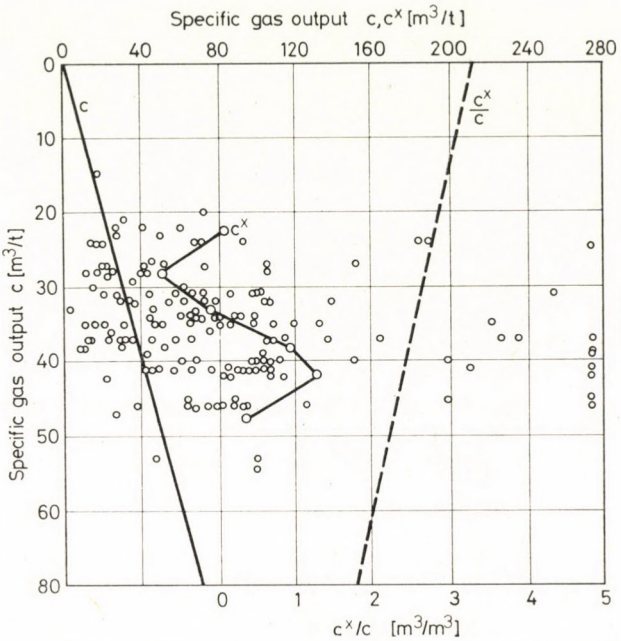

Fig. 2. Variation of the specific gas output and the ratio c^x/c at Pécsbánya

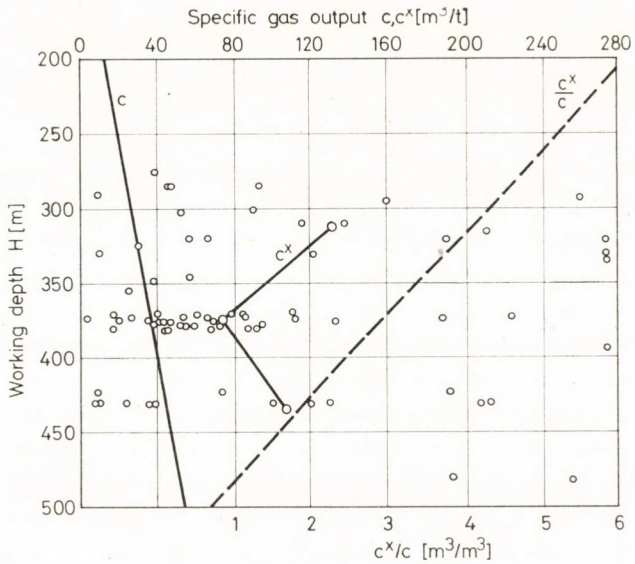

Fig. 3. The specific gas output and the ratio c^x/c as a function of the working depth at Szabolcs

pared with the total thickness of seams. The ratio of the secondary gas output is high, this is why in this case the value of c^x/c becomes less than 1. When making comparisons based on the value c^x, the parameters are not determined for

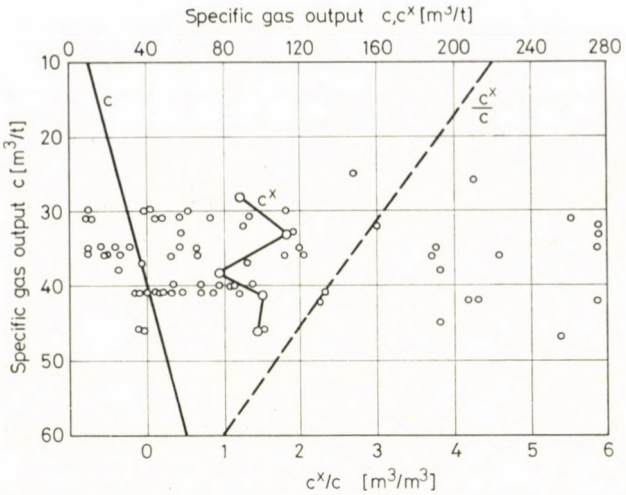

Fig. 4. Variation of the specific gas output and the ratio c^x/c at Szabolcs

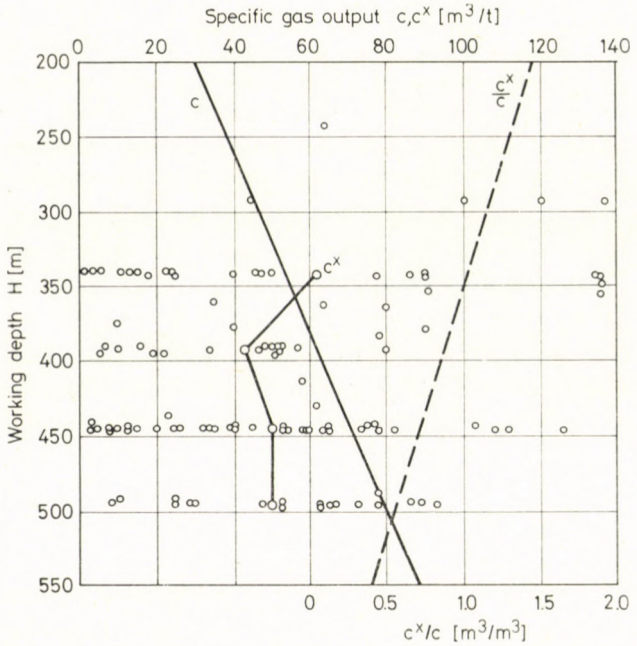

Fig. 5. The specific gas output and the ratio c^x/c as a function of the working depth at Vasas

single outbursts or outbursts in some given layer, but for all events of the working unit. Therefore, in the theoretical investigations of deterioration, the values derived from the data should be regarded as approximate.

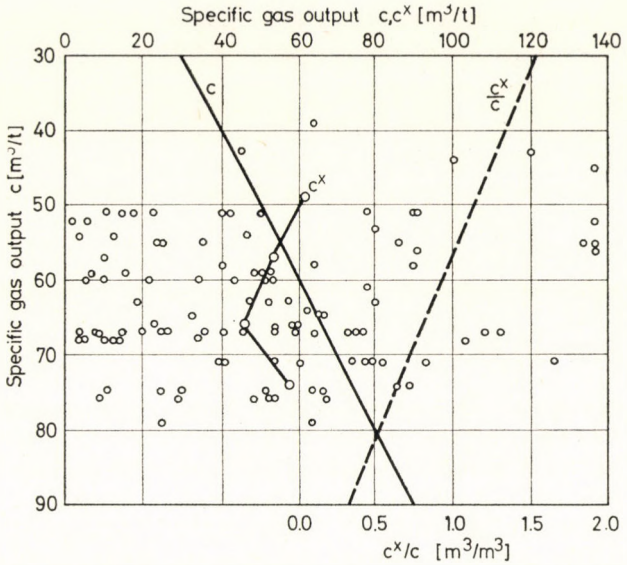

Fig. 6. Variation of the specific gas output and the ratio c^x/c at Vasas

The specific gas output c^x of the outbursts is also known with a limited accuracy. The continuous and accurate recording of the released gas volume (the methane content of the mine air) has not been solved as yet either during the outburst or in its various periods. Even if some instrumental observation is used, it only indicates values between certain concentration limits. The amount of the released gas is only determined by indirect or approximate methods. This deficiency and the subjectivism of the estimation and calculation show, however, a random character. Consequently, the error can be both positive and negative and it can be observed in all areas (mines, basins, countries). The average values calculated from the available statistical data can be accepted as fair approximate ones, since the systematic errors of the specific values caused by different properties (seam thickness and intensity) are considerably smaller than the random errors compensating each other.

From the analysis of the values c and c^x or the ratio c^x/c, comparisons can be made, laws obeyed by the trends can be formulated and the results of regression analysis can be utilized.

Within the investigated depth range (250—300 m) the original strength of the rocks does not vary by such a degree as to bring about a major change in the deterioration conditions. The ratios c^x/c for Pécsbánya and Szabolcs are nearly the same: 2.64 and 2.80, respectively. This value is, however, considerably smaller in the Vasas area where the average specific gas output of the outbursts is lower than the average gas release. The value c^x/c is 0.85 for this mine. According to the available data, this deviation is not due to the average seam

strength. Rather, it depends on the ratio of the worked and the total seam thickness on the one hand and on further geological characteristics, on the other.

These special characteristics are dealt with in [4]. It is pointed out that the degree of coalification is optimum in the layers of the Vasas mine from the point of view of methane release. The porosity of the coal is highly increased due to thermometamorf effects, while their sorption capability remains essentially unchanged. The porosity of the contact seam parts of the Vasas area amounts to 25—27% and this value leads to practically the same conditions for the outburst danger as does the 3—9% porosity in the Szabolcs mine. The tectonical conditions, contact effects and the thermal anomaly are responsible for the fact that the natural degradation (defined as the percentage fraction of the particles less than 0.5 mm) at Vasas does not characterize the outburst danger so unambiguously as in the Pécsbánya and Szabolcs areas.

During the investigations reported in [3] we have been lead to the conclusions that there is a correlation between the average gas output released during mining operations and the average specific methane output of outbursts. For increasing gas outputs, the conditions of the outbursts (deterioration) are more easily brought about and the amount of excess gas produced or accumulated in the place of the outbursts is smaller. Correlation can be found between the strength of the seams on the one hand, and the gas output and the specific gas output of the outburst on the other. In cases of smaller rock strength, the deterioration can also be initiated by a smaller gas content or pore pressure.

The above statements are supported by the analysis of statistical data. From the data of gas outbursts in the three Pécs mines, the ratio of the specific gas output c^x of the outbursts and the gas output c released by mining operations has been determined for each district. Figure 7 illustrates the values c^x/c (+ stands for Pécsbánya, 0 for Szabolcs and x for Vasas). The corresponding data for the Zobák mine in the Komló region were taken from the gas outbursts N° 5, 6, 7, 10, 12, 13, 14 and 16 (represented by ⊗ in Fig. 7). Data from abroad have been furnished by the literature. The data of the Kuznetsk basin is taken from Fig. 1 and Table 2 of [5]. In one set of data referring to 15 outbursts, the average of c is 17.1 m³/t and that of c^x/c 5.87. In another region, the gas output produced by mining operations is 16.5 m³/t and the average c^x/c amounts to 6.06 according to data from 23 outbursts. The study referred to points out that the value c^x/c ranges between 3 and 15 in the outbursts of the basin. Data for the Donets basin can be found in [6]. The average of the specific gas output is 9.5 m³/t in a given depth, the average gas output of the outbursts being $c^x = 31$ m³/t and the value $c^x/c = 3.26$. In [7] there are data about the Ruhr region: $c = 15$ m³/t, $c^x = 50$ m³/t and $c^x/c = 3.33$.

On Figure 7 Soviet and German data are also plotted. Even without any regression analysis it can be stated that the ratio of the specific gas output, produced by the outbursts and the mining operations, decreases considerably

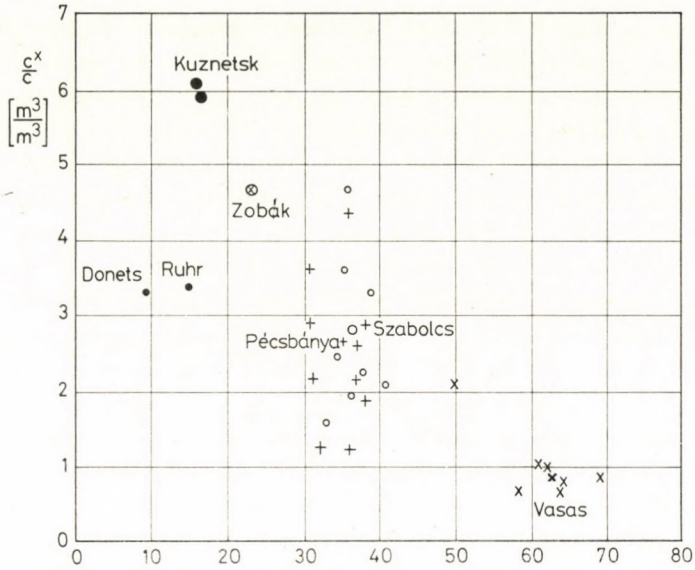

Fig. 7. The ratio c^x/c as a function of the specific gas release

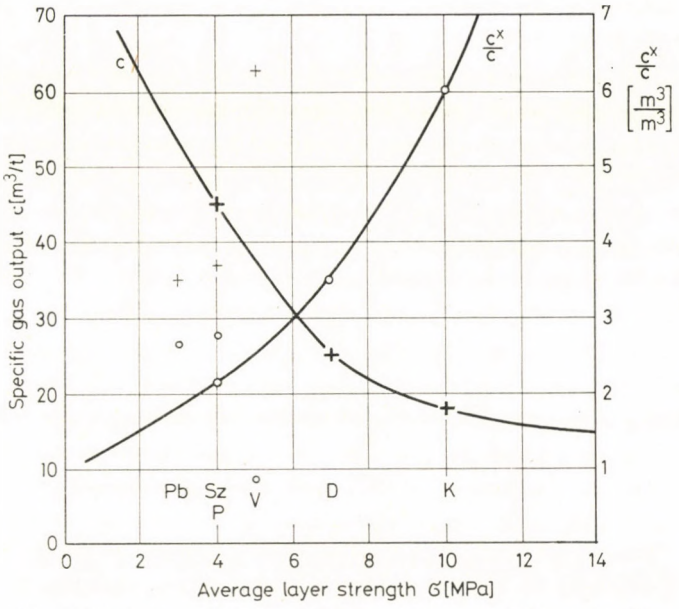

Fig. 8. Variation of the specific gas release c and the ratio c^x/c

with increasing gas output. In cases of higher gas output, even a smaller amount of excess gas content is sufficient to cause deterioration.

Studies analysing the geological circumstances and conditions leading to gas outburst danger often come to the conclusion that the specific gas content

of the layers or the amount of accumulated methane increases with the reduction of seam strength (i.e. for greater degradation). At the same time, in coal seams of greater strength, the specific gas flow of the outbursts exceeds several times the amount of gas continuously during mining operations.

This statement will be illustrated with approximate data from three regions, in Fig. 8. The data should be considered as rough average values, for in the Soviet literature seam strength is generally characterized by Protodiakonoff's number which has to be converted into strength. For gas outputs produced by mining operations, only approximate data have been available and it was not possible to identify the place of origin inside the basin for strength and gas output data. The estimated average values are as follows:

Area	Average strength [MPa]	Specific gas output c[m³/t]	c^x/c Ratio [m³/m³]	Notation
Donets (SU)	7	25	3.50	D
Kuznetsk (SU)	10	18	6.00	K
Pécsbánya (Hungary)	3	35	2.64	Pb
Szabolcs (Hungary)	4	37	2.80	Sz
Vasas (Hungary)	5	62	0.85	V
Pécs (Hungary)	4	45	2.13	P

From Fig. 8 it can be seen that the specific gas output produced by the mining operations has a tendency to decrease with increasing coal seam strength. Also, the deterioration responsible for outbursts occurs only if the gas content exceeds the average by several times. One of the essential conditions of outbursts that the pore gas pressure or gas content should be considerably greater than the average values. Relying upon the data of Figs 7 and 8, the conclusion of studies [1] and [2] based on theoretical principles, can be considered as verified. According to this conclusion, the pore gas pressure or gas content influences rock strength to a great extent and reduces the safety against deterioration.

In what follows we shall briefly review the technical literature concerning the above questions. The problems of gas content — gas outburst danger, gas content — rock strength, gas content — deterioration, porosity — gas outburst danger, sorption properties and grade of degradation etc. are dealt with in these studies.

ETTINGER, in Section III. of his monography [18] presents a thorough analysis of these questions. He describes the strength-reducing effect of adsorption, called the Rebinder phenomenon. The adsorbed molecules intrude

into the microsplits in the deformed zone of the solid. This effect encourages the deformation of the solid both in the elastic and the plastic fields at the same load (stress). At the same time, the critical yield, strength, breaking and deterioration values diminish.

Even a negligibly small amount of surface-active material can cause a strong reduction in the mechanical strength of the rocks. According to experiments, CO_2 brings about the greatest reduction in strength. Methane has the second strongest effect of this kind. The strength-reducing effect depends upon the sorption capability of the gas.

The strength-reduction of coal layers is also related to the grade of coalification or metamorphosis. Anthracite and young long-flame coal are the hardest ones. They possess an increased sorption capability. The degree of strength-reduction is greatest in these types of coal, it amounts to 25—30%. The attrition of certain coal sorts in a carbondioxide atmosphere may reduce the strength by as much as 50%.

In coals with a disintegrated structure and full of microsplits, this phenomenon has an increased effect. The strength of loose coals can decrease under favourable adsorption conditions by as much as 50% or its value as measured in the air. Of further importance as regards deterioration is the fact that active gases with good sorption capability decrease the strength more rapidly.

The author of study [8] points out, on the basis of an analysis of the role of tectonical effects and gas content, that the active parts of the tectonical structure are areas of increased gas output, tectonical stresses encourage extraordinary gas evaporation.

The metamorphosis of coal layers increases the methane content. The danger-increasing effect of thermal factors (even 3—5 °C excess temperature) can be positively indicated. Outbursts are always characterized by a certain amount of excess gas output which exceeds in some cases the natural gas content of the layers by many times. Proportionally to the increase of gas content, the danger of unexpected outbursts increases.

Based on the research results of MAKNII, the author of [9] reports that the principal factors affecting outburst danger are rock pressure and the physico-mechanical properties of gas and coal. As to the interaction of these three parameters it is stated, on the basis of experiments, that the saturation of coal with methane brings about a strength-reduction of the coal samples. On the other hand, observation proves that coal is easier to win and comminute at faces filled with gas than in properly ventilated gas-free places. Relying upon these facts, the author emphasizes that in the investigations of the strength and deformation properties in the analysis of the outburst danger and the deterioration of coal layers due care should be taken of the effect of gas.

Experiences of working the Pécs region in southern Hungary which coincide with French observations, tell us that an increase of the gas content in

the coal face reduces strength. On the other hand, layers affected by gas drainage or workings beneath or above the layer are more stable. Similar practical experiences are also listed in book [18].

In their simple equation describing the condition of deterioration and rock separation, the authors of study [14] make use of the pore volume, pore pressure and the tensile strength of the coal. Doing so, they attribute a basic role to these factors in bringing about outburst conditions. According to them, the method of protection layers and loosening blasts exert their danger-reducing effect mostly by reducing pore pressure. If water injection is used, a smaller amount of the pore volume is exposed to the pore gas pressure and the gas storing capability also reduces.

Research workers of the Moscow Mining University [10] report that the gas outburst danger is exceptionally high in areas where the layer contains a great amount of sorbed methane and the permeability is low.

Australian experiences [15] point to the fact that with increasing depth the gas content of the layers and the amount of gas relieved during working increase. In areas with accumulated stress, especially near dislocations with sliding, the coal is comminuted, its inner surface increases, the gas storing capability is greater than average. Thus, a much greater amount of gas is relieved in course of outbursts than generally during working. From this, it is concluded that the tectonical stresses contribute to the increased gas evaporation and accumulation.

Investigations in Belgium [16] show that rock stress and deterioration depend on gas pressure and rock permeability. The author also reports results stating that with increasing depth and stress, the permeability of coal layers decreases and the danger increases.

The connection of gas content and deterioration is also dealt with in book [17]. Based on experimental results, the author states that the increase of gas sorption increases the rate of deterioration. He claims, however, that the pore pressure and gas pressure gradient have a more important effect on the fracture process than the gas content and gas sorption. Further results prove that with increasing coal strength, the rate of deterioration decreases.

Many authors investigated analogous problems in connection with sandstones, also affected by gas outburst danger.

The authors of study [11] reporting on research results of Donets sandstones exposed to outburst danger, point out that the level of gas content influences the properties of the rocks and their behaviour under loading. According to their statements, the strength and fragility of sandstones vary under the influence of methane saturation. The gas content affects and determines the state of stress and deformation.

The role played by the gas in the initiation and further course of the outbursts consists in increasing the inner stresses, reducing the strength prop-

erties of the material and throwing out the deteriorated material into the mine space.

From the analysis of the properties of sandstones affected by gas outburst danger, the authors draw the conclusion that the porosity of sandstones subject to gas outburst danger is twice as great while their strength only half that measured in non-dangerous areas.

Similar sandstone data are published in study [7] for the Ruhr district. The porosity of non-dangerous sandstones is 2.7—6.9% while it is 9.9—14.1% and 10.2—14.3%, respectively, in areas with gas outburst danger.

Stress and deterioration investigations concerning rock and gas outbursts carried out in the Donetsk Physical-Technical Institute [12] lead to the following results.

Gas content and gas pressure considerably affect the amount of surface energy of sandstones, and this modifies to a large extent the value of the limit rupture stress. At a given state of stress the gas factor encourages deterioration and increases the gas outburst danger. The methane content and gas pressure modify the deterioration of fracture energy of sandstones.

On the basis of experimental data it has been established that methane does much more than simply splitting rock parts apart by pore pressure. In case of great gas content and gas pressure the increase of the actual surface energy proves that the methane filling the pores and splits makes the rock more brittle. Brittleness, however, reduces tensile and fracture strength. At splits and dislocations the stress concentration increases which results in an increased deterioration.

Study [13] also summarizes observations and experimental data about the deterioration problems of sandstone side-rocks exposed to gas outburst danger in the Donets basin.

According to the authors' opinion one of the characteristic parameters concerning gasdynamical phenomena is the porosity of sandstones. Their investigations have shown that the porosity of sandstones affected by outburst danger is in average by 50% greater than that of non-dangerous ones. With increasing depth porosity decreases, the rate of decrease being 2.5% for every 100 m at small depths (100—400 m). In greater depths the rate of change becomes less: the gradient amounts to 0.4—0.3% at 1300—1600 m. Similar depth-porosity correlation is published by the author of study [4], based on data from Saarbrucken. The decrease of pore volume is 2—4% for 100 m.

In Donetsk detailed investigations have been carried out to determine the correlations between gas saturation, gas content and the strength and deterioration properties of sandstones. It has been proved experimentally that the strength of sandstones, in zones subject to outburst danger, decreases in the average by 30% under the effect of 2—6 MPa pressure. At the same time, however, no similar effect has been observed for rock materials without out-

burst danger. Similar results were obtained by the analysis of the deformation characteristics. The degree of deformation of the sandstone specimens considerably increased with increasing gas saturation.

The laboratory tests were supplemented by *in-situ* investigations to measure the strength factor of sandstones with and without outburst danger. Using drillability data, Protodiakonoff's number was 8—9 in sections under gas pressure in zones subject to outburst danger, while for non-dangerous zones it was 11—12. After removing the gas from the dangerous places and relieving the pressure by working above the layer, the strength factor increased to 12—13.

The different behaviour of dangerous and non-dangerous areas in the gas-saturated state, i.e. the selective effect is believed to be due to the composition and structural properties of rocks. On the basis of experiments and observations, rock and gas outbursts are treated as dynamical problems from the theoretical point of view.

Summing up the experimental and practical results about coal layers subject to gas outburst danger [8, 9, 10, 14, 15], the following main statements can be made.

An active tectonical structure, stress and metamorphosis and the comminuted coal resulting from these produce an increased gas output and greater gas content. The pore volume, pore pressure and the strength of the coal layer decisively affect the deterioration and gas outburst danger. The increase of the gas content and pore pressure reduces the strength of the coal layer and encourages deterioration. Rock stress (depth) decreases the pore volume and permeability on the one hand and increases the danger of deterioration and outburst, on the other.

As for sandstones subject to outburst danger [4, 7, 11, 12, 13], it can be stated that in the dangerous areas porosity is twice as great while the strength half that found in the non-dangerous parts of the layer. Gas content and gas pressure reduce the strength of sandstones, they modify to a great extent the limit tensile stress, disadvantageously influence deterioration circumstances and increase outburst danger.

The practical and experimental results considerably support the theoretical conclusion of studies [1] and [2]. Gas content and pore gas pressure play a decisive role in creating the conditions of deterioration. Gas pressure reduces the strength of the coal layer or rocks, increasing the danger of deterioration. Stress decreases the pore volume and permeability, increasing the danger of outburst.

There is a difference in the parameters of outburst danger for coal layers and for the side-rocks subject to gas outbursts. Experience and theoretical considerations show that for coal layers a small porosity is disadvantageous from the point of view of the outburst danger. The effect of depth on the in-

crease of stress, gas content and pore gas pressure is much more disadvantageous in encouraging deterioration if the pore volume is small. The ratio of the effective and total stress varies in the wrong direction. For sandstones, however, practical data show that porosity is by 50—100% greater in areas subject to gas outburst danger than in non-dangerous ones [7, 11, 13].

When evaluating the degree of outburst danger for rocks with various properties it should be taken into consideration that to a great rock porosity, generally, a small strength belongs. If the Young's modulus of the rock is small, i.e. its capability for deformation is great, the danger-increasing effect of the small porosity is stronger than the effect of the great strength which reduces the danger of outburst. This is the case for coals with small Young's moduli and generally low strength. If the Young's modulus of the rock is great, i.e. its capability for deformation is small, the effect of great porosity decreasing the outburst danger is weaker than that of the small strength increasing the danger. This is the case for sandstones with high value of Young's modulus and great strength.

Figures 7 and 8, constructed on the basis of our investigations, also seem to prove the theoretical discoveries of studies [1] and [2]. If the gas content of the layer is great, a small increase in the pore pressure is satisfactory for deterioration. The amount of excess gas output released at outbursts is moderate. With increasing strength of the layer its specific gas content decreases the safety against deterioration consequently increases, and a manifold of the average gas content is needed to encourage outbursts.

The review of the technical literature and the reported investigations prove that in order to determine the conditions leading to gas outbursts, and to improve the methods of combatting them, one has to carry on the theoretical investigations based on physical, mechanical and gas-dynamical principles and to evaluate the accumulating experimental and practical data. In course of this work, the effect of the working depth on rock strength, gas content, gas pressure, porosity and other gas-dynamical parameters has to be analysed in a simplex way. The correlations between porosity — gas pressure, porosity — degree of comminution, and porosity — water content — gas characteristics should be investigated. A detailed analysis will be needed to determine the effect of gas content and pore pressure on the strength and — similarly — on the loading and deterioration conditions of the rock-gas and rock-gas-water systems.

REFERENCES

1. Somosvári, Zs.: Investigation of the deterioration of the rock-gas systems to clarify the cause of rock and gas outbursts. *Acta Geod. Geoph. Mont. Hung.*, 15 (1980), 257—269.
2. Somosvári, Zs.: Investigation of the load assumption of rock-gas systems, aiming at the detection of the causes of rock and gas outbursts. *Acta Geod. Geoph. Mont. Hung.*, 15 (1980), 271—294.

3. KOVÁCS, F.: Determination of the Expected Measure of Gas Outburst Danger and Evaluation of its Economical Consequences. Doctor's Thesis. Hungarian Academy of Sciences, 1975.
4. FEJÉR, L.: Details of the Geology of Mine Gases. Combat of the Mecsek Coal Mines against unexpected coal and gas outbursts in 1973—74. (3). Műszaki Könyvkiadó. Budapest. 1977. p. 150—164.
5. HASHIN, V. N.—LUDZISH, V. S.: Some characteristics of the phenomena of sudden outbursts in mines of the Prokopieff area of the Kuznetsk basin. Physical Technical Problems of Working Mineral Deposits. Academy of Sciences of the Sovietunion, Siberian Section. 1974. No. 2. 100—107.
6. Mining Encyclopaedia. Vol 6. p. 39. 267.
7. PAUL, K.: Outbursts of sandstone and methane from the adjacent strata of coal seams in the Federal Republic of Germany. Economic Comission for Europe Coal Committee. Symposium on Sudden Coal and Gas Outbursts. Donetsk, 1974.
8. VEREDA, V. S.: Present tectonical stresses as causes of unexpected coal and gas outbursts and consequences drawn from this hypothesis. Economic Comission for Europe Coal Committee. Symposium on Sudden Coal and Gas Outbursts. Donetsk, 1974.
9. NIKOLIN, V. I.: Unexpected coal and gas outbursts and forecast of outburst danger in coal mines. (Common report.) Economic Comission for Europe Coal Committee. Symposium on Sudden Coal and Gas Outbursts. Donetsk, 1974.
10. RZHEVSKI, V. V.—BURCHSKOFF, A. S.—MOSKALENKO, S. M.—NOSHKIN, N. V.: Theory and practice of controlling stability of rock massifs for combat of principal dangers in coal mines. Economic Comission for Europe Coal Committee. Symposium on Sudden Coal and Gas Outbursts. Donetsk, 1974.
11. NIKOLIN, V. I.—BOLISHINSKI, M. I.: Basic solutions of the forecast of outburst danger and combat of rock and gas outbursts in deep mines of the Donetsk Basin. Economic Comission for Europe Coal Committee. Symposium on Sudden Coal and Gas Outbursts. Donetsk, 1974.
12. ALEKSEIEFF, A. D.—POLIAKOFF, N. S.: Research of the institutes of the Academy of Sciences of the Soviet Union on coal, rock and gas outbursts. Economic Comission for Europe Coal Committee. Symposium on Sudden Coal and Gas Outbursts. Donetsk, 1974.
13. ARRAMOFF, F. A.—DIHTIAR, A. A.—ZABIGAILO, V. E.—POLUIANSKI, S. A.—HARITONOFF, V. N.—SHEVELEFF, G. A.: Investigations into rock and gas outbursts in mines of the Donetsk Basin, development of forecast methods and possibilities of protection against them. Economic Comission for Europe Coal Committee. Symposium on Sudden Coal and Gas Outbursts. Donetsk, 1974.
14. PETUHOFF, I. M.—LINKOFF, A. M.—SIDOROFF, V. S.: Theory, practical use and evaluation of the efficiency of protection layers. Economic Comission for Europe Coal Committee. Symposium on Sudden Coal and Gas Outbursts. Donetsk, 1974.
15. GRIFFITHS, L.: Outburst of coal and gas in the southern district of the New South Wales coalfield. Economic Comission for Europe Coal Committee. Symposium on Sudden Coal and Gas Outbursts. Donetsk, 1974.
16. STASSEN, I. J.: Combat of methane outbursts in Belgium. Economic Comission for Europe Coal Committee. Symposium on Sudden Coal and Gas Outbursts. Donetsk, 1974.
17. SZIRTES, L.: Combat of Coal and Gas Outbursts. Műszaki Könyvkiadó, Budapest. 1971. p. 88—89.
18. ETTINGER, I. L.: Sudden Coal and Gas Outbursts and the Structure of Coal. Nedra. Moscow. 1969.

О СВЯЗИ ГАЗОНОСНОСТИ И ПРОЧНОСТИ ВЫБРОСООПАСНЫХ ПОРОД

Ф. КОВАЧ

РЕЗЮМЕ

В статье на основе обработки литературных материалов и анализа данных выбросов газа в шахтах горы Мечек исследуется: каким образом влияют пористость, газоносность, давление газа и прочность на вероятность выбросов газа. Автор устанавливает, что упомянутые природные параметры имеют решающее значение при появлении выбросов.

Активная тектоническая структура (метаморфоз) способствует измельчению угля, усиливает выделение газа, создаёт большую газоносность. Увеличение объёма и давления пор уменьшает прочность залежа угля, способствуют его разорению. Увеличение глубины и напряжения пород уменьшает объём пор и проницаемость, увеличивает вероятность выбросов газа.

Исследуя естественно-геологические условия выбросоопасных песчанников можно установить, что на опасных участках пористость в два раза больше, а на безопасных участках прочность в два раза меньше. Газоносность и давление газа уменьшают прочность песчанников и отрицательно влияют на процессы разорения, увеличивают опасность выбросов газа.

С ростом прочности залежа угля средняя газоносность уменьшается, вследствии чего безопасность от разорения увеличивается, для наступления выбросов необходимо газоносность в несколько раз выше.

Acta Geodaet., Geophys. et Montanist. Acad. Sci. Hung. Tomus 16 (1), pp. 131—149 (1981)

INVESTIGATION OF THE ROCK-GAS SYSTEM IN FRONT OF THE FACE OF WORKINGS IN ORDER TO DETERMINE THE CAUSE OF ROCK AND GAS OUTBURSTS

ZS. SOMOSVÁRI

TECHNICAL UNIVERSITY OF HEAVY INDUSTRY, MISKOLC

[Manuscript received January 5, 1979]

Based on investigations of the interaction of rock-gas system, it is proved that rock and gas outbursts cannot occur in working if the Poisson ratio is small, i.e. near 2. In this case, namely, the basic condition of outbursts, derived in our previous study, does not hold according to which an outburst needs a reduction in the rock volume in front of the face. This result explains the general experience that at extremely small coal strength, outbursts are concentrated in the headings and they only occur in workings in case of great coal strength i.e. for great Poisson ratio.

It is shown that the initial pore gas pressure, the primary vertical stress $H\gamma$, the Poisson ratio of the layer, the angle of internal friction, the compressive strength and the change of the compressive strength have major effect on the danger of outburst. The layer strength (uniaxial compressive strength) necessary to avoid the outbursts is derived as a function of the aforementioned principal parameters. This connection will explain, among others, the experience that the frequency of outbursts increases with depth and that in some cases, outbursts may occur even at very small (0.3—0.4 MPa) pore gas pressure while in other cases, they do not come about at all, even for much greater pore gas pressures. Also, the same formula will explain why outbursts, in general, occur in layers of small strength, and how it is that in certain cases they also may occur in layers of great compressive stress.

The results presented further corroborate that, as we have previously reported, the outburst is a sudden, explosion-like process of deterioration of the load-bearing rock-gas system catalysed by the pore gas pressure. The basic cause of outbursts is the strength-reducing effect of the pore gas pressure. This effect initiates a chain-reaction-like process which accelerates the deterioration and makes it explosion-like. At the same time, the load is transferred from the solid structure of the deteriorated rock to the pore gas. This brings about a great gas pressure which throws out the solid phase into the open space. Simultaneously, a great amount of gas flows into the mine, as an explosion, because the major part of the bound (adsorbed) gas phase gets relieved due to the decreased gas pressure.

Symbols

B	Brinke's number
e_0	initial void ratio
E	Young's modulus
H	depth beneath the surface
l_x, l_0	semi-width of the cave
m	Poisson's ratio
M	thickness of layer under working
p	pore gas pressure
p_0	initial pore gas pressure
s	convergence factor
$\Delta V/V$	specific change of volume
x	distance measured from the face
γ	average unit weight
$\varepsilon_x, \varepsilon_y, \varepsilon_z$	deformations
$\varkappa$	polytropic exponent
σ', τ'	effective stresses
σ_c	uniaxial compressive strength
σ'_c	uniaxial compressive strength in presence of pore gas pressure

σ_T	tensile strength
σ_t	total stress
$\overline{\sigma}_x$	primary horizontal stress
σ_x	secondary horizontal stress
$\overline{\sigma}_z$	primary vertical stress
σ_z	secondary vertical stress
$\overline{\tau}$	primary shear stress
τ	secondary shear stress, shear limit stress
$\Delta\sigma_x$	horizontal deformation stress
$\Delta\sigma_z$	vertical deformation stress
$\Delta\tau$	shear deformation stress

The problems concerning unexpected rock and gas outbursts can be divided into two major categories: the phenomena before and after the beginning of the outburst. The description of the phenomena after the beginning of the outburst, i.e. the actual process of the rock and gas outburst, is of practical importance from the point of view of the development of the mechanical effect. Since unexpected gas and rock outbursts always create an acute danger for human lives and fortune, the processes preceding the outburst, and the cause of the outburst, are for the every-day practice much more important than the outburst itself. That is why our choice fell on the investigation of the cause of outbursts, a problem even today not wholly understood. Despite enormous efforts and expenses to reduce danger, unexpected gas and rock outbursts occur in our country as well, causing loss of human lives.

This study, similarly to [3] and [4], presents an analysis of the mechanical interactions of the load-bearing rock-gas system in order to determine the cause of outbursts. It is realized, of course, that beside the mechanical interactions between the two phases in question thermal and physico-chemical interactions also occur. Thermal effects begin to influence the rock-gas system starting from the chemical process of gas expansion since gas expansion is controlled by thermodynamical conditions. The physico-chemical properties of the free and adsorbed gas in the splits of the rocks depend on the thermodynamical parameters. Also, the variations of gas pressure, temperature and amount of bound and free gas obey thermodynamical laws. These variations are caused by changes of volume of the free gas connected with the deformations and change of volume of the surrounding rock around mine excavations. Consequently, the rise and development of the outbursts is accompanied by thermodynamical effects. Nevertheless, the essential feature of the rise of rock and gas outbursts is, to our belief, the mechanical interaction of the dual system. This hypothesis is based on the fact that in the rocks surrounding mine excavations, mechanical phenomena (stress rearrangements, deformations, movements) occur in the first place and outbursts are always triggered by mine excavations. Also, the phenomenon itself cannot come about without the mechanical deterioration of the solid structure of the rock. Regarding the nature of the phenomenon, no analysis of the mechanical interactions could have been carried out without taking account of the thermodynamical interactions, since

the variation of the gas pressure required for the mechanical investigations, is determined by thermodynamical interactions. For this reason, the thermal effects will be considered as well.

In the study, necessarily, some approximate assumptions will be made. Since these are generally accepted in rock-mechanical, soil-mechanical or geomechanical calculations, their justifications does not seem necessary.

The main results of the previous studies [3, 4] can be summarized as follows.

The outburst is a sudden, explosion-like deterioration process of the rock-gas system. Its basic cause is the strength-reducing effect of the pore gas pressure. If the specific volume of the rock decreases during deteriorations, the pore gas pressure accelerates the deterioration process and gives it an explosion-like character.

It is important to distinguish between deterioration processes characterized by a specific volume reduction, and those where the specific volume increases. If the rock deterioration is combined with a specific volume increase, no outburst can ensue because during the process the pore gas pressure decreases, the strength increases, thus the deterioration process is slowed down. On surfaces of drifts or shafts, far from the face, outbursts never occur because in these areas a specific volume increase takes place during rock deterioration. The effect of working with protective layer can also be explained as due to the specific volume increase.

According to experience, gas outbursts always begin at faces (roadhead, working place or shaft sole). The reason of this, as explained in [3, 4] is that a specific volume reduction proceeds in front of the face during rock deterioration combined with outburst.

1. Mechanism of the rise of rock-gas outbursts

According to our previous reports [3, 4] the mechanism of the rise of outbursts can be outlined as follows. The rock in front of the face of excavations (roadhead or shaft sole), is exposed to transferred rock pressure. In this part of the rock, the specific volume change is reduction. The volume reduction occurs to a large extent at the expense of the pore volume. Thus, in this area, the initial pore gas pressure increases. The solid structure of the rock has to bear a greater load due to transferred rock pressure. The strength, however, decreases because of the increased pore gas pressure, and the condition of deterioration easily arises. With the inset of deterioration, the load is transferred from the solid structure to the pore gas, consequently, the pore gas pressure increases. While the pore gas pressure increases, the strength reduces still further and the condition of deterioration will be fulfilled in the stronger rock parts as well and

the deterioration proceeds further on. Accordingly, a chain-reaction-like process ensues during which the rock is deteriorated in form of an explosion and, with simultaneous increase of the pore gas pressure to many times of its initial value. This procedure produces a great gas pressure and a solid rock which has hardly any internal resistance. An intensive gas flow begins towards the free space, combined with the out-throw of the solid material. During this out-throw, the adsorbed gas phase is relieved from the surface of the deteriorated rock pieces and pores because of the gas pressure reduction. So, a very great amount of gas flows into the surrounding mine excavations.

In what follows, this mechanism will also be described numerically, in case of workings.

2. Experiences about gas and rock outbursts in workings

It is a common experience that, in some areas, the majority of outbursts (90—99 per cent) occurred during drifting while it hardly ever happened in workings. In other areas, however, a considerable amount of outbursts (30—40 per cent) is observed in workings [1, 2]. In the Balkan Basin in Bulgaria 84—89% of the outbursts, in Poland 95%, in France 94%, in England 60%, in the Donets Basin 65%, in the Kuznetsk Basin 62%, in the Pechora Basin 90%, in the Pécs Region (Hungary) 99% of the outbursts occurred at drifting, the remaining percentage in workings. It can be shown that the above figures are in connection with the layer strength [2]. The decisive majority of outbursts (90—100%) occurs at drifting in that case if the coal strength is extraordinary small. This ratio is shifted towards the workings if the uniaxial compressive strength is great. Also, we have to take into account that two drifts are required to each longwall face, i.e. the number or roadheads is about twice the number of working faces. This fact modifies the frequency of outbursts, independently of all other circumstances, towards drifting. When evaluating outbursts, this should also be taken into account.

Aceordingly, no or hardly any outburst occur in workings if the coal strength is small. In case of great coal strength, however, outbursts are rather frequent in workings, too. At the same time, the practical observation also holds that outbursts are concentrated in areas of small layer strength.

3. Stress of the rock domain in front of wide-face working

The mechanical behaviour of the rock domain in front of faces (shaft sole, roadhead or working) is hardly dealt with in rock-mechanical literature, the results can only be used for qualitative analysis. In o der to obtain quanti-

tative results, we have to investigate the mechanical behaviour of the rock domain in front of the face.

In the middle of a wide-face working, the state of deformation can be assumed as planar, whereas the plane of deformation is vertical and perpendicular to the face. Assuming elastic conditions the following primary stresses are present in the investigated rock domain before opening excavations, if the pore gas pressure is $p_0 = 0$:

$$\bar{\sigma}_z = H\gamma\,; \quad \sigma_x = \frac{H\gamma}{m-1}\,; \quad \bar{\tau}_{x2} = \bar{\tau}_{zx} = \bar{\tau} = 0 \tag{1}$$

where

H = depth beneath the surface
γ = average unit weight
m = Poisson's ratio
$\bar{\sigma}_z$ = vertical principal stress
$\bar{\sigma}_x$ = horizontal principal stress
$\bar{\tau}$ = shear stress.

This state of stress is modified by the effect of excavations, when the secondary stresses σ_z, σ_x, $\tau_{x,z} = \tau_{z,x} = \tau$ arise. The equilibrium condition for a volume element of thickness dx (Fig. 1) is:

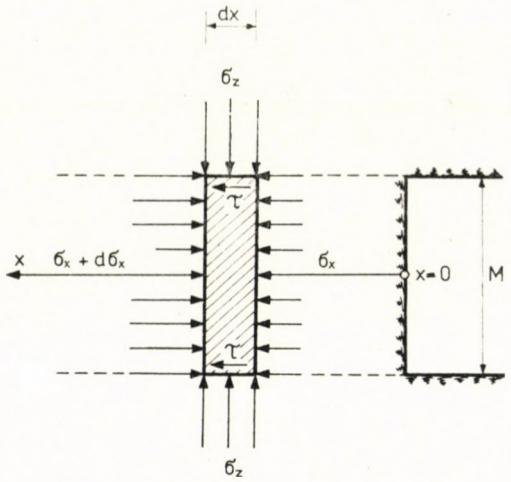

Fig. 1. Stresses on a rock element of infinitesimal thickness in front of the working face

$$\sigma_x M - (\sigma_x + \mathrm{d}\,\sigma_x) M + 2\,\tau\,\mathrm{d}x = 0. \tag{2}$$

Hence

$$\frac{\mathrm{d}\,\sigma_x}{\mathrm{d}x} = \frac{2\,\tau}{M}\,. \tag{3}$$

The secondary stresses can be written as

$$\sigma_z = \bar{\sigma}_z + \Delta\sigma_z;\ \sigma_x = \bar{\sigma}_x + \Delta\sigma_x;\ \tau = \bar{\tau} + \Delta\tau \tag{4}$$

where $\Delta\sigma_z$, $\Delta\sigma_x$ and $\Delta\tau$ are deformational or induced stresses. Since $\bar{\tau} = 0$ thus $\tau = \Delta\tau$, consequently, the shear stress is a deformational one.

Since the deformations causes by opening excavations are always intercorrelated, the deformational stresses calculated from the deformations, are also in a functional correlation with each other, i.e. $\tau = f(\Delta\sigma_x)$ and $\Delta\sigma_x = f(\Delta\sigma_2)$. The deformational stresses are caused by the same effect, *viz.* by opening the excavations, thus their functional description in the area investigated should be similar. Let us assume that these correlations have the form $\tau = -A\Delta\sigma_x$, $\Delta\sigma_z = -C\Delta\sigma_x$. Thus

$$\tau = -A\left(\sigma_x - \frac{H\gamma}{m-1}\right) \tag{5}$$

$$\sigma_z = -C\left(\sigma_x - \frac{H\gamma}{m-1}\right). \tag{6}$$

Using these equations, the linear differential equation

$$\frac{\mathrm{d}\sigma_x}{\mathrm{d}x} + \frac{2A}{M}\sigma_x = \frac{2A}{M}\frac{H\gamma}{m-1} \tag{7}$$

is obtained. The solution to this differential equation (subject to the initial conditions $x = 0$ and $\sigma_x = 0$) is

$$\sigma_x = \frac{H\gamma}{m-1}\left(1 - e^{-\frac{2A}{M}x}\right); \qquad \Delta\sigma_x = -\frac{H\gamma}{m-1}e^{-\frac{2A}{M}x}. \tag{8}$$

Using this solution

$$\tau = A\frac{H\gamma}{m-1}e^{-\frac{2A}{M}x} = \Delta\tau \tag{9}$$

$$\sigma_z = H\gamma + c\frac{H\gamma}{m-1}e^{-\frac{2A}{M}x} = H\gamma\left(1 + \frac{c}{m-1}e^{-\frac{2A}{M}x}\right) \tag{10}$$

$$\Delta\sigma_z = \frac{CH\gamma}{m-1}e^{-\frac{2A}{M}x}. \tag{11}$$

The value of parameter C can be determined from equation (10) since at the face $x = 0$

$$\sigma_z (x = 0) = H\gamma \left(1 + \frac{C}{m - 1}\right). \tag{12}$$

The stress at the face can be calculated by taking account of the excavation created until the first breakage. Under the effect of any further increase of the worked-out area, the vertical stress at the face remains, practically, unchanged. The vertical section of the mining excavation can be replaced by an ellipse for the description of the stress in the roof until the first breakage. The reaction of the supports used in workings amounts to about 0.6 MPa. This is negligibly small compared with $H\gamma$ (5—10 MPa). For this reason, the excavation can be considered, from our point of view, as having no support. The tangential stress in the roof point of the excavation is

$$(\sigma_x)_R = \frac{H\gamma}{m - 1}\left(m - 2 - \frac{M}{l_x}\right) \tag{13}$$

where M denotes the height of the working and

l_x is the semi-width of the excavation.

If the tensile strength in the surrounding of the roof point is σ_z than an advance of

$$2\,l_0 = \frac{2\,M}{m - 2 - (m - 1)\,\dfrac{\sigma_z}{H\gamma}} \tag{14}$$

is required until the first breakage sets in. The tensile strength, in the majority of cases, is negligible compared with $H\gamma$, thus

$$2\,l_0 = \frac{2\,M}{m - 2}. \tag{15}$$

The vertical stress at the face cannot be described by means of the elliptic section because of the great difference in curvature. The working has to be regarded as a quadrangle, at the side-point of which, i.e. at the face there arises a stress

$$\sigma_z(x = 0) = H\gamma\left[\frac{m - 2}{m - 1} + f\left(\frac{2\,l_0}{M}\right)\right]. \tag{16}$$

For the roof $m = 2.5—4$, is, in general, characteristic which gives $2l_0/M = 2 - 4$. For this interval $f(2l_0/M) = 0.9—1.9$ is valid. In what follows, $f(2l_0/M) = 1.5$ will be assumed. Thus we have

$$\sigma_z\,(x=0) = H\gamma\left(\frac{m-2}{m-1}+1.5\right). \tag{17}$$

On the other hand

$$\sigma_z(x=0) = H\gamma\left(1+\frac{C}{m-1}\right). \tag{18}$$

From these two equations

$$C = 1.5\,m - 2.5. \tag{19}$$

Further, from the equilibrium

$$\int_{-\infty}^{+\infty} \Delta\,\sigma_z\,\mathrm{d}x = 0 \tag{20}$$

i.e.

$$\int_0^{\infty} \Delta\,\sigma_z\,\mathrm{d}x = C\frac{H\gamma}{m-1}\int_0^{\infty} e^{-\frac{2A}{M}x}\,\mathrm{d}x = \frac{C\,H\gamma}{m-1}\frac{M}{2A} = T \tag{21}$$

is a definite value. This equation is suitable to determine the connection between the parameters A and C. The sum of the total transferred vertical stress on the rock domain in front of the face and the total pressure on the goaf up to the semi-width of the worked-out area, should be equal to the weight of the prismatic rock body above the semi-widths of the worked-out area. The transfer of load is well characterized by the subsidence which can be seen even on the surface above the working. The ratio of the volumes of the subsidence trough and extracted mineral, is proportional to the pressure on the goaf. Since the area of the vertical section of the subsidence trough can be calculated as $Ms\,2l_x$ in case of a wholly worked-out area [5], the area corresponding to the extracted mineral is $M\,2l_x$. Thus, the sum of the vertical stresses transferred to one side, is proportional to $1 - s$, i.e.

$$T = (1-s)\,H\,\gamma\,l_x \tag{22}$$

where s denotes the subsidence factor ($s < 1$).

The semi-width of the total worked-out area is $l_x = 8\,H/k$ [5], and, in general, $k = 8$. Using this value

$$T = (1-s)\,H\,\gamma\,H\,. \tag{23}$$

The subsidence factor, usually is $s = 0.85$. Consequently

$$T = 0.15\,H\,\gamma\,H. \tag{24}$$

Since the semi-width of a working is essentially smaller than $H = 200-500$ m, the stresses transferred beside the working should also be taken into account. This means that the calculations should be carried out using one third of the aforementioned value of T, i.e. $T = 0.05\, H\, \gamma\, H$. Thus,

$$A = \frac{C\, H \gamma}{m-1} \frac{M}{2T} = \frac{10\, C}{m-1} \frac{M}{H}. \tag{25}$$

4. Specific volume change in the rock domain in front of the working

In the first part of this study it has been explained how important it is whether the specific volume change is an increase or decrease.

The specific volume change can be written as

$$\frac{\Delta V}{V} = \varepsilon_x + \varepsilon_y + \varepsilon_z \tag{26}$$

where ε_x, ε_y and ε_z denote deformations. $\Delta V/V < 0$ means volume reduction, $\Delta V/V > 0$ a volume increase. Among the deformations, $\varepsilon_y = 0$ because the state of deformation is planar. The deformational (induced) stresses are those which are correlated with the deformations. Using HOOKE's law

$$\varepsilon_x = \frac{1}{E}\left(\frac{m^2-1}{m^2}\Delta\sigma_x - \frac{m+1}{m^2}\Delta\sigma_z\right) \tag{27}$$

$$\varepsilon_y = 0 \tag{28}$$

$$\varepsilon_z = \frac{1}{E}\left(\frac{m^2-1}{m^2}\Delta\sigma_z - \frac{m+1}{m^2}\Delta\sigma_x\right). \tag{29}$$

Substituting $\Delta\sigma_2 = C\,\Delta\sigma_x$

$$\varepsilon_x = -\frac{\Delta\sigma_z}{E}\left(\frac{m^2-1}{m^2}\frac{1}{C} + \frac{m+1}{m^2}\right) \tag{30}$$

$$\varepsilon_z = \frac{\Delta\sigma_z}{E}\left(\frac{m^2-1}{m^2} + \frac{m+1}{m^2}\frac{1}{C}\right). \tag{31}$$

Thus, the specific volume change becomes

$$\frac{\Delta V}{V} = \frac{\Delta\sigma_z}{E}\frac{(m+1)(m-2)}{m^2}\frac{C-1}{C} = \frac{\Delta\sigma_z}{E}\frac{(m+1)(m-2)}{m^2}\frac{1.5\,m-3.5}{1.5\,m-2.5} \tag{32}$$

The specific volume change, $\Delta V/V$, is 0 if $m = 2.33$; it is a volume reduction if $m > 2.33$, while an increase if $m < 2.33$. This result immediately explains the fact that in certain areas no outburst occurs in workings while they occur in other areas. If the Poisson ratio for the coal layer is smaller than 2.33, the layer undergoes a volume increase due to the transferred pressure. In this case, no outburst can arise in workings. However, if the Poisson ratio for the coal layer is greater than 2.33, the volume change of the layer due to the transferred pressure is a reduction. Thus, one of the conditions for outburst is satisfied. If the other conditions are also met, the outburst sets in. The Poisson ratio is in correlation with the strength. In general rocks of great strength have great Poisson ratio. The Poisson ratio for rocks of extraordinary small strength is around 2. This explains the observation that no gas outbursts occur in workings carried out in layers of extraordinary small compressive strength.

Next, the mechanical state of the rock domain in front of the face will be investigated by taking into account the pore gas pressure p.

5. Stress of the rock domain in front of the working in the presence of pore gas pressure

If pore gas is present, the so-called effective stress (σ') in the solid rock structure and the pore gas pressure or neutral stress (p) have to be distinguished. The sum of these two stresses is called the total stress (σ_t).

Before opening excavations, the following stresses rise in the solid structure of the rock [3, 4]:

$$\bar{\sigma}'_z = H\gamma - p_0\,, \quad \bar{\sigma}'_x = \frac{\bar{\sigma}'_z}{m-1} = \frac{H\gamma - p_0}{m-1} \tag{33}$$

where p_0 denotes the pore gas pressure before opening the excavations. If excavations are opened in an intact area, p_0 equals the initial pore gas pressure. In case of rock pillars, p_0 is greater than the initial pore gas pressure.

The equilibrium of the volume element of thickness $\mathrm{d}x$ (Fig. 2) can be described in the rock domain investigated by the equation:

$$\Delta\sigma'_x M - [\Delta\sigma'_x + \mathrm{d}(\Delta\sigma'_x)]M + [\Delta p + \mathrm{d}(\Delta p)]M - \Delta p M + 2\tau'\mathrm{d}x = 0. \tag{34}$$

Hence:

$$\frac{\mathrm{d}(\Delta\sigma'_x)}{\mathrm{d}x} - \frac{\mathrm{d}(\Delta p)}{\mathrm{d}x} = \frac{2\tau'}{M}\,. \tag{35}$$

The change of pore gas pressure (Δp) due to opening excavations is approximately proportional to the specific change of volume of the rock. The specific change of volume, however, is linearly proportional to the horizontal deforma-

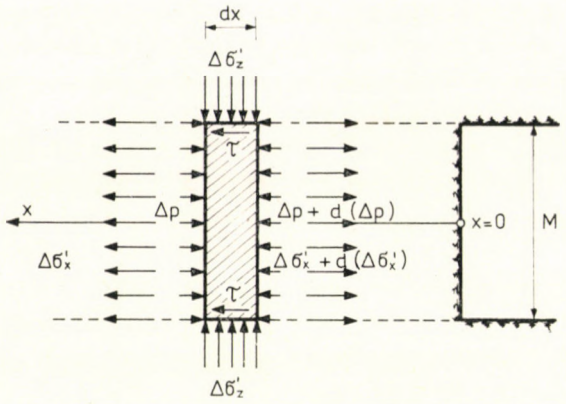

Fig. 2. Effective and neutral deformational stresses on a rock element of infinitesimal thickness in front of the working face

tional stress ($\Delta\sigma'_x$), for this reason the change of the pore gas pressure can be written as $\Delta p = -D\Delta\sigma'_x$. Substituting, we get the differential equation

$$(D+1)\frac{\mathrm{d}(\Delta\sigma'_x)}{\mathrm{d}x} = \frac{2\tau'}{M} \tag{36}$$

whose general solution is

$$\Delta\sigma'_x = F\, e^{-\frac{2A}{M(D+1)}x}. \tag{37}$$

For $x = 0$ we should have $\Delta\sigma'_x = \dfrac{H\gamma - p_0}{m-1}$, thus

$$F = -\frac{H\gamma - p_0}{m-1} \tag{38}$$

i.e.

$$\Delta\sigma'_x = -\frac{H\gamma - p_0}{m-1} e^{-\frac{2A}{M(D+1)}x}. \tag{39}$$

Consequently, the stresses in the solid structure of the rock can be written in the secondary state as

$$\sigma'_x = \frac{H\gamma - p_0}{m-1}\left(1 - e^{-\frac{2A}{M(D+1)}x}\right) \tag{40}$$

$$\tau' = A\frac{H\gamma - p_0}{m-1} e^{-\frac{2A}{M(D+1)}x} \tag{41}$$

$$\sigma'_z = (H\gamma - p_0)\left(1 + \frac{C}{m-1} e^{-\frac{2A}{M(D+1)}x}\right). \tag{42}$$

It should be noted that the values of parameters A and C are not affected by the pore gas pressure, they are the same as in the previous case.

The determination of parameter D requires special attention. The specific volume change in front of the face is

$$\frac{\Delta V}{V} = -\frac{\Delta \sigma_x'}{E}\frac{(m+1)(m-2)(1.5\,m-3.5)}{m^2} \tag{43}$$

The change of the pore gas pressure, expressed with the specific change of volume [4] is

$$\Delta p = p_0\left\{\left[\frac{e_0}{e_0 - \frac{\Delta V}{V}(1+e_0)}\right]^{\varkappa} - 1\right\}; \qquad \frac{\Delta V}{V} < \frac{e_0}{1+e_0} \tag{44}$$

where e_0 denotes the void ratio of the rock corresponding to the initial pore gas pressure (p_0) and $\varkappa$ is the polytropic exponent.
For methane $1 \leq \varkappa \leq 1.3$. The value $\varkappa = 1$ stands for isothermic change of state, i.e. for the case when the heat exchange is maximum for a constant temperature. If $\varkappa = 1.3$, the change of state is adiabatic, i.e. no heat exchange takes place but the change of temperature is maximum. Regarding the fact that $\varkappa$ varies within a very limited interval, it is of no decisive importance to which ideal change of state the actual polytropic change is nearer. It would be no major error if we used either $\varkappa = 1$ or $\varkappa = 1.3$ in the calculations.

If the specific volume change is small, the function $p(\Delta V/V)$ can be replaced by its tangent taken at $\Delta V/V = 0$. The equation of the tangent is

$$p = \varkappa p_0 \frac{1+e_0}{e_0}\frac{\Delta V}{V}; \qquad \frac{\Delta V}{V} < \frac{e_0}{e_0+1}. \tag{45}$$

Since the use of the tangent instead of the function means an approximation from below, we shall take $\varkappa = 1.3$ which gives an approximation from above. In this way the differences compensate each other to some extent. Eventually, the parameter to be determined becomes

$$D = 1.3\,p_0\frac{1+e_0}{e_0}\frac{(m+1)(m-2)(1.5\,m-3.5)}{E\,m^2}. \tag{46}$$

The equations show that the stress on the solid structure of the rock does not depend on the change of the pore gas pressure Δp, due to the effect of the excavation. The initial pore gas pressure (p_0) relieves the solid structure from load. The greater the pore gas pressure, the smaller becomes the stress in the solid

structure. This effect is advantageous from the point of view of deterioration, and explains the observation that in many cases layers with great pore gas pressure are not subject to outburst danger. It is also evident that the greater the initial pore gas pressure p_0, the greater is Δp. This fact has a very disadvantageous effect on rock strength. Correspondingly, the increase of the initial pore gas pressure reduces the load on the solid structure but also reduces the rock strength. The analysis of these two principal and controversial effects deserves a special treatment.

The variation of stresses will be illustrated by an example. Let $m = 4$, i.e. a value which can cause an outburst. In the calculations we shall use $B = 4$, $E = 400$ MPa and $e_0 = 0.05$, characteristic of stronger coals. Further, we assume $H = 400$ m, $\gamma = 25$ kN/m^3 and $M = 2.5$ m. In this case, the parameters become $C = 3.5$, $A = 0.073$, $D = 0.01\ p_0$ and $2\ A/M = 0.058$. The stresses and gas pressure can now be written as

$$\sigma'_x = \frac{100 - p_0}{3}\left(1 - e^{-\frac{0.058}{0.01\ p_0+1}\ x}\right) \tag{47}$$

$$\sigma'_z = (100 - p_0)\left(1 + 1.17\ e^{-\frac{0.058}{0.01\ p_0+1}\ x}\right) \tag{48}$$

$$\tau' = 0.058(100 - p_0)\ e^{-\frac{0.058}{(0.01\ p_0+1)}\ x} \tag{49}$$

$$p = p_0 - D\ \Delta\ \sigma'_x = p_0\left[1 + 0.01\frac{100 - p_0}{3}\ e^{-\frac{0.058}{(0.01\ p_0+1)}\ x}\right]. \tag{50}$$

The stresses are illustrated for $p_0 = 0$. 1 and 2 MPa in Fig. 3. It is seen that the shear stress (τ') is small, even at the working face, and it quickly diminishes with increasing distance from the face.

6. Deterioration of the rock domain in front of the working in the presence of pore gas pressure

In the presence of pore gas pressure the strength of the rock decreases. The equation of the linear fracture limit line is [3]:

$$\tau = \frac{\sigma_c}{2\sqrt{B}}\left[1 + \frac{B - 1}{\sigma_c}(\sigma_t - p)\right] \tag{51}$$

where σ_c denotes the uniaxial compressive strength measured without gas pressure and

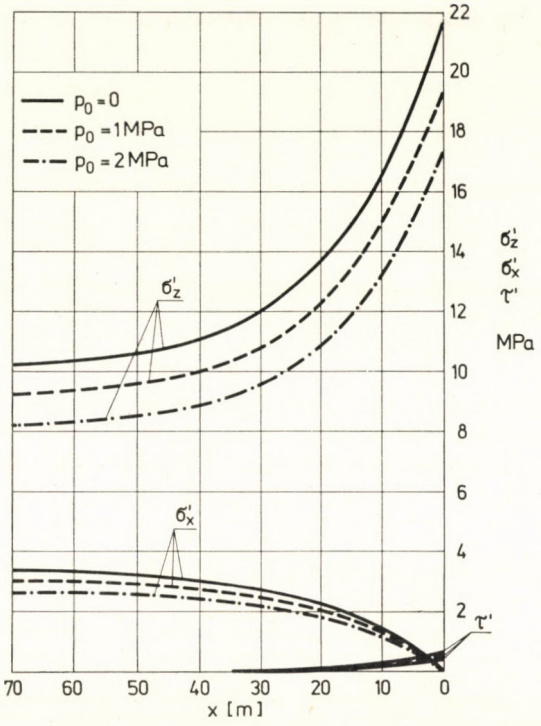

Fig. 3. Effective stresses in front of the working face

B is Brinke's number.
Brinke's number is defined as

$$B = \left| \frac{\sigma_c}{\sigma_T} \right| = \mathrm{tg}^2 \left(45° + \frac{\varphi}{2} \right) \tag{52}$$

where σ_T is the tensile strength and
φ the angle of internal friction.

Taking into account pore gas pressure, the uniaxial compressive strength becomes

$$\sigma'_c = \sigma_c - (B - 1)p. \tag{53}$$

The extremal principal stresses in the rock domain in front of the working face are

$$\sigma'_1 = \frac{\sigma'_x + \sigma'_z}{2} + \sqrt{\left(\frac{\sigma'_z - \sigma'_x}{2} \right)^2 + \tau'^2} \tag{54}$$

$$\sigma'_3 = \frac{\sigma'_x + \sigma'_z}{2} - \sqrt{\left(\frac{\sigma'_z - \sigma_x}{2} \right)^2 + \tau'^2} \,. \tag{55}$$

Assuming a straight line for the linear fracture limit curve, the condition of the occurrence of deterioration that the equation

$$\sigma_1' = \sigma_c' + B\,\sigma_3' = \sigma_c - (B-1)p + B\sigma_3' \tag{56}$$

should be satisfied, where $p = p_0 + \Delta p$. Keeping in mind that τ' is small even at the face and quickly diminishes, we can write

$$\sigma_z' = \sigma - (B-1)p + B\sigma_x'. \tag{57}$$

Further, D can be neglected beside the unity. Thus, the uniaxial compressive strength just required to prevent deterioration is

$$\sigma_{c\,\mathrm{req}} = (H\gamma - p_0)\left[\frac{e^{-\frac{2A}{M}x}}{m-1}(1.5\,m - 2.5 + B) + 1 - \frac{B}{m-1}\right] + (B-1)p_0 \tag{58}$$

where

$$\frac{2A}{M} = \frac{1.5\,m - 2.5}{0.05(m-1)\,H}. \tag{59}$$

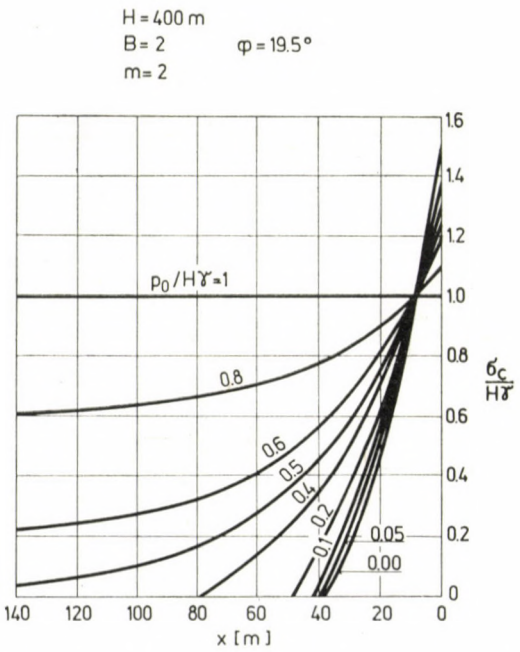

Fig. 4. Variation of the compressive strength required to avoid deterioration in front of the working face

Equation (58) shows that the greater $H\gamma$, the greater becomes the compressive strength which could prevent deterioration. This explains why the frequency of outburst increases with depth. The greater the required compressive strength to prevent deterioration, the more common it would be that this condition were not satisfied.

Figures 4—6 show the compressive strength required to prevent deterioration in front of the working face, as function of the pore gas pressure, Poisson ratio and BRINKE's number, respectively. It is seen from the figures that the compressive strength required to prevent deterioration quickly decreases to zero with the distance from the face, if the pore gas pressure is small. The zero value of the required compressive strength means that the internal friction alone is sufficient to prevent deterioration. If the pore gas pressure is greater, the compressive strength which prevents deterioration does not decrease to zero. Such cases are disadvantageous from the point of view of the outburst danger. With increasing Brinke's number and Poisson ratio, the coal strength, as a rule, also increases. The figures show that a greater compressive strength is required to prevent deterioration if the values B and m are great. So, nature

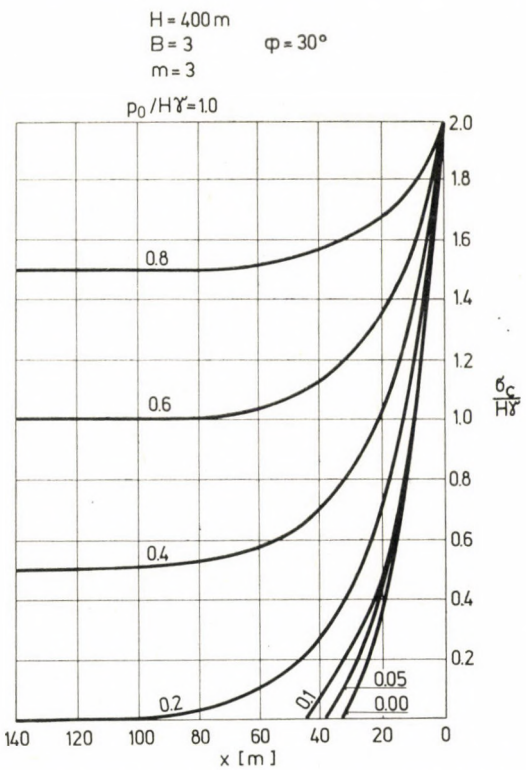

Fig. 5. Variation of the compressive strength required to avoid deterioration in front of the working face

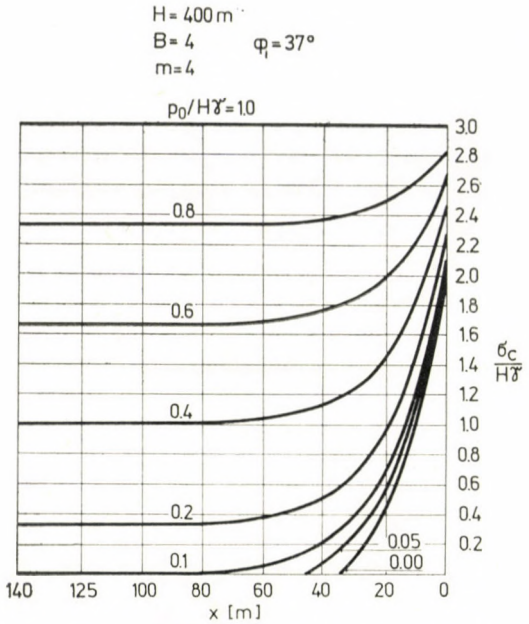

Fig. 6. Variation of the compressive strength required to avoid deterioration in front of the working face

reveals again a compensation phenomenon which can be observed so frequently.

If the compressive strength of the layer at or near the face is smaller than that required to prevent deterioration, a rock deterioration ensues in the area of the face. This, however, does not bring about outburst automatically because the pore gas and the evaporating adsorbed gas can leave the rock through the great surface of the face. So, the pore gas pressure has no possibility to increase. However, if the deterioration penetrates into great distances behind the face, in case of $m > 2.33$ the pore gas pressure has the possibility to increase. Thus, the deterioration process accelerates and an outburst comes about. The situation is especially dangerous if the coal strength decreases more quickly with the distance from the face than the compressive strength which would prevent the deterioration. These circumstances come about near fault zones. Here, rock deterioration ensues far from the face and pore gas pressure increases. The intact rock mass of the face prevents the gas from escaping and during advancing, gas pressure suddenly throws out the face from its place. This explains why the outbursts at fault zones are combined with such large mechanical effects.

It should be noted that pore gas pressure values greater than 0.4—0.5 $H\gamma$ among those of $p_0 = (0.0—1.0)H\gamma$ in Figs. 4—6, have no practical importance. Experience, namely, shows that pore gas pressure falls within the limits

0 and 5 MPa, in many cases even within 0.5 and 1 MPa. The figures are computed for a layer depth of $H = 400$ m where, in general, approximately $H\gamma = 10$ MPa. From Fig. 6 it can be read that at $p_0/H\gamma = 0.4$ i.e. at a pore gas pressure $p_0 = 4$ MPa, $\sigma_c/H\gamma = 1$ is valid even at great distance from the working face. This means that a compressive strength of $\sigma_c = 10$ MPa is required to prevent rock deterioration. In case of a greater angle of internal friction (BRINKE's number) and Poisson ratio, an even greater compressive strength is required to avoid deterioration. This explains how outburst can occur even in case of great layer strengths.

7. Conclusions

The results of the investigations carried out in this study are in concordance with the results of our previous investigations, and experience, as well. At the same time, further statements can be made about the cause of outbursts on the basis of our latest results.

No outburst can occur in wide-face workings if the Poisson ratio for the layer is approximately $m < 2.3$. Such is the case for extraordinarily small coal strengths. However, if the Poisson ratio is approximately $m > 2.3$, outbursts have exactly the same chance to come about in wide-face working as at drifting.

Outbursts can happen in workings if $\sigma_c < \sigma_{c\,\mathrm{req}}$ farther from the face. Such cases can be usually observed in or near the areas of fault zones.

Beside the pore gas pressure and the compressive strength, the danger of outburst is strongly affected by the Poisson ratio and the angle of internal friction (BRINKE's number) of the layer. In possession of these four data, the danger of outburst can be determined by means of the equations of Section 6.

For coals for which the angle of internal friction and the Poisson ratio is greater, a considerable compressive strength is required to avoid deterioration if pore gas is present. This explains the frequent outbursts even in layers of great compressive strength.

In the Pécs Coal Basin (Hungary) 99% of the outbursts happened in roadheads and not in workings. This is due to the fact that the layers are disturbed, their strength and Poisson ratio are extraordinarily small. Consequently, a specific volume increase ensues in front of the working face which does not increase the pore gas pressure, so the rock deterioration does not take place explosion-like.

REFERENCES

1. SZIRTES, L.: Combat of Coal and Gas Outbursts. Műszaki Könyvkiadó. Budapest. 1971.
2. KOVÁCS, F.: Connection between the gas content and strength of rocks exposed to gas outburst danger. *Acta Geod. Geoph. Mont. Hung.* , 16 (1981), 115—130.
3. SOMOSVÁRI, ZS.: Investigation of the deterioration of the rock-gas system to clarify the cause of rock and gas outbursts. *Acta Geod. Geoph. Mont. Hung.*, 15 (1980), 257—269.

4. Somosvári, Zs.: Investigation into the loading of multicomponent rock-gas systems to determine the cause of rock and gas outbursts. *Acta Geod. Geoph. Mont. Hung.*, 15 (1980), 271—294.
5. Somosvári, Zs.: Determination of the Displacement Field of Pseudohorizontal Overburden Layers Above Workings. Ph. D. Thesis. Miskolc. 1973.

ИССЛЕДОВАНИЕ ОБЛАСТИ ПЕРЕД ЛИНИЕЙ ОЧИСТНЫХ ЗАБОЕВ В СИСТЕМЕ ПОРОДА-ГАЗ ДЛЯ ВЫЯСНЕНИЯ ПРИЧИН ВЫБРОСОВ ГАЗА И ПОРОДЫ

Ж. ШОМОШВАРИ

РЕЗЮМЕ

На основании исследований взаимодействий системы порода-газ покажем, что при забоях в таких случаях, когда число Пуассона для залежа мало, его значение близко к двум, выброс породы и газа невозможен потому, что не выполняется основное условие выброса, установленного нами раньше, — что перед линией очистних забоев должно произойти уменьшение объёма породы.

Этот результат объясняет тот общеизвестный эмпирический факт, что при чрезвычайно маленьких прочностях угля выбросы концентрируются на прохождение выработок и только при больших прочностях угля и вместе с этим при больших числах Пуассона происходят и в отбое.

Покажем, что вероятность выброса решающим образом определяется оригинальным давлением газа пор, вертикальным первичным напряжением ($H\gamma$), числом Пуассона, углом внутреннего трения, прочностью на сжатие залежи.

Выводим формулу, которой в зависимости от упомянутых существенных параметров определяется прочность залежи (однонаправленная прочность на сжатие), необходимая во избежании выброса. Это соотношение, между прочим, объясняет тот опытный факт, что частость выбросов растет с глубиной, кроме того в некоторых случаях выбросы происходят и при совсем малых давлениях газа пор (3—4 кр/см^2), а в других случаях и при более больших давлениях газа пор выбросы не происходят.

Вышеупомянутая зависимость объясняет и тот опытный факт, что выбросы обычно происходят в залежах с маленькими прочностями, в тоже время в некоторых случаях могут произойти и в залежах с большими прочностями. Полученные результаты снова подтверждают наши предыдущие выводы, что выброс является ничем иным, как внезапным взрывообразным процессом разрушения системы порода-газ, несущая нагрузку катализированным давлением газа пор. Основной причиной выбросов является влияние давления газа пор на прочность, которое при разрушении вызывает процесс подобно цепной реакции. Этот процесс ускоряет разрушение, делает его взрывообразным. В тоже время нагрузка с твердой каркасной структурой внезапно возлагается на давление газа пор, возникает большое давление газа, которое бросает твердую фазу в свободное пространство, причем взрывообразно огромное количество газа течет в выработанное пространство ввиду того, что из-за уменьшения давления газа большая часть связанной (адсорбированной) фазы газа выделяется.

Acta Geodaet., Geophys. et Montanist. Acad. Sci. Hung. Tomus 16 (1), pp. 151—160 (1981)

PROCESS CONTROL SYSTEM WITH FEEDFORWARD FOR GRINDING-SEPARATING CYCLES

SZ. PETHŐ

TECHNICAL UNIVERSITY OF HEAVY INDUSTRY, MISKOLC

[Manuscript received February 2, 1979]

The study deals with a computer process control system ensuring a feedforward for the pneumatic separator. At the same time, it reduces the time loss of the mill to minimum. This makes prossible for the product to have a constant and prescribed quality as well as maximum mass, even in case of changing grindability.

1. Introduction

The control task for ball mills with a closed cycle can be as follows [1, 2]: "A product of prescribed particle-size distribution and minimum cost has to be produced so as to gain maximum product output." This maximum amount can vary first of all because of the grindability of the material. That is why the authors of the quoted studies suggest an adaptive optimum control. They give a rather general flowsheet for the optimum control of the mill. At the same time, however, they do not exclude the possibility of other solutions (1).

2. Principal scheme of the process control system

Figure 1 illustrates schematically the optimum control enabling quantitative and qualitative steering. A feeder belt to measure and transport fresh feed R is required. Mass M of the product leaving the mill is measured by recording belt scales. Then, the product is sampled and the samples are continuously analyzed by a particle-size analyzer. At the 1975 Nuremberg Congress on Particle Size Analysis, a device was introduced which was capable to produce various fractions [5]. The particle size distribution and mass of the mill product and the quality specifications for the end-product (e.g. the mass fraction coarser than a given particle size) form the input data for the process control computer.

Another input signal is the mill characteristics as shown in Fig. 2. This mill characteristics differs to some extent from those in studies [1] and [2], but it can be derived from them. In the studies cited, the endproduct which

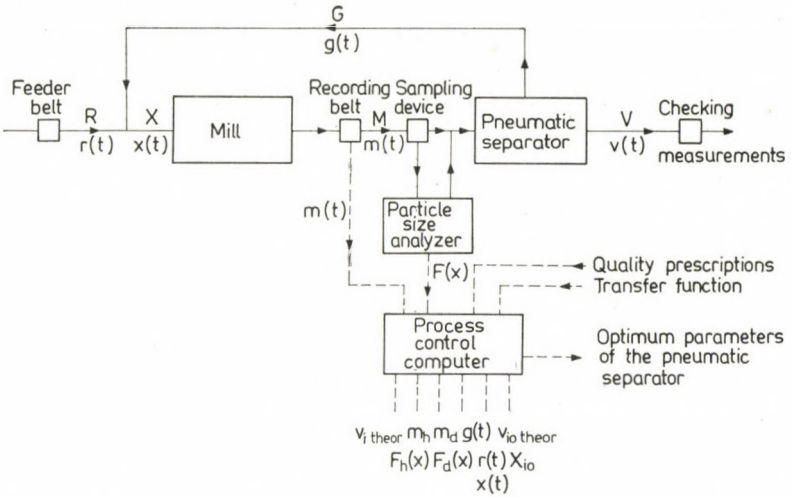

Fig. 1. Principal scheme of a process control system with feedforward

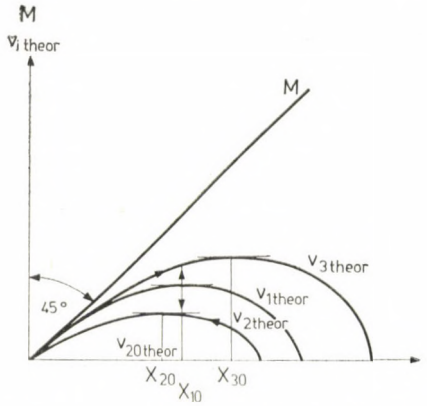

Fig. 2. Mill characteristics mass $V_{i,\,\text{theor}}$ of the end-product versus mass X_i of the material fed into the mill

can actually be separated by a pneumatic separator has been illustrated as a function of mill feed X. The mill characteristics suggested here enables us to determine the variation of the endproduct $V_{i,\,\text{theor}}$ $(i = 1, 2, \ldots, n)$, to be obtained by a perfect separation, *versus* mill feed X.

A pneumatic separator with changeable parameter operates inside the system. The parameter which can be changed in modern pneumatic separators during operation is the revolution per minute. If the particle size distribution of the product, however, changes permanently, the number of blades can also be changed. It is a rather essential criterium for the design of an optimum control system that we have to know the partition curve for the various operational parameters of the separator.

The partition curves furnish the transfer function of the pneumatic separator and form a further input signal for the process control computer.

The process control computer supplies the following "service":

It determines and sums for any given period (e.g. shifts, days etc.) the mass and particle size distribution of the product and masses $V_{i,\ \mathrm{theor}}$ and $V_{i0,\ \mathrm{theor}}$, respectively. The latter masses mean the "useful material" actually present in the product and its maximum (see Fig. 2), i.e. the product finer than a given particle size.

The computer calculates the results of the pneumatic separation for all parameter values of the pneumatic separator using the recovery values of the partition curve and the particle size distribution of the product [3]. The computed results are the masses of the end-product and the circulating duff (or the number of cycles) and their particle size distributions. From among these processes the computer selects the particular separation which can produce the end-product of prescribed quality in the greatest possible amount (i.e. with the smallest possible number of cycles). Its mass and particle size distribution are summed and averaged, respectively. If needed, the expected specific surface of the end-product is calculated, as well.

The computer selects those parameters of the pneumatic separator (e.g. the number of revolutions) which ensure the optimum separation. The mass G and the particle size distribution of the duff product at the optimum separation are calculated. From the difference $X - G$ the mass of fresh feed R is also determined ($R = X - G$), this will be the input signal for the feeder belt shown in Fig. 1.

The process control carried out as suggested above has the following advantages.

1. The end-product can be produced so as to ensure a prescribed and constant quality and maximum mass even in case of changing grindability.

2. By a weighing the product, continuously determining its particle size distribution and, also knowing the mill characteristics, the grindability function of the material becomes known within the shortest possible time. Thus the optimum mill feed X_{i0} can be adjusted within a minimal time loss (Fig. 2).

3. The optimum control of the pneumatic separator is carried out by means of the so-called feedforward. This requires in the present case the knowledge of the particle size distribution of the raw material and the transfer function of the pneumatic separator. (The algorithm of the calculation will be presented later in this paper.) In case of feedforward there is no time loss: the pneumatic separator operating at the optimum parameters "expects" the material with the altered particle size distribution. The quality prescriptions can always be fulfilled accurately, unlike in case of feedback. The possible minimum amount of fine product is in circulation, consequently, the processing capacity of the system can be further increased.

3. Practical solution of the process control

Systematical experiments have been carried out on a WEDAG pneumatic separator at the Department of Mineral Dressing, Technical University of Heavy Industry. The cross-section of the classifying chamber of the pneumatic separator was 0.07 m^2. It can be operated at 2300, 2000, 1700, 1500 and 1100 r.p.m. and either without any or with 2, 3 and 6 blades. The blades can be radial or backwards arched at an angle of 15°, 30°, 45°, 60°, 70° or 90°. As a result of experiments clinker sorts of several Hungarian cement factories have been classified with most of the above parameters. Since the particle size distributions of the products of the pneumatic separator have also been determined, the partition curves could have been established.

3.1 *Transfer function of the pneumatic separator and quality prescriptions for the end-product*

Table I contains the transfer function of the pneumatic separator, i.e. the parameters and the corresponding partition curves which can arise in case of clinker classification. Fractions indicate the various parameter values (e.g. 2300/2) the numerator giving the revolutions per minute, the denominator for the radial blade number. No other parameter values are included in the Table since they cannot be taken into consideration for clinker classification because of the low separation particle size. Backwards arching blades have hardly any effect on the partition curve as compared with the radial ones. That is why these parameter values are not contained in the Table, either. The last two rows of the Table give two characteristic numbers for the partition curves. $M(\bar{X})$ is the expected value of the equalizing parameter. This gives the parameter of the separation. The ratio $M(F)/M(\bar{X})$ characterizes the *sharpness* of the separation. Table II makes clear the calculation of these two numbers by the example of the partition curve values for the parameter 1100/0 [4], while Fig. 3 helps in the interpretation. The equalizing parameter ensures the construction of a partition curve with a perfect separation, the area under which would be equal to that under the actual partition curve. The horizontal side of the partition curve with a perfect separation gives $M(\bar{X})$. Between the two functions two error areas $M(F)$ of the same size can be obtained. The ratio $M(F)/M(\bar{X})$, i.e. that of the error area to the area under the partition curve, characterizes the sharpness of separation.

With the aid of the above explanation the calculation methods illustrated in Table II should be easy to follow [4]. First, particle size intervals Δx are formed, which are multiplied with the recovery values. Their sum gives the value $M(\bar{X})$. In order to calculate the error areas, $M(\bar{X})$ is taken for one of the

Table I

Transfer Function and Separation Numbers of the Pneumatic Separator

Particle Size μm	Recoveries				
	2300/0	2000/0	1500/0	1100/0	2300/2
<63	0.82335	0.80962	0.79906	0.65110	0.64565
63—90	0.57906	0.53965	0.53586	0.23414	0.14735
90—160	0.40726	0.33957	0.31900	0.07449	0.02569
160—200	0.26572	0.19741	0.16718	0.02102	0.00882
200—315	0.18738	0.13598	0.08356	0.00900	0.00310
315—500	0.08850	0.08861	0.04691	0	0
500 <	0.03915	0.03629	0	0	0
$M(\bar{X})$	148.48	132.90	112.11	54.43	47.16
$M(F)/M(\bar{X})$	0.6467	0.3970	0.3590	0.3489	0.3543

Particle Size μm	Recoveries			
	2000/2	1500/2	2300/3	2300/6
<63	0.61526	0.56173	0.54949	0.53264
63—90	0.08974	0.06032	0.06989	0.01450
90—160	0.01826	0.00164	0.01596	0.00342
160—200	0.00434	0.00134	0.01323	0.00189
200—315	0.00122	0.00086	0.00206	0.00100
315—500	0	0	0	0
500 <	0	0	0	0
$M(\bar{X})$	42.78	37.49	38.78	34.37
$M(F)/M(\bar{X})$	0.3848	0.4383	0.4505	0.4674

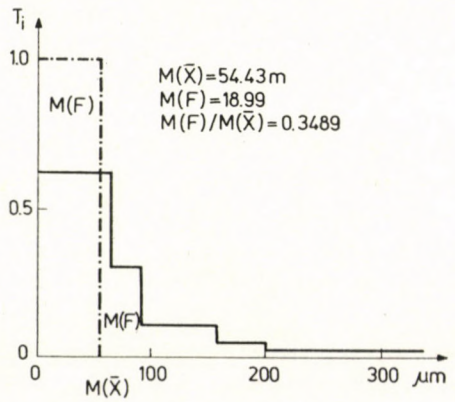

Fig. 3. Partition curve of the pneumatic separator

Table II

Calculation Method of the Numbers of the Partition Curve 1100/0

Particle size μm	Recovery T_i	Particle size interval Δx_i	$T_i \Delta x_i$
<63	0.65110	63	41.0193
63—90	0.23414	27	6.3218
90—160	0.07449	70	5.2143
160—200	0.02102	40	0.8408
200—315	0.00900	115	1.0350
			$M(\bar{X}) = 54.4312$

Particle size μm	$1 - T_i$	T_i	Δx_i	$(1 - T_i)\Delta x_i$	$T_i \Delta x_i$
<54.43			54.43		
54.43—63	0.34890	0.65110	8.57	18.9906	5.5799
69—90		0.23414	27		6.3218
90—160		0.07449	70		5.2143
160—200		0.02102	40		0.8408
200—315		0.00900	115		1.0350
				$M(F) = 18.9906$	$M(F) = 18.9918$

particle size limits. The transfer function together with the quality prescription form input signals for the process control computer. Let the following prescription be valid for the composition of the end-product: the ratio of the particles coarser than 90 μm should not exceed 7% and the recovery of the particles smaller than 90 μm in the fine product be as high as possible.

3.2 *Determination of the particle size distribution of the product and the value* $V_{i,\,\mathrm{theor}}$ *of the mill characteristics*

Let us now assume that three different particle size distributions have been established by an on-line particle size analyzer under steady conditions. They are denoted by A, B and C in Table III. Relying upon the quality prescriptions the mass fraction finer than 90 μm is considered as the useful part of the product. The mass contents finer than 90 μm are in the three products 59.06; 48.56 and 81.89%, respectively. These contents represent various grindability and multiplying them with mass M of the product yields the points $V_{i,\,\mathrm{theor}}$ of the mill characteristics (in this case $V_{1,\,\mathrm{theor}} = 0.5906$ M, $V_{2,\,\mathrm{theor}} = 0.4856$ M and $V_{3,\,\mathrm{theor}} = 0.8189$ M).

Table III

Particle Size Distributions of Three Clinker Products (A, B and C)

Particle size μm	*A*	*B*	*C*
	Δm, %	Δm, %	Δm %
1	2	3	4
<63	46.98	38.95	61.14
63—90	12.08	9.61	20.75
90—160	18.13	23.15	9.17
160—200	6.98	5.87	3.35
200—315	8.62	15.84	3.04
315—500	5.28	3.73	1.51
500<	1.93	2.85	1.04
	100.00	100.00	100.00

3.3 *Calculation of the expected results of the pneumatic separation and selection of the most suitable alternative*

The computer calculates the expected results of the separation for all parameter values of the pneumatic separator, making use of the transfer function and the particle size distribution of the product [3]. The separation results of product A are contained in Table IV, for the 1100 r.p.m. and no blade case. Multiplying the direct mass fractions and the recoveries one gets the so-called reduced mass fractions Δm_{red} of the fine product, while the multiplication of the mass fractions with the complementary recoveries yield Δm_{red} of the coarse product. The respective sums represent the mass recoveries m_h and m_d of the fine and coarse product, their sum adds up to 100%. The direct distribution values Δm and the cumulative ones $F_h(x)$ and $F_m(x)$ can also be found in the Table. The last column gives the number of cycles $100/m_h$ (2.86), the mass fraction coarser than 90 μm in the end-product 4.50% and the recovery of the particles smaller than 90 μm in the fine product 0.6811. The specific surface of the fine product can also be calculated from the results of the particle size analysis [5].

Table V helps in the selection of the most appropriate alternative. Here, the principal parameters of the pneumatic separation are illustrated for seven parameter values of the pneumatic separator (the values 2300/3 and 2300/6 are not included, in contradiction with Table I) and for all three particle size distributions. The principal parameters are as follows: mass recovery m_h, the number of cycles $100/m_h$, mass fraction $100 - F_h(90)$ of the particles coarser than 90 m in the end-product and the recovery k (90) of the particles smaller than 90 μm.

Table IV

Calculation of the Expected Values of the Pneumatic Separation

Particle size μm	Product A Δm, %	Recoveries (1100/0)	Fine product		
			Δm_{red}	Δm	$F_h(x)$
<63	46.98	0.65110	30.589	87.42	87.42
63—90	12.08	0.23414	2.828	8.08	95.50
90—160	18.13	0.07449	1.349	3.86	99.36
160—200	6.98	0.02102	0.147	0.42	99.78
200—315	8.62	0.00900	0.078	0.22	100.00
315—500	5.28	0	0	0	
500<	1.93	0	0	0	
	100.00		$m_h = 34.991$	100.00	

Particle size μm	Coarse product			Some parameters
	Δm_{red}	Δm	$F_m(x)$	
<63	16.391	25.22	25.22	$\frac{100}{34.991} = 2.86 = 100/m_h$
63—90	9.252	14.23	39.45	
90—160	16.781	25.81	65.26	$100 - 95.50 = 4.5 = 100 - F_h(90)$
160—200	6.833	10.51	75.77	$\frac{30.589 + 2.828}{46.98 + 12.08} = 0.6811$
200—315	8.542	13.14	88.91	
315—500	5.280	8.12	97.03	
500<	1.930	2.97	100.00	
	$m_d = 65.009$	100.00		

The calculation of these parameters can be carried out by the method illustrated in Table IV.

The process control computer calculates the differences between the prescription for the mass fraction of the part coarser than 90 μm (in this case 7%) and 100 — F_h (90). It choses that particular parameter value which keeps the difference with positive sign at minimum or at zero. If identical differences are obtained the computer choses that parameter value which ensures maximum recovery for the part finer than 90 μm in the end-product.

This solution ensures the fulfilment of the purpose outlined in the Introduction. The pneumatic separator can be operated at the parameter value ensuring the most effective separation even in case of changing particle size distribution of the product. By the time the product with the altered particle size distribution gets to the pneumatic separator, the new parameter will

Table V

Principal Parameters of the Pneumatic Separation for Various Revolution Numbers

Sample and separation parameters	2300/0	2000/0	1500/0	1100/0
	m_h	57.07	53.80	51.93	34.99
A	$100/m_h$	1.75	1.86	1.93	2.86
	$100-F_h(90)$	19.97	17.18	15.25	4.50
	$k(90)$	0.7734	0.7544	0.7452	0.6811
	m_h	52.04	48.33	46.14	29.60
B	$100/m_h$	1.92	2.07	2.17	3.38
	$100-F_h(90)$	27.67	24.02	21.38	6.72
	$k(90)$	0.7752	0.7562	0.7470	0.5686
	m_h	67.73	65.06	63.78	45.45
C	$100/m_h$	1.48	1.54	1.57	2.20
	$100-F_h(90)$	7.92	6.71	5.98	1.72
	$k(90)$	0.7614	0.7412	0.7324	0.5454

Sample and separation parameters	2300/2	2000/2	1500/2
	m_h	32.67	30.36	27.17
A	$100/m_h$	3.06	3.29	3.68
	$100-F_h(90)$	1.70	1.23	0.17
	$k(90)$	0.5437	0.5078	0.4592
	m_h	27.26	25.29	22.52
B	$100/m_h$	3.67	3.95	4.44
	$100-F_h(90)$	2.55	1.84	0.27
	$k(90)$	0.5470	0.5112	0.4625
	m_h	42.81	39.67	35.62
C	$100/m_h$	2.34	2.52	2.81
	$100-F_h(90)$	0.65	0.47	0.06
	$k(90)$	0.5194	0.4821	0.4347

already have been adjusted. — According to Table V the separation of material A is the most effective without blades and at 1100 r.p.m. The discussed difference is now $7-4.5 = 3.5\%$, recovery becomes 0.6811. Material C is best sepa-

rated at 2000 r.p.m., without blades. In this case the mass fraction of the clinker coarser than 90 μm amounts to 6.71%, recovery being 0.7412. The most suitable separation parameters are specially marked in the Table.

According to the suggested solution the computer calculates the absolute mass of the duff led back to the mill with the equation $G = m_d M$. If a material with constant mass is fed to the system the mass of fresh feed can also be calculated with the correlation $R = X - G$.

In order to keep the system at its optimum the previous knowledge of the mill characteristics is required. It should, however, be noted that the adjustment of X_{i0} and $V_{i0,\,\mathrm{theor}}$ is made in the direction of the arrows and the control of the pneumatic separator is carried out so as to take account of these values.

4. Consequences

For the sake of the process control the transfer functions of the pneumatic separators applied in the industry have to be established by means of representative measurements. The stability of these functions should be made sure. The continuous analysis of the particle size distribution [7] is to be developed for various particle size fractions. The mill characteristics is proposed to be formed as outlined in the study. It has to be checked continuously during operation.

REFERENCES

1. Hilger, M.—Kolostori, J.: A comparative analysis of control systems used for ball mills with closed circulation. *Építőanyag*, 28 (1976), 437—440.
2. Csáki, F.—Kis, P.—Hilger, M.—Reviczky, L.—Kolostori, J.: A solution for maximum-minimum-control of closed-looped mills. *Mérés és automatika*, 25 (1977), 10—13.
3. Pethő, Sz.: On the computer control of the gravitational separation. Technical Economical Publications of the Tatabánya Coal Mines. *Tatabányai Szénbányák Műszaki-Közgazdasági Közleményei*, 1975, 45—50.
4. Pethő, Sz.—Tompos, E.: On the transfer function and new numbers of the classification. *Építőanyag*, 27 (1975), 241—247.
5. Metzger, K. L.—Leschonski, K.: Investigation of a cross-stream separator for on-line particle size analysis. 1st European Congress on Particle Size Analysis, Nuremberg. 1975, 77—94.
6. Pethő, Sz.—Schultz, Gy.—Tompos, E.: Particle size measurement, comminution and classification in the glass industry. Manuscript. 1977.
7. Pethő, Sz.—Schultz, Gy.: Investigation of the continuous particle size measurement. Zement-Kalk-Gips, 1974, 75—85.

СИСТЕМА УПРАВЛЕНИЯ ДРОБИЛЬНОГО СЕПАРАТОРА С ЗАМКНУТОЙ ЦИРКУЛЯЦИЕЙ

С. ПЕТЁ

РЕЗЮМЕ

В работе можно познакомиться с такой системой программного управления, которая осуществляет «обратную связь» воздушного сепаратора, а по отношению мельницы уменьшает до минимума мёртвое время. Это делает возможным и в вслучае переменной размолоспособности обеспечение максимальной массы продукта постоянного и предписанного качества.

Acta Geodaet., Geophys. et Montanist. Acad. Sci. Hung. Tomus 16 (1), pp. 161—166 (1981)

RECENSIONES

Hamid N. Al-Sadi

SEISMIC EXPLORATION (TECHNIQUE AND PROCESSING)
LMW/A 7, ASTRONOMISCH-GEOPHYSIKALISCHE REIHE, BD. 7

Birkhäuser, Basel—Boston—Stuttgart 1979, 220 pages, sFr. 49.—

This book is a comprehensive, relatively short and up-to-date review of the physics and mathematics involved in seismic exploration. The text is very clearly written, all important information is given and nothing of importance for the understanding is omitted. It is therefore well suited both as a textbook for students and as a handbook for anybody dealing with seismic exploration in practice.

Chapter 1 of the book deals with the theory of wave motion, propagation of waves and influences of the media traversed. Chapter 2 is devoted to seismic waves, their types and propagation. Chapters 3 and 4 offer the mathematical background of the seismic processing methods, both in time and frequency domain. This part can be even used in non-seismic problems, due to its excellent presentation. Chapter 3, Time series analysis, is divided into parts on digital functions, time-domain processes and filtering, Chapter 4, Spectral analysis, into a short historical review, spectral analysis of periodic functions, spectral analysis of transient functions and basic theorems for the Fourier-transform. Chapters 5 and 6 deal with seismic prospecting in a strict sense, giving descriptions on seismic methods, reflection field technique, and detection and recording of seismic signals. Chapter 6 discusses digital processing of reflection data, including digital processing technique, data reduction and stacking, signal resolution, determination of processing parameters, interpretation processing and a processing example. This example illustrates the effect of different processing manipulations.

The book is a welcome addition to the library of all exploration geophysicists.

J. Verő

TIDAL FRICTION AND THE EARTH'S ROTATION

Editor: *P. Brosche, J. Sündermann*

Springer, Berlin, Heidelberg, New York 1978, 252 pages, 81 figs, DM 48.—

It is quite unusual that the editor should passionately praise the topic of his book as here is the case: "Tidal friction and the Earth's rotation ... is one of the most fascinating books — not merely chapters! — of the modern history of science". I think that this is nevertheless no exaggeration as the book is also in the real sense of the word fascinating. It is a collection of papers presented by representants of different disciplines at a meeting hold in 1977 at Bielefeld.

The papers can be grouped below the following headings:

1. Did tidal friction cause measurable changes in historical times?
2. What is the importance of the tides of the solid Earth in comparison to those of the oceans?
3. Does any reliable computation exist about tidal friction for the system Earth-Moon?

The first paper by T. R. STEVENSON reviews the results of pre-telescopic astronomical observations. From an analysis of total and near-total solar eclipses he concludes that the lunar acceleration $\dot{n}$ measured in ephemeris time (ET) remained practically constant in the last three thousand years.

In the second paper L. V. MERRISON deals with tidal deceleration of the Earth's rotation from the results of astronomical observations in the period A. D. 1600 to the present. Due to tidal friction the rotation velocity of the Earth decreases and the Moon's orbit expands. The orbital velocity of the latter decreases, but its orbital angular momentum increases so that the rotational angular momentum due to the Earth's rotation decreases in favour of the orbital angular momentum. This decrease cannot be found in astronomical measurements over the past three centuries as the fluctuations due to the transfer of angular momentum between the core and mantle cause greater effects in a somewhat shorter period range. The decrease of the Earth's rotation velocity can be obtained, however, from measurements of the decrease of the Moon's angular velocity using telescopic observations over the past three centuries. The velocity decrease of the Moon is from data observed since 1600 according to the author:

$$\dot{n} = -26 \pm 2''/\text{century}^2$$

and the change of the rotational velocity:

$$\dot{w}/w = -29 \pm 2 \cdot 10^{-3}/\text{century}$$

where w denotes the Earth's angular velocity.

The third paper (H. ENSLIN) is devoted to the present determination of the Earth's rotation. The determination of the Earth's rotation includes the determination of the Earth's rotation with respect to a celestial frame of reference, further the determination of the position of the rotation axis with respect to the Earth's crust — i.e. the determination of Universal Time (UT) and polar motion. This can be realized only in an international cooperation supervised by the Bureau International de l'Heure (BIH) in Paris and by the International Polar Motion Service (IPMS) in Mizusawa. The paper describes phenomena connected to these fields. It reviews such notions as equatorial system, astronomical longitude and latitude, different time scales (astronomical time, atomic time). Observational aids and methods are also reviewed (optical measurements, Doppler satellite observations). Then the work done in the mentioned centres (BIH, IPMS) is dealt with and some illustrative figures offered for the changes of the days' length and for the polar motion in recent years.

O. CALAME and J. D. MULHOLLAND investigate in the fourth paper the tidal effect on the basis of laser and distance measurements. They summarize the tidal phenomenon and point out possible consequences: change of the length of the day and of the angular position and geocentric distance of the Moon. Modern techniques, as e.g. Doppler measurements, VLBI and laser ranging have several consequences. The latter is discussed in more details. At present there are 5 laser refractors on the Moon (3 American, 2 Soviet ones). From a 7 years measurement series, about two thousand reliable values are available with a typical accuracy of 15 cm, but the best measurements have an accuracy of 5 cm. The determination of the lunar acceleration from measurement data is discussed, the difficulties of interpretation are summarized.

The author of the fifth paper is M. BONATZ. He discusses the tides of the solid Earth from gravimetric measurements. His paper is based on the material of the 8th International Symposium on Earth Tides held 1977 in Bonn and summarizes the most recent results presented there. After a short review of the static tidal theory, actual problems of the terrestrial tidal research are treated. These are the following: present theoretical models do not consider inhomogeneities, the measurements are influenced by unknown local and secondary effects, further by the effects of the oceans. The author hints at a recommendation of the mentioned symposium which emphasizes the necessity of a study of these problems.

J. ZSCHAU's paper is a detailed, comprehensive review of the phenomenon of tidal friction. It is outstanding not only due to its length, but it can be recommended to everybody interested in tidal friction not only on the level of a phenomenon. The dissipation energy in the tidal friction is discussed, both for the tides of the solid Earth and for that of the oceans. The text is illustrated by numerical computations and measurement results.

The seventh paper (K. LAMBECK) considers tidal dissipation in the oceans. It concludes that the greatest part of the tidal energy is dissipated in the oceans, but the dissipation mechanism is at present unknown.

W. ZAHEL's eighth paper investigates the effect of the deformation of the solid Earth by diurnal and semidiurnal oceanic tides. This is even now an open question, and ZAHEL gives a correct review on our present knowledge. Computations are made using a $4° \times 4°$ net presented by the author in 1970. The result of computations for the M_2 and K_1 waves are presented. The results obtained in the $4° \times 4°$ net are more correct with consideration of the tide of the solid Earth than without it, but worse than those obtained in the $1° \times 1°$ net without solid Earth tides.

In the ninth paper, J. SÜNDERMANN and P. BROSCHE analyze numerical computations of tidal friction for ancient and present oceans. Hydrodynamical equations and numerical models for the problem are presented. Both application to present oceans and to ancient ones are treated. The authors suggest that such computations may solve the contradiction between computations of the changes of the rotational energy and measured values.

K. LAMBACH deals in the tenth paper with the paleorotation of the Earth. In the framework of this, conclusions are drawn from ancient organic material about the rotation of the Earth. Bivalves, corals and stromatolites enable conclusions on three periodicities:

1. the number of days per year,
2. the number of days per synodic month,
3. the number of synodic months per year.

The three types of fossiles are treated at first separately, then combined results are presented.

The length of the day and month is discussed by C. T. SCRUTTON in the eleventh paper by considering fossile growth features. The author gives a detailed analysis of bivalve, coral and stromatolite growth features, their investigation methods and the data obtained. The following conclusions are drawn:

1. The Moon has been in orbit around the Earth for the last 3000 million years at least.
2. There has been a gradual decrease in the number of days per year during the Phanerozoic and probably before.
3. There has been also a gradual decrease in the number of days per lunar month in the same time, but the number of lunar months per year remained constant.
4. The decrease of the rotation rate of the Earth support the hypothesis of tidal friction.

In the last paper, J. D. A. PIPER outlines a magnific panorama on dynamics and hydrosphere of Precambrian continents on the basis of geological and geophysical data.

In conclusion this short summary will perhaps evoke the reader's interest for this really exciting book.

G. Bartha

TERRESTRIAL HEAT FLOW IN EUROPE

Editor: *V. Čermak* and *L. Rybach*

Springer Verlag, Berlin—Heidelberg—New York, 1979. 151 figs, 47 tab., 1 twelve-color map. VIII, 328 p. Cloth DM 89, U.S. $ 49

This book is the result of an international cooperation in the framework of the Inter-Union Commission of Geodynamics to construct a 1 : 5 000 000 heat flow map of the continent. In the last decade the number of heat flow measurements increased considerably. The book contains some 3000 heat flow data from Europe and from the surrounding marine areas. It is a great merit of the editor that they brought together this vast amount of data and succeeded in constructing a heat flow map of Europe with considerable details. The coverage is naturally changing, there are regions where practically no data exist, while in other cases the strong local changes cause greater problems. In any case the book and the included map is a welcome addition to earlier heat flow reviews with a significantly increased amount of data.

The first part of the book contains 11 papers on general problems. Roughly the half refers closely to the map, describing or supplementing it, drawing conclusions from comparisons between the heat flow data and conductivity anomalies, fault tectonics, crustal thickness and recent vertical movements. The other half deals mainly with correction problems, e.g. in sea and lake bottom sediments due to sedimentation, topography and hydrology.

The second part contains national reports from 21 countries in which the authors describe the data, their acquisition, error sources etc. It seems that the problem of corrections is still a major source of inaccuracies; the editors have chosen the way that they do include as few corrections as possible, while the topographic, climatic, glaciation corrections, effects due to circulating waters, sedimentation and denudation, problems in the determination of the heat conductivity in loose sediments are treated in individual papers or in certain national reports.

The book contains not only valuable information on heat flow in Europe both in form of numerical data and of a map constructed with long-time practice and very great carefulness, but also yields a very interesting picture on the present state of heat flow investigations by enabling a comparison of many national reports in which the authors emphasize and discuss a fascinating variety of problems related to heat flow problems.

J. Verő

E. Grafarend—H. Heister—R. Kelm—H. Kropff—B. Schaffrin

OPTIMIERUNG GEODÄTISCHER MESSOPERATIONEN (OPTIMATION OF GEODETIC MEASUREMENTS)

Herbert Wichmann Verlag, Karlsruhe, 1979, 499 p., 88 DM

A new book has been published on a most interesting field of geodesy, on the optimation of geodetic measurements. In addition to an analysis of the accuracy and reliability of geodetic measurements, the authors investigate the importance of qualitative and quantitative problems in the construction of geodetic networks. Expenses and time demand are also taken into account in the optimation. The book contains six Parts.

Part 1 deals with the basic mathematical problems of the optimation of geodetic measurements. The chapters of this Part deal additionally with linear spaces, transformation problems, problems of the definiteness, further in the framework of optimation with the simplex method, with the approximative method, and with the convex, quadratic and dynamic methods.

Part 2 deals with optimation problems of geodetic networks, thus with the configuration of the networks, with the optimum use of the instruments, further with optimum expenses. Having finished the measurements, the actual accuracies in the network are studied diagnostically. Its chapters deal with the aim-functions of the optimation, criteria of utilization and accuracy (trilateration networks, traverses, including inner orientations, — further the optimation of different intersection and resection problems). The problems of the defects of the matrix ranks and of the computation of different type pseudoinverses are also treated.

Part 3 deals with first order optimation (optimation methods according to the form of the network), where — depending on the accuracy demand of the coordinates to be determined — the gradient method, the method using the graph theory, further the indirect methods (network simulation, electric analogies) are discussed. As theoretical examples the optimum resection, optimum satellite geodetic networks, very long base radio-interferometric measurements, further the problems of networks produced by navigational methods are offered. Further the use of implicite functions, determinants, and of the Laplace-theorem are also discussed in the geometric optimation.

Part 4 discusses second order optimation (optimation of the measurement plan), including measurement weights of geodetic networks, the criterion matrix method (KRONECKER, KHATRI-RAO), and indirect solutions. Scalar aim-functions, optimum planning of continuous observations (movement investigations) and optimation of the manpower demand are reserved. In this Part planning of two-dimensional networks, further of gravimetric measurements are treated, too.

Part 5 deals with third-order planning (network optimation with supplementary measurements). Mathematical problems of the supplementary control measurements, further of the weight changes, and of the changes of the variance-covariance matrix are treated. A theoretical example is presented with the use of Neumann-series for triangulation, trilateration and combined networks.

In Part 6 the problems of the hybrid planning of networks are discussed. The optimation methods (as methods according to the form of the network, to the determination plan) described in previous chapters are combined with the method of the Neumann-series.

This list shows that the authors discuss a wide range of optimation problems in geodetic measurements. The book has a more theoretical character, nevertheless a number of practical problems are also discussed in connection with certain problems. The investigations are based on random errors, though it would be desirable to study regular (model) errors inevitable in networks, too. There are only some hints to such problems. Little attention is paid in the optimation e.g. to refraction errors, calibration problems of the instruments, optimation of intermediate orientations and regular errors in connection with them. The references are rather exhaustive in spite of some hiatuses which are probably due to the cooperation of several authors. The most striking hiatus is that of the collocation being advantageously utilizable in optimation, further that of some analogous physical-electrical methods.

It can be said that the authors deal with the optimation problems of geodetic networks on a very high mathematical level, using the most up-to-date mathematical methods. The technical production of the book is of high standard, too, thus it can be recommended to anybody dealing with the optimation of geodetic networks on a scientific and practical basis.

F. Halmos

H. Moritz

ADVANCED PHYSICAL GEODESY

Herbert Wichmann Verlag, Karlsruhe and Abacus Press, Tumbridge Wells, Kent, 1980, 500 p., 80 DM

An excellent book dealing with the problems of the theoretical geodesy and its use has been published written by a prominent representant of the physical geodesy, H. MORITZ, Professor at the Technical University Graz. It was published in a very short time (one and half years between the first letters of the manuscript and the publication) with the cooperation of two publishing houses. It includes in 4 Parts and 55 Chapters the recent developments in this field based partly on the excellent work by HEISKANEN and MORITZ (Physical geodesy, Freeman, San Francisco, 1967) and on other works. The material is presented with the well-known pedagogical sense of the author, in a clear and continuous line of thoughts which enables even for the less experienced reader to gain new knowledge in this field.

Part A deals with the basic ideas of physical geodesy. Part B includes least squares collocation, Part C its practical use. Part D discusses the boundary-value problem of geodesy and problems in connection with it. The book is restricted to "classical" physical geodesy, i.e. it considers the figure of the earth and its gravitational field as being independent of time. This is true down to an accuracy of 10^{-7} what is compatible with present accuracy possibilities. For an even higher precision, mainly for geodynamical purposes, time variations must be also taken into account. This problems are reviewed in a short chapter. It is remarked in the introduction that the geodetic aspects of geodynamics would be worth of a separate part, or even of a complete book. In the discussion of the boundary value problem of geodesy, the four-dimensional treatment is also used. It can be therefore supposed that the author intends to write a work dealing in details with the problems of geodynamics, offering a four-dimensional treatment.

The present book is didactically, pedagogically and practically of outstanding value for the geodesy.

The parts have the following content:

Part A discusses the mathematical background of physical geodesy (spherical harmonics describing the gravity field of the Earth, linear operators, convergence problems, etc.).

Part B deals with the determination of the anomalies of the gravitational field of the Earth using the least-squares collocation. Equations are presented for the connection of different kinds of geodetic computations. The structure of this Part is based on simple models starting from which the author reaches through statistical and analytical structures collocation interpretation and prediction. On hand of elementary examples, the notions of random and regular errors, "noises" are clarified. In addition to this logical structure, the great number of illustrative examples from the physical-geodesy is to be emphasized which promote an easy understanding. For the solution of very great linear equation systems a stepwise method is proposed. The determination of the covariance functions is treated in details, being a problem of utmost importance for the least-square collocation. Mathematical and numerical questions in this connection are also analyzed. This part includes the author's own results achieved through many years.

Part C deals with the geometric basis of the least-squares collocation by representing the Hilbert spaces with kernel functions. It is proved that this gives a unique solution for the figure of the Earth and its gravitational field. The statistical background of the solution with collocation, the stochastic principles of the determination of gravity anomalies are also investigated. A separate chapter yields the proof that the spherical approximation is sufficient for the solution with collocation, as ellipsoidic formulae cause only slight changes against the spherical ones, but they cause a significant increase of computational work.

In connection with the boundary-value problem of the geodesy, discussed in Part D, a detailed analysis is given on MOLODENSKY's, BROVAR's and other solutions which are based on mathematical series (convergence, equivalence problems, etc.). From recent solutions, HÖRMANDER's, KRARUP's and SANSO's methods are discussed. A theoretical basis of these computations is given. The complexity of HÖRMANDER's solution is emphasized. SANSO's solution which is based on the Legendre-transformation is recommended as a new, original and very effective solution. The time dependence of the reference systems, tidal effects, further geodynamical aspects are shortly summarized. Special attention is paid to the importance of the absolute g determinations from the point of view of the four-dimensional geodesy. The importance of tidal studies, polar motion and inertial systems are shortly reviewed.

The book is supplemented by exhaustive references. The citations in the text give considerable help for the less experienced reader for a more detailed study of certain problems. The mathematics of the book is clear, simple and of a logical structure. A harmony of form and content is characteristic for the book for what all geoscientists, especially all geodesists owe the author thanks. A special merit of the author and the publisher is that they produced the book in a very short space of time enabling a text including recent results on this field of science. This should be a model for other publishing houses, too.

F. Halmos

P. Schmidt

SEISMOLOGIE UND MEDAILLEN VOM 17. JAHRHUNDERT BIS IN UNSERE ZEIT

Jahrbuch der Staatlichen Kunstsammlungen Dresden 1976—1977. S. 193—208.

Es ist interessant und nützlich, daß der Verfasser die Medaillen über große Erdbeben vom 17. Jahrhundert an zusammengesucht und veröffentlicht hat. Die erste Medaille bezieht sich auf das niederländische Erdbeben vom 18. September 1692; die letzte auf das italienische Erdbeben vom 28. Dezember 1908. Es werden aber auch Medaillen behandelt, die von wissenschaftlichen Institutionen für seismische Forschungsarbeiten verliehen wurden und werden.

Der Verfasser regt mit Recht an, in Anbetracht der großen Bedeutung der Seismologie und Seismik solche Medaillen auch in der Zukunft herauszugeben.

Die Arbeit stellt eine wertvolle Bereicherung unserer Wissenschaft dar.

A. Tárczy-Hornoch

INDEX

Printed in Hungary

A kiadásért felel az Akadémiai Kiadó igazgatója — Műszaki szerkesztő: Zacsik Annamária

A kézirat nyomdába érkezett: 1980. XI. 10. — Terjedelem: 14,70 (A/5) ív, 77 ábra

81.8942 Akadémiai Nyomda, Budapest — Felelős vezető: Bernát György

Acta Geodaetica, Geophysica et Montanistica, eine Halbjahresschrift der Ungarischen Akademie der Wissenschaften. Sie veröffentlicht Originalbeiträge aus dem Bereich der Geodäsie, Geophysik und des Bergbaus in deutscher, englischer, französischer oder russischer Sprache.

Redaktion: H-9400 Sopron, Múzeum u. 6.

Bestellbar bei »Kultura« Außenhandelsunternehmen (1389 Budapest 62, P.O.B. 149) oder seinen Auslandsvertretungen.

Acta Geodaetica, Geophysica et Montanistica est une revue biannuelle de l'Académie Hongroise des Sciences publiant des essais originaux du domaine de la géodésie, géophysique et des sciences minières en français, anglais, allemand ou russe.

Rédaction: H-9400 Sopron, Múzeum u. 6.

On peut s'abonner à l'Entreprise du Commerce Extérieur « Kultura » (1389 Budapest 62, P.O.B. 149) ou chez représentants à l'étranger.

Acta Geodaetica, Geophysica et Montanistica выходят два раза в год в издании Академии наук Венгрии. В журнале публикуются оригинальные исследования по проблемам геодезии, геофизики и горного дела на русском, английском, немецком и французском языках.

Адрес редакции: H-9400 Sopron, Múzeum u. 6.

Заказать журнал через Внешнеторговое предприятие «Kultura» (1389 Budapest 62, P.O.B. 149) или через его заграничные представительства.

Reviews of the Hungarian Academy of Sciences are obtainable at the following addresses:

AUSTRALIA
C.B.D. LIBRARY AND SUBSCRIPTION SERVICE, Box 4886 G.P.O. *Sydney N.S.W. 2001*
COSMOS BOOKSHOP, 135 Ackland Street, *St. Kilda (Melbourne), Victoria 3182*

AUSTRIA
GLOBUS Höchstädtplatz 4 *1200 Wien* XX

BELGIUM
OFFICE INTERNATIONAL DE LIBRAIRIE, 30 Avenue Marnix *1050 Bruxelles*
LIBRAIRIE DU MONDE ENTIER, 162 Rue du Midi. *1000 Bruxelles*

BULGARIA
HEMUS. Bulvar Ruszki 6, *Sofia*

CANADA
PANNONIA BOOKS, P.O. Box 1017, Postal Station "B", *Toronto, Ontario M5T 2T8*

CHINA
CNPICOR, Periodical Department, P.O. Box 50, *Peking*

CZECHOSLOVAKIA
MAD'ARSKÁ KULTURA, Národní třida 22, *115 66 Praha*
PNS DOVOZ TISKU, Vinohradská 46, *Praha 2*
PNS DOVOZ TLAČE, *Bratislava 2*

DENMARK
EJNAR MUNKSGAARD, Norregade 6, *1165 Copenhagen*

FINLAND
AKATEEMINEN KIRJAKAUPPA, P.O. Box 128, *SF-00101 Helsinki 10*

FRANCE
EUROPERIODIQUES S. A., 31 Avenue de Versailles, *78170 La Celle St.-Cloud*
LIBRAIRIE LAVOISIER, 11 rue Lavoisier, *75008 Paris*
OFFICE INTERNATIONAL DE DOCUMENTATION ET LIBRAIRIE, 38 rue Gay-Lussac, *75240 Paris Cedex 05*

GERMAN DEMOCRATIC REPUBLIC
HAUS DER UNGARISCHEN KULTUR, Karl-Liebknecht-Strasse 9, *DDR-102 Berlin*
DEUTSCHE POST ZEITUNGSVERTRIEBSAMT, Strasse der Pariser Kommüne 3—4, *DDR-104 Berlin*

GERMAN FEDERAL REPUBLIC
KUNST UND WISSEN ERICH BIEBER, Postfach 46, *7000 Stuttgart 1*

GREAT BRITAIN
BLACKWELL'S PERIODICALS DIVISION, Hythe Bridge Street, *Oxford OX1 2ET*
BUMPUS, HALDANE AND MAXWELL LTD., Cower Works, *Olney, Bucks MK46 4BN*
COLLET'S HOLDINGS LTD., Denington Estate, *Wellingborough, Northants NN8 2QT*
W.M. DAWSON AND SONS LTD., Cannon House, *Folkestone, Kent CT19 5EE*
H. K. LEWIS AND CO., 136 Gower Street, *London WC1E 6BS*

GREECE
KOSTARAKIS BROTHERS, International Booksellers, 2 Hippokratous Street, *Athens-143*

HOLLAND
MEULENHOFF-BRUNA B.V., Beulingstraat 2, *Amsterdam*
MARTINUS NIJHOFF B.V., Lange Voorhout 9—11, *Den Haag*
SWETS SUBSCRIPTION SERVICE, 347b Heereweg, *Lisse*

INDIA
ALLIED PUBLISHING PRIVATE LTD., 13/14 Asaf Ali Road, *New Delhi 110001*
150 B-6 Mount Road, *Madras 600002*
INTERNATIONAL BOOK HOUSE PVT. LTD., Madame Cama Road, *Bombay 400039*
THE STATE TRADING CORPORATION OF INDIA LTD., Books Import Division, Chandralok, 36 Janpath, *New Delhi 110001*

ITALY
EUGENIO CARLUCCI, P.O. Box 252, *70100 Bari*
INTERSCIENTIA, Via Mazzé 28, *10149 Torino*
LIBRERIA COMMISSIONARIA SANSONI, Via Lamarmora 45, *50121 Firenze*
SANTO VANASIA, Via M. Macchi 58, *20124 Milano*
D. E. A., Via Lima 28, *00198 Roma*

JAPAN
KINOKUNIYA BOOK-STORE CO. LTD., 17-7 Shinjuku-ku 3 chome, Shinjuku-ku, *Tokyo 160-91*
MARUZEN COMPANY LTD., Book Department, P.O. Box 5056 Tokyo International, *Tokyo 100-31*
NAUKA LTD., IMPORT DEPARTMENT, 2-30-19 Minami Ikebukuro, Toshima-ku, *Tokyo 171*

KOREA
CHULPANMUL, *Phenjan*

NORWAY
TANUM-CAMMERMEYER, Karl Johansgatan 41—43. *1000 Oslo*

POLAND
WĘGIERSKI INSTYTUT KULTURY, Marszałkowska 80, *Warszawa*
CKP I W ul. Towarowa 28 *00-958 Warsaw*

ROMANIA
D. E. P., *Bucureşti*
ROMLIBRI, Str. Biserica Amzei 7 *Bucureşti*

SOVIET UNION
SOJUZPETCHATJ — IMPORT, *Moscow* and the post offices in each town
MEZHDUNARODNAYA KNIGA, *Moscow G-200*

SPAIN
DIAZ DE SANTOS, Lagasca 95, *Madrid 6*

SWEDEN
ALMQVIST AND WIKSELL, Gamla Brogatan 26, *101 20 Stockholm*
GUMPERTS UNIVERSITETSBOKHANDEL AB, Box 346, *401 25 Göteborg 1*

SWITZERLAND
KARGER LIBRI AG, Petersgraben 31, *4011 Basel*

USA
EBSCO SUBSCRIPTION SERVICES, P.O. Box 1943, *Birmingham, Alabama 65201*
F. W. FAXON COMPANY, INC., 15 Southwest Park, *Westwood. Mass, 02090*
THE MOORE-COTTRELL SUBSCRIPTION AGENCIES, *North Cohocton, N. Y. 14838*
READ-MORE PUBLICATIONS, INC., 140 Cedar Street, *New York, N. Y 10003*
STECHERT-MACMILLAN, INC., 7250 Westfield Avenue, *Pennsauken* N. J. 08110

VIETNAM
XUNHASABA, 32, Hai Ba Trung, *Hanoi*

YUGOSLAVIA
JUGOSLAVENSKA KNJIGA, Terazije 27 *Beograd*
FORUM, Vojvode Mišića 1, *21000 Novi Sad*

4. IX. 1981 HU ISSN 0374—1842 Index: 26.031

Acta GEODAETICA, GEOPHYSICA et MONTANISTICA

ACADEMIAE SCIENTIARUM HUNGARICAE

AKADÉMIAI KIADÓ, BUDAPEST

TOMUS 16
FASCICULI 2–4
1981

ACTA GEODAETICA, GEOPHYSICA et MONTANISTICA

Academiae Scientiarum Hungaricae

A Magyar Tudományos Akadémia Föld- és Bányászati Tudományok Osztályának folyóirata

Szerkesztőség: H-9400 Sopron, Múzeum u. 6.
Kiadja az Akadémiai Kiadó, 1054 Budapest, Alkotmány utca 21.

Az *Acta Geodaetica, Geophysica et Montanistica* eredeti tanulmányokat közöl a geodézia, geofizika és a bányászati tudományok tárgyköréből, angol, német, francia vagy orosz nyelven. Félévenként jelenik meg, évi egy, kb. 400—500 oldalas kötetet alkotva.

Megrendelhető az Akadémiai Kiadónál (1363 Budapest Pf. 24.), a külföld részére pedig a „Kultura" Külkereskedelmi Vállalatnál (1389 Budapest 62, P.O.B. 149).

Acta Geodaetica, Geophysica et Montanistica is a semiannual review of the Hungarian Academy of Sciences, publishing papers on geodesy, geophysics and minings in English, German, French or Russian.

Editorial Office: H-9400 Sopron. Múzeum u. 6.

Orders may be placed with "Kultura" Foreign Trading Company (1389 Budapest 62. P.O.B. 149) or its representatives abroad.

FOREWORD

This issue of Acta Geodaetica, Geophysica et Montanistica celebrates the twenty-fifth anniversary of the foundation of the present Geodetic and Geophysical Research Institute of the Hungarian Academy of Sciences as two independent laboratories. The collected papers aim to give informations about the investigations made in the Institute in recent years, and correspond to the level reached in 1980, thus individual manuscripts do not bear any datum. The picture given in these papers could not be considered as a complete one, nevertheless they include the most important items of the last years.

Sopron, December 29, 1980

József Somogyi
Director

Acta Geodaet., Geophys. et Montanist. Acad. Sci. Hung. Tomus 16 (2—4), pp. 169—178 (1981)

DAS 25-JÄHRIGE BESTEHEN DES GEODÄTISCHEN UND GEOPHYSIKALISCHEN FORSCHUNGSINSTITUTES (GGKI) DER UNGARISCHEN AKADEMIE DER WISSENSCHAFTEN

J. SOMOGYI

DOKTOR DER TECHNISCHEN WISSENSCHAFTEN

Geodätische und geophysikalische Forschungen wurden in Sopron bereits vor dem Krieg ausgeübt. Am Lehrstuhl für Geodäsie und Markscheidewesen bzw. am Lehrstuhl für forstliches Vermessungswesen der von Selmecbánya (heute Banska Stiavnica) nach Sopron übersiedelten Hochschule für Bergbau und Forstwesen wurde nebst Unterricht auch nennenswerte Forschungstätigkeit geleistet. Die Forschungsergebnisse wurden in zahlreichen in- und ausländischen Zeitschriften, sowie in den fremdsprachigen Veröffentlichungen der Hochschule publiziert. Dadurch hatte Sopron bereits zu dieser Zeit Verbindungen zu heimischen und internationalen wissenschaftlichen Kreisen.

Nach 1945 nahmen — wie alle Wissensgebiete — auch die geodätischen und geophysikalischen Forschungen einen wesentlichen Aufschwung.

Im Jahre 1947 wurde mit der Ausbildung von Bergbau-Forschungsingenieuren mit einem hauptsächlich auf Geowissenschaften ausgerichtetem Studium begonnen und damit verbunden nahm in demselben Jahr eine geodätische und geophysikalische Arbeitsgemeinschaft ihre wissenschaftliche Tätigkeit in Sopron auf. 1949 begann ebenfalls in Sopron die Ausbildung der Vermessungsingenieure, 1951 die der Ingenieure für Geophysik.

Die Gründer der Arbeitsgemeinschaft waren die Professoren István Hazay, Károly Kántás, Antal Tárczy-Hornoch und Miklós Vendel. Daraus entwickelte sich im Jahre 1955 das Geodätische bzw. das Geophysikalische Forschungslaboratorium der Ungarischen Akademie der Wissenschaften unter der Leitung von Tárczy-Hornoch bzw. Kántás. Im Herbst 1956 übernahm Tárczy-Hornoch — nach Ausscheiden von Kántás — auch die Leitung des Geophysikalischen Forschungslaboratoriums; seither konnten beide Institutionen unter einer einheitlichen Führung arbeiten. 1971 wurden beide Forschungslaboratorien sowie das Seismologische Observatorium in Budapest auch organisatorisch in ein einheitliches Forschungsinstitut vereinigt. Akademiemitglied Tárczy-Hornoch wirkte bis 1. Jänner 1972 als Institutsdirektor.

Beide Forschungslaboratorien begannen ihre Tätigkeit mit je 4—5 Mitarbeitern. Das Geodätische Forschungslaboratorium war in den ersten Jahren in einem Zimmer des Lehrstuhls für Geodäsie und Markscheidewesen der Technischen Universität Sopron untergebracht. Das Geophysikalische Forschungslaboratorium arbeitete unter verhältnismäßig günstigeren Umständen, in selbständigen Räumlichkeiten. Eine für Grundlagenforschungen sowie für Instrumentenentwicklung unerläßlich notwendige mechanische Werkstatt konnte daher im Geophysikalischen Forschungslaboratorium schon am Anfang eingerichtet werden. Die Mechaniker des Geodätischen Forschungslaboratoriums konnten nur in der Werkstatt des Lehrstuhls arbeiten. Eine eigene mechanische Werkstatt wurde hier erst nach der Umsiedlung der Technischen Universität nach Miskolc eingerichtet. Nachdem im Juni 1960 auch das Forschungslaboratorium für Erdölgewinnung der U. A. d. W. nach Miskolc verlegt wurde, konnten beide Laboratorien in einem selbständigen Gebäude untergebracht werden. Die Unterbringung war aber bereits 1960 zu eng. Derzeit arbeiteten in beiden Forschungslaboratorien 16 wissenschaftliche Mitarbeiter, die Anzahl aller Beschäftigten betrug 30. Bis 1970 erhöhte sich die Zahl der wissenschaftlichen Mitarbeiter nur auf 17. Die mechanische Werkstatt der Geophysiker und die Garage blieben an ihrer früheren Stelle. Die Probleme der Unterbringung konnten endgültig erst 1973, nach der Fertigstellung eines neuen Institutsgebäudes gelöst werden. Im neuen Gebäude hat jeder wissenschaftliche Mitarbeiter ein selbständiges Arbeitszimmer. Die Bibliotheken beider Forschungslaboratorien konnten vereinigt werden. Das neue Rechenzentrum und die Instrumentenprüfhalle entsprechen weitgehend den Voraussetzungen der modernen Forschungstätigkeit. Im alten Gebäude konnten die Werkstätten für Mechanik und Elektronik sowie das Fotolaboratorium untergebracht werden. Hier sind auch Räume für Freizeitunterhaltung und Sport eingerichtet. Der Personalstand des Institutes ist derzeit 110, die Zahl der wissenschaftlichen Mitarbeiter 33.

Geowissenschaften, besonders Geodäsie und Geophysik haben Tradition in Ungarn. Die Instrumentenproduktion auf beiden Gebieten kann bis zum vorigen Jahrhundert zurückgeführt werden. Geodätische Instrumente werden in Ungarn seit 1872 hergestellt, die Erzeugung der Eötvösschen-Drehwaage begann ebenfalls im vorigen Jahrhundert. Nach 1945 setzte sowohl in der geodätischen als auch in der geophysikalischen Instrumentenproduktion ein großer Aufschwung ein. Erfolgreiche Instrumentenentwicklung kann ohne hochstehende Grundlagenforschungen nicht verwirklicht werden. Diese Forschungen müssen die zu erwartenden Entwicklungsrichtungen, sowie die Prüfung und den Vergleich der Leistungsfähigkeit der verschiedenen Instrumententypen erfassen. In der Forschungstätigkeit der Soproner Laboratorien haben seit der Gründung auch solche Untersuchungen eine bedeutende Rolle gespielt, da man dessen bewußt war, daß eingehende Grundlagenforschungen

unmittelbar einen doppelten Nutzen bringen können. Einerseits können die Ergebnisse der Grundlagenforschungen des fraglichen Gebietes das wissenschaftliche Ansehen des Landes erhöhen, wodurch das Vertrauen zu den erzeugten Instrumenten zunehmen wird; andererseits können Forschungsergebnisse bei den Instrumentenentwicklungen auch unmittelbar angewendet werden.

Das Geodätische Forschungslaboratorium begann seine Tätigkeit im Jahre 1955 mit 5 Mitarbeitern (GYULA ALPÁR wiss. Abteilungsleiter, ferner LÁSZLÓ GEREBEN, FERENC HALMOS, JÓZSEF SOMOGYI und GYULA SZÁDECZKY-KARDOSS). Diese Zahl erhöhte sich 1957 mit zwei weiteren Mitarbeitern (ERNŐ CZUCZOR und ALADÁR ORBÁN). Zwei Feinmechaniker (ANTAL BUMMER und GYULA ULLRICH) arbeiteten in der Werkstatt, ferner war eine administrative Kraft und ein PKW-Fahrer angestellt.

Diese kleine Gruppe von Wissenschaftlern befaßte sich außer den geodätischen, meßtechnischen, rechentechnischen, fehlertheoretischen und physikalisch-geodätischen Grundlagenforschungen (Ausgleichungsrechnung, Anwendung der Matrix-Algebra, Genauigkeitsprüfungen, Projektionsberechnungen, numerische Probleme der Photogrammetrie, Gravitation, Astrogeodäsie) auch sehr intensiv mit instrumententechnischen Problemen. Dies wurde durch den Umstand bedingt, daß die Ungarischen Optischen Werke (MOM) in der Mitte der fünfziger Jahre die geodätische Instrumentenproduktion recht stark und erfolgreich förderten. Eine enge Zusammenarbeit mit den Ungarischen Optischen Werken (MOM) bestand seit 1958. Die Prüfung sämtlicher Versuchsexemplare und die der Prototype wurde in unserem Forschungslaboratorium in enger Zusammenarbeit mit den oft auch persönlich anwesenden Konstrukteuren durchgeführt. Hauptzweck dieser Zusammenarbeit war das Anpassen dieser Instrumente jenem technischen Niveau, das dem der von führenden ausländischen Firmen hergestellten Instrumenten entsprach. Für diese auch als Heldenepoche bezeichenbare Periode war jene Begeisterung charakteristisch, die dazu führte, daß Diskussionen über die Klärung aufregender Probleme bzw. Arbeiten zur Verwirklichung von Konstruktionsänderungen oft bis spät in die Nacht dauerten, oder oft auch an Ruhetagen fortgeführt wurden.

Außerdem bestand auch mit dem Bergbau eine wirksame Zusammenarbeit. So wurden z. B. gemeinsam mit den Mitarbeitern des Lehrstuhls für Geodäsie und Markscheidewesen für den Ausbau neuer Gruben im Kohlenrevier Mecsek geodätische Richtungsmessungen zum Durchbruch zweier von verschiedenen Flözen ausgetriebenen Strecken durchgeführt. Man kann ruhig behaupten, daß die Forschungslaboratorien die im Jahre 1968 erlassene wirtschaftspolitische Forderung, wonach die Wissenschaft neben Grundlagenforschungen eine unmittelbare Produktivkraft werden soll, bereits 1956 verwirklicht und praktiziert hat.

Es wurden in der mechanischen Werkstatt spezielle der Grundlagenforschung dienende Instrumente gebaut (z. B. verschiedene halbautomatische, automatische Libellenprüfer, astrogeodätische Instrumente) daneben aber auch Hilfsgeräte zur Prüfung neuer geodätischer Instrumente (z. B. Kreisteilungsprüfer, Stehachsenschwankungsprüfer, Diagrammprüfer, usw.) hergestellt. Die zur Prüfung geodätischer Instrumente entwickelten neuen Methoden wurden auch von der internationalen Fachliteratur übernommen.

Im Jahre 1959 begann die regelmäßige geographische Breitenbestimmung zur Untersuchung der Polschwankungen im Observatorium bei Nagycenk. 1968 wurde in Sopronbánfalva ein Observatorium zwecks Messung von Erdgezeiten mit der selbstlosen Hilfe des Kohlenbergwerks Oroszlány fertiggestellt.

1955 waren vier wissenschaftliche Mitarbeiter im Geophysikalischen Forschungslaboratorium angestellt (VILMOS AUER wiss. Abteilungsleiter, ferner ANTAL ÁDÁM, PÁL BENCZE und ÁKOS WALLNER). 1957 kamen dazu — nebst Ausscheiden von V. AUER — JUDIT CZUCZOR, FERENC MÄRCZ und JÓZSEF VERŐ, wiss. Abteilungsleiter wurde ANTAL ÁDÁM; weiters waren zwei Kräfte für Verwaltung und Administration und zwei PKW-Fahrer angestellt. In der Werkstatt arbeiteten zwei Mechaniker (GYULA SIMON und GYŐZŐ MÄRCZ).

Die ersten Aufgaben des Laboratoriums zur Gründungszeit war u. a. die Untersuchung der Anwendungsmöglichkeit der tellurischen Methode in Erdölforschungen, was vornehmlich auf dem Gebiete der Erdölstruktur Nagylengyel in Südwestungarn durchgeführt wurde; Konstruktion eines Erdstrommeßgerätes, sowie einer Induktionssonde für Bohrlochmessungen. Das tellurische Instrument wurde im Winter 1955/56 auf einer Ausstellung in der Volksrepublik China gezeigt. Als Ergebnis wurden 50 Instrumente bestellt, zu derer Herstellung die Budapester Fabrik Geophysikalischer Meßgeräte 1956 in Sopron eine Abteilung mit 20 Arbeitern gegründet und diese unter die unmittelbare Leitung des Geophysikalischen Forschungslaboratoriums gestellt hat. In dieser Abteilung wurden später noch aufgrund mehrerer Konstruktionen des Laboratoriums geoelektrische und geomagnetische Instrumente sowohl zur Deckung des heimischen Bedarfs als auch für Exportzwecke hergestellt.

Eine wichtige Aufgabe bedeutete derzeit auch die Vorbereitung des Internationalen Geophysikalischen Jahres 1957/58. Die Hauptaufgabe bestand in der Errichtung eines elektromagnetischen Observatoriums. Dafür wurde aufgrund von Probemessungen als geeigneter Ort ein Gebiet bei Nagycenk ausgewählt. Darauf folgte der Bau der notwendigen Gebäuden und die Ausstattung mit den nötigen Instrumenten größtenteils im Eigenbau. Der Observatoriumsbetrieb begann im August 1957 mit den tellurischen Registrierungen, die seither laufend durchgeführt werden. Die Registrierung der geomagnetischen Elemente wurde im Jahre 1961 aufgenommen. Die Tätigkeit des Obser-

vatoriums wurde 1962 mit Ionosphären-Forschungen erweitert. Die Veröffentlichung der Meßergebnisse des Observatoriums geschieht in Jahrbüchern. Das Observatorium und dessen Umgebung stehen unter Naturschutz, was die Ungestörtheit der Forschungstätigkeit sichert.

Aus den bereits erwähnten geht es schon hervor, daß im Geophysikalischen Forschungslaboratorium seit ihrer Gründung ebenfalls nebst Grundlagenforschungen auf volkswirtschaftlichen Nutzen unmittelbar ausgerichtete Forschungen durchgeführt worden sind. Auf diesem Gebiet sind noch einige hydrologische Forschungen sowie geoelektrische Messungen am Fertő-See zu erwähnen.

Die Umrisse der heutigen geodätischen und geophysikalischen Forschungen wurden schon in den sechziger Jahren festgelegt und diese bestimmten auch größtenteils die Gestaltung der wissenschaftlichen Abteilungen, bei der Reorganisierung in ein einheitliches Institut. Selbstverständlich war dabei auch die Wirkung der auf die ganze Welt sich erstreckenden technisch-wissenschaftlichen Revolution unserer Fachgebiete ein bedeutender Faktor. Die Verbreitung und Anwendung der zeitgemäßen Rechentechnik zur Lösung geodätischer und geophysikalischer Probleme bedeutet nicht nur einen Zeitgewinn, sondern auch die Untersuchung jener neuen Probleme, deren Lösung früher unvorstellbar war. Instrumente, die aufgrund verschiedener neuer Prinzipien arbeiten und die die Meßgenauigkeit mit Größenordnungen steigern, sowie die Automatisierbarkeit der Messungen, ermöglichen die Inbetrachtnahme von Parametern, die die Skale der Prüfungen erweitern. Das Erscheinen der künstlichen Satelliten war Ausgangspunkt eines neuen Fachgebietes sowohl in der Geodäsie als auch in der Geophysik. Mit ihrer Hilfe können die auf die Erde und die Atmosphäre bezogenen Kenntnisse erweitert werden.

Die geodätischen Forschungen wurden in Sopron auf folgende Hauptgebiete konzentriert:

Steigerung der geodätischen Rechenkultur; Lösung geodätischer Probleme aufgrund moderner mathematischer Methoden; Ausarbeitung von Rechenprogrammen für praktische Anwendung;

Forschungen auf dem Gebiet der physikalischen Geodäsie (gravimetrische und astrogeodätische Messungen zur Untersuchung der Erdkruste; Anwendung der Daten der künstlichen Satelliten zu geodynamischen Zwecken; Untersuchung lokaler geodynamischer Phänomene);

Entwicklung spezieller Instrumente für die eigenen Forschungen; Ausarbeitung moderner Methoden der Instrumentenprüfung.

Die geophysikalischen Forschungen in Sopron wurden auf folgende Hauptgebiete konzentriert:

Forschungen der Pulsationen sowie der zeitlichen und räumlichen Eigenschaften des geomagnetischen Feldes; Theorie der Entstehung und der Ver-

breitung der Pulsationen; die Bestimmung der Parameter der Magnetosphäre und des interplanetaren Raumes aufgrund der Observatoriumsdaten;

Untersuchung der atmosphärischen Elektrizität; Beschreibung der Eigenschaften der unteren Ionosphäre, Untersuchung der Erscheinung der sonnenphysikalischen Effekte in deren Parametern, sowie der Dynamik der unteren Ionosphäre;

Weiterentwicklung elektromagnetischer Induktionsmethoden wie Tellurik, Magnetotellurik und geoelektrischer Methoden sowie Instrumentenbau auf diesen Gebieten; Bestimmung der regionalen Eigenschaften der elektrischen Leitfähigkeitsverteilung im Ungarischen Becken; Beschreibung allgemeiner geophysikalischer Zusammenhänge zwischen der elektrischen Leitfähigkeitsverteilung und anderen geophysikalisch-tektonischen Parametern.

Der Generalsekretär der Ungarischen Akademie der Wissenschaften hat mit seinem Erlaß von 1971 zwecks organisierter und zeitgemäßer Durchführung der theoretischen und empirischen geodätischen und geophysikalischen Forschungen in Ungarn, aus beiden Laboratorien sowie der seismologischen Forschungsgruppe des Lehrstuhls für Geophysik der Loránd Eötvös Universität in Budapest das Geodätische und Geophysikalische Forschungsinstitut der U. A. d. W. (GGKI) ins Leben gerufen. Zu den Hauptaufgaben des Institutes gehört die Durchführung der bedeutenden geodätischen und geophysikalischen Grundlagenforschungen in Ungarn, die Entwicklung von wissenschaftlichen Instrumenten, die Inbetriebhaltung eines Observatoriums-Netzes, eine enge Zusammenarbeit mit der Industrie, eine aktive Teilnahme in der Tätigkeit der internationalen wissenschaftlichen Organisationen, die Organisierung wissenschaftlicher Veranstaltungen, usw.

Das Institut besteht aus zwei wissenschaftlichen Hauptabteilungen:

a) Hauptabteilung für Geodäsie
b) Hauptabteilung für Geophysik
Beide sind in je drei Abteilungen gegliedert:

Die Hauptabteilung für Geodäsie besteht aus:

1. Abteilung für mathematische Geodäsie
2. Abteilung für physikalische Geodäsie
3. Abteilung für Instrumententechnik.

Die Hauptabteilung für Geophysik besteht aus:

1. Abteilung für Geomagnetismus
2. Abteilung für Aeronomie
3. Abteilung für Seismologie.

Wir möchten hier kurz auch die Vergangenheit und die derzeitige Lage der seismologischen Forschungen in Ungarn überblicken.

Die organisierten seismologischen Forschungen Ungarns begannen zwar erst vor 75 Jahren, als RADÓ KÖVESLIGETHY das Seismologische Observatorium bzw. das Institut für Erdbebenforschung gründete, einige beachtenswerte Ergebnisse liegen aber schon aus früherer Zeit vor, z. B. ein Erdbebenkatalog aus dem Jahre 1783 und die Bearbeitung des Erdbebens von Mór vom Jahre 1810 durch KITAIBEL und TOMCSÁNYI die bereits Isoseiten konstruierten.

Der erste international bekannte Wissenschaftler der ungarischen Erdbebenforschung war RADÓ KÖVESLIGETHY, dessen Fachtätigkeit in der internationalen Literatur auch heute noch geschätzt wird. Das von ihm gegründete Institut baute ein seismologisches Observatoriumsnetz aus und wies gute Entwicklung in der Forschung auf. Durch die Zerstörungen des zweiten Weltkrieges erlitt es jedoch einen schweren Rückfall und organisatorische Änderungen wirkten in den fünfziger Jahren eher ungünstig.

Ein bedeutender neuer Aufschwung der ungarischen Erdbebenforschung ist mit dem Namen von LÁSZLÓ EGYED verbunden, der mit Recht als der zweite Begründer der seismologischen Forschungen in Ungarn angesehen wird. Im Rahmen der neben dem Lehrstuhl für Geophysik der Loránd Eötvös Universität arbeitenden seismologischen Forschungsgruppe der U. A. d. W. vereinigte er die seismologische Forschung in Ungarn und unternahm Schritte zur Modernisierung und zum Weiterausbau des seismologischen Observatoriumsnetzes. Als LÁSZLÓ EGYED 1970 plötzlich starb, bestand die Arbeitsgruppe aus 5 Wissenschaftlern und 10 anderen Angestellten und hatte 4 Observatorien in Betrieb. Seit 1971 bildet sie die Abteilung für Seismologie unseres Institutes.

Nennenswerte Ergebnisse der seismologischen Forschung sind: die Ausarbeitung einer neuen Methode zur Bestimmung der Magnitude aufgrund des Zeitraumes der Oberflächenwelle, Berechnung von Platten-Oszillationen aus Coda-Wellen, die Bestimmung der LVL in Europa, ingenieurseismologische Untersuchungen, seismische Vibrationsmessungen in Bergwerken, die aufgrund der Tektonik konstruierte Seismizitäts-Karte Ungarns, usw.

Zurzeit arbeiten das Zentralobservatorium Sashegy, sowie die Observatorien Piszkéstető, Jósvafő und Sopron, deren moderne Instrumente teilweise von den Fachleuten der Abteilung angefertigt wurden. Zwecks Modernisierung des Beobachtungsnetzes begann 1976 der Ausbau eines telemetrischen Netzes, d. h. die telemetrische Weiterleitung der Meßsignale der einzelnen seismologischen Observatorien in das Zentralobservatorium Sashegy. Das System ist zwischen Piszkéstető und Budapest bereits funktionsfähig. Als nächste wird eine in der Umgebung von Pécs neu erbaute Station an das System angeschlossen werden.

Die Forschungstätigkeit auf dem Gebiet der Geowissenschaften ist ohne ein Observatoriumsnetz unvorstellbar. Wie bereits erwähnt, wurde als erstes der Ausbau des Observatoriums bei Nagycenk im Jahre 1957 in Angriff

genommen. Hier werden die Daten der Geoelektrizität, des Geomagnetismus, der atmosphärischen Elektrizität und der Astrogeodäsie registriert. Modernisierungs- und Erneuerungsarbeiten im Observatorium bei Nagycenk wurden 1979 durchgeführt. Es wurde ein neues Gebäude für Verwalterwohnung gebaut und sämtliche alten Gebäuden wurden erneuert. Zurzeit ist die Digitalisierung der Datensammlung im Ausbau.

Das unterirdische Observatorium von Sopronbánfalva wurde ursprünglich als Beobachtungsstation für Erdgezeiten und Seismologie erbaut. Ergänzt mit dem 1976 fertiggestelltem neuen Meßturm bildet es die geodynamische Station unseres Institutes, wo außer den bereits erwähnten Untersuchungen auch astrogeodätische Messungen und Doppler-Satellitenbeobachtungen zur Bestimmung globaler geodynamischer Phänomene durchgeführt werden. Ferner ist diese Station ein Punkt für die mit dem Institut für Weltraumforschung der Österreichischen Akademie der Wissenschaften gemeinsam durchgeführten regionalen geodynamischen Messungen (Bewegungsuntersuchung der Ost-Alpen).

Der Ausbau internationaler Kontakte begann bereits in den fünfziger Jahren. Die Zusammenarbeit mit der Technischen Universität Dresden und der Bergakademie Freiberg begann bereits im Jahr 1958. Bald danach wurde eine bis heute bestehende Zusammenarbeit mit dem Zentrallaboratorium für Geodäsie der Bulgarischen Akademie der Wissenschaften entwickelt. Weiters entstand bilaterale Zusammenarbeit mit dem Zentralinstitut für Physik der Erde Potsdam, mit dem Institut für Geophysik Prag, mit den geodätischen Instituten der Technischen Universitäten Graz und Wien, sowie mit dem Lehrstuhl für Geophysik der Technischen Universität Wien. Im Jahre 1979 wurden gemeinsame Forschungstätigkeiten mit finnischen Institutionen auf dem Gebiete der Geodäsie und der Geophysik konkretisiert. Mit dem Moskauer Institut für Physik der Erde wird derzeit eine langfristige Zusammenarbeit im Thema der Erdbebenprognose ausgebaut. Außerdem stehen wir mit zahlreichen ausländischen Instituten und Universitäten in gegenseitigem Informationsaustausch. Seit 1966 besteht eine Zusammenarbeit mit den betreffenden Institutionen beinahe sämtlicher sozialistischer Länder im Rahmen der KAPG-Organisation der Akademien der Wissenschaften der sozialistischen Länder.

Die Organisierung von Symposien und Konferenzen in verschiedenen Themenkreisen dient ebenfalls der Festigung der internationalen Kontakte. Unser Institut war in der vergangenen Periode Gastgeber zahlreicher kleinerer und größerer Veranstaltungen. Außer den verschiedenen Arbeitssitzungen im Rahmen der KAPG haben wir 1970 und 1978 die Plenarsitzungen der KAPG und die damit verbundenen Symposien organisiert. Im Jahre 1973 fand in Sopron im Rahmen der IAG eine internationale Erdgezeiten-Konferenz statt. 1976 organisierte das Institut ein Workshop des im Rahmen der IUGG wirken-

den IAGA, 1977 ein IAG-Symposium. Im Herbst 1978 war das Institut Gastgeber für eine internationale Konferenz über Probleme der System-Analyse, im Herbst 1979 fand eine gemeinsame KAPG-INTERKOSMOS Veranstaltung im Thema der Anwendung der Doppler-Technik für geodätische und geodynamische Zwecke statt.

Im Interesse der engen Zusammenarbeit mit heimischen Fachkreisen wird jährlich auch eine die fachliche Weiterbildung fördernde Vortragsreihe veranstaltet, zu der stets namhafte ausländische Experten eingeladen werden. So wurden in der vergangenen Zeit z. B. folgende aktuelle Themen behandelt. analytische Photogrammetrie, Beobachtungen von künstlichen Satelliten für geodätische Zwecke, remote sensing, usw. Die Mitarbeiter des Institutes nehmen mit Vorträgen an sämtlichen bedeutenden heimischen Veranstaltungen teil.

Eine wesentliche Hilfe für die Forschungstätigkeit des Institutes ist das Rechenzentrum, bestehend aus einem Kleincomputer des Typs HP 2100 mit entsprechender Datenspeicherung und den erforderlichen Peripherien. Der Großteil der Rechenaufgaben kann damit gelöst werden, daher sind wir kaum gezwungen Maschinenstunden am zentralen Großcomputer der Akademie in Anspruch zu nehmen. Eine weitere große Hilfe bedeuten die Dienstleistungen der Werkstätten für Elektronik und Feinmechanik. Außer der Entwicklung und dem Bau der zu den Forschungen nötigen Spezialinstrumenten werden von den Werkstätten die Arbeiten zur Digitalisierung des Observatoriumsnetzes, sowie die benötigten Service-Arbeiten ausgeführt.

Die Forschungsergebnisse des Institutes werden — abgesehen von den für Auftraggeber verfertigten Berichten und Studien — über Instrumentenentwicklungen sowie experimentelle Feld- und Laboratoriumsmessungen in erster Linie in Form von Abhandlungen und Dissertationen realisiert. In den letzten 25 Jahren haben die Mitarbeiter mehr als 800 wissenschaftliche Abhandlungen veröffentlicht. Mehr als 600 Arbeiten erschienen in Fremdsprachen in etwa 150 ausländischen Fachzeitschriften. (Diese Statistik enthält nicht die Publikationstätigkeit des ersten Direktors TÁRCZY-HORNOCH. Er selbst schrieb insgesamt mehr als 300 wissenschaftliche Arbeiten und sechs Bücher.) Die Zahl der von den Mitarbeitern des Institutes geschriebenen bzw. redigierten Bücher und Monographien beträgt 5.

Das Institut selbst publiziert Observatoriumsjahrbücher, ferner einige Spezialausgaben, die die Ergebnisse größerer Forschungen enthalten.

Die wissenschaftliche Tätigkeit unseres Institutes ist durch den auf den Zeitraum 1976—80 zusammengestellten und genehmigten mittelfristigen Plan bestimmt. Im Plan haben wir uns an die Hauptforschungsrichtungen und Forschungszielprogramme des Landes angeschlossen. Die Themen unserer Grundlagenforschungen stehen einerseits in Zusammenhang mit den angewandten Forschungen der Fachgebiete des Zentralamtes für Geologie, des

Lóránd Eötvös Geophysikalischen Institutes, der Ungarischen Optischen Werke, des staatlichen Unternehmens für Erdöl- und Gasindustrie, des Landesamtes für Vermessungswesen und Kartographie, des Kohlenbergbaus, usw. Andererseits sind die Forschungen an solche internationale wissenschaftliche Programme angeschlossen die aufgrund der Initiative von internationalen Organisationen der sozialistischen Länder (KAPG, INTERKOSMOS) bzw. von weltweiten internationalen Organisationen (ICSU, IUGG) angeregt wurden. Forschungen für angewandte Zwecke und Entwicklung werden meistens im Rahmen von Verträgen durchgeführt.

Die Forschungsthemen des Institutes sind laut mittelfristigem Plan die folgenden:

I. Untersuchung von mathematischen Modellen zur Bestimmung der zeitgemäßen geodätischen Grunddaten und deren Speicherung;

II. Geodynamische Forschungen;

III. Prüfung und Weiterentwicklung geodätischer Instrumente;

IV. Untersuchung der zeitlichen Änderungen des elektromagnetischen Feldes der Erde vom Gesichtspunkt der Magnetosphäre und des interplanetaren Feldes aus;

V. Untersuchung der geoelektrischen Struktur im Ungarischen Becken;

VI. Untersuchung der zeitlichen und räumlichen Änderungen der Ionosphäre;

VII. Seismologische Forschungen.

In dieser Planperiode standen bzw. stehen wir mit mehreren größeren Institutionen auf dem Gebiete der industriellen Forschungs- und Entwicklungs-Arbeit in Verbindung. Eigens erwähnt sei die Zusammenarbeit mit den Ungarischen Optischen Werken (MOM), mit dem Ungarischen Geodätischen Dienst, mit den Ungarischen Kohlenbergwerken, mit den Mecseker Kohlenbergwerken, mit dem Kartographischen Institut, mit dem staatlichen Unternehmen für Erdöl- und Gasindustrie, mit dem Staatlichen Ungarischen Geophysikalischen Institut Loránd Eötvös und mit dem Zentralamt für Geologie. Unsere angewandten Forschungen stehen in vollem Einklang mit unserer Tätigkeit auf dem Gebiete der Grundforschungen, sie tragen zur unmittelbaren Lösung der Aufgaben volkswirtschaftlicher Bedeutung bei und erweitern die Forschungsbasis.

Acta Geodaet., Geophys. et Montanist. Acad. Sci. Hung. Tomus 16 (2—4), pp. 179—190 (1981)

REMARKS ON UNBIASED FREE NET ADJUSTMENT

B. BARÓTHY—M. VERŐ-HETÉNYI

GEODETIC AND GEOPHYSICAL RESEARCH INSTITUTE OF THE HUNGARIAN ACADEMY OF SCIENCES, SOPRON

A linear algebraic view of biased parameter estimations in singular linear systems is given. A general theorem is proved for biased to non-biased estimation transformations. A free net example is computed to apply this theorem.

1. The best linear minimum bias estimator

We can describe the free net adjustment problem by the following general model:

$$\mathbf{A}\mathbf{x} = \hat{\mathbf{b}} + \mathbf{v}, \quad \exp(\mathbf{x}) = \mathbf{x}_0, \quad \exp(\hat{\mathbf{b}}) = \mathbf{A}\mathbf{x}_0 \quad \operatorname{cov}(\hat{\mathbf{b}}) = s^2\mathbf{P}^{-1}; \qquad (1)$$

where $\operatorname{rank}(\mathbf{A}) = \mathbf{r} < \min(m, n)$; $\mathbf{P}$ is hermitian positive definite; $\mathbf{A}$, $\hat{\mathbf{b}}$ and $\mathbf{P}$ are known; $\mathbf{x}$ and $\mathbf{v}$ are unknown; $\mathbf{x}_0$ and s^2 are to be estimated.

It is useful to start with reflecting to the geometric background of the problem. There are two linear spaces given: E^m the space of observation vectors with the semi-norm $\mathbf{P}$; and E^n the space of unknown vectors with the usual euclidean norm. Let $\mathcal{O}(\mathbf{A})$ be the column-space of $\mathbf{A}$, i.e. the subspace of rank r in E^m spanned by the column-vectors of $\mathbf{A}$. It is evident $\mathbf{A}\mathbf{x} \in \mathcal{O}(\mathbf{A})$ for all $\mathbf{x} \in E^m$, but in general $\mathcal{O}(\mathbf{A})$ does not contain the vector $\hat{\mathbf{b}}$ also given in E^m.

Therefore it is a very reasonable step to choice that unique vector $\widehat{\mathbf{A}\mathbf{x}} \in \mathcal{O}(\mathbf{A})$ which minimizes the distance between $\hat{\mathbf{b}}$ and $\mathcal{O}(\mathbf{A})$ in the sense of the $\mathbf{P}$-norm; i.e. let $\widehat{\mathbf{A}\mathbf{x}}$ be the result of the $\mathbf{P}$-orthogonal projection of $\hat{\mathbf{b}}$ onto $\mathcal{O}(\mathbf{A})$.

Because of the rank defect of $\mathbf{A}$ there is an $(n - r)$-dimensional hyperplane $\mathfrak{L}(\widehat{\mathbf{A}\mathbf{x}})$ in E^n containing the end points of all those vectors $\mathbf{x} \in E^n$ for which $\mathbf{A}\mathbf{x} = \widehat{\mathbf{A}\mathbf{x}}$. It is also reasonable to choice the shortest $\mathbf{x}$ pointing into the hyperplane $\mathfrak{L}(\widehat{\mathbf{A}\mathbf{x}})$. Let this unique vector be denoted by $\hat{\mathbf{x}}$.

Figure 1 shows the simple case of $m = 3$, $n = 2$, $r = 1$ and $\mathbf{P} = \mathbf{I}$ (unit matrix).

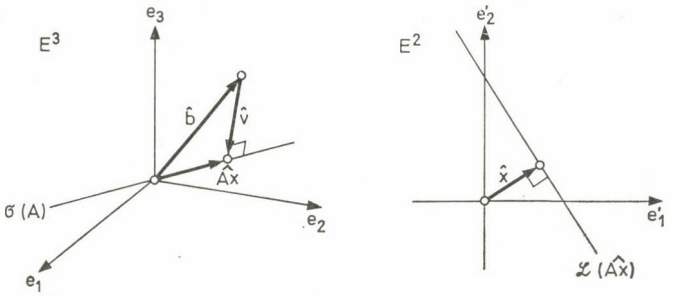

Fig. 1. $\mathbf{A} : E^2 \to \mathcal{O}(\mathbf{A})$; $\mathbf{A} : \mathfrak{L}\hat{\mathbf{Ax}}) \to \hat{\mathbf{Ax}}$

It is proved (see [1]) the solution of this double projection or double minimization task should be given in the form

$$\underset{n,1}{\hat{\mathbf{x}}} = \underset{n,m}{\mathbf{A}_{PI}^{+}} \underset{m,1}{\hat{\mathbf{b}}} \tag{2}$$

where $\mathbf{A}_{PI}^{+}$ denotes the Moore-Penrose **P** — **I**-inverse of the singular matrix **A**, accepting the **P** positive definite semi-norm in E^m and the **I** unit-norm in E^n. In the following we use the notation $\mathbf{A}_P^{+}$ instead of $\mathbf{A}_{PI}^{+}$.

Summarizing, this so-called **P** — **I**-generalized solution of (1) has the following property:

$$|| \hat{\mathbf{x}} || = \min \left\{ || \mathbf{x} || \;\middle|\; || \mathbf{Ax} - \hat{\mathbf{b}} ||_P = \min \{ || \mathbf{Ax} - \hat{\mathbf{b}} ||_P \;|\; \mathbf{x} \in E^n \} \right\}. \tag{3}$$

The procedure described above shows how to derive the solution (2) from the linear model (1) using only purely algebraic methods and aiming at the reasonable geometric property (3).

In order to apply this result in geodetic problems we have to investigate the stochastic properties of solution (2). Therefore we regard **x**, $\hat{\mathbf{b}}$ and **v** in model (1) as random variables; $\mathbf{x}_0$ and s^2 as distribution parameters to be estimated. The estimators (e.g. $\hat{\mathbf{x}}$) must also be random variables, having their own distribution parameters.

The mathematical statistical properties of estimator $\hat{\mathbf{x}}$ are collected in the abbreviation BLMBE, which means the random vector-variable $\hat{\mathbf{x}}$ is the "Best Linear Minimum-Bias Estimator" of $\mathbf{x}_0 = \exp(\mathbf{x})$. To give a complete view of this question we prove the validity of this statement (see also [1]).

a) The vector $\hat{\mathbf{x}}$ is a *linear* estimator, because $\mathbf{A}_P^{+}\hat{\mathbf{b}}$ is a linear vector-valued function of $\hat{\mathbf{b}}$.

b) The linear estimator $\hat{\mathbf{x}}$ gives a *biased* estimation for $\mathbf{x}_0$, because $\exp(\hat{\mathbf{x}}) = \exp(\mathbf{A}_P^{+}\hat{\mathbf{b}}) = \mathbf{A}_P^{+} \exp(\hat{\mathbf{b}}) = \mathbf{A}_P^{+}\mathbf{A}\mathbf{x}_0 \neq \mathbf{x}_0$ in general. Its bias is $|| (\mathbf{I} - \mathbf{A}_P^{+}\mathbf{A})\mathbf{x}_0 ||$.

c) The biased linear estimator $\hat{\mathbf{x}}$ gives a *minimum-bias* estimation for $\mathbf{x}_0$. Let $\mathbf{H}$ be an arbitrary $(n \times m)$ matrix, then the linear estimator $\mathbf{H}\hat{\mathbf{b}}$ has the bias

$$f(\mathbf{H}) = (\mathbf{x}_0 - \mathbf{H}\mathbf{A}\mathbf{x}_0)^*(\mathbf{x}_0 - \mathbf{H}\mathbf{A}\mathbf{x}_0) = \mathbf{x}_0^*\mathbf{x}_0 - \mathbf{x}_0^*\mathbf{H}\mathbf{A}\mathbf{x}_0 - \\ - \mathbf{x}_0^*\mathbf{A}^*\mathbf{H}^*\mathbf{x}_0 + \mathbf{x}_0^*\mathbf{A}^*\mathbf{H}^*\mathbf{H}\mathbf{A}\mathbf{x}_0\,, \tag{4}$$

where the asterisk denotes the conjugate transpose. Let us minimize this scalar-matrix function:

$$\frac{\partial f}{\partial \mathbf{H}} = -\mathbf{x}_0\mathbf{x}_0^*\mathbf{A}^* - \mathbf{x}_0\mathbf{x}_0^*\mathbf{A}^* + 2\mathbf{H}\mathbf{A}\mathbf{x}_0\mathbf{x}_0^*\mathbf{A}^* = \mathbf{0}\,, \tag{5}$$

$$\frac{\partial^2 f}{\partial \mathbf{H}^2} = \mathbf{A}\mathbf{x}_0\mathbf{x}_0^*\mathbf{A}^*. \tag{6}$$

From (5) we have:

$$\mathbf{H}\mathbf{A}\mathbf{x}_0\mathbf{x}_0^*\mathbf{A}^* = \mathbf{x}_0\mathbf{x}_0^*\mathbf{A}^* \tag{7}$$

and this equation should be valid for any $\mathbf{x}_0$. It means $\mathbf{A}^*$ is invariant for the transformation combined from $\mathbf{HA}$ and any one-rank hermitian singular transformation. Consequently $\mathcal{O}(\mathbf{A}^*)$ is invariant for $\mathbf{HA}$. The matrix $\mathbf{A}_P^+\mathbf{A}$ is the orthogonal $\mathbf{P}$-projector onto $\mathcal{O}(\mathbf{A}^*)$ therefore $\mathbf{HA} = \mathbf{A}_P^+\mathbf{A}$ satisfies the equation (7) and $\mathbf{H} = \mathbf{A}_P^+$ is a solution of (5). This solution gives the minimum of function f because the matrix in (6) is a positive semi-definite one. Thus

$$\min_H f(\mathbf{H}) = f(\mathbf{A}_P^+) = ||(\mathbf{I} - \mathbf{A}_P^+\mathbf{A})\mathbf{x}_0||$$

what agrees with the bias of estimator $\hat{\mathbf{x}}$.

d) The minimum-bias linear estimator $\hat{\mathbf{x}}$ is the *best* one in the sense of having the minimal variance among all minimum-bias linear estimators. Let us examine the covariance matrix of an arbitrary minimum-bias linear estimator $\mathbf{H}\hat{\mathbf{b}}$:

$$\operatorname{cov}(\mathbf{H}\hat{\mathbf{b}}) = \mathbf{H}\operatorname{cov}(\hat{\mathbf{b}})\mathbf{H}^* = s^2\mathbf{H}\mathbf{P}^{-1}\mathbf{H}^*. \tag{8}$$

From a basic property of $\mathbf{A}_P^+$ it is evident:

$$\mathbf{A}_P^+\mathbf{A}\mathbf{A}^* = \mathbf{A}^*(\mathbf{A}_P^+)^*\mathbf{A}^* = \mathbf{A}^*(\mathbf{A}^*)_{IP^{-1}}^+\mathbf{A}^*, \text{ i.e. } \mathbf{A}_P^+\mathbf{A}$$

is the $\mathbf{P}$-orthogonal projector onto $\mathcal{O}(\mathbf{A}_P^+)$ and $\mathcal{O}(\mathbf{A}^*)$ too, and therefore $\mathcal{O}(\mathbf{A}^*) = \mathcal{O}(\mathbf{A}_P^+)$.

We have seen above for any minimum-bias estimator $\mathbf{H}\hat{\mathbf{b}}$ the space $\mathcal{O}(\mathbf{A}^*)$ is invariant for the transformation $\mathbf{HA}$. Consequently $\mathcal{O}(\mathbf{A}_P^+)$ is also

invariant and $\mathbf{HAA}_P^+ = \mathbf{A}_P^+$. Applying the identity $\mathbf{A}_P^+ = (\mathbf{A^*PA})^+\mathbf{A^*P}$ we have:

$$\mathbf{HP}^{-1}(\mathbf{A}_P^+)^* = \mathbf{HP}^{-1}\mathbf{PA}(\mathbf{A^*PA})^+ = \mathbf{HAA}^+\mathbf{P}^{-1}(\mathbf{A^*})^+ = \mathbf{A}^+\mathbf{P}^{-1}(\mathbf{A^*})^+ = (\mathbf{A^*PA})^+,$$

$$\mathbf{A}_P^+\mathbf{P}^{-1}\mathbf{H^*} = (\mathbf{A^*PA})^+\mathbf{A^*PP}^{-1}\mathbf{H^*} = \mathbf{A}^+\mathbf{P}^{-1}(\mathbf{A^*})^+\mathbf{A^*H^*} = \mathbf{A}^+\mathbf{P}^{-1}(\mathbf{A^*})^+ = (\mathbf{A^*PA})^+,$$

$$\mathbf{A}_P^+\mathbf{P}^{-1}(\mathbf{A}_P^+)^* = (\mathbf{A^*PA})^+\mathbf{A^*PP}^{-1}\mathbf{PA}(\mathbf{A^*PA})^+ = (\mathbf{A^*PA})^+\mathbf{A^*PA}(\mathbf{A^*PA})^+ = (\mathbf{A^*PA})^+.$$

Using these identities the expression (8) could be transformed to the following equation:

$$\begin{aligned}\operatorname{cov}(\mathbf{H}\hat{\mathbf{b}}) &= s^2[(\mathbf{A^*PA})^+ + \mathbf{HP}^{-1}\mathbf{H^*} - \mathbf{HP}^{-1}\mathbf{PA}(\mathbf{A^*PA})^+ - \\ &- (\mathbf{A^*PA})^+\mathbf{A^*PP}^{-1}\mathbf{H^*} + (\mathbf{A^*PA})^+\mathbf{A^*PP}^{-1}\mathbf{PA}(\mathbf{A^*PA})^+] = \\ &= s^2[(\mathbf{A}_P^+\mathbf{P}^{-1}(\mathbf{A}_P^+)^* + (\mathbf{H} - \mathbf{A}_P^+)\mathbf{P}^{-1}(\mathbf{H} - \mathbf{A}_P^+)^*].\end{aligned} \tag{9}$$

It means the variances, i.e. the diagonal elements of the covariance matrix are sums of two non-negative values; one of them is a constant, the other is a function of **H**. The sum is minimum if and only if this function of **H** reaches its own minimum, consequently when $\mathbf{H} = \mathbf{A}_P^+$ is valid. Thus the variance matrix belonging to the minimum-variance minimum-bias linear estimator $\hat{\mathbf{x}}$ is:

$$\operatorname{cov}(\hat{\mathbf{x}}) = s^2\mathbf{A}_P^+\mathbf{P}^{-1}(\mathbf{A}_P^+)^* = s^2(\mathbf{A^*PA})^+. \tag{10}$$

The other stochastic properties of BLMBE are:

$$\exp(\hat{\mathbf{x}}) = \mathbf{A}_P^+\mathbf{Ax}_0, \tag{11}$$

$$\hat{\mathbf{v}} = \mathbf{A}\hat{\mathbf{x}} - \hat{\mathbf{b}} = (\mathbf{AA}_P^+ - \mathbf{I})\hat{\mathbf{b}}, \tag{12}$$

$$\exp(\hat{\mathbf{v}}) = \mathbf{AA}_P^+\mathbf{Ax}_0 - \mathbf{Ax}_0 = \mathbf{0},$$

$$\begin{aligned}\operatorname{cov}(\hat{\mathbf{v}}) &= \operatorname{cov}(\mathbf{A}\hat{\mathbf{x}} - \hat{\mathbf{b}}) = \operatorname{cov}\left((\mathbf{AA}_P^+ - \mathbf{I})\hat{\mathbf{b}}\right) = \\ &= (\mathbf{AA}_P^+ - \mathbf{I})\operatorname{cov}(\hat{\mathbf{b}})(\mathbf{AA}_P^+ - \mathbf{I})^* = \\ &= s^2[\mathbf{AA}_P^+\mathbf{P}^{-1}(\mathbf{A}_P^+)^*\mathbf{A^*} - \mathbf{P}^{-1}(\mathbf{A}_P^+)^*\mathbf{A^*} - \mathbf{AA}_P^+\mathbf{P}^{-1} + \mathbf{P}^{-1}] = s^2\mathbf{P}^{-1}(\mathbf{I} - \mathbf{AA}_P^+),\end{aligned} \tag{13}$$

$$\begin{aligned}\exp[(\hat{\mathbf{v}})^*\mathbf{Pv}] &= \exp[\operatorname{trace}(\mathbf{P}\hat{\mathbf{v}}(\hat{\mathbf{v}})^*)] = \operatorname{trace}[\exp(\mathbf{P}\hat{\mathbf{v}}(\hat{\mathbf{v}})^*] = \\ &= \operatorname{trace}[\mathbf{P}\operatorname{cov}(\hat{\mathbf{v}})] = s^2 \cdot \operatorname{trace}(\mathbf{I} - \mathbf{AA}_P^+) = s^2 \cdot [\operatorname{trace}(\mathbf{I}) - \operatorname{trace}(\mathbf{A}_P^+\mathbf{A})] = \\ &= s^2[m - \operatorname{trace}(\mathbf{B^*B})] = s^2(m - r),\end{aligned} \tag{14}$$

(we note $\mathbf{A}_P^+\mathbf{A}$ is a hermitian orthogonal projector and thus there is an $(n\times r)$ unitary matrix $\mathbf{B}$ for which $\mathbf{A}_P^+\mathbf{A} = \mathbf{BB}^*$ and $\mathbf{B}^*\mathbf{B} = \mathbf{I}_r$, where $\mathbf{I}_r$ is the r-rank unit matrix)

$$\widehat{s^2} = \frac{(\mathbf{v})^*\mathbf{Pv}}{m-r}\,;\ \exp(\widehat{s^2}) = s^2 \text{ (unbiased)}, \tag{15}$$

$$\widehat{\operatorname{cov}(\hat{\mathbf{v}})} = \frac{(\hat{\mathbf{v}})^*\mathbf{P}\hat{\mathbf{v}}}{m-r}\,\mathbf{P}^{-1}(\mathbf{I} - \mathbf{AA}_P^+)\,. \tag{16}$$

2. The biased to non-biased estimation transformation

It was the study of E. GRAFAREND and B. SCHAFFRIN [2] which directed the attention of geodesists to the bias of estimator $\hat{\mathbf{x}}$. At the same time the authors explained a lemma used as base for our further investigations. This lemma could be generalized for the **P**-normed case in the following way.

Lemma:

Let $\hat{\mathbf{x}}$ be the generalized solution (2) of equation (1), then for any $(k\times n)$ matrix $\mathbf{T}$ (k is arbitrary):

$$\exp(\mathbf{T}\hat{\mathbf{x}}) = \mathbf{T}\mathbf{x}_0 \tag{17}$$

if and only if

$$\mathbf{T} = \mathbf{T}(\mathbf{A}^*\mathbf{PA})^+(\mathbf{A}^*\mathbf{PA})\,. \tag{18}$$

Proof

$$\hat{\mathbf{x}} = \mathbf{A}_P^+\hat{\mathbf{b}} = (\mathbf{A}^*\mathbf{PA})^+\mathbf{A}^*\mathbf{P}\hat{\mathbf{b}},$$

$$\exp(\mathbf{T}\hat{\mathbf{x}}) = \mathbf{T}(\mathbf{A}^*\mathbf{PA})^+\mathbf{A}^*\mathbf{P}\exp(\hat{\mathbf{b}}) = \mathbf{T}(\mathbf{A}^*\mathbf{PA})^+(\mathbf{A}^*\mathbf{PA})\mathbf{x}_0 = \mathbf{T}\mathbf{x}_0$$

being $\mathbf{x}_0$ arbitrary, this is equivalent with

$\mathbf{T} = \mathbf{T}(\mathbf{A}^*\mathbf{PA})^+(\mathbf{A}^*\mathbf{PA})$; and inversely.

The matrix $\mathbf{T}$ was called the *difference operator* in [2] and computed examples were given for the basic types of geodetic free nets.

In the following we give a general explicit formulation for the transformation matrices satisfying the equivalent conditions (17) and (18).

The task is to create a new linear model using the known components $(\mathbf{A}, \hat{\mathbf{b}}, \mathbf{P})$ which could offer an unbiased minimum-variance linear estimator for the expectation-value parameter of its unknown. Let the new model be:

$$\underset{m,k}{\mathbf{C}}\ \underset{k,1}{\mathbf{y}} = \underset{m,1}{\hat{\mathbf{b}}} + \underset{m,1}{\mathbf{w}}\,. \tag{19}$$

Since $r = \text{rank}(\mathbf{A})$ is the greatest possible number of unknowns that would be unbiasedly estimable we restrict the problem for the case of $k = r$. Then the detailed version of model (19) is:

$$\begin{gathered} \underset{m,r}{\mathbf{C}} = \underset{m,n}{\mathbf{A}} \; \underset{n,r}{\mathbf{S}} \; ; \; \underset{r,1}{\mathbf{y}} = \underset{r,n}{\mathbf{T}} \; \underset{n,1}{\mathbf{x}}; \; \mathbf{Cy} = (\mathbf{AS})(\mathbf{Tx}) = \hat{\mathbf{b}} + \mathbf{w}; \\ \exp(\mathbf{y}) = \mathbf{Tx}_0; \; \exp(\hat{\mathbf{b}}) = \mathbf{Ax}_0; \; \operatorname{cov}(\hat{\mathbf{b}}) = s^2\mathbf{P}^{-1}. \end{gathered} \tag{20}$$

According to the previous conditions **C** must be a fullrank matrix, i.e. column-regular. Therefore **S** is also column-regular and **T** is row-regular.

The BLUE (Best Linear Unbiased Estimator) of the model (20) is given by $\hat{\mathbf{y}} = \mathbf{C}_P^+\hat{\mathbf{b}}$. Thus the condition for unbiasedness is:

$$\exp(\hat{\mathbf{y}}) = \exp[(\mathbf{AS})_P^+\hat{\mathbf{b}}] = (\mathbf{AS})_P^+ \exp(\hat{\mathbf{b}}) = (\mathbf{S^*A^*PAS})^{-1}\mathbf{S^*A^*PAx}_0 = \mathbf{Tx}_0. \tag{21}$$

Considering this equation for all $\mathbf{x}_0$ we have:

$$\mathbf{T} = (\mathbf{S^*A^*PAS})^{-1}\mathbf{S^*A^*PA}, \tag{22}$$

therefore $\mathbf{TS} = \mathbf{I}_r$ (the r-rank unit matrix). Since **T** and **S** are full rank matrices

$$\begin{aligned} \mathbf{S} &= \mathbf{T}^+ = \mathbf{T^*}(\mathbf{TT^*})^{-1}, \\ \mathbf{T} &= \mathbf{S}^+ = (\mathbf{S^*S})^{-1}\mathbf{S^*}. \end{aligned} \tag{23}$$

Consequently from Eq. (22);

$$\mathbf{T} = (\mathbf{AT}^+)_P^+\mathbf{A} = \mathbf{QA}, \qquad \text{where} \qquad \mathbf{Q} = (\mathbf{AT}^+)_P^+ \tag{24}$$

is an $r \times m$ full rank matrix. Let us choice a set of r linearly independent column vectors of **A**. For any choice there is a permutation matrix **M** of order n, dividing the matrix **A** for two partitions:

$$\underset{m,r}{(\mathbf{R}} \mid \underset{m,n-r}{\mathbf{Z}}) = \underset{m,n}{\mathbf{A}} \; \underset{n,n}{\mathbf{M}}, \qquad \mathbf{M}^2 = \mathbf{I}_n \tag{25}$$

where **R** is the column regular matrix containing the chosen columns and **Z** linearly depends on **R**. Thus there is an $r \times (n - r)$ matrix **U**:

$$\mathbf{Z} = \mathbf{RU} \qquad \text{and} \qquad \mathbf{U} = \mathbf{R}_P^+\mathbf{Z} = (\mathbf{R^*PR})^{-1}\mathbf{R^*PZ}. \tag{26}$$

With this notation:

$$\mathbf{A} = (\mathbf{R} \mid \mathbf{Z})\mathbf{M} = \mathbf{R}(\mathbf{I} \mid \mathbf{U})\mathbf{M} \tag{27}$$

$$\mathbf{T} = \mathbf{QA} = \mathbf{QR}(\mathbf{I} \mid \mathbf{U})\mathbf{M}. \tag{28}$$

Since both **Q** and **R** are full rank matrices and **Q** is arbitrary we can introduce the notation:

$$\underset{r,r}{\mathbf{D}} = \underset{r,m}{\mathbf{Q}} \quad \underset{m,r}{\mathbf{R}}, \tag{29}$$

where **D** is an arbitrary regular matrix. (Naturally the matrices **D** and **Q** are not arbitrary simultaneously.) Then in the model (20):

$$\mathbf{C} = \mathbf{A}\mathbf{T}^{+} = \mathbf{R}(\mathbf{I} \mid \mathbf{U})\mathbf{M}\mathbf{M}(\mathbf{I} \mid \mathbf{U})^{+}\mathbf{D}^{-1} = \mathbf{R}\mathbf{D}^{-1} \tag{30}$$

and

$$\mathbf{y} = \mathbf{T}\mathbf{x} = \mathbf{D}(\mathbf{I} \mid \mathbf{U})\mathbf{M}\mathbf{x}\,.$$

The BLUE is:

$$\hat{\mathbf{y}} = \mathbf{C}_P^{+}\hat{\mathbf{b}} = \mathbf{D}\mathbf{R}_P^{+}\hat{\mathbf{b}} = \mathbf{D}(\mathbf{R}^{*}\mathbf{P}\mathbf{R})^{-1}\mathbf{R}^{*}\mathbf{P}\hat{\mathbf{b}}\,, \tag{31}$$

what reduces the biased estimation to an unbiased one and the singular matrix computations to a regular one. Let us summarize the results:

Theorem

Let $\mathbf{A}\mathbf{x} = \hat{\mathbf{b}} + \mathbf{v}$; $\exp(\mathbf{x}) = \mathbf{x}_0$; $\exp(\hat{\mathbf{b}}) = \mathbf{A}\mathbf{x}_0$, $\operatorname{cov}(\hat{\mathbf{b}}) = s^2\mathbf{P}^{-1}$ a linear model and

$\mathbf{A} = \mathbf{R}(\mathbf{I} \mid \mathbf{U})\mathbf{M}$ an arbitrary rank-partitioning of **A** according to (25) and (26). Then **T** is a biased to unbiased transformator if and only if $\mathbf{T} = \mathbf{D}(\mathbf{I} \mid \mathbf{U})\mathbf{M}$ for any regular matrix **D**.

If **T** satisfies this condition then

$\widehat{\mathbf{T}\mathbf{x}} = \mathbf{T}\hat{\mathbf{x}} = \mathbf{D}(\mathbf{R}^{*}\mathbf{P}\mathbf{R})^{-1}\mathbf{R}^{*}\mathbf{P}\hat{\mathbf{b}}$ is the best linear unbiased estimator for $\mathbf{T}\mathbf{x}_0$.

From this infinite number of different transformations we can choice a unique one by fixing a particular rank-partitioning of **A** and a particular regular matrix **D**. The simplest choice is what follows. Let $\mathbf{R}(\mathbf{I} \mid \mathbf{U})\mathbf{M}$ be the rank partitioning produced by the Gram-Schmidt orthogonalization method executed in **P**-norm sense from left to right on the columns of **A** and let $\mathbf{D} = \mathbf{I}_r$.

An economic way for rank-partitioning with G-S method was given in [3]. This method produces the required matrices after the simultaneous execution of orthogonalization on the matrices **A** and $\mathbf{I}_n$:

$$\mathbf{A} \xrightarrow{\text{G-S}} (\mathbf{V} \mid \mathbf{0})\mathbf{M} \tag{32}$$

and

$$\mathbf{I}_n = \begin{pmatrix} \mathbf{I}_r & \mathbf{0} \\ \mathbf{0} & \mathbf{I}_{n-r} \end{pmatrix} \xrightarrow{\text{G-S}} \mathbf{M} \begin{pmatrix} \mathbf{Y} & \mathbf{X} \\ \mathbf{0} & \mathbf{I}_{n-r} \end{pmatrix} \mathbf{M}, \tag{33}$$

where

$$\mathbf{U} = -\mathbf{X}, \quad \mathbf{R}_P^+ = \mathbf{YV}^* \tag{34}$$

and the permutation matrix $\mathbf{M}$ is defined by the indices of null-vectors in $(\mathbf{V} \mid \mathbf{0})\mathbf{M}$.

In the case of the proposed simplest transformation $\mathbf{T} = (\mathbf{I} \mid \mathbf{U})\mathbf{M}$. The related estimators are:

$$\hat{\mathbf{y}} = \mathbf{T}\hat{\mathbf{x}} = \mathbf{R}_P^+ \hat{\mathbf{b}} \tag{35}$$

and

$$\hat{\mathbf{w}} = \mathbf{C}\hat{\mathbf{y}} - \hat{\mathbf{b}} = (\mathbf{R}\mathbf{R}_P^+ - \mathbf{I})\hat{\mathbf{b}}. \tag{36}$$

Using the Eqs (10), ..., (16) the statistical character of these estimators could be given as follows:

$$\operatorname{cov}(\hat{\mathbf{y}}) = \operatorname{cov}(\mathbf{R}_P^+ \hat{\mathbf{b}}) = s^2(\mathbf{R}^*\mathbf{P}\mathbf{R})^{-1}, \tag{37}$$

$$\exp(\hat{\mathbf{y}}) = \mathbf{R}_P^+ \mathbf{A}\mathbf{x}_0 = \mathbf{T}\mathbf{x}_0 \text{ (unbiased)}, \tag{38}$$

$$\exp(\hat{\mathbf{w}}) = (\mathbf{R}\mathbf{R}_P^+\mathbf{R} - \mathbf{R})(\mathbf{I} \mid \mathbf{U})\mathbf{M}\mathbf{x}_0 = \mathbf{0}, \tag{39}$$

$$\operatorname{cov}(\hat{\mathbf{w}}) = s^2\mathbf{P}^{-1}(\mathbf{I} - \mathbf{R}\mathbf{R}_P^+), \tag{40}$$

$$\exp[(\hat{\mathbf{w}})^*\mathbf{P}\hat{\mathbf{w}}] = s^2(m - r), \tag{41}$$

$$\widehat{s^2} = \frac{(\hat{\mathbf{w}})^*\mathbf{P}\hat{\mathbf{w}}}{m - r}, \quad \exp(\widehat{s^2}) = s^2 \text{ (unbiased)}, \tag{42}$$

$$\widehat{\operatorname{cov}(\hat{\mathbf{w}})} = \frac{(\hat{\mathbf{w}})^*\mathbf{P}\hat{\mathbf{w}}}{m - r}\mathbf{P}^{-1}(\mathbf{I} - \mathbf{R}\mathbf{R}_P^+). \tag{43}$$

It is very important to emphasize the matrices determined in the above theorem transform not only the biased estimator to a non-biased one but also the object of estimation. Therefore there is not any guarantee for the reasonable geodetic meaning of a transformed unknown.

After the estimation procedure described above we have a new linear model for the original unknowns:

$$\mathbf{T}\mathbf{x} = \hat{\mathbf{y}} + \mathbf{z}; \quad \exp(\mathbf{x}) = \mathbf{x}_0; \quad \exp(\mathbf{y}) = \mathbf{T}\mathbf{x}_0; \quad \operatorname{cov}(\hat{\mathbf{y}}) = s^2(\mathbf{R}^*\mathbf{P}\mathbf{R})^{-1}. \tag{44}$$

Since $\mathbf{T}$ is row-regular all solutions of this model give biased estimators. That makes more clear the fact: the examined transformation does not provide any possibility to construct an unbiased estimation for the original unknowns.

3. An example for practical computations

For the geodetic application of this method, the following example is shown. The triangle in the example has been determined by distance- and angular measurements (see Fig. 2).

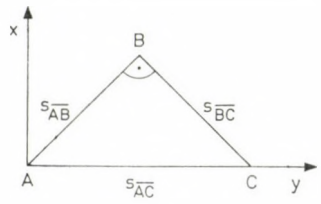

Fig. 2.

The approximative coordinates are the following:

$$A\begin{cases} x^0 = 0 \\ y^0 = 0 \end{cases} \qquad B\begin{cases} x^0 = 10 \\ y^0 = 10 \end{cases} \qquad C\begin{cases} x^0 = 0 \\ y^0 = 20\,. \end{cases}$$

The functions containing the unknowns have been linearized by introducing approximative coordinates ($x = x^\circ + \delta x$) and by series expansion. The correction equations obtained are the following:

$$\begin{aligned} c_{AB}\,\delta x_B + d_{AB}\,\delta y_B - c_{AB}\,\delta x_A - d_{AB}\,\delta y_A &= b_{\overline{AB}} + v_{\overline{AB}} \\ c_{AC}\,\delta x_C + d_{AC}\,\delta y_C - c_{AC}\,\delta x_A - d_{AC}\,\delta y_A &= b_{\overline{AC}} + v_{\overline{AC}} \\ c_{BC}\,\delta x_C + d_{BC}\,\delta y_C - c_{BC}\,\delta x_B - d_{BC}\,\delta y_B &= b_{\overline{BC}} + v_{\overline{BC}} \end{aligned}$$

$$\begin{aligned} &\frac{\varrho''}{s^0_{AC}} d_{AC}\delta x_A - \frac{\varrho''}{s^0_{AC}} d_{AC}\delta x_C - \frac{\varrho''}{s^0_{AC}} c_{AC}\delta y_A + \frac{\varrho''}{s^0_{AC}} c_{AC}\delta y_C = b_{(AC)} + v_{(AC)} \\ &\frac{\varrho''}{s^0_{AB}} d_{AB}\delta x_A - \frac{\varrho''}{s^0_{AB}} d_{AB}\delta x_B - \frac{\sigma''}{s^0_{AB}} c_{AB}\delta y_A + \frac{\varrho''}{s^0_{AB}} c_{AB}\delta y_B = b_{(AB)} + v_{(AB)} \\ &\frac{\varrho''}{s^0_{BC}} d_{BC}\delta x_B - \frac{\varrho''}{s^0_{BC}} d_{BC}\delta x_C - \frac{\varrho''}{s^0_{BC}} c_{BC}\delta y_B + \frac{\varrho''}{s^0_{BC}} c_{BC}\delta y_C = b_{(BC)} + v_{(BC)} \end{aligned} \tag{45}$$

where

$$c_{ij} = \frac{x^0_j - x^0_i}{s^0_{ij}}\,; \quad d_{ij} = \frac{y^0_j - y^0_i}{s^0_{ij}} \tag{46}$$

mean the coefficients, $b_{\overline{ij}}$ the free terms referring to the distances, $b_{(ij)}$ those referring to the directions.

Taking into account that no data are supposed to be errorfree in the correction equations of the three distance- and three angular measurements, the triangle is overdetermined and one has the case of a free adjustment. The matrix to be inverted is naturally singular.

The correction equations are on basis of Eq. (45) in a matrix form:

$$\mathbf{Ax} = \hat{\mathbf{b}} + \mathbf{v}.$$

In order to simplify the computations a triangle has been chosen (Fig. 2) for the numerical test for which the form matrix **A** of the correction equations can be split into a matrix product $\mathbf{A} = \mathbf{K} \cdot \mathbf{A}'$ in a way that the first term is a quadratic matrix with non-zero elements only in the main diagonal, the second term contains only positive and negative units as elements.

$$\mathbf{K} \cdot \begin{bmatrix} -1 & -1 & +1 & +1 & 0 & 0 \\ 0 & -1 & 0 & 0 & 0 & +1 \\ 0 & 0 & +1 & -1 & -1 & +1 \\ +1 & 0 & 0 & 0 & -1 & 0 \\ +1 & -1 & -1 & +1 & 0 & 0 \\ 0 & 0 & +1 & +1 & -1 & -1 \end{bmatrix} \cdot \begin{bmatrix} \delta x_A \\ \delta y_A \\ \delta x_B \\ \delta y_B \\ \delta x_C \\ \delta y_C \end{bmatrix} = \begin{bmatrix} b_{\overline{AB}} \\ b_{\overline{AC}} \\ b_{\overline{BC}} \\ b_{(AC)} \\ b_{(AB)} \\ b_{(BC)} \end{bmatrix} + \begin{bmatrix} v_{\overline{AB}} \\ v_{\overline{AC}} \\ v_{\overline{BC}} \\ v_{(AC)} \\ v_{(AB)} \\ v_{(BC)} \end{bmatrix}$$

where the matrix **K** is:

$$\mathbf{K} = \begin{bmatrix} \frac{1}{\sqrt{2}} & 0 & 0 & 0 & 0 & 0 \\ 0 & 1 & 0 & 0 & 0 & 0 \\ 0 & 0 & \frac{1}{\sqrt{2}} & 0 & 0 & 0 \\ 0 & 0 & 0 & \varrho'' \cdot 0.05 & 0 & 0 \\ 0 & 0 & 0 & 0 & \varrho'' \cdot 0.05 & 0 \\ 0 & 0 & 0 & 0 & 0 & \varrho'' \cdot 0.05 \end{bmatrix}$$

In the following the computations are carried out with the matrix $\mathbf{A}'$ instead of **A** without forgetting the matrix **K**. The number of the defects is in the present case two; the matrix **K** has full rank (as a diagonal matrix), therefore $\mathbf{A}'$ can be split according to Eq. (27) as:

$$\mathbf{A}' = (\mathbf{R} \mid \mathbf{Z})\mathbf{M},$$

and then one gets:

$$\mathbf{A} = (\mathbf{KR} \mid \mathbf{KZ})\mathbf{M} = \mathbf{K}(\mathbf{R} \mid \mathbf{Z})\mathbf{M} = \mathbf{KA}'$$

$$\mathbf{R} = \begin{bmatrix} -1 & -1 & +1 & +1 \\ 0 & -1 & 0 & 0 \\ 0 & 0 & +1 & -1 \\ +1 & 0 & 0 & 0 \\ +1 & -1 & -1 & +1 \\ 0 & 0 & +1 & +1 \end{bmatrix} \quad \text{and} \quad \mathbf{Z} = \begin{bmatrix} 0 & 0 \\ 0 & +1 \\ -1 & +1 \\ -1 & 0 \\ 0 & 0 \\ -1 & -1 \end{bmatrix}.$$

Thus the permutation matrix **M** does not play here any role, as no column- and row interchanges are necessary.

For the computation of the matrix **U** of Eq. (26) one needs the inverse $\mathbf{R}^+$ for which the following is valid:

$$\mathbf{R}^+ = \begin{bmatrix} -\frac{1}{4} & 0 & +\frac{1}{4} & +\frac{1}{2} & +\frac{1}{4} & +\frac{1}{4} \\ -\frac{1}{4} & -\frac{1}{2} & -\frac{1}{4} & 0 & -\frac{1}{4} & +\frac{1}{4} \\ +\frac{1}{8} & 0 & +\frac{3}{8} & +\frac{1}{4} & -\frac{1}{8} & +\frac{3}{8} \\ +\frac{1}{8} & -\frac{1}{4} & -\frac{3}{8} & 0 & +\frac{1}{8} & +\frac{3}{8} \end{bmatrix}$$

now one can compute the matrix **U**:

$$\mathbf{U} = \begin{bmatrix} -1 & 0 \\ 0 & -1 \\ -1 & 0 \\ 0 & -1 \end{bmatrix}.$$

At last according to the theorem the computation of **T** can be made as follows:

$$\mathbf{T} = (\mathbf{I} \mid \mathbf{U}) = \begin{bmatrix} 1 & 0 & 0 & 0 & -1 & 0 \\ 0 & 1 & 0 & 0 & 0 & -1 \\ 0 & 0 & 1 & 0 & -1 & 0 \\ 0 & 0 & 0 & 1 & 0 & -1 \end{bmatrix}.$$

The matrix **K** which has been introduced in order to simplify the computations must be taken again into account when the unknowns are computed according to Eq. (35), and the corrections according to Eq. (36).

$$\mathbf{y} = \mathbf{T}\hat{\mathbf{x}} = (\mathbf{RK})^+\hat{\mathbf{b}} = \mathbf{K}^+\mathbf{R}^+\hat{\mathbf{b}}$$

$$\hat{\mathbf{y}} = \begin{bmatrix} -0.1768 & 0 & +0.1768 & +0.000048 & +0.000024 & +0.000024 \\ -0.1768 & -0.3535 & -0.1768 & 0 & -0.000024 & +0.000024 \\ +0.08839 & 0 & +0.2651 & +0.000024 & -0.000012 & +0.000036 \\ +0.08839 & -0.1768 & -0.2651 & 0 & +0.000012 & +0.000036 \end{bmatrix} \cdot \begin{bmatrix} b_{\overline{AB}} \\ b_{\overline{AC}} \\ b_{\overline{BC}} \\ b_{(AC)} \\ b_{(AB)} \\ b_{(BC)} \end{bmatrix}.$$

The corrections are as follows:

$$\hat{\mathbf{w}} = \big((\mathbf{KR})(\mathbf{KR})^{+} - \mathbf{I}\big)\hat{\mathbf{b}} = (\mathbf{KRR}^{+}\mathbf{K}^{+} - \mathbf{I})\hat{\mathbf{b}} =$$

$$= (\mathbf{RR}^{+}\mathbf{KK}^{+} - \mathbf{I})\hat{\mathbf{b}} = (\mathbf{RR}^{+} - \mathbf{I})\hat{\mathbf{b}}$$

$$\hat{\mathbf{w}} = \frac{1}{4}\begin{bmatrix} -1 & +1 & 0 & -1 & 0 & +1 \\ +1 & -2 & +1 & 0 & +1 & -1 \\ 0 & +1 & -1 & +1 & -1 & 0 \\ -1 & 0 & +1 & -2 & +1 & +1 \\ 0 & +1 & -1 & +1 & -1 & 0 \\ +1 & -1 & 0 & +1 & 0 & -1 \end{bmatrix} \cdot \begin{bmatrix} b_{\overline{AB}} \\ b_{\overline{AC}} \\ b_{\overline{BC}} \\ b_{(AC)} \\ b_{(AB)} \\ b_{(BC)} \end{bmatrix}.$$

REFERENCES

1. Rao, C. R.—Mitra, S. K.: Generalized Inverse of Matrices and its Applications. John Wiley and Sons, Inc., New York 1971.
2. Grafarend, E.—Schaffrin, B.: Unbiased Free Net Adjustment. Survey, Review, 22 (1974). 171, 200—218.
3. Rust, B.—Burrus, W. R.—Schneeberg, C.: A Simple Algorithm for Computing the Generalized Inverse of a Matrix. *Comm. of ACM*, 9/5 (1966), 381—387.

ЗАМЕЧАНИЯ О НЕИСКАЖЕННОМ УРАВНИВАНИИ СВОБОДНЫХ СЕТЕЙ

Б. БАРОТИ—М. ВЕРЁ-ХЕТЭНИ

РЕЗЮМЕ

В статье дается рассмотрение методами линейной алгебры об оценке искаженных параметров в сингулярных линейных системах. Доказывается общая теорема для преобразования искаженных оценок в неискаженные. Для иллюстрации применения теоремы вычисляется пример в отношении свободных сетей.

Acta Geodaet., Geophys. et Montanist. Acad. Sci. Hung. Tomus 16 (2—4), pp. 191—207 (1981)

ON THE TRANSFORMATION OF GEODETIC NETWORKS USING LEAST SQUARES ADJUSTMENT

F. HALMOS†

DOCTOR OF TECHN. SCI.

GEODETIC AND GEOPHYSICAL RESEARCH INSTITUTE OF THE HUNGARIAN ACADEMY OF SCIENCES, SOPRON

Transformations between geodetic networks can be most easily carried out by using least squares adjustment. The problem is at present of special importance for the common adjustment of Doppler-satellite geodetic networks, and of terrestrial triangulation and leveling networks. In the investigations described here a solution for the common adjustment of the geodetic networks of several countries is looked for, whereby the deduction of independent transformation parameters for each network is justified. Basically a solution based on the Helmertian block-adjustment is proposed, but other methods are also shortly reviewed. Formulae for the computations and for the adjustment are given.

1. Introduction

When connecting mathematically networks referring to different planar and spatial coordinate systems, the contradictions must be resolved by transformations. There are several known methods for the determination of the transformation parameters; corresponding comprehensive analyses can be found e.g. in BURSA (1962), WOLF (1963), MORITZ (1973), SIGL (1978), HALMOS (1980).

From the transformation models, the Bursa-model (also known as Bursa—Wolf model), the two methods proposed by MOLODENSKY (also denoted as Molodensky—Badekas method), the Veis-model, the Krakiwsky—Thomson method and the Wells—Vanicek method should be mentioned. It can be easily shown that the models of BURSA, MOLODENSKY and VEIS have many similarities or common points. The adjustment based on the collocation principle can also be used if the elements of the variance-covariance are *a priori* well known.

The results of terrestrial geodetic triangulation and leveling measurements can be easily transformed into spatial geocentric coordinates, and then adjusted three-dimensionally. This can be connected with the three-dimensional Doppler-adjustment [VINCENTY, 1980; WOLF, 1980]. It can also be found a solution where the original triangulation observations appear in the adjustment model [WOLF, 1980], but in that case caution must be preserved to the introduction of the height data into the adjustment. It is obvious that the accuracy

of the rigorous leveling supplemented by gravimetric measurements is very high. It should not be forgotten, however, that due to the connection to different absolute sea level differences of some tens of cm-s (in certain cases even of about 1 m) can be experienced. From this point of view it should be considered whether it would be useful to compare the relative height differences with Doppler observations having an accuracy of $\pm 0.3-0.5$ m, and to introduce them as constraints into the adjustment. An other solution would be to adopt the Doppler or other satellite geodetic heights.

In the following the problems of the so-called 7 parameters transformation (3 rotational, 3 translational elements and 1 scaling factor) based on the similarity transformation are analyzed on the basis of the least squares adjustment. Some special transformation problems shall also be mentioned mainly for the sake of comparison. The solutions of the connection of several networks by using the Helmertian block adjustment are studied in details.

2. General problems of the transformations between coordinate systems

2.1 *Systems of coordinates*

The coordinates characterizing the position of geodetic points with respect to each other can be either local or global ones. For the determination of the coordinates, different kinds of geodetic or satellite geodetic measurements can be used. Since the measurement results are referring to the physical surface of the Earth, the gravitational force and its changes supplement the originally purely geometric problem with physical—geophysical aspects.

From the point of view of the functional models, the following two kinds of coordinate systems can be distinguished: Natural coordinate systems are used for the description of the point coordinates on the basis of geodetic measurement results, while traditional or conventional coordinate systems are used for the description of the Earth's surface. Recently, for latter purpose the use of three-dimensional coordinate systems gains importance. In certain cases the changes of coordinates with time must also be studied (geodynamics) which leads us to four-dimensional coordinate systems. In national survey and in industrial survey two-dimensional planar coordinates and separate one-dimensional height coordinates are mostly used.

The global geocentric coordinate systems (their origin is the mass centre of the Earth, the Z-axis points towards the mean pole, the X-axis towards the mean Greenwich meridian, thus the plane XY is the equipotential plane and the plane XZ is the Greenwich meridional plane) and the local astronomic coordinate systems (their origin in a three-dimensional system is the chosen initial point or topocentre, the vertical axis is the plumb line in the direction

of the astronomical zenith, the x-axis points towards the astronomical meridian, i.e. towards North, the y-axis perpendicularly to it towards East) are natural coordinate systems.

Traditional or conventional coordinate systems include the global ellipsoidic systems (the origin in the centre of the ellipsoid, the axis $\overline{Z}$ lies in the rotational axis of the ellipsoid, the axis $\overline{X}$ points towards the zero, initial meridian (Greenwich ellipsoidic meridian), the axis $\overline{Y}$ is perpendicular to it in a right hand system) and the local ellipsoidic coordinate systems (the origin is in an arbitrary basic point, the axis $\bar{z}$ lies in the normal of the ellipsoid, i.e. in the geodetic zenith, the axis $\bar{x}$ is the rotational axis of the ellipsoid, i.e. the geodetic meridian, the axis $\bar{y}$ points perpendicularly to them towards East).

In order to be able to carry out transformations between coordinates given in different coordinate systems, several transformation methods can be used [e.g. HALMOS 1980]. With respect to the present satellite observation techniques it is a general practice to carry out computations and adjustment in a geocentric coordinate system. On the basis of the ellipsoidic latitude B_i, ellipsoidic longitude L_i and ellipsoidic height $\overline{H}_i$ of the point i, the coordinates in the spatial geocentric system $\overline{X}$, $\overline{Y}$, $\overline{Z}$ can be obtained by means of the following formula:

$$\overline{\mathbf{R}}_i = \begin{bmatrix} \overline{X}_i \\ \overline{Y}_i \\ \overline{Z}_i \end{bmatrix} = \begin{bmatrix} (N_i + \overline{H}_i) \cos B_i \cos L_i \\ (N_i + \overline{H}_i) \cos B_i \sin L_i \\ \left(N_i \frac{b^2}{a^2} + \overline{H}_i\right) \sin B_i \end{bmatrix} \tag{1}$$

where $\overline{H}_i = H_i + h_i$, and the following notations are used:

H_i is the height of the point i above sea level,
h_i is the height of the geoid in the point i above the ellipsoid,
$\overline{H}_i$ is the height of the point i above the ellipsoid,
a, b are the major and minor semi-axes of the ellipsoid,
N_i is the radius of the cross curvature.

It follows from Eq. 1 that for the determination of geocentric Cartesian coordinates on the basis of ellipsoidic coordinates uniform heights above sea level and geoid heights determined with an adequate accuracy are needed. Since an accuracy of $\pm 0.3-0.5$ m can already be reached in the determination of the spatial points coordinates even in a greater area, it follows that in the future a more precise determination of the geoid will be needed.

It should be mentioned supplementarily that a satellite geodetic or Doppler network in itself is undetermined together with the transformation parameters, but the combination with a terrestrial geodetic network resolves this undeterminedness.

2.2 *Determination of the transformation parameters between coordinate systems with adjustment in case of two kinds of networks*

The results of terrestrial geodetic measurements and of Doppler observations are often computed in a common adjustment model [ÁDÁM et al., 1979; HALMOS, 1980]. There are systematic deviations between the two kinds of networks partly due to deviations in the scale factor and of the orientation of the two systems, partly due to differences in the origin of the coordinate systems. Let us denote the scale factor according to WOLF (1980) by $(1 + \Delta)$ (it is sometimes denoted by $(1 + k)$, too), the rotational factor between the three axis by $\delta\varepsilon$, if the deviation between the systems is very small in consequence of the introductions of well-adopted approximative vector ε, and the translation vector in the origin by $\delta\mathbf{r}_0$, if it is also very small due to the introduction of a well-adopted approximative value $\mathbf{r}_0$. It should be mentioned that all these factors, i.e. the unknown one scale factor, the three rotational factors, and the three translational factors refer to the system determined by Doppler measurements. This means that the task is to transform the Doppler data into the terrestrial geodetic coordinate system, i.e. the latter is accepted as a general reference system. If there are some *a priori* informations about the accuracy of the values Δ and $\delta\varepsilon$, their weights $\mathbf{P}_\Delta$ and $\mathbf{P}_\varepsilon$ can also be introduced into the adjustment.

From the point of view of the adjustment let us consider as one of the blocks the system of correction equations deduced from the terrestrial geodetic measurements, and as the other block the system deduced for the Doppler observations. The system of normal equations for both blocks must be reduced as long as the unknown coordinates of the Doppler stations will be reached including now of course the transformation parameters. All other not common unknowns have already been eliminated by the reduction of the normal equations. Thus, among others the orbital elements from the satellite observations, the refraction unknowns and other parameters, too [WOLF, 1980]. A considerable amount of computations in the reduction and inversion can be spared by using the splitting into Helmertian blocks [WOLF, 1978].

When neglecting the orbital and other parameters, the correction equation for the Doppler satellite observations is [WOLF, 1980; HALMOS, 1980]:

$$\mathbf{v} = \mathbf{r}_D(1 + \Delta) + \mathbf{A}\delta\varepsilon + \mathbf{B}\delta\mathbf{r}_0 - (\mathbf{r}^0 + \delta\mathbf{r}) \tag{2}$$

where $\delta\varepsilon = [\varepsilon_x, \varepsilon_y, \varepsilon_z]^T$ are the rotational elements for all the three axes,
$\delta\mathbf{r}_0 = [\Delta X_0, \Delta Y_0, \Delta Z_0]^T$ the translational values of the origin for the three directions,
$\mathbf{r}_{D_i} = [\ldots[X_D, Y_D, Z_D]\ldots]_T$ the coordinates deduced from the adjustment of the Doppler observations ($i = 1, 2, \ldots n$), n is the number of

Doppler stations, $\delta\mathbf{r} = \mathbf{r} - \mathbf{r}^0$ are the coordinate changes resulting from common adjustment, $\mathbf{r}$ is the final coordinate,
$\mathbf{r}^0$ the adopted approximative value,
$\mathbf{v}$ = the values of the corrections.

Further according to the Bursa-model [HALMOS, 1980]:

$$\mathbf{A}^T = [\mathbf{A}_1^T, \mathbf{A}_2^T \ldots \mathbf{A}_i^T \ldots \mathbf{A}_n^T]$$

$$\mathbf{A}_i = \begin{bmatrix} 0 & Z_i & Y_i \\ -Z_i & 0 & X_i \\ Y_i & -X_i & 0 \end{bmatrix} \tag{3}$$

$\mathbf{B}^T = [\mathbf{I}, \mathbf{I} \ldots \mathbf{I}]$ where $\mathbf{I}$ is the unit matrix.

If the changes of the coordinates $\delta\mathbf{r}$ are brought to the first places, as made by WOLF, then:

$$\mathbf{v} = -\delta\mathbf{r} + \mathbf{r}_D\Delta + \mathbf{A}\delta\varepsilon + \mathbf{B}\delta\mathbf{r}_0 + \mathbf{l}_D \tag{4}$$

where $\mathbf{l}_D = \mathbf{r}_D - \mathbf{r}^0$. The value $\mathbf{r}_D$ is received after elimination of all unknowns with the exception of the unknown coordinates. If the reduced matrix is denoted by $\mathbf{N}_D$ and the condition

$$\mathbf{v}^T\mathbf{N}_D\mathbf{v} = \min \tag{5}$$

is introduced, where $\mathbf{N}_D$ can be manipulated as a weight matrix of $\delta\mathbf{r}$, then the following reduced normal matrix can be written on the basis of Eq. 4 together with the transformation parameters [WOLF, 1980]:

$$\begin{bmatrix} \mathbf{N}_D, & -\mathbf{N}_D\mathbf{r}_D, & -\mathbf{N}_D\mathbf{A}, & -\mathbf{N}_D\mathbf{B} \\ -(\mathbf{N}_D\mathbf{r}_D)^T, & (\mathbf{r}_D\mathbf{N}_D\mathbf{r}_D+\mathbf{P}_\Delta), & \mathbf{r}_D^T\mathbf{N}_D\mathbf{A}, & \mathbf{r}_D^T\mathbf{N}_D\mathbf{B} \\ -(\mathbf{N}_D\mathbf{A})^T, & (\mathbf{r}_D^T\mathbf{N}_D\mathbf{A})^T, & (\mathbf{A}^T\mathbf{N}_D\mathbf{A}+\mathbf{P}_\varepsilon), & \mathbf{A}^T\mathbf{N}_D\mathbf{B} \\ -(\mathbf{N}_D\mathbf{B})^T, & (\mathbf{r}^T\mathbf{N}_D\mathbf{B})^T, & (\mathbf{A}^T\mathbf{N}_D\mathbf{B})^T, & \mathbf{B}^T\mathbf{N}_D\mathbf{B} \end{bmatrix} \begin{bmatrix} \delta\mathbf{r} \\ \Delta \\ \delta\varepsilon \\ \delta\mathbf{r}_0 \end{bmatrix} + \tag{6}$$

$$+ \begin{bmatrix} \mathbf{l}_D \\ -\mathbf{r}_D^T\mathbf{l}_D \\ -\mathbf{A}^T\mathbf{l}_D \\ -\mathbf{B}^T\mathbf{l}_D \end{bmatrix} = 0$$

where the a priori weights $\mathbf{P}_\Delta$ and $\mathbf{P}_\varepsilon$ are also taken into account. It is supposed that the changes Δ and δ in the adjustment are very small and therefore their products as well as the second- and higher order terms can be neglected [HALMOS, 1980].

The Doppler coordinate system X_D, Y_D, Z_D with the origin OD can be seen in Fig. 1 with respect to the coordinate system of the terrestrial geodetic network having the origin OG. As it has been already mentioned it is advantageous to transform the Doppler system into the terrestrial geodetic coordinate system.

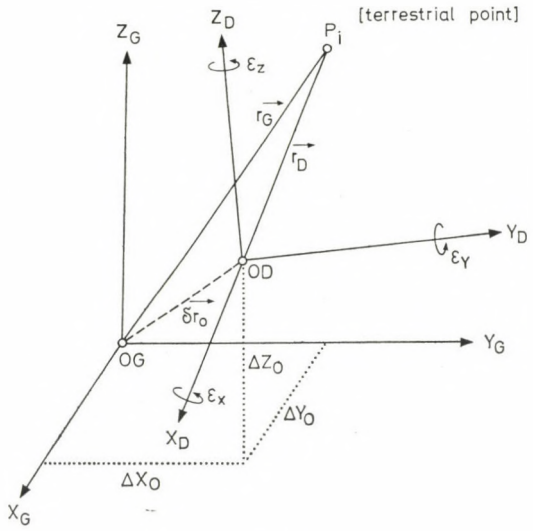

Fig. 1.

Let us suppose that in the adjustment of the geodetic network the points of the Doppler observations are at the same time triangulation points, therefore the reduction of the normal matrix must be done till the unknowns of the Doppler points. The reduced normal matrix of the geodetic three-dimensional adjustment [WOLF, 1980] is on the basis of the existing correction equations [HALMOS, 1980]:

$$\mathbf{N}_g \delta\mathbf{r} + \mathbf{l}_g = 0 \tag{7}$$

where $\mathbf{N}_g$ ist ehe coefficient matrix, $\mathbf{l}_g$ is the free term. A combination of the Eqs 6 and 7 gives the normal matrix obtained from terrestrial geodetic and Doppler-satellite measurements in the following form:

$$\begin{bmatrix} (\mathbf{N}_g + \mathbf{N}_D), & -\mathbf{N}_D\mathbf{r}_D, & -\mathbf{N}_D\mathbf{A}, & -\mathbf{N}_D\mathbf{B} \\ -(\mathbf{N}_D\mathbf{r}_D)^T, & (\mathbf{r}_D^T\mathbf{N}_D\mathbf{r}_D + \mathbf{P}_\Delta), & \mathbf{r}^T\mathbf{N}_D\mathbf{A}, & \mathbf{r}^T\mathbf{N}_D\mathbf{B} \\ -(\mathbf{N}_D\mathbf{A})^T, & (\mathbf{r}_D^T\mathbf{N}_D\mathbf{A})^T, & (\mathbf{A}^T\mathbf{N}_D\mathbf{A} + \mathbf{P}_\varepsilon), & \mathbf{A}^T\mathbf{N}_D\mathbf{B} \\ -(\mathbf{N}_D\mathbf{B})^T, & (\mathbf{r}_D^T\mathbf{N}_D\mathbf{B})^T, & (\mathbf{A}^T\mathbf{N}_D\mathbf{B})^T, & \mathbf{B}^T\mathbf{N}_D\mathbf{B} \end{bmatrix} \begin{bmatrix} \delta\mathbf{r} \\ \Delta \\ \delta\varepsilon \\ \delta\mathbf{r}_0 \end{bmatrix} + \tag{8}$$

$$+ \begin{bmatrix} (\mathbf{l}_g + \mathbf{l}_D) \\ -\mathbf{r}_D^T\mathbf{l}_D \\ -\mathbf{A}^T\mathbf{l}_D \\ -\mathbf{B}^T\mathbf{l}_D \end{bmatrix} = 0.$$

The inversion of the matrix yields the unknown coordinate-changes, the transformation parameters as well as their variance-covariance matrix.

2.3 *Transformation by the connection of several networks by adjustment*

If one has not only one terrestrial geodetic network, but several networks or systems of networks, and all the networks must be interpreted as independent units, the already mentioned seven transformation parameters must be determined for each network. For the coverage of a greater area, a Doppler observation system can be used. According to this, the transformation of the Doppler measurements into the geodetic network yields different parameters of the different cases. The method for the deduction of the equations, further the normal matrices obtained on the basis of the terrestrial geodetic measurements and of the Doppler observations can be reduced till the common unknowns. In the following, a partitioning is advantageous, as the transformation parameters are different for the networks or network parts, respectively.

Before deducing the connections it is worth illustrating the terrestrial and Doppler measurements in the networks (Fig. 2), and the transformation problems in connection with the coordinate systems (Fig. 3). Figure 2 shows six geodetic networks with different orientations and scales, which are stiffened by the Doppler network denoted by full dots. The coordinate systems of the terrestrial geodetic networks and the coordinate system of the Doppler network is illustrated in Fig. 3. There are two possible solutions.

The first case occurs in consequence of the decision that the observation, the orientation, the scale and the position of the Doppler network are more reliable, and therefore the Doppler network is accepted. In that case the coordinate systems of the terrestrial geodetic measurements must be transformed into the Doppler system. Now there are $7 \times 6 = 42$ transformation parameters

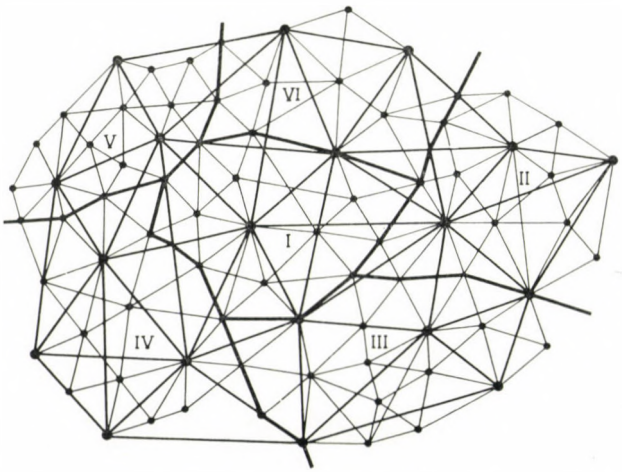

Fig. 2.

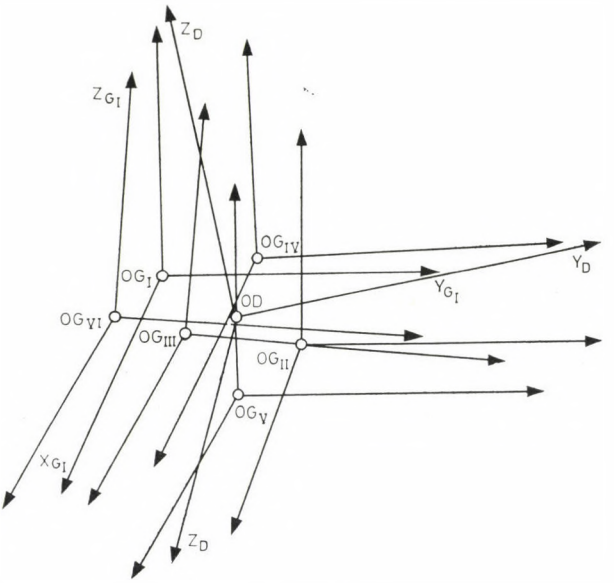

Fig. 3.

to be determined supplementarily. The aim is in such a case the deduction of a uniform common three-dimensional network.

In the second case the single national networks are to be accepted and accordingly the data concerning the Doppler coordinate system must be transformed into the terrestrial geodetic network. In this case the number of the transformation parameters is again 42.

Let us consider the latter case taking into account that from the point of view of the theoretical basis the two solutions are similar. As it can be seen from Fig. 2, the individual network parts do not include all Doppler connection points. Further, it is obvious, from the structure of the system of equations (8) that if all network parts obtain independent transformation parameters, the matrix will be stepwise full. Taking all these into account let us denote the coefficients and unknown parameters of the normal matrix reduced till the common unknowns of the Doppler point coordinates of the different (geodetic and Doppler) networks as follows:

$$[(\mathbf{N}_g + \mathbf{N}_D)_I, (\mathbf{N}_g + \mathbf{N}_D)_{II}, \ldots, (\mathbf{N}_g + \mathbf{N}_D)_m] = \mathbf{N}$$

$$[-(\mathbf{N}_D\mathbf{r}_D)_I] = \mathbf{R}_I, [-(\mathbf{N}_D\mathbf{r}_D)_{II}] = \mathbf{R}_{II}, \ldots, [-(\mathbf{N}_D\mathbf{r}_D)]_m = \mathbf{R}_m \tag{9}$$

$$[\delta\mathbf{r}_I, \delta\mathbf{r}_{II}, \ldots, \delta\mathbf{r}_m]^T = \delta\,. \tag{10}$$

Further one has:

$$\begin{bmatrix} (\mathbf{r}_D^T\mathbf{N}_D\mathbf{r}_D + \mathbf{P}_\Delta), & \mathbf{r}_D^T\mathbf{N}_D\mathbf{A}, & \mathbf{r}_D^T\mathbf{N}_D\mathbf{B} \\ (\mathbf{r}_D^T\mathbf{N}_D\mathbf{A})^T, & (\mathbf{A}^T\mathbf{N}_D\mathbf{A} + \mathbf{P}_\varepsilon), & \mathbf{A}^T\mathbf{N}_D\mathbf{B} \\ (\mathbf{r}_D^T\mathbf{N}_D\mathbf{B})^T, & (\mathbf{A}^T\mathbf{N}_D\mathbf{B})^T, & \mathbf{B}^T\mathbf{N}_D\mathbf{B} \end{bmatrix}_I = \mathbf{M}_I$$

$$\vdots \qquad (11)$$

$$\begin{bmatrix} (\mathbf{r}_D^T\mathbf{N}_D\mathbf{r}_D + \mathbf{P}_\Delta), & \mathbf{r}_D^T\mathbf{N}_D\mathbf{A}, & \mathbf{r}_D^T\mathbf{N}_D\mathbf{B} \\ (\mathbf{r}_D^T\mathbf{N}_D\mathbf{A})^T, & (\mathbf{A}^T\mathbf{N}_D\mathbf{A} + \mathbf{P}_\varepsilon), & \mathbf{A}^T\mathbf{N}_D\mathbf{B} \\ (\mathbf{r}_D^T\mathbf{N}_D\mathbf{B})^T, & (\mathbf{A}^T\mathbf{N}_D\mathbf{B})^T, & \mathbf{B}^T\mathbf{N}_D\mathbf{B} \end{bmatrix}_m = \mathbf{M}_m$$

and

$$\begin{aligned} [\Delta_I, \quad \delta\varepsilon_I, \quad \delta\mathbf{r}_{0I}]^T &= \delta_I \\ &\vdots \\ [\Delta_m, \quad \delta\varepsilon_m, \quad \delta\mathbf{r}_{0,m}]^T &= \delta_m \end{aligned} \qquad (12)$$

$$\begin{aligned} &[(\mathbf{l}_g + \mathbf{l}_D)_I, \quad (\mathbf{l}_g + \mathbf{l}_D)_{II}, \quad \ldots, \quad (\mathbf{l}_g + \mathbf{l}_D)_m]^T = \mathbf{L} \\ &[-(\mathbf{r}_D^T\mathbf{l}_D)_I, \quad -(\mathbf{A}^T\mathbf{l}_D)_I, \quad -(\mathbf{B}^T\mathbf{l}_D)_I] = \mathbf{L}_I \\ &\quad \vdots \qquad (13) \\ &[-(\mathbf{r}_D^T\mathbf{l}_D)_m, \quad -(\mathbf{A}^T\mathbf{l}_D)_m, \quad -(\mathbf{B}^T\mathbf{l}_D)_m] = \mathbf{L}_m . \end{aligned}$$

Taking all these into account, the reduced geodetic and Doppler system of normal equations for a system consisting of $(I - m)$ parts has the following form:

$$\left[\begin{array}{c|cccc} \mathbf{N} & \mathbf{R}_I & \mathbf{R}_{II} & \ldots & \mathbf{R}_m \\ \hline \mathbf{R}_I^T & \mathbf{M}_I & \mathbf{0} & \ldots & \mathbf{0} \\ \mathbf{R}_{II}^T & \mathbf{0} & \mathbf{M}_{II} & \ldots & \mathbf{0} \\ \vdots & \vdots & \vdots & & \vdots \\ \mathbf{R}_m^T & \mathbf{0} & \mathbf{0} & & \mathbf{M}_m \end{array}\right] \left[\begin{array}{c} \delta \\ \hline \delta_I \\ \delta_{II} \\ \vdots \\ \delta_m \end{array}\right] + \left[\begin{array}{c} \mathbf{L} \\ \hline \mathbf{L}_I \\ \mathbf{L}_{II} \\ \vdots \\ \mathbf{L}_m \end{array}\right] = \mathbf{0} . \qquad (14)$$

The basis of the solution is the partitioning of the unknowns, and consequently of the coefficient matrix into two groups. The first is the system of equations containing the coordinate unknowns (δ), the second is the equation group containing the transformation elements $\delta_I(\delta_I\delta_m)$. The unknown coordinate changes δ are immediately correlated with the transformation parameters or groups of parameters, the latter are, however, according to our supposition uncorrelated between themselves, i.e. the coefficient elements for the covariances are equal zero. If there are no a priori estimations for the values $\mathbf{P}_\Delta$ and $\mathbf{P}_\varepsilon$, they are equal zero, too.

If the number of the coordinate unknowns is n, the dimension of the matrix $\mathbf{N}$ is (n, n). As all groups of the transformation parameters contain

7 variables δ_i, the dimension of the $\mathbf{R}_i$-s is $(n, 7)$, and that of the $\mathbf{M}$-s (7, 7). The dimension of the δ_i-s is (7, 1) and similarly of the $\mathbf{L}_i$-s (7, 1). Depending on the unknowns for which the solution is looked for, either the form given in the structure of the normal matrix (14) can be used, or if the δ unknown coordinate changes are to be found immediately, then this group of equations is to be left at the end of the normal matrix [HALMOS, 1975]. The blocks $\mathbf{M}_i$ appearing in the Eqs 14 form a diagonal block-matrix. On the basis of the diagonality, the following solution is evident for the unknowns and for the transformation parameters:

$$\delta = (\mathbf{N} - \mathbf{R}\mathbf{M}^{-1}\mathbf{R}^T)^{-1}(\mathbf{L} - \mathbf{R}_i\mathbf{M}_i^{-1}\mathbf{L}_i) \tag{15}$$

where $\mathbf{R}$ and $\mathbf{M}$ contain all the elements, and

$$\delta_i = \begin{bmatrix} \delta_I \\ \delta_{II} \\ \vdots \\ \delta_m \end{bmatrix} = - \begin{bmatrix} \mathbf{M}_I^{-1} & \mathbf{0} & \dots & \mathbf{0} \\ \mathbf{0} & \mathbf{M}_{II}^{-1} & \dots & \mathbf{0} \\ \vdots & \vdots & & \vdots \\ \mathbf{0} & \mathbf{0} & \dots & \mathbf{M}_m^{-1} \end{bmatrix} \begin{bmatrix} \mathbf{L}_I \\ \mathbf{L}_{II} \\ \vdots \\ \mathbf{L}_m \end{bmatrix} - \\ - \begin{bmatrix} \mathbf{M}_I^{-1} & \mathbf{R}_I^T \\ \mathbf{M}_{II}^{-1} & \mathbf{R}_{II}^T \\ & \vdots \\ \mathbf{M}_m^{-1} & \mathbf{R}_m^T \end{bmatrix} \delta . \tag{16}$$

The variance matrix referring to δ is on the basis of Eq. 15:

$$\mathbf{Q}_{\delta\delta} = (\mathbf{N} - \mathbf{R}\mathbf{M}^{-1}\mathbf{R}^T)^{-1}. \tag{17}$$

Similarly it can be found for the δ_i-s:

$$\mathbf{Q}_{\delta_i\delta_i} = \mathbf{M}_i^{-1} + \mathbf{M}_i^{-1}\mathbf{R}_i^T (\mathbf{N} - \mathbf{R}\mathbf{M}^{-1}\mathbf{R}^T)^{-1}(\mathbf{M}_i^{-1}\mathbf{R}_i^T)^T \tag{18}$$

and

$$\mathbf{Q}_{\delta_i\delta_j} = \mathbf{M}_i^{-1}\mathbf{R}_i^T(\mathbf{N} - \mathbf{R}\mathbf{M}^{-1}\mathbf{R}^T)^{-1}(\mathbf{M}_j^{-1}\mathbf{R}_j^T)^T \tag{19}$$

where $i \neq j$. Using any known inversion method, the parameters together with the elements of the variance covariance are obtained immediately.

If one does not succeed in grouping the coordinate unknowns (δ) according to blocks, there are also product terms in the second part of the normal matrix due to connections with the neighborous parts of the network. In such

a case the normal matrix reduced till the common unknowns gets the following form in analogy of Eq. 14:

$$\left[\begin{array}{c|cccccc} \mathbf{N} & \mathbf{R}_I & \mathbf{R}_{II} & \mathbf{R}_{III} & \mathbf{R}_{IV} & \cdots & \mathbf{R}_m \\ \hline \mathbf{R}_I^T & \mathbf{M}_I & \mathbf{S}_{I,II} & \mathbf{S}_{I,III} & \mathbf{S}_{I,IV} & \cdots & \mathbf{S}_{I,m} \\ \mathbf{R}_{II}^T & \mathbf{S}_{I,II}^T & \mathbf{M}_{II} & \mathbf{S}_{II,III} & \mathbf{0} & \cdots & \mathbf{0} \\ \mathbf{R}_{III}^T & \mathbf{S}_{I,III}^T & \mathbf{S}_{II,III}^T & \mathbf{M}_{III} & \mathbf{S}_{II,IV} & \cdots & \mathbf{0} \\ \vdots & \vdots & & & & & \\ \mathbf{R}_m^T & \mathbf{S}_{I,m}^T & \mathbf{0} & \mathbf{0} & \mathbf{0} & \mathbf{S}_{m-2,m-1}^T \mathbf{S}_{m-1,m}^T & \mathbf{M}_m \end{array}\right] \left[\begin{array}{c} \delta \\ \hline \delta_I \\ \delta_{II} \\ \delta_{III} \\ \vdots \\ \delta_m \end{array}\right] + \left[\begin{array}{c} \mathbf{L} \\ \hline \mathbf{L}_I \\ \mathbf{L}_{II} \\ \mathbf{L}_{III} \\ \vdots \\ \mathbf{L}_m \end{array}\right] = \mathbf{0}. \tag{20}$$

The matrix formulation in Eq. 20 is valid if the grouping between the single networks is as shown in Fig. 2. If the network part I has no central situation, the second part of the coefficient matrix in Eq. 20 is the band matrix (belonging to the δ_i-s).

The advantageous solution is in this case the elimination of the unknown coordinate changes δ, and then the solution of the reduced normal matrix is for the vectors δ_i:

$$\left[\begin{array}{ccccccc} \mathbf{M}_I & \bar{\mathbf{S}}_{I,II} & \bar{\mathbf{S}}_{I,III} & \bar{\mathbf{S}}_{I,IV} & \cdots & \bar{\mathbf{S}}_{I,m} \\ \bar{\mathbf{S}}_{I,II}^T & \bar{\mathbf{M}}_{II} & \bar{\mathbf{S}}_{II,III} & \mathbf{0} & \cdots & \mathbf{0} \\ \bar{\mathbf{S}}_{I,III}^T & \bar{\mathbf{S}}_{II,III}^T & \bar{\mathbf{M}}_{III} & \bar{\mathbf{S}}_{II,IV} & \cdots & \mathbf{0} \\ \vdots & \vdots & \vdots & \vdots & & \vdots \\ \bar{\mathbf{S}}_{I,m}^T & \mathbf{0} & \mathbf{0} & \mathbf{0} & \bar{\mathbf{S}}_{m-2,m-1}^T \bar{\mathbf{S}}_{m-1,m}^T & \bar{\mathbf{M}}_m \end{array}\right] \left[\begin{array}{c} \delta_I \\ \delta_{II} \\ \delta_{III} \\ \vdots \\ \delta_m \end{array}\right] + \left[\begin{array}{c} \bar{\mathbf{L}}_I \\ \bar{\mathbf{L}}_{II} \\ \bar{\mathbf{L}}_{III} \\ \vdots \\ \bar{\mathbf{L}}_m \end{array}\right] = \mathbf{0} \tag{21}$$

where the upper sign denotes reductions.

Having made the general reduction one gets:

$$\bar{\mathbf{M}}_m^{(m)} \delta_m + \bar{\mathbf{L}}_m^{(m)} = \mathbf{0} \tag{22}$$

where the upper index (m) denotes again reduction. According to the procedures of the adjustment, the variance-covariance matrix of the unknown parameters can also be computed. Depending on the Doppler network, the matrix (21) can also be fully filled. Its solution, inversion means no problem, as the number of the parameters to be determined has at most an order of a magnitude of some hundred:

$$\left[\begin{array}{ccccc} \bar{\mathbf{M}}_I & \bar{\mathbf{S}}_{I,II} & \bar{\mathbf{S}}_{I,III} & \cdots & \bar{\mathbf{S}}_{I,m} \\ \bar{\mathbf{S}}_{I,II}^T & \bar{\mathbf{M}}_{II} & \bar{\mathbf{S}}_{II,III} & \cdots & \bar{\mathbf{S}}_{II,m} \\ \bar{\mathbf{S}}_{I,III}^T & \bar{\mathbf{S}}_{II,III}^T & \bar{\mathbf{M}}_{III} & \cdots & \bar{\mathbf{S}}_{III,m} \\ \vdots & \vdots & \vdots & & \vdots \\ \bar{\mathbf{S}}_{I,m}^T & \bar{\mathbf{S}}_{II,m}^T & \bar{\mathbf{S}}_{III,m}^T & \cdots & \bar{\mathbf{M}}_m \end{array}\right] \left[\begin{array}{c} \delta_I \\ \delta_{II} \\ \delta_{III} \\ \vdots \\ \delta_m \end{array}\right] + \left[\begin{array}{c} \bar{\mathbf{L}}_I \\ \bar{\mathbf{L}}_{II} \\ \bar{\mathbf{L}}_{III} \\ \vdots \\ \bar{\mathbf{L}}_m \end{array}\right] = \mathbf{0}. \tag{21a}$$

If there are significant differences in the accuracy of the observations of different parts in the network, a "homogenization" (weighting) can be used for the solution. For the solution of linear equations to be partitioned into blocks the Helmertian method is the optimal one [WOLF, 1978]. It is advisable that one group should consist of the "inner" unknowns, eliminated in the first step, i.e. the coordinates of the network points, the unknowns introduced for the elimination of the refraction and other regular error sources or in case of Doppler or other satellite networks the orbital elements and correction factors. The "outer", connecting unknowns are the common terrestrial geodetic and satellite geodetic coordinates for Doppler or other satellite points, further the transformation parameters.

In order to enable the transformation between the networks, at least three common points, i.e. Doppler or other satellite geodetic and terrestrial geodetic points are necessary.

The case when only superficial geodetic coordinates (e.g. B and L geodetic ellipsoidic data) are at disposal, but no height data, will not be treated here [WOLF, 1980]. It should be remarked, however, that in such a case spatial coordinates can be computed from the ellipsoidic data B and L (eventually taking into account the variance-covariance matrix, too), and the Doppler height datum is accepted. The number of the transformation parameters is 4 when using ellipsoidic coordinates (one scale factor, 1 orientational rotation and 2 coordinate translations in the directions of δB_0 and δL_0). According to WOLF (1980) in such a case one has instead of the three rotational parameters one orientation (rotational) parameter (δA_0) in the chosen point P_0.

$$\begin{bmatrix} \varepsilon_x \\ \varepsilon_y \\ \varepsilon_z \end{bmatrix} = \begin{bmatrix} \cos B_0 \cos L_0 \\ \cos B_0 \sin L_0 \\ \sin B_0 \end{bmatrix} \delta A_0. \tag{23}$$

In such a case $\mathbf{P}_\Delta$ and $\mathbf{P}_\varepsilon$ are equal zero. The scale factor and the rotational parameters get *a priori* weights and accepting the Doppler height datum as a constraint, a solution with 7 transformation parameters is given by WOLF (1980). If the *a priori* weights $\mathbf{P}_\Delta = \infty$ and $\mathbf{P}_\varepsilon = \infty$ are introduced, this means practically that the scale factor and orientation of the axis of the Doppler system of coordinates is accepted as a final one.

It can occur that both the geodetic and Doppler observations contain ellipsoidic coordinates. In this case similarly to Eq. (4) one gets:

$$\mathbf{v}^E = \mathbf{D}^E \delta \mathbf{r} + \mathbf{r}_D^E \Delta + \mathbf{A}^E \delta \varepsilon + \mathbf{B}^E \delta \mathbf{r}_0 \mathbf{C}^E \delta \mathbf{E} + \mathbf{l}_D^E \tag{24}$$

where the upper index E means ellipsoidic system:

$$\mathbf{A}^E = a \begin{bmatrix} \sin L & -\cos L & 0 \\ -\sin B \sin L & -\sin B \sin L & \cos B \\ 0 & 0 & 0 \end{bmatrix},$$

$$\mathbf{D}^E = \begin{bmatrix} a \\ \cos B \\ 1 \end{bmatrix}, \qquad \delta\mathbf{r} = \begin{bmatrix} \delta B \\ \delta L \\ \delta H \end{bmatrix},$$

$$\mathbf{B}^E = \begin{bmatrix} -\sin B \cos L & -\cos B \sin L & \cos B \\ \sin L & \cos L & 0 \\ \cos B \cos L & \cos B \sin L & \sin L \end{bmatrix}, \tag{25}$$

$$\delta\mathbf{r}_0 = \begin{bmatrix} \delta B_0 \\ \delta L_0 \\ \delta H_0 \end{bmatrix},$$

$$\mathbf{C}^E = -\begin{bmatrix} 0 & \sin^2 B \\ 0 & 0 \\ 1 & \sin^2 B \end{bmatrix}, \qquad \delta\mathbf{E} = \begin{bmatrix} \delta a \\ a\delta f \end{bmatrix}.$$

Here δa is the change of the major axis of the ellipsoid and δf that of its obliquity. The values $\mathbf{r}_D^E$ and $\mathbf{l}_D^E$ should be expressed by ellipsoidic coordinates, too.

2.4 *The determination of the transformation parameters in case of a number of parameters differing from the previous values*

There are together 8 transformation parameters in the Wells—Vanicek model (1975) [HALMOS, 1980]. A general terrestrial system with the origin OF (and axes X, Y, Z), a satellite or Doppler system of coordinates with the origin OD (and with the axes X', Y', Z') and a geodetic system of coordinates

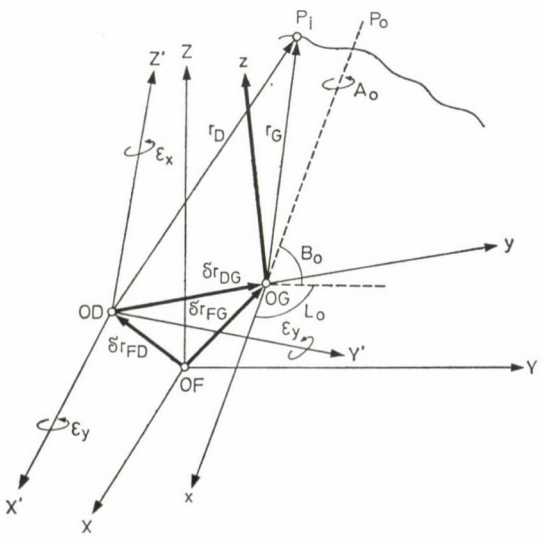

Fig. 4.

(also called geodetic datum-system, and connecting the previous ones) with the origin OG (and axes x, y, z, with a rotation A_0 around the normal of the ellipsoid in the origin if it is related to the terrestrial system (Fig. 4)) occur here. In order to transform the results of the Doppler observations into a terrestrial coordinate system, the following transformation equation is given taking into account that in all cases one has geocentric systems being rather similar to each other:

$$[\mathbf{Q}(\varepsilon_x, \varepsilon_y, \varepsilon_z) - \mathbf{Q}(\mathbf{A}_0) - \Delta]\,\mathbf{r}_D - \delta\mathbf{r}_{DG} + \mathbf{r}_D - \mathbf{r}_G = \mathbf{v} \tag{26}$$

with the rotational matrix $\mathbf{Q}$ being similar to that in Eq. (3) ε, with the rotational elements $\varepsilon_x\varepsilon_y$, ε_z and A_0, with the change in the scale factor Δ, and with the three translational factors $\delta\mathbf{r}_{DG}$ (together 8 parameters). By expressing the **v**-s, one gets similarly to Eq. 2 the following correction equations in a matrix form:

$$\mathbf{v} = -\delta\mathbf{r} + \mathbf{r}_D(1 + \Delta) + \mathbf{A}\delta\varepsilon + \mathbf{B}\delta\mathbf{r}_{DG} + \mathbf{C}\delta A_0 + \mathbf{l}_D \tag{27}$$

where

$$\mathbf{C} = \begin{bmatrix} 0 & \sin B_0 & -\cos B_0 \sin L_0 \\ -\sin B_0 & 0 & \cos B_0 \cos L_0 \\ \cos B_0 \sin L_0 & \cos B_0 \cos L_0 & 0 \end{bmatrix}. \tag{28}$$

Equation 28 can also be deduced from Eq. 23, as here δA_0 is the orientational rotation, and B_0, L_0 are again the ellipsoidic coordinates of the origin. A common adjustment of the terrestrial geodetic network measurements and of the results of Doppler or other satellite observations yields again the reduced system of normal equations (14) or (20) by taking into account the transformation parameters. The change results only from the introduction of the new rotational parameter δA_0.

The Krakiwsky—Thomson model (1974) differs from the Wells—Vanicek model by the introduction of three rotational parameters for the geodetic system in addition to those of the satellite and Doppler coordinate system, respectively, further one more scale factor if necessary and three translational parameters. Correspondingly, the number of the transformation parameters is 13 or 14 depending on the new scale factor. This solution can be especially advantageous in networks with great extension, where differing transformation parameters appear. In such cases it is to be considered whether it would not be more advantageous to use the MORITZ collocation method (1973), or the seven parameter solution with a separation of the network into smaller regional parts proposed by HALMOS. The structure of the common transformation parameter adjustment using the Krakiwsky—Thomson model is else identical with our general model, if regionally separated network parts are

considered. For an unambiguous solution one needs with the Krakiwsky—Thomson model at least 3—3 points with known spatial coordinates, too.

In addition to the cases already treated it can occur that besides the solutions using 7 or more parameters, the transformation is made with the introduction of only 4 parameters (e.g. the change of the scale factor Δ and the translational change consisting of 3 elements $\delta \mathbf{r}_0$). In case of an other solution, when the origin of two systems of coordinates coincide, the parameters Δ and $\delta\varepsilon$ for the transformation can be computed from the adjustment. An adjustment on the basis of the least squares yields similar or identical results, only the number of the unknowns decreases.

In cases when the parts of terrestrial geodetic networks refer to a common system of coordinates, and regional or local changes of the parameters cannot be supposed among them, the number of the supplementary transformational unknowns in the adjustment will be 7 when connecting the Doppler and the terrestrial geodetic network.

If the terrestrial geodetic ellipsoidic coordinates refer to different ellipsoids in different networks, or the origin of the ellipsoids is different, this situation must be taken into account at the determination of the spatial three dimensional coordinates. If the transformational parameters are good approximations, and the geodetic latitude and longitude are known, the translational parameters between the origine of the ellipsoid centres can also be introduced as unknowns.

In certain cases, the use of the affine transformation is also recommended besides the similarity transformations [MODENOV and PARKHOMENKO, 1961].

4. Conclusions

The indeterminedness or defect of the Doppler networks can be resolved by adjustment in a common model of the terrestrial geodetic network measurements and of the Doppler satellite observations, and by the introduction of suitable transformation parameters.

For the determination of the spatial three dimensional coordinates of traditional terrestrial geodetic measurements and for an increase of the accuracy, it is necessary to uniformize the height values referring to several mean sea levels, to know more accurate geoid heights or to introduce a uniform global equipotential surface.

For a determination of the transformation parameters by adjustment, more than three points must be known by their coordinates in both systems.

If several networks (e.g. national ones) are to be connected (they are called in such cases datum-systems), in each new system the three dimensional coordinates of at least two common points must be known. As a general rule

the coverage with common points should be as uniform in the whole area as possible.

An adjustment on the basis of the least squares principle supposes significantly more than the minimum of common points with known coordinates or where measurements were made.

Both the introduction of the different type transformation parameters into the adjustment, or the neglection of a part of them necessitates a previous significance test in order to test if the used mathematical model corresponds to the physical reality.

In the present situation of the accuracy, the mean square error of the network coordinates deduced from Doppler observations is around $\pm 0.3-0.5$ m [HALMOS, 1978, 1979]. This value already necessitates to carry out the adjustment of the terrestrial and Doppler or other satellite geodetic data in a common model. Always practical points of view decide in the connection of the transformation parameters with the corresponding coordinate system. According to experiences gained hitherto, the scale factor and orientation of the terrestrial networks is more reliable than those of the Doppler networks. Therefore, quite recently work is done on the solution of the scale factor and orientation problem of satellite geodetic networks (combined solutions with laser and very long base interferometry measurements).

Having finished the adjustment, it is advisable to carry out an analysis of the accuracy and reliability tests on the basis of the variance-covariance elements.

If there is only one terrestrial network, but it is inhomogeneous, then the regional transformation parameters can be determined by collocation or by selecting the already mentioned regions and introducing for each region 3 rotational elements and 1 scale factor.

REFERENCES

ÁDÁM, J.—HALMOS, F.—VARGA, M. 1979: On the concepts of combination of Doppler satellite and terrestrial geodetic networks. International Doppler Seminar held in Sopron. *Acta Geod. Geophys. et Mont. Hung.* (in press).

BURSA, M. 1962: The theory of the determination of the nonparallelism of the minor axis of the reference ellipsoid, polar axis of inertia of the Earth and initial astronomical and geodetic meridians from observations of artificial Earth satellites. *Geophysica et Geodaetica*, 6.

HALMOS, F. 1975: Analyse der kombinierten kosmisch-geodätischen Beobachtungsmethoden. Observations of Artificial Earth Satellites, 14, 183—200.

HALMOS, F. 1978: Methodische Fragen der geodätischen Anwendung von Dopplerschen Satelliten-Beobachtungen. *Acta Geod. Geoph. Mont. Hung.*, 13, 305—325.

HALMOS, F. 1979a: Einige Fragen der Versteifung und Berechnung geodätischer Netze. *Vermessungstechnik*, 27, 42—45.

HALMOS, F. 1979b: Geodinamical evaluation of Doppler satellite observations. *Acta Geod. Geoph. Mont. Hung.*, 14, 3—16.

HALMOS, F. 1979c: Connection between the structure, densification and computation of geodetic networks. Proceedings of the Second International Symposium on Problems

Related to the Redefinition of North American Geodetic Networks. NOAA, National Ocean Survey, 487—506.

HALMOS, F. 1980: Mathematical models of the transformations between geodetic networks (in Hungarian). *Geodézia és Kartográfia*, 32, 97—104.

KRAKIWSKY, E. I.—THOMSON, D. B. 1974: Mathematical models for the combination of terrestrial and satellite networks. *The Canadian Surveyor*, 28, 606—615.

MODENOV, P. S.—PARKHOMENKO, A. S. 1961: Geometric transformations. Vol. I: Euclidean and affine transformations. (Translation from Russian) Academic Press, New York and London.

MORITZ, H. 1973: Eine Methode der kleinsten Quadrate zur Koordinatentransformation. Academia Sc. Bulgaria, Vl. K. Hristov Septuagenario, 107—116.

SIGL, R. 1978: Zur Transformation von Datumskoordinaten. Wiss. Arbeiten der Lehrstühle für Geodäsie, Photogrammetrie und Kartographie der TU Hannover. Nr. 83, 148—154.

VINCENTY, I. 1980: Height-controlled three-dimensional adjustment of horizontal networks. *Bulletin Géodésique*, 54, 37—43.

WELLS, D. E.—VANICEK, P. 1975: Alignment of geodetic and satellite coordinate systems to the average terrestrial system. *Bulletin Géodésique*, 49, 241—256.

WOLF, H. 1963: Geometric connections and re-orientation of three-dimensional triangulation nets. *Bulletin Géodésique*, 68, 165—169.

WOLF, H. 1978: The Helmert block method — its origin and development. Proceedings of the Second International Symposium on Problems Related to the Redefinition of North American Geodetic Networks. NOAA, National Ocean Survey, 319—326.

WOLF, H. 1980: Scale and orientation in combined Doppler and triangulation nets. *Bulletin Géodésique*, 54, 45—53.

ПРЕОБРАЗОВАНИЕ ГЕОДЕЗИЧЕСКИХ СЕТЕЙ НА ОСНОВЕ УРАВНИВАНИЯ ПО СПОСОБУ НАИМЕНЬШИХ КВАДРАТОВ

Ф. ХАЛМОШ

РЕЗЮМЕ

Преобразование геодезических сетей целесообразно осуществлять применением метода наименьших квадратов. Этот вопрос особенно актуален с точки зрения взаимного уравниваниях допплеровских, наземных триангуляционных и нивелирных сетей. В наших исследованиях изыскается такое решение, когда речь идет о взаимном уравнивании геодезических сетей разных стран, и для каждой из них установление самостоятельных трансформационных параметров считается непременно обоснованным. В первую очередь излагается метод Гельмерта, основанный на уравнивании блоков, но кратко упоминаются и другие решения. Приводятся соответствующие зависимости исчислений и уравниваний.

Acta Geodaet., Geophys. et Montanist. Acad. Sci. Hung. Tomus 16 (2—4), pp. 209—235 (1981)

COMPENSATION OF SYSTEMATIC ERRORS IN BLOCKADJUSTMENT WITH INDEPENDENT MODELS

J. SOMOGYI
DOCTOR OF TECHN. SCI.

L. BATTA—I. NAGY
GEODETIC AND GEOPHYSICAL RESEARCH INSTITUTE OF THE HUNGARIAN ACADEMY OF SCIENCES, SOPRON

1. Introduction

In photogrammetric point determinations, the accuracy can be increased only if systematic errors are correctly detected and eliminated. In Hungary, blockadjustment with independent models is used in the practice. Thus the investigations described in this paper are concentrated on the elimination of the systematic errors in blockadjustment with independent models. When using adequate additional parameters, an accuracy increase of 20—25% can be reached in the blockadjustment.

The accuracy of certain measurement technical tasks can be only increased if systematic errors are eliminated. This holds also for photogrammetry. Together with computer tools and methods, the photogrammetric aerotriangulation methods significantly developed in recent years both theoretically and practically and up-to-date blockadjustment methods were proposed. The increase of accuracy demands directed the interest toward systematic errors. The continuous presence of systematic image errors sets a limit to the accuracy of the determination of photogrammetric control points. A further increase of the accuracy can be reached only by detecting the sources of systematic errors and by eliminating them. Such investigations have already been discussed at the ISP Congress in Ottawa, 1972. At the Helsinki Congress in 1972, the importance of this topic was generally acknowledged and a working group (WG III/3) created for these studies inside of Commission III. The activity of this working group has been reported by KILPELÄ at the 1980 Hamburg Congress [1]. At the same congress, ACKERMANN [2] summarized the different self-calibration methods mostly used for the elimination of the systematic errors.

2. Aims of the present investigations

The theoretical investigations in connection with blockadjustment with additional parameters refer mainly to bundle adjustment. This can be easily understood as the effect of the systematic image distorsions appears immediately in the image coordinates being the basis for the bundle adjustment.

The situation is more complicated in case of the method of the independent models. A first neglection is that the independence of the model coordinates being the basis of the blockadjustment is only a supposition. A further problem is that the effect of the systematic image distorsions can be hardly traced. That is perhaps why this problem has been less treated up to now (e.g. [3, 4]).

In the Hungarian practice blockadjustment with independent models is used. Therefore the possibilities for an accuracy increase should be looked for in such blockadjustments. The Geodetic and Geophysical Research Institute of the Hungarian Academy of Sciences has been lead by these considerations — in addition to the immanent interest for the problem — when it joined WG III/3.

In our investigations, the material of the test area Jämijärvi in Finland has been used. The investigation included following items taking into account the aims of WG III/3:

a) Application of mini-computer systems

b) The effect of the overlapping between strips on the accuracy

c) The effect of different type additional parameters on the systematic errors

d) The connection of the control points appearing in the adjustment and the additional parameters.

3. Preparation

The comparator coordinates of flight No 77 215 measured with PSK-1 have been handled in the following way:

a) The comparator coordinates are transformed to the four fiducials with affin transformation.

b) Radial distorsion is numerically corrected according to calibration report.

c) Refraction is corrected according to Bertram's formula.

With the corrected image coordinates, analytical relative orientation was carried out to get independent models. The models belonging to the single

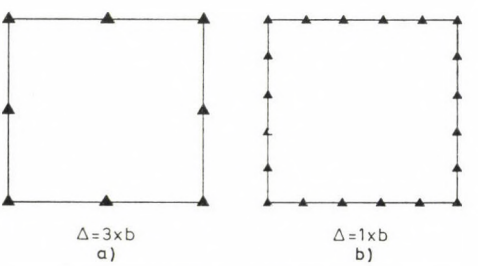

Fig. 1a. Control point patterns

strips have been transformed in a strip system using the coordinates of projection centres. For each strip we determined the approximate ground coordinates with help of control points on the first models of the corresponding strips. These coordinates serve as input data to the blockadjustment.

The blocks were composed in two different ways for the computations. The first variant consisted of 6 strips with a 60% sidelap, the second of three strips with 20% sidelap. The overlapping inside the strips between individual images was 60%. The combinations for the control points used in the blockadjustment can be seen in Fig. 1a (8 and 20 control points, respectively).

4. Computation

4.1 *Description of the programs applied*

The blockadjustment was carried out by the two-dimensional independent model method. To compensate the systematic model deformations the program was completed with additional parameters. Two variations have been worked out:

a) conformal polynomials
b) free polynomials.

The terms of the conformal polynomials are:

$$\begin{aligned} X &= ax + by + p_1(x^2 - y^2) + 2\,p_2xy \\ Y &= -ay + bx + 2\,p_1xy + p_2(x^2 - y^2)\,. \end{aligned} \tag{1}$$

The terms of the free polynomials are:

$$\begin{aligned} X &= ax + by + a_1x^2 + a_2xy + a_3a^2 \\ Y &= -ay + bx + b_1x^2 + b_2xy + b_3y^2\,. \end{aligned} \tag{2}$$

The linear terms of the additional parameters are common for the whole block, the non-linear terms are used for the strips.

The programs can be divided into four groups:

a) Construction of strips from measured data: neighbouring models are linked through 3 common points, the second model is transformed into the coordinate system of the first, using the Caley—Euler matrix. At the end of the procedure all the models in the strip are given in the coordinate system of the very first model of the strip. Then the whole strip is transformed into the ground coordinate system, yielding the approximate ground coordinates.

All computations are done in double precision (12 significant digits). Data storage: disc and magnetic tape.

b) Construction of the matrix of normal equations, according to the type of adjustment applied. Matrix elements are stored on disc in single precision (7 significant decimal digits). Construction of the right hand side of the system of normal equations.

c) Solution of the system of normal equations by the Cholesky factorization. At the end, iterative refinement of the solution is applied, until machine precision is attained (2.4E-7).

Inner products are computed in double precision. For time efficiency 4 buffers were used on disc. Using the formula $\mathbf{A} = \mathbf{L}\mathbf{L}^T$, both **A** and **L** were stored in row sequential as well as line sequential format. Run-time was about 4 hours in case of 260 unknowns. Determination of the unknowns.

d) Computation of coordinate discrepancies, standard deviations (μ_{xy}).

5. Informations on hardware and software

5.1 *Hardware*

The whole computational procedure was made on a Hewlett-Packard mini-computer system. This system is based on an HP 2100A CPU with 24 Kwords of operative memory and an HP 7900A disc with 4.8 M byte of mass memory capacity. The cycle time of the CPU is 960 ns. (Fig. 1b shows the configuration of the system).

The punched tape reader was used as primary input unit for original (distributed and measured) source data.

The tape punch unit was used as auxiliary output unit.

The secondary input data, the intermediary data and most of the final data were handled as disc-resident files.

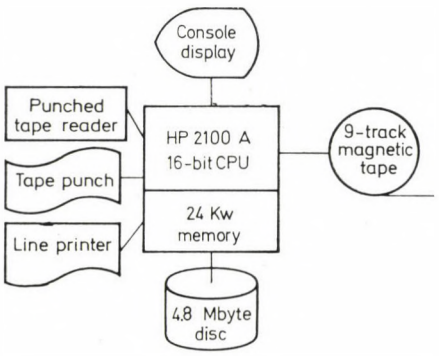

Fig. 1b

The 9-track magnetic tape was used for storage of some kinds of final data.

The run-time parameters were inserted through the console display or from pseudo-disc batch file.

5.2 *Software*

The computer system described in the hardware section was used in a disc based operating system environment. This software system was the HP-DOS-III [5].

All programs were written in the HP representation of standard NSI FORTRAN-IV programming language [6].

6. Results

In the following, the results for the block composed of flight 77,215, strips 7—12 shall be shown in different combination. The notations for the different versions can be seen in Table I.

It should be remarked that the improving effect of the additional parameters of the free polynomials did not appear in the present case using few control points, or even the results were deteriorated by them. Therefore this version has been omitted using few control points.

The coefficient matrix of the normal equations was inverted in the adjustment, thus the weight coefficients of the unknowns could be also computed. Using the computed mean square errors of the unknown tie points, informations were obtained about the planimetric accuracy of the adjusted blocks and on the distribution of the systematic errors without using the check points. Figures 2 to 6 show the mean square errors (μ_{xy}) of the tie points with 60/60 overlapping, Figs 7 to 10 those with overlapping 60/20 from the adjustments related to the image scale.

Table I

Versions of blockadjustment				
Overlaps	Number of control points	without add. p.	with add. p.	
			conformal p.	free p.
60/60	8	A_1	C_1	—
60/60	20	A_2	C_2	F_2
60/20	8	A_3	C_3	—
60/20	20	A_4	C_4	F_4

These figures show that if few control points are used (versions A_1, C_1, C_3) the reliability generally decreases toward the boundaries of the blocks in accordance with the theory. It can be concluded from this result that the homogeneity of the blocks is weakest at the boundaries and in the corners, respectively. Greater discrepancies inside the blocks indicate the presence of systematic errors. The increase of the number of control points increases

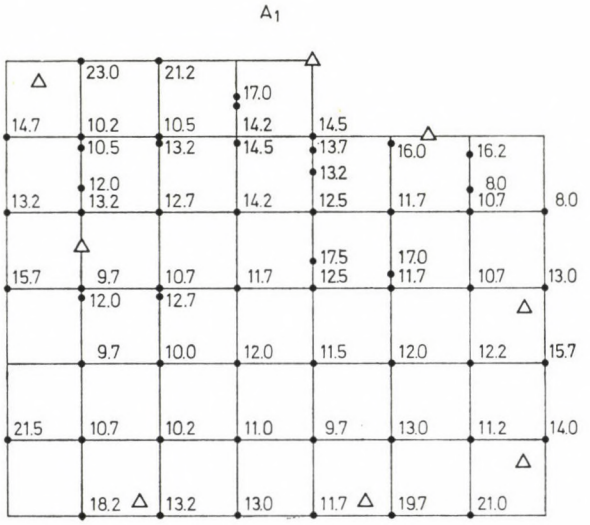

Fig. 2.

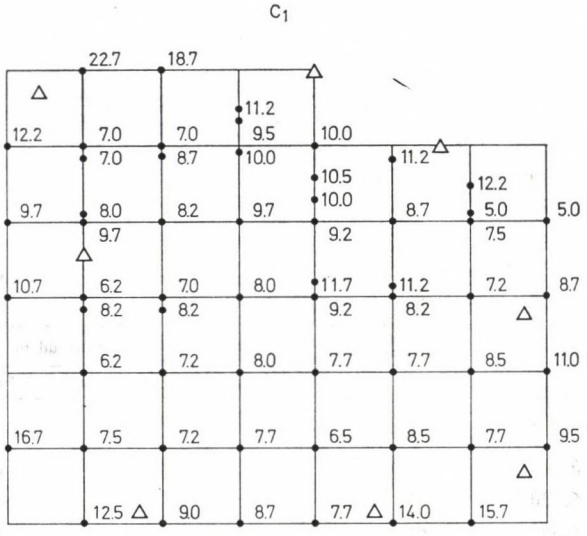

Fig. 3.

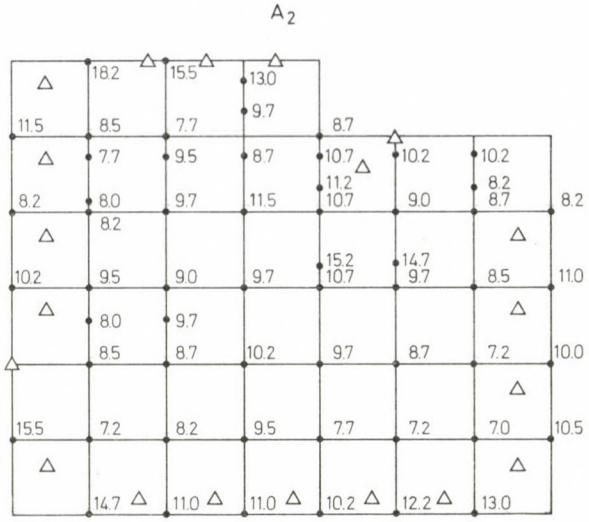

Fig. 4.

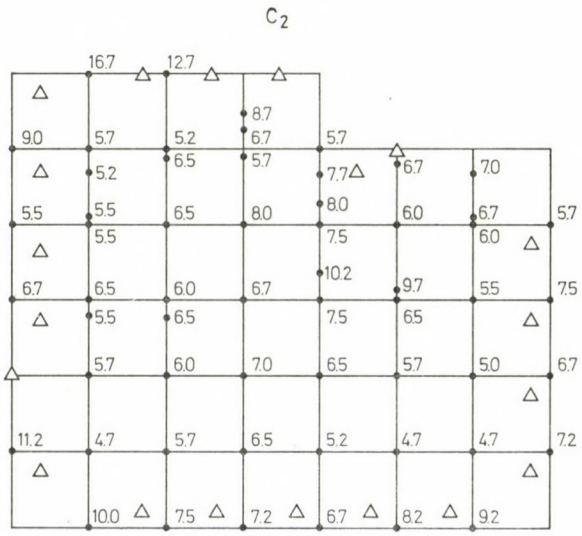

Fig. 5.

the homogeneity of the blocks, but the maximum coordinate differences do not appear in the centre of the block. In case of adjustment without additional parameters it can be clearly seen how the 60% overlapping between strips increase the accuracy (cf. Figs 2 and 7, or Figs 4 and 9). In case of an adjustment with additional parameters, however, the difference of the overlapping between strips does not influence the reliability of the determination.

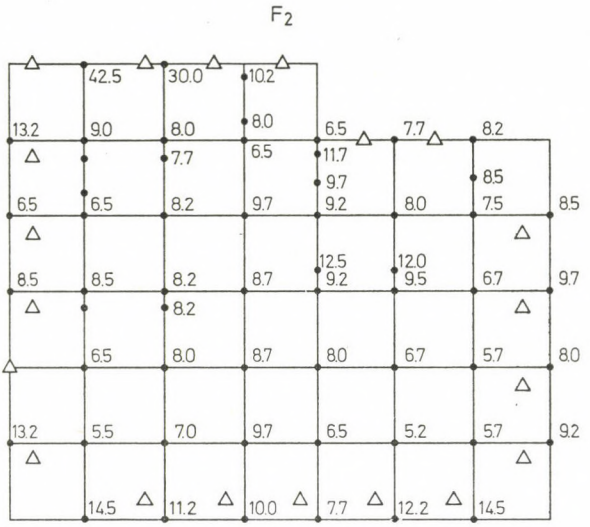

Fig. 6.

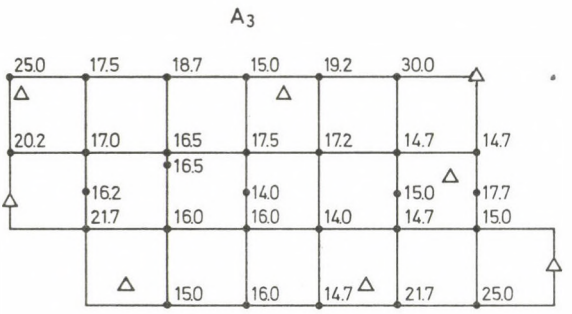

Fig. 7.

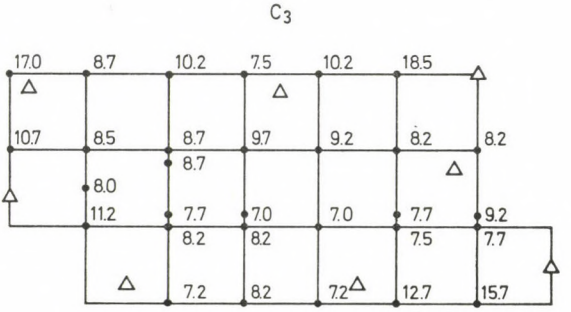

Fig. 8.

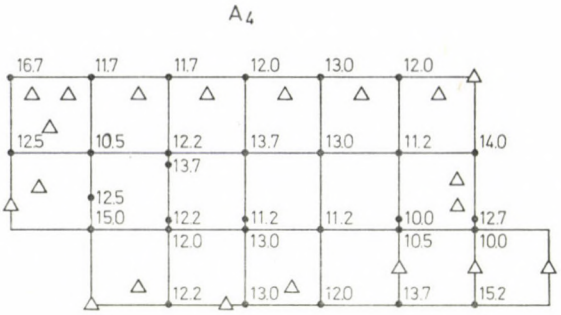

Fig. 9.

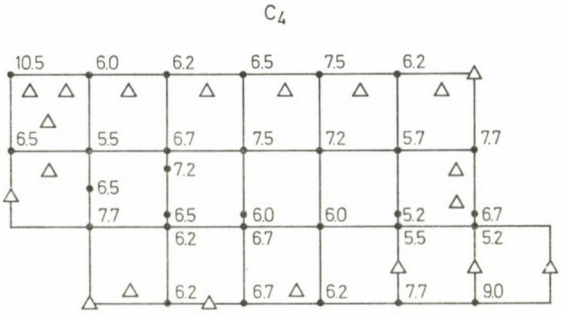

Fig. 10.

The use of additional parameters increases the accuracy of the adjustment and the homogeneity of the blocks. Conformal polynomial are more effective than free polynomials.

Figures 11 to 20 show the vector diagrams of the coordinate differences computed from the check points of the test area for the different adjustments. A certain correlation can be found here with previous figures. The effect of the systematic errors can be easily seen after adjustments without additional parameters. Greatest vectors can be found at the boundaries and in the corners. The improving effect of the additional parameters — mainly that of the version with conformal polynomials — is well illustrated. It can be also seen that conformal polynomials yield better results even in case of less control points. In the vector diagrams of the simple adjustments, the effect of the overlapping between strips is also significant. When using free polynomials, the effect of regular errors can be detected even if 20 control points are used in the adjustment.

The accuracy data for the different adjustments can be seen from Table II.

Let us consider first the values δ_0, meaning the standard deviations of the model coordinates. In case of versions without additional parameters

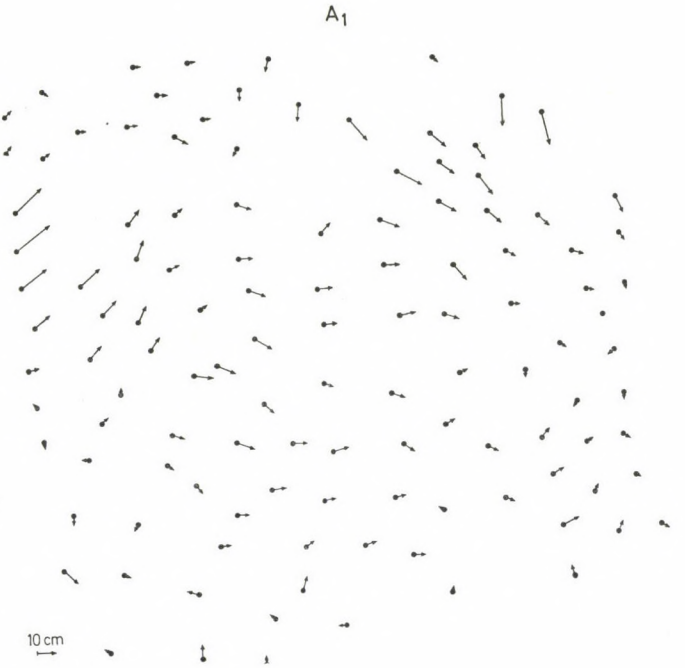

Fig. 11.

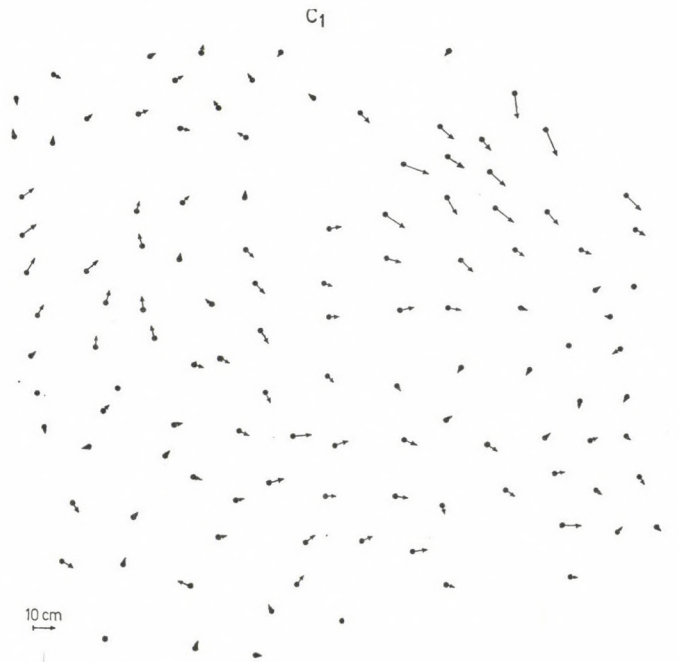

Fig. 12.

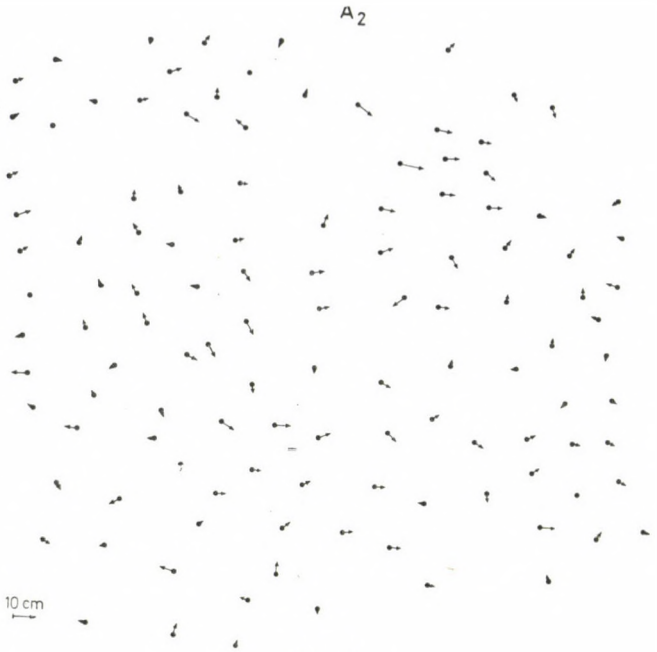

Fig. 13.

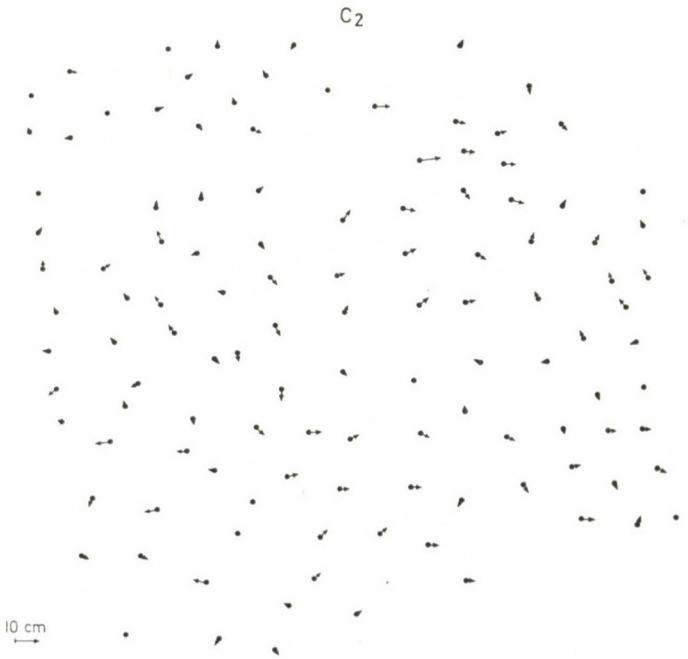

Fig. 14.

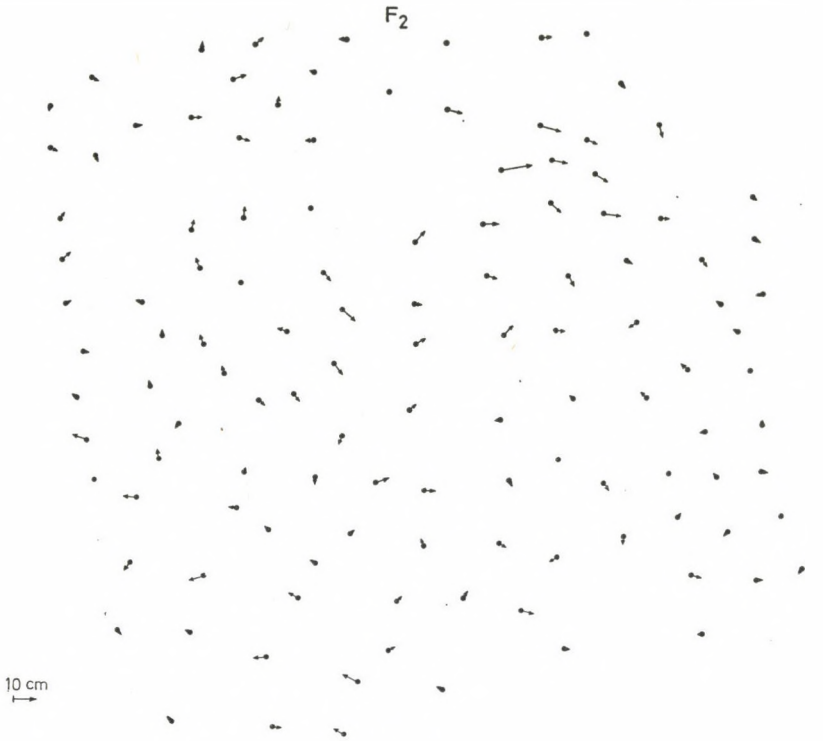

Fig. 15.

Fig. 16.

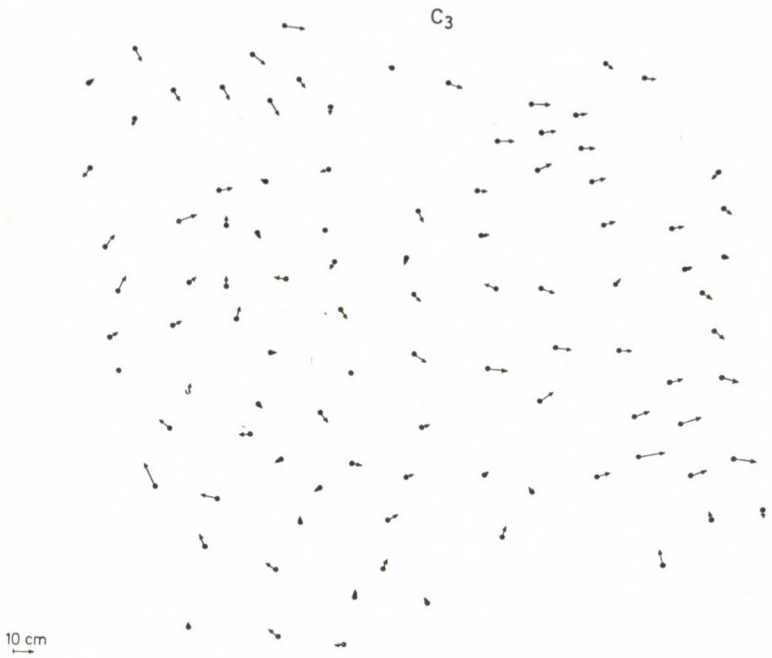

Fig. 17.

Fig. 18.

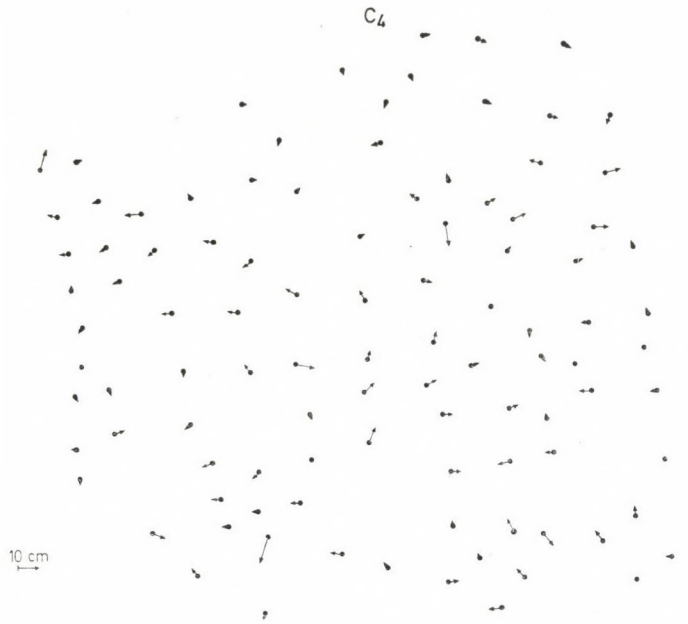

Fig. 19.

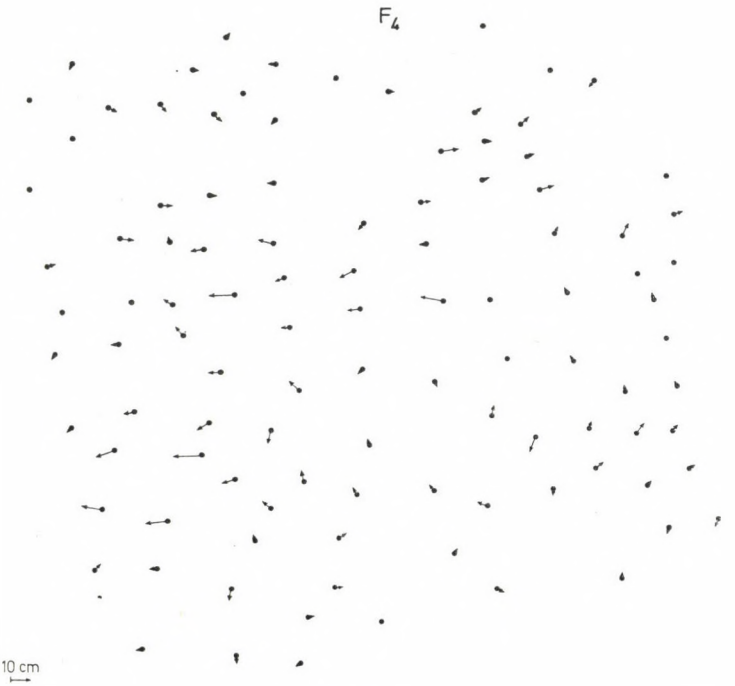

Fig. 20.

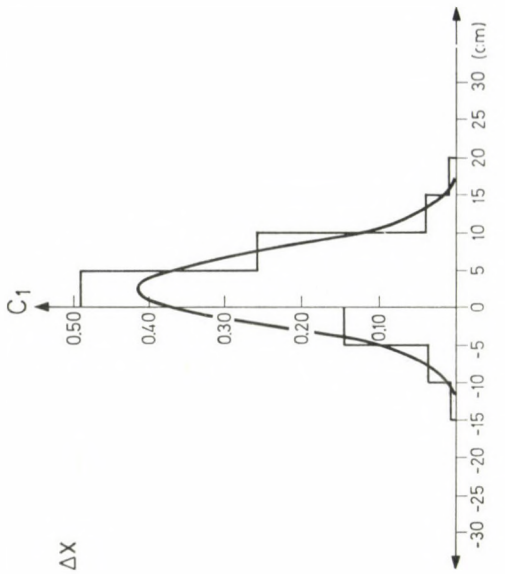
C1
ΔX
0.50
0.40
0.30
0.20
0.10
-30 -25 -20 -15 -10 -5 0 5 10 15 20 25 30 (cm)

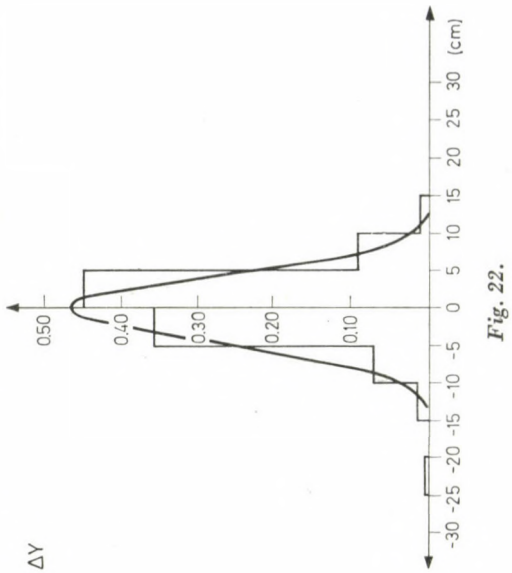
ΔY
0.50
0.40
0.30
0.20
0.10
-30 -25 -20 -15 -10 -5 0 5 10 15 20 25 30 (cm)

Fig. 22.

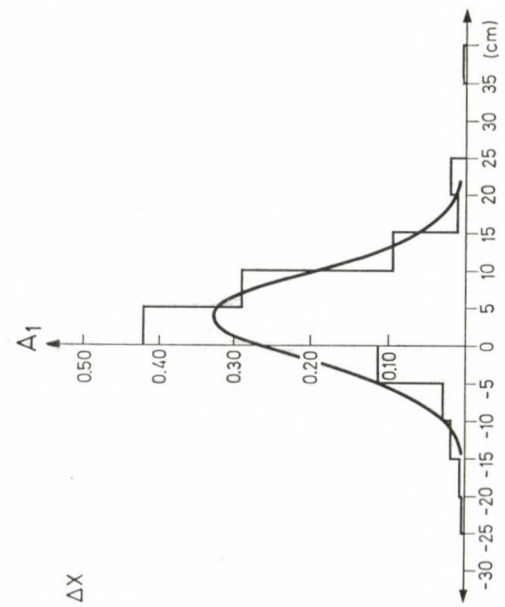
A1
ΔX
0.50
0.40
0.30
0.20
0.10
-30 -25 -20 -15 -10 -5 0 5 10 15 20 25 30 35 (cm)

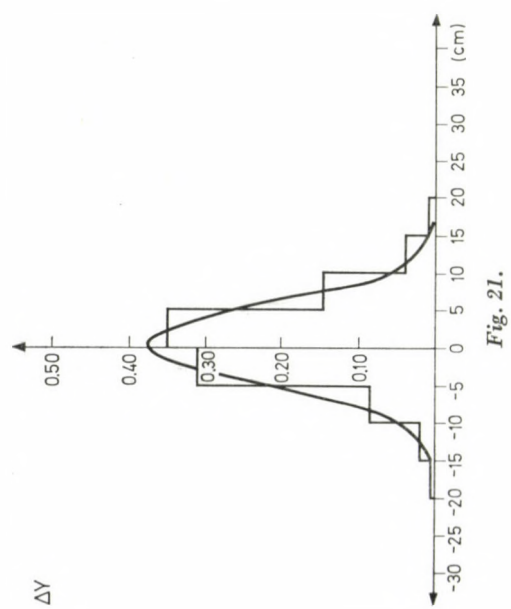
ΔY
0.50
0.40
0.30
0.20
0.10
-30 -25 -20 -15 -10 -5 0 5 10 15 20 25 30 35 (cm)

Fig. 21.

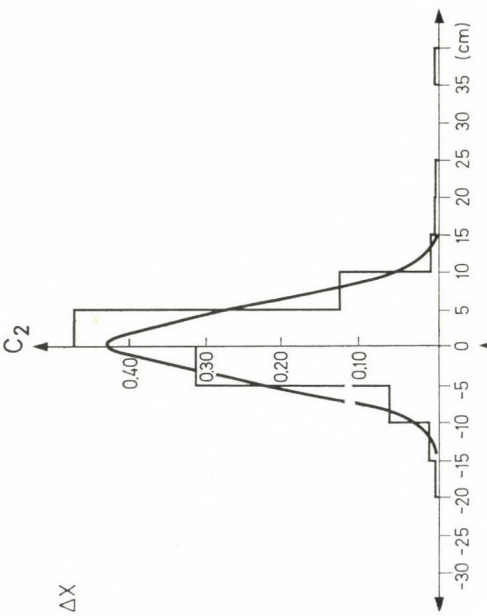
C2
ΔX
0.40
0.30
0.20
0.10
-30 -25 -20 -15 -10 -5 0 5 10 15 20 25 30 35 (cm)

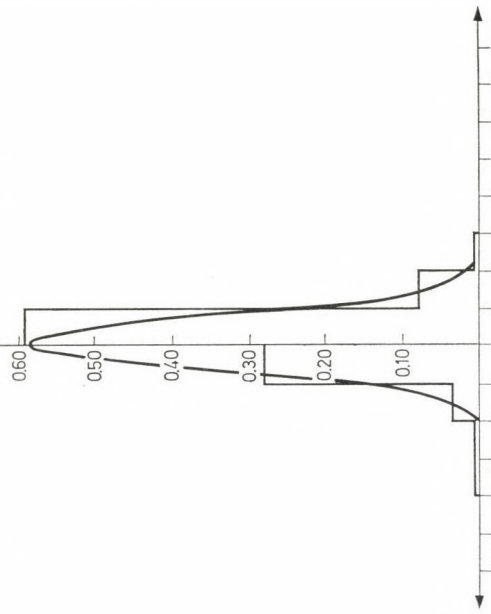
ΔX
0.60
0.50
0.40
0.30
0.20
0.10
-30 -25 -20 -15 -10 -5 0 5 10 15 20 25 30 35 (cm)

Fig. 24.

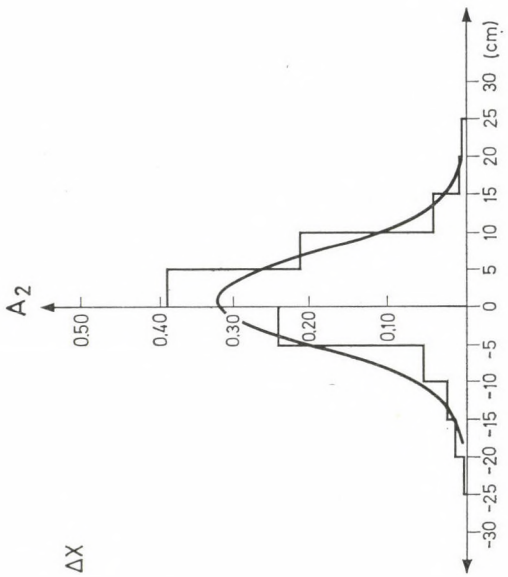
A2
ΔX
0.50
0.40
0.30
0.20
0.10
-30 -25 -20 -15 -10 -5 0 5 10 15 20 25 30 (cm)

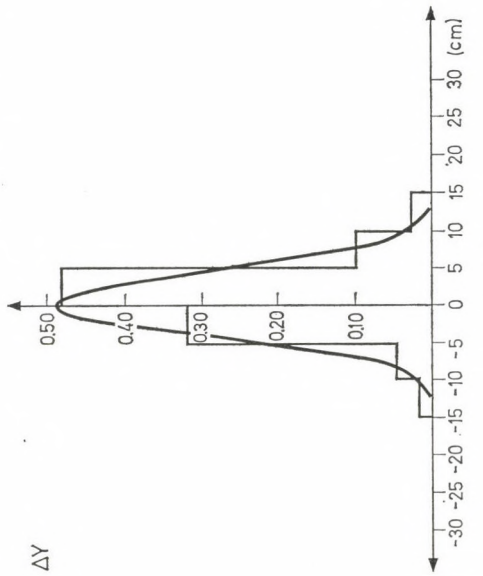
ΔY
0.50
0.40
0.30
0.20
0.10
-30 -25 -20 -15 -10 -5 0 5 10 15 20 25 30 (cm)

Fig. 23.

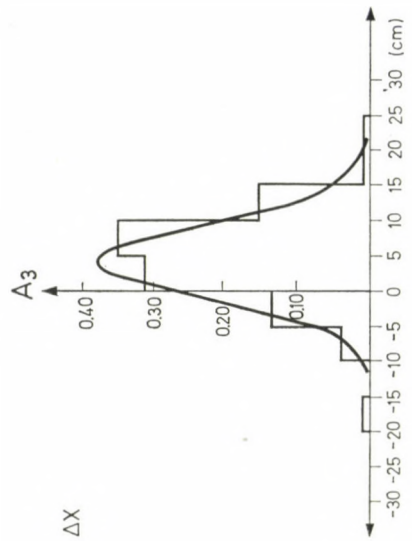
A3
ΔX
0.40
0.30
0.20
0.10
-30 -25 -20 -15 -10 -5 0 5 10 15 20 25 30 (cm)

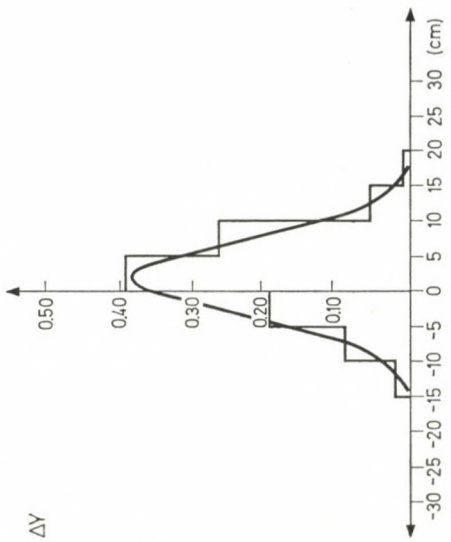
ΔY
0.50
0.40
0.30
0.20
0.10
-30 -25 -20 -15 -10 -5 0 5 10 15 20 25 30 (cm)

Fig. 26.

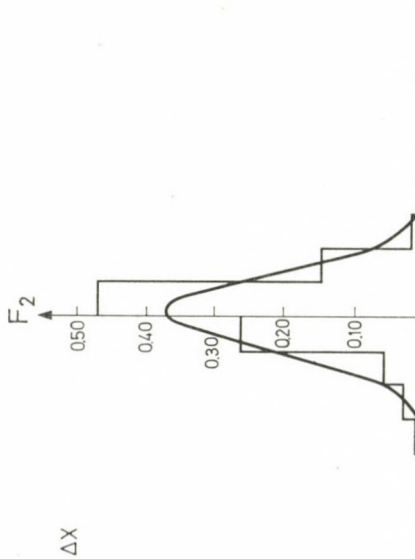
F2
ΔX
0.50
0.40
0.30
0.20
0.10
-30 -25 -20 -15 -10 -5 0 5 10 15 20 25 30 35 (cm)

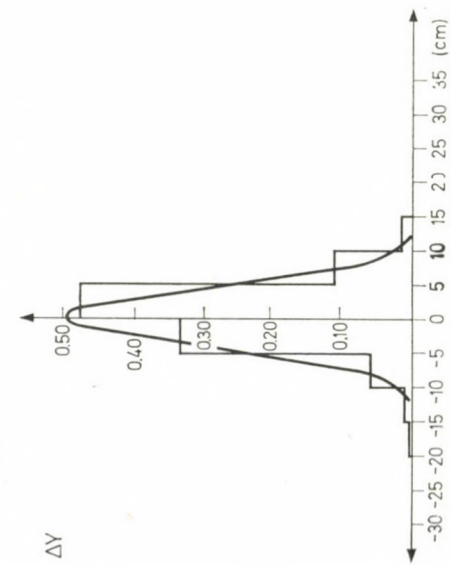
ΔY
0.50
0.40
0.30
0.20
0.10
-30 -25 -20 -15 -10 -5 0 5 10 15 20 25 30 35 (cm)

Fig. 25.

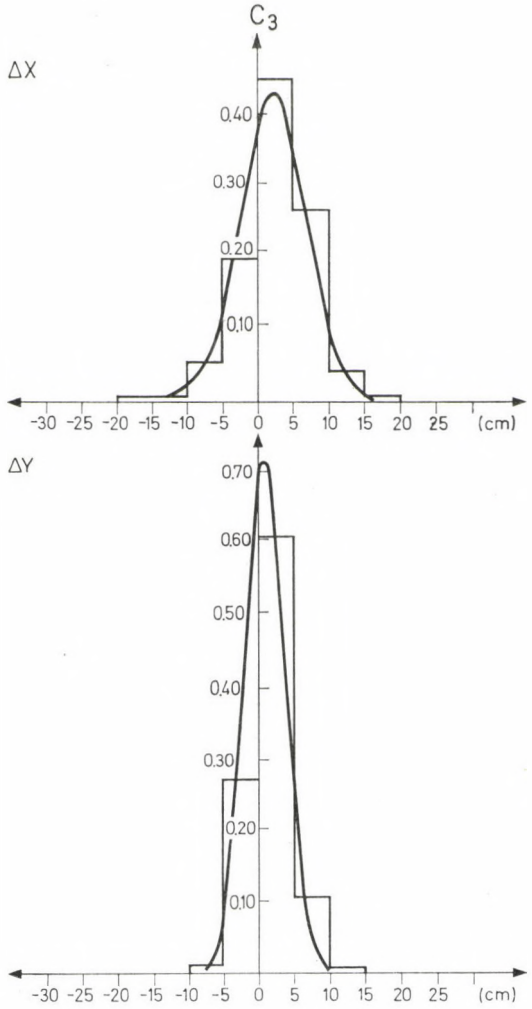
C3
ΔX
0.40
0.30
0.20
0.10
-30 -25 -20 -15 -10 -5 0 5 10 15 20 25 (cm)
ΔY
0.70
0.60
0.50
0.40
0.30
0.20
0.10
-30 -25 -20 -15 -10 -5 0 5 10 15 20 25 (cm)

Fig. 27.

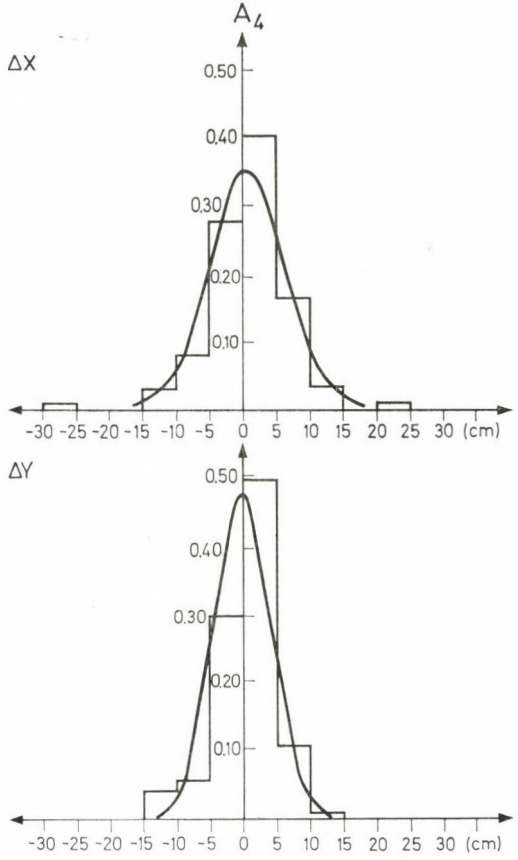
A4
ΔX
0.50
0.40
0.30
0.20
0.10
-30 -25 -20 -15 -10 -5 0 5 10 15 20 25 30 (cm)
ΔY
0.50
0.40
0.30
0.20
0.10
-30 -25 -20 -15 -10 -5 0 5 10 15 20 25 30 (cm)

Fig. 28.

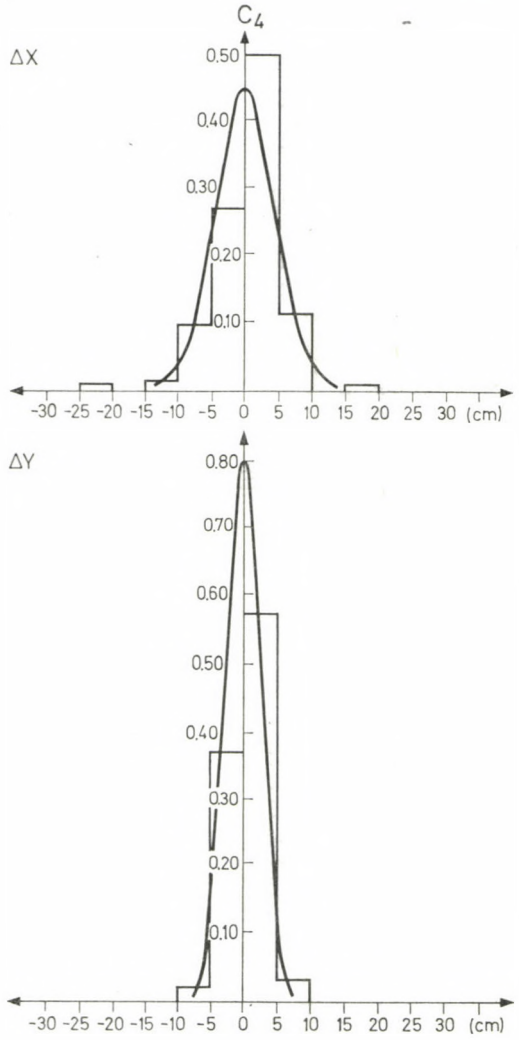
C4
ΔX
0.50
0.40
0.30
0.20
0.10
-30 -25 -20 -15 -10 -5 0 5 10 15 20 25 30 (cm)
ΔY
0.80
0.70
0.60
0.50
0.40
0.30
0.20
0.10
-30 -25 -20 -15 -10 -5 0 5 10 15 20 25 30 (cm)

Fig. 29.

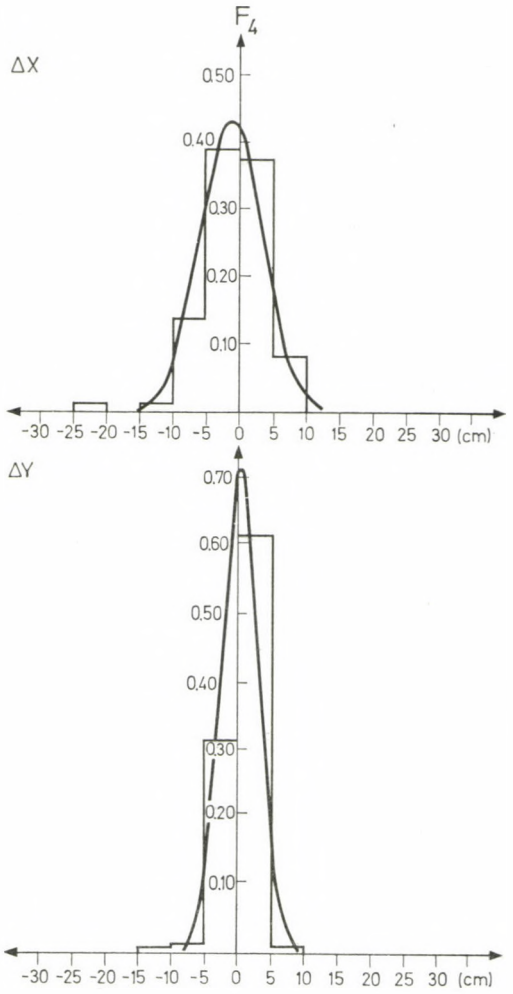
F4
ΔX
0.50
0.40
0.30
0.20
0.10
-30 -25 -20 -15 -10 -5 0 5 10 15 20 25 30 (cm)
ΔY
0.70
0.60
0.50
0.40
0.30
0.20
0.10
-30 -25 -20 -15 -10 -5 0 5 10 15 20 25 30 (cm)

Fig. 30.

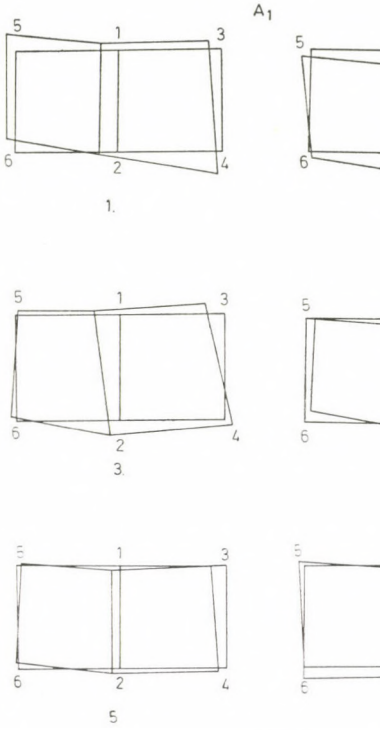

Fig. 31.

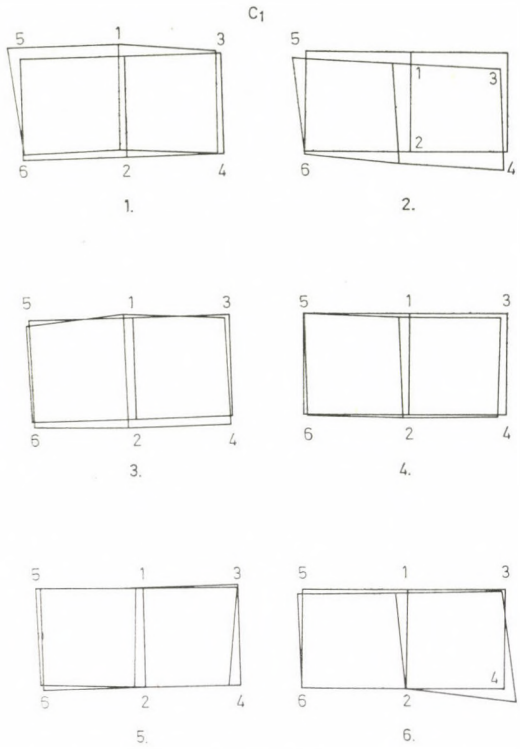

Fig. 32.

they are more scattered and depend on the distribution of control points, further on the overlapping between strips of the block. This fact proves the absence of systematic errors and supports our previous conclusions. In case of the use of additional parameters this scatter and the dependence on the number of control points and on overlapping decreases significantly. Further the values of δ_0 decrease themselves significantly in case of adjustments with additional parameters (a decrease of 30—40%).

Table II

Overlaps	Control points	*A*		*C*		*F*	
		σ_0	μ_{xy}	σ_0	μ_{xy}	σ_0	μ_{xy}
60/60	8	12.7	14	8.0	11	—	—
60/60	20	11.5	12	7.5	9	8.2	11
60/20	8	15.5	16	7.5	11	—	—
60/20	20	13.5	12	7.0	9	6.0	10

Table III

Discrep. cm	A_1		C_1	
	x	y	x	y
24—20	1			
19—15	1	1	1	
14—10	10	4	4	1
9—5	29	15	26	9
4—0	42	37	49	45
—1—5	11	31	15	36
—6—10	3	9	4	7
—11—15	2	2	1	2
—16—20	1	1		

The absolute accuracy of the blockadjustment can be estimated based on the RMS coordinate errors of check points, μ_{xy}. The Table shows clearly the improving effect of the additional parameters (in average by 20—25%),

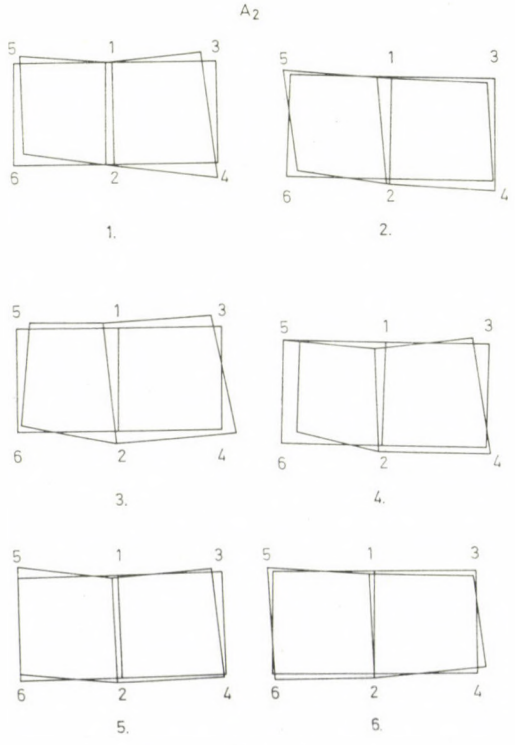

Fig. 33.

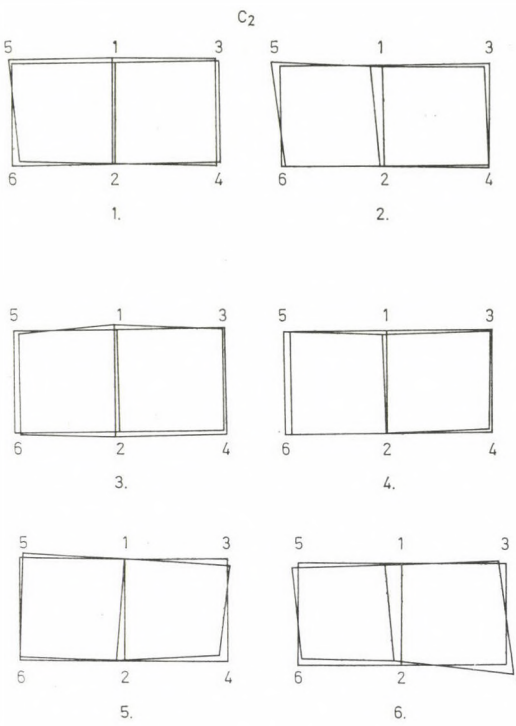

Fi g. 34.

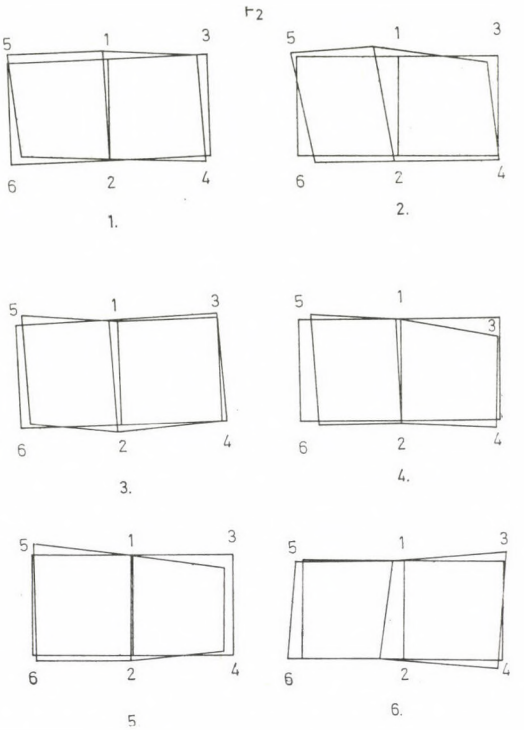

Fig. 35.

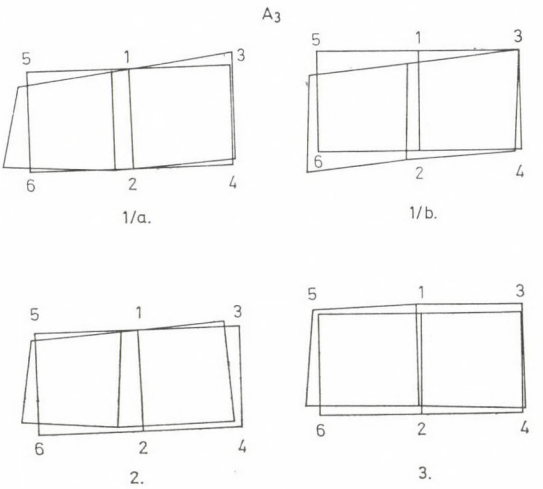

Fig. 36.

further the fact that the increase in accuracy is greater if the number of control points and the overlapping between strips are less. The results show further that the improving effect of the additional parameters from conformal polynomials was stronger than that of the parameters from free polynomials. These conclusions are consistent with the conclusions drawn from Figs 2 to 10.

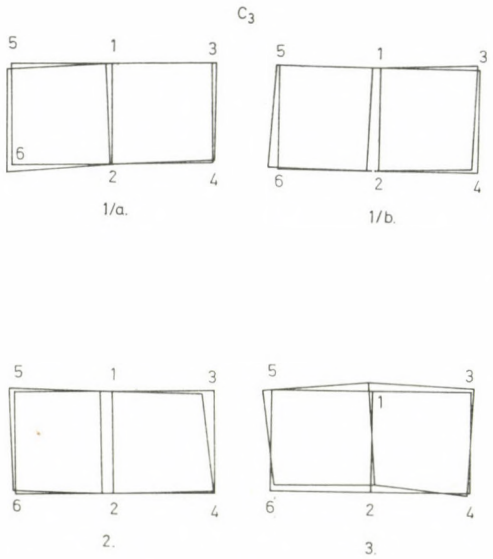

Fig. 37.

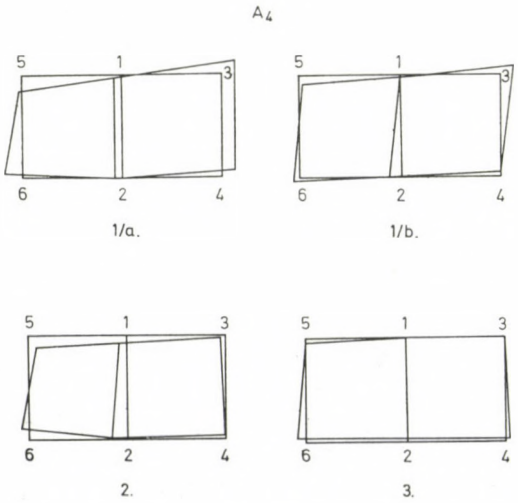

Fig. 38.

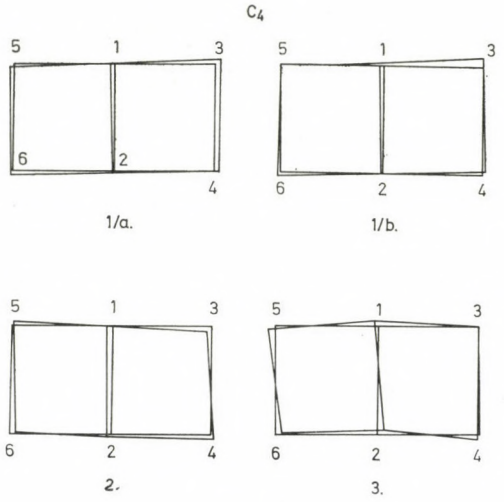

Fig. 39.

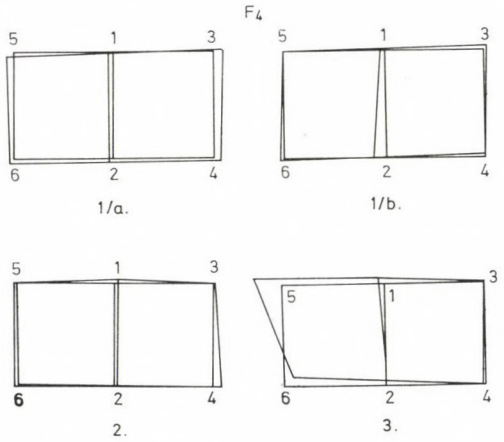

Fig. 40.

Tables III to VI show the deviations of the adjusted coordinates from the given values of the coordinates x and y of the check points in per cents in 5 cm intervals.

The curves of the relative occurrence frequencies of the deviations in x and y directions in 5 cm intervals can be seen in Figs 21 to 30. The data of the Tables and the frequency distribution curves confirm the previous conclusions.

The distribution curves of the deviations in direction x are in all cases more flat than the distribution curves y. If additional parameters are used,

Table IV

Discrep. cm	A_2		C_2		F_2	
	x	y	x	y	x	y
24—20	1					
19—15	1		1			
14—10	4	3	1	1	2	1
9—5	22	10	13	8	15	11
4—0	39	48	47	59	47	48
—1—5	24	32	31	28	26	33
—6—10	6	5	6	4	6	6
—11—15	2	2	1		3	1
—16—20	1				1	

Table V

Discrep. cm	A_3		C_3	
	x	y	x	y
15—19	1	1	1	
10—14	15	5	4	1
5—9	35	26	26	11
0—4	31	39	44	60
—1—5	13	19	19	27
—6—10	4	8	5	1
—11—15	0	2	1	
—16—20	1			

Table VI

Discrep. cm	A_4		C_4		F_4	
	x	y	x	y	x	y
24—20	1					
19—15	0		1			
14—10	3	1	0			
9—5	17	10	12	3	8	6
4—0	40	50	50	58	37	61
—5—5	28	30	27	37	39	31
—6—10	8	5	9	2	14	1
—11—15	2	4	1		1	1
—16—20	0				0	
—21—25	0				1	
—26—30	1					

this difference even increases. That means that the determination of the coordinates y was in all cases more accurate. This effect is very likely to be connected with the direction of flight.

Figures 31 to 40 show the average distortion of the strips of the different blocks after adjustment.

7. Conclusions

Any generally valid conclusions can be hardly expected from experiments made on test areas. Anyway the following conclusions seem to be justified in accordance with other investigations:

The use of additional parameters increases the homogeneity and accuracy of the points determined by the blockadjustment. The choice of adequate additional parameters is very important as ill-chosen parameters may result in certain complications. In case of blockadjustment with independent models, it is sufficient to attribute the additional parameters to the strips which the block consists of.

The improving effect of the additional parameters is more significant in case of few control points than in case of many control points.

The effect of free polynomial parameters is not unambiguous. In case of few control points, e.g. in case of the present version with 8 control points, its effect can be even a negative one.

For the qualification of practical blockadjustments with few check points it is advisable to invert the coefficient matrix of the normal equations. The mean square errors of the tie points yield information of the homogeneity of the adjusted blocks and on the effect of the systematic errors on the blocks.

REFERENCES

1. KILPELÄ, E.: Compensation of Systematic Errors of Image and Model Koordinates. Int. Archives of Phot., Vol XXIII, Part B9, Hamburg, 1980.
2. ACKERMANN, F.: Blockadjustment with Additional Parameters, Int. Archives of Phot. Vol. XXIII, Part B3, Hamburg, 1980.
3. EBNER, H.—SCHNEIDER, W.: Simultaneous Compensation of Systematic Errors with Block Adjustment by Independent Models. Bildmessung und Luftbildwesen, 1975.
4. EBNER, H.: Automatische Kompensation systematischer Fehler bei der Blockausgleichung mit unabhängigen Modellen. Schriftenreihe, Institut für Photogrammetrie der Universität Stuttgart, Heft 1, 1976.
5. HP 24307 DOS-III Disc Operating System Reference Manual. Hewlett-Packard Company.
6. Fortran IV Reference Manual, Hewlett-Packard Company.

КОМПЕНСАЦИЯ СЛУЧАЙНЫХ ОШИБОК В УРАВНИВАНИИ ПО БЛОКАМ ПРИ ПОМОЩИ НЕЗАВИСИМЫХ МОДЕЛЕЙ

Й. ШОМОДИ—Л. БАТТА—И. НАДЬ

РЕЗЮМЕ

Повышение точности в фотограмметрическом определении точек возможно только выявлением и исключением систематических ошибок. В Венгрии уравнивание по блокам при помощи независимых моделей получило практическое применение. Поэтому исследования, изложенные в статье концентрируются на исключении систематических ошибок в уравнивании по блокам при помощи независимых моделей. При применении соответствующих дополнительных параметров достигается повышение точности в уравнивании по блокам.

Acta Geodaet., Geophys. et Montanist. Acad. Sci. Hung. Tomus 16 (2—4), pp. 237—244 (1981)

DIGITAL MAP CONSTRUCTION USING BICUBIC SPLINE INTERPOLATION

J. ZÁVOTI

GEODETIC AND GEOPHYSICAL RESEARCH INSTITUTE OF THE HUNGARIAN ACADEMY OF SCIENCES, SOPRON

For the illustration of the classification of the elements in a data system contour maps are widely used in geosciences. Here a method is presented which enables the automatic construction of contour maps using digital computers. The isolines produced by this method fit to the given discrete data — without being influenced by the spatial distribution of the points —, but the contour map produced by the computer does not contain any kind of information not present in the original data.

In recent years, methods for the construction of contour maps have been proposed by CRAIN and BHATTACHARYYA (1967), KRAUS and STANGER (1975), ASSMUS (1976), EBNER (1980) and KOCH (1973).

The method proposed in the present paper is based on the advantageous characteristics of the two-variable spline interpolation.

1. Two-dimensional third order spline functions

For sake of simplicity let us chose the rectangular domain $T = [a, b] \times [c, d]$ as area of interpolation, and distribute it into a rectangular grid:

$$\{T = (x_i, y_k)/a \leq x_i \leq b,\ c \leq y_k \leq d;\ \ i = 0, 1, \ldots M;\ \ k = 0, 1, \ldots N\}. \quad (1)$$

[In case of a connected, non-rectangular interpolation domain the spline interpolation can also be used, if the graph obtained by a connection of the neighborous points of the data system is topologically equivalent with a rectangular grid of the dimension $(M + 1) \times (N + 1)$.] Let us suppose that the values of a two-variable, continuous function $f(x, y)$ are known in the grid points. By defining third order polynomials in both variables in the dots of the rectangular block

$$x_{i-1} \leq x \leq x_i;\quad y_{k-1} \leq y \leq y_k \quad (2)$$

in the form:

$$g_{ik} = \sum_{m=0}^{3} \sum_{n=0}^{3} a_{mn}^{i,k} (x - x_{i-1})^m (y - y_{k-1})^n . \quad (3)$$

The coefficients a_{mn}^{ik} can be obtained with the following supposition: the surface elements are connected smoothly, they exactly fit to the given points,

and the surface obtained by the composition of the surface elements is double derivable in both variables continuously, the second derivative in normal direction disappears at the boundary of the domain.

It can be proved [MARCSUK, 1976] that a function $g(x, y)$ fulfilling these conditions exists, it is unique and it is the solution of the following variation problem:

$$\int_T \left[\left(\frac{\partial^2 g}{\partial x^2}\right)^2 + \left(\frac{\partial^2 g}{\partial y^2}\right)\right] \mathrm{d}T \to \min_{W_2^2}$$
$$g(x_i, y_k) = f(x_i, y_k) \quad \begin{matrix} i = 0, 1, \ldots M \\ k = 0, 1, \ldots N \end{matrix} \tag{4}$$

— where W_2^2 denotes the space of the double derivable, quadratically integrable functions.

The amount of computations can be considerably decreased when determining the coefficients a_{mn}^{ik} if the values of the following derivates are known in the boundary points of each dot:

$$p_{ik} = f_x(x_i, y_k), \; g_{ik} = f_y(x_i, y_k), \; s_{ik} = f_{xy}(x_i, y_k). \tag{5}$$

According to the boundary condition, the following conditions are valid:

$$g_{xx}(x_i, y_j) = 0 \quad \begin{cases} i = 0, M \\ j = 0, 1, \ldots N \end{cases} \tag{6}$$

$$g_{yy}(x_i, y_j) = 0 \quad \begin{cases} i = 0, 1, \ldots N \\ j = 0, N \end{cases} \tag{7}$$

In case of all the straight lines $j = 0, 1, \ldots N$ the derivates p_{ij} have to fulfill the following system of equations:

$$p_{i+1,j} + 4p_{i,j} + p_{i-1,j} = 3(g_{i+1,j} - g_{i-1,j}) \;\; i = 1, 2, \ldots M - 1 . \tag{8}$$

The boundary condition according to Eq. 6 ensures the necessary equations for the unique determination of the derivates p_{ij}.

For the determination of the derivates g_{ij} the equations can be written similarly for all straight lines $i = 0, 1, \ldots M$

$$g_{i,j+1} + 4g_{i,j} + g_{i,j-1} = 3[g_{i,j+1} - g_{i,j-1}] \;\; j = 1, 2, \ldots N - 1 . \tag{9}$$

The supplementary equations necessary for the determination of the derivates g_{ij} can be obtained from Eq. 7.

For the determination of the mixed derivates s_{ij} the previously determined derivates p_{ij} and g_{ij} can be used. If $j = 0$ or $j = N$, and the boundary

condition is being used, the system of equations:

$$s_{i+1,j} + 4s_{i,j} + s_{i-1,j} = 3[g_{i+1,j} - g_{i-1,j}] \quad i = 1, \ldots M-1 \tag{10}$$

can be solved. In the inner grid points $i = 0, 1, \ldots M$ the lacking derivates s_{ij} can be obtained by using the derivates p_{ij}:

$$s_{i,j+1} + 4s_{i,j} + s_{i,j-1} = 3[p_{i,j+1} - p_{i,j-1}] = \quad j = 1, 2, \ldots N-1\,. \tag{11}$$

For the solution of such equation systems, the algorithm developed for the one-dimensional spline interpolation can be advantageously used [ZÁVOTI, 1978].

Having determined the derivates p_{ij}, g_{ij}, s_{ij} it is easy to determine the coefficients a_{mn}^{ik} of the two variables, being in each dot third order spline polynomials.

The mathematical principles of the spline interpolation are dealt with more detailed by DE BOOR (1962), ALBORG et al. (1967) and SÜNKEL (1977).

2. Fourier transformation of bicubic spline functions

The bicubic spline interpolation of data observed in discrete points can be used for the determination of the direct and inverse Fourier transforms in the spatial or frequency domain. It is a very important and advantageous result that the amplitude and phase spectrum obtained by the spline functions has a sufficient correspondence with the real spectrum at low frequencies [SÜNKEL, 1977].

This fact explaines the exceptional accuracy reached by spline interpolation in the computation of second- and higher order derivates of the potential of gravitational anomalies. The small and large amplitudes i.e. the peaks of gravitational anomalies are exactly reflected in the interpolation. The gradient vector of the field is not distorted significantly. All these facts show that bicubic spline fitting is a reliable and exact interpolation method for the practice.

The general model for the representation of a given data set by bicubic spline functions is given by Eq. 3, which can be analytically expressed in the following form:

$$g(x,y) = \sum_{i=0}^{M-1} \sum_{k=0}^{N-1} \left\{ \sum_{m=0}^{3} \sum_{n=0}^{3} a_{mn}^{i,k} (x - x_i)^m (y - y_k)^n \cdot \right.$$
$$\left. \cdot [\delta(x - x_i) - \delta(x - x_{i+1})]\, [\delta(y - y_k) - \delta(y - y_{k+1})] \right\} \tag{12}$$

— where δx is the so-called unit-step function.

After lengthy computations using the theses of the Fourier transformation, the following formula can be received for the Fourier transform of the bicubic spline functions:

$$G(u,v) = \int_{-\infty}^{\infty}\int_{-\infty}^{\infty} g(x,y)\, e^{-j(ux+vy)}\mathrm{d}x\,\mathrm{d}y =$$

$$= \sum_{i=0}^{M-1}\sum_{k=0}^{N-1}\left\{\sum_{m=0}^{3}\sum_{n=0}^{3} a_{mn}^{ik}\, e^{-j(ux_i+vy_k)}\cdot\right.$$

$$\left.\cdot\left[\frac{m!}{(ju)^{m+1}} - e^{jn}\sum_{r=0}^{m}\frac{m!}{r!(ju)^{m-r+1}}\right]\cdot\left[\frac{n!}{(jv)^{n+1}} - e^{jv}\sum_{s=0}^{n}\frac{n!}{s!(jv)^{n-s+1}}\right]\right\}. \tag{13}$$

Having determined the bicubic spline coefficients of a data system given in grid points, this equation can be used for the determination of the phase and amplitude spectrum of the anomalous potential.

3. Collocation

Most methods for the automatic construction of contour maps determine a data system regularly given in the grid points of a rectangular grid from the original data irregularly distributed. The selection of the prediction method for this purpose is an arbitrary one, but the maps produced by different methods differ in important parameters. The different properties of the different prediction methods can be used for the filtering of data systems. In the practice the transformation of the arbitrarily distributed data is mostly carried out by collocation using the methods proposed by Koch (1973) and Ebner (1980).

In these methods it is supposed that the measured values include random errors, therefore the surface fitted to the predicted points does not contain in all cases the original measured data.

The collocation based on the least squares principle is a prediction method which yields from among linear estimations the best undistorted estimate of the predicted values. The method is not treated here, as it has been described several times [Moritz, 1972].

The basic equations is:

$$u = [C(PP_1), C(PP_2), \ldots C(PP_n)]\begin{bmatrix} C(P_1P_1) & C(P_1P_2) & \ldots & C(P_1P_n) \\ C(P_2P_1) & \ldots & & \\ \vdots & & & \\ C(P_nP_1) & \ldots & & C(P_nP_n) \end{bmatrix}^{-1}\begin{bmatrix} h_1 \\ h_2 \\ \vdots \\ h_n \end{bmatrix} =$$

$$= \mathbf{c}\,\mathbf{C}^{-1}\mathbf{h}\,. \tag{14}$$

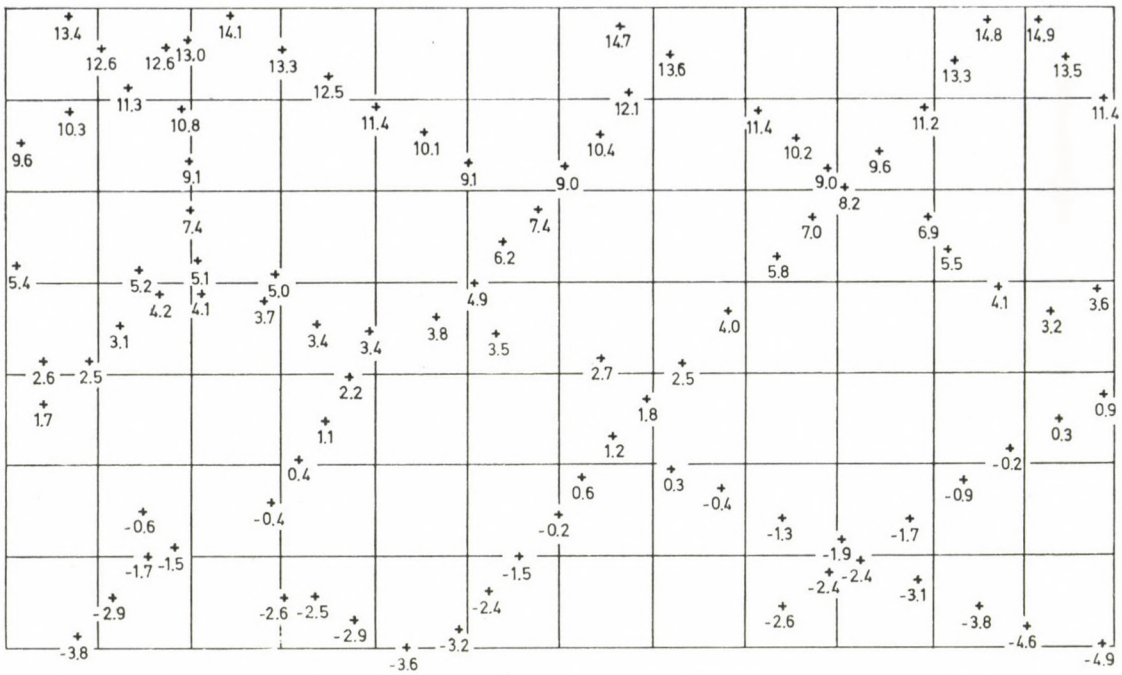

Fig. 1. Map of Bouguer-anomalies

The quantity u is the predicted value of a grid point P and the quantities h_i are the data appearing in the prediction. The vector **c** yields the covariances of the point P and the measuring points P_i, i.e. the statistical dependence. Matrix **C** contains the covariances of the measurement points P_i. The covariance $C(P_iP_k)$ expresses how the points influence each other. It is supposed that it is sufficient to use the value of the covariance $C(P_i\,P_k)$ as a function of the distance between the points. That means that the distribution of the points is homogeneous and isotropic.

Several functions can be recommended as covariance functions. The following types of these functions have been recommended:

$$
\begin{aligned}
c(r) &= \sigma_0^2\, e^{-\frac{2r}{a^2}} \quad \text{Gaussian} \\
c(r) &= \sigma_0^2\, e^{-\frac{2r}{a}} \quad \text{exponential} \\
c(r) &= \frac{\sigma_0^2}{1+r^2} \quad \text{Hirvonen-type.}
\end{aligned}
\tag{15}
$$

The unknown parameters of these covariance functions can be estimated on the basis of greater quantities of measured data.

4. Numerical example

The practical application of the proposed method is presented in form of the representation of a gravimetric field. The original data were provided by H. SÜNKEL.

Figure 1 shows the anomaly distribution in a practical exploration area with the network of the measurement stations (number of the measured stations is 97). The stations are denoted by + — signs. The measurements were made along highways. There are rather big areas between the measured sites where no measurements were made. On the basis of these data, a digital surface model consisting of 13×8 points has been produced (the distance between the grid points is 3 km). The anomalies in the grid points of the quadratic network have been predicted by collocation having estimated the statistical parameters of the measurements. The regularized values obtained

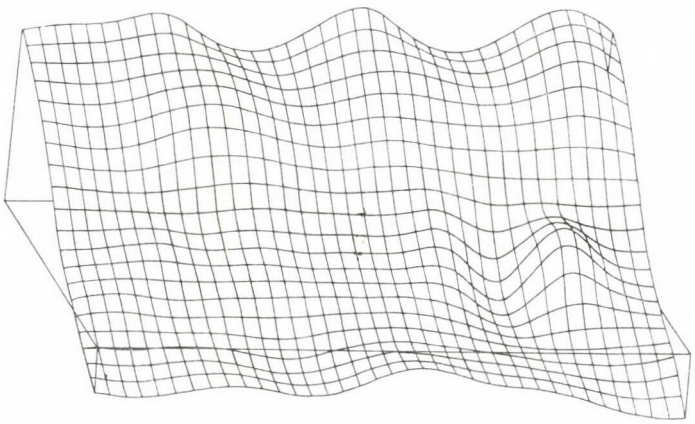

Fig. 2. Perspectivic view of a gravimetric surface

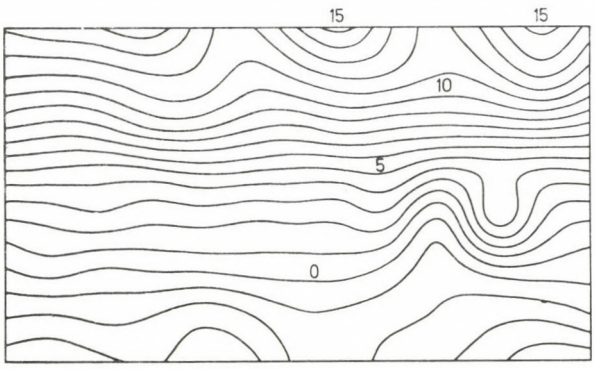

Fig. 3. Isolines map of the anomalies, scale 1 : 250,000

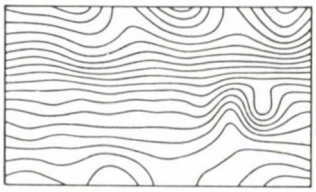

Fig. 4a. Generalized isoline map of the anomalies, scale 1 : 500,000

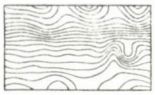

Fig. 4b. Generalized isoline map of the anomalies, scale 1 : 1,000,000

by this method are the initaial data of the bicubic spline interpolation. A perspective view of the fitted surface can be seen in Fig. 2.

The intersection points of an arbitrary plane $z = H$ and the surfaces g_{ik} defined by Eq. 3 can be found easily for the construction of the isolines. In case of given values $x - x_{i-1} < x < x_i$ and for all $i = 1, 2, \ldots M$, $k = 1, 2, \ldots N$ the roots of the third order equation

$$\sum_{n=0}^{3}\left[\sum_{m=0}^{3} a_{mn}^{ik}\,(x - x_{i-1})^m\right](y - y_{k-1})^n = H \tag{16}$$

are to be found for which $y_{k-1} < y < y_k$ is valid.

The plotter connected to the computer plots these roots, thus the isoline map of the interpolating surface is automatically constructed. Figure 3 shows an isoline map with the scale 1 : 250,000.

Maps with smaller scale can be similarly obtained, thus this method solves the problem of map generalization, too. Figure 4a shows a map with the scale 1 : 500,000, Fig. 4b that with a scale 1 : 1,000,000.

REFERENCES

Assmus, E. 1976: Berücksichtigung von Geländekannten im Stuttgarter Höhenlinienprogram. *Geowiss. Mitt.* 8, 51—63.

Alborg, J. H.—Nilson, E. N.—Walsch, I. L. 1967: The theory of splines and their applications. Academic Press, London.

Boor, C. 1962: Bicubic spline interpolation. *J. Math. Phys.*, 41, 212—218.

Crain, I. K.—Bhattacharyya, B. K. 1967: Treatment of non equispaced two-dimensional data with a digital computer. *Geoexplor.*, 5, 173—194.

Ebner, H. 1980: HIFI — A minicomputer program package for height interpolation by finite elements. Congress of the international society for photogrammetry, Hamburg.

Koch, K. R. 1973: Digitales Geländemodell und automatische Höhenlinienzeichnung. *ZfV*, 8, 346—352.

MARCSUK, G. I. 1976: A gépi matematika numerikus módszerei (Numerical methods of computer mathematics). Műszaki Könyvkiadó, Budapest.
MORITZ, H. 1972: Advanced least-squares methods. *Reports of the Department of Geodetic Science*, No. 175.
STANGER, W.—KRAUS, K. 1975: Ein allgemeines digitales Geländemodell — Das Stuttgarter Höhenlinienprogram. Numerische Photogrammetrie, H. Wichmann Verlag, Karlsruhe.
SÜNKEL, H. 1977: Die Darstellung geodätischer Integralformeln durch bikubische Spline-Funktionen. Mitt. der geod. Institute der TU Graz.
ZÁVOTI, J. 1978: A spline interpoláció alkalmazása a geodéziában (The use of spline interpolation in geodesy) Kozmikus Geodézia. Hungarian Astronautical Society.

СОСТАВЛЕНИЕ ЦИФРОВЫХ КАРТ ПРИ ПОМОЩИ ИНТЕРПОЛЯЦИИ ФУНКЦИЯМИ БИКУБИЧЕСКИХ СПЛАЙНОВ

Й. ЗАВОТИ

РЕЗЮМЕ

В геодезии для иллюстрации разделения элементов системы данных на классы широко испльзуются уровенные карты. Описывается метод, позволяющий при помощи ЭВМ автоматическое составление карт с изолиниями. Линии уровней созданные таким образом, хорошо подходят к заданным дискретным данным — независимо от пространственного распределения точек —, но карта с изолиниями созланная при помощи ЭВМ не содержит никакой новой информации по сравнению с исходными данными.

В последнее время Крейн и Баттачария [1], Краус и Штангер [2], Ассмус [3], Эбнер [4] и Кох [5] опубликовали методы автоматизированного составления карт с изолиниями.

Предлагаемый нами метод основывается на выгодных свойствах интерполяции сплайнов с двумя переменными.

Acta Geodaet., Geophys. et Montanist. Acad. Sci. Hung. Tomus 16 (2—4), pp. 245—257 (1981)

DETERMINATION OF POLAR MOTION COORDINATES FROM DOPPLER OBSERVATIONS OF A SINGLE STATION

GY. SZÁDECZKY-KARDOSS

CAND. TECHN. SCI.

GEODETIC AND GEOPHYSICAL RESEARCH INSTITUTE OF THE HUNGARIAN ACADEMY OF SCIENCES, SOPRON

The paper presents a method for the deduction of the polar motion coordinates x, y from the data of Doppler measurements made at a single station during longer time. Formulae are given for the computation of the changes of geographical longitudes and latitudes, then of the coordinates of the polar motion. Formulae are also deduced for the determination of geographical coordinates from spatial Cartesian ones, further for the determination of the mean pole position. Lastly in a complete numerical example the coordinates of the polar motion are computed from fictitious measurement results.

1. Introduction

If measurements are made continuously for a longer time with a Doppler receiver set up stably in a geodynamic station, series of the sets X, Y, Z of orthogonal spatial coordinates can be computed. Such measurements are carried out in a number of stations in different parts of the globe, and from a common processing of the data, polar motion coordinates are deduced.

The question can be raised whether polar motion coordinates could be deduced from Doppler observations of a single station, carried out continuously during longer time, for the time interval of the measurements. The present paper deals with this question.

It is naturally accepted that the polar motion coordinates x, y deduced from the measurements of a single station cannot be as accurate as the values determined from the measurements of several stations.

2. Computation of $\Delta\varphi$ and $\Delta\lambda$ from Doppler observations

The spatial orthogonal coordinates of the ellipsoid of rotation, X, Y, Z can be computed — as generally known — by the formulae:

$$X = (N + h) \cos \varphi \cos \lambda \tag{1}$$

$$Y = (N + h) \cos \varphi \sin \lambda \tag{2}$$

$$Z = \left(N \frac{b^2}{a^2} + h\right) \sin \varphi \tag{3}$$

where φ and λ are geographic coordinates, N is the radius of curvature in the prime vertical, and h is the height above the ellipsoid.

In a first step it is supposed that the value of h does not change, but N is changing due to changes in $\Delta\varphi$. In this case the change of the geographic latitude due to the polar motion can be deduced from a derivation of Eq. 3:

$$\mathrm{d}z = \left(N \frac{b^2}{a^2} + h\right) \cos \varphi \, \mathrm{d}\varphi + \sin \varphi \, \mathrm{d}N$$

where (4)

$$N = a (1 - e^2 \sin^2 \varphi)^{-\frac{1}{2}}$$

and

$$\mathrm{d}N = e^2 \frac{N^3}{a^2} \sin \varphi \cos \varphi \, \mathrm{d}\varphi \tag{5}$$

then $\mathrm{d}\varphi$ can be written after some simple algebra:

$$\mathrm{d}\varphi'' = \frac{\mathrm{d}z \varrho''}{Z \operatorname{ctg} \varphi + \dfrac{e^2}{a^2} N^3 \sin^2 \varphi \cos \varphi}. \tag{6}$$

The formula for the change of the geographic longitude $d\lambda$ can be deduced in two different ways. The first is obtained from a derivation of Eq. 1:

$$\mathrm{d}\lambda'' = -\frac{\mathrm{d}x \varrho''}{Y} - \operatorname{ctg} \lambda \operatorname{tg} \varphi \, \mathrm{d}\varphi'' + \frac{e^2 N^3}{a^2} \frac{\sin \varphi \cos^2 \varphi \cos \lambda \, \mathrm{d}\varphi''}{Y}. \tag{7}$$

The second way for the computation of $d\lambda$ is obtained from a derivation of Eq. 2. From this one gets:

$$\mathrm{d}\lambda'' = \frac{\mathrm{d}y \, \varrho''}{X} + \operatorname{tg} \varphi \operatorname{tg} \lambda \, \mathrm{d}\varphi'' - \frac{e^2 N^3}{a^2} \frac{\sin \varphi \cos^2 \varphi \sin \lambda \, \mathrm{d}\varphi''}{X}. \tag{8}$$

In the following the formula of the change of the geographic longitude for the case when h is changing will also be necessary. Thus, from a derivation of Eq. 3 one gets:

$$\mathrm{d}\varphi_i = \frac{\mathrm{d}z_i \, \varrho'' - \sin \varphi_1 \varrho'' \left(\dfrac{b^2}{a^2} \, \mathrm{d}N_i + \mathrm{d}h_i\right)}{Z_1 \operatorname{ctg} \varphi_1} \tag{9}$$

and from the derivation of Eq. 2:

$$d\lambda_i = \frac{dy_i\,\varrho''}{X_1} + \frac{Y_1}{X_1}\operatorname{tg}\varphi_1\,d\varphi_i'' - \frac{\cos\varphi_1 \sin\lambda_1\,\varrho''}{X_1}(dN_i + dh_i)\,. \qquad (10)$$

In the practice Eqs 6—10 are used if the differences Δx_i, Δy_i and Δz_i relating to certain terms X_1, Y_1, Z_1 of the series X_i, Y_i, Z_i are computed, then the values of $d\varphi_i$, one gets from the Eqs 6 or 9 and, the values of $d\lambda_i$ from Eqs 8 and 10. Concerning dimensions it is to be remarked that the values of dx_i, dy_i, dz_i, X, Y, Z, dN_i and dh_i are substituted in meter, the values of $d\varphi_i$ and $d\lambda_i$ in seconds of arc, and the value

$$\varrho'' = 206\,264.806''.$$

3. Deduction of the coordinates x, y of the polar motion from the values of $\Delta\varphi$, $\Delta\lambda$ computed from X, Y, Z coordinates of Doppler receiver measurements

Let P_0 be the mean pole with reference to CIO, P_i the true pole. The equations of the polar motion are if the Eastward values of the geographic longitude are taken positive [MUELLER, 1969; Eqs 4.39 and 4.40, p. 87]:

$$\left.\begin{aligned} \Delta\varphi_{0i} &= \varphi_i - \varphi_0 = x'' \cos\lambda - y'' \sin\lambda \\ \Delta\lambda_{0i} &= \lambda_i - \lambda_0 = x'' \sin\lambda \operatorname{tg}\varphi + y'' \cos\lambda \operatorname{tg}\varphi \end{aligned}\right\}. \qquad (11)$$

From these two equations the values of the unknown coordinates x, y of the polar motion can be computed. After lengthy computations and trigonometric transformations, the final results is:

$$x_i'' = \Delta\lambda_{0i}'' \operatorname{ctg}\varphi \sin\lambda + \Delta\varphi_{0i}'' \cos\lambda \qquad (12)$$

$$y_i'' = \Delta\lambda_{0i}'' \operatorname{ctg}\varphi \cos\lambda - \Delta\varphi_{0i}'' \sin\lambda\,. \qquad (13)$$

The correctness and usefulness of these deductions can be illustrated on hand of a practical example. Starting from the CIO coordinates φ_0 and λ_0 of a station, the changes of the coordinates $\Delta\varphi_i$, $\Delta\lambda_i$ have been computed from Eq. 11 with an accuracy of 0.001″ on the basis of the polar coordinates x, y for each tenth day of the Chandler period between January 1.0, 1979, and April 5.0, 1980 [BIH, 1980; p. B21—B22] (see column 2,3 in Table I). Using these values and further φ_0, λ_0, the values of φ_i and λ_i have been computed, latters are valid each tenth day. Now from Eqs 1—4, the spatial coordinates X_i, Y_i, Z_i for each tenth day have been computed with an accuracy of 1 mm in the WGS—72 system (see columns 4—6 of Table I).

Table I

Date 1979		$\Delta\varphi$	$\Delta\lambda$	X_i 4 123 700+	Y_i 1 226 200+	Z_i 4 693 300+	$dx = X_i - X_0$	$dy = Y_i - Y_0$	$dz = Z_i - Z_0$
Jan.	1.0	+.112	+.124	57.933	71.650	80.210	−3.189	+1.750	+2.329
	11.0	+.093	+.105	58.462	71.393	79.815	−2.660	+1.493	+1.934
	21.0	+.072	+.090	59.011	71.230	79.378	−2.111	+1.330	+1.497
	31.0	+.046	+.076	59.663	71.120	78.837	−1.459	+1.220	+0.956
Feb.	10.0	+.018	+.068	60.323	71.142	78.255	−0.799	+1.242	+0.374
	20.0	−.015	+.064	61.070	71.277	77.569	−0.052	+1.377	−0.312
Mar.	2.0	−.050	+.064	61.835	71.505	76.841	+0.713	+1.605	−1.040
	12.0	−.084	+.072	62.533	71.886	76.134	+1.411	+1.986	−1.747
	22.0	−.113	+.087	63.078	72.375	75.531	+1.956	+2.475	−2.350
Apr.	1.0	−.140	+.106	63.556	72.930	74.970	+2.434	+3.030	−2.911
	11.0	−.163	+.131	63.911	73.580	74.492	+2.789	+3.680	−3.389
	21.0	−.182	+.155	64.184	74.183	74.097	+3.062	+4.283	−3.784
May	1.0	−.197	+.180	64.364	74.781	73.784	+3.242	+4.881	−4.097
	11.0	−.208	+.203	64.468	75.312	73.556	+3.346	+5.412	−4.325
	21.0	−.217	+.227	64.522	75.851	73.368	+3.400	+5.951	−4.513
	31.0	−.222	+.250	64.495	76.343	73.264	+3.373	+6.443	−4.617
Jun.	10.0	−.221	+.277	64.313	76.876	73.286	+3.191	+6.976	−4.595
	20.0	−.218	+.304	64.086	77.396	73.348	+2.964	+7.496	−4.533
	30.0	−.213	+.330	63.822	77.884	73.451	+2.700	+7.984	−4.430
Jul.	10.0	−.206	+.354	63.526	78.318	73.597	+2.404	+8.418	−4.284
	20.0	−.192	+.376	63.089	78.667	73.889	+1.967	+8.767	−3.992
	30.0	−.171	+.398	62.499	78.970	74.325	+1.377	+9.070	−3.556
Aug.	9.0	−.148	+.418	61.876	79.220	74.803	+0.754	+9.320	−3.078
	19.0	−.123	+.435	61.228	79.397	75.323	+0.106	+9.497	−2.558
	29.0	−.100	+.449	60.641	79.527	75.801	−0.481	+9.627	−2.080
Sep.	8.0	−.074	+.456	60.031	79.498	76.342	−1.091	+9.598	−1.539
	18.0	−.052	+.461	59.519	79.455	76.799	−1.603	+9.555	−1.082
	28.0	−.033	+.459	59.115	79.291	77.195	−2.007	+9.391	−0.686
Oct.	8.0	−.019	+.454	58.839	79.100	77.486	−2.283	+9.200	−0.395
	18.0	−.007	+.448	58.612	78.902	77.735	−2.510	+9.002	−0.146
	28.0	+.005	+.438	58.408	78.624	77.985	−2.714	+8.724	+0.104
Nov.	7.0	+.019	+.424	58.185	78.253	78.276	−2.937	+8.353	+0.395
	17.0	+.034	+.404	57.976	77.755	78.588	−3.146	+7.855	+0.707
	27.0	+.044	+.382	57.887	77.250	78.796	−3.235	+7.350	+0.915
Dec.	7.0	+.049	+.358	57.921	76.738	78.900	−3.201	+6.838	+1.019
	17.0	+.052	+.336	57.986	76.279	78.962	−3.136	+6.379	+1.081
	27.0	+.052	+.315	58.111	75.859	78.962	−3.011	+5.959	+1.081
Jan.	6.0	+.051	+.294	58.257	75.446	78.941	−2.865	+5.546	+1.060
	16.0	+.045	+.274	58.508	75.085	78.816	−2.614	+5.185	+0.935
	26.0	+.036	+.252	58.835	74.703	78.629	−2.287	+4.803	+0.748
Feb.	5.0	+.026	+.234	59.161	74.409	78.421	−1.961	+4.509	+0.540
	15.0	+.021	+.220	59.354	74.161	78.318	−1.768	+4.261	+0.437
	25.0	+.015	+.209	59.551	73.980	78.193	−1.571	+4.080	+0.312
Mar.	6.0	+.008	+.203	59.739	73.906	78.047	−1.383	+4.006	+0.166
	16.0	−.007	+.202	60.074	73.984	77.735	−1.048	+4.084	−0.146
	26.0	−.026	+.202	60.490	74.107	77.340	−0.632	+4.207	−0.541
Apr.	5.0	−.051	+.204	61.025	74.310	76.820	−0.097	+4.410	−1.061

Table II

	Date 1979	$dx_i = X_i - X_1$	$dy_i = Y_i - Y_1$	$dz_i = Z_i - Z_1$	$\Delta\varphi_i$	$\Delta\lambda_i$
Jan.	1.0	0.000	0.000	0.000	0.000	.00000
	11.0	+0.529	−0.257	−0.395	−0.019	−.01904
	21.0	+1.078	−0.420	−0.832	−0.040	−.03403
	31.0	+1.730	−0.530	−1.373	−0.066	−.04800
Feb.	10.0	+2.390	−0.508	−1.955	−0.094	−.05602
	20.0	+3.137	−0.373	−2.641	−0.127	−.06001
Mar.	2.0	+3.902	−0.145	−3.369	−0.162	−.06000
	12.0	+4.600	+0.236	−4.076	−0.196	−.05201
	22.0	+5.145	+0.725	−4.679	−0.225	−.03700
Apr.	1.0	+5.623	+1.280	−5.240	−0.252	−.01803
	11.0	+5.978	+1.930	−5.718	−0.275	+.00700
	21.0	+6.251	+2.533	−6.113	−0.294	+.03097
May	1.0	+6.431	+3.131	−6.426	−0.309	+.05600
	11.0	+6.535	+3.662	−6.654	−0.320	+.07898
	21.0	+6.589	+4.201	−6.842	−0.329	+.10301
	31.0	+6.562	+4.693	−6.946	−0.334	+.12599
Jun.	10.0	+6.380	+5.226	−6.924	−0.333	+.15297
	20.0	+6.153	+5.746	−6.862	−0.330	+.17996
	30.0	+5.889	+6.234	−6.759	−0.325	+.20600
Jul.	10.0	+5.593	+6.668	−6.613	−0.318	+.22999
	20.0	+5.156	+7.017	−6.321	−0.304	+.25200
	30.0	+4.566	+7.320	−5.885	−0.283	+.27399
Aug.	9.0	+3.943	+7.570	−5.407	−0.260	+.29399
	19.0	+3.295	+7.747	−4.887	−0.235	+.31098
	29.0	+2.708	+7.877	−4.409	−0.212	+.32497
Sep.	8.0	+2.098	+7.848	−3.868	−0.186	+.33199
	18.0	+1.586	+7.805	−3.411	−0.164	+.33700
	28.0	+1.182	+7.641	−3.015	−0.145	+.33498
Oct.	8.0	+0.906	+7.450	−2.724	−0.131	+.32999
	18.0	+0.679	+7.252	−2.475	−0.119	+.32399
	28.0	+0.475	+6.974	−2.225	−0.107	+.31399
Nov.	7.0	+0.252	+6.603	−1.934	−0.093	+.29999
	17.0	+0.043	+6.105	−1.622	−0.078	+.27997
	27.0	−0.046	+5.600	−1.414	−0.068	+.25796
Dec.	7.0	−0.012	+5.088	−1.310	−0.063	+.23398
	17.0	+0.053	+4.629	−1.248	−0.060	+.21200
	27.0	+0.178	+4.209	−1.248	−0.060	+.19099
Jan.	6.0	+0.324	+3.796	−1.269	−0.061	+.17001
	16.0	+0.575	+3.435	−1.394	−0.067	+.15000
	26.0	+0.902	+3.053	−1.581	−0.076	+.12796
Feb.	5.0	+1.228	+2.759	−1.789	−0.086	+.11000
	15.0	+1.421	+2.511	−1.892	−0.091	+.09597
	25.0	+1.618	+2.330	−2.017	−0.097	+.08496
Mar.	6.0	+1.806	+2.256	−2.163	−0.104	+.07898
	16.0	+2.141	+2.334	−2.475	−0.119	+.07800
	26.0	+2.557	+2.457	−2.870	−0.138	+.07796
Apr.	5.0	+3.092	+2.660	−3.390	−0.163	+.07998

In the following, every term of this fictitious series has been subtracted from the values of the spatial coordinates corresponding to the position P_0:

$$X_0 = 4\,123\,761.\ 122\ \text{m}$$
$$Y_0 = 1\,226\,269.\ 900\ \text{m}$$
$$Z_0 = 4\,693\,377.\ 881\ \text{m}\,.$$

Thus columns 7—9 of Table I have been obtained.

After these preparatory calculations, the changes of the geographic coordinates $\Delta\varphi$ and $\Delta\lambda$ are computed with the help of Eqs 6—8. These coincide within a maximum deviation of $\pm 0.0004''$ with the values in columns 2 and 3 of Table I. Lastly using Eqs 12—13, the polar coordinates x and y are computed, which agree within a maximum deviation of $\pm 0.0006''$ with the values of [BIH, 1980]. This experimental computation proves that if the spatial coordinates X, Y, Z are homogeneous and sufficiently accurate, then the polar coordinates can be computed from the data of a Doppler station using the equations in Chapters 2 and 3. Naturally, the computed results cannot have better accuracy than that of the coordinates X, Y, Z.

In the next experimental computation it will be shown that even if the mean pole P_0 is unknown, the deviations $\Delta\varphi_i$ and $\Delta\lambda_i$ corresponding to an arbitrarily chosen pole position P_i are real. Let us take as reference point the values of X_1, Y_1, Z_1 for January 1.0, 1979, and compute the differences

$$\left.\begin{aligned} \mathrm{d}x_i &= X_i - X_1 \\ \mathrm{d}y_i &= Y_i - Y_1 \\ \mathrm{d}z_i &= Z_i - Z_1 \end{aligned}\right\} \tag{14}$$

from these values (columns 2—4 of Table II), then similarly to the previous case, the values of $\Delta\varphi_i$ and $\Delta\lambda_i$ referring to the position P_1 can be obtained by means of Eqs 6 and 8. It can be seen from columns 5 and 6 of Table II that the differences of the geographic coordinates referring to P_1 coincide within $\pm 0.00004''$ with the values in columns 2 and 3 of Table I, and even these differences are due to rounding-off in the computations.

4. Computation of geographic coordinates and of h from spatial orthogonal coordinates

For the following the values of φ_i, λ_i and h_i of the points P_i are needed if the spatial orthogonal coordinates X_i, Y_i and Z_i are known, i.e. inverses of Eqs 1—3. For the computation several formulae have been proposed, the

most recent ones are proposed by HALMOS (1980, Eq. 14 on p. 9). For sake of completeness the following equation can be obtained from Eqs 1—2:

$$\operatorname{tg} \lambda = \frac{Y}{X}. \tag{15}$$

For the computation of the geographic latitude I propose a new solution which can be used most advantageously on microcomputers. One gets from Eqs 2—3:

$$\operatorname{tg} \varphi = \frac{Z}{Y} \sin \lambda \left(\frac{1 + \dfrac{h}{N}}{\dfrac{b^2}{a^2} + \dfrac{h}{N}} \right) \tag{16}$$

and in a first approximation one has:

$$\operatorname{tg} \varphi_0 = \frac{Z}{Y} \sin \lambda \left(\frac{b^2}{a^2} \right)^{-1}. \tag{16a}$$

The approximation in Eq. 16a is the better the smaller the quotient h/N is. From the value of φ_0 obtained so one can compute in the following:

$$W_i = 1 - e^2 \sin^2 \varphi_i \tag{17}$$

$$N_i = a/W_i \tag{18}$$

and using Eqs 1—2 one has:

$$N_i + h_i = \frac{X}{\cos \varphi_i \cos \lambda} = \frac{Y}{\cos \varphi_i \sin \lambda}. \tag{19}$$

Using these equations, an approximative value for the height above the ellipsoid can be calculated. By substituting these values into Eq. 16, a better approximation can be reached for φ, which is then used again in Eqs 17—19.

In case of the present numerical example, the values of φ and h are obtained with the following differences:

iteration 1: $\Delta\varphi = 0.0405''$, $\Delta h = 1.377$ m
iteration 2: $\Delta\varphi = 0.0002''$, $\Delta h = 0.004$ m
iteration 3: $\Delta\varphi = 0.0000''$, $\Delta h = 0.001$ m.

5. Determination of the mean pole

In the next numerical example it is supposed that datum values (a, b^2/a^2, e^2, mean pole) are unchanged, but the measured values of the coordinates X_i, Y_i and Z_i have measurement errors. In this numerical experiment the measurement errors are simulated using a subroutine which generates pseudo-random numbers on the computer HP2100A of the Institute (BARÓTHY) using which a measurement error series having uniform distribution in the interval -0.5 m and $+0.5$ m has been produced by KALMÁR. By adding the values of this error series to the orthogonal coordinates in columns 4—6 of Table I, the series of values X_i, Y_i and Z_i in columns 2—4 of Table III is obtained which can be taken as quasi measurement results. From this series the geographic coordinates φ_0 and λ_0 referring to the mean pole P_0 can be computed most advantageously with the following method. Let the original data be the values X_1, Y_1 and Z_1 for January 1.0, 1979, which are then subtracted from columns 2—4 of Table III according to Eq. 14, which yields then the series of the coordinate differences $\mathrm{d}x_i$, $\mathrm{d}y_i$, $\mathrm{d}z_i$.

For a number n of the times T_i chosen in well separated intervals (e.g. 3—4 times in one year) one obtains:

$$\varphi_0 = \varphi_1 + \mathrm{d}\varphi_i - \Delta\varphi_{0i} = \varphi_1 + \mathrm{d}\varphi_i - x_i \cos\lambda + y_i \sin\lambda \tag{20}$$

and

$$\lambda_0 = \lambda_1 + \mathrm{d}\lambda_i - \Delta\lambda_{0i} = \lambda_1 + \mathrm{d}\lambda_i - x_i \sin\lambda \operatorname{tg}\varphi - y_i \cos\lambda \operatorname{tg}\varphi \,. \tag{21}$$

With these equations, the value n of the mean pole can be determined, and the average of these values approximates rather well the mean pole.

In the numerical example n equals 4 according to column 1 of Table IV. In Eqs 20—21 the values of the differences of the geographical coordinates $\mathrm{d}\varphi_i$ and $\mathrm{d}\lambda_i$ can be found in columns 2 and 5 of Table IV. They are computed from Eqs 6—8 using the values of $\mathrm{d}x_i$, $\mathrm{d}y_i$, $\mathrm{d}z_i$ from the present experiment. The geographical coordinates φ_1, λ_1 are computed with a maximum of three iterations from the spatial coordinates X_1, Y_1, Z_1 of January 1.0, 1979, see columns 2—4 of Table III using Eqs 15—19. The polar coordinates x and y for Eqs 20—21 are taken e.g. from [BIH, 1980] but only for the time moment n used in the averaging. As the lowest part of columns 4 and 7 in Table IV shows, the mean pole can be determined by this method with an accuracy of $-0.0080''$ in the geographical latitude, and of $+0.0015''$ in the geographical longitude. With these one gets:

$$\varphi_1 - \varphi_0 = +0.1122'' \tag{22}$$

$$\lambda_1 - \lambda_0 = +0.1135'' \tag{23}$$

Table III

Date 1979		X_i 4 123 700+	Y_i 1 226 200+	Z_i 4 693 300+	$d\varphi_i$	$d\lambda_i$	x_i	y_i
Jan.	1.0	57.719	71.326	80.261	.0000	.00000	+.1370	+.0671
	11.0	58.748	71.428	80.154	−.0051	+.00344	+.1330	+.0715
	21.0	59.154	70.855	79.455	−.0388	−.03619	+.0904	+.0465
	31.0	59.449	71.059	78.743	−.0730	−.03712	+.0574	+.0555
Feb.	10.0	60.254	70.650	78.504	−.0845	−.06133	+.0401	+.0377
	20.0	61.081	71.378	77.405	−.1373	−.04210	−.0055	+.0695
Mar.	2.0	62.018	71.039	77.118	−.1511	−.06355	−.0243	+.0547
	12.0	62.033	71.683	75.774	−.2158	−.05241	−.0834	+.0831
	22.0	62.936	72.851	75.378	−.2348	−.00017	−.0881	+.1338
Apr.	1.0	63.701	73.111	74.790	−.2631	+.00362	−.1142	+.1452
	11.0	63.560	73.882	74.288	−.2872	+.03434	−.1294	+.1789
	21.0	64.277	73.863	73.992	−.3015	+.02873	−.1445	+.1781
May	1.0	64.579	74.646	73.489	−.3257	+.06002	−.1596	+.2123
	11.0	64.419	74.878	73.237	−.3378	+.06768	−.1692	+.2224
	21.0	64.791	75.963	73.607	−.3200	+.12775	−.1366	+.2698
	31.0	64.050	76.421	73.065	−.3460	+.14219	−.1577	+.2898
Jun.	10.0	64.722	76.834	73.441	−.3280	+.16871	−.1336	+.3078
	20.0	64.044	76.940	73.576	−.3215	+.17613	−.1255	+.3124
	30.0	63.387	78.025	73.918	−.3050	+.23577	−.0941	+.3598
Jul.	10.0	63.793	78.773	73.851	−.3083	+.27211	−.0879	+.3924
	20.0	63.109	78.628	73.712	−.3140	+.26300	−.0957	+.3861
	30.0	62.719	79.140	74.474	−.2783	+.30023	−.0518	+.4084
Aug.	9.0	61.515	79.091	74.792	−.2630	+.30276	−.0365	+.4063
	19.0	61.579	79.595	75.415	−.2330	+.33774	−.0013	+.4282
	29.0	60.494	79.374	75.954	−.2077	+.33492	+.0248	+.4186
Sep.	8.0	60.495	79.299	75.937	−.2079	+.33111	+.0237	+.4153
	18.0	59.124	79.137	76.488	−.1814	+.33163	+.0492	+.4082
	28.0	59.071	79.674	77.476	−.1339	+.37396	+.1057	+.4317
Oct.	8.0	58.634	78.757	77.476	−.1339	+.32809	+.0938	+.3916
	18.0	58.277	78.898	77.641	−.1260	+.33772	+.1039	+.3977
	28.0	58.739	78.187	78.014	−.1081	+.30798	+.1055	+.3690
Nov.	7.0	57.690	78.165	77.796	−.1185	+.30349	+.1022	+.3657
	17.0	57.521	77.665	78.949	−.0631	+.29652	+.1535	+.3438
	27.0	58.117	77.001	78.778	−.0713	+.26064	+.1363	+.3148
Dec.	7.0	57.895	76.553	79.042	−.0586	+.24237	+.1437	+.2953
	17.0	58.261	75.912	78.481	−.0856	+.20151	+.1072	+.2673
	27.0	58.490	75.818	79.297	-.0464	+.20958	+.1469	+.2632
Jan.	6.0	58.558	75.008	78.780	−.0712	+.16099	+.1105	+.2279
	16.0	58.403	75.324	78.334	−.0927	+.16979	+.0922	+.2417
	26.0	58.998	74.580	78.688	−.0756	+.13815	+.1004	+.2092
Feb.	5.0	59.582	74.025	78.615	−.0792	+.10921	+.0894	+.1850
	15.0	58.918	74.462	78.453	−.0869	+.12856	+.0871	+.2041
	25.0	59.644	73.744	77.758	−.1204	+.08174	+.0428	+.1727
Mar.	6.0	59.718	74.282	77.729	−.1218	+.10820	+.0483	+.1962
	16.0	59.617	73.868	77.237	−.1454	+.07981	+.0183	+.1782
	26.0	60.435	74.525	77.718	−.1223	+.12019	+.0510	+.2068
Apr.	5.0	61.305	74.362	77.069	−.1535	+.10188	+.0163	+.1998

Table IV

	Date 1979	$d\varphi_{0i}$	$-\Delta\varphi_{0i}$	φ_0 47°40′+	$d\lambda_{0i}$	$-\Delta\lambda_{0i}$	λ_0 16°33′+
Jan.	1.0	.000	−.112	53.158	.0000	−.124	38.628
Jun.	10.0	−.328	+.221	53.163	+.1687	−.277	38.644
Nov.	7.0	−.118	−.019	53.133	+.3035	−.424	38.632
Apr.	5.0	−.154	+.051	53.168	+.1020	−.204	38.650
Mean				53.158			38.6385
Diff.				−0.008			+0.0015

By adding these values to the known φ_1 and λ_1, the coordinates φ_0 and λ_0 of the mean pole are obtained. After this, the computation is carried out with the method outlined previously, i.e. to the values of $d\varphi_i$ and $d\lambda_i$ calculated with the help of formulae 20 and 21 the values from Eqs 22—23 are added. Thus values of $d\varphi$ and $d\lambda$ are obtained:

$$d\varphi_i + \varphi_1 - \varphi_0 = d\varphi \tag{24}$$

$$d\lambda_i + \lambda_1 - \lambda_0 = d\lambda \tag{25}$$

using which Eqs 12—13 yield the coordinates x_i and y_i of the polar motion (columns 7 and 8 of Table III).

By comparing these values with those from the publication [BIH, 1980], the greatest deviation found in x_i is $+0.030''$, that in y_i + $0.026''$. These deviations are naturally not totally the result of rounding-off errors, but they are partially the consequence of measurement errors up to 0.5 m in the coordinates X_i, Y_i, Z_i.

6. Practical computations

In the computations presented upto Chapter 5, it has been supposed that the heights above the ellipsoid h remain unchanged. This is no more valid in case of the computational method presented here, as due to the measurement errors the value of h is also burdened with errors, therefore a more exact solution is reached if Eqs 9 and 10 are used instead of Eqs 6 and 8. Using these equations, the coordinates x_i and y_i of the polar motion can be computed from the Doppler observation of a single station with the following method:

Let us start from the spatial coordinates X, Y, Z computed from the Doppler transits in a single station which have been observed during a longer

time interval, e.g. in a complete Chandler period. From the series of the three coordinates, averages are computed for each 10 days interval e.g. with the Orlov method [ORLOV, 1961]. The time moments of these averages are the central points of the intervals. Let us denote the 10 days-averages by X_i, Y_i, Z_i. In an experimental example the values from columns 2—4 of Table III are used. Let us further use the same $n = 4$ value and compute the values φ_i, λ_i, dN_i and dh_i from the quantities of Eqs 15—19 after three iterations. dN_i and dh_i denote the deviations from point P_1, their values can be found in Table V. With these values and Eqs 9—10, the values $d\varphi_{0i}$ and $d\lambda_{0i}$ are computed which can be found in columns 2 and 5 of Table VI. The values of φ_0 and λ_0 referring to the mean pole computed with Eqs 20—21 differs from φ_0 by $-0.0052''$, from λ_0 by $+0.0031''$. One gets referring to $n = 1$ measurements:

$$\varphi_1 - \varphi_0 = +0.1150'' \tag{26}$$

$$\lambda_1 - \lambda_0 = +0.1151''. \tag{27}$$

The following computations are summarized in Table VII: the value of $\Delta\varphi_i$ is computed from Eq. 6, that of $\Delta\lambda_i$ from Eq. 8 (columns 2 and 3 of Table VII). Then the value of $d\varphi_i$ is computed with Eq. 20, and that of $d\lambda_i$ with

Table V

Date 1979	dN_i	dh_i	dy_i	dz_i
Jan. 1.0	.000	.000	.000	.000
Jun. 10.0	−.036	+.534	+5.508	−6.820
Nov. 7.0	−.010	−.528	−2.465	+6.839
Apr. 5.0	−.018	+.536	−3.192	+3.036

Table VI

Date 1979	$d\varphi_{0i}$	$-\Delta\varphi_{01}$	φ_0 47°40′+	$d\lambda_{0i}$	$-\Delta\lambda_{01}$	λ_0 16°33′+
Jan. 1.0	.0000	−.112	53.1582	.0000	−.124	38.6280
Jun. 10.0	−.3470	+.221	53.1442	+.1574	−.277	38.6324
Nov. 7.0	−.0998	−.019	53.1514	+.3146	−.424	38.6426
Apr. 5.0	−.1541	+.051	53.1671	+.0965	−.204	38.6445
Mean			53.1552			38.6369
Diff.			−0.0052			+0.0031

Table VII

Date 1979		$\Delta\varphi_i$	$\Delta\lambda_i$	$d\varphi_i$	$d\lambda_i$	x_i	y_i
Jan.	1.0	.0000	.00000	+.1150	+.1151	+.1401	+.0677
	11.0	−.0051	+.00344	+.1099	+.1185	+.1361	+.0721
	21.0	−.0388	−.03619	+.0762	+.0789	+.0935	+.0471
	31.0	−.0730	−.03712	+.0420	+.0780	+.0605	+.0561
Feb.	10.0	−.0845	−.06133	+.0305	+.0538	+.0432	+.0383
	20.0	−.1373	−.04210	−.0223	+.0730	−.0024	+.0701
Mar.	2.0	−.1511	−.06355	−.0361	+.0516	−.0212	+.0553
	12.0	−.2158	−.05241	−.1008	+.0627	−.0803	+.0835
	22.0	−.2348	−.00017	−.1198	+.1149	−.0850	+.1344
Apr.	1.0	−.2631	+.00362	−.1481	+.1187	−.1112	+.1458
	11.0	−.2872	+.03434	−.1722	+.1494	−.1263	+.1795
	21.0	−.3015	+.02873	−.1865	+.1438	− 1414	+.1787
May	1.0	−.3257	+.06002	−.2107	+.1751	−.1565	+.2129
	11.0	−.3378	+.06768	−.2228	+.1827	−.1661	+.2230
	21.0	−.3200	+.12775	−.2050	+.2429	−.1335	+.2704
	31.0	−.3460	+.14219	−.2310	+.2573	−.1546	+.2904
Jun.	10.0	−.3470	+.15740	−.2320	+.2725	−.1517	+.3040
	20.0	−.3215	+.17613	−.2065	+.2912	−.1224	+.3130
	30.0	−.3050	+.23577	−.1900	+.3509	−.0911	+.3604
Jul.	10.0	−.3083	+.27211	−.1933	+.3872	−.0848	+.3930
	20.0	−.3140	+.26300	−.1990	+.3781	−.0926	+.3867
	30.0	−.2783	+.30023	−.1633	+.4153	−.0487	+.4090
Aug.	9.0	−.2630	+.30267	−.1480	+.4179	−.0334	+.4069
	19.0	−.2330	+.33774	−.1180	+.4528	+.0044	+.4288
	29.0	−.2077	+.33492	−.0927	+.4500	+.0279	+.4192
Sep.	8.0	−.2079	+.33111	−.0929	+.4462	+.0268	+.4159
	18.0	−.1814	+.33163	−.0664	+.4467	+.0523	+.4088
	28.0	−.1339	+.37396	−.0189	+.4891	+.1088	+.4323
Oct.	8.0	−.1339	+.32809	−.0189	+.4432	+.0969	+.3922
	18.0	−.1260	+.33772	−.0110	+.4528	+.1070	+.3983
	28.0	−.1081	+.30798	+.0069	+.4231	+.1164	+.3673
Nov.	7.0	−.0998	+.31460	+.0152	+.4297	+.1161	+.3707
	17.0	−.0631	+.29652	+.0519	+.4116	+.1566	+.3444
	27.0	−.0713	+.26064	+.0437	+.3757	+.1394	+.3154
Dec.	7.0	−.0586	+.24237	+.0564	+.3575	+.1468	+.2959
	17.0	−.0856	+.20151	+.0294	+.3166	+.1103	+.2679
	27.0	−.0464	+.20958	+.0686	+.3247	+.1500	+.2638
Jan.	6.0	−.0712	+.16099	+.0438	+.2761	+.1136	+.2285
	16.0	−.0927	+.16979	+.0223	+.2849	+.0953	+.2423
	26.0	−.0756	+.13815	+.0394	+.2533	+.1035	+.2098
Feb.	5.0	−.0792	+.10921	+.0358	+.2243	+.0925	+.1856
	15.0	−.0869	+.12856	+.0281	+.2437	+.0902	+.2047
	25.0	−.1204	+.08174	−.0054	+.1968	+.0459	+.1733
Mar.	6.0	−.1218	+.10820	−.0068	+.2233	+.0514	+.1968
	16.0	−.1454	+.07981	−.0304	+.1949	+.0214	+.1788
	26.0	−.1223	+.12019	−.0073	+.2353	+.0541	+.2074
Apr.	5.0	−.1541	+.09650	−.0391	+.2116	+.0174	+.1958

Eq. 21 (columns 4 and 5 in Table VII). Finally the x_i coordinate of the polar motion is computed with Eq. 12 and the y_i coordinate with Eq. 13 (columns 6 and 7 of Table VII). If the values computed in the last step are compared with the corresponding values in [BIH, 1980], the greatest deviation in x_i is $-0.027''$ (June 30.0, 1979), that in y_i $-0.026''$ (March 22.0, 1979).

According to this numerical example even in the case of measurement errors up to ± 0.5 m, the coordinates of the polar motion can be computed from the continuous Doppler observations of a station with a maximum error of $\pm 0.027''$.

REFERENCES

MUELLER, I. I. 1969: Spherical and Practical Astronomy. Frederick Ungos, New York.

BIH (Bureau International de l'Heure) 1980: Annual Report for 1979 Paris, and BIH Circular D160—D162.

HALMOS, F. 1980: Geoid determination on the basis of satellite observations *Acta Geod. Geoph. Mont. Hung.*, 15, 5—16.

ORLOV, A. YA. 1961: Izbrannye Trudy Tom 1, Kijev reprinted in: Analiz rezultatov shirotnikh nablyudenii Akad. Nauk Uzbekskoi SSR, Tashkent, 1966.

ОПРЕДЕЛЕНИЕ КООРДИНАТ ДВИЖЕНИЯ ПОЛЮСА ИЗ ДОППЛЕРОВСКИХ НАБЛЮДЕНИЙ ОДНОЙ СТАНЦИИ

ДЬ. САДЕЦКИ-КАРДОШ

РЕЗЮМЕ

В статье излагается метод исчисления координат x, y движения полюса из допплеровских измерений проведенных на одной станции за длительный промежуток времени. Даются формулы для исчисления изменений географических долгот и широт и после этого для координат движения полюса. Приведены формулы также для определения географических координат из пространственных прямоуголных координат и для определения среднего положения полюса. Наконец приведен полный численный пример для исчисления координат движения полюса из фиктивных результатов измерения.

Acta Geodaet., Geophys. et Montanist. Acad. Sci. Hung. Tomus 16 (2—4), pp. 259—263 (1981)

DIE LICHTGESCHWINDIGKEIT UND DIE DARAUF BERUHENDE DEFINITION DES METERS IN DER GEODÄSIE

G. FELSŐ

GEODÄTISCHES UND GEOPHYSIKALISCHES FORSCHUNGSINSTITUT DER UNGARISCHEN AKADEMIE DER WISSENSCHAFTEN, SOPRON

The speed of light c as a fundamental constant of nature — which plays an important role in many branches of natural science — has been the source of an impressive development in experimental and theoretical physics. Due to the possibility of highly accurate optical frequency measurements, c can now be determined to an accuracy limit inherent in the present wavelength standard for the meter. In addition, c is proven to be constant and to be independent of frequency till a prodigious accuracy.

It was suggested by BAY that, instead of redefining the meter on the basis of a new wavelength standard, it would be more advantageous to create a unified time-length measurement system in which the definition of the second and the meter are connected by a defined value of the speed of light. The necessity of the introduction of this new standard in some geodetical measurements is underlined.

Das Produkt der Frequenz (ν) und der Wellenlänge (λ) der in Vakuum sich fortpflanzenden elektromagnetischen Welle ergibt die Lichtgeschwindigkeit in Vakuum

$$\nu\lambda = c\,. \tag{1}$$

Ausdruck (1) ist eine Definition, d. h. jede der darin auftretenden Größen wird von den beiden anderen eindeutig bestimmt. Bei der Definition der Maßsysteme schien es zweckmäßig, die Frequenz (oder die Zeit) und die Wellenlänge zu standardisieren und die Geschwindigkeit als abgeleitete Größe zu betrachten. Mit der Entwicklung der Meßmethoden konnten für die fundamentalen Größen neue Eichmaße eingeführt werden, wodurch auch die abgeleitete Größe genauer bestimmt werden kann.

Das Comité International des Poids et Mesures hat im Jahre 1960 anstatt des Urmeters und 1967 anstatt der auf der Erdrotation beruhenden Sekunde neue Standarddefinitionen festgelegt.

Demnach ist

$$1 \text{ Meter} = 1\,650\,763{,}73\ \lambda_0\,,$$

wo λ_0 die im Vakuum gemessene Wellenlänge eines bestimmten Überganges des ungestörten ^{86}Kr Atoms bedeutet. Ferner ist

$$1 \text{ Sekunde} = 9\,192\,631\,770\ \tau_0\,,$$

wo τ_0 die Periode des zu einem bestimmten Übergang des ^{133}Cs Atoms gehörende Schwingung bedeutet.

Bereits im XIX. Jahrhundert begann man zu erkennen, daß unter den Naturkonstanten die Lichtgeschwindigkeit eine bevorzugte Stellung einnimmt. Im Jahre 1856 haben Kohlrausch und Weber erstmals die Proportion der elektromagnetischen und elektrostatischen Maßeinheiten gemessen. MAXWELL erkannte, daß diese Proportion durch die Lichtgeschwindigkeit bestimmt ist. Daraufhin hat er den Wert c in die elektromagnetische Grundgleichungen eingeführt.

Die spezielle Relativitätstheorie hat die bevorzugte Stellung der Lichtgeschwindigkeit noch mehr in den Vordergrund gestellt.

Es folgt aus der Invarianz der Gleichungen der Mechanik gegenüber der Lorentz-Transformation, daß prinzipiell keine Bewegungsgleichung (folglich auch keine jederlei physikalisches Phänomen beschreibende Gleichung) exakt aufgestellt werden kann, ohne den Wert c nicht zu enthalten.

Mit einer größeren Geschwindigkeit als die Lichtgeschwindigkeit kann keine Informations-, Material-, und Energietransport verwirklicht werden. Das Quadrat der Lichtgeschwindigkeit stellt die Verbindung zwischen den Maßeinheiten der Energie und der Masse her. Die Einstein-Minkowskische Raumzeit hat eine derartige Struktur, daß unabhängig von der Geschwindigkeit des Systems c ein Invariant ist. Ähnliches Gesetz gilt für die Einsteinsche allgemeine Relativitätstheorie. Hier ändert sich zwar die Lichtgeschwindigkeit für irgendwelchen Beobachter von Punkt zu Punkt (in Abhängigkeit vom Gravitationspotential), aber dennoch erhält jeder Beobachter, der in seiner lokalen Umgebung die Lichtgeschwindigkeit mißt, denselben invarianten Wert c, falls er seine lokalen Koordinaten verwendet.

PLANCK schlug 1906 (ein Jahr nach Aufstellung der spezialen Relativitätstheorie) vor, die physikalische Maßeinheiten mit Hilfe der grundlegenden Naturkonstanten festzulegen [1]. Durch Zuschreibung von Einheitswert für die Konstanten c, h, G und K (d. h. für Lichtgeschwindigkeit, Plancksche, Gravitations- und Boltzmann-Konstante) können die natürlichen Einheiten von Zeit, Länge, Masse und Temperatur definiert werden.

Dieser Vorschlag war zwar theoretisch von großer Bedeutung, konnte aber damals nicht in die Praxis umgesetzt werden, da die Ungenauigkeit der damals bekannten Werte der Grundkonstanten in die Bestimmung der Maßeinheiten übergegangen wäre.

PLANCKs Vorschlag könnte auch heutzutage nicht verwirklicht werden, mit Ausnahme der Einheiten von Zeit und Länge.

Das ist dadurch möglich, daß in der Dimension der Lichtgeschwindigkeit nur Zeit und Länge vorkommen und daß durch c eine Verbindung zwischen diesen Einheiten besteht.

Während die Präzision des Meterstandards 10^{-8} beträgt, erreicht die

Präzision des Sekundestandards 10^{-12}. Es wäre auch aus praktischen Gründen wichtig, diese Differenz von vier Größenordnungen zu überbrücken. Früher wurden die Frequenzen, mit Hilfe des bekannten Wertes der Lichtgeschwindigkeit, aus Wellenlängenmessungen berechnet. Die auf diese Weise erhaltenen Frequenzwerte konnten jedoch die Genauigkeit der Lichtgeschwindigkeit nicht überschreiten.

Derzeit kann man die Frequenz mit größerer Genauigkeit messen als die Lichtgeschwindigkeit, weil die Messung der Schwingungszahlen eine durch die Genauigkeit der Atomuhren bestimmte Zeitmessung ist, wogegen die Genauigkeit der Lichtgeschwindigkeit von der jeweiligen Meterdefinition abhängt.

Nach Erscheinen des Lasers hat TOWNES darauf aufmerksam gemacht, daß durch die Messung optischer Frequenzen die Maßeinheiten von Länge und Zeit mit Hilfe der Lichtgeschwindigkeit miteinander in Verbindung gebracht werden können [2].

Ein auf der Lichtgeschwindigkeit beruhender einheitlicher Zeit- und Längestandard wurde von BAY und LUTHER vorgeschlagen [3, 4].

Die Grundidee dieses Vorschlages besteht darin, daß anstatt der Bestrebung die Genauigkeit der Meterdefinition zu erhöhen, die Lichtgeschwindigkeit als Grundkonstante aufgefaßt werden sollte, wodurch das Meter eine neue Definition erhält. Die vom Licht in einer Sekunde zurückgelegte Entfernung, d. h. die sog. »Lichtsekunde« soll in Meter ausgedrückt, und diese Meterzahl von einem internationalen Ausschuß ein für allemal bestimmt werden. Demnach wird die Genauigkeit der Meterdefinition immer dieselbe sein, als die der Definition der Sekunde, d. h. sie erreicht die Genauigkeit der jeweiligen Atomuhren.

Es ist eine grundsätzliche Frage zu klären, ob die Fortpflanzung des Lichtes im Vakuum frequenzabhängig ist oder nicht. Eine eventuelle Vakuumdispersion würde die Einführung des neuen Systems verhindern, weil dann die Lichtgeschwindigkeit mit einer konstanten Zahl nicht charakterisiert werden könnte.

Aufgrund der Zeitspiegelungssymmetrie wird von der allgemeinen Dispersionstheorie die Bedingung gestellt, daß eine eventuelle Vakuumdispersion der Lichtgeschwindigkeit nur von den geradzahligen Potenzen der Frequenz abhängig sein kann. Die spezielle Relativitätstheorie beruht (unter anderen) auf der konstanten Lichtgeschwindigkeit.

Mit Hilfe der Lorentz-Transformation haben BAY und WHITE nachgewiesen, daß die Verallgemeinerung der Theorie eine Änderung des Brechungsindizes nach der Formel

$$n^2 = 1 + \frac{A}{\nu^2} \tag{2}$$

zuläßt (wo A konstant ist).

Dieses Ergebnis ist für alle sich im Vakuum fortpflanzenden Wellen gültig, weil nichts von Art und Quantisierung der Wellen vorausgesetzt wurde. Formel (2) gilt auch für die quantisierten de Broglie-Wellen; in diesem Falle ist

$$A = -(m_0 c^2/h)^2 ,$$

wo m_0 die Ruhemasse des Teilchens bedeutet, d. h. Formel (2) ist auch für ein Photon mit einer endlichen Ruhemasse gültig.

Würde in der Dispersionsformel ein Glied vom Typ Bv^2 vorkommen, würde dies das Relativitätsprinzip verletzen. Dennoch haben BAY und WHITE für die Auswertung der auf eine Frequenzabhängigkeit der Lichtgeschwindigkeit hinweisenden Daten, die Formel

$$n^2 = 1 + \frac{A}{v^2} + Bv^2 \tag{3}$$

angewendet, weil die Gültigkeit der Einsteinschen Relativitätstheorie bei sehr kleinen Wellenlängen von manchen Forschern in Frage gestellt wird. Aufgrund der modernsten Meßergebnisse haben BAY und WHITE nach Festlegung von Obergrenzen für die Koeffizienten A und B der Formel (3) nachgewiesen, daß vom Bereich der Mikrowellen bis zu dem der ultravioletten Strahlen die Dispersion des Lichtes nicht größer als 10^{-20} sein kann.

Die praktischen Voraussetzungen der Einführung eines einheitlichen Raum-Zeit Meßsystems wurde von BAY mit den folgenden zwei Bedingungen angegeben:

1. Die Lichtgeschwindigkeit muß bis zur Genauigkeit des Kryptonstandardes bekannt sein.

2. Es müssen die Voraussetzungen dazu geschaffen werden, daß die Messung der optischen Frequenzen in allen Bereichen des Spektrums auf die Standardfrequenz bezogen werden können.

Mit der Entwicklung neuer, sowie mit der Verbesserung alter Meßmethoden können diese Bedingungen in nächster Zukunft erfüllt werden.

Im Jahre 1973 schlug das Comité International des Poids et Mesures drei Möglichkeiten für die Einführung des neuen Meters vor: mit Hilfe eines infraroten Lasers (mit einer Vakuumwellenlänge von $\lambda = 3\,392\,231{,}40 \cdot 10^{-12}$ m), mit Hilfe eines rotfarbigen Lasers (mit einer Vakuumwellenlänge von $\lambda = 632\,991{,}399 \cdot 10^{-12}$ m), oder durch die Annahme eines neuen Wertes für die Lichtgeschwindigkeit ($c = 299\,792\,458$ m sec^{-1}). Die Unsicherheit bei jeden dieser drei Werte beträgt $4 \cdot 10^{-9}$. Es muß betont werden, daß diese nur vorgeschlagene, nicht aber angenommene Werte sind.

Die Frage eines einheitlichen Raum-Zeit Meßsystems ist noch nicht entschieden, da das Komitee sich bisher jeder Stellungnahme darüber enthielt,

durch welches dieser drei Werte das Meter definiert werden soll. Bemerkenswert ist aber der Vorschlag des Meterkomitees, wonach im Falle der Annahme eines neuen Meterstandards der derzeit vorgeschlagene Wert der Lichtgeschwindigkeit nicht geändert werden soll.

Es sei noch erwähnt, daß bei den planetarischen Radar-Experimenten der von FROMME gemessene c-Wert als ein angenommener Wert ohne Unsicherheit ($c = 299\,792\,500$ m sec^{-1} mit $3 \cdot 10^{-7}$ relativer Ungewißheit) verwendet wird, obwohl die Genauigkeit dieses Wertes mit zwei Größenordnungen niedriger ist als die des gegenwärtigen Wertes. FROMMES Messung wurde im Jahre 1958 auf einer Wellenlänge von 4 mm durchgeführt [5].

Es sei hier der Standpunkt vertreten, daß der von BAY und LUTHER vorgeschlagene Meterstandard bei einigen Messungen von höchster Genauigkeit der kosmischen Geodäsie bereits jetzt eingeführt werden soll, überwiegend bei jenen Messungen, wo die atmosphärische Refraktion keine wesentliche Rolle spielt, z. B. bei der Einmessung des auf den Mond aufgestellten Laserspiegels, oder bei der sogenannten satellite-to-satellite tracking-Methode.

Würde die von PONTECORVO vorausgesagte Neutrino-Konversion sich als wahr erweisen, wird es nicht ausgeschlossen sein, daß — obzwar mit einem riesigen Kostenaufwand — Entfernungsmessungen von höchster Genauigkeit zwischen zwei Punkten mit Hilfe von, die Erde durchdringenden Neutrinoströmen durchgeführt werden können. In diesem Falle wird der Gebrauch des einheitlichen Raum-Zeit Systems unvermeidlich sein.

SCHRIFTTUM

1. PLANCK, M.: Theorie der Wärmestrahlung. f. A. Barth, Leipzig, 1906.
2. TOWNES, C. H.: Advances in Quantum Electronics. f. R. Singer, New York, 1961.
3. BAY, Z.: Internal NBS Report, 1965.
4. BAY, Z.—LUTHER, G. G.: Appl. Phys. Letters, No. 9. 13 (1968), 303—.
5. FROMME, K. D.: Proc. Roy. Soc., A247 (1958), 109—.

СКОРОСТЬ СВЕТА И НОВЫЙ МЕТР В ГЕОДЕЗИИ

Г. ФЕЛЬШЁ

РЕЗЮМЕ

Огромное развитие в области теоретической и экспериментальной физики выдвигало скорость света c как фундаментальный константа, который имеет большое значение во многих отраслях науки. В результате возможности высокоточных измерений оптических чатот, c можно определить с точностью эталона метра. Кроме этого скорость света оказалась с поразительной точностью постоянной и независимой от частоты.

По предложению Баи вместо нового определения метра на основе нового эталона расстояния, предпочтительно создать единую систему измерения времени и расстояния, где определение секунды и метра проводится взаимосвязанно через определенное значение скорости света. Подчеркивается необходимость введения этого нового стандарта в некоторых геодезических измерениях.

Acta Geodaet., Geophys. et Montanist. Acad. Sci. Hung. Tomus 16 (2—4), pp. 265—268 (1981)

EARTH TIDES IN GEODYNAMICS

G. BARTHA

CAND. OF TECHN. SCI.

GEODETIC AND GEOPHYSICAL RESEARCH INSTITUTE OF THE HUNGARIAN ACADEMY OF SCIENCES, SOPRON

A short mathematical description is given about the composition of a tidal record. Geodynamic informations included in tidal records are reviewed. To obtain these informations, it is necessary to improve the evaluation methods and the cotidal maps as well as to carry out a greater number of parallel measurements.

The instruments recording the Earth tides effect measure both the change of the magnitude of the gravity vector and the direction change of the gravity vector:

$$\Delta\mathbf{g}(\Delta\mathbf{r}, \Delta t) = \mathbf{g}(\mathbf{r}_0 t_0) - \mathbf{g}(\mathbf{r}, t) \tag{1}$$

where the vectors $\mathbf{r}_0$, $\mathbf{r}$ are the position vectors of the observation point at epoch t_0 and epoch t, respectively.

If the Earth is modelled as a rigid body, then:

$$\Delta\mathbf{r}(t) = 0$$

and

$$\Delta g(\mathbf{r}_0, \Delta t) = \mathbf{T}_E(\mathbf{r}_0, \Delta t) + \vec{\Phi}(\mathbf{r}_0, \Delta t) \tag{2}$$

where the vectors $\mathbf{T}_E$ and $\vec{\Phi}$ denote the Earth tides effect and the non-lunisolar global effect (planetary, cosmic, etc.), respectively. The vector $\mathbf{T}_E$ is usually called theoretical Earth tides. Generally, the following relation is valid between this two effects:

$$|\,\mathbf{T}_E\,| \geqslant |\,\vec{\Phi}\,|\,. \tag{3}$$

If the Earth is assumed as a perfect elastic body, then:

$$\Delta\mathbf{r}(t) \neq 0 \tag{4}$$

i.e. the observation point moves periodically in consequence of the elastic deformation. With respect to the relation (3) the non-lunisolar global effect can

be neglected, because the change of the gravity vector is:

$$\Delta \mathbf{g}\,(\Delta \mathbf{r}_0, \Delta t) = \mathbf{T}_E(\mathbf{r}_0, \Delta t) + \mathbf{T}_D(\mathbf{r}_0) + \mathbf{T}_A(\mathbf{r}_0, \Delta t) \tag{5}$$

where vector $\mathbf{T}_D$ denotes the effect caused by the deformation and vector $\mathbf{T}_A$ that caused by the mass rearrengement. According to Love the Earth tides can be described with a poliharmonical series:

$$\Delta \mathbf{g}(t, \vec{\varphi}_i) = \mathbf{T}_E(\omega_i t + \vec{\varphi}_i) + \mathbf{T}_D(\omega_i t + \vec{\varphi}_i) + \mathbf{T}_A(\omega_i t + \vec{\varphi}_i)\,. \tag{6}$$

According to Love's theory the vectors $\mathbf{T}_D$ and $\mathbf{T}_A$ can be expressed as the linear combination of the vector $\mathbf{T}_E$:

$$\Delta \mathbf{g} = \mathbf{T}_E + \mathbf{K}_0\, \mathbf{T}_E = (\mathbf{E} + \mathbf{K}_0)\mathbf{T}_E \tag{7}$$

where matrix $\mathbf{E} + \mathbf{K}_0$ is a diagonal matrix, and its valuable elements are the linear combinations of the Love numbers. They are the so-called Earth tides factors.

If an elastic-plastic Earth model is taken — which is the best approximation for the real Earth — a phase lag ε_i appears in the term of the deformation as well as in that of the rearrangement:

$$\mathbf{T}_D = \mathbf{T}_D(\omega_i t + \vec{\varphi}_i + \vec{\varepsilon}_i) \tag{8}$$

and

$$\mathbf{T}_A = \mathbf{T}_A(\omega_i t + \vec{\varphi}_i + \vec{\varepsilon}_i)\,.$$

In consequence of this effect there is a distortion in the Earth tides factor, further a phase lag in comparison to the perfect elastic model. In addition to these an indirect effect (loading effect $\mathbf{T}_L$) appears as a result of the ocean tides, too:

$$\Delta \mathbf{g}(t, \vec{\varphi}_i) = \mathbf{T}_E(\omega_i t + \vec{\varphi}_i) + \mathbf{K}_0\mathbf{T}_E(\omega_i t + \vec{\varphi}_i + \varkappa_i) + \mathbf{T}_L(\omega_i t + \vec{\varphi}_i + \varkappa_i)\,. \tag{9}$$

Equation (9) includes all the effects of lunisolar origin recorded with our instruments. At the same time the instruments react not only to the lunisolar effect but also to other effects arised by local or regional reasons such as crustal movements, local movements, movements due to artifical activities, etc. Our instruments record them together with the lunisolar effect. Therefore, Eq. (9) should be transformed into the following form:

$$\Delta \mathbf{g}(t) = \mathbf{T}(t) + \mathbf{S}(t) \tag{10}$$

where vector **T** denotes the lunisolar effect and vector **S** the local effect. These gravity changes are real changes from the point of view of the measurement technique. However, some non-real effects such as temperature, air pressure and inner changes in the instrument have also an influence on the output signal. Thus, a signal recorded by an Earth tidal instrument consists of three parts:

$$1(t) = T(t) + S(t) + D(t) . \tag{11}$$

Here the term $D(t)$ denotes the non-real part.

Summarized, the global and regional/local geodynamic informations are included in the recorded signal. Although the global informations represented by tidal factors concern primarily to the inner elastic properties of the global Earth, but experiences show that the value of these factors depend on the geographical site of the observation point, too. Therefore, the informations about the tectonical structure are involved into the distribution of the tidal factors.

For the use of the tidal records for geodynamic purposes it is essential to separate the three terms as sharply as possible. This separation can be achieved by two steps. The first step is the separation of the lunisolar and the non-lunisolar part, and the comparison of the recorded lunisolar part with the theoretical tides. This comparison yields the tidal factors and the phase lags. The several existing methods can be classified to three groups [WENZEL, 1977]:

1. deterministic methods, in which the records are only described by a deterministic model (e.g. Fourier analysis),

2. stochastic methods, in which the recorded data are handled as stochastic variables,

3. mixed methods, in which a deterministic model is applied to describe the records, but a superposed white noise is also assumed.

The methods of the third group are most frequently applied to evaluate the tidal records. These methods can also be used for the evaluation of the gappy data series in contradiction to the other ones. It is well known that the tidal data series have often gaps in consequence of technical and other reasons. In these methods a determinated function is assumed for the description of the non-lunisolar part (e.g. Venedikov method) [VENEDIKOV, 1966.] Therefore, the non-lunisolar part is forced into an appropriate form. To get a more correct form of the lunisolar part the methods based on the operations of data differences are preferred [USANDIVARAS and DUCARME, 1969; BARTHA, 1973]

The first step yields the tidal factors and the phase lags from the lunisolar part independently from the applied method. Further it yields a data series including the non-lunisolar real effects and the non-real effects, respectively (non-tidal part).

Let us see the tidal factors and the phase lags from the point of view of geodynamics. Accepting an Earth tidal model anomalies can be got between the model and the tidal parameters. These anomalies can be interpreted as the loading effect and they considerably depend on the tectonical structure between the observing point and the loading area. By modelling the structure and applying the finite element methods, the tectonic model itself can be tested. Nowadays the first step of the development of this technique can be observed [BEAUMONT, 1972], but better cotidal maps are essential for its success.

In respect of the separated non-tidal part the essential problem is to separate the real and non-real terms. One of the possible solutions of this problem is to determine an analytical form for the non-tidal part. If parallel recording has been carried out with different instruments on the same place, there is a chance to get the real part based on the common part of the analytical forms [BARTHA, 1979].

After this short review it is clear that the tidal records include many interesting informations on geodynamic effects, but for obtaining them it should be necessary:

— to improve the cotidal maps,
— to improve the modelling of the lateral inhomogeneities,
— to increase the number of the recording instruments to carry out more parallel recordings,
— to improve the evaluation technique of the non-tidal part.

REFERENCES

BARTHA, G. 1973: Evaluation of earth-tide records by sectionwise approximation of the instrumental drift. *Acta Geod. Geoph. Mont. Hung.*, 8, 445—450.

BARTHA, G. 1979: A method for evaluation of local tilting. — *BIM*, 81, 4982—4984.

BEAUMONT, C.—LAMBERT, A. 1972: Crustal Structure from Surface Load Tilts, Using a Finite Element Model. *Geophys. J. R. astr. Soo.*, 29, 203—226.

USANDIVARAS, J. C.—DUCARME, B. 1969: Analyse des enregistrements de marée terrestre par la méthode des moindres carrés. — ORB, Serie B, Nr. 45, Bruxelles.

VENEDIKOV, A. P. 1966: Une method pour l'analyse der marées terrestres a partir d'enregistrements de longuer arbitraire. ORB Nr 250., Bruxelles.

WENZEL, H. G. 1977: Estimation of accuracy for the earth tide analysis results. — *BIM*, 76, 4427—4445.

ЗЕМНЫЕ ПРИЛИВЫ В ГЕОДИНАМИКЕ

Г. БАРТА

РЕЗЮМЕ

Дается краткое математическое описание о составляющих регистрации земных приливов. Рассматриваются геодинамические информации, полученные в процессе регистраций. Для получения этих информаций необходимо улучшить обработку данных и котидальных карт, а также произвести большего числа параллельных измерений.

Acta Geodaet., Geophys. et Montanist. Acad. Sci. Hung. Tomus 16 (2—4), pp. 269—280 (1981)

HORIZONTAL PENDULUM WITH CAPACITIVE TRANSDUCER

GY. MENTES

GEODETIC AND GEOPHYSICAL RESEARCH INSTITUTE OF THE HUNGARIAN ACADEMY OF SCIENCES, SOPRON

The paper deals with the digitizing problems of the pendulum recordings. It describes new horizontal pendulums supplied with capacitive transducers. A detailed description of the test to investigate the effect of different capacitive transducers on the operation of pendulums is given.

1. Introduction

The effect of the Earth tides is the result of two forces, i.e. the attractive force deriving from the mass of the Earth and the centrifugal force deriving from the rotation of the Earth acting at each point of the surface (Fig. 1). The resultant is the force of gravity with a periodic change in consequence of the rotation of the Earth. This periodic change brings about a periodic deformation on each point of the surface of the Earth. The magnitude of the deformation depends on the construction and elasticity of the Earth. Hence, the recording of the change of gravity force can give informations on the elasticity of the Earth and likely on the tectonic construction of the Earth's crust. Further, the effect of the Earth tides must be taken into account at precision geodetic measurements. These problems require the more exact measurement of the Earth tides. In the history of Earth tides measurements the first attempts were to measure any changes produced by Earth tides effect in the direction of the gravity vector by means of vertical pendulums. The sensitivity of these pendulums, however, was not enough to measure the Earth tides. HENGLER solved the problem in 1832 by inventing the horizontal pendulum with a much greater mechanical amplification as that of the vertical pendulum. In 1872 the horizontal pendulum was improved by ZÖLLNER with the special suspension of the pendulum arm. Zöllner's suspension has been worldwide used. The Zöllner pendulum (Fig. 2) consists of a bracket fixed on a very rigid base plate; latter stands on a fixed point and on two levelling screws L_1 and L_2. At the points A and B two metal wires are clamped and their other ends are fixed at the points C and D to a horizontal metal arm.

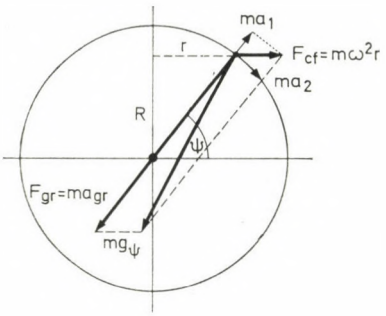

Fig. 1.

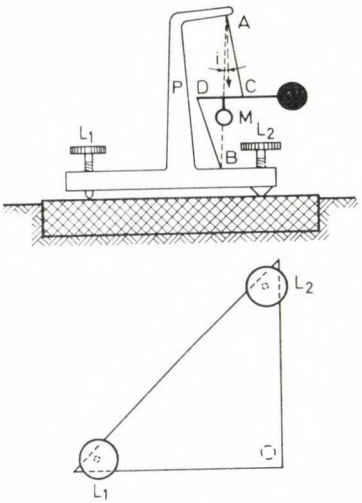

Fig. 2.

Points A, B, C, D lie on the same vertical plane. Thus, the rotation axis of the arm is the line $A-B$ which can be set almost vertical by suitable manipulation of the levelling screws. The levelling screws are situated at the tips of a right-angled triangle. L_1 is the "sensitive screw" and L_2 the "drift screw". By turning L_1 one modifies the angle i and so the sensitivity of the pendulum will be changed. By turning the screw L_2 one can change the equilibrium position of the pendulum arm.

The moving of the pendulum arm can be recorded photographically by means of a light beam reflected from a mirror fixed on the pendulum arm to the photographic paper on a drum rotating around its horizontal axis. The disadvantages of this recording are:

1. The record becomes visible only after the development of the photographic paper.

2. To get the required optical amplification a distance of about 4—5 m between mirror and photodrum and so a rather large room for recording is necessary.

3. Each change of the photographic paper disturbes the pendulums.

4. Checking and adjusting of the pendulums must be done in darkness.

5. The analogous records of the pendulums must be read out and typed into a computer giving occasion to a lot of mistakes.

The disadvantages and the development of the computing techniques requires the development of pendulum recording, too. The main problems are to read out the analogous records of the pendulums and to type the data into a computer. The solution of this problem is the digitizing of the pendulum records.

2. Methods of digitizing Earth tides records

There are two ways to get a digital signal from a horizontal pendulum:

1. Indirect digitizing (Fig. 3).

An analogous record e.g. a photorecord made by a photodrum or a record made by an electric strip chart recorder can be digitized by means of a curve digitizer and can be processed directly by a computer. In this case the irregularities of the record can be corrected manually, however, the evalu-

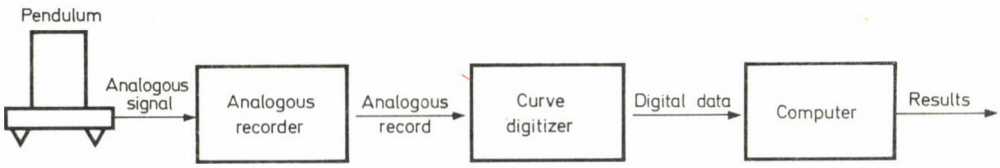

Fig. 3.

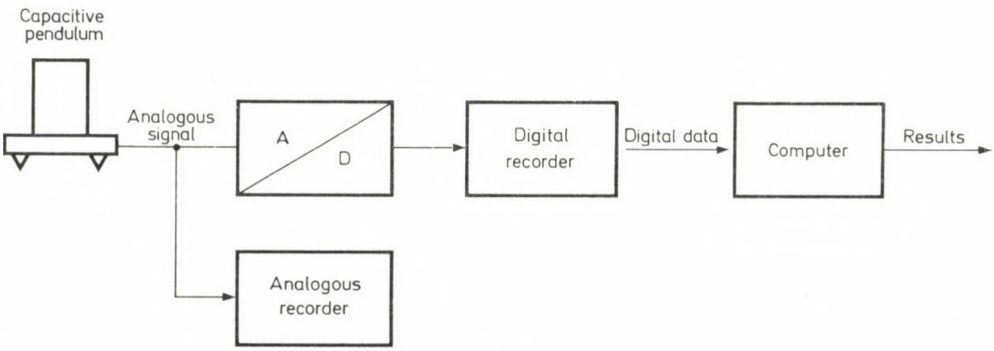

Fig. 4.

ation of the record is a very tiring work. Moreover, this method has a disadvantage: the digital data contain the error of the analogous recorder of about 0.5—2%, too.

2. Direct digitizing (Fig. 4).

This method requires horizontal pendulums with digital signal output. This can be reached by means of a transducer transforming the mechanical rotation of the pendulum arm, i.e. an angle into an electric signal. This analogous output signal of the pendulum can be directly digitized by means of an $A-D$ converter and recorder on a punch or a magnetic tape. For observing the irregularities of the record it is advisable to record also the analogous signal of the pendulum.

Since 1971 experiments were made in the Geodetic and Geophysical Research Institute of the Hungarian Academy of Sciences to develop such a pendulum [1].

3. Construction of the capacitive pendulum

The principle of the construction of the pendulum is similar to that shown in Fig. 2. It has a Zöllner suspension as the Tomaschek—Ellenberger pendulums. The dimension of this suspension is shown in Fig. 5, where all sizes are given in mm. The weight of the pendulum arm together with the moving plate of the capacitive transducer is 47 g its centre of gravity is S. The moving plate of the differential condenser is mounted on the pendulum arm (Fig. 6), and its working principle is based on the change of the surfaces of the opposite-standing plates. The inner construction of the pendulum

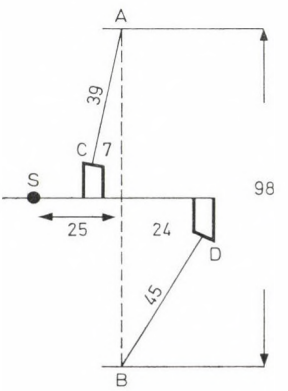

Fig. 5.

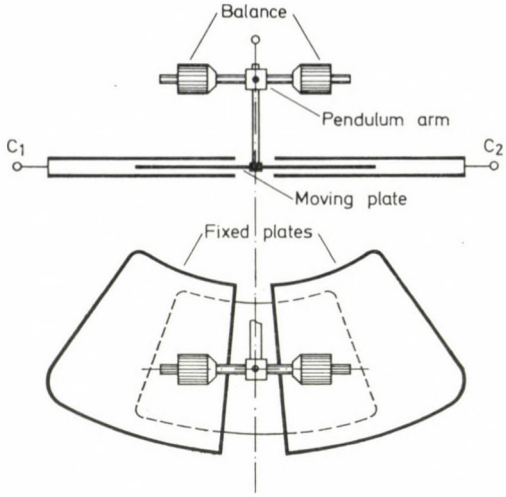

Fig. 6.

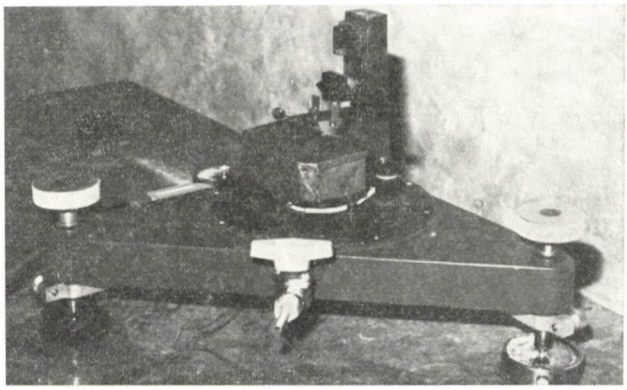

Fig. 7.

together with the shielded capacitive transducer and preamplifier is shown in Fig. 7.

To understand it easier why a differential condenser is needed and what kind of problems can arise by the adaptation of the capacitive transducer, let us see the formula of the capacity of a single plate-condenser:

$$C = \varepsilon_0 \varepsilon_r \frac{A}{d} \tag{1}$$

where

C = the capacity of the condenser

ε_0 = the dielectric constant of the vacuum

ε_r = the relative dielectric constant of the dielectric between the plates

A = the surface of the opposite-standing plates

d = the distance between the plates.

As Eq. (1) shows the capacity of the transducer can be changed by the change of the dielectric constant and the distance, too. For this reason these values must be kept constant. The change of the dielectric constant is the reason of the most problems, because its value depends very strongly on the changes of environmental parameters (temperature, humidity). Although the application of the differential condenser reduces this effect, it will not be eliminated totally.

The principle of our capacitive pendulum is the following (Fig. 8): The differential condenser has been completed to a bridge circuit by two capacitances of equal value. The supply voltage of this bridge is produced by a sine-wave oscillator. The amplitude of the supply voltage is 20 V and its frequency 15 kHz. The output voltage of the bridge is detected by an amplifier having a high input and a low output resistance. The preamplifier is placed near to the transducer and it transforms the high output impedance of the bridge to a low one. So, the output voltage of the bridge can be transmitted on a small impedance to the separate electronical unit to ensure a lower noise-sensitivity. The preamplifier is followed by a selective amplifier and a phase-sensitive rectifier which enables the sign-correct measurement of the deviation of the pendulum arm from its zero position. Its output signal contains yet the free oscillation of the pendulum. The phase-sensitive rectifier is followed by a low-pass filter for the filtering of the free oscillation of the pendulum. Both the phase-sensitive rectifier and the low-pass filter are followed by a D.C. amplifier where the clock signal is superposed to the filtered and unfiltered output signals. The unfiltered output is necessary for the measurements of the eigenperiod of the pendulum at the installation and of course at the recording of the unfiltered signal, too, because the unfiltered signal

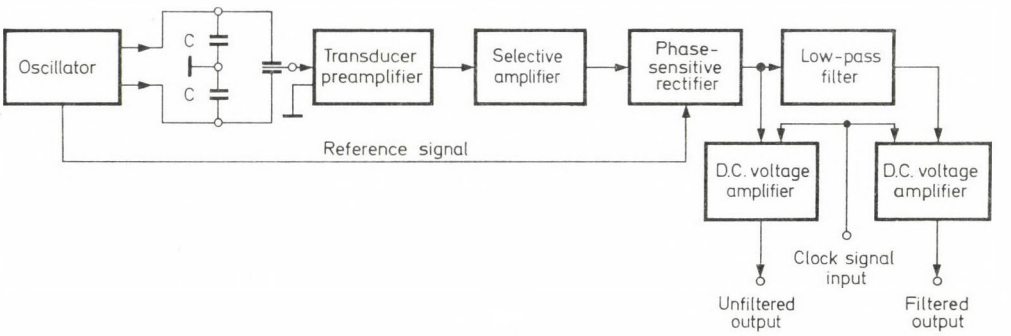

Fig. 8.

contains yet all informations. The filtered output is also necessary because earth movements independent from the Earth tides also excite the pendulum and increase very much the magnitude of the free oscillation, and that would saturate the D.C. amplifier having a greater amplifying than the one of unfiltered output. The filter has a cut-off frequency of 0.005 Hz. This output gives a smooth signal easy to digitize.

Two pairs of pendulums were built, in the first the capacitive transducer has an air dielectric, in the second an oil dielectric. Some measurements were made to investigate the changes caused by the adaptation of the capacitive transducers to the pendulums.

4. Test of the capacitive pendulum with air dielectric

The dielectric of the transducer has no significant effect on the damping of the moving of the pendulum arm and so the eigenperiod of the pendulum arm can be measured. The test of the pendulum was made as follows: a small known tilt was given to the pendulum by means of a crapoudine [2] placed under the drift screw, and the displacement of the pendulum arm at different eigenperiods was optically and electrically measured. The results compared with other pendulums can be seen in Fig. 9a where:

$$N = \frac{\Phi}{\varphi} = kT_H^2 \tag{2}$$

N = the static sensitivity of the pendulum
Φ = the angle of the deviation of the pendulum arm
φ = the angle of the tilt of the pendulum
k = the constant of the instrument
T_H = the horizontal eigenperiod.

The deduction of the above mentioned formula can be found in [3].

The angle Φ was measured optically and the results show that the different pendulums have similar characteristics, and the instrument constant is practically the same as at other pendulums. HI-175 and HI-175/1 are capacitive pendulums with different clamping of the suspensory wire.

In Fig. 9b the angle Φ is plotted against the eigenperiod T_H measured electrically. The sensitivity of the capacitive transducer was got from these measurements:

$$S = 1.698 \frac{\text{mV}}{\text{sec. of are}}.$$

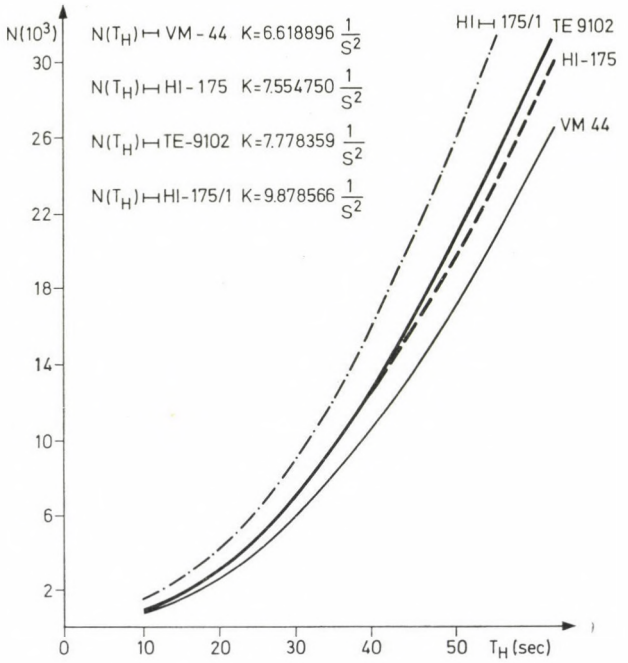
N(10³)
30
26
22
18
14
10
6
2
0
10
20
30
40
50
T_H (sec)
N(T_H) ⊢ VM - 44 K=6.618896 1/S²
N(T_H) ⊢ HI - 175 K=7.554750 1/S²
N(T_H) ⊢ TE-9102 K=7.778359 1/S²
N(T_H) ⊢ HI-175/1 K=9.878566 1/S²
HI ⊢ 175/1
TE 9102
HI-175
VM 44

Fig. 9a.

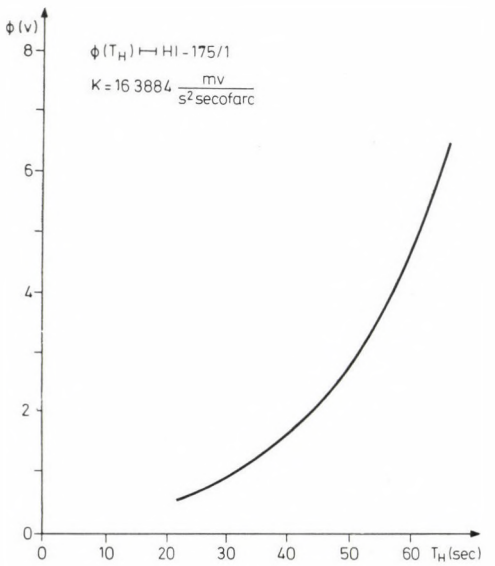
ϕ(v)
8
6
4
2
0
0
10
20
30
40
50
60
T_H (sec)
ϕ(T_H) ⊢ HI - 175/1
K = 16 3884 mv / s² secofarc

Fig. 9b.

5. Test of the capacitive pendulum with oil dielectric

The relative dielectric constant of air is 1, that of water 80, therefore a change in the air humidity can cause great disturbances in the Earth tides record. For insulating the capacitive transducer from humidity it is the best to place it into oil. The oil between the plates of the condenser ensures an aperiodic damping which is further advantageous for the filtering of the free oscillation of the pendulum and of the microseismic activity.

For showing the influence of the oil to the pendulum let us solve the differential equation of the horizontal pendulum in a different way as given in [3]. Figure 10 gives schematic horizontal and vertical views of the suspended pendulum arm and of the forces acting on it. The vertical line Z and the rotation axis of the pendulum arm i.e. the line AB form a small angle i which determines the sensitivity of the pendulum. The differential equation of the pendulum is:

$$\Theta \frac{\mathrm{d}^2\Phi}{\mathrm{d}t^2} + k \frac{\mathrm{d}\Phi}{\mathrm{d}t} + mg \sin i \cdot \sin \Phi + \eta\Phi = mgs\varphi \tag{3}$$

where

$k \dfrac{\mathrm{d}\Phi}{\mathrm{d}t}$ = the damping term

$mg \sin i \cdot \sin \Phi$ = the restoring moment of the gravity

$\eta\Phi$ = the restoring moment of the suspensory wires

$mgs\varphi$ = the moment derived from the deviation of the vertical in the plane perpendicular to the plane Z and AB

Θ = the moment of inertia

m = the mass of the pendulum arm

s = the distance between the centre of gravity and the axis of rotation

Φ = the angle of rotation of the pendulum arm

φ = the angle of rotation of the vertical.

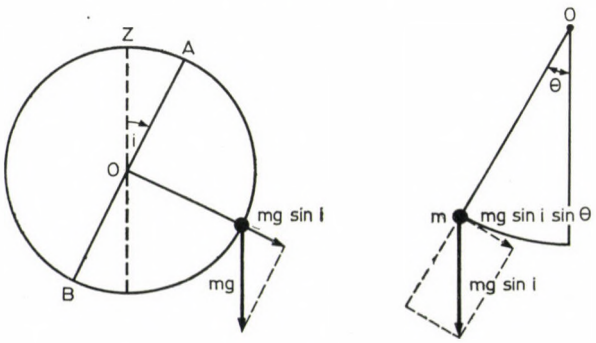

Fig. 10.

The differential equation can be written as follows

$$\frac{\mathrm{d}^2\Phi}{\mathrm{d}t^2} + 2\beta\frac{\mathrm{d}\Phi}{\mathrm{d}t} + \omega_i^2 \cdot \Phi = \frac{g}{l_0} \cdot \varphi \tag{4}$$

where

$$2\beta = \frac{K}{\Theta}; \quad \sin\Phi \approx \Phi; \quad \frac{\Theta}{ms} = l_0; \quad \omega_i^2 = \frac{g}{l_0}\sin i + \frac{\eta}{\Theta}.$$

The homogeneous part of (4) describes the movement of the pendulum arm in the transient period:

$$\Phi'' + 2\beta\Phi' + \omega_i^2\Phi = 0. \tag{5}$$

The solution of this homogeneous differential equations is

$$\Phi = \frac{\omega_0}{\lambda_1 - \lambda_2}(e^{\lambda_1 t} - e^{\lambda_2 t});$$

where $\lambda_1 = -\beta + \sqrt{\beta^2 - \omega_i^2}; \quad \lambda_2 = -\beta - \sqrt{\beta^2 - \omega_i^2}.$

If the damping is great enough:

$$\beta > \omega_i; \quad \beta_2 \gg \omega_i^2 \quad \text{and} \quad \lambda_1 \approx 0; \quad \lambda_2 \approx -2\beta.$$

This approximation is possible because the eigenperiod of the pendulum without damping is between 50 s and 120 s.

Therefore the solution will be

$$\Phi = \frac{\omega_0}{2\beta}\left(1 - e^{-2\beta t}\right) = \omega_0 \cdot \tau\left(1 - e^{-\frac{t}{\tau}}\right) \tag{6}$$

where

$$\tau = \frac{1}{2\beta}$$

ω_0 = the angle velocity of the pendulum arm at crossing of the zero position of the pendulum arm

τ = the time constant of the pendulum.

Equation (6) is the transient function of the horizontal pendulum and it is plotted in Fig. 11. This equation will describe the movement of the pendulum arm, when a known tilt ($\varphi = 1$) is given to the pendulum by means of a crapoudine placed under the drift screw.

The static sensitivity of the pendulum can be calculated from Eq. (6) too. In the stabile state when $t \to \infty$ itt will be

$$\Phi = \omega_0 \cdot \tau$$

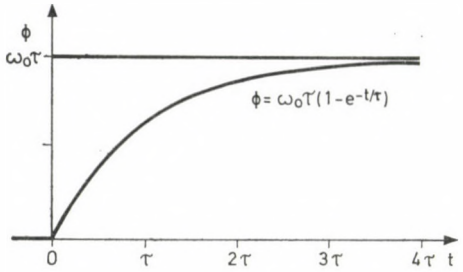

Fig. 11.

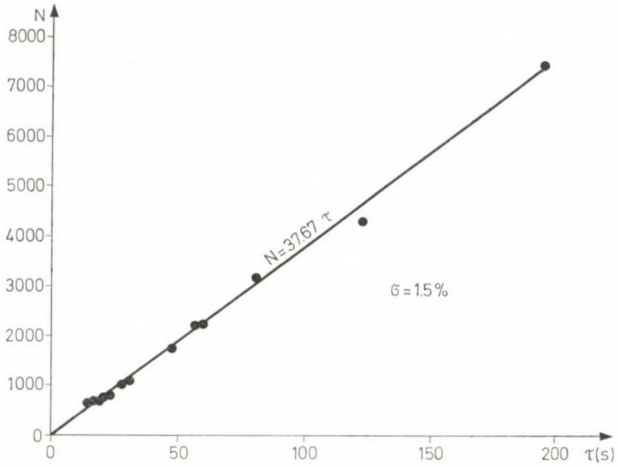

Fig. 12.

Because $\varphi = 1$ the static sensitivity of the pendulum is:

$$N = \frac{\Phi}{\varphi} = \omega_0 \cdot \tau \,. \tag{7}$$

The values of the time constant τ and the sensitivity N can be determined directly from the output record as demonstrated in Fig. 11. In Fig. 12 the sensitivity N is plotted against the time constant τ. The results of these measurements prove the correctness of the above approximations because the measured and calculated function of the static sensitivity is the same.

Equation (7) is very interesting because it gives a possibility to calibrate the pendulum in an indirect way, by means of measuring the time constant τ. The accuracy of the indirect calibration does not surpass the accuracy of the direct calibration, but it can be very useful at the installation of the pendulums.

This capacitive pendulum with oil dielectric gives a very smooth output signal without any filtering. The signal can be digitized very easy.

The main advantage of this pendulum is the insensibility of the transducer to the changes of environmental parameters. The systematic error arisen from damping can be avoided by means of a correction of the pendulum records at the evaluation.

6. Conclusion

It has been shown that the capacitive transducer especially that with oil dielectric is a reliable transducer for horizontal pendulums. Such pendulums are suitable for the development of a "zero method tiltmeter" with an electric (piezoelectric, magnetostrictive) dilatable crapoudine where the harm effect of the suspensory wires can be avoided. In consequences of the accuracy of the measurement with capacitive pendulums may be somewhat greater than that of the traditional Earth tides recording. The data processing will be faster and more reliable although the record of the analogous signal remains further necessary, since this one contains all the informations.

REFERENCES

1. MENTES, GY.: Development of horizontal pendulum recordings. *Acta Geod. Geoph. et Mont. Hung.*, 14 (1979), 101—109.
2. MELCHIOR, P.: The tides of the planet Earth Pergamon Press, Oxford—New York—Toronto—Sydney—Paris—Frankfurt, 1978.
3. MITTELSTRASS, G.: Konstruktionsprinzipien von Horizontaleinfachpendeln. Wissenschaftliche Arbeiten der Lehrstühle für Geodäsie, Photogrammetrie und Kartographie an der Technischen Hochschule, Hannover, Nr. 26, 1968.

НАКЛОНОМЕР С ЕМКОСТНЫМ ПРЕОБРАЗОВАТЕЛЕМ

Д. МЕНТЕШ

РЕЗЮМЕ

В статье рассматриваются проблемы преобразования регистрации наклономеров в цифровую форму. Описывается новый наклономер с емкостным преобразователем. Дается детальное описание теста для исследования влияния разных емкостных преобразователей на режим наклономера.

Acta Geodaet., Geophys. et Montanist. Acad. Sci. Hung. Tomus 16 (2—4), pp. 281—294 (1981)

ABOUT THE CALIBRATION OF INVAR LEVELING RODS

J. SOMOGYI
DOCTOR TECHN. SCI.

J. ZÁVOTI
GEODETIC AND GEOPHYSICAL RESEARCH INSTITUTE OF THE HUNGARIAN ACADEMY OF SCIENCES, SOPRON

D. BESSKÓ
HUNGARIAN OPTICAL WORKS, BUDAPEST

For increasing the accuracy of the leveling the systematic errors of the invar leveling rods must be taken into account. It is expedient to perform the calibration of the rods in two steps (laboratorium and field calibration). For such a two step testing of leveling rods a field comparator device is required which is conveniently manageable in field conditions and assures an accuracy of 2 to 3 μm. Furthermore a special mathematical solution is needed too, to get the wanted corrections.

The application of new, up-to-date instruments and methods of metrology exerts an influence also on the accuracy requirements of surveying measurements. The enhanced measurement accuracy renders possible the solution of such tasks that were regarded impossible so far. The increase in measurement reliability, however, involves certain difficulties. Besides random errors, the measurement results may carry systematic errors, too that may act against the enhancement of accuracy and the diminution of their effect constitutes a basic requirement.

The value ± 1.5 mm/km has been internationally accepted as the limit of error for precision leveling. With this limit considered, systematic errors may not exceed 0.2 to 0.3 mm/km. In special leveling tasks — as e.g. in the investigation of vertical crustal movements, determination of vertical deformations during the construction of nuclear power plants or of valley dams, etc. — this accuracy requirement may be increased even further up to 0.1 to 0.5 mm per km. In case of such high requirements, the effect of systematic errors in leveling — thus the errors of the leveling rods, too — must be taken into account in order to obtain reliable values from the measurements.

Calibration methods for leveling rods can be distributed into two main groups. In the methods of investigation pertaining to the *first of the categories* a normal metre standard is compared to partial intervals of rod graduation. From series of observations taken from different places of the rod the correction of the average rod metre related to one metre length is derived. Then, by adding the value thereby obtained to the "desired" metre length, the average rod metre is attained. These comparators, utilizing the optical principle

of operation can be divided into two main groups from the point of view of design as follows:

a) comparators with fixed measuring microscope;

b) double image comparators (by coincidence principle).

A more detailed treatment of these instruments is provided in References [1, 2, 3] and [4, 5, 6, 7], respectively.

As in this method rod sections are measured, therefore it is a drawback of this method that no information is obtained on individual graduation errors, instead, the differences between the graduation errors of individual sections is obtained and their sum gives information on the order of regular errors and on the tendency thereof.

To counterbalance this disadvantage various procedures of measurement and calculation were elaborated. The simplest solution is to determine the scale factor for the rod graduation (average metre) in function of the position along the rod taking the readings e.g. by every metre. For this purpose the 0.5 metre long comparison base can be advantageously used as it has been proposed for a more reliable control of leveling rods by CSATKAI [5]. If a suitable number of graduation intervals are measured, then the corrections for the part graduations can be calculated by some suitable mathematical method as for example by the method of HANSEN as described e.g. MARZAHN in [3].

SCHLEMMER [10] and WITTE [13] give solutions for calculating the correction of rod graduations by integrating rod metre corrections. That is feasible because a correction of the rod metre can be regarded as the difference between two graduation corrections.

In the test methods pertinent to the *second group* the distance of each of the graduations is measured from an initial point, or zero point. This way, the error of each graduation of the rod can be determined with respect to the zero point. This kind of measurement can be carried out with laser interferometer with a high accuracy maintained.

Both methods of standardization are applied in laboratory conditions. Consequently, the results attained also refer to laboratory conditions only. In field measurement, the mechanical and physical effects encountered by the rods may change the parameters of standardization. To measure these influence directly and to take them in consideration is not an easy task, their uncertain estimation may even lead to the determination of erroneous corrections.

The increased accuracy requirement demands the possible most reliable estimation of the systematic errors of leveling. For this purpose it seems advisable to change the calibration methods applied so far.

Systematic error sources of leveling rods may be divided into two groups as follows:

1. errors in the graduation process like erroneous template, and error in the graduating machine, etc.;

2. changes of external physical and mechanical influences, as those of temperature, of tape pull force, mechanical deformations, etc.

While graduation errors may be considered steady for a longer period, external physical and mechanical influences and the systematic errors caused by them are changing from time to time. Accordingly, it is expedient to perform the calibration of the rod in two steps. The first is the determination of rod graduations by a laser interferometric comparator in laboratory environment. This information can be stored either in numerical or in graphical form supposing that the relative position of graduations on the invar tape is rather steady and does not alter its position to a significant extent upon external physical and mechanical influences. The change in the scale thus caused can be determined by means of a simple field comparator simultaneously with field measurements. So the graduation errors determined by a laboratory calibration process that can be considered steady for a longer period may be modified with the application of field calibration data.

By mathematical methods, the original graduation errors can be modified so as to approximate the curve interpolated to these graduation errors with the measurement data of field standardization calculating thereby the modified graduation errors.

In the following treatment a mathematical method will be given for the modification of the original graduation errors after a comparison performed in the field.

Let us denote the deviation of the graduations of a leveling rod from the nominal values

$$x_0 < x_1 < \ldots < x_n \tag{1}$$

respectively, by

$$f_0, f_1, \ldots f_n. \tag{2}$$

In our model of rod comparison all l_i reading values are built up of two components: the actual value x_i of the rod graduation and the pertinent correction f_i

$$l_i = x_i + f_i \quad i = 0, 1, 2, \ldots n. \tag{3}$$

Denote the length unit of the meter standard incorporated in the field comparator by L. In a comparison of such a character the differences between the graduation errors will be obtained:

$$l_{L+k-1} - l_{k-1} = (x_{i+k-1} - x_{k-1}) - (f_{L+k-1} - f_{k-1}); \; k = 1, 2, \ldots n - L + 1. \tag{4}$$

The precondition is that the graduation corrections (2) of the graduations (1) are known. The corrections may be defined as a function of graduation values as independent variables:

$$f = f(x) . \tag{5}$$

Let us consider the derivatibes in the dividing points:

$$f(x_{L+k-1}) = \frac{f(x_{L+k-1}) - f(x_{k-1})}{L} = \frac{f_{L+k-1} - f_{k-1}}{L} = \frac{Y_k}{L}$$
$$k = 1, 2, \ldots n - L + 1. \tag{6}$$

From the theorem of mean values of differential calculus it may be stated that in the interval (x_{L+k-1}, x_{k-1}) there exists at least one point were the derivate assumes the value (6). In the following, it will be supposed that this point is the halving point of the interval.

Consequently, by performing the field comparison, informations are obtained from the derivate function of graduation errors. The task to be performed is as follows: from the behaviour of the derivate function known in discrete points conclusions should be drawn about the local characteristics of the prime function. This way, modified correction values should be assigned to each individual graduation according to field comparison results.

The mathematical model applied here is as follows:

The each part-interval

$$[x_{i-1}, x_i] \qquad i = 1, 2, \ldots n \tag{7}$$

of the leveling rod third-order polynomials, so-called spline functions are laid

$$g_i(x) = a_0^i + a_1^i(x_i - x) + a_2^i(x_i - x)^2 + a_3^i(x_i - x)^3 \qquad i = 1, 2, \ldots n . \tag{8}$$

Be the interpolated function an element of the function class $C^2(x_0, x_n)$, being this way continuous as well as its first and second derivatives.

Now, the task to be performed is to determine the coefficients

$$[a_0^i, a_1^i, a_2^i, a_3^i] \qquad i = 1, 2, \ldots n . \tag{9}$$

Equations required for the determination of the coefficients may be obtained from the conditions that assure the continuity of the interpolated function as well as its first and second derivatives in the grid points and from the boundary conditions.

As on the base of the above considerations no fixed values are given in the graduations x_i $(i = 0, 1, \ldots n)$ to be assumed by the spline functions, therefore further equations are required. Further connections may be derived by the application of field comparison measurement results

$$g_{k+L-1}(x_{k+L-1}) - g_k(x_{k-1}) = Y_k \quad k \in I \tag{10}$$

in which I is the set of indices of field comparison instrumens.

The set of indices I can be selected arbitrarily. Therefore it is sufficient to perform the field comparison only in some positions along the rod, as e.g. in the lowest, middle and upper sections, that is, in three positions.

Whenever any variations are revealed by the field comparison then, upon their effect, the correction of graduations determined by laboratory measurement, as defined in Eq. 2, will also be subject to change.

$$Y_k = \tilde{f}_{k+L-1} - \tilde{f}_{k-1} \qquad k \in I. \tag{11}$$

Using the values obtained in the field comparison the spline functions best fitting to the laboratory comparison values are to be determined by least square technics.

Our task can be reduced to the solution of the following problem of extremes (see [14] for detailed deduction and proof):

$$\left(f_0 - a_0^1 - a_1^1 h_1 - \frac{2}{3} a_2^1 h_1^2\right)^2 + \sum_{i=1}^{n} (f_i - a_0^i)^2 \to \min_{[a_0^1, a_0^2 \ldots a_0^n, a_1^1]}$$

$$a_0^{k+L-1} - a_0^{k-1} = Y_k \qquad k \in I - \{1\} \tag{12}$$

$$a_0^2 - a_0^1 - a_1^1 l_1 - \frac{2}{3} a_2^1 h_1^2 = Y_1 .$$

To find the extremes Lagrange's multiplicator procedure can be applied.

The solution is the following:

For each individual graduation of the leveling rod it can be decided whether there has been a measurement performed during the field comparison or not (or whether the graduation has been an end point of the length compared to the standard metre or not). Rod graduation can be classified on the base whether there exist such indices $k_1 \in I_1 k_2 \in I$ (not necessarily different ones) whose rod comparison Y_{k1} and Y_{k2} have at least one common terminal point.

If a graduation has no pertinent $k \in I$, then this graduation should form a separate class.

This way, the set of Y_k $(k \in I)$ measurement results will split into disjunct chains.

Be the length of such a chain m and be I' the set of indices for the comparison values Y'_k figuring in the chain. It can be supposed that

$$\{I' = 1, 2 \ldots m\}.$$

The form the following vectorial series:

$$P_0 = (-m, -m + 1, \ldots 1) \tag{13}$$

$$P_i^i = P_{i+1}^i + \delta_{ij}(m + 1) \qquad i = 1, 2, \ldots m \qquad j = 1, 2, \ldots m \tag{14}$$

in which δ_{ij} is the known Kronecker symbol.

The following values are assigned as corrections to the graduations of the leveling rod:

$$[a_0^i = \frac{1}{m+1}\left(\sum_{j=0}^{m} f_j + \sum_{j=1}^{m} P_{i-1}^j Y_j\right) \qquad i = 1, 2, \ldots m. \tag{15}$$

This assignment entails the feature that if

$$Y_j = f_{j+L-1} - f_{j-1} \qquad j \in I^1 \tag{16}$$

then

$$a_0^i = f_i. \tag{17}$$

On the base of [15] and [12] the still missing coefficients of the spline polynomials can be determined.

In the following, numerical examples will be given to illustrate the above expounded procedure. For the examples the measurements treated in [10] will be utilized. Field comparison was simulated by the use of the data so that average rod metres were taken with a step distance of 0.5 m, (this corresponds to five measurements). In Fig. 1 that case is illustrated when there was no deviation between laboratory and field measurements. In this case the corrections for the graduation calculated from the field comparison are practically not different from the laboratory measurement results. Figure 2 shows that case when the deviation of field measurements from laboratory ones is linear. Graduation corrections because of non-linear variations are indicated in Fig. 3.

If only a comparator equipped with a standard meter is available for laboratory comparison then the correction values pertinent to the individual graduations can be determined only in an indirect way, by means of calculations. Similar to the procedures described by SCHLEMMER and WITTE, the method given here can also be modified for the determination of graduation corrections on the base of measured differences.

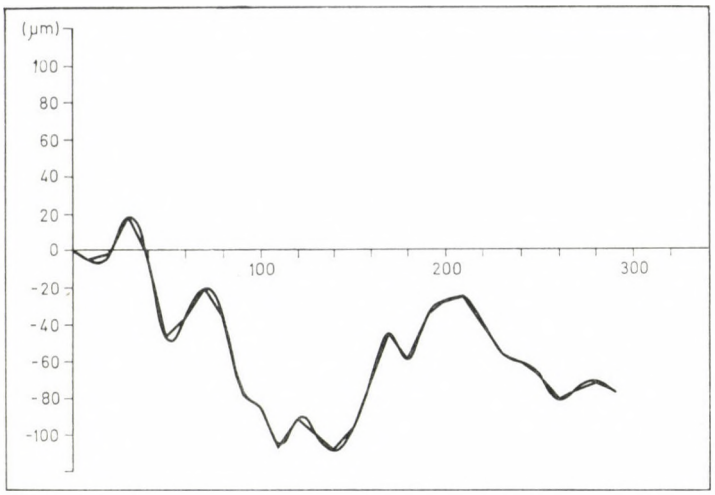

Fig. 1.

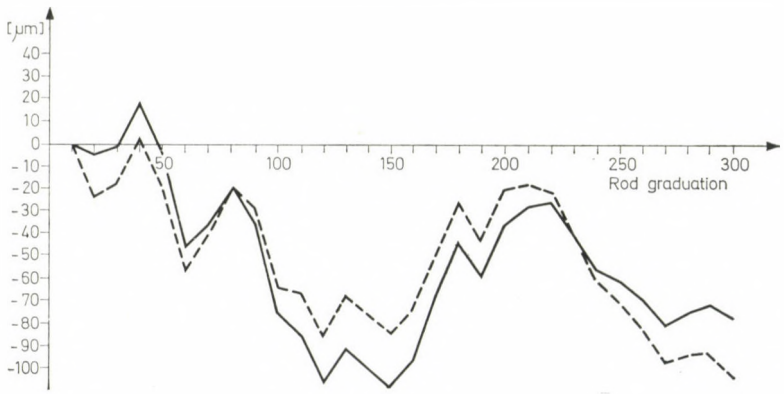

Fig. 2.

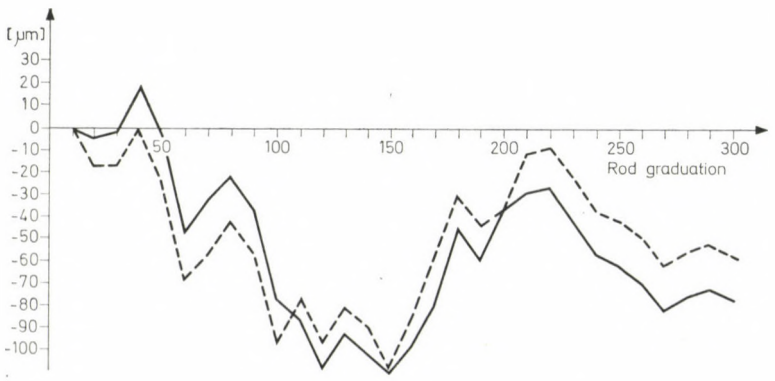

Fig. 3.

Connection 15 that serves to estimate the graduation errors of the leveling rod are composed of two terms:

$$a_0^i = \frac{1}{m+1}\left(\sum_{j=0}^{m} f_j + \sum_{j=1}^{m} P_{i-1} Y_j\right) \quad i = 1, 2, \ldots m. \tag{18}$$

Consequently, if a consistent estimate is available for the expectable value of the average of graduation errors, then a sufficient estimate can be given for graduation corrections also on the base of the rod metre correction values.

The expected value of the arithmetic mean of graduation errors can be estimated by the following statistics:

$$f = \frac{1}{n}\left(\sum_{i=1}^{n-L\left[\frac{n}{L}\right]+1} f_{i-1} + \left[\frac{n-1}{L}\right]\sum_{i=1}^{L} f_{i-1} + \sum_{i=1}^{n-L\left[\frac{n}{L}\right]+1}\sum_{j=1}^{\left[\frac{n-1}{L}\right]} Y_{(j-1)L+i} + \right.$$
$$\left. + \sum_{j=1}^{\left[\frac{n-1}{L}\right]-1}\left(\left[\frac{n-1}{L}\right] - j\right)\sum_{i=1}^{L} Y_{(j-1)L+i}\right). \tag{19}$$

From the above expression it can be stated that hereinafter it will prove sufficient to estimate merely the sum of the graduation corrections f_i $i = 0, 1, \ldots L-1$ and by this the formerly expounded procedure will be rendered readily applicable.

To estimate the first $i = 0, 1, \ldots L-1$ values of graduation corrections the method given by SCHLEMMER in [10] will be applied.

If the discrete comparison values Y_k $(k = 1, 2, \ldots n-L-1)$ are interpolated by a higher-order adjustment polynomial, then to integrate this polynomial will involve no serious difficulties. In this case, using Eqs 5 and 6, the corrections pertinent to each individual graduation will be obtained. To decide about the order of the trend polynomial the criterion of least square of deviations may be used. The integration constant can be determined in the following manner: no error may be assigned to the first graduation of the leveling rod because of physical considerations, that is, $f_0 = 0$. By this, the value of the graduation correction will be known in point $L/2$ and therefore the integration constant for this place can be determined directly.

The graduation corrections of the first and last part of $L/2$ length in the leveling rod can be determined from the rod comparison values Y_k and from the graduation corrections already determined by integration.

As, according to Eq. 6, rod comparison is corresponding to a derivation and because the operation of derivation is basically a filtering process, therefore this operation cuts off not only the higher frequencies but attenuates

also those slower variations that are interesting for our purposes. Therefore, with the aim of reestablishing the original form of graduation corrections, the smoothed function should be subjected to a "restoration" process. BRACEWELL [16] gives the following connection for the restoration:

$$f(x_i) = \frac{1}{6} f(x_i - L/2) + \frac{4}{3} \underline{f}(x_i) - \frac{1}{6} (x_i + L/2) \,. \tag{20}$$

In the following, some numerical examples will be given for this solution, too. In the figures the continuous line indicates the real graduation corrections, the dot-dash line pertains to those obtained by the polynomial solution while the dashed line shows graduation corrections as calculated by the spline functions. Figure 4 gives the correction curves for the approximate graduation errors calculated with the numerical data published in SCHLEMMER's paper [10]. The figure clearly shows the enhancement of accuracy attained by the application of the spline function. By the method, the mean errors of the calculated graduation corrections can be determined by the deviations from the original value. In Figs 5, 6, 7, 8 and 9 one can distinguish the curves of approximate graduation corrections calculated according to graduation errors of different character. All five figures clearly indicate that the method here described approximates the actual value more closely. Consequently, from the so calculated informations one can obtain a closer view on the character of the graduation errors of the leveling rod investigated.

For such a two-step testing of leveling rods a field comparator device is required that is conveniently manageable in field conditions, too, and assures the required 2 to 3 m of accuracy. SCHLEMMER [10] expounds those sources of error in comparators applying a metre standard for standardization

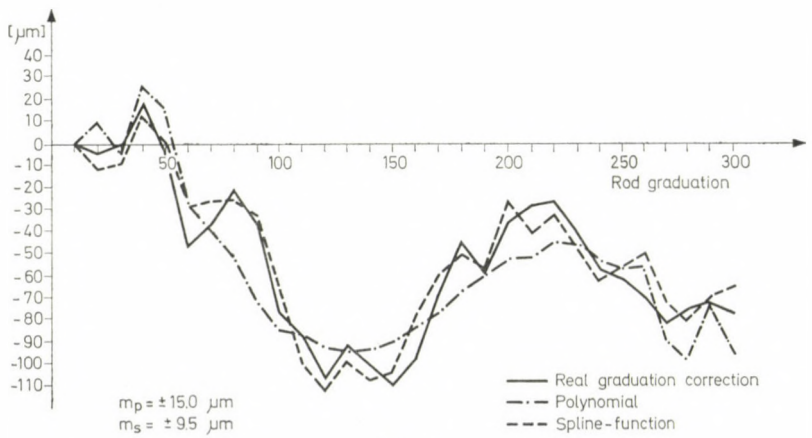

Fig. 4.

due to errors the required accuracy can be but hardly attained. These are the thermal expansion of the normal metre applied, the drift of the comparator upon the influence of thermal changes and the application of one metre base length for standardization.

In the Geodetic and Geophysical Research Institute of the Hungarian Academy of Sciences the development of comparators is a subject that has already some background. An earlier design was described by HALMAI [11].

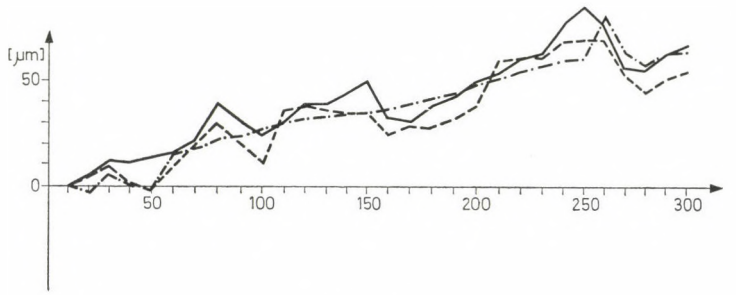

Fig. 5.

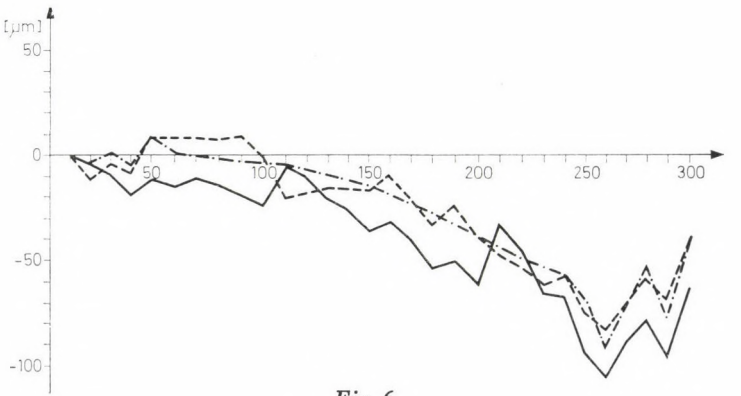

Fig. 6.

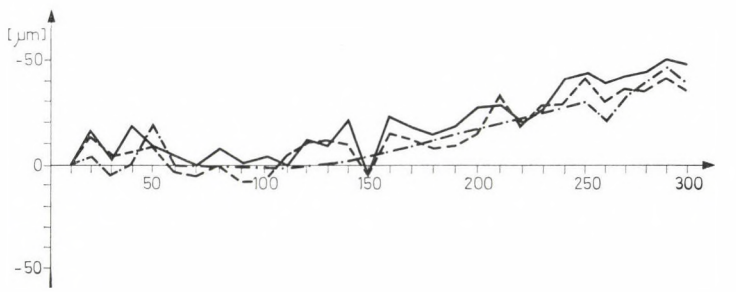

Fig. 7.

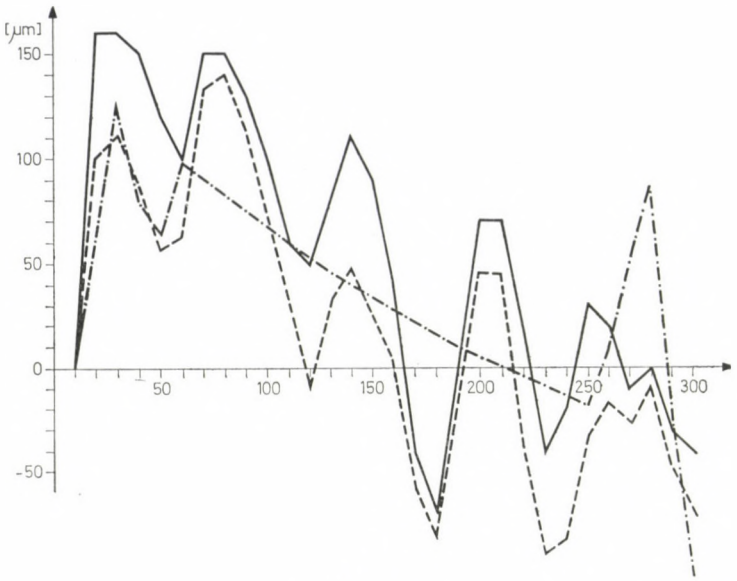

Fig. 8.

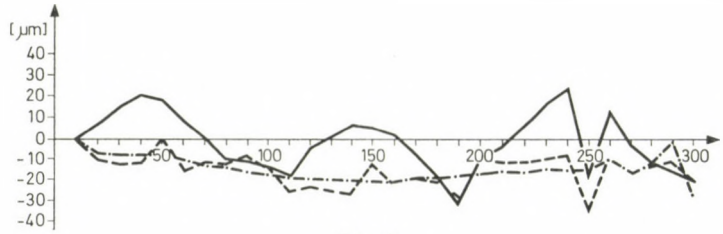

Fig. 9.

Even at the first type, to assure the required measurement accuracy, due care was taken to eliminate the previously listed sources of errors. That is why the standard rod used for the comparison has been made of a ceramic material and its base length is 0.5 metre. On the base of our control measurements the thermal expansion coefficient of the ceramic rod is so low that it can be neglected for the measurements. To eliminate the thermal drift of the comparator structure, the optical components were fastened on a beam made of invar material. Using the experiences obtained from the first instrument the design was further developed. Keeping the accuracy requirements, the main objective of the work was to decrease the weight of the device, to facilitate easy handling in the field and to render possible its application for various types of rods.

The comparator (Fig. 10) is an optical measuring tool with a length standard incorporated in the equipment. Its optical arrangement is shown in Fig. 11. The optical system serves to project the image of the rod gradu-

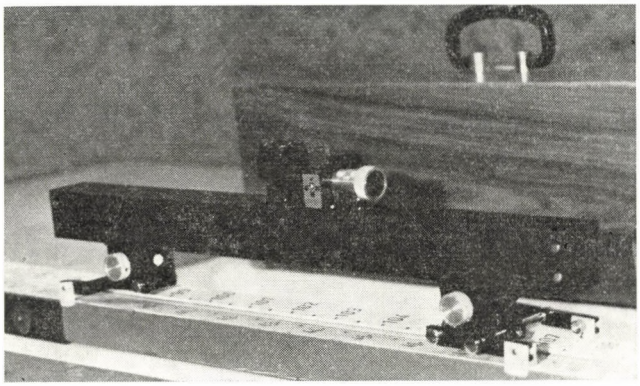

Fig. 10.

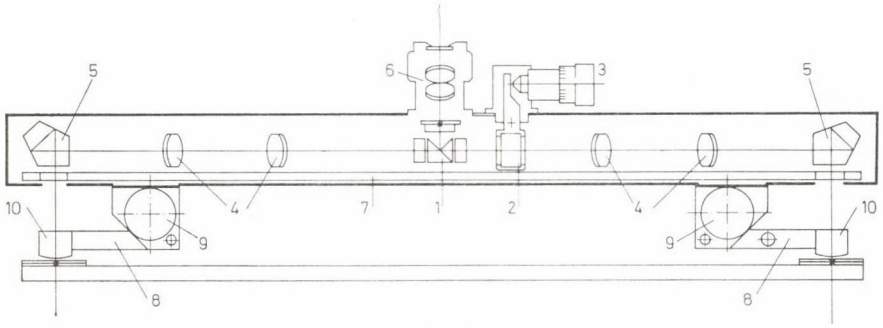

Fig. 11.

ations or those of the length standard from both ends of the longitudinal structure to coincidence prism(1) in the centre. The left side of the optical system simply projects the image to the centre while the right side includes plan-parallel glass plate (2), too, tiltable around a horizontal axis, its position readable by a micrometer screw fitted with a graduated drum (3). Lenses (4), at the left side and those at the right diminish the rod image by a factor of 0.7. Pentagon prisma (5) maintain the optical axes parallel to each other in spite of any occasional distorsion of the device. The images appearing in the respective windows of the coincidence prism are viewed from above through ocular lens (6), of the eyepiece resulting in a total magnification of $7\times$.

The optical system, with the exception of the parallel plate micrometer, is mounted on an invar steel rod (7) of a very low thermal expansion coefficient. The complete system is accommodated inside an aluminium alloy housing provided with legs below to be supported on the frame of the leveling rod. Two of the legs (8) are fixed together and can be moved together by turning

left focusing knob (9) to lift up or descend the left side of the comparator. The other two legs (8) can also be moved in the same way by right focusing knob (9) to focus the right side of the image, however, they are not fastened together but connected through an equalizing mechanism. This mechanism maintains the average height of the two legs fixed but, with this condition observed, the two legs can move freely. So, by lifting up one of the legs the other is caused to descend and inversely. This provision is necessary to eliminate the instability because of the irregularity of the rod frame surface.

The four legs are fitted with plastic shoes (10) by which the comparator can be positioned with respect to the rod. The plastic shoes belong to a certain cross-section of rod. For measuring another rod of different size the set of four shoes can be interchanged for another set. With the comparators the following rod types can be tested: Wild, C. Zeiss Jena, Rost and Kern.

For transport and storage the comparator is housed in a wooden transport case. In the bottom part of the transport case the length standard is incorporated. The length of the standard is measured between the lines engraved on glass plates adhered at the ends of the ceramic rod. The lower part of the case accommodates the comparator as well, and in this position one can observe the end marks of the ceramic rod through the eyepiece of the comparator in the respective halves of the coincidence prism (Fig. 3).

In the course of test measurements with the comparator we got for the coincidence of the lines of length standard an accuracy of ± 1.2 μm and for good quality lines of leveling rods ± 2 μm. The behaviour of the instrument was separately tested on effect of larger temperature changes. Test measurements in conditions when the temperature was changed between -10 °C $+25$ °C were unable to discover provable deviations in the measuring accuracy of the comparator. One can get more information about the calibration results with the field comparator from [17].

REFERENCES

1. Peschel, H.: Untersuchungen von Invarnivellierlatten der Firma C. Zeiss. *Zeitschrift für Instrumentenkunde*, Heft 2, 1938.
2. Ochsenhirt, H.: Zur Untersuchung von Feinnivellierlatten mit Invarband. *ZfV*, Heft 3, 1956.
3. Marzahn, K.: Untersuchungen an Invarband Nivellierlatten. *DGK*, Reihe C, Nr. 22, 1957.
4. Regőczi, E.: Neuer Nivellierlattenkomparator. *Geodézia és Kartográfia*, Nr. 2. 1957.
5. Csatkai, D.: Steigerung der Genauigkeit bei der Bestimmung der Komparationverbesserung in der Nivellierung. *Acta Technica Hungaricae*, 37, 1961.
6. Peschel, H.: Komparator für Invarband-Nivellierlatten. *Vermessungstechnik*, Heft 8, 1963.
7. Witte, B.: Über die Genauigkeit der Kalibrierung im Basis- und Nivellierlatten mit den Breithauptschen Doppelbildkomparatoren. *ZVV*, Heft 7. 1969.
8. Manteuffel, H.: Systematische Fehler des Maßstabes und der Teilung Nivellierlatten. Geodätische und Geophysikalische Veröffentlichungen, DDR, Reihe III, Heft 14, 1969.
9. Takalo, M.: The laser Rod Comparator. Report of the Finnish Geodetic Institute. Helsinki, 1974.

10. SCHLEMMER, H.: Laser-Interferenzkomparator zur Prüfung von Präzisionsnivellierlatten. *DGK*, Reihe C, Nr. 210, 1975.
11. HALMAI, E.: Feldkomparator für Invarband-Nivellierlatten. *Acta Geod., Geoph. Mont. Hung.*, 13 (1978), 144—152.
12. ZÁVOTI, J.: Anwendung von Spline-Functionen in Geodäsie. Kosmische Geodätische Seminar in Sopron, 1978.
13. WITTE, B.: Zur Prüfung von Invarbandlatten. *AVN*, 1978.
14. SOMOGYI, J.—ZÁVOTI, J.: Anwendung von Spline-Functionen zur Prüfung von Invarbandnivellierlatten, *AVN*, 1981.
15. MARCSUK, G. I.: A gépi matematika numerikus módszerei. Műszaki Könyvkiadó, Budapest, 1976.
16. TAUBENHEIM, J.: Statistische Auswertung geophysikalischer und meteorologischer Daten. Akademische Verlagsgesellschaft, Leipzig 1969.
17. VÁMOSI, S.: Calibration Procedures for Invar Levelling Rods in Canada, Second International Symposium on Problems Related to the Redefinition of North American Vertical Geodetic Networks, Ottawa, Canada 1980.

О КАЛИБРОВАНИИ ИНВАРНОЙ НИВЕЛИРНОЙ РЕЙКИ

Й. ШОМОДИ—Й. ЗАВОТИ—Д. БЕШКО

РЕЗЮМЕ

Для повышения точности нивелирования необходимо учитывать систематические ошибки инварных нивелирных реек. Калибрование целесообразно произвести в двух шагах (лабораторное калибрование и калибрование при полевых условиях). Для осуществления такого калибрования в двух шагах необходимо применять компаратор, который удобно используется при полевых условиях. Необходимая точность компаратора 2—3 μм. Кроме этого для достижения желаемой коррекции требуется специальное математическое решение.

Acta Geodaet., Geophys. et Montanist. Acad. Sci. Hung. Tomus 16 (2—4), pp. 295—305 (1981)

NEUE STEREOKAMMER, MESS- UND RECHENMETHODE IM UNTERTAGEBAU

L. BATTA—E. HALMAI—J. SOMOGYI

GEODÄTISCHES UND GEOPHYSIKALISCHES FORSCHUNGSINSTITUT DER UNGARISCHEN AKADEMIE DER WISSENSCHAFTEN, SOPRON

Zur Ermittlung der Konvergenz bzw. der Deformation eines Tunnelteiles mit etwa 15 m Länge, wurde eine schlagwettersichere, gut transportable photogrammetrische Stereokammer mit fixer Basis, eine schlagwettersichere Punktmarkierungsanlage für Untertagebau, eine automatisierte Meß- und Rechenmethode der Nahbereichsphotogrammetrie entwickelt.

Die Anlage, die Meß- und Rechenmethode kann im Untertagebau und auch im Straßen- und Eisenbahntunnelbau günstig eingesetzt werden.

Die Anwendung der Photogrammetrie im Bergbau wurde in Ungarn bereits im vergangenen Jahrhundert an der Akademie zu Selmecbánya (Banska Stiavnica) und späteran der Königlichen Ungarischen Akademie für Bergbau-, Hütten- und Forstwesen zu Sopron in den Vorlesungen behandelt. Im Jahre 1913 schrieb Prof. FINKEY in der Zeitschrift »Berg- und Hüttenmännische Blätter« über die Wichtigkeit der Photogrammetrie im Bergbau. Im Jahre 1932 deutete Prof. A. TÁRCZY-HORNOCH in seinem Vortrag vor der Gesellschaft der Ungarischen Photogrammeter, »Photogrammetrie im Dienste des Bergbaues« auf die neue, durch die Photogrammetrie angebotene Meßtechnik hin. Nach dem zweiten Weltkrieg, in Folge des großen wissenschaftlich-technischen Aufschwunges, entstanden neue meß- und rechentechnische Methoden, wobei die Photogrammetrie eine wesentliche Rolle spielte. Die Erfolge in der Rechentechnik, die modernen Rechenzentren, die genauen Auswertegeräte bieten uns auch gegenwärtig die Möglichkeit um die Instrumente der markscheiderischen Photogrammetrie weiterzuentwickeln. Der Einsatz der Photogrammetrie im Bergbau war für eine lange Zeit nur zur Lösung vermessungstechnischer Aufgaben im Tagebau vorstellbar. Der rasche Fortschritt in Wissenschaft und Technik, die rasch zunehmenden Ansprüche veränderten diese Auffassung allmählich. In dieser Beziehung ist in Ungarn die Tätigkeit des Kohlenbergbau-Trustes und dessen Abteilung für Markscheidewesen am bedeutendsten.

In der Fachliteratur gibt es gegenwärtig über Photoapparate, Aufnahmeanlagen, Mono- und Stereokammern der Nahbereichsphotogrammetrie viel zu lesen. Es gibt serienmäßig hergestellte Mono- und Stereokammern, die mehr oder weniger zur Lösung universaler Zwecke dienen sollen (UMK-10, SMK 5,5 usw.), kaum gibt es aber handelsübliche Stereokammern und Punkt-

markierungsanlagen, die auch schlagwettersicher sind und den ungünstigen Bedingungen im Untertagebau entsprechen. Im Einklang mit dem Bedarf der Markscheider haben wir im Institut für Geodäsie und Geophysik der U. A. d. W. in Sopron eine Stereokammer entwickelt, die auch in schlagwettergefährlichen Räumlichkeiten im Untertage zugelassen werden kann.

Beim Bau der Aufnahme-Anlage haben wir folgende Ziele gesetzt:

1. Das Gerät soll photogrammetrische Aufnahmen der Objektpunkte im Stollen von 5—20 m Entfernung ermöglichen.

2. Der mittlere Fehler der drei errechneten Koordinaten eines Raumpunktes darf den Wert von ± 2 cm nicht überschreiten.

3. Kammer und Punktmarkierung soll schlagwettersicher sein.

4. Transport und Handhabung der Anlage soll den Bedingungen im Untertagebau entsprechen.

5. Die Berechnung der Raumkoordinaten der photographierten Punkte soll mit einer Rechenanlage automatisch berechnet werden können (EDV).

6. Die in verschiedenen Zeitpunkten verfertigten Aufnahmen sollen zur Messung und Darstellung der Konvergenz bzw. der Deformation eines Stollenteiles anwendbar sein.

7. Die Bilder sollen im Stereo, mit einem Stereokomparator ausgewertet werden und ein Lochstreifen für EDV soll automatisch gelocht werden.

Abb. 1 zeigt das in unserem Institut entwickelte Aufnahmegerät auf ein geodätisches Stativ montiert. Das Instrument kann aber auch an ein Hängestativ (Firstenstativ) oder in vertikaler Lage an ein Seitenstativ (Seitenarm) montiert werden. Die Basislänge ist fix in 0,75 m abgestimmt, die Kammerkonstante ebenfalls fix montiert. Letztere wurde so eingestellt, d. h. das Objektiv wurde so montiert, daß eine Schärfentiefe von 5 m bis 20 m entstand. Die Kammern erzeugen die Bilder auf die bekannte 9×12 cm² Topoplatte TO-1.

Abb. 1

Das Instrument wird mit Hilfe der drei Fußschrauben horizontal eingestellt. Zur Kontrolle der Einstellung dienen die beiden quer zueinander eingebauten Röhrenlibellen, die sich am mittleren Teil des Instrumentes befinden. Hier sind weiters ein kleines Sucherfernrohr, der Schalter der Rahmenmarkenbeleuchtung und die Batterie untergebracht. Die Justierschrauben sind an den beiden Enden der Basis, womit man die Kammerachsen dem Normalfalls entsprechend justieren kann.

Das Objektiv ist eine handelsübliche Meopta Anaret Linse mit eingebauter Blende. Die Fokuslänge beträgt 105 mm.

Der Verschluß konnte in Folge der unempfindlichen Negative sehr einfach ausgeführt werden.

Die Kasetten der Negative sind ebenfalls handelsübliche Elemente des Instrumentes.

Die Beleuchtung der Rahmenmarken ist mit Hilfe von 2×4 LED Dioden gelöst, eine neunte dient zur Kontrolle. Der Schalter des Stromkreises (Abb. 2) ist ein vakuummagnetischer Schalter, ein sog. Reed Relais. Auch die handelsüblichen Batterien werden schlagwettersicher eingebaut (Abb. 3).

Mit dem justierten Instrument können Normalstereogramme gefertigt werden. Die beiden Kammern müssen aber einzeln kalibriert werden. Zu diesem Zweck haben wir im Labor ein Testfeld — mit 70 Punkten — aufgebaut und die Raumkoordinaten der Punkte mit einer Genauigkeit von $\pm 0{,}2$ mm mit geodätischen Methoden festgestellt. Zur Berechnung der inneren und äußeren Orientierungselemente verwendeten wir die perspektiven Beziehungen der Punkte des Objektraumes und Bildraumes.

Ausgehend von den Grundgleichungen der Zentralprojektion

$$x - x_0 = c \frac{a_{11}(X - X_0) + a_{21}(Y - Y_0) + a_{31}(Z - Z_0)}{a_{12}(X - X_0) + a_{22}(Y - Y_0) + a_{32}(Z - Z_0)} \tag{1}$$

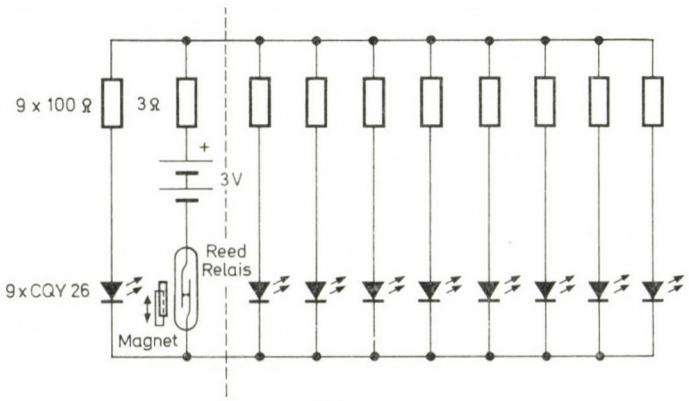

Abb. 2

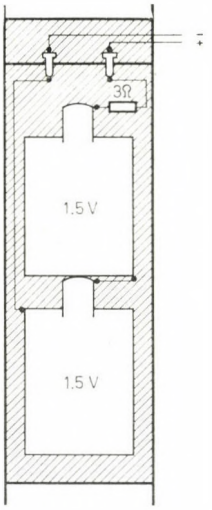

Abb. 3

und analog

$$z - z_0 = c \frac{a_{13}(X - X_0) + a_{23}(Y - Y_0) + a_{33}(Z - Z_0)}{a_{12}(X - X_0) + a_{22}(Y - Y_0) + a_{32}(Z - Z_0)} \tag{2}$$

wurden die Verbesserungsgleichungen der Tabelle I hergeleitet, woraus die Normalgleichungen und weiters die Verbesserungen der Näherungswerte berechnet werden können. Auch die mittleren Fehler der Unbekannten werden ermittelt.

Der Verzeichnungsfehler des Objektives wird mit dem Computer berechnet und auch zeichnerisch dargestellt (Abb. 4).

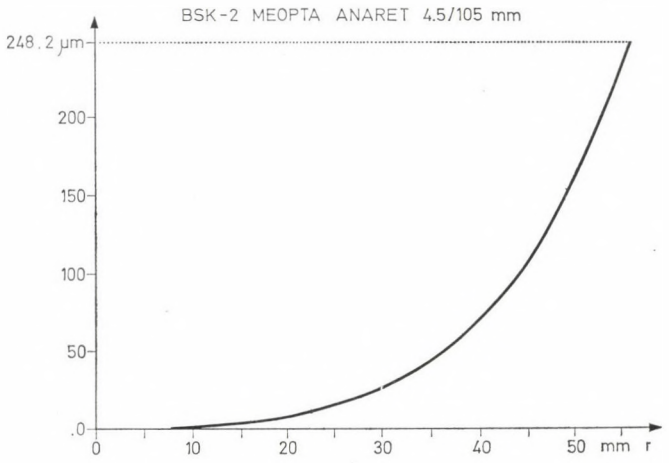

Abb. 4

Tabelle I

START
KAMMERKALIBRIERUNG

INPUT: x_o, z_o, c_o, X_o, Y_o, Z_o Näherungswerte
$\omega = \varphi = \varkappa = a_3 = a_5 = p_1 = p_2 = dm = d\beta = \emptyset$
und die Koordinaten der Raum- und Bildpunkte mit den Identifizierdaten
I_i, X_i, Y_i, Z_i
I_i, x_i, z_i

Die Verbesserungsgleichungen:

$$x = x_o + dx_o + \frac{X-X_o}{Y-Y_o}\,dc - \frac{c}{Y-Y_o}\,dX_o + \frac{X-X_o}{(Y-Y_o)^2}\,cdY_o - \frac{(X-X_o)(Y-Y_o)}{(Y-Y_o)^2}\,cd\omega -$$
$$- \frac{Z-Z_o}{Y-Y_o}\,cd\varphi + \left[1+\left(\frac{X-X_o}{Y-Y_o}\right)^2\right]cd\varkappa + \frac{X-X_o}{Y-Y_o}\,c(a_3 r^2 + a_5 r^4) +$$
$$+ p_1\left[r^2 + 2(x_s - x_o)^2\right] + p_2\, 2(x_s - x_o)(z_s - z_o)$$

und

$$z = z_o + dz_o + \frac{Z-Z_o}{Y-Y_o}\,dc + \frac{Z-Z_o}{(Y-Y_o)^2}\,cdY_o - \frac{c}{Y-Y_o}\,dZ_o -$$
$$- c\left[1+\left(\frac{Z-Z_o}{Y-Y_o}\right)^2\right]d\omega + c\,\frac{X-X_o}{Y-Y_o}\,d\varphi + c\,\frac{(X-X_o)(Z-Z_o)}{(Y-Y_o)^2}\,d\varkappa +$$
$$+ \frac{Z-Z_o}{Y-Y_o}\,c(a_3 r^2 + a_5 r^4) + 2p_1(x_s - x_o)(z_s - z_o) + p_2\left[r^2 + 2(z_s - z_o)^2\right] +$$
$$+ (z_s - z_o)\,dm + (x_s - x_o)\,d\beta$$

wo $x_s = x_o + \frac{X-X_o}{Y-Y_o}\,c$, $z_s = z_o + \frac{Z-Z_o}{Y-Y_o}\,c$, $r^2 = (x_s - x_o)^2 + (z_s - z_o)^2$
bedeutet.

Aufbau und Lösung der Normalgleichungen
$Ax = b \rightarrow A^T Ax = A^T b$ woraus $x = (A^T A)^{-1} A^T b$

Verbesserung der Näherungswerte, Berechnung des mittleren Fehlers der Unbekannten.

Aufzeichnen der Verzeichnungfehlerkurve mit der Beziehung
$dr = r^3(a_3 + r^2 a_5)$

END

Im Normalgleichungssystem sind 15 Unbekannten vorhanden, und zwar in der angewandten Reihenfolge:

x_0, z_0, c_0 = innere Orientierungselemente
X, Y, Z = Raumkoordinaten des Objektives
$\omega, \varphi, \varkappa$ = Drehwinkel

a_3, a_5 = Koeffizienten des radialen Verzeichnungspolynomes
p_1, p_2 = Koeffizienten der tangentialen Verzeichnung
$dm, d\beta$ = Koeffizienten der Bildschrumpfung.

Nach der Lösung der Normalgleichungen und Verbesserung der Näherungswerte können mit den nun schon gut bekannten Kammern auch im Untertage Bilder aufgenommen werden, wenn die aufzunehmenden Punkte entsprechend der Blendezahl und der Empfindlichkeit der Negative beleuchtet werden. Die schlagwettersichere Punktmarkierung geschieht bei unserem System mit ringförmigen, zentralsymmetrischen Zielzeichen. Sie werden mit der elektrischen Lampe eines Markscheiders von hinten durchleuchtet (Abb. 5). Die Punktsignale werden mit Hilfe einer Schraube und einer Ankerung an dem eisernen Versicherungsring befestigt oder magnetisch angebracht; sie können aber auch an Stangen oder Röhre, die in den Felsen einragen, befestigt werden; man kann aber auch »sich kontinuierlich bewegende« Punktsignale verwenden.

Die Punktsignale werden im Stollen an einem oder an mehreren nacheinander folgenden Querschnitten (Sicherungsringen) angebracht und während der Aufnahme von hinten durchleuchtet. Die entstandenen Bilder werden an Ort und Stelle entwickelt und erst später im Stereokomparator stereographisch ausgewertet. Gleichzeitig wird ein Lochstreifen gelocht, womit man die Daten in den Computer überführt. Zu diesem Zweck eignet sich unter anderen das Stekometer C des VEB Carl Zeiss Jena am besten.

Abb. 5

Da der Komparator die Bildkoordinaten in einem eigenen Koordinatensystem mißt, müssen sie in das Bildkoordinatensystem umgerechnet werden (Programm 1.).

Weil die Bildkoordinaten mit den Verzeichnungsfehlern des Objektives belastet sind, müssen sie verbessert werden (Programm 2.).

Mit den so ermittelten Bildkoordinaten berechnen wir die Raumkoordinaten mit Hilfe der Gleichungen des Normalfalles, wo auch die Ungleichheit der beiden Kammerkonstanten und der Koordinaten der beiden Bildhauptpunkte einbezogen werden (Programm 3.).

$$X = \frac{bc''(x' - x_0')}{c''(x' - x_0') - c'(x' - x_0'')} \tag{3}$$

$$Y = \frac{bc'c''}{c''(x' - x_0') - c'(x'' - x_0'')} \tag{4}$$

$$Z = \frac{b}{(x' - x_0') - (x'' - x_0'')} \cdot \frac{z' + z''}{2} \tag{5}$$

wo

b = Länge der Basis
c' = Kammerkonstante der linken Kammer
c'' = Kammerkonstante der rechten Kammer
x', z' = verbesserte Bildkoordinaten des linken Bildes
x'', z'' = verbesserte Bildkoordinaten des rechten Bildes
x_0' = Bildkoordinate des linken Bildhauptpunktes
x_0'' = Bildkoordinate des rechten Bildhauptpunktes

Zur Ableitung der a priori Fehler nimmt man $c' = c''$ und $x' = x'' = 0$, bildet die totalen Differentialgleichungen der Gleichungen (3)—(5) mit einem Übergang zum mittleren Fehler und durch Vereinfachungen erhält man:

$$\mu_X = X \sqrt{\left(\frac{\mu_b}{b}\right)^2 + \left(\frac{\mu_x}{x}\right)^2 + \left(\frac{\mu_p}{p}\right)^2} \tag{6}$$

$$\mu_Y = Y \sqrt{\left(\frac{\mu_b}{b}\right)^2 + \left(\frac{\mu_y}{y}\right)^2 + \left(\frac{\mu_p}{p}\right)^2} \tag{7}$$

$$\mu_Z = Z \sqrt{\left(\frac{\mu_b}{b}\right)^2 + \left(\frac{\mu_z}{z}\right)^2 + \left(\frac{\mu_p}{p}\right)^2}. \tag{8}$$

Praktisch kann man

$$\left(\frac{\mu_b}{b}\right)^2 = \left(\frac{\mu_x}{x}\right)^2 = \left(\frac{\mu_y}{y}\right)^2 = \left(\frac{\mu_z}{z}\right)^2 = 0 \tag{9}$$

annehmen, so vereinfachen sich die Ausdrücke wesentlich, und wenn wir weiterhin $\mu_p = \pm 0{,}004$ mm und $p_{\min} = 4$ mm einsetzen, so gehen die mittleren Fehlergleichungen in

$$\mu_X = \pm X \cdot 10^{-3} \text{ mm} \tag{10}$$

$$\mu_Y = \pm Y \cdot 10^{-3} \text{ mm} \tag{11}$$

$$\mu_Z = \pm Z \cdot 10^{-3} \text{ mm} \tag{12}$$

über.

Mit unseren Abmessungen der Praxis, bei

$$X_{\max} = 5 \text{ m} \tag{13}$$

$$Y_{\max} = 20 \text{ m} \tag{14}$$

$$Z_{\max} = 5 \text{ m} \tag{15}$$

wird

$$\mu_X = \pm 5 \text{ mm}$$

$$\mu_Y = \pm 2 \text{ cm}$$

$$\mu_Z = \pm 5 \text{ mm}$$

nicht überschritten.

Mit Gleichungen (3)—(5) berechnen wir die Raumkoordinaten der stereographisch ausgewerteten Bildpunkte. Diese Koordinaten beziehen sich auf das im Raume willkürlich stehende Basis-Koordinaten-System. Richtungen X und Y wurden zwar mit den Libellen horizontiert, die Richtungen der Achsen entsprechen aber der Richtung der Aufnahmebasis bzw. quer zu dieser. Der Ursprung des Koordinatensystems liegt im vorderen Hauptpunkt des linken Objektives.

Der Ursprung dieses Koordinatensystems wird zunächst in einen Punkt der gemessenen Raumpunkte, z. B. P1, I. (Abb. 6) versetzt und zusätzlich um die Achse Z so verdreht, daß die Richtung Y das Lot eines zweiten Fixpunktes P2, II (Abb. 6) trifft.

Die Möglichkeit um Aufnahmen zu verfertigen und Raumkoordinaten zu berechnen ist in verschiedenen Zeitpunkten T_1, T_2, T_3, usw. gegeben. Reduzieren wir alle Koordinaten auf P1, I und P2, II, so erhalten wir die zur T_1, T_2, T_3 gehörenden Raumkoordinaten in ein und demselben Bezugssystem. Die Abweichungen der entsprechenden Raumkoordinaten sind die Konvergenzgrößen bezogen auf P1, I und P2, II.

Instrument, Meß- und Rechenverfahren wurden an Hand von Aufnahmen die in einem Kohlenbergwerk in 260 m Untertagebau verfertigt wurden, erfolgreich erprobt. Mit dieser Methode wurden nicht nur Konvergenzgrößen, sondern auch Deformationen mit allen räumlichen Richtungen festgestellt.

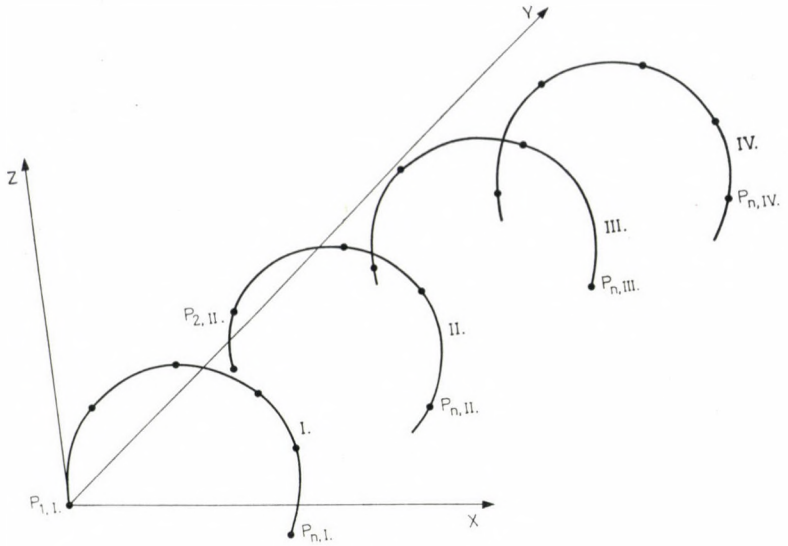

Abb. 6

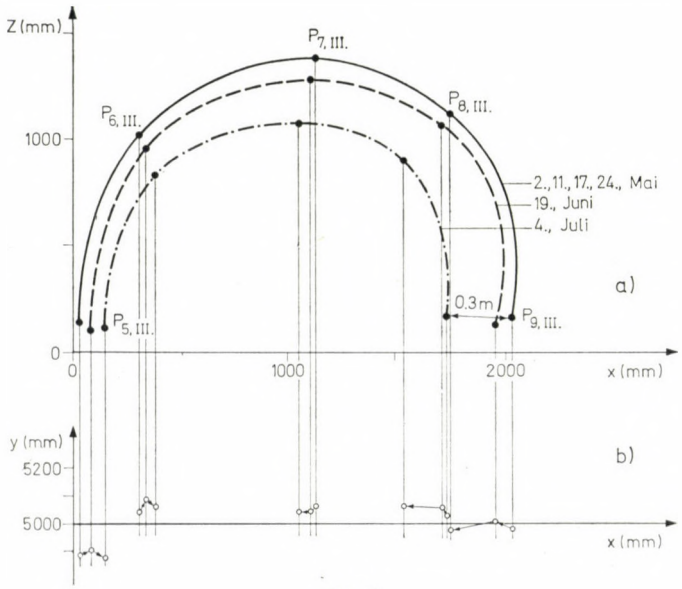

Abb. 7

Den mit III bezeichneten Querschnitt des untersuchten Stollenteiles zeigt Abb. 7a—b. Der äußerste Ring entspricht den Daten der Aufnahmen vom 2., 11., 17. und 24. Mai. Die Konvergenz begann erst nachdem sich die quer zur Stollenrichtung arbeitende Förderkette näher als 20 m zum untersuchten Querprofil angenähert hat. Der mittlere Ring der Abb. 7 wurde von den Aufnahmen vom 19. Juni, der innerste vom 4. Juli abgeleitet. (Derzeit

war der Bau unmittelbar bei diesem Querschnitt.) Abb. 7b zeigt die Punktbewegungen in der Ebene XY, diese sind aber bedeutungslos und klein. Ähnlich wurden bei unseren Testaufnahmen auch die anderen vermessenen Profile behandelt und die Konvergenz bzw. die Deformation ermittelt. Die Raumkoordinaten der Punkte der einzelnen Querschnitte wurden mit dem Computer ermittelt und aufgezeichnet und die Verbindungslinie mit Gleichungen der »Spline-Funktionen« beschrieben.

Das Instrument ist auch beim Bau von Straßen- und Eisenbahntunneln, zur Herstellung von Schnitten verschiedener Richtungen, zu Volumenberechnungen, usw. anwendbar. Der Zweck der Messungen im Untertagebau ist entweder die Bestimmung der Form, oder Formänderungen, oder die Ermittlung jener Spannungskräfte, die die Formänderungen hervorrufen. Auf Grund des Hook'schen Gesetzes sind die Kräfte und Spannungen im Gebirge aus den Konvergenz- und Deformationswerten ermittelbar. Kennen wir die Kräfte des Gebirges bzw. des Flözes, so können die Entfernungen der nachbarlichen Sicherungselemente (Sicherungsringe) so ermittelt werden, daß deren Einbau preisgünstig, aber trotzdem zuverlässig sein soll. Zur Ermittlung der Deformationen im Tagebau kann die Luftbildmessung eingesetzt werden. Die Bewegungen im Untertage und Obertage sind in der Regel verknüpft. Zur Erklärung der zwischen diesen Bewegungen bestehenden Gesetzmäßigkeiten können die photogrammetrischen kontinuierlichen Messungen dieser Bewegungen eine große Hilfe leisten. Die Anwendung der photogrammetrischen Methoden im Bergbau kann gut an die Konzeption der bergbaulichen Datenbank angepaßt werden, da die von den Lichtbildern gemessenen Daten digitalisiert und direkt in die Rechenanlage eingegeben werden können. Mit Hilfe einer zentralen EDV-Anlage und mit ausgebauten Terminal-System können die Daten jederzeit für die Verbraucher gut zugänglich gemacht werden.

SCHRIFTTUM

GREIFF, R. 1970: Über stereophotogrammetrische Deformationsbestimmung unter Tage. *ZfV*, 95, 337—344.

GRUMPELT, H. 1973: Ein analytisches Verfahren der Bündelverknüpfung in der Nahbildmessung, angewandt auf Deformationsmessungen an einer Tunnelröhre im Bergbaugebiet. DGK Reihe C. Nr. 189.

HAGGREN, H.—VÄÄTÄINEN, S. 1979: A test wall for the close-range photogrammetric calibration. *The Photogr. Journal of Finnland*, 1, 57—62.

MÜLLER, B.-G. 1974: Zum Aufnahmeproblem der ingenieurgeodätischen Nahbereichsphotogrammetrie. *VR*, 9—10, 362—382.

MÜLLER, B.-G. 1975: Zur geodätisch-photogrammetrischen Querschnittsüberwachung in Tunneln und bergmännischen Strecken. *BuL.* 43, 62—69.

STIPA, V. 1966: Eine im Berliner Markscheide Institut gebaute Doppelmesskammer. *Festschrift Hilbig.* 7—14.

TORLEGARD, K. 1967: On the Determination of Interior Orientation of close-up Cameras under Operational Conditions Using Three-Dimensional Test-Objects. Diss. Stockholm.

VLCEK, J. 1976: Die Photogrammetrie im Untertagebau. *Jenaer Rundschau*, 21, 93—100.

WÖLPERT, D. 1969: Untersuchung zur Abstimmung und inneren Orientierung fokussierbarer Messkammern. Diss. DGK. Reihe C. Heft 131.

НОВАЯ СТЕРЕОКАМЕРА, МЕТОД ИЗМЕРЕНИЯ И ВЫЧИСЛЕНИЯ В ПОДЗЕМНОЙ ДОБЫЧЕ

Л. БАТТА—Э. ХАЛМАИ—Й. ШОМОДИ

РЕЗЮМЕ

Для определения конвергенции и деформации участка туннеля длиной 15 м были разработаны газобезопасная транспортабельная стереофотограмметрическая камера с постоянной базой, газобезопасное маркировочное приспособление для подземной добычи, автоматизированный метод измерения и вычисления краткодистанционной стереофотограмметрии.

Устройство, метод измерения и вычисления применяются также в железнодорожном и шоссейном туннелировании.

Acta Geodaet., Geophys. et Montanist. Acad. Sci. Hung. Tomus 16 (2—4), pp. 307—317 (1981)

INTERFEROMETRIC ANGLE MEASURING SYSTEM OPERATING IN SMALL ANGULAR RANGE

B. J. INCZÉDY—K. KRAUSZ

GEODETIC AND GEOPHYSICAL RESEARCH INSTITUT OF THE HUNGARIAN ACADEMY OF SCIENCES, SOPRON

The paper describes an interferometric angle measuring instrument operating in a small angular range (about 1°). It is a modified version of the Michelson interferometer. The principle of the instrument is presented, the accuracy demands in the construction of the interferometer discussed and the obtainable accuracy of the system given.

Geodynamic studies necessitate measuring methods ensuring higher accuracy than those used hitherto. Special attention is to be paid to angular measurements as the greatest part of the geodynamic phenomena can be observed by a small amount (less than 1°) of inclination or rotation of some kind of surfaces or lines (e.g. surface of the Earth, vertical direction etc.). For the measurement of small angular changes different kinds of instruments can be used. The traditional ones are levels, collimators, autocollimators and different kinds of pendulums, but recently electronic inclinometers are also getting more and more into use.

A common characteristic of these instruments is that they are not calibrated as angular measuring devices, as no corresponding angular etalons are at disposal. The accuracy of the instruments measuring small angles reach the value of 0.1—1 second of arc, therefore devices enabling the detection of 0.01—0.05 secs of arc rotation are needed for their calibration.

The measurement of angles is an important problem also from the point of view of metrology, as no angular etalons exist, and consequently the angular measurements must be reduced anyway to length measurements. The accuracy of angular measurements depends on the accuracy of these distance measurements.

At present, the most exact method to measure distances is the laser interferometry. The interferometric distance-measuring method, which enabled some 20—30 years ago the measurement of distances of only some cm-s under laboratory conditions, developed recently in a way due to a rapid improvement of the laser technics and of the electronics that an instrument is produced in great series which enables a relative accuracy of 10^{-7} in case of distances of 60 m.

This large-scale development of the interferometric distance meters made possible to develop interferometric angle measuring devices. The basic idea is to reduce the measurement of the angular rotation by the use of a trigonometric function to a distance measurement, whereby the latter is made by an interferometer with high accuracy. Such a method ensures a very quick and accurate determination of angles.

The disadvantage of the method is that the angle to be measured is received indirectly, as a trigonometric function of the angle i.e. as the ratio of two distance values. One of the distances is measured directly, the other cannot be directly determined, it is an instrumental constant corresponding to the given instrumental construction.

According to that said above a solution of the calibration problems in angular measurements can be awaited from the interferometric measurement methods. Consequently the intention has been to construct a basic instrument which can be used under laboratory conditions for a large scale of purposes.

For the investigation and calibration of the precision levels or so-called second-levels used in geodesy level triers have been developed, where the necessary angular rotation is set on an arm rotable around a horizontal axis by means of a vertically movable precision measuring screw.

A level trier of the Geodetic and Geophysical Research Institute of the Hungarian Academy of Sciences has been manufactured in 1953, at which the pitch of the measuring screw is 0.40 mm, the distance between the rotation axis and the supporting point of the measuring screw, i.e. the length of the balance arm 463 mm [1]. The measuring screw can be rotated by means of a drum of 120 mm diameter with a scale of grades. By means of the drum the value of the inclination can be simply set: it follows from the geometry of the level trier that due to a 1° rotation of the drum, the height of the screw changes by 1.1 μm, and the balance arm is dipped by an angle of 0.5 sec of arc. Rigorously taken the level trier measures not the rotation angle itself but its tangent, the error due to this omission, however, is within 1° negligible.

A greater problem is the error caused by the uncontrollable inaccuracies of the pitch of the measuring screw: an error in the linearity of 1 μm which is a rather good value causes already an error of 0.5 sec of arc.

If the lift of the measuring screw is controlled interferometrically both the angular resolution and the accuracy of the measurement can be increased. Level triers controlled by multiple beam interferometers were reported by DELMONTE [2] in 1949 and by KANNGIESSER and SCHUHR [3] in 1976. The balance arm was chosen as 30 cm, thus a lift by about 1.5 μm caused an inclination of 1 sec of arc. The error of the angular rotation produced by the screw and controlled by the interferometer could be reduced to 0.05 and 0.004 secs of arc according to experiments carried out by these authors in a range of 1 min of arc and 30 secs of arc, respectively.

The level trier of our Institute has been controlled by a Michelson-interferometer. The results were reported in 1977 [4]. The level trier has been studied in a range of 30 secs of arc, and an accuracy of 0.04 secs of arc could be reached.

The accuracy data quoted are theoretically sufficient to enable a precise calibration of the instruments measuring small angular changes, i.e. the interferometric technics ensures sufficient resolution and measurement accuracy. A great disadvantage of the mentioned arrangements is, however, that while the lift produced by the screw is controlled with interferometric accuracy the rotation axis is at the same time supposed to be ideal. Due to its construction procedure, a perfect rotation axis cannot be produced, and the errors resulting from this are practically uncontrollable. Therefore it was necessary to choose an arrangement, where the accuracy of the rotation axis does not influence the accuracy of the measurements.

The interferometer for angular measurements shown in Fig. 1 fulfils these requirements. Such an instrument has been manufactured by J. G. MARZOLF in 1964 for spectroscopic purposes [5]. The instrument is a modified version of the Michelson interferometer. A parallel light beam reaches from the laser light source the plate-type beam splitter. One half of the beam is reflected from here by mirror M_1, the other half by mirror M_2 parallel to each other through the corner cube reflectors C_1 and C_2, respectively, to mirror M_3. The incident beams are reflected from mirror M_3 into themselves and thus interfere having met at the beam splitter 0. Similarly to the Michelson interferometer the interference is produced in the apparent air slot between the end mirrors of the two arms, but in this case the virtual pictures of M_3 are the two border plains of the air slot.

The moving part of the interferometer consists of the corner cube reflectors C_1 and C_2 being fixed with respect to each other, but can be tilted together around the rotation axis a. In this arrangement an arbitrary translational movement of the rotating part does not change the order of the interference, i.e. the observed interference picture remains unchanged. The practical advantages are the following: the operation of the instrument is independent from

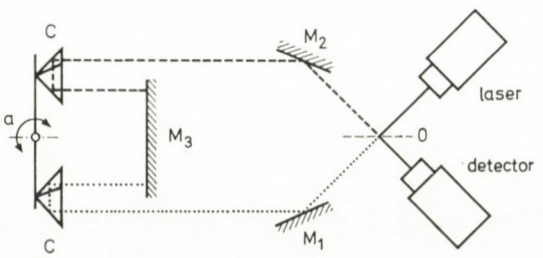

Fig. 1.

the position of the rotation axis; the position of the momentaneous rotation axis, its parallel movements during the measurements do not influence the accuracy of the angular measurements. The operational equation of the system is:

$$\sin \varphi = \frac{d}{r} \tag{1}$$

where φ is the angle of rotation, d the relative motion of the corner prisms in direction of the parallel light beams incident on the rotating part and r (an instrumental constant) the distance between the optical centres of the corner cubes. Thus the movement d is measured interferometrically, and when knowing the instrumental constant r the value of the angular change can be unambiguously determined.

For the construction of the interferometric level trier the existing level trier has been used as basis. The optical system and the light paths have been chosen so that on the one hand any kind of devices, instruments etc. could be mounted on the tiltable arm, on the other the possibilities for the unvoluntary interruption of the beam should be avoided.

The beam path lays in a plane parallel with the rotation plane of the tiltable arm, and the light beams propagate partly below the basis, partly along its two sides (Fig. 2). The two corner cubes are mounted on the moving arm, all other optical elements are mounted on the basis. A beamsplitter covered by a semipermeable layer and a pentaprism are mounted on one side, a pentaprism, a right-angle prism and a mirror on the other. Of course all these optical elements can not be put into their operational position during the mounting, since the possibility of a small change of their position is necessary for the regulation and calibration of the optical system. This task has been solved by the use of the mechanical devices shown in Fig. 3. The two triangular plates are held together by three screws, and the distance between

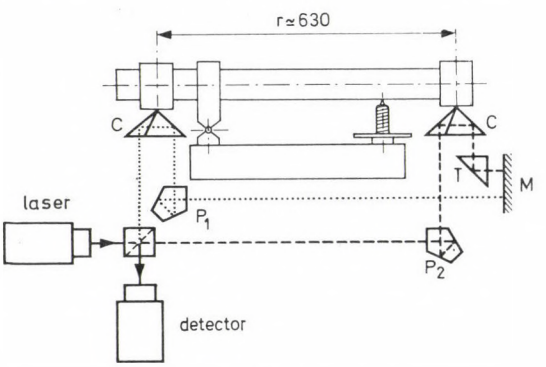

Fig. 2.

the sheets is ensured by a ball. The whole device is mounted on the bearer with a pin so that it can be rotated. With the help of the screws the upper plate can be tilted around two axes, and the rotation around the third axis is ensured by the pin mounting.

The position of the optical elements must be very carefully set with suitable apparatus in order to keep regular setting errors due to uncorrect

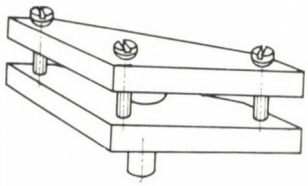

Fig. 3.

position at a minimum [6]. The choice of corner cubes needs very great care, the other optical elements have not to fulfil special requirements.

In the angle measuring interferometer the beam path is the following: the light leaves the laser, crosses a collimator and reaches the beamsplitter cube as parallel beam of a diameter of about 7 mm. The beam splitter cube halves the light beam, one half of the flux reaches through the corner cube C_1 and the pentaprism P_1 the mirror M and there it is reflected into itself; the other half of the flux crosses the pentaprism P_2, the corner cube C_2 and the right-angle prism T, then it reaches the mirror M and is also reflected into itself. The two returning beams meet at the beamsplitter cube and interfere; the interference can be visually observed or detected by a suitable instrument. In case of ideal optical elements and perfectly plane wave front perfectly bright and black fringes would occur in the interference picture. Since it is very difficult to fulfil this condition in the practice, such a setting is aimed at where only either maximum intensity or minimum intensity should appear in the sight field at once: such an interference picture can be easily detected electronically.

The angle measuring interferometer is enlighted by the frequency stabilized laser of the distance measuring instrument Metra Blansko typ LA 3000. Since a circularly polarized light beam leaves the laser and the collimator built together with it, the observation of the stripe movement due to the change of the position of the balance arm and its counting is made in the way as with the Czechoslovakian instrument [7]. The detector projected is shown in Fig. 4. The light beam returning from the arms of the interferometer, and united at the beamsplitter cube 0 is cut into two with the beamsplitter 0', and the two beams are transmitted to the photodetectors through polarization filters. The polarization filters transmit the components of the circularly

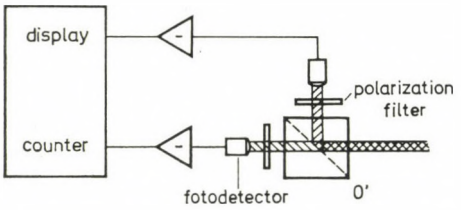

Fig. 4.

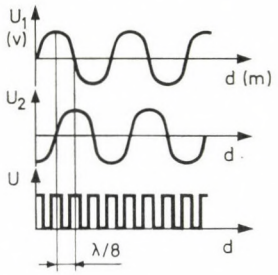

Fig. 5.

polarized light beam being perpendicular to each other, thus the signals produced by the photodetectors and proportional with the intensity of the incident light differ from each other by 90° (Fig. 5). The signals detected so are processed electronically and thus a direction-dependent counting of the interference stripes is enabled with an accuracy of 1/4 period [8].

The relative motion d of the corner cube in a direction being parallel with the incident light beams causes a change in the length of the optical path $4d$. The change can be measured by means of the electronic transformation in units of $\lambda/4$ (λ is the wave-length of the light), i.e.:

$$d = n\frac{\lambda}{16} \quad (n = 0, \pm 1, \pm 2, \ldots), \tag{2}$$

using which the operational equation (1) gets the form:

$$\sin\varphi = n\frac{\lambda}{16r} \qquad (n = 0, \pm 1, \pm 2, \ldots). \tag{3}$$

In the measuring range of the interferometric level trier (about ± 30 min) it can be supposed that

$$\sin\varphi \cong \varphi\,. \tag{4}$$

As the error in case of end deflection is only:

$$\Delta\varphi\Big|_{\varphi=30\,\text{min}} = 0.024 \text{ secs of arc} \tag{5}$$

the operational equation will be:

$$\varphi = n\frac{\lambda}{16r}. \tag{6}$$

By substituting $n = 1$, $\lambda = 0.63$ μm and $r \approx 63$ cm, the resolution power of the angle measurements will be:

$$f = 0.012 \text{ secs of arc}. \tag{7}$$

When the interference stripes are counted electronically, the error due to the digital output ($\Delta n = \pm 1$) is:

$$\Delta\varphi_a = 0.025 \text{ secs of arc}. \tag{8}$$

The sources of regular errors at the interferometric level trier and their effect on the angular measurements are summarized in Table I. The error due to incorrect adjustment is according to this table:

$$\Delta\varphi_j = \sum_{i=1}^{6} \Delta\varphi_i = 0.015 \text{ secs of arc} \tag{9}$$

in the whole operational range.

It follows from operational equation (6) that the incorrect determination of the distance of the edge prisms causes an error of the following value:

$$\Delta\varphi_r = n\frac{\lambda}{16r^2}\cdot\Delta r. \tag{10}$$

In order to reach $\Delta\varphi_r < 0.01$ sec of arc, the distance between the optical centres of the corner cubes must be determined with an accuracy of

$$r = 1.7 \ \mu\text{m}.$$

A direct measurement of a distance with such an accuracy is impossible, hence an other method must be looked for, i.e. the instrument has to be calibrated with known angular values. As the angle measuring interferometer has an operational range of 1° and the output of the interferometer as well as the tilt

Table I

The source of the regular error	Value of the regular error		
Inaccuracy of the wave length	$\Delta\varphi = 5 \cdot 10^{-11}$ mm	$\Delta\varphi = \frac{n}{16r}\Delta\lambda$	$\Delta\varphi_1 = 3 \cdot 10^{-4}$ sec
Non-parallel incident light beams on the rotating part	$v = 120$ sec	$\Delta\varphi = v^2 \frac{\tan\varphi}{2}$	$\Delta\varphi_2 = 6 \cdot 10^{-4}$ sec
Non-perpendicularity of the rotation axis and the incident beam	$\eta = 60$ sec	$\Delta\varphi = \eta^2 \frac{\tan\varphi}{2}$	$\Delta\varphi_3 = 1.5 \cdot 10^{-4}$ sec
Different heights of the corner cubes	$\Delta h = 0.1$ mm	$\Delta\varphi = \frac{\Delta h \cdot 16\mu\left(\frac{\varphi^2}{2\mu} - \frac{\varphi^2}{2\mu^2}\right)f}{\lambda}$	$\Delta\varphi_4 = 1.5 \cdot 10^{-3}$ sec
Different refractivity of the corner cubes	$\Delta\mu = 5 \cdot 10^{-4}$	$\Delta\varphi = \frac{\Delta\mu \cdot 8h\varphi^2 \cdot f}{\lambda \cdot \mu^2}$	$\Delta\varphi_5 = 5.2 \cdot 10^{-4}$ sec
The corner cubes are of different	$\alpha = 30$ sec	$\Delta\varphi = \frac{\alpha \cdot 16 \cdot h \cdot \varphi \cdot (\mu - 1) \cdot f}{\mu \cdot \lambda}$	$\Delta\varphi_6 = 1.2 \cdot 10^{-2}$ sec

In this Table

$n = 3 \cdot 10^5$	the counter gets n impulses in the complete range,
$r = 63$ cm	the distance of the corner cubes,
$\lambda = 0.63$ μm	the wave length of the He—Ne laser,
$\varrho = 1°$	range of the level trier,
$\mu = 1.5$	refractivity index of the corner cube,
$f = 0.012$	resolution power of the interferometer,
$h = 5$ cm	height of the corner cube.

of the arm can be supposed as linear within the error limits given by Eq. 5, it is sufficient to produce an angular rotation of ± 30 mins of arc with respect to the central position. As no suitable detector has been at our disposal, we only give the method usable for the calibration.

The simplest calibration method can be made by means of an autocollimator. A mirror is mounted on the moving arm of the level trier as shown

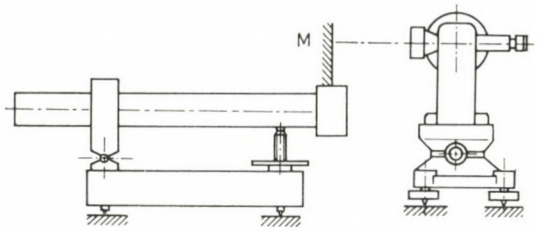

Fig. 6.

in Fig. 6 and the autocollimator picture in the infinite is pointed with a telescope. Then the telescope is rotated around its horizontal axis both in positive and negative directions by 30 mins of arc. In both cases the autocollimator picture is set by the dipping of the balance arm. If the balance arm is moved the optical path and together with it, the order of the interference changes, and the stripe transits are detected by the electronic instrument.

During a dip of 1°, the counter counts about $n = 3 \cdot 10^5$ impulses; the ratio of these two values yields the resolution power of the instrument ($f = 0.012$ secs of arc).

The error of the angle measurement with the autocollimator method is about 0.5 secs of arc which value divided by the number of impulses ($n \approx \approx 3 \cdot 10^5$) yields the error of the resolution power of the interferometer due to the calibration method

$$\Delta\varphi_{\text{res}} = 1.6 \cdot 10^{-6} \text{ secs of arc}. \tag{11}$$

The error of the resolution power due to the incorrect adjustment is:

$$\Delta\varphi_{\text{adj}} = \frac{\Delta\varphi_j}{n} = 5 \cdot 10^{-8} \text{ sec of arc}. \tag{12}$$

The sum of the two regular errors is:

$$\Delta\varphi_{\text{reg}} = \Delta\varphi_{\text{res}} + \Delta\varphi'_{\text{adj}} \cong 1.7 \cdot 10^{-6} \text{ sec of arc}.$$

The accuracy of the interferometric level trier can be obtained from the sum of the errors analyzed hitherto:

$$\delta\varphi = n \cdot \Delta\varphi_{\text{reg}} + \Delta\varphi_{\text{dig}}. \tag{13}$$

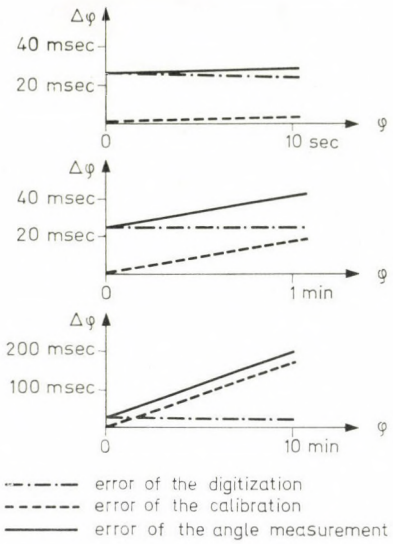

Fig. 7.

Thus, the accuracy of the instrument contains a term independent from the measuring range ($\Delta\varphi_{dig}$) and an other depending on it ($n\Delta\varphi_{reg}$).

Figure 7 shows the error function described by Eq. 13 in different measuring ranges. It can be seen that in case of small (around 10 secs of arc) angles the error of the digital values plays the greater role, while in a greater range the error due to $\Delta\varphi_{reg}$ a more and more important role, meanly in consequence of the increasing influence of the inaccuracy of the calibration.

It can be concluded that the accuracy of the level trier has been significantly increased, therefore this instrument is now suitable to solve problems with higher accuracy requirements in case of laboratory measurements.

REFERENCES

1. TÁRCZY-HORNOCH, A.: Egy tanszéki műhely a műszerellátás szolgálatában (A university workshop in the service of instrument supply). *Bányászai Lapok*, 10 (1955), 195—205.
2. DELMONTE, R.: Un metodo interferenciale per la taratura delle livelle. *Bulle in Geodésique*, 1949, 73—77.
3. KANNGIESSER, E.—SCHUHR, W.: Nacheichung eines Hannoverschen Libellenprüfers. *Allgemeine Vermessungsnachrichten*, 33 (1976), 173—175.
4. INCZÉDY, J.: Libellamérleg vizsgálata Michelson-interferométerrel (Checking of a level trier with Michelson-interferometer). *Geodézia és Kartográfia*, 29 (1977), 332—334.
5. MARZOLF, J. G.: Angle Measuring Interferometer. *Review of Scientific Instruments*, 35 (1964), 1212—1215.
6. DEBLER, E.: Winkelmessungen mit Laser-Interferometern, Mehrfachreflexionen und Dreirosetten-Meßverfahren. PTB — Bericht Me-8. Oktober, 1975.
7. LA 3000 Universal Längenmess-System. Technical Manual 1977.
8. PECK, E. R.—OBETZ, S. W.: Wave length or Length Measurement by Reversible Fringe Couting. *Journal of the Optical Society of America*, 43 (1953), 505—509.

ИНТЕРФЕРОМЕТРИЧЕСКИЙ УГЛОМЕР, ДЕЙСТВУЮЩИЙ В МАЛОМ ИНТЕРВАЛЕ

Я. ИНЦЕДИ—К. КРАУС

РЕЗЮМЕ

В статье описывается интерферометрический прибор для измерения углов, действующий в малом интервале (примерно 1°).

Описывается принцип действия инструмента, который можно считать модификацией интерферометра Майкелсона. Рассматриваются критерии точности при сборке интерферометра и достижимая точность измерений углов этим инструментом.

Acta Geodaet., Geophys. et Montanist. Acad. Sci. Hung. Tomus 16 (2—4), pp. 319—332 (1981)

DAS PRÜFEN DER KIPPACHSEN VON THEODOLITEN

A. ORBÁN

GEODÄTISCHES UND GEOPHYSIKALISCHES FORSCHUNGSINSTITUT DER UNGARISCHEN AKADEMIE DER WISSENSCHAFTEN, SOPRON

Die Prüfung der Kippachse des Theodolits hat in erster Reihe nicht für die Geodäsie, sondern vor allem für die Instrumententechnik eine große Bedeutung. Die Änderung der Kippachsenlage kann nämlich Ursprung mehrerer anderer Instrumentenfehler sein.

Nach deren Erörterung werden weitere Bemerkungen hinsichtlich der Wirkung des Kippachsenfehlers auf die horizontale Winkelmessung und Punktablotung gemacht. Die Wirkung des Kollimationsfehlers und des Stehachsenfehlers auf die Prüfung der Kippachse wird eingehend erörtert. Die zweckmäßigsten Prüfmethoden und Prüfinstrumente werden besprochen (Justierkollimator).

In diesem Zusammenhang wird auf einige in der Fachliteratur vorkommende Fehlbemerkungen hingewiesen. Zum Schluß werden die mit Reitlibelle durchgeführten Prüfungen der Kippachse und die Kritik dieser Methode angeschnitten.

Einleitung

Der Kippachsenfehler von Theodoliten kann — wie bekannt — durch das Messen in zwei Fernrohrlagen eliminiert werden. Deswegen ist die Kippachsenprüfung in geodätischer Hinsicht hauptsächlich nur dann erforderlich, wenn die Messungen aus irgendeinem Grund, sei es aus Zeit- oder Platzmangel, oder eventuell wegen der Bauart des Meßgerätes nur in der einen Fernrohrlage durchgeführt werden können.

Hingegen gehört bei der *Erzeugung oder Reparaturen* von Theodoliten die Kippachsenprüfung zu den wesentlichsten instrumentellen Untersuchungen; es empfiehlt sich sogar, sie in der Reihenfolge der Untersuchungen unter die ersten zu setzen. Der Grund hierfür liegt darin, daß bei den modernen Theodoliten der Kippachsenfehler mehrere andere Instrumentenfehler nach sich ziehen kann. Als solche wären zu erwähnen: Rektifikationsfehler der Alhidadenlibelle, Vergrößerungs- und Schärfefehler der Ableseeinrichtung, Fadenkreuzschiefe im Fernrohr, Projizierungsfehler des optischen Lotes usw. Die Eliminierung dieser Fehler vor der Prüfung der Kippachsen kann sich sogar als eine überflüssige Arbeit erweisen, da ja gegebenenfalls diese Fehler durch die Rektifikation der Kippachse ev. automatisch verschwinden können.

Bei der Untersuchung und der Beseitigung des Kippachsenfehlers ist es durchaus nicht immer nötig, den effektiven Wert der Schräglage zu kennen. Oft genügt die Kenntnis schon jener Wirkung, welche von der Schrägheit auf die horizontale Winkelmessung oder das Herabloten eines hochgelegenen Punktes ausgeübt wird. In solchen Fällen muß die Rektifizierung mit schrittweiser Annäherung solange fortgesetzt werden, bis der Fehlereinfluß erlöscht.

Die Bestimmung des *numerischen Wertes* des Kippachsenfehlers wird in erster Linie nur zur Kontrolle der Konstruktion benötigt, wenn man sich über jene Veränderungen zu informieren wünscht, die sich im späteren Gebrauch an der Kippachse einstellen werden. Die bekannteren Prüfmethoden sind hierbei folgende: Untersuchung durch horizontales Winkelmessen oder Punkt-Herablotung, Kollimator-Prüfung usw. (Die Prüfung durch Visieren eines mechanischen Lotes ist nur zum Nachweisen des Vorhandenseins eines Kippachsenfehlers geeignet.)

Sehr wesentliche Gesichtspunkte bei der Wahl der besten Untersuchungsmethode bestehen darin, daß der Kippachsenfehler möglichst von der Wirkung anderer Instrumentenfehler getrennt werden könne, ferner, daß das Messen und das Auswerten einfach sei.

Für den Geodäten scheint es am nächstliegendsten zu sein, die Kippachsenprüfung mit der horizontalen Winkelmessung zu verrichten, da hierbei die Untersuchung ohne irgendwelche Hilfseinrichtungen mit dem zu prüfenden Theodolit selbst durchgeführt werden kann. Deswegen soll diese Methode hier an erster Stelle behandelt werden.

Der Einfluß des Kippachsenfehlers auf das horizontale Winkelmessen

Ist i der Wert des Kippachsenfehlers, dann erhält man den Wert des bei der horizontalen Winkelmessung begangenen Ablesungsfehlers δ_h auf Grund der aus der sphärischen Geometrie bekannten Ableitung aus der Formel

$$\delta_h = i \operatorname{tg} \alpha,$$

worin α der Höhenwinkel der Ziellinie ist.

Obzwar nun diese Beziehung aus der Fachliteratur [1] allgemein bekannt ist, erachten wir es — mit Rücksicht auf unsere späteren Darlegungen — doch für wichtig, hier folgendes festzulegen:

— Der Fehler δ_h erscheint in der Horizontalebene.
— Die Formel gilt nur dann, wenn die Stehachse des Theodolits während des Messens vertikal ist (mithin die Kippachsenneigung nicht durch das Schiefstehen der Stehachse verursacht wird).
— Schließlich hat die Formel nur Geltung, wenn die Fernrohrziellinie normal zur Kippachse ist, d. h. der Theodolit keinen Kollimationsfehler hat.

Ein vorhandener Kollimationsfehler kann sehr störend sein, da es — ohne seinen numerischen Wert vorher zu kennen — sehr schwer fallen dürfte zu sagen, in welchem Ausmaß der Ablesefehler am Horizontalkreis von der Kollimation, beziehungsweise von dem Kippachsenfehler abhängig ist. Wert und Vorzeichen der beiden Fehler können sich sogar so ergeben, daß sie einander bei gewissen Höhenwinkeln löschen.

Herablotung des Höhenpunktes auf die Horizontalebene

Der in Winkelmaßeinheiten ausgedrückte Wert des Fehlers, der beim Herabloten des Punktes auf die Horizontalebene begangen wird, stimmt seiner Natur gemäß mit jenem Fehler überein, den der Kippachsenfehler auf die Horizontalkreisablesung ausübt. Mit der Projiziermethode kann der Fehler δ_h sehr einfach abgeleitet werden.

In Abb. 1 sei angenommen, daß der Schnittpunkt der Kippachse f und des Fernrohrs t des zu prüfenden Theodolits auf den Punkt A entfällt, und daß das Fernrohr keinen Kollimationsfehler hat. Das Herabloten des als natürliches Signal benützten Höhenpunktes P auf die Horizontalebene kann auf zweifache Weise erfolgen: Bei dem Herabloten wird das Fernrohr zunächst um eine gedachte horizontale Kippachse verdreht (PB ist die Projiziergerade), danach aber um eine Kippachse verdreht, die um den Winkel i zur Horizontalen geneigt ist (Projiziergerade ist PC). Wenn kein Kollimationsfehler vorliegt, dann ist die Fernrohrziellinie normal zur Kippachse. Demzufolge ist von den beiden, aus dem Punkt P ausgehenden Projizierlinien PB normal auf die horizontale Kippachse, PC aber normal auf die um i geneigte Kippachse. Somit ist auch der von den beiden Geraden am Punkt P eingeschlossene Winkel gleich i.

Nach dem Projizieren durch Verdrehung um die gedachte horizontale Kippachse bzw. um die i-geneigte Kippachse schließen die Ziellinien der beiden in *horizontaler Stellung befindlichen Fernrohre* miteinander einen Winkel δ_h ein, der mit jener, vom Kippachsenfehler i auf die Horizontalkreis-Ablesung ausgeübten Wirkung übereinstimmt.

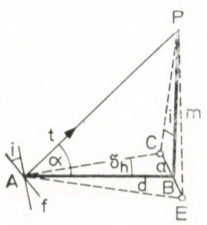

Abb. 1

Die Berechnung des Winkels δ_h (Abb. 1) lautet wie folgt:

Aus $$ABC\triangle \quad \delta_h'' = \varrho'' \frac{a}{d}. \tag{1}$$

Aus $$ABP\triangle \quad d = \frac{m}{\operatorname{tg} \alpha}. \tag{2}$$

Aus $$CBP\triangle \quad a = \frac{i \cdot m}{\varrho}. \tag{3}$$

Wird (2) und (3) in (1) eingesetzt, so erhält man:

$$\delta_h = i \operatorname{tg} \alpha .$$

Ist der Projizierwinkel $\alpha = 45°$, dann ist die Wirkung des Kippachsenfehlers auf die Horizontalkreisablesung gleich dem Schrägheitswert der Kippachse. Diese bekannte Feststellung trifft jedoch nur dann zu, wenn die Fernrohrziellinie normal zur Kippachse ist, mithin kein Kollimationsfehler vorliegt. Die vom Kollimationsfehler (c) auf die Horizontalkreisablesung ausgeübte Wirkung δ_k ändert sich nämlich — wie bekannt — gleichfalls als Funktion des Höhenwinkels, laut Beziehung

$$\delta_k = \frac{c}{\cos \alpha}$$

Beim Herabloten des Punktes auf die Horizontalebene weicht die nur mit Kollimation behaftete Ziellinie in beiden Fernrohrlagen mit dem gleichgroßen absoluten Winkelwert, doch mit entgegengesetztem Vorzeichen von der richtigen Projizierrichtung ab. Deswegen besteht zwischen den beiden Projektionen von P in der Horizontalebene *selbst dann eine lineare Abweichung, wenn die Kippachse horizontal ist.* Ist auch die Kippachse schief, dann muß man, um die Fehler zu trennen, den Kollimationsfehler bei horizontaler Fernrohrlage gesondert bestimmen, (wobei hier die Wirkung der Kippachsenneigung gleich null ist); danach aber muß ihre Wirkung rechnerisch berücksichtigt werden, indem man es an die Formel des Kippachsenfehlers anknüpft ([2] S. 142., Formel 87).

Projizierung von gleichem Höhen- und Tiefenwinkel

Ein, mit einem Kollimationsfehler c behaftetes Fernrohr bewegt sich beim Drehen um die Kippachse auf einem Kegelmantel (Abb. 2). Die Ziellinie des Fernrohrs beschreibt dabei in der zur Kippachse parallelen Vertikalebene

eine Hyperbel. Die unter gleichem Höhen- und Tiefenwinkel sichtbaren Punkte der Hyperbel P und P' fallen (in beiden Fernrohrlagen) in *eine* Vertikale, vorausgesetzt, daß die Kippachse horizontal war.

Wenn also das Herabloten in der Weise erfolgt, daß der zu projizierende Punkt eben so hoch über der Horizontalen zu sehen ist, wie der projizierte

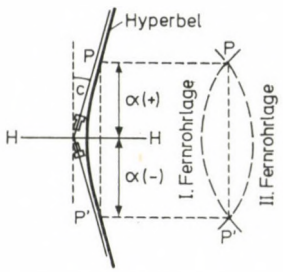

Abb. 2

Punkt (P') darunter liegt, dann ist die Projizierung frei von jeglicher Kollimationswirkung. (Der zu projizierende und der projizierte Punkt liegen in diesem Falle in gleichem Abstand von der vertikalen Symmetrieachse der Hyperbel.) (Abb. 3a)

Liegt aber außer dem Kollimationsfehler auch noch ein Kippachsenfehler vor, dann steht auch die vorhin noch senkrecht angenommene Symmetrieachse der Hyperbel schräge, und die projizierten Punkte gleichen Höhen- und Tiefenwinkels entfallen nicht mehr auf *eine* Vertikale. Doch selbst in diesem Falle wird die Wirkung der Kippachsenneigung bei der Projizierung durch den Kollimationsfehler nicht verzerrt, da der zu projizierende und der projizierte Punkt P und P' von der Gerade a', b' in gleichem Abstand bleiben. Das ist so vorzustellen, als ob sich die Punkte P und P' auf der die wirkliche Schrägheit der Kippachse angebenden Gerade a' b' befänden (Abb. 3b).

Bei einer derartigen Punktherablotung kann das Ausscheiden des Kollimationsfehlers auch auf Grund der aus der sphärischen Geometrie bekannten Ableitung des Kollimations-Effektes erläutert werden.

Demgemäß wird die Wirkung des Kollimationsfehlers (c) auf den nur in einer Fernrohrlage gemessenen Horizontalwinkel $\Delta\delta_k$ durch die Formel

$$\Delta\delta_k = \frac{c}{\cos \alpha_1} - \frac{c}{\cos \alpha_2}$$

ausgedrückt, worin α_1 und α_2 die Höhenwinkel der angezielten Punkte bedeuten. Diese Formel ist im ausländischen Fachschrifttum selten anzutreffen [2, S. 140]; in den ungarischen Lehrbüchern aber ist sie sogar an zwei Stellen

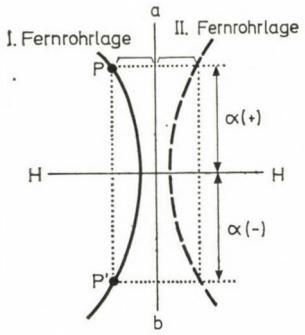

Abb. 3a

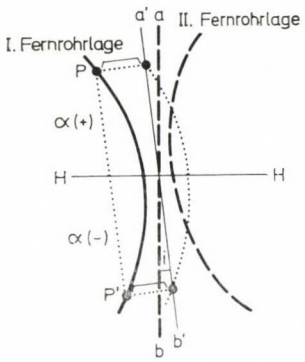

Abb. 3b

angeführt. Die in [3], (S. 385) dieser Formel beigefügte Erklärung lautet folgendermaßen: »Ist $\alpha_1 = \alpha_2$, mithin der Höhenwinkel der räumlichen Richtungen der Winkelschenkel einander gleich, dann ist $\Delta\delta_k = 0$, d. h. man erhält den gemessenen Winkel fehlerfrei.« Nach der Formelerklärung in [4, I. 287] aber gilt: »Wenn Winkel gemessen werden, und dabei die beiden Richtungen nicht unter dem gleichen Neigungswinkel liegen, dann wird der Wert des gemessenen Winkels falsch sein; und zwar wird der Fehler umso größer, je größer der Unterschied zwischen den Neigungswinkeln ist.«

Beide Erklärungen der Formel bedürfen einer Ergänzung. Es ist nämlich aus den vorhergehenden Erörterungen, wie auch daraus, daß $\cos(-\alpha) = \cos\alpha$ ist, offensichtlich, *daß ein in der einen Fernrohrlage gemessener Horizontalwinkel auch dann frei von Kollimationswirkung ist, wenn die Höhenwinkel der angezielten Punkte die gleichen Werte, aber entgegengesetzte Vorzeichen haben.*

Zu der Formel

$$(c) = \frac{c}{\sin Z_1} - \frac{c}{\sin Z_2},$$

welche in [2], (S. 140) für den Zenitwinkel mitgeteilt ist, wurde folgendes hinzugeführt: »Der Einfluß des Zielachsenfehlers auf den in einer Fernrohrlage gemessenen Winkel ist um so kleiner, je kleiner der Unterschied der beiden Zenitwinkel (Höhenwinkel) ist. Bei gleichen Absolutwerten der Zenitwinkel ist er gleich Null.«

Es ist jedoch klar, daß auch diese Formelerklärung einer Ergänzung bedarf: Die erwähnte Wirkung ist nämlich auch dann gleich Null, wenn

$$Z_2 = 180° - Z_1 \text{ ist}.$$

Die Wichtigkeit dieser Ergänzungen ist u. a. gerade zum Verständnis des für die Prüfung des Kippachsenfehlers gebauten, und später noch näher erörterten Justierkollimators erforderlich.

Die Prüfeinrichtung besteht aus zwei Kollimatoren, die zur Horizontalen um den gleichen Höhen- und Tiefenwinkel geneigt sind und vor welchen der zu prüfende Theodolit aufgestellt wird. Im Gesichtsfeld des oberen Kollimators ist ein einfaches Fadenkreuz, in dem unteren aber eine Horizontalskala zu sehen.

Das Prüfen besteht nun darin, daß der Mittelpunkt des oberen, einfachen Fadenkreuzes in zwei Fernrohrlagen auf die untere Kollimatorskala herabprojiziert wird. Fallen dabei die beiden Projizierungen auf verschiedene Skalenteilungen, dann ist die Kippachse schief. Der Wert dieser Schrägheit kann an einer geeichten Skala auch direkt in Winkelmaßeinheiten bestimmt werden.

Diese einfache Prüfmethode ist in den allgemein gebrauchten Lehrbüchern nicht beschrieben, trotzdem sie — nach den Informationen aus den Geräteprospekten — von den Werken für geodätischen Gerätebau in weitem Umfang benützt wird. Bisher gelang es nur in einer Dissertation [5] von OCHSENHIRT aus 1962 eine kurze Beschreibung der Vorzüge dieser Methode zu finden, und an gleicher Stelle wird auch an einem Beispiel aufgezeigt, auf welche Weise der Wert des Kippachsenfehlers numerisch bestimmt werden kann. Letzterer bedarf aber einer Korrektur und einer Ergänzung. Und dies gab den Anlaß dazu, daß wir uns mit der Theorie dieser Methode eingehender befassen sollen.

Die Vorzüge dieser Prüfmethode sind:

a) Im Gegensatz zu mehreren anderen Prüfmethoden ist hier keine Winkel- und Entfernungsmessung nötig. (Besonders bei Labormessungen, die in einem relativ kleinen Raum durchgeführt werden müssen, kann das Prüfergebnis durch die Fehler der Winkel- und Entfernungsmessung sehr ungenau werden.)

b) Wegen des Anzielens der Kollimatoren ist das Prüfergebnis unabhängig vom Fehler der Fernrohrexzentrizität und der Negativlinse-Führung. (Die visierten Signale liegen im Unendlichen.)

c) Wegen der bei gleichen Höhen- und Tiefenwinkel erfolgenden Herablotung ist diese Methode frei von jeglichem Kollimationsfehlereinfluß.

d) Bei der Prüfung erübrigt es sich, die Theodolit-Stehachse genau vertikal einzustellen.

Prüfen wir nun zuerst, welcher Fehler bei der Bestimmung des Kippachsenfehlers entsteht, wenn während der Herablotung in zwei Fernrohrlagen die Stehachse des Theodolits nicht vertikal ist.

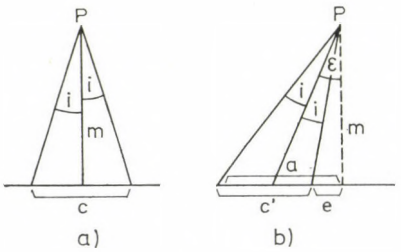

Abb. 4

In Abb. 4a ist die Projizierung des Punktes P mit Hilfe eines Theodolits von vertikaler Stehachse in zwei Fernrohrlagen durchgeführt worden. Der Abstand der beiden projizierten Punkte ist c. Abb. 4b zeigt die mit einer Schiefe ε der Stehachse erfolgende Projizierung. Hier ist der Abstand der projizierten Punkte c'. Berechnen wir nun jenen Projizierungsfehler ($\Delta c = c' - c$), der aus dem Stehachsenfehler oder aus dem gleichgroßen zusätzlichen Kippachsenfehler erwächst.

Auf Grund von Abb. 4a ist $c = 2m \operatorname{tg} i$ (worin m die Höhe des Punktes P, i aber den Kippachsenfehler bedeutet).

Auf Grund von Abb. 4b ist:

$$a = m \operatorname{tg} (\varepsilon + i); \qquad e = m \operatorname{tg} (\varepsilon - i)$$

$$c' = a - e = m[\operatorname{tg} (\varepsilon + i) - \operatorname{tg} (\varepsilon - i)]$$

$$\Delta c = c' - c = m[\operatorname{tg} (\varepsilon + i) - \operatorname{tg} (\varepsilon - i) - 2 \operatorname{tg} i].$$

Ohne eine eigene Abbildung sei angenommen, daß der zu prüfende Theodolit im Abstand d von der vertikalen Projizierungsebene stehe. Von dieser Entfernung erscheint der Punkt P unter dem Höhenwinkel α, und der Abstand Δc unter dem parallaktischen Winkel $\Delta_h'' = \varrho'' (\Delta c/d)$. Der Winkel Δ_h'', d. h. die auf die Winkelmessung bezogene Wirkung des *doppelten* Wertes des zusätzlichen Kippachsenfehlers, ist auf dem Horizontalkreis des Theodolits meßbar.

Wird die für Δc erhaltene Gleichung in die Formel Δ_h'' eingesetzt und berücksichtigt, daß $\operatorname{tg} \alpha = m/d$ ist, dann erhält man:

$$\Delta_h'' = \varrho'' \operatorname{tg} \alpha \left[\operatorname{tg} (\varepsilon + i) - \operatorname{tg} (\varepsilon - i) - 2 \operatorname{tg} i\right].$$

Der Fehler (Δi) der Bestimmung des *einfachen* Kippachsenfehlers i lautet auf Grund der bekannten Beziehung ($\delta_h = i \operatorname{tg} \alpha$):

$$\Delta i = \frac{\Delta_h}{2 \operatorname{tg} \alpha} = \varrho'' \frac{\operatorname{tg} (\varepsilon + i) - \operatorname{tg} (\varepsilon - i) - 2 \operatorname{tg} i}{2}.$$

Es seien $\varepsilon = 7°$; $i = 60''$; dann ist $\Delta i = 0{,}9''$.

Wenn also die Stehachse des Theodolits um 7° schief ist, und der Kippachsenfehler $60''$ beträgt, dann ist die Bestimmung des Kippachsenfehlers nur mit einem Fehler kleiner als $1''$ behaftet.

Diese Darlegungen gelten auch für die mit dem Kollimator erfolgende Punktherablotung, wenn der Punkt in die horizontale Ebene projiziert wird.

Es stellt sich ferner noch die Frage, wie groß soll der Neigungswinkel der Kollimatoren zum Horizontalen sein. Diesbezüglich wird von OCHSENHIRT 45° vorgeschlagen. Bei den sog. Justierkollimatoren der Ungarischen Optischen Werke (MOM) werden 30° benützt, während im sowjetischen GOST Standard [6] — obzwar diese Prüfung auf der horizontalen Winkelmessung beruht — Winkel nicht kleiner als 20° vorgeschrieben werden.

Der Kippachsenfehler kann prinzipiell mit Kollimatorpaaren von vielerlei Neigungswinkel bestimmt werden. Bei kleinerem Neigungswinkel ist das Prüfergebnis weniger genau; bei großem Neigungswinkel aber ist das Messen sehr unbequem; bei manchen Theodolittypen sogar unmöglich.

Die Verwendung von bevorzugten Neigungswinkeln vereinfacht aber den Untersuchungsgang. Ein solcher Neigungswinkel ist beispielsweise der bereits erwähnte, und auch in [5] mitgeteilte Winkel $+45°/-45°$, bei welchem der vierfache Wert der Kippachsenschräge am Horizontalkreis des Theodolits direkt gemessen werden kann.

Betreffs des anderen bevorzugten Neigungswinkels $+30/-30°$, der auch bei den Justierkollimatoren, Bauart MOM Verwendung findet, konnten wir im Fachschrifttum keine Hinweise finden.

Dieser Neigungswinkel wird auf Grund unserer eigenen Nachforschungen deswegen bevorzugt, da das Dreieck APB — wie es auf Abb. 5 zu erkennen ist — gleichseitig ist und deshalb der Abstand 2a zwischen den Punkten C und B sowohl von P, wie auch von A aus unter dem gleichen Winkel erscheint. Demzufolge kann der in Punkt P erscheinende Wert i der Kippachsenschräge aus Punkt A einfach bestimmt werden ($i = \varphi$).

Diese Darlegungen gelten auch für Prüfungen, die mit dem Herabloten von natürlichen Punktsignalen durchgeführt werden, doch ist es dann wesent-

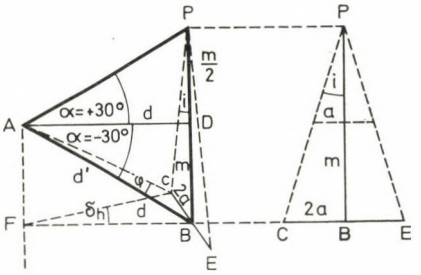

Abb. 5

lich, daß dabei die Gerade d, welche den bei Punkt A befindlichen Winkel 2α halbiert, normal auf die vertikale Projektionsebene (in Punkt D) sei. Bei einer solchen Anordnung kann auf Grund von Abb. 5 sogar errechnet werden, mit welchem Höhen- oder Tiefenwinkel man projizieren muß damit i gleich φ werde.

$$\varphi'' = \varrho'' \frac{2a}{d'} \tag{4}$$

$$i'' = \varrho'' \frac{2a}{m} \tag{5}$$

$$m = 2\mathrm{d}\,\mathrm{tg}\,\alpha \tag{6}$$

$$d' = \frac{d}{\cos(-\alpha)} = \frac{d}{\cos\alpha}\,. \tag{7}$$

Aus (4) und (5) ist zu ersehen, daß i'' dann gleich φ'' wird, wenn d' gleich m ist. Werden die mit den Gleichungen (6) und (7) gegebenen Werte m und d' einander gleichgesetzt, und die so erhaltenen Gleichungen nach α aufgelöst, so erhält man:

$$2\,\mathrm{tg}\,\alpha = \frac{1}{\cos\alpha}$$

$$\frac{\sin\alpha}{\cos\alpha} = \frac{1}{2\cos\alpha}$$

$$\sin\alpha = \frac{1}{2}$$

$$\alpha = 30°.$$

Demnach sind die Winkel i und φ dann einander gleich, wenn $\alpha = 30°$ ist.

Der Winkel φ ist in einer schrägen Ebene gelegen, sodaß er am Horizontalkreis des Theodolits direkt nicht gemessen werden kann. Der Horizontalkreis liegt in der durch den Punkt A gelegten Ebene. (In Abb. 5 zu sich parallel in den Punkt F verschoben.) Am Horizontalkreis ist anstatt φ der zwischen den durch die Punkte C und B gelegten, einander in AF schneidenden Vertikalebenen gebildete Winkel δ_h meßbar.

Wie verhält sich nun der Wert δ_h zu dem in einer schrägen Ebene erscheinenden φ? Auf Grund von Abb. 5 ist:

$$\delta_h'' = \varrho'' \frac{2a}{d}; \quad \varphi = \varrho'' \frac{2a}{d'}; \quad \frac{\delta_h''}{\varphi''} = \frac{d'}{d}$$

$$\varphi'' = \delta_h'' \frac{d}{d'} \qquad \frac{d}{d'} = \cos \alpha$$

$$\varphi'' = \delta_h'' \cos \alpha .$$

In der Horizontalebene wird ein größerer Winkel gemessen, als in der schrägen Ebene (Punkt F liegt näher der Entfernung $2a$ als Punkt A). Die Prüfmethode, welche die $+/-30°$ Projizierung benützt, ist also gegenüber der $+/-45°$ Projizierung im Nachteil, da hier die Kippachsenschrägheit am Horizontalkreis des Theodoliten direkt nicht gemessen werden kann.

Anders verhält es sich, wenn in der Projizierungsrichtung $-30°$ ein mit einer mm-Skala, oder mit einem Okularmikrometer versehener Meßkollimator von bekannter Brennweite steht. Mit dem Meßkollimator können Winkel auch in schräger Ebene gemessen werden. Somit kann der, der Kippachsenschrägheit gleiche Winkel i direkt bestimmt werden.

Auf Grund des Vorhergehenden kann betreffs der Kippachsenprüfung folgendes festgestellt werden:

— Wird der parallaktische Winkel zwischen den in zwei Fernrohrlagen herabgeloteten Punkten am *Horizontalkreis des zu prüfenden Theodolits*, oder am Horizontalkreis eines Hilfstheodoliten gemessen, welch letzterer als Kollimator gegenüber dem zu prüfenden Theodoliten aufgestellt ist, dann muß der Projizierwinkel $+45°$ und $-45°$ sein.

— Wird der in einer *schrägen Ebene* erscheinende Winkel zwischen den in zwei Fernrohrlagen herabgeloteten Punkten mit dem Meßkollimator gemessen, dann muß der Projizierwinkel $+30°$ und $-30°$ sein.

— Von Ochsenhirt [5] wurde eine Projizierung von $+45°$ und $-45°$ angewendet. Der Winkel zwischen den beiden herabgeloteten Punkten wurde von ihm in schräger Ebene gemessen (besser gesagt: auf Grund der im Kollimator vorgesehenen mm-Skala und der bekannten Brennweite des Kollimators berechnet). Doch im Sinne des Vorhergesagten erhielt er auf diese Weise nicht die richtigen i-Werte, da diese bei der Projizierung von $+45°$ zu $-45°$

in der Horizontalebene erscheinen. Die in der schrägen Ebene ermittelten Werte sind kleiner als die wirklichen Winkelwerte, so daß diese noch durch cos 45° (= 0,707) dividiert werden müssen. Somit sind in [5] die Formeln (69) und (70) unrichtig, und ebenso unrichtig die aus diesen errechneten Werte (Tabelle 44 und 45).

— Um bei der Kippachsenprüfung festzustellen, welches Achsenende höher liegt, kann folgende einfache Methode empfohlen werden: Nach dem Herabloten des Höhenpunktes in zwei Fernrohrlagen beobachtet man, welche Fernrohrstütze aus der Vertikalrichtung gedrückt werden muß, um die Fernrohr-Ziellinie zur Mittellinie der beiden Projizierpunkte hin zu verschieben. Dieses Kippachsenende liegt nämlich höher. Mit dieser Prüfmethode fallen dann alle die zur Kippachsen-Rektifizierung erforderlichen Vorzeichenprobleme automatisch weg.

— Zwischen den horizontalen Winkelwerten, die bei Kippachsenfehler mit Anzielung der Punkte unter verschiedenen Höhenwinkeln in zwei Fernrohrlagen gemessen wurden, ergibt sich eine von der Größe des Höhenwinkels abhängige, variable Differenz (Scheinbare Kollimationsfehler-Änderung). Dieser Umstand macht darauf aufmerksam, daß es nicht in jedem Falle ratsam ist, selbst bei Theodoliten mit diametraler Ablesung, die Güte der im Gelände durchgeführten Messungen auf Grund der Änderung des Kollimationsfehlers zu kontrollieren und beurteilen.

— Bei Projizierungen, die bei gleichem Höhen- und Tiefenwinkel erfolgen, fällt die Wirkung des Kollimationsfehlers — wie wir sahen — aus. Nicht dasselbe geschieht aber in dem Fall, wenn mit einem mit Kollimations- und Kippachsenfehler behafteten Theodolit Horizontalwinkel durch das Anzielen von unter gleichen Höhen- und Tiefenwinkeln erscheinenden Punkten, in zwei Fernrohrlagen gemessen werden. Der Unterschied der in zwei Fernrohrlagen gemessenen Winkelwerte ist nämlich in der Aufwärts- und Abwärtsrichtung nicht gleich groß. Der Grund hierfür liegt darin, daß die Winkelwerte durch die Kollimationsfehler oben und unten mit dem gleichen Vorzeichen, während durch die Kippachsenfehler mit entgegengesetztem Vorzeichen beeinflußt werden. Die Wirkung der Kollimation wird demnach einmal zum Kippachsenfehler hinzuaddiert, ein andersmal aber von diesem subtrahiert. Demzufolge meldet sich die scheinbare Änderung des Kollimationsfehlers auch bei dem Anzielen von Punkten gleichen Höhen- und Tiefenwinkels.

— Nach der Eliminierung des in der horizontalen Fernrohrlage bestimmbaren wirklichen Kollimationsfehlers müßten eigentlich die scheinbaren Kollimationsfehler der Punkte gleichen Höhen- und Tiefenwinkels einander gleich sein. Bemerkt man trotzdem eine Abweichung, so muß daraus auf einen Taumelfehler der Kippachse, eventuell auf ihre Ovalität gefolgert werden.

Für das Prüfen des Kippachsenfehlers durch Winkelmessung werden in der Fachliteratur im allgemeinen solche Prüfmethoden beschrieben, die nur

mit *einem* Höhenwinkel erfolgen. Eine Prüfung bei nahezu gleichen Höhen- und Tiefenwinkeln wird nur im Standard GOST 20063-74 vorgeschlagen [6], doch auch hier werden die Vorteile dieser Methode nicht dargelegt.

Zur Verminderung der vorher erwähnten Fehler ist es zweckmäßig, die Untersuchungen der Kippachse bei gleichem Höhen- und Tiefenwinkel durchzuführen, und dann aus den erhaltenen Ergebnissen die Mittelwerte zu bilden. Nach unseren Erfahrungen nähern sich die auf diese Weise erzielten Kippachsenfehlerwerte am besten den mit dem Justierkollimator bestimmten Werten. Die Ergebnisse der nur mit den Höhenwinkeln $+\alpha$, oder $-\alpha$ durchgeführten Prüfungen wichen hiervon in Einzelfällen selbst um $10''-15''$ ab. Bezüglich der Größe der Ursachen, welche diese Abweichung bewirken, sei hier folgendes bemerkt: Wenn sich das eine Ende einer 10 cm langen Kippachse beim Drehen im Lager nur um 0,01 mm hebt, dann ändert sich die Kippachsenschrägheit um 20,6″. Durch diese Kippachsenfehler kann beim Anzielen unter einem Höhenwinkel von $\alpha = 30°$ der am Horizontalkreis abgelesene Wert um 12″ falsch sein.

Prüfung mit Reitlibelle

Die Kippachsenschrägheit kann bei einzelnen Theodoliten auch mit der Reitlibelle geprüft werden [7], (S. 154). Nach unseren Erfahrungen aber weicht der auf diese Weise ermittelte Wert der Achsenschiefe gegebenenfalls von den mit anderen Methoden bestimmten Werten ab. Dieser Unterschied kann u. a. auch dadurch verursacht werden, daß die Aufliegefläche der Kippachse im Lager zum Laufring der Reitlibelle nicht parallel ist. Außerdem kann auch das Taumeln der Kippachse und die Ovalität der Achse Abweichungen verursachen. Die erwähnten Fehlerquellen können mit der Reitlibelle so geprüft werden, daß die Libelle bei verschiedenen Größen der Fernrohrneigung auf die Kippachse aufgesetzt wird. Wegen der Unsicherheit des Aufliegens und der völlig nicht vermeidbaren Kreuzungsfehler der Libelle hat aber diese Prüfung an sich keine befriedigende Genauigkeit mehr. Betreffs der Autokollimatorprüfung der Auflagefläche der Reitlibelle ist ein leicht ausführbarer Vorschlag in [8] zu finden. Eine elegante Kippachsenprüfmethode ist noch in [9] beschrieben.

SCHRIFTTUM

1. Jordan, W.—Eggert, O.: Handbuch der Vermessungskunde, Band II. J. B. Metzlersche Verlagsbuchhandlung, 1950.
2. Deumlich, F.: Instrumentenkunde der Vermessungstechnik. VEB Verlag für Bauwesen, Berlin, 1974.
3. Sárdy, A.: Geodéziai alapismeretek I. kötet. (Grundkenntnisse der Geodäsie, Band I. BME Építőmérnöki Kar (Technische Universität, Budapest, Lehrstuhl für Bauingenieure). Tankönyvkiadó, 1977.

4. SÉBOR, J.: Általános geodézia I. (Allgemeine Geodäsie, I.) Mezőgazdasági Kiadó, 1953.
5. OCHENHIRT, H.: Prüfen und Justieren moderner geodätischer Instrumente und Geräte mit Hilfe von Kollimatoren im Laboratorium. Dissertation. Technische Hochschule Hannover, Nr. 19, 1952.
6. GOST 13424-68, 10528-70, 20063-74. Landesstandarde. Sowjetunion.
7. FIALOVSZKY, L.: Geodéziai műszerek (Geodätische Instrumente). Műszaki Könyvkiadó, Budapest, 1979.
8. GÖHLER, H.: Laufringuntersuchung mit Autokollimationsfernrohr. *Vermessungstechnik*, 18 (1970), 59—61.
9. MATTHIAS, H.: Umfassende Behandlung der Theodolitachsenfehler auf vektorieller Grundlage unter spezieller Berücksichtigung der Taumelfehler der Kippachse. Mitteilungen aus dem geodätischen Institut an der Eidgenössischen Technischen Hochschule, Zürich, Nr. 10. 1961.

ПРОВЕРКА ГОРИЗОНТАЛЬНОЙ ОСИ ТЕОДОЛИТОВ

А. ОРБАН

РЕЗЮМЕ

Проверка горизонтальной оси теодолитов имеет значение в первую очередь не с геодезической, а приборостроительной точки зрения, так как изменение положения горизонтальной оси может вызывать некоторые другие виды погрешности инструмента.

Наряду с изложением этих, сделаем дальнейшие замечания по поводу известного влияния ошибки горизонтальной оси на горизонтальные измерения углов и проектирования точек. Подробно рассматриваются влияния коллимационной ошибки и наклона вертикальной оси на проверку горизонтальной оси. Излагается наиболее подходящий метод и прибор (регулировочный коллиматор) для проверки.

В связи с этим обращается внимание на некоторые ошибочные представления, встречающиеся в литературе. Наконец вкратце упоминается проверка горизонтальной оси при помощи накладного уровня и критика этого метода.

Acta Geodaet., Geophys. et Montanist. Acad. Sci. Hung. Tomus 16 (2—4), pp. 333—351 (1981)

THE GEOPHYSICAL OBSERVATORY NEAR NAGYCENK

I. ELECTROMAGNETIC MEASUREMENTS AND PROCESSING OF DATA

A. ÁDÁM—J. VERŐ
DOCTORS OF SCIENCES

J. CZ. MILETITS—L. HOLLÓ—Á. WALLNER
GEODETIC AND GEOPHYSICAL RESEARCH INSTITUTE OF THE HUNGARIAN ACADEMY OF SCIENCES, SOPRON

In the first part of the paper the geological-geophysical structure below the observatory near Nagycenk is reviewed. A detailed analysis is given on the determination of the magneto-telluric sounding curves and on the geoelectric layer sequence. In the second part, earth current (telluric) and magnetic instruments of the observatory are described, and the parameters of the recording summarized. Finally the processing of the data is outlined with an estimation on the reliability of the different parameters and indices on a routine basis. Some effects disturbing the recordings are also reviewed.

Introduction

Since the beginning of the International Geophysical Year (IGY) in mid-1957, earth currents, since 1961, geomagnetic elements have been recorded at the geophysical observatory near Nagycenk in Hungary, situated 15 km to the East from the town Sopron at the Southern shore of the Lake Fertő. A study of the atmospheric electric parameters began in 1960, the ionospheric research with the recording of the absorption of radiowaves in 1966. The present paper reviews earth current and geomagnetic studies carried out in the observatory and supplements earlier descriptions [ÁDÁM and VERŐ, 1958; ÁDÁM et al., 1967]. It contains informations on the geological-geophysical structure, on instrumentation and principles of data processing methods.

Geological and geophysical structure of the observatory site

The crystalline schist mountains of Sopron is thrust into a depth of about 2000 m along a NE—NW striking fault towards SE from Sopron, in the line Balf—Kópháza—Magyarfalva. The deep range beginning here is closed towards E by a high corresponding to the Mihályi gravitational maximum. The crystalline basement has an amphitheater-like structure open towards SW in the vicinity of the village Nagycenk. The observatory lies on the Northern slope of this local deep. The thickness of the sediments is here about

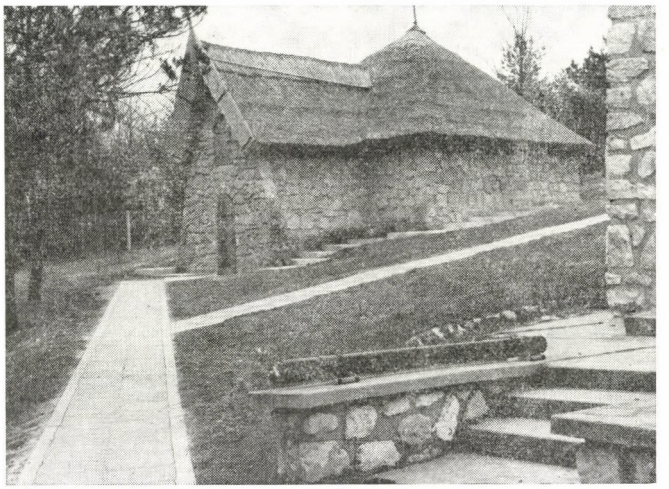

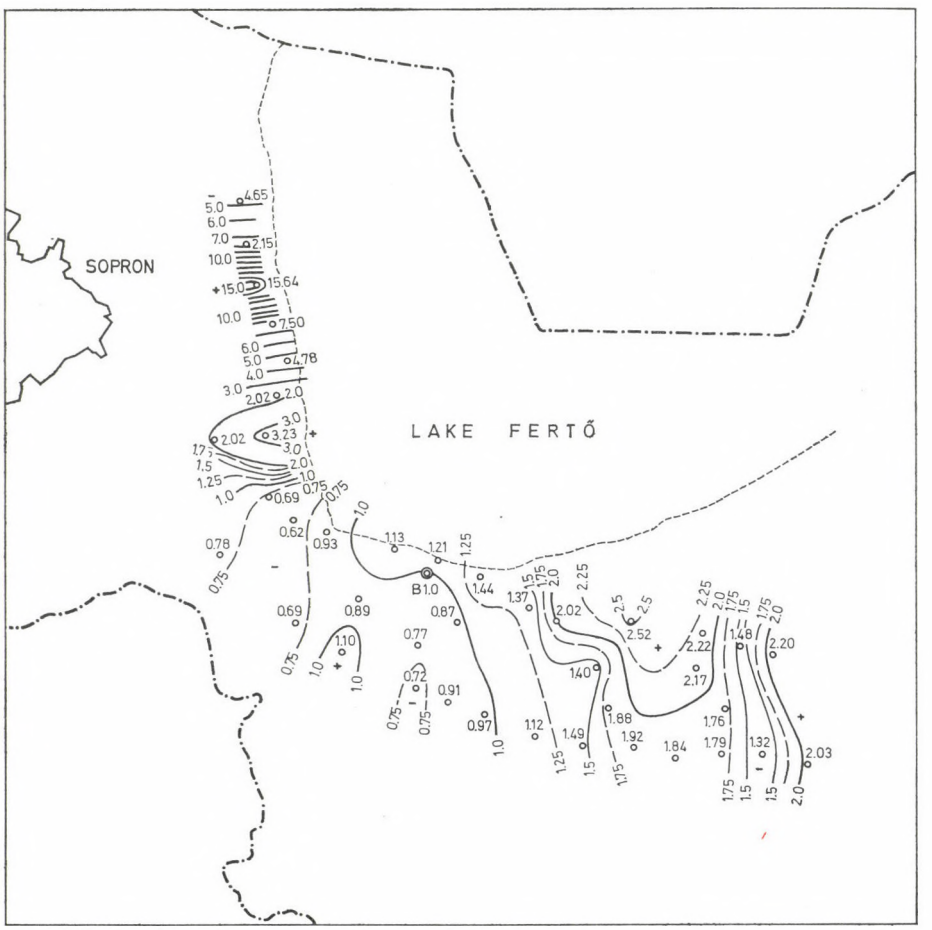

Fig. 1. Telluric isoarea map. = isoarea lines, o measuring point and its area value (area of the relative telluric ellipse)

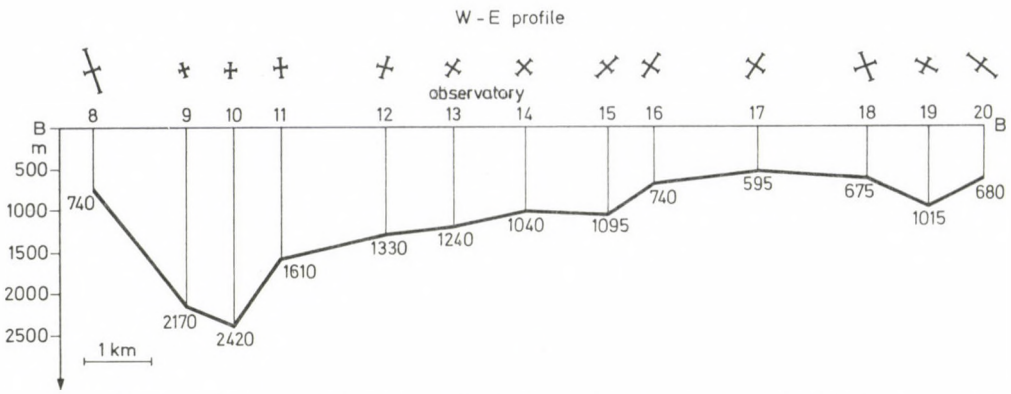

Fig. 2. Basement depths deduced from telluric measurements along a profile S of Lake Fertő with the axes of the relative ellipses

1500 m. The relief of the basement has towards East several deeps and lows etc.

The crystalline basement is in a significant physical contrast with respect to the loose sediment overlaying it. It can be traced by gravimetric, seismic and geoelectric methods, and from the results of prospecting works with these methods, the main changes of its depth are rather well known. So e.g. in connection with the planning of the regional water supply of the Sopron area a detailed geological-geophysical survey has been carried out at the W and S shores of Lake Fertő in 1977. The relief of the basement was determined by seismic and geoelectric methods and the results of the two methods were well correlated. Figure 1 presents the geoelectric (telluric) isoarea map along the shore of the Lake Fertő; Fig. 2 the geoelectric E—W profile to the South of the Lake [WALLNER, 1977]. The basis station of the telluric measurements was in the observatory lying roughly near the centre of the profile. On the top of the profile, the axes of the relative ellipses can be seen which reflect the depth changes of the basement by direction changes. This geological situation is important for the observatory, as at least a part of the anisotropy observed in the frequency range of the pulsations can be explained by these near-surface structures.

Deep electric conductivity-distribution

If connections characteristic for the upper atmosphere and represented by the primary electromagnetic field are to be deduced from the time series of an electromagnetic observatory, the induction effect in the subscil must be taken into account. This effect can be described by the transfer function

between the geomagnetic field and the electric field in function of the frequency of the electromagnetic variations. From the transfer function, the distribution of electric conductivity can be determined by using e.g. the magnetotelluric (MT) method.

The first magnetotelluric data from the observatory Nagycenk were published at the beginning of the sixties [ÁDÁM, 1962, 1963]. The first sounding curves computed in the directions N—S (x) and E—W (y) were later expanded from the frequency range of the pulsations to the low harmonics of the daily variation, S_q and computed with a higher accuracy [ÁDÁM and VERŐ, 1967]. The layer sequence corresponding to the ϱ_x-curve was approximated by a theoretical 1D model [ÁDÁM, 1968]. As in the seventies a change has been observed in the values of ϱ_x and ϱ_y at periods shorter than 100 s, a repeated determination of the sounding curves was necessary, now using the MT data processing program of the Institute [VERŐ, 1972]. This program yields the extrema of ϱ (Fig. 3, ϱ_{max} and ϱ_{min}) together with their directions (Figs 4 and 5). The reliability of the values is given by the RMS error corresponding to the medians for ϱ, and for α, by the scatter of the individual averages.

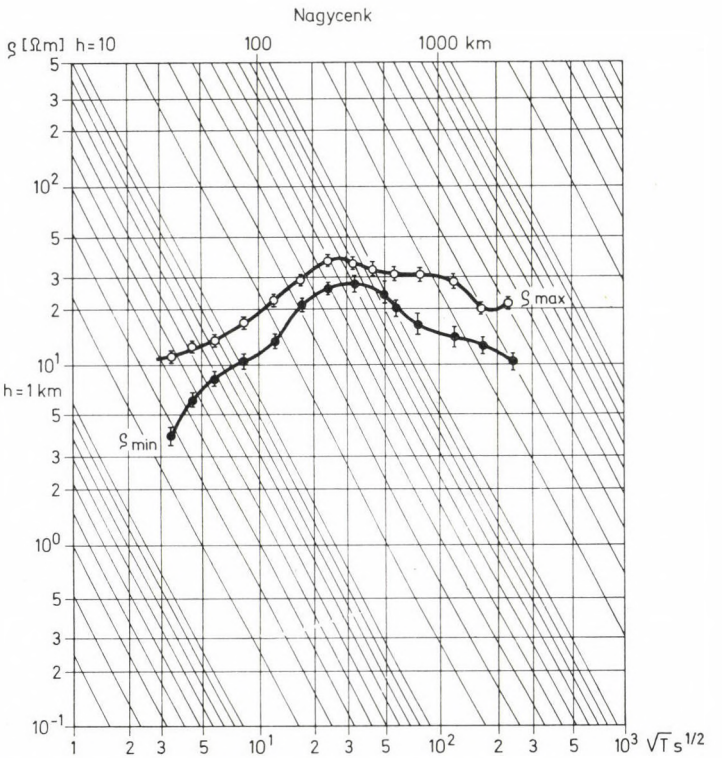

Fig. 3. Magnetotelluric ϱ_{max}- and ϱ_{min}-curve of the Observatory Nagycenk

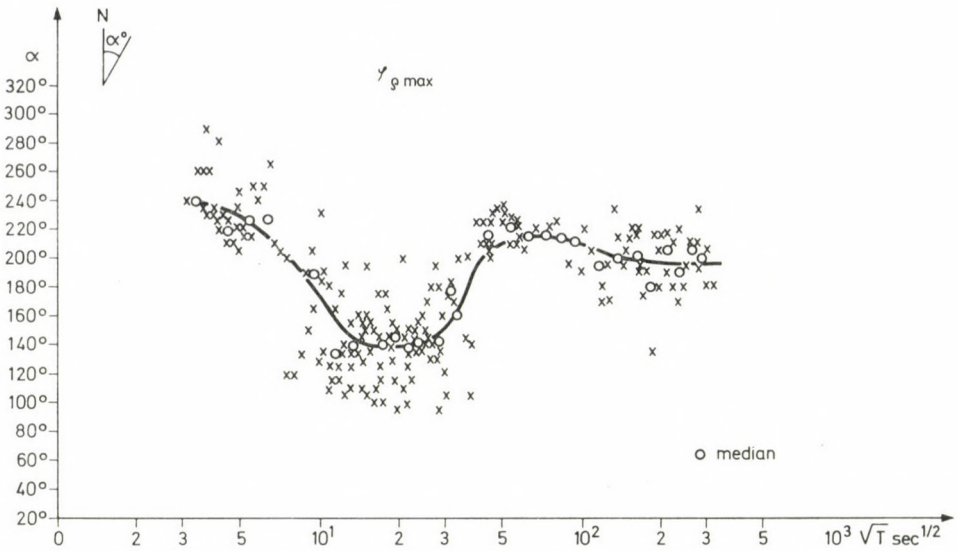

Fig. 4. Directions of the MT ϱ_{max}-values in the Observatory Nagycenk

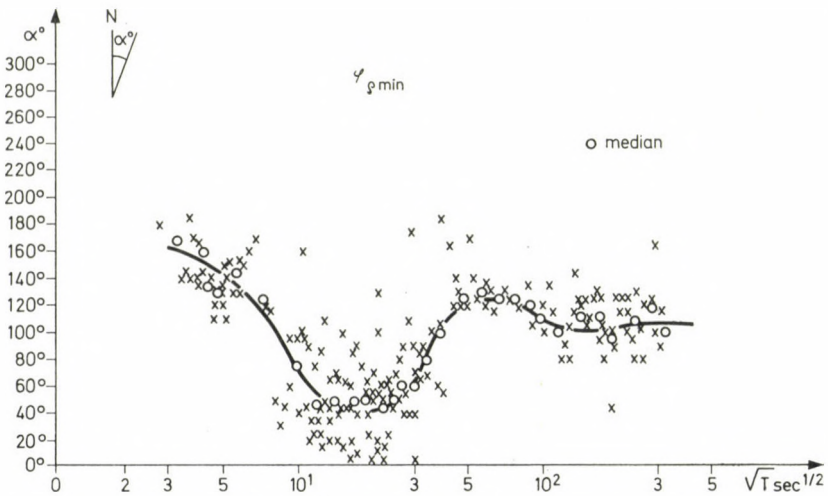

Fig. 5. Directions of the MT ϱ_{min}-values in the Observatory Nagycenk

The sounding curves have been obtained from three types of records:

— in the frequency range of the pulsations, $\sqrt{T} = 3-50\ s^{1/2}$, with magnetic sensors MTV-2, the observatory plumb electrodes, and a common photorecorder with a paper speed of 6—20 mm/m;

— in the frequency range of substorms, $\sqrt{T} = 45-100\ s^{1/2}$, with an Askania variograph (paper speed 20 mm/h) and earth currents recorder (26 mm/h);

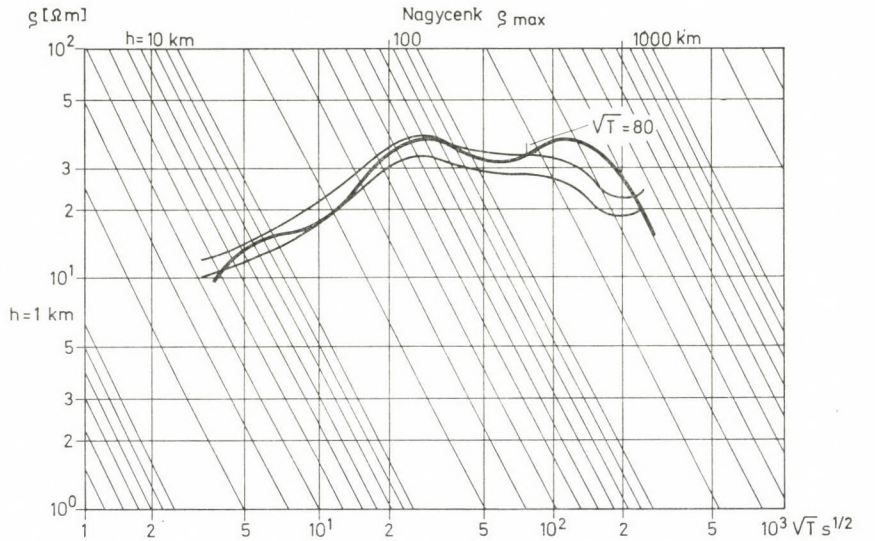

Fig. 6. Error limits of MT ϱ_{max}-curve of Nagycenk in comparison with the theoretical 1D model (thick line 1D model curve, thin lines error limits of ϱ_{max} curve)

— the harmonics of the daily variation (S_q) ($\sqrt{T} > 100 s^{1/2}$) with La Cour type variometers (15 mm/h) and with the same earth currents recorder (26 mm/h).

All earth current measurements were made on the plumb electrodes of the observatory, being in use since about 20 years (distance of electrodes 500 m).

In case of the first two ranges, the records have been digitized with an appropriate digitizing interval (between 0.3 and 3 mm on the record), in case of S_q, the hourly mean values were used.

The sections of the curve determined with different instruments overlap each other quite well. The maximum RMS error of the ϱ_{min} values is $\pm 14\%$, that of the ϱ_{max} values $\pm 9\%$.

It can be seen from Fig. 6 that the 1D MTS curve determined in the sixties lies between the error limits of the ϱ_{max} curve till a period of $\sqrt{T} = 80\ s^{1/2}$. In the frequency range corresponding to the harmonics of S_q, the model curve differs from ϱ_{max}, but intersect each other only at the first harmonics of S_q. Thus the depth of the first conducting layer in the upper mantle of the asthenosphere is according to the new curves the same within the error interval as in the previous model, while the conducting layer supposedly corresponding to the phase transition of the rocks is nearer to the surface. The inaccuracies of the MT values computed from the S_q harmonics were already studied in 1963 [ÁDÁM, 1963, 1965].

The 1D models computed from the curves ϱ_{max} and ϱ_{min} are given in Table I. By changing the parameters so that the curves remain within the

error limits, the inaccuracies of the layer sequence have also been studied. It is evident that the parameters of the model are intercorrelated i.e. a change in the MTS curve can be approximated by the change of several parameters. In the present error computations these correlations are not taken into account, each parameter has been individually changed, therefore they are only approximative values. As a summary it can be concluded that a conductivity increase appears in three depth ranges in accordance with the previous model: in the crust (at 17.6 km from $\varrho_{\min}$), in the asthenosphere (at

Table I

Geoelectrical layer sequences of 1D model computed from the curves $\varrho_{\min}$ and $\varrho_{\max}$ of the Observatory Nagycenk

Layer	Thickness Δh [km]	Resistivity ϱ [Ωm]	
1	1.60	2.30	$S_1 = 690 \pm 70\ \Omega^{-1}$
			($\Delta h_2 = 1.6\ ^{+1.6}_{-1.2}$ km)
2	16.00 ± 2.50	$200.00\ ^{+500}_{-60}$	
3	1.00	1.50	$S_3 = 650 \pm 120\ \Omega^{-1}$
			($\Delta h_3 = 1 \pm {}^{10}_{1}$ km)
4	60.000 ± 9.0	80.00 ± 50.00	
5	230.00 ± 40.00	6.00 ± 0.80	
6		0.10	

Layer	Thickness Δh [km]	Resistivity ϱ [Ωm]	
1	1.50 ± 0.40	8.00 ± 1.00	
2	4.00 ± 1.50	16.00 ± 3.00	
3	8.00 ± 3.00	28.00 ± 5.00	
4	15.00 ± 15.00	45.00 ± 10.00	
5	55.00 ± 10.00	$90.00\ ^{+50.00}_{-25.00}$	
6	15.00	8.00	$S_6 = 1900 \pm 1250\ \Omega^{-1}$
			($\Delta h_6 = 15\ ^{+13}_{-8}$ km)
7	200.00 ± 25.00	20.00 ± 4.00	
8		0.10	

78 km from ϱ_{min}, and at 83 km from ϱ_{max}), respectively, further in the depth range of the phase transition of the rocks (?) (at 310 km from ϱ_{min}, and at 300 km from ϱ_{max}, respectively).

As it has been shown earlier [ÁDÁM, 1963], the direction of ϱ_{max} changes in the period range studied. From ENE—WSW it turns towards N—S, and in the period range of substorms and S_q, it reaches the latter direction.

In addition to this direction change, there is a clear change in the direction of ϱ_{max} in the Pc 3 range around 25 s which has been observed at several stations in the Carpathian Basin, therefore it is connected with the regional MT anisotropy of the area (see on the intersection of the ϱ_x and ϱ_y curves in ÁDÁM (1969)).

The instruments of the observatory

The electromagnetic recording instruments of the observatory have mostly been produced in the Institute, with the exception of some generally used magnetic instruments (La Cour-type variometers). These have been described in earlier publications, here the main characteristics are summarized in tables (see Tables II and III).

Absolute magnetic measurements are made in the observatory only with control purposes about biweekly using Danish QHM and BMZ instruments and a magnetic theodolite. The magnetic basis observatory in Hungary is the Observatory Tihany where the absolute values are regularly compared with neighborous countries and the observatory Nagycenk.

Geomagnetic data processing

The most important data of the records made in the observatory have been determined continuously since the beginning, possibly with the same method, and a part of them is also published in the observatory reports. These data are not the same as determined and published by other observatories, as we consider our main task a continuous monitoring of shorter period variations. The determination of the secular variation, i.e. the measurement of the absolute magnetic elements is carried out only by comparing them to neighborous observatories, as mentioned earlier.

The main aim of the processing of shorter period variations is to produce time series in a possibly wide range of frequencies with good time resolution. For this purpose different kinds of instruments are necessary (see Tables II and III). The observatory data contain inevitably local influences, such as geographic situation: latitude and longitude, geologic structure, etc. In order

Table II

Telluric (earth current) instruments
(Distance of the electrodes: 500 m)

Task	Mode of operation, paper speed	Type of the instrument	Components recorded	Scale value mV/km/mm	Reference
Recording of longer period variations (Normal recording)	continuous, 20 mm/h	T9	2	0.18	ÁDÁM, 1956
Recording of the geomagnetic pulsations (Rapid run)	continuous 6 mm/min	T14A	2	0.15	ÁDÁM, et al., 1962
High resolution recording of pulsations (ultraquick recording)	on world days 20 mm/min	T9	2	0.15	ÁDÁM, et al., 1962

Table III

Magnetic instruments

Task	Mode of operation paper speed	Type of the instrument	Components recorded	Scale value	Reference
Recording of longer period variations (Normal recording)	continuous 15 mm/h	La Cour-systems normal system sensitive system	 3 2 (no D)	 4—5 nT/mm 1.5 nT/mm	
Recording of Pc 1 type pulsations	pen recorder continuous during night time, analogue magnetic tape recorder on special intervals	induction coil	1 (N—S)	max. $2 \cdot 10^{-4}$ nT/mm between 0.8—1.5 Hz	ÁDÁM et al., 1977
Digital system with 1 min sampling interval	experimental	magnetic variometers MTV-2	3	$1 \cdot 10^{-2}$ nT, linear below 1 Hz	for the magnetic instrument, ÁDÁM and HORVÁTH, 1976

to eliminate these effects a greater observatory network would be necessary (e.g. the effect of the local time can be eliminated from pulsations data using 3—4 longitudinally well distributed stations). As long as such a station network does not exist, our observatory data are published in local time, or more correctly in Central European Time, approximating rather closely the local time (CET = LT — 7 min).

The use of CET does not cause considerable errors in this case, as the basic interval of the data is either 1 hour or 30 minutes, thus a transformation into UT does not mean any problem.

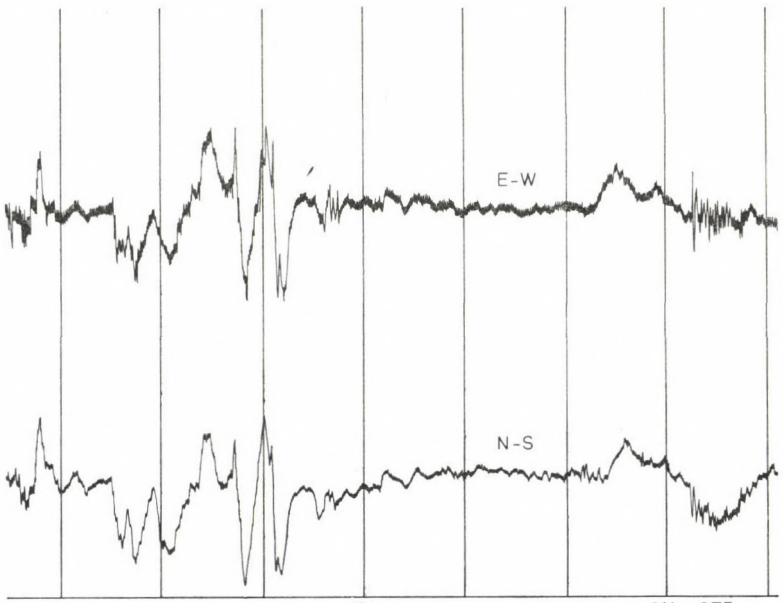

August 9, 1980

Amplitudes in the North-South component / in 0.18 mV/km/

0- 2 min	1	-	-	1	-	-	1
2- 6 min	-	-	1	1	-	1	2
6-12 min	2	3	2	2	2	1	1
12-24 min	8	-	8	3	-	-	-
24-60 min	-	28	-	-	-	4	12

Amplitudes in the East-West component / in 0.18 mV/km/

0- 2 min	1	1	-	-	-	-	1
2- 6 min	1	1	2	-	-	-	4
6-12 min	2	2	2	2	2	1	2
12-24 min	7	5	9	3	2	2	5
24-60 min	-	30	-	-	-	7	-

Fig. 7. A sample of the earth current normal record from August 9, 1980, and the corresponding part of the processing with the amplitudes in the 5 period ranges. The amplitudes in each hour are given below in mm of the original record corresponding to 0.18 mV/km

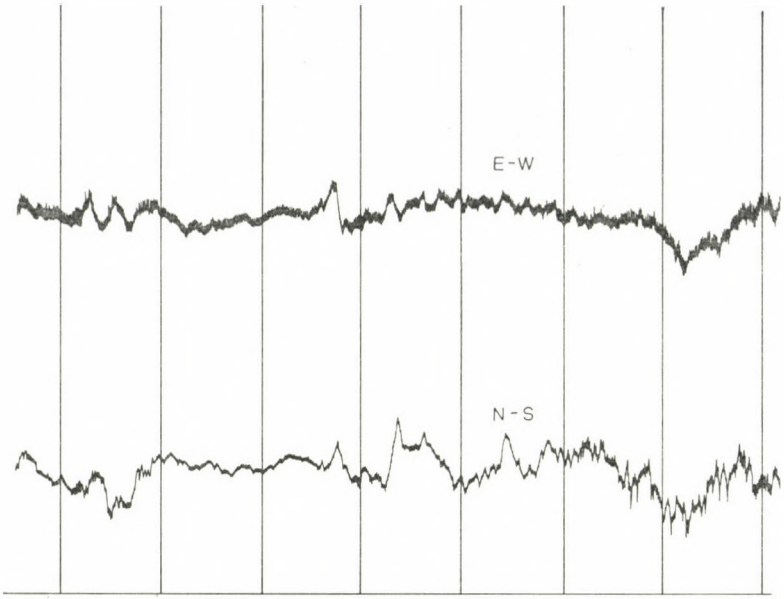

Amplitudes in the North-South component /in 0.18 mV/km/

0- 2 min	-	-	1	1	-	1	1
2- 6 min	2	1	1	1	1	1	1
6-12 min	2	1	-	2	2	1	2
12-24 min	3	3	2	-	3	2	4
24-60 min	5	-	3	11	4	6	-

Amplitudes in the East-West component / in 0.18 mV/km/

0- 2 min	1	-	1	1	-	-	2
2- 6 min	1	1	1	-	-	1	1
6-12 min	2	2	1	2	2	1	2
12-24 min	6	2	-	3	2	2	5
24-60 min	-	2	4	-	-	2	-

Fig. 8. A sample of the earth current normal record from August 10, 1980. Notations as in Fig. 7

The daily variation of the geomagnetic elements is determined on the usual way from the results of the recording with La Cour-type magnetic variometers and T9 type telluric instruments. The daily variation of the 3 magnetic components and of the 2 electric components is averaged for individual months, years, quiet and disturbed days. For the latter, days are chosen by taking into account the telluric current activity, too, i.e. by considering with higher weight the shorter period variations, and not by accepting the international *D* and *Q* days.

From the earth currents records, activity in five period ranges is con-

tinuously determined for each hour by subjective estimation. The average hourly amplitudes are estimated in the following period ranges:

K1	0— 2 min
K2	2— 6 min
K3	6—12 min
K4	12—24 min
K5	24—60 min.

On the basis of the hourly amplitudes, daily averages are computed, which are then converted into daily activity indices using Table IV.

In addition to daily averages, the daily variation of the activity is determined separately for each month, for the year, for quiet and disturbed days.

The occurrence frequencies of the indices for each range had been identical in a basic interval in the first years of the observatories; since then the occurrence frequencies have not been any more identical partly due to changes in the geomagnetic activity, partly due to changes in the subjective scale of the person making the estimation.

The following should be remarked in connection with these activity indices K1—K5 and their basic material:

The index K1 and the period range 0—2 min is mainly characterized by the pulsations of the type Pc 3—4. The night time Pi 1—2 impulses influence the index only insignificantly, but they cause some slight increase of the average amplitude around midnight.

The index K2 and its range 2—6 min has somewhat the character of a mixture, including long period, Pc 5—6 type pulsations, short (si-type) impulses, etc. Anyway, this band is closely correlated with the geomagnetic activity; its scale is, however, too high, most likely due to a change in the subjective estimation, i.e. the daily indices are generally very small.

Table IV

Limits between K-values
Values in 10^{-5} *V/km*

	0—1	1—2	2—3	3—4	4—5	5—6	6—7	7—8	8—9
K1	2	4	7	13	18	23	29	41	54
K2	9	13	18	23	29	34	41	56	90
K3	16	22	25	32	38	45	56	83	120
K4	34	43	54	70	85	101	124	151	202
K5	29	43	67	88	110	131	191	234	339

The third band, K3 with 6—12 min, has clearly, noise-character. The average amplitudes lie mostly between 0.3—0.4 mV/km, the index is then 4. Lower activity is very exceptional, higher one occurs only on very disturbed days. Here both the noise-character and some subjective influence are present.

The index K4 and the activity of the corresponding band is similar to K3, the variability of the index, however, much greater. It can be said in general that the index K4 (and K3, too) is greater in the descending part of the geomagnetic activity [VERŐ, 1959].

The index K5 with the period range 24—60 min contains essentially the substorm-type activity.

In our opinion these indices can be distributed into 3 groups: the most reliable ones are K1 and K5; K2 and K4 can be practically used, and K3 is of little value. As the indices are now determined for two solar cycles, it is not intended to change the method for their determination taking into account that in the rather near future they should be determined digitally. For this purpose, several experiments have already been made.

On the basis of the 6 mm/min earth current record, pulsation data are determined in a greater time resolution. Here 12 period bands are used:

P1: 1—5 s, P2: 5—10 s, P3: 10—15 s, P4: 15—20 s, P5: 20—25 s, P6: 25—30 s, P7: 30—40 s, P8: 40—60 s, P9: 60—90 s, P10: 90—120 s, P11: 2—5 min, P12: 5—10 min.

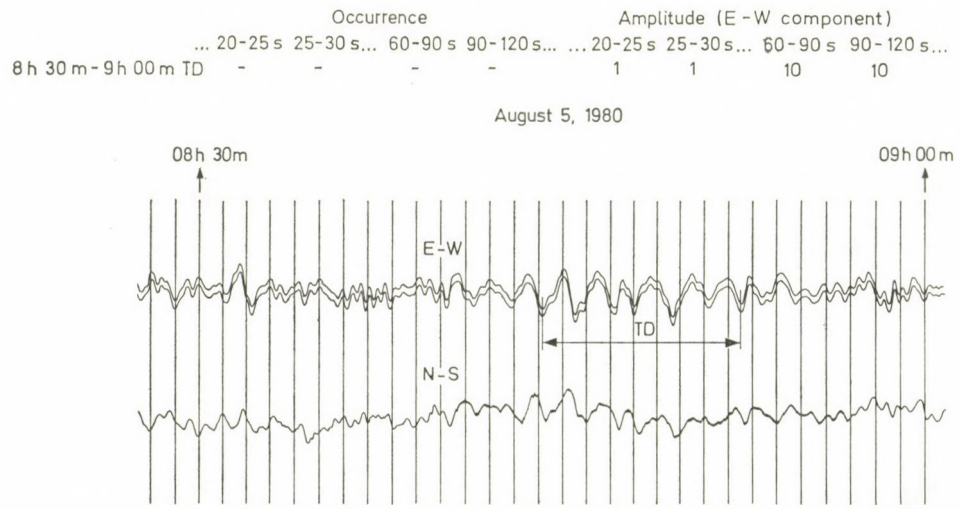

Fig. 9. A sample of the earth current quick run record from August 5, 1980, and the corresponding part of the processing with occurrence frequencies and amplitudes (in 0.18 mV/km) in the 12 period ranges (here only period ranges, in which activity was noted, are shown). The chosen part of the half hour interval is denoted, all the values are taken from this part of the record

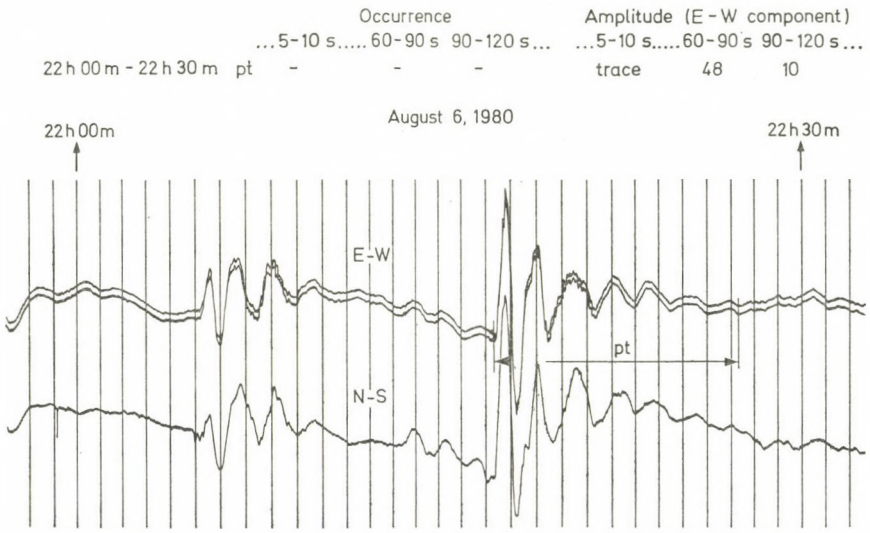

Fig. 10. A sample of the earth current quick run record from August 6, 1980. Notations as in Fig. 9

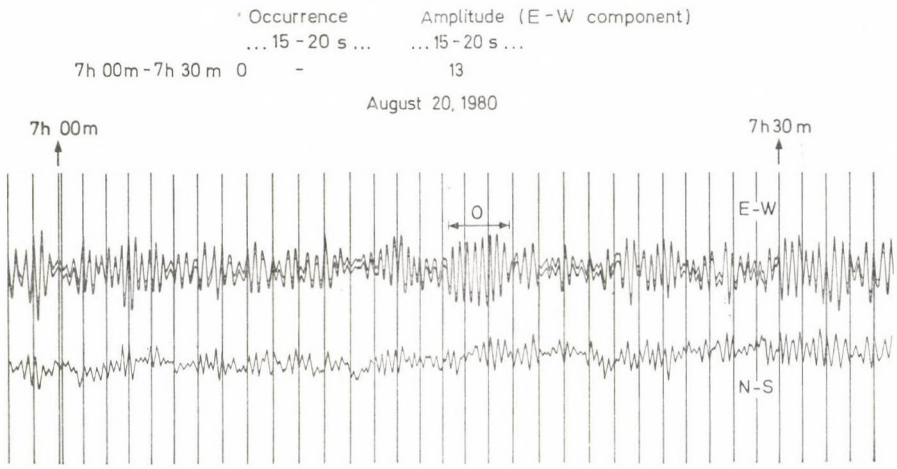

Fig. 11. A sample of the earth current quick run record from August 20, 1980. Notations as in Fig. 9

The presence of any activity in these bands is examined in 30 min intervals, and in all such intervals, where an activity of a certain band is present, its amplitude is also found. These data constitute the pulsation catalogue which is therefore a description of the pulsation activity in all 30 min intervals using the most typical part of the interval. The catalogue also contains descriptive letters for the characterization of the pulsations. Occurrence and

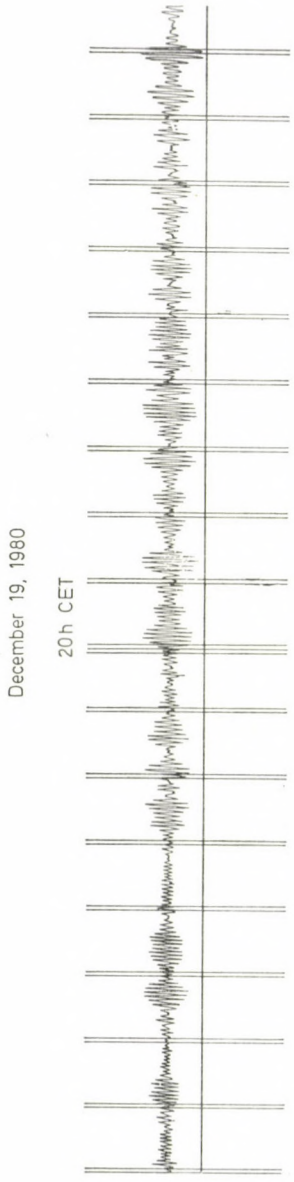

Fig. 12. A sample of Pcl-records from December 19, 1980. The scale value at the frequency of this event is about 10^{-2} nT/mm. North—South component is shown here

amplitude data are summed daily, and based on these sums, a daily activity index having the values 1—5 is attributed to all bands. The published indices are determined on the basis of the occurrence frequency; amplitude indices are also determined, but they are not published, as they are somewhat less reliable than occurrence-type indices. The occurrence frequency of the 5 possible different indices was equal in a basis interval; later changes in the subjective estimation of the activity were eliminated by changes of their scales. Such changes are inevitable in case of personal changes. Therefore the pulsation indices P1—P12 are comparable only within one year.

The indices P1—P2 are rather unsure in consequence of the parameters of the recording, even the uniform distribution could not be reached in the basis interval, as the activity of these bands is often absent during full days, i.e. the index has a priori the value 1. A similar but less strong uncertainty has been observed in case of the indices P11—P12, which are too long in comparison to the recording speed.

Data on the Pc 1 activity from recording with the induction coil are at disposal from a comparatively short time. For comparison, a catalogue is being made also from these data, which contains the occurrence time and amplitude of all Pc 1-events, and on the basis of the total daily occurrence, daily Pc 1-indices are also determined. This experimental Pc 1 will substitute the P1 index of the quick-run earth current recording with the difference that the Pc 1-index contains only regular variations (no Pi 1), while P1 all variations in the corresponding period range.

Observatory data include in addition to the already listed ones special events found in magnetic and earth current normal or quick-run records (ssc, b, pi, si, and short impulses, i.e. so-called "needles"). Fourier-coefficients of the daily variations of the 5 electromagnetic components are also computed and published.

For inner use, local activity indices are determined on the basis of the maximum 3-hour amplitudes of the magnetic and electric components neglecting the daily variation (M and T, respectively). As the scales are linear, they can be compared to local ap indices, but their possible values are 0—9, i.e. for activities greater than corresponding the limit of the index 9, the final index is always 9. These indices are used exclusively for investigations where local time + activity appear together.

From the data mentioned, the indices K1—K5 and their original data are at disposal since August 1957, the indices P1—P12 and the catalogue with somewhat more interruption since 1966, but yearly averages cannot be compared in these cases due to already mentioned causes. Pc 1 recording is operating with several interruptions since 1976.

Two questions can be raised in connection with these indices. At first, they are deduced with the exception of the Pc 1 index from earth current

measurements; how does this fact influence the results? The second question concerns the long-term stability of the subjective estimation of these indices.

Let us consider the first question. Figure 3 shows that the ratio of the extremal magnetotelluric resistivities is generally less than 2; the value of the impedance changes between periods of 10 and 1000 s by a factor of 1.5, above 1000 s, the changes are significantly greater reaching the factor 3. It seems therefore to be justified to substitute the magnetic components with the corresponding earth current ones bearing in mind the possible differences of the values given here.

The constancy of the subjective estimation can be controlled among others by comparing its values to some interplanetary parameters. A comparison of the 23 years long K1 series with solar wind data (from about 16 years) has shown that the level suffered no significant changes. In case of the P1—P12 indices, the levels are in each year different, as explained earlier.

The reliability of the system earth current instruments + cables + electrodes can also be evaluated on the basis of 23 years of experiences. The area of the Nagycenk observatory is exceptional in Hungary, as it is practically free of electric noises from a frequency of about 1 Hz to DC, or more exactly, if there are noises, then these are produced by the observatory itself. Such noises are mostly due to faulty electric network, not corresponding to the inner prescriptions and they can be in the majority of cases eliminating the grounding of the neutral point. The observatory area is anyway a nature preservation area and the consent of the Institute is necessary for all buildings in the neighbourhood.

The scale values of the instruments can slightly change during longer time. In case of a change of 5% they are eliminated by the change of resistivities (a change can cause certain changes in the subjective estimation). Such a stability is necessary to exclude the changes due to scale value differences in the subjective estimations. Such changes are necessary once in about 4—5 years.

The cables were laid down in 1963. They are armoured cables; earlier simple cables had been used without outer protection. During the 17 years, no problem was detected with the cables. At present, the cables on the humid part should be exchanged due to a decrease in their insulation.

The total resistivity between electrodes is regulated to a constant value with the help of a Wheatstone-bridge. Thus changes in the resistivity of the circle do not influence the scale value of the recording. The electrodes themselves are lead plates with a surface of 2 m^2; they have been buried since 1963 between two layers of clay. An electrode has been buried out since then for control purposes, but no remarkable changes were found not regarding some corrosion, and the measurements remained also unaffected by electrode problems. In our opinion the lifetime of such electrodes is about 35—40 years.

Some meteorological effects influenced the measurements of earth currents. One of such effects is heavy rainfall (about 50 mm rain in two days) or strong thaw with a comparable amount of water. In such cases the electrodes are most likely inondated by water or they lie in streaming water, and the potential of the electrodes changes after such events for a maximum of 30—50 days rather strongly. The changes are normally about of a value of 0.01 mV/day, after such heavy rains they are by one or several orders of magnitude higher, reaching a value of 1 mV/day in certain cases. Such great water quantities are rather seldom, as an average one case in five years can be given.

The second meteorological influence is the lightning stroke. Due to them, sudden potential differences appear either by electrochemical processes or by static loading. The impulse like change decays in about 2—4 hours, maximally in one day. Such near lightning stroke occur in summer months about once in each month.

On the basis of all these, we can characterize the indices of the Nagycenk observatory as follows:

Long, reliable data series: K1, K5, P3—P10

Less reliable, long data series: K2, K4, P2, P11, P12

Unsure indices: K3, P1

Short data series: Pc 1-indices

Local indices, long series: T and M.

As it has been already mentioned, experiments to begin with the digital recording are for a longer time being carried out. We should like to determine similar indices from the digital data. It is clear that the methods of determination cannot be equivalent, nevertheless the experiments are aimed to reach the possible best overlapping.

REFERENCES

ÁDÁM, A. 1956: Ein neues tellurisches Messinstrument. *Bányamérnöki és Földmérőmérnöki Karok Közleményei*, 19, 1—7.

ÁDÁM, A. 1962: Magnetotelluric anisotropy. *Magyar Geofizika*, 3, 69—80. (in Hungarian).

ÁDÁM, A. 1963: Study of the electrical conductivity of the Earth's crust and upper mantle. Methodology and results. Dissertation (Cand.), 111 pp. Sopron. (in Hungarian).

ÁDÁM, A. 1965: Uncertainty of the magnetotelluric values computed from the harmonics of the Sq variation. *MTA Műszaki Tud. Oszt. Közleményei*, 35, 133—147. (in Hungarian).

ÁDÁM, A. 1968: Electric conductivity structure of the upper mantle in the Hungarian Basin. The problem and specialities of its determination. Dissertation (Doctor Sci.), 179 pp. Sopron. (in Hungarian).

ÁDÁM, A. 1969: Appearance of electrical inhomogeneity and anisotropy in the results of the complex electrical exploration of the Carpathian Basin. *Acta Geod. Geoph. Mont. Hung.*, 4, 187—197.

ÁDÁM, A.—HORVÁTH, J. 1976: The development of magnetic sensors in the Geodetical and Geophysical Research Institute of the Hungarian Academy of Sciences. Proceedings of the 20th Geophys. Symposium Budapest—Szentendre (15—19. 9. 1975). OMKDK Technoinform Budapest, 703—710.

ÁDÁM, A.—VERŐ, J. 1958: Das Erdstromobservatorium bei Nagycenk (Ungarn). *Geofisica pura e applicata*, 39, 126—151.
ÁDÁM, A.—VERŐ, J. 1967: Latest results of electromagnetic measurements in Hungary. *Geofizikai Közlemények*, 16, 25—52. (in Hungarian).
ÁDÁM, A.—ERKEL, A.—SZABADVÁRY, J. 1962: Neue ungarische geoelektrische Instrumente. *Geofisica pura e applicata*, 52, 127—138.
ÁDÁM, A.—VERŐ, J.—WALLNER, Á. 1967: Tellurische und erdmagnetische Messungen im Observatorium bei Nagycenk. Observatoriumsberichte Nagycenk, 1966, 129—141.
ÁDÁM, A.—CZ. MILETITS, J.—HORVÁTH, J.—VERŐ, J. 1977: Pc 1 type pulsations. Recording system — data processing. Geophys. Obs. Reports Nagycenk, Year 1976, 121—130.
CZ. MILETITS, J.—HOLLÓ, L.—TÁTRALLYAY, M.—VERŐ, J. 1978: Experimental results with the characterization of geomagnetic micropulsations VI. Summary of results, recommendations. *Acta Geod. Geoph. Mont. Hung.*, 13, 231—238.
HOLLÓ, L.—TÁTRALLYAY, M.—VERŐ, J. 1972: Experimental results with the characterization of geomagnetic micropulsations. I. The methods of characterization used in the investigations. *Acta Geod. Geoph. Mont. Hung.*, 7, 155—166.
HOLLÓ, L.—VERŐ, J. 1972: Experimental results with the characterization of geomagnetic micropulsations. II. Micropulsation index. Auto- and cross-correlation functions of micropulsations and geomagnetic activity. *Acta Geod. Geoph. Mont. Hung.*, 7, 167—176.
TAKÁCS, L. 1975: Experimental results with the characterization of geomagnetic micropulsations. V. Comparison of the geomagnetic pulsation activity at the observatories Nagycenk, Niemegk and Sodankylä. *Acta Geod. Geoph. Mont. Hung.*, 10, 307—320.
TÁTRALLYAY, M.—VERŐ, J. 1973: Experimental results with the characterization of geomagnetic micropulsations. IV. Comparison of occurrence frequency and amplitude spectra from different type records. *Acta Geod. Geoph. Mont. Hung.*, 8, 217—224.
VERŐ, J. 1959: Earth-current variations of different period in the observatory near Nagycenk. *J. Atm. Terr. Phys.*, 13, 375—376.
VERŐ, J. 1972a: Experimental results with the characterization of geomagnetic micropulsations. III. Effect of the geomagnetic activity on pc 3—4 and pi-2 type geomagnetic micropulsations. *Acta Geod. Geoph. Mont. Hung.*, 7, 177—190.
VERŐ, J. 1972b: On the determination of the magnetotelluric impedance tensor. *Acta Geod. Geoph. Mont. Hung.*, 7, 333—351.
WALLNER, Á. 1977: Report on the telluric measurements made between Fertőrákos and Fertőszentmiklós. Manuscript (in Hungarian).

ЭЛЕКТРОМАГНИТНАЯ ОБСЕРВАТОРИЯ В НАДЬЦЕНКЕ

А. АДАМ—Й. ВЕРЁ—Й. Ц. МИЛЕТИЧ—Л. ХОЛЛО—А. ВАЛНЕР

РЕЗЮМЕ

В первой части работы рассматриваются геолого-геофизические условия подпочвы обсерватории в Надьценке, и подробно излагаются методы определения магнитотеллурических кривых зондирований, а также данные геоэлектрической свиты. Во второй части в виде таблиц представляются теллурические и магнитные приборы обсерватории и параметры наблюдательной и регистрационной техники. В заключение описывается стандартная обработка данных с оценками надежности разных параметров и показателей.

Рассматриваются некоторые пертурбационные эффекты по поводу записывания данных.

Acta Geodaet., Geophys. et Montanist. Acad. Sci. Hung. Tomus 16 (2—4), pp. 353—357 (1981)

THE GEOPHYSICAL OBSERVATORY NEAR NAGYCENK
II. ATMOSPHERIC ELECTRIC AND IONOSPHERIC MEASUREMENTS

P. BENCZE
CAND. GEOSCI.
F. MÄRCZ
GEODETIC AND GEOPHYSICAL RESEARCH INSTITUTE OF THE HUNGARIAN ACADEMY OF SCIENCES, SOPRON

The measuring site, the equipments used for atmospheric electric and ionospheric measurements in the Geophysical Observatory near Nagycenk, as well as the processing of the records are described. The scaling of the instruments and supplementary measurements, necessary for the control of the recordings, are also discussed.

Introduction

Since it was planned that in the observatory all six components and possibly the whole spectrum of the geoelectromagnetic field should be recorded, in addition to the components of the geomagnetic field and earth currents the measurement of the vertical electric component in the air, i.e. that of the atmospheric electric potential gradient has been started in 1961. During disturbed periods (cloudy weather, thunderstorms) if the field strength reaches the breakdown voltage, point discharge current, proportional to the field strength, occurs. For the investigation of such periods the recording of point discharge currents has been started already in 1960.

The geoelectromagnetic field is influenced at a given recording site not only by the structure of the underground, but also by the state of the ionosphere. Thus, the measurement of ionospheric absorption of radio waves as a complementary investigation has been carried out since 1966.

The brief description of the site and the instruments was published earlier [1]. In this paper a review of the atmospheric electric and ionospheric measurements will be given, as well as the description of the measuring technique and the data processing in [1] will be completed.

The measuring site

Reliable atmospheric electric and ionospheric measurements can only be made in an undisturbed environment. Atmospheric electric investigations require a possibly flat ground far from high-voltage power lines and sources

of air pollution. As regards ionospheric measurements, the noise level should be small at the observing station. Efforts were made to meet these requirements in the observatory. The boiler, assuring the heating in the observatory is mounted in the dwelling located north—eastwards from the measuring site, while the prevailing wind direction is west—north—west. To avoid inhomogeneous ionization of the air due to the radiation of enrichments of radioactive materials in the soil, the place assigned for the mounting of the atmospheric electric measuring gauges was surveyed by means of a Geiger counter. Anomalies indicating the presence of such enrichments have not been found. The observatory is supplied with electric power from the nearest village, the cable in the vicinity of the observatory is buried.

Atmospheric electric measurements

The vertical electric component of the geoelectromagnetic field can be measured in the air. The vertical electric component is, however, the resultant of field components of different origin. Besides the slowly varying field due to the global atmospheric electric circuit, fluctuations attributable mostly to local sources (clouds, air parcels having an ion concentration different from their surroundings and drifting with wind, rainfall, fog, snow) are recorded. There occur variations, for which a connection with the geomagnetic pulsations of extraterrestrial and magnetospheric origin can be proved. Finally, with increasing frequency the sources of the geoelectromagnetic field become lightning discharges. The study of these different contributions to the vertical electric component can be achieved with different methods and equipments.

At present only the slowly varying field is recorded. A radioactive collector is used to equalize the potential appearing in an altitude of 1 m above the surface of the ground and that of the input of the equipment. The radioactive collector has a time constant of ~ 30 s and cannot follow variations of a period less than 30 s. According to our investigations [2] the radioactive preparation corresponds to a transitional resistance of $1.7 \cdot 10^{12}\ \Omega$ in the substituting circuit of the apparatus. The case containing the radioactive preparation and attached to a vertical rod is held by a double walled insulator with an insulation resistance of $4 \cdot 10^{13}\ \Omega$. The input resistance of the measuring apparatus is another important factor in case of the recording of the atmospheric electric potential gradient, as the voltage of a power supply of high inner resistance has to be determined. The measuring apparatus consists of a triode, the anode of which is connected with the radioactive potential equalizer and the potential of the anode controls the grid current. This circuit has an input resistance of $1 \cdot 10^{13}\ \Omega$. Both the filament voltage (4 V) and the voltage (250 V) necessary to hold the grid-cathode system at a positive poten-

tial as compared to the anode are supplied by a stabilized power supply unit. The variations of the grid current due to the changes of the atmospheric electric field are recorded photographically by means of a sensitive galvanometer. The equipment is scaled weekly by putting the collector in an artificial electric field. This is produced by a regulated high voltage power supply between the ground and a metallic net. The latter is placed over the case containing the radioactive preparation. Moreover, the scaling net is also placed over the collector and grounded every day for some minutes to mark the zero field on the record by a zero line. The sensitivity of the equipment is adjusted so that a deflection of 10 mm on the record corresponds to 100 V. The speed of the recording is 20 mm/hour. Hourly time signals are given by the central digital clock, which is continuously controlled by comparing it with the markers of the time-signal transmitter Mainflingen (FRG).

The point discharge currents are observed by means of a tip made from stainless steel. This is insulated and attached to the top of a vertical boom mounted on the roof of a 3.5 m high building. Thus, the tip is in a height of about 7 m above the ground. The currents flowing through the tip during disturbed periods are recorded photographically with a sensitive galvanometer. The recording speed is 20 mm/hour.

Processing of atmospheric electric records

Since atmospheric electric investigations in the Institute are mostly connected with the study of the global atmospheric electric circuit, the records of the atmospheric electric potential gradient are processed as described below. First the hourly average deflection as compared to the zero line are determined. The zero line can be drawn by connecting the parts of the record corresponding to the times when the grounded scaling net was placed above the collector. Besides the determination of the hourly averages, the differences between the largest and smallest deflection occuring within periods of three hours and proportional to the atmospheric electric activity are also read. The value of the potential gradient is obtained by multiplying the deflection in mm with the scaling factor in V/m/mm, which is determined on the basis of the weekly scaling.

Point discharge current records can be used for the determination of the charge exchange between the ground and the atmosphere. The quantities of positive and/or negative charges transported by point discharge, which occurred within the interval of an hour are determined. They result from the multiplication of an area (formed by the recording trace, the hourly time markes and the zero line) with the charge sensitivity of the equipment. The charge sensitivity can be obtained by multiplying the current producing

a unit deflection (A/mm) with the reciprocal of the recording speed (s/mm). The various features appearing on point discharge current records and their interpretation are discussed in detail in [3].

Ionospheric measurements

Nowadays, first of all the use of ground based methods is reasonable, which allow the investigation of the lower ionosphere, i.e. the region inaccessible by direct satellite measurements. In the observatory one of these methods, the measurement of the absorption of radio waves obliquely incident on the ionosphere (method A3) is used. For the measurements transmitters of long wave (LF) and medium wave (MF) bands have been chosen. They have to be located in suitable distances from the observatory, i.e. the condition of an one hop reflection should be given and the field strength of the reflected wave must be comparable with that of the ground wave. At present the field strength of the reflected wave of the transmitter Československo (272 kHz) is continuously recorded and in addition the transmitter Bratislava (1098 kHz) is experimentally received.

The apparatus for the measurement of ionospheric absorption of radio waves with the method A3 consists of an antenna system, a receiver and a recorder. The antenna system is a vertical loop aerial combined with a vertical rod antenna for the removal of the voltage, which remains, when the loop aerial is set perpendicular to the vertical plane passing through the transmitter and the receiver (minimum position). The receiver is a three stage amplifier with two outputs of different sensitivity [4]. The less sensitive channel is used for the determination of the night time absorption. The more sensitive channel can be used for the study of the daytime absorption. The recorder, connected with the output of the receiver is a compensograph with a recording speed of 60 mm/hour. The apparatus is scaled daily by turning the loop aerial from its minimum position into both directions by steps of five degrees till 30° and by steps of ten degrees from 30° till 90° whereby the appropriate deflections on the recorder are read. Thus, the records are scaled by means of the ground wave. The scaling is performed near noon, when the contribution of the field strength of the reflected wave to the total field strength is the smallest and its elimination is easier. Hourly time signals breaking the connection between receiver and recorder as well as giving a small negative voltage to the recorder are supplied by the central digital clock.

For the control of the ionospheric absorption measurements the absolute values of the field strength of the earlier mentioned transmitters are measured daily.

Processing of records for the determination of ionospheric absorption

The records of the relative field strength of the reflected wave are processed according to international agreements [5]. The amplitudes are read at times corresponding to predetermined solar zenith angles (40°, 50°, 60°, 66.4°, 72.5°, 78.5°, 85°, 90°, 100°). Since the recorded curve consists of fluctuations in accordance with the rotation of the plane of polarization, the average of the maximum deflections (envelope) for the period ranging from 10 minutes before to 10 minutes after the time corresponding to a given solar zenith angle is taken. On the basis of the daily scalings these averages are expressed in units of the ground wave field strength (i.e. the average deflections are given on the basis of the daily scaling with the angles, by which the frame antenna should have been turned away from its minimum position to produce these deflections on the record). At first the conversion coefficient is determined by using the computed field strength ratios and an appropriate factor. This factor can be computed on the basis of the propagation path as well as in knowledge of the characteristics of the antenna and of the power of the transmitter. It is supposed that neither the electrical properties of the ground along the propagation path, nor the power of the transmitter do change and the reflection height does not significantly vary. Finally, from the conversion coefficient the corresponding absorption value is computed.

REFERENCES

1. Bencze, P.—Märcz, F.: Atmosphärisch-elektrische und ionosphärische Messungen im Observatorium bei Nagycenk. Observatoriumsberichte des Geophysikalischen Forschungslaboratoriums der Ungarischen Akademie der Wissenschaften vom Jahre 1966, Sopron, 1967, 143—152.
2. Bencze, P.—Märcz, F.: Determination of the scaling factor for the computation of the absolute value of the potential gradient in the Geophysical Observatory near Nagycenk. Geophysical Observatory Reports of the Geodetical and Geophysical Research Institute of the Hungarian Academy of Sciences, Year 1979, Sopron, 1980, 129—133.
3. Bencze, P.: The annual variation of the ratio of the quantities of negative to positive charge transported by point discharge. *Acta Geod. Geoph. Mont. Hung.*, 1 (1966), 93—105.
4. Bencze, P.—Horváth, J.—Märcz, F.: A new equipment for the measurement of ionospheric absorption. Geophysical Observatory Reports of the Geodetical and Geophysical Research Institute of the Hungarian Academy of Sciences, Year 1975, Sopron, 1976, 111—118.
5. Lauter, E. A.: Method A3(b): Oblique incidence field strength observations on frequencies in and below the MF broadcasting band. In: Manual on Ionospheric Absorption (Ed. K. Rawer). Report UAG-57, Washington, D.C., 1976, 147—163.

ГЕОФИЗИЧЕСКАЯ ОБСЕРВАТОРИЯ В НАДЬЦЕНКЕ II. АТМОСФЕРНО-ЭЛЕКТРИЧЕСКИЕ И ИОНОСФЕРИЧЕСКИЕ ИЗМЕРЕНИЯ

П. БЕНЦЕ—Ф. МЕРЦ

РЕЗЮМЕ

Изложены место наблюдения, приборы, применимые для атмосферно-электрических и ионосферических измерений в Надьценкской геофизической обсерватории, а также обработка регистраций. Калибровка приборов и добавочных измерений, необходимых для контроля регистраций, тоже приведены в статье.

Acta Geodaet., Geophys. et Montanist. Acad. Sci. Hung. Tomus 16 (2—4), pp. 359—380 (1981)

ANALOGUE MODEL FOR STUDYING GEOELECTRIC METHODS IN THE GEODETIC AND GEOPHYSICAL RESEARCH INSTITUTE OF THE HUNGARIAN ACADEMY OF SCIENCES

A. ÁDÁM—J. PONGRÁCZ—L. SZARKA
GEODETIC AND GEOPHYSICAL RESEARCH INSTITUTE OF THE HUNGARIAN ACADEMY OF SCIENCES, SOPRON

P. KARDEVÁN—L. SZABADVÁRY
HUNGARIAN GEOPHYSICAL INSTITUTE EÖTVÖS LORAND

Z. NAGY—I. ZIMÁNYI
GEOPHYSICAL EXPLORATION COMPANY

I. KORMOS—P. RÉGENI
INDUSTRIAL RESEARCH INSTITUTE FOR ELECTRONICS, BUDAPEST

As geoelectric and electromagnetic methods play a significant role in geophysical prospecting in Hungary, it became necessary to solve the interpretation of complicated geological structures.

The electromagnetic modeling laboratory built up in the Geodetic and Geophysical Research Institute of the Hungarian Academy of Sciences in cooperation with several Hungarian institutions serves this purpose.

To meet the modeling requirements an extremely wide frequency band modeling apparatus was to be planned. This involves in its present form instrument packages for modeling artifical frequency soundings using electric dipoles and for modeling some DC methods as well.

The large quantity of the measured data and the requirements for parameter calculations made it necessary to use computerized data processing.

This modeling apparatus has been used for investigations of high conductivity dykes related to faulting zones in the Transdanubian conductivity anomaly. We have used this apparatus in the bauxite exploration work of the Eötvös Lorand Geophysical Institute and for modeling frequency soundings above inhomogenous basement structures for the Geophysical Exploration Company.

Future developments involve a plane-wave field generation as well as developing of magnetic sensing coil systems.

Aims for a model construction in Hungary

Geoelectric and electromagnetic methods play a significant role in geophysical prospecting in Hungary. There are three fields of exploration where an increase of effectivity of these methods is especially justified in view of both economic and scientific aspects.

1. Exploration of the Earth's crust and upper mantle i.e. of deep structures by *electromagnetic induction* soundings (magnetotelluric and geomagnetic soundings). The geophysical information received by these methods is used for formulating the geological exploration concepts and for implementing the exploration strategies. Moreover, this information has also basic theoretical value.

2. Determination of the topography of the high resistivity basement of the Pannonian sedimentary basin and of the sediment parameters in the basin for the purpose of hydrocarbon exploration by *artificial frequency soundings*.

3. Exploration of shallow (less than a few hundred meters thick) sedimentary basins in the Hungarian Middle Mountains Range and its foothills for the purpose of bauxite ore and coal exploration by *low frequency, mainly DC geoelectric methods*.

All in the listed exploration fields geoelectric methods have supplied useful, in numerous respects requisite results. The basic mathematical—physical formulas of these methods are deduced only for quite simplified models (usually only for one- or two-dimensional structures). Nature is much more complex. The simple models may be regarded as rare limiting cases that describe nature with various ambiguity. For this reason general acceptance has been gained by analogue modeling in the interpretation process of geoelectric (electromagnetic) data beside recent numerical methods generally used in the interpretation of 2D structures.

To meet the requirements an extremely wide frequency band modeling apparatus had to be planned. This in its present form involves two basic instrument packages:

a) DC modeling apparatus

b) Apparatus for artifical frequency soundings (conductive model).

Media for modeling purposes (salt solution and model bodies) are contained in all cases in the same large size plastic container (tank). The apparatus for excitation and sensore may change according to the modeling requirements. The mechanical tools for positioning and determination of spatial location (coordinates) are always the same.

The paper describes the modeling apparatus and also shows some characteristic results gained in the exploration fields described above.

Modeling laws

The laws of modeling are based on the Maxwell-equations. For sake of completeness they are presented here in Dosso's (1967) formulation:

$$\mathbf{rot}\,\mathbf{E} + \frac{\partial \mathbf{B}}{\partial t} = \mathbf{0} \tag{1}$$

$$\mathbf{rot}\,\mathbf{H} - \mathbf{j} - \frac{\partial(\varepsilon\varepsilon_0\mathbf{E})}{\partial t} = \mathbf{0} \tag{2}$$

where

$$\mathbf{B} = \mu \cdot \mu_0 \mathbf{H} \quad \text{and} \quad \mathbf{j} = \sigma \mathbf{E}$$

$$\varepsilon_0 = \frac{1}{4\pi} \frac{10^{-9}}{9} \frac{F}{m}$$

$$\mu_0 = 4\pi\, 10^{-7}\, H/m.$$

Let us make the following substitutions:

$$\mathbf{E} = e_0 \mathbf{E}'; \ \mathbf{H} = h_0 \mathbf{H}'; \ \sigma = \sigma_0 S; \ D = d_0 D' \text{ and } t = t_0 T,$$

where $\mathbf{E}'$, $\mathbf{H}'$, D' and T as well as μ and ε are dimensionless quantities; e_0, h_0, σ_0, d_0 and t_0 as well as μ_0 and ε_0 are units of electric and magnetic fieldstrengths, electric conductivity, length and time, vacuum magnetic premeability and dielectric factor, respectively.

The Maxwell-equations 1 and 2 take thus the following form:

$$\mathbf{rot}\, \mathbf{E}' + \alpha \frac{\partial \mathbf{H}'}{\partial T} = \mathbf{0} \tag{3}$$

$$\mathbf{rot}\, \mathbf{H}' - \beta \frac{\partial \mathbf{E}'}{\partial T} - \gamma \mathbf{E}' = \mathbf{0} \tag{4}$$

where

$$\alpha = \frac{d_0 \mu \mu_0}{t_0} \left(\frac{h_0}{e_0} \right) \tag{5}$$

$$\beta = \frac{d_0 \varepsilon \varepsilon_0}{t_0} \left(\frac{e_0}{h_0} \right) \tag{6}$$

$$\gamma = d_0 \sigma_0 S \left(\frac{e_0}{h_0} \right). \tag{7}$$

Equations 3 and 4 are invariant in case of changes in the units if the dimensionless quantities α, β, γ are invariant.

Assuming that $\varepsilon\varepsilon_0$ and $\varepsilon\varepsilon_0$ are vacuum values and $\varepsilon = \mu = 1$, e_0/h_0 can be eliminated from the equations. As a result one gets the following invariance condition in case of changes in the units:

$$\sigma_0 f_0 d_0^2 = \text{const} \tag{8}$$

that has to be fulfilled in natural ("t" index) and model ("m" index) circumstances. Thus one gets

$$\sigma_m f_m d_m^2 = \sigma_t f_t d_t^2. \tag{9}$$

Measuring technology of the conductive frequency sounding model

Model experiments are carried out in a NaCl-solution with suitable specific resistivity.[1] The electrolite solution is contained in a 4 · 3 · 0.5 cu.m. poliester tank. Structures of the basement are represented by high resistivity model bodies. For the conductive measurements a selective measuring system has been developed mainly for dipole—dipole electric frequency soundings.

The most important requirements for the measuring system were as follows:

1. Generation of an earth-symmetric constant inducing current in the 10 kHz—10 MHz frequency range.
2. Measurement of the electric field by a selective microvoltmeter produced on the surface of the electrolite.
3. Comfort in the operation.
4. Possibility for automatization of measurements.
5. Possibility to determine the relative phase of the measured signal.

These requirements were met by a synthesizer generator and a synchronously tuned (tracking) receiver unit. The synthesizer generator can produce an output voltage of constant amplitude in 100 Hz steps [KORMOS et al., 1978]. This voltage controls a current generator as output stage that is built together with the generating electrode pair. The proximity of the current generator output to the generator electrodes is an important factor because already a shunt capacity of some 10 pF would deteriorate the output impedance of the current generator on a frequency of 10 MHz.

The selective microvoltmeter is a heterodyne receiver converting the frequency of the measured signal three times [RÉGENI et al., 1978]. The automatic synchronizing with the generator unit is enabled by the fact that the signal of the first oscillator of the receiver is the same as one of the signals that control the generator output. Namely the output signal of the generator is produced by mixing: it is the difference between the signals of a fixed frequency oscillator (being the same as the 1. IF frequency of the receiver) and a synthesized digitally programable oscillator. The frequency of the generator output and of the receiver input may be written as

$$f_{\text{out}} = f_{\text{in}} = f_{\text{prg}} - f_{\text{IF}} \,.$$

This solution fulfills requirements 3 and 4.

To meet requirement 5 it is necessary that the generator frequency and all oscillator frequencies in the receiver should be synchronized to the same reference signal i.e. these signals must be coherent.

[1] The specific resistivity of the solution can be controlled with an error of $\pm 2\%$ by an OK 102/1 conductivity-meter using normal KCl-solutions as standards.

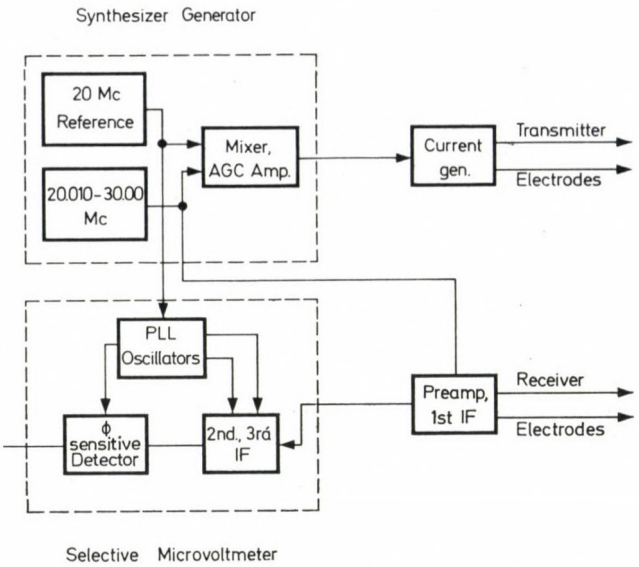

Fig. 1. Simplified block diagram of the generator and the receiver

This requirement has been fulfilled by *phase locked loop* arrangements. Signal detection is carried out by multiple phase sensitive detectors.

Just like in the case of the generator, the front end of the receiver must be in close proximity to the measuring electrodes. This is necessary due to low signal levels (μV range) and to a large input impedance. (A current loading on the measuring electrodes would distort the field strength distribution.)

So the pre-amplifier, mixer 1 and the 1st IF amplifier of the receiver have been built in a separate unit close to the measuring electrodes.

The simplified block diagram of the generator and the receiver is shown in Fig. 1.

Although the modeling apparatus was carefully constructed the first experiments were unsuccessful because of the geometry of the measuring layout.

At higher frequencies (above 1 MHz) quite large disturbances occurred that were by several orders of magnitude higher than the signal itself. These disturbances were created by the common mode (asymmetric) current component flowing from the generating electrodes to the ground (electrolyte). The generator can be set to an optimum symmetry in the low frequency domain. At higher frequencies the compensation deteriorates due to parasite capacitances in the circuit and a common mode signal component appears also on the output. This common mode signal current component can flow to the ground only through the grounding of the generator—receiver complex. The ground-loop where the disturbance current flows can be seen in Fig. 2.

The common mode component flows along the loop shown in this figure and produces a voltage drop corresponding to the loop impedance between the electrolyte and the ground of the current generator. As the ground of the generator and of the preamplifier are shorted galvanically and from the high frequency point of view as well (the coaxial cables are running side by side

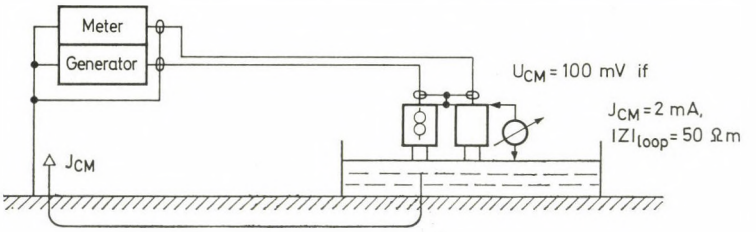

Fig. 2. Ground-loop where the disturbance current flows

for 10 meters) the voltage drop described earlier reaches also the differential inputs of the preamplifier as an unwanted common mode signal. The common mode rejection of the preamplifier (CMR) is 40—46 dB (up to 10 MHz).

Since this value could not be significantly improved in the 10 MHz bandwidth of the instrument, the common mode component had to be attenuated in a great extent. To this end the following modifications had to be done:

1. The preamplifier grounding was to be separated from the grounding of the system and of the current generator and it had to be connected to the electrolyte.

2. The current generator must be grounded to the electrolyte through a connection of a low impedance to shunt the large ground loop. Since some capacitance remained between the current generator and the grounding of the preamplifier, it is advisable to decrease the common mode disturbance on the ground of the current generator as much as possible.

In practice the followings were carried out:

Power to the preamplifier was supplied from ground independent sources (batteries). This way the preamplifier could be grounded to the electrolyte. Besides both signal lines had to be provided with coupling transformers of low capacitance. This was achieved by small size high frequency toroidal transformers. The capacitance between the primary and secondary coils of the transformers could be reduced to a value of 1.5 pF. Some problems were encountered at the stray inductance of the transformers. In case of the 20 MHz signal it could be eliminated by resonant tuning. In case of the oscillator signal this method could not be used because of the varying frequencies in the 20—30 MHz band. Since the stray inductance had caused some 6—10 dB change in the signal level of the oscillator, a limiter amplifier had to be used to remedy the problem.

Grounding to the electrolyte was performed with an electrode that is placed in the neutral centre between the two measuring electrodes. To ground the current generator a relatively large electrode was required. It could not be placed between the two transmitter electrodes since it would have also distorted the potential distribution. To solve this problem the grounding electrode was placed in the symmetry axis of the two transmitter electrodes on the opposite side of the receiver. The distance to the grounding electrodes was chosen so that the current flowing through it should not interfere significantly the electric field. (This distance must be greater than that of the wall effect.)

As a result of the low capacitive coupling only a small fraction of the common mode signal can reach the ground of the preamplifier. The attenuation is governed by the ratio of the coupling impedance (stray capacitance) and

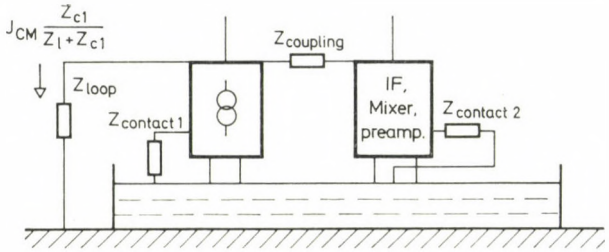

Fig. 3. To the computation of the resulting disturbance rejection

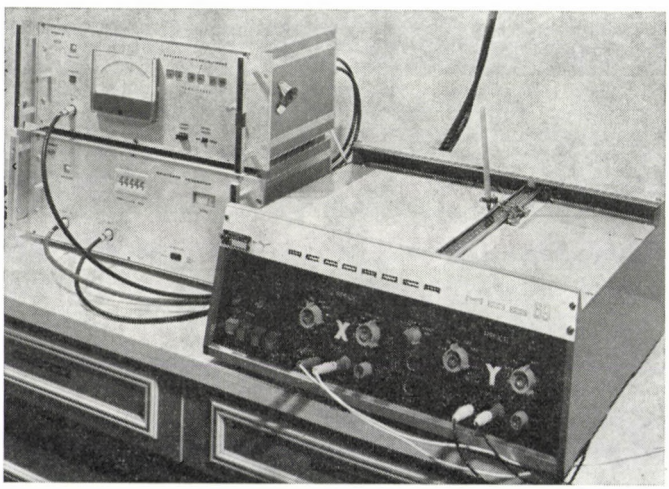

Fig. 4. Selective microvoltmeter and synthesiser generator (left) and x—y coordinate plotter used for the profile measurements

the contact resistance of the grounding electrode. Other factors in the noise reduction are the ratio of ground-loop impedance (it can be several hundred ohms, since it has a resonance at about 6 MHz) and the "grounding" contact resistance of the current generator. The resultant noise attenuation is the product of the two factors (Fig. 3).

The apparatus described above can be seen in Fig. 4 (lefthand side).

Electrode moving apparatus

The transmitter and measuring unit can be moved with suitable accuracy along the tank by rolling bridge structures on which carriages can move crosswise. The electrode holding rods are fixed on these carriages.

Most of the mechanical parts of the modeling apparatus (Fig. 5) are made of plastic materials (ongroplast, bonamide, textile-bakelite, polymethylacrylate and polyester resin). Since only these materials proved to be suitable for easy carriage movement in spite of long span, they are corrosion resistant and suitable also for carrying out MT-modeling experiments.

The determination of the location and resetting to a given point is done by the measuring tapes along the two coordinates with ± 0.5 mm accuracy. (In points above the tank where the coordinates on the measuring tapes are not known, the accuracy of setting is ± 1 mm.)

Z-coordinates of the transmitter and receiver can be continuously changed by the vertical setting apparatus on the electrode holding carriage (Fig. 6). Setting error of the Z-axis is ± 0.05 mm.

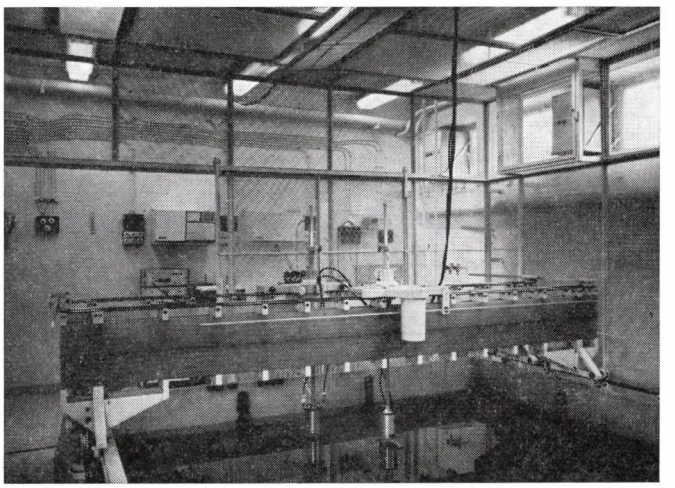

Fig. 5. Apparatus for moving the electrodes above the tank in a Faraday-cage and the measuring panel

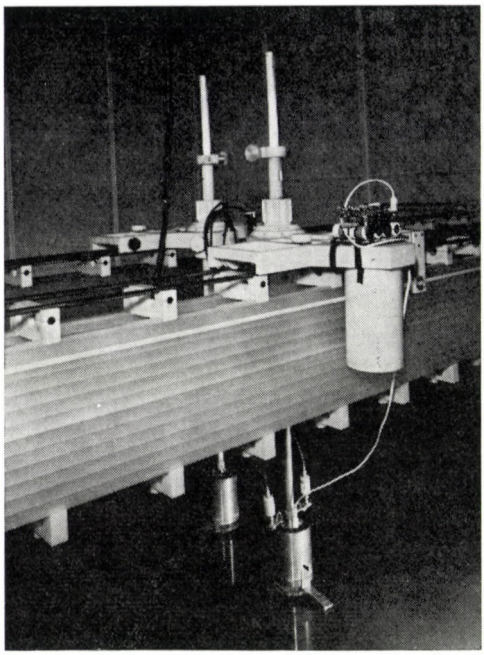

Fig. 6. Rods for holding the electrodes on the bridge frame

The electrode holding rods may be turned by 90 degrees. Platinum electrodes are used. Their length is 2 mm, the diameter at the generator electrodes (A, B) is 2 mm, at the measuring electrodes 1 mm.

Conductive alternating current modeling

The operation of the apparatus is simple and so the model measurements are very productive.

In case of one point frequency sounding having determined the measuring configuration — model structures, electrode system — the frequency is digitally changed between 10 kHz and 10 MHz in at least 100 Hz steps then the microvoltmeter is read. The measuring limit is set by hand or in case of larger range it is automatically set between 1 μV and 300 mV in 8 steps. The current generator supplies 50 mA via the A, B electrodes to the electrolite regardless of the frequency so no regulation is required.

In the other often used measuring method i.e. in the *profiling* the frequency is set to a required value. The distance between the receiver and transmitter is set to a constant value and the whole system is simultaneously moved above the model structure. The profile is plotted by an x — y recorder

unit. The position of the measuring unit is determined by the voltage values taken from resistivity lines placed along the tank and along the transverse bridges.

Apparatus for DC measurements

The lower limit of the frequency sounding band of the conductive modeling apparatus is 10 kHz. By taking into account all other geoelectric parameters of the system (specific resistivity, linear dimensions) this frequency is enough for modeling DC methods, but because of the possibility of a technical simplification of measurement at lower (audio) frequencies it seemed to be reasonable to use an other apparatus for this aim.

An audiofrequency generator with maximum 10 W power-output (Type TR 0161) set at 300—500 Hz is used as a generator. The current flowing through the A, B electrodes into the electrolite is held on a specified value within 0.3% by regulating the voltage on a resistance of 1 abs. ohm (by a TR 1660 digital multimeter) as it is seen in Fig. 7.

The potential difference of the MN-dipole is measured by a voltmeter (Bruel and Kjaer Te 2107) tuned to the frequency of the output signal. The sensitivity of the instrument in the least measuring range is 300 mm/mV.

The electrode system fulfils the requirements of the method. The movement of the electrode system is carried out with the same apparatus as used in case of the conductive frequency sounding modeling.

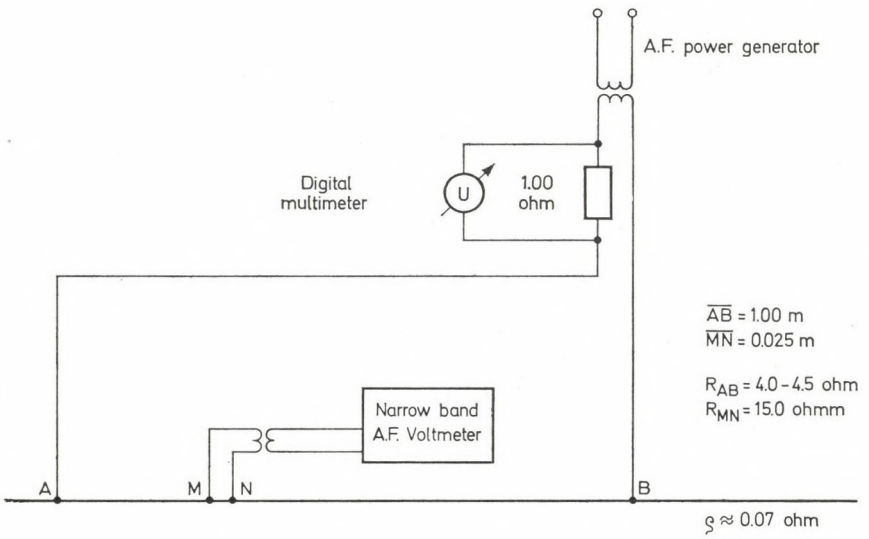

Fig. 7. Block diagram of the DC modeling unit

Fig. 8. Ratio of the measured and computed potential differences in potential mapping (PM) on the surface of a two layer half-space. *A* and *B* are the feeding electrodes (SZARKA, 1980)

The measuring program involves the potential mapping (PM) and underground potential mapping (UPM) methods as well as conventional geoelectric soundings.

In case of the potential mapping, the largest relative deviation of the measured and computed field intensities is 3% on the surface of a half-space containing two layers, with ϱ_∞ basement (Fig. 8).

Processing of model data

In order to determine the rules, all model experiments are carried out by varying certain parameters of the structure to be explored. In general tens of thousands of ΔU_{MN} voltage measurements are needed to solve one model problem.

The geophysical interpretation is carried out by evaluating certain derived quantities (T, ϱ_ω, S, computed depth values, etc.).

The large quantity of the measured data, the requirements for the parameter calculation and a possible future need for a new kind of data processing made it necessary to use for the processing a computer, the HP-2100A of the Geodetic and Geophysical Institute (MTA GGKI). The measured data are stored on punchtapes.

All data-processing programs are written in FORTRAN. Interpretation algorithms owned by other cooperative institutions are programmed and MTA GGKI mathematical programs are used for solving special problems.

The MTA GGKI computing centre is equipped with all usual peripherical units. The computed quantities — depth maps, sounding curves etc., — can be plotted on the plotter of the computer. These plots are fast and descriptive tools of the interpretation as shown by the following examples:

Figure 9 illustrates an anomaly map of electric field intensity vectors around a 3D high resistivity uplift as obtained by DC current modeling. The electrode configuration is shown on a sketch in Fig. 9.

A vector anomaly $(\mathbf{E} - \mathbf{E}_0)/|\mathbf{E}_0|$ maps is determined comparing the $\mathbf{E}_0(x, y)$ field intensity which was measured by the same electrode configuration over a horizontally homogeneous two-layer model. This map shows the location of the anomaly and its characteristics.

Figure 10 illustrates the curves above a 3D step-like structure obtained by two different electrode configurations. The points of sounding curves were determined at 19 frequencies. The measured $\sqrt{T} - \varrho_\omega$ pairs of values were joined by a special cubic polynomial (spline function). The interpolation made in this manner is quite satisfactory. The plot is made in a scale corresponding to a 62.5 mm mode log-log sheet. In this way the manual drawing of sounding curves is eliminated. A program is also available for the numerical solution

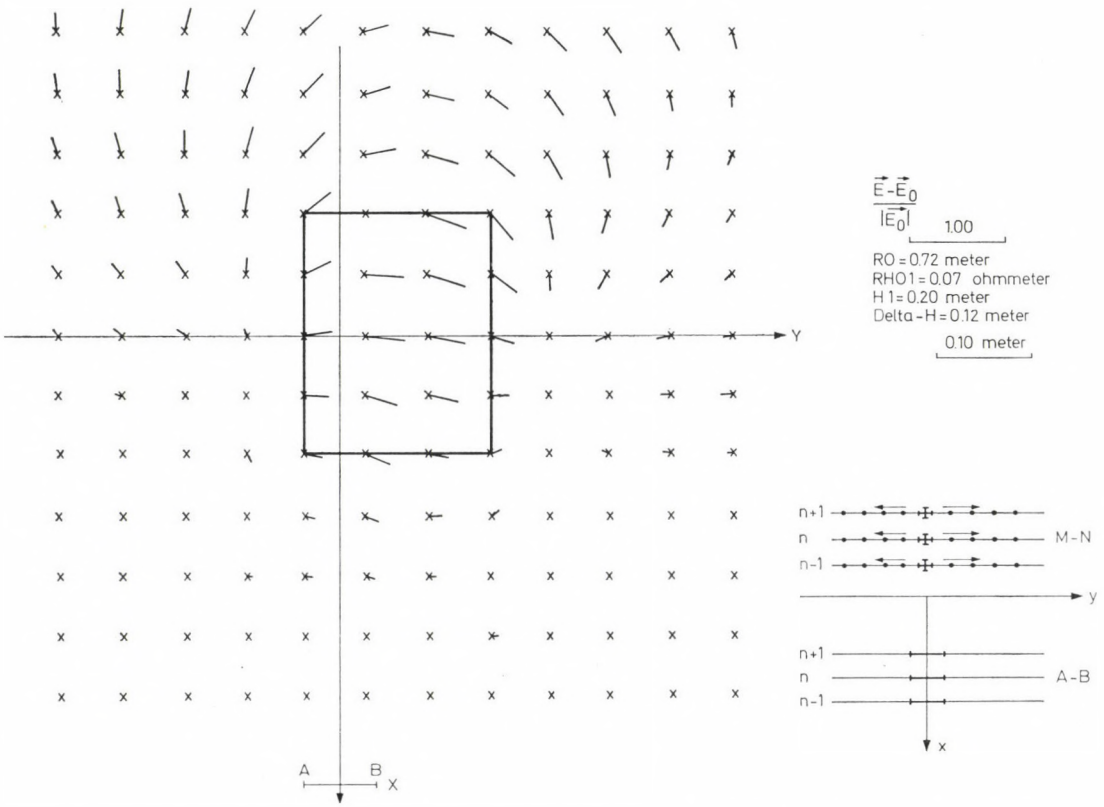

Fig. 9. Anomaly map of the electric field intensity vector around a 3D high resistivity uplift (see the electrode configuration right side bottom of the figure)

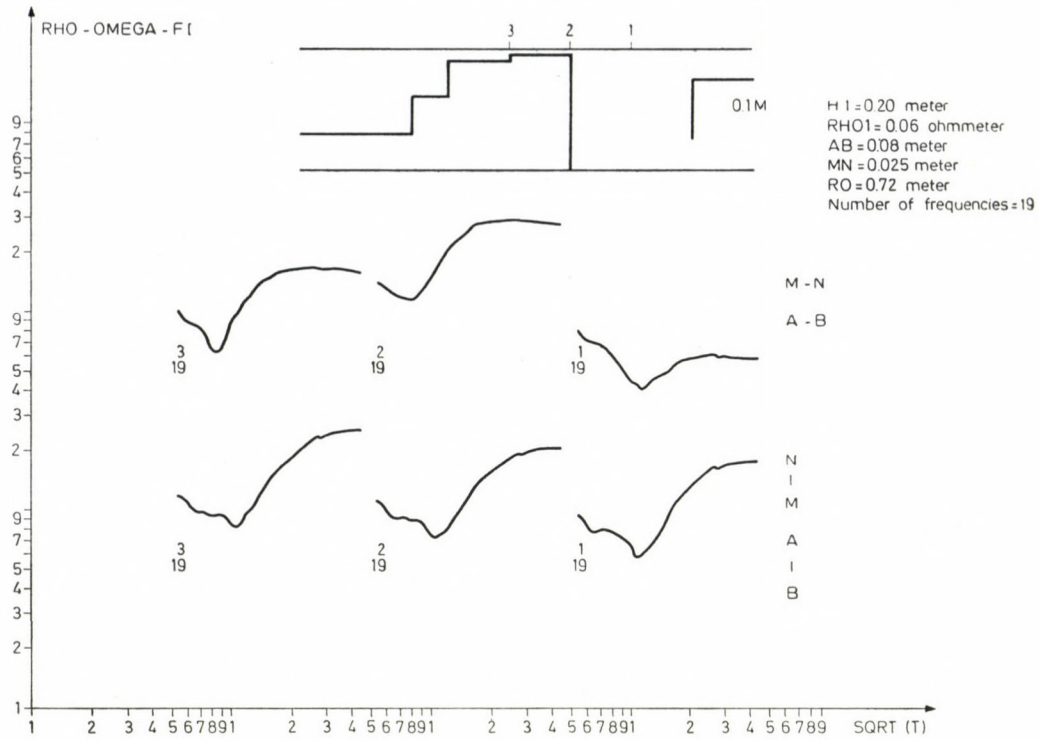

Fig. 10. Frequency sounding curves measured by dipole equatorial and axial configuration above a 3D step-like structure

of the graphical interpretation applied by the Geophysical Exploration Company.

In Fig. 10 the profile of the MN-dipole crosses a high resistivity uplift. The locations of the measuring points are denoted by 1, 2 and 3.

Analysis of geological-geophysical problems by modeling

a) *Modeling of the high conductivity bodies in Transdanubia*

Conductivity anomalies (Fig. 11) observed in the Transdanubian Middle Mountains (Hungary) and its foothills were explained by conductive material in the faults of the Earth's crust under several km thick Mesozoic and Palaeozoic media. It was assumed that this material consists of graphite, graphitic shale (whose veins predetermined the tectonics, and as a result the Earth's crust has been broken up along these tectonic lines during the basin's isostatic subsidence), or of some other high temperature electrolyte [ÁDÁM, 1977]. The connection between the tectonic lines on the surface (fault zones) and

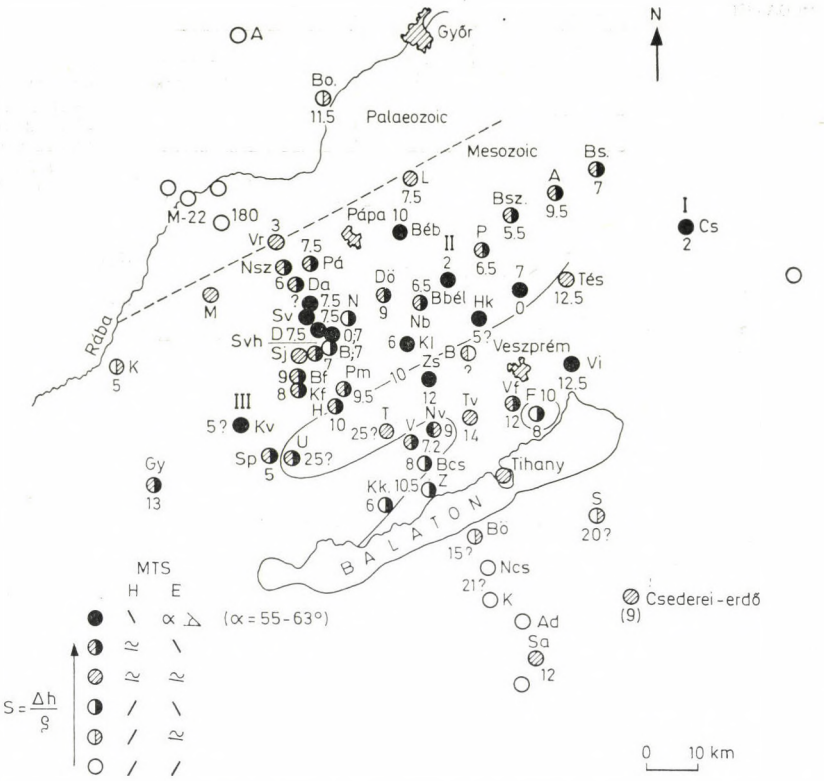

Fig. 11. Indications of the Transdanubian conductivity anomaly on the basis of ϱ_{max} and ϱ_{min} MTS curves (ϱ_{min} corresponds to the E polarization). The half circles (according to the key on the left side) indicate the existence of a decreasing part on MTS curves depending on the S-value of the high conductivity layer (ÁDÁM, 1977)

the EM induction directional quantities ($Z_{xy\,max}$ impedance, direction of the Wiese-vector) were proven by statistical analysis [ÁDÁM, 1980].

Suitable geoelectric methods were selected by modeling that (beside natural electromagnetic induction soundings) would make it possible to analyse dykes related to faulting zones, but covered with high resistivity rocks.

Due to the screening effect of high resistivity materials, DC methods could not be used. For this reason induced frequency soundings were applied in dipole equatorial configuration with electric excitation and electric sensing.

The high conductivity dyke was represented by a vertical metal plate set in an insulator base, which was placed in the electrolyte of the model tank. The metal plate was covered by an insulator plate. The measurements were carried out in various parameter combinations to determine the characteristics and size of the anomaly. Soundings and profilings were carried out above the different structures with the high conductivity dyke, without dyke, with and without insulator.

Figure 12 illustrates the sounding curves with various solution thicknesses (h_1) in case of uncovered dyke. Significant points on the sounding curve e.g. minimum points are shifted along the frequency axis vs. solution depth. The low and high frequency parts of the sounding curves with dyke or without dyke shift in opposite directions. For comparison the effect of the covered dyke in the case of the smaller solution thickness is shown in Fig. 13. It can be stated that the electric dipole—dipole system is quite insensitive for tracing such insulated dykes.

The above statements were also proven by profiling on low (0.1 MHz) and high (4 MHz) frequencies (Fig. 14). A high conductivity dyke reduces

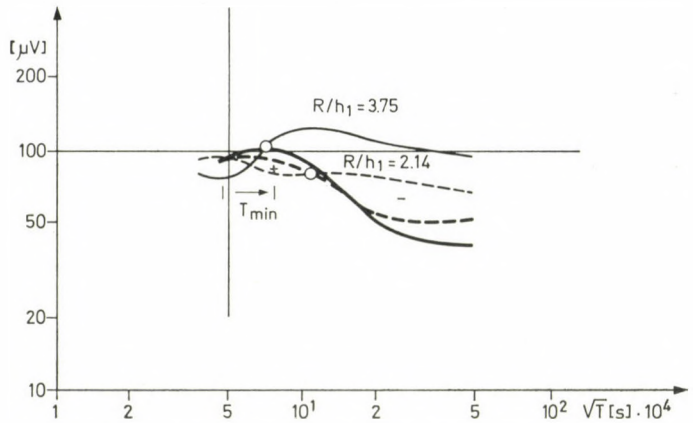

Fig. 12. Dipole—dipole equatorial frequency sounding curves above a highly conductivity dyke placed in insulator media with various electrolite overburden thicknesses (h_1), (R = distance between the dipoles = const)

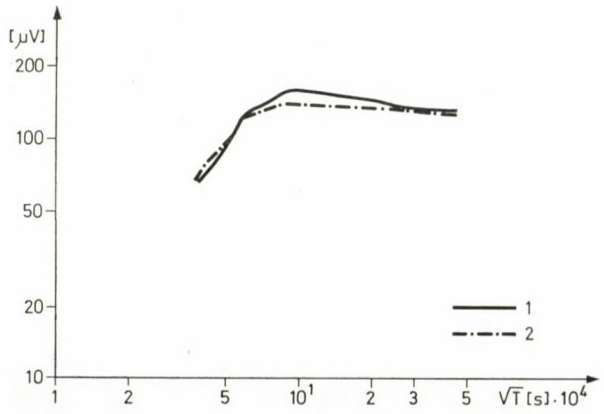

Fig. 13. Effect of the high conductivity dyke covered by an insulating layer (2) on sounding curves as compared to the effect of the same structure but without the dyke

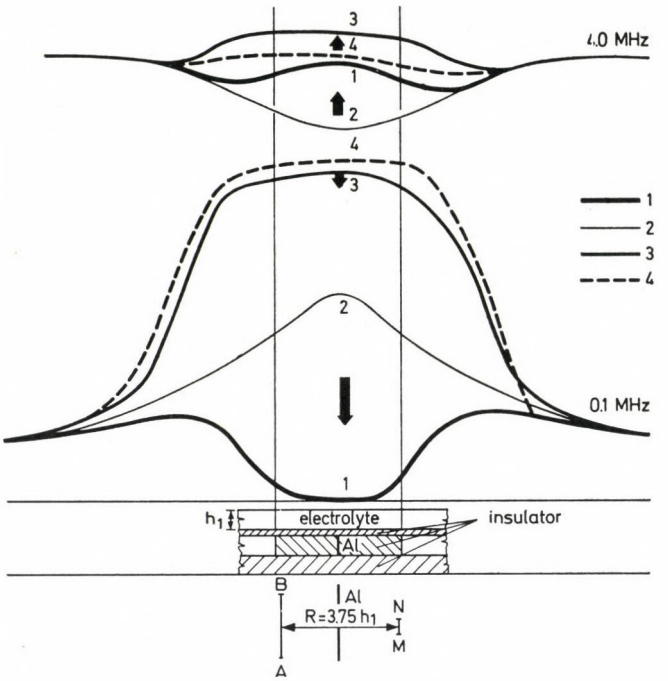

Fig. 14. Profiling with dipole—dipole equatorial configuration on frequencies 0.1 and 4 MHz in the case of highly conductive uncovered dyke (1), dyke covered by an insulator layer (2), and in the case of similar structures but without highly conductive dyke

at low frequencies and increases at high frequencies the field intensity. These effects are significantly reduced due to the presence of a screening layer as it was shown in the case of sounding.

b) *Modeling of potential mapping (PM) for bauxite exploration*

"Bauxite bodies explored or assumed to be present in the Western part of the Bakony Mountains are small in size and are located in tectonically preformed dolomite trenches and depressions of 50—100 meters diameter. Karstic well or canyon like structures can also be found. These small size structures are economically important since the bauxite deposits are quite thick (30—50 m), and of high quality that can be mined from the surface without danger of karstic water flood (MÁELGI, 1975 Report)."

The aims of the geophysical survey are

1. exploration of the Triassic dolomite (and limestone) outcrops;

2. determination of basement structures under 30—300 m thick overburden.

The aim is in both cases to prospect for the structures. For this reason complex geophysical exploration is carried out. One of the significant methods

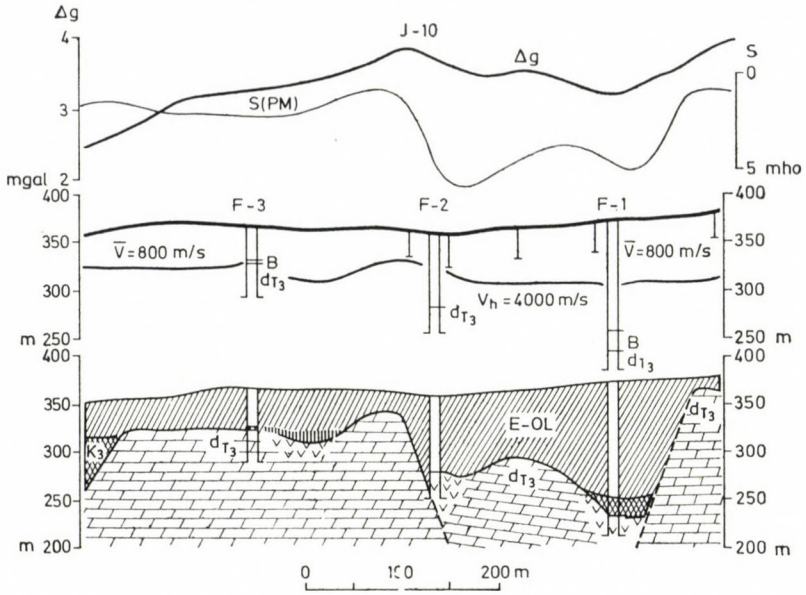

Fig. 15. Potential mapping (S/PM/) above bauxite bearing dolomite blocks and the geological profile based on gravity profile (Δg) with the geological structure reconstructed from borehole (F) informations (MÁELGI, 1975)

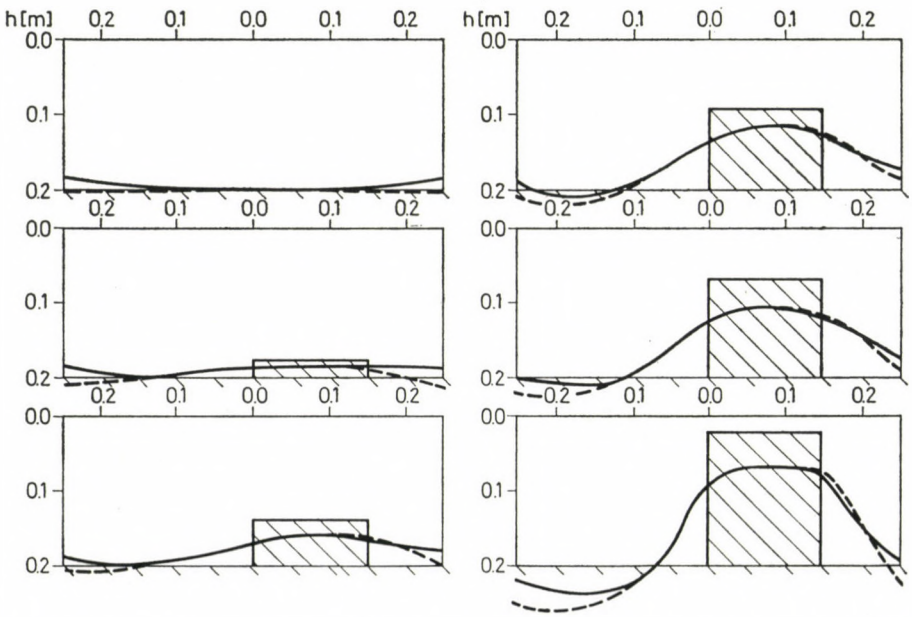

Fig. 16. Relation between computed depth values (h) from DC potential mapping (PM) and the real structures. Continuous lines represent depth values in the S-interval. Broken lines represent depth values outside of the S-interval at the margins (SZARKA, 1980)

in this is the potential mapping. E.g. as it is seen on the profile J-10 (Fig. 15) the shape of trench-like structure can be easily interpreted on the corrected S-profile. The depth values can only be verified by borehole data.

It can be determined by modeling how the PM anomaly reflects the effect of subsurface horizontal inhomogeneities (faults, trenches, uplifts, etc.). Moreover, information concerning to the depth deformation can also be derived about the high resistivity basement on the basis of S-values by assuming a linear relationship. Figure 16 illustrates the deformation effect above a 2D model series representing uplift structures [SZARKA, 1980]. As it can be seen, the depth values computed from measured data contain some distortion. By neglecting this fact, the computed depth values would also contain this distortion. At present modeling studies are carried out above trench-like structures.

c) *Modeling of frequency soundings above inhomogeneous basement structures*

Modeling of frequency soundings has been an important experimental tool in the planning of frequency soundings and interpretation of their measured data concerning to the hydrocarbon exploration in the Paleogene belt of the Northern Pannonian Basin.

In the Paleogene basin the triassic limestone basement structures (in some cases together with thin Eocene structures) form under Miocene and Oligocene sediments an ideal marker horizon of high specific resistivity for geoelectric prospecting. The inhomogenous basement structures are characterized by faults of great dislocations and blocks of small horizontal extensions.

The theory of frequency soundings is available for horizontally homogenous, horizontally stratified layers. Informations about inhomogenous media are not complete or only very simple models have been investigated [ISAEV et al., 1970]. Results of earlier published analogue model investigations can be used in some cases for inhomogenous basement structures [KUZNETSOV et al., 1972, 1974].

By modeling of frequency soundings many problems of the field explorations were solved and the experiences gained with modeling were profitably put into practice in the exploration of the Paleogene belt of the basin.

Modeling problems shown on Figs 9 and 10 yielded clues about the correct location of the transmitting dipoles in the sounding runs. Moreover, they also supplied clues to the interpretation of frequency sounding curves above fault zones.

Figures 17, 18 and 19 illustrate some results gained in the Vatta—Maklár area of the Paleogene belt. Modeling results were applied in the field measurement and interpretation as well.

Fig. 17. Location of the measuring lines of the frequency soundings as compared to the gravity anomalies

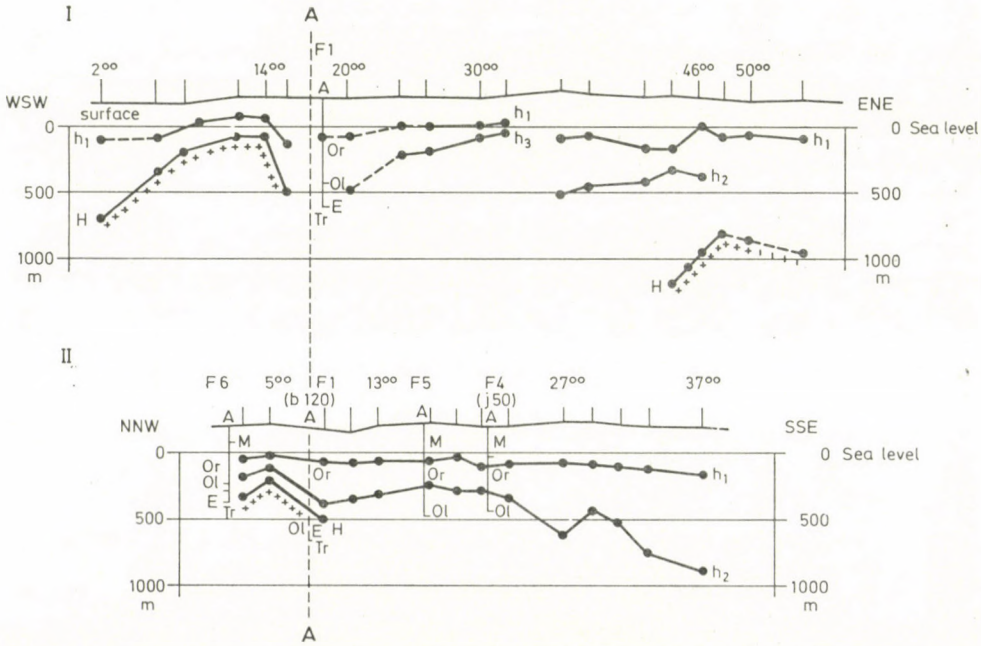

Fig. 18. Depth profile of the frequency sounding profiles shown in Fig. 17. H is the surface of Triassic limestones, h_1 and h_2 are Miocene and Oligocene layers. $A-A$ is the projection of the crossing of the measuring profiles. $F1$, $F2$, etc. are boreholes

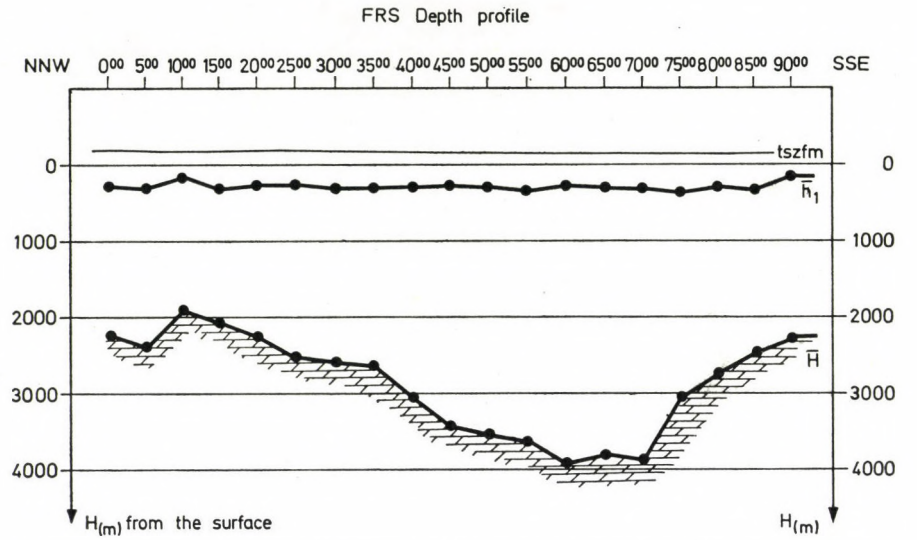

Fig. 19. Frequency sounding profile across the Vatta—Maklár trench. H values have been interpreted from the soundings as surface data of the Triassic limestone, h_1 is the reference level (1st layer)

Figure 17 shows the location of frequency sounding profiles on a filtered gravity anomaly map. The faults determined by frequency soundings are also shown on the figure.

Figure 18 shows the depth profile of the two frequency sounding lines in Fig. 17. Horizon H is interpreted as the surface of the Triassic limestone, h_1 and h_2 as those of layers in the Miocene and Oligocene sediments. Because of the employed relatively small transmitter-receiver spacing only the locations of the fractures could be primarily determined. In the shallower zones of the basin, the basement could also be followed. An example for continuous mapping of the basement can also be seen on Fig. 19.

Some important methodical conclusions could be drawn from the model measurements e.g. if the frequency sounding profile agrees with the direction of dip and the dipole-radius R between the transmitter and receiver dipoles is nearly parallel with the direction of strike, the rules valid for horizontally homogeneous layers can be used with the assumption that there is no uplift of the basement between the transmitter and receiver (feeding and measuring dipoles) that could create a "screening side-effect". To avoid these effects special attention is to be paid to the selection of the location of the transmitter. To identify these effects a "multifold" sounding system was developed in hydrocarbon prospecting. In this system the length and position of (fen-like) profiles to one transmitter location further repeated measurements from other transmitter locations are planned on the basis of some methodical aspects also considering the modeling results.

Future developments

— One of our aims is to develope a magnetic sensing coil system for frequency soundings in addition to the measurement of the electric components. Experiments have proved that in certain cases the measurements of the magnetic components may supply better results (e.g. to indicate a high conductivity body between insulating layers).

— In the near future means for plane-wave generation will be developed beside conductive excitation by building a suitable aerial system to study the problems of magnetotellurics [Dosso, 1967].

REFERENCES

ÁDÁM, A. 1977: The Transdanubian crustal conductivity anomaly. *Acta Geod. Geoph. Mont. Hung.*, 12, 73—79.

ÁDÁM, A. 1980: Statistische Zusammenhänge zwischen elektrischer Leitfähigkeitsverteilung und Bruchtektonik in Transdanubien (Westungarn). *Acta Geod. Geoph. Mont. Hung.*, 16, 97—114.

БЕРДИЧЕСКИЙ, М. Н.—КУЗНЕЦОВ, А. Н.—ЗАВАДСКАЯ, Т. Н. 1972: Дипольное электромагнитное зондирование горизонтально-неоднородных сред (Electromagnetic sounding of horizontally inhomogeneous media with dipole configuration). *Prikladnaya Geofizika*, 67.

DOSSO, H. V. 1967: Analytical and analogue methods of studying electromagnetic variations at the Earth's surface. Vol. I—II. Inst. of Earth Sciences, The University of B.C. pp. 212.

ФОМИНА, В. И.—КУЗНЕЦОВ, А. Н.—КОЧАРЯНЦ, Е. Б. 1972: Частотные зондирования под моделю ступени опорного электрического горизонта. (Frequency soundings above step-like model of the geoelectric basement). *Prikladnaya Geofizika*, 68.

ИСАЕВ, Г. А.—КАУФМАН, А. А.—РАБИНОВИЧ, Б. И.—ШАТОХИН, В. Н. 1970: Теория электромагнитных полей применяемых в разведочной геофизике (Influence of dipping layers to electromagnetic fields in geoelectric prospecting). Monography, Nauka, Novosibirsk.

KAKAS, K.—NYITRAI, T.—REZESSY, G.—SZABADVÁRI, L. 1976: Complex geophysical exploration in the Transdanubian Mountains Range. MÁELGI 1975 Report, 11—22.

KORMOS, I.—RÉGENI, P. 1978: Some problems of the indirect frequency synthesis. HIKI — 25 Years 1978. Conference Proceedings, 3, 55—58.

КУЗНЕЦОВ, А. Н.—ЗАВАДСКАЯ, Т. Н. 1974: Дипольное электромагнитное зондирование горизонтально-неоднородных сред, включающих непроводящие экраны. (Electromagnetic soundings by dipol configurations above inhomogeneous media containing non-conducting screening layer). *Prikladnaya Geofizika*, 68.

RÉGENI, P.—MONÁCSI, I. 1978: A tracking selective microvoltmeter. HIKI — 25 Years 1978. Conference Proceedings Vol. 3 pp. 60—63.

SZARKA, L. 1980: Potenciáltérképezés analóg modellezéssel. (Analogue modeling of potential mapping). *Magyar Geofizika*, 21, 193—200.

АНАЛОГОВОЕ МОДЕЛИРОВАНИЕ ДЛЯ ИССЛЕДОВАНИЯ ГЕОЭЛЕКТРИЧЕСКИХ МЕТОДОВ В ГЕОДЕЗИЧЕСКОМ И ГЕОФИЗИЧЕСКОМ ИССЛЕДОВАТЕЛЬСКОМ ИНСТИТУТЕ АКАДЕМИИ НАУК ВНР

А. АДАМ—Я. ПОНГРАЦ—Л. САРКА—П. КАРДЕВАН—Л. САБАДВАРИ—З. НАДЬ—И. ЗИМАНИ—И. КОРМОШ—П. РЕГЕНИ

РЕЗЮМЕ

Поскольку в Венгрии геоэлектрические и электромагнитные методы имеют важное значение в геофизической разведке, стало необходимым решать интерпретацию сложнейших трехразмерных геологических структур.

Для этой цели служит электромагнитная моделирующая лаборатория, которая была создана в Шопроне в Геодезическом и Геофизическом Исследовательском Институте совместной работой нескольких венгерских учреждений.

Чтобы удовлетворить требованиям моделирования, было необходимо планировать установку, работающую в экстремально широкой области частот.

Эта установка в нынешнем этапе развития состоит из группы инструментов, которые пригодны для моделирования искусственных частотных зондирований электрическими диполями и для моделирования нескольких электроразведочных методов постоянными токами.

Большое количество измеряемых данных и потребность в вычислении разных параметров сделали необходимым применение ЭВМ.

До сих пор эта моделирующая установка была применена в исследовании дайков с хорошей электрической проводимостью находящихся в разломных зонах на территории аномалий с электрическими проводимостями Задунайского Края. Установка тоже применялась в боксит-разведочной работе Геофизического Института им. Этвеша и с ней моделировали для Геофизического Разведочного Предприятия частотные зондирования над основаниями геологических бассейнов.

Acta Geodaet., Geophys. et Montanist. Acad. Sci. Hung. Tomus 16 (2—4), pp. 381—395 (1981)

PC 3—4 TYPE GEOMAGNETIC PULSATION PERIODS ALONG A MERIDIONAL CHAIN IN CENTRAL EUROPE

J. CZ. MILETITS

GEODETIC AND GEOPHYSICAL RESEARCH INSTITUTE OF THE HUNGARIAN ACADEMY OF SCIENCES, SOPRON

A summary is given on the investigations of the latitude dependence of geomagnetic pulsation periods. A detailed study of the latitude dependence of Pc 3—4 periods has been carried out using one month data of a meridional chain of stations consisting of 4 stations at the latitudes $\Phi = 42.9 - 52.2°$ N. As the latitude dependence of pulsation periods is strongly connected with the origin of the pulsations, theories of pulsation excitation are also reviewed. Latitude dependence may yield clues for the control of the theories, therefore enables a better understanding of the near-Earth space.

Geomagnetic pulsations play an important role in a better understanding of magnetospheric processes. In recent years, the determination of certain pulsation parameters proved to be an effective tool for the surface monitoring of magnetospheric and interplanetary phenomena. It is, however, unclear how the pulsation activity is influenced by magnetospheric parameters, and a theoretical determination of the pulsation periods did not succeed so far, either. The dependence of the periods of the geomagnetic pulsations on the geographic latitude can contribute significantly to an understanding of these connections.

For a study of the latitude dependence of pulsation periods simultaneous geomagnetic or earth current records from different stations are necessary. It is generally accepted that the period of the Pi-type pulsations does not change with the latitude, at least at middle latitudes, while there is no uniform view on the latitude dependence of Pc-type pulsations.

The first studies of the latitude dependence were made by OBAYASHI and JACOBS (1958) with the result that periods get longer at higher latitudes. The same result was confirmed by DUNCAN (1961) and VOELKER (1963). The latter used in the FRG three instruments of the same type at different latitudes, therefore the first reliable proof for the latitude dependence has been received by his study. Later pulsations with latitude dependent periods were identified by BOL'SHAKOVA and ZYBIN (1964), FANSELAU (1966, 1968), ELEMAN (1967), VERŐ (1969), SAITO (1969), ORR and MATTHEW (1971). On the contrary, ELLIS (1961), HERRON and HEIRTZLER (1966), BARANSKY et al. (1969) did not found any latitude dependence of the periods.

In an earlier experiment [CZ. MILETITS, 1971] the average periods of Pc-type pulsations were determined from the records of 30 observatories distributed at different parts of the Earth, whereby a period-increase with latitude from the geomagnetic equator towards higher latitudes, till the auroral zone was found. The rate of increase has shown three frequency peaks at rates of 0 (i.e. no latitude dependence), 4 and 10 percent increase for one degree of geomagnetic latitude.

For the investigations carried out in several steps the results of the synchronous measurements organized by the KAPG completed with the data of more and more observatories were used [ÁDÁM et al., 1972, 1976; CZ. MILETITS, 1975]. It has been also dealt with the problem whether the period change is continuous or stepwise. Indications were found that pulsations have periods being in harmonic relations to each other, but the basic period remained uncertain. For the following investigations, pulsation spectra were used.

In a next step the microstructure of the pulsations was studied, i.e. coherence and amplitude spectra of pulsation events recorded at distant stations were compared [CZ. MILETITS and VERŐ, 1975; CZ. MILETITS, 1977, 1978]. It was found again that the peaks of both types of spectra can be considered as harmonics of a basic period of several minutes.

The latitude dependence of the pulsation periods is in connection with the origin of the pulsations. There are several possible excitation mechanisms, which could be controlled by it. Such a theory would significantly contribute to a better understanding of the Earth's environment. Pulsations were always supposed to originate outside of the rigid Earth. Some theories considered the ionosphere as the source region, while variations in the equatorial ring current were also regarded as possible sources at least for a part of the pulsations. DUNGEY (1954) as first pointed out the possibility of the inner-magnetospheric origin of pulsations by certain field line resonances. The resonant period would naturally depend on the geomagnetic latitude. The form of this dependence changes with the magnetospheric model adopted.

In this connection the idea of the harmonic structure of the pulsation spectra seemed to be of interest. The basic period would be in the period range of Pc 5 [CZ. MILETITS and VERŐ, 1965]. The Pc 5-type pulsation is excited at the magnetopause by a Kelvin—Helmholtz instability due to inhomogeneities in the solar wind. The harmonics of the basic period propagate inwards together with the basic wave and get into resonance with particular field lines [STUART and USHER, 1966]. Our results were not in contradiction to this theory, but the determination of the basic period proved to be very uncertain [CZ. MILETITS and VERŐ, 1975; CZ. MILETITS, 1977].

DUNGEY's idea in a somewhat modified form of resonating magnetic shells has been widely accepted. Such a shell consists of field lines crossing the equatorial plane at identical distances, and it can resonate independently of

neighborous shells with the period corresponding to DUNGEY's theory. In the framework of this theory an explanation can be found for the different rates of the period change in our investigations (0, 4 and 10%/°). The footprint of a resonating shell has everywhere the same pulsation period, then it changes stepwise to the period corresponding to the next shell. According to recent estimations the width of a shell is 150—200 km, and in such distances the period can remain constant, or change by a value corresponding to neighborous shells, etc. Thus the period can change with the latitude in different rates, the typical values were found by us, but their occurrence frequency differs according to the frequency of momentaneous situations [CZ. MILETITS, 1971].

In recent years it became obvious that a great part of Pc 3—4 type pulsations originate outside of the magnetosphere, in the space at and before the magnetopause. In case of the outer-magnetospheric origin the harmonic structure cannot be maintained, but inner magnetospheric resonances are possible.

The idea of the outer magnetospheric origin of pulsations is supported by connections between pulsation parameters and parameters of the interplanetary space. The pulsation periods have approximately a value of $T(s) = 160/B$, where B is the interplanetary magnetic field in nT. This connection was found by GUL'ELMI (1974) and he was among the firsts to propose a hypothesis of the excitation of the pulsations before the magnetopause and the shock wave. The excitation mechanism he considered was proton cyclotron instability in the solar wind due to reflected protons from the magnetosheath. GUL'ELMI et al. (1976) investigated numerically this cyclotron instability supposing Maxwellian distribution for both the solar wind and the reflected protons. An instability in the range of Pc 3 seemed to be possible.

KOVNER et al. (1977) have supposed Kelvin—Helmholtz instability at the plasmapause as the source of long period pulsations, and at the magnetopause as that of shorter period pulsations.

If pulsations are excited outside of the magnetosphere in the region before the magnetopause, it must be re-evaluated how latitude-dependent periods originate. Several possibilities can be taken into consideration.

One possibility is that only primary spectra are determined by the source region, and when propagating through the magnetosphere, the signals change due to e.g. shell resonances. In this case, however, the validity of the connection $T = 160/B$ at different latitudes is not clear.

An other possibility is to suppose that only a part of the pulsations have extra-magnetospheric origins, namely those which have latitude-independent periods. It is further possible that pulsations originating outside and inside the magnetosphere are mixed; even pulsations with identical periods at different latitudes may originate at the plasmapause. ORR (1973) supposes that pulsations with latitude-dependent periods may originate from the plasma-

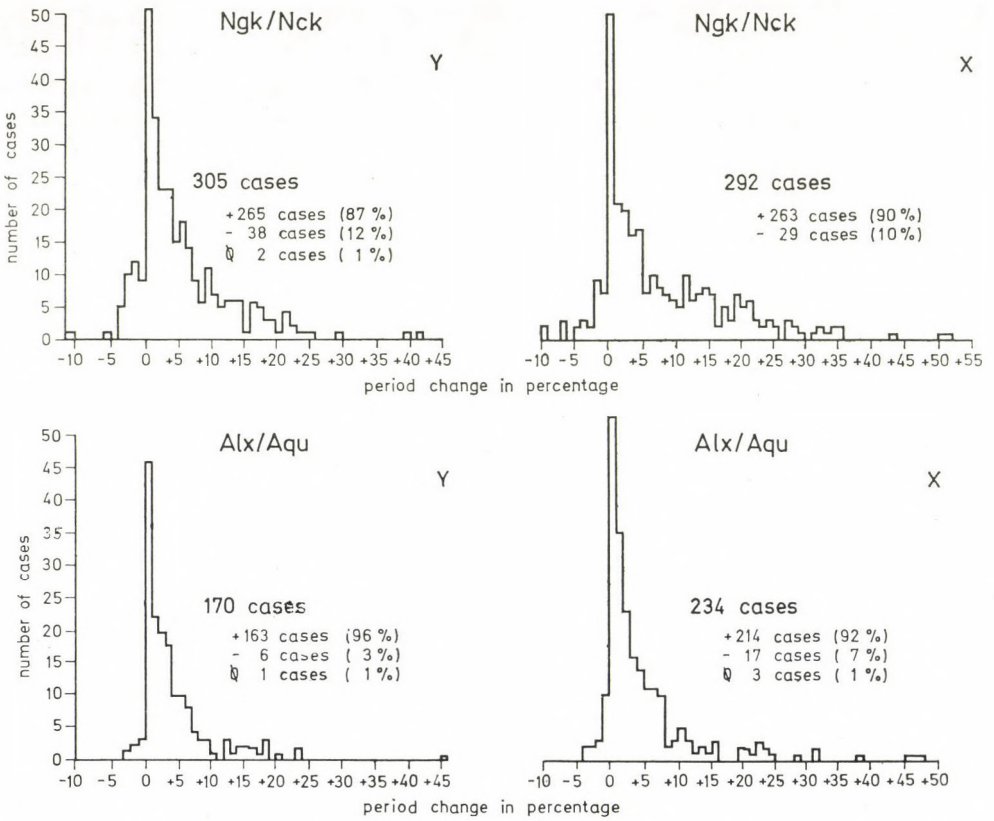

Fig. 1. **Period changes in per cents between the observatory pairs Ngk/Nck and Alx/Aqu for both components (magnetic or telluric)**

pause, too. From practical experience it is clear, however, that at least a part of the extramagnetospheric signals have latitude-dependent periods at the surface. So, it is inevitable to suppose a mechanism in the magnetosphere which selects different periods from the primary spectrum at different latitudes. The most likely mechanism seems to be the shell-resonance.

Anyway, it is rather paradoxical that while the pulsation periods are determined by the interplanetary magnetic field, their periods still depend on the latitude [Cz. MILETITS, 1980b].

For a study of these problems the microstructure of the latitude dependence of pulsation periods may yield an important contribution. For this purpose a meridional chain of stations was established with the Nagycenk observatory in the centre, one Northern (Niemegk) and one Southern (L'Aquila) station lying farther away, and a temporary station (Alexandra) lying some 180 km to the South of the observatory. Data of the stations are shown in

Table I

Station	Code	Geographical coordinates		Geomagnetic coordinates	
		φ	λ	Φ	Λ
Niemegk	Ngk	52°04′ N	12°41′ E	52.2°	96.5°
Nagycenk	Nck	47°38′	16°43′	47.2°	98.3°
Alexandrapuszta	Alx	46°05′	17°30′	45.6°	98.8°
L'Aquila	Aqu	42°23′	13°19′	42.9°	93.0°

Table I. Records from about one month (March—April 1977) were collected, including earth current (in Hungary and in Ngk) and magnetic components (in Aqu). For each typical Pc-event (about 300 events at all) the average

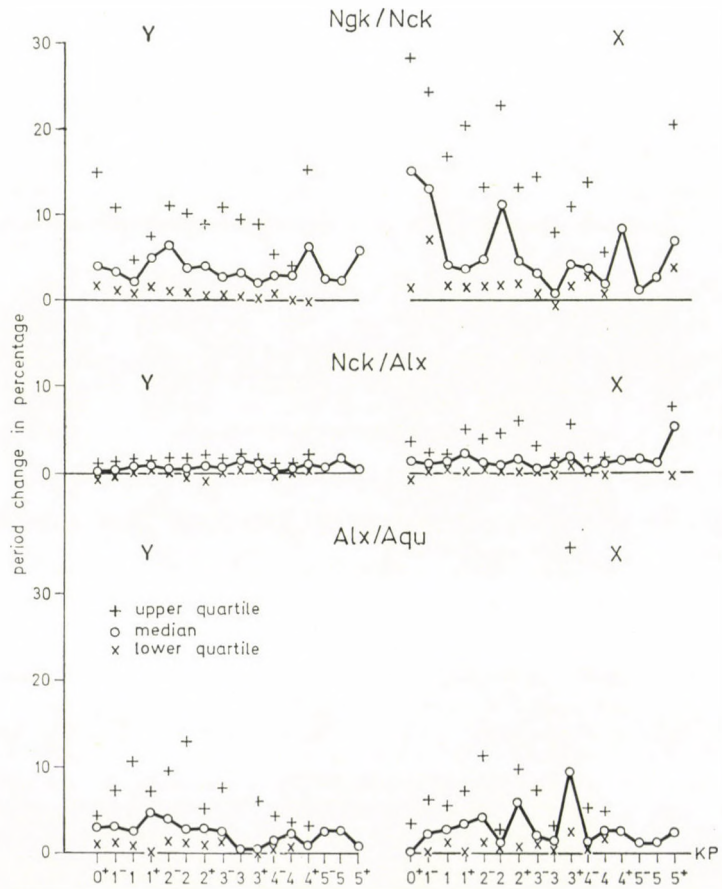

Fig. 2. Period changes in function of the geomagnetic activity (Kp) for the pairs of observatories Ngk/Nck, Nck/Alx, Alx/Aqu

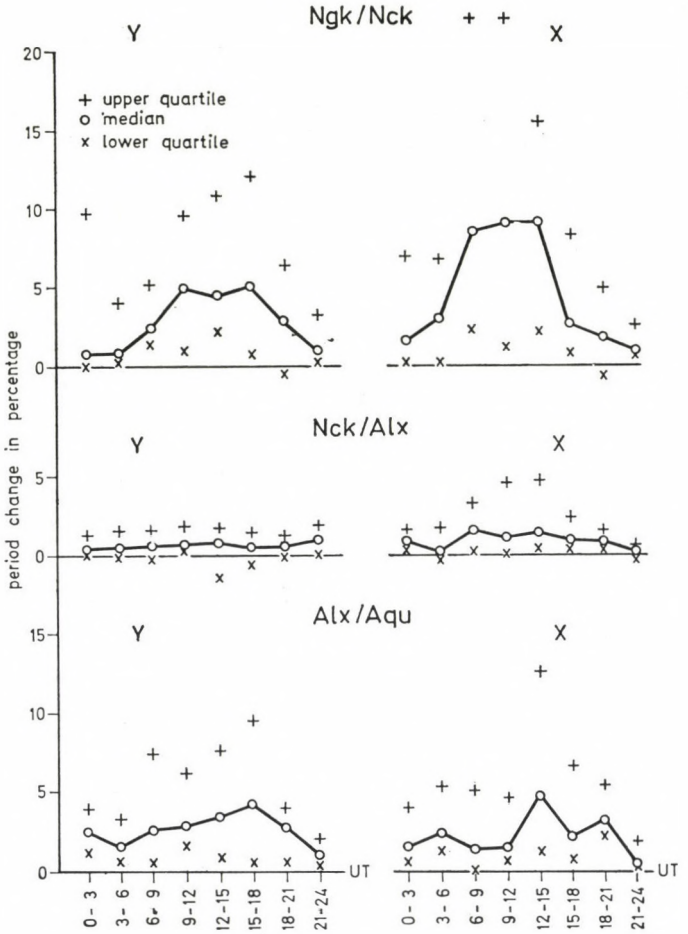

Fig. 3. Period changes in function of local time for the same pairs of observatories

period was computed at each station. Such an event contained at least 5, but generally about 10 individual cycles of rather regular shape. About 90% of the events were of Pc 3-type, the others of Pc 4-type. From these averages the rate of the period change was determined between each pairs of observatories.

One of the first results of this investigation was that period changes could be proved even between stations lying in N—S direction only 180 km far from each other. In both components the average periods were longer in Nagycenk than in the more Southern station Alexandra. The rate of the period change is greater in the X (earth current E—W or magnetic N—S) components than in the Y (earth current N—S or magnetic E—W) components [Cz. MILETITS, 1979].

The rates of period changes have not a normal distribution (Fig. 1), but they can be well approximated with the sum of two normal distributions. There is a distinct maximum between 0 and 1% (positive values indicate periods increasing with increasing latitude), and several smaller maxima at higher rates, too. The average rate depends approximately linearly on the distance between the stations.

No differences were found in the latitude dependence in function of geomagnetic activity as illustrated by Fig. 2 where the rate of the period change is shown for all the three station pairs *vs.* geomagnetic activity. The station pairs are formed in decreasing order of latitude. For sake of simplicity quartiles and medians are represented here. This independence is in contradiction with several other investigations.

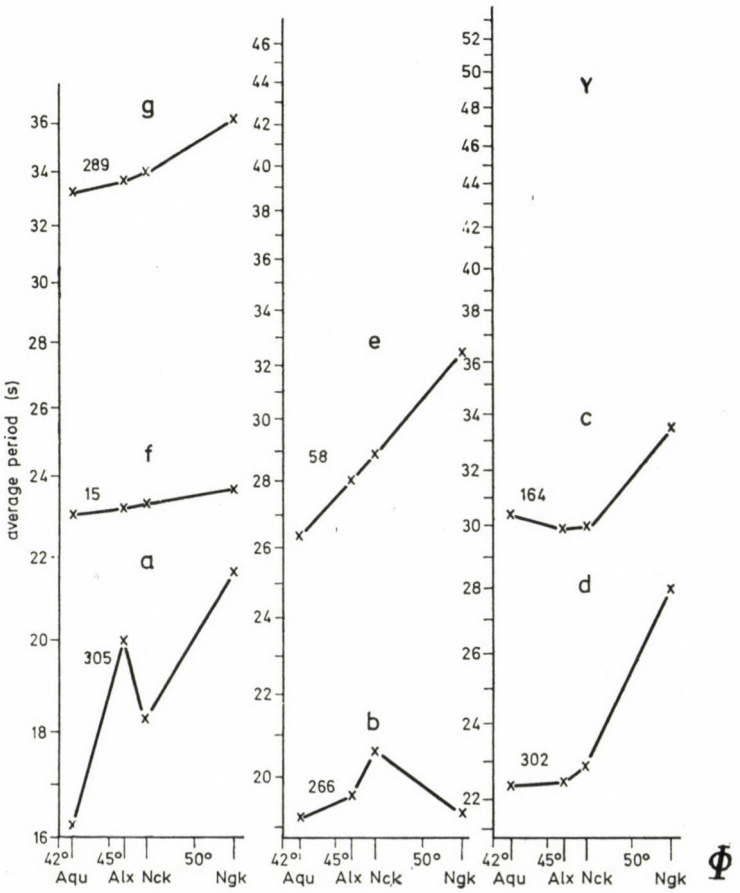

Fig. 4. Different types of the latitude dependence of periods. (*Y* components). Explanation see in text

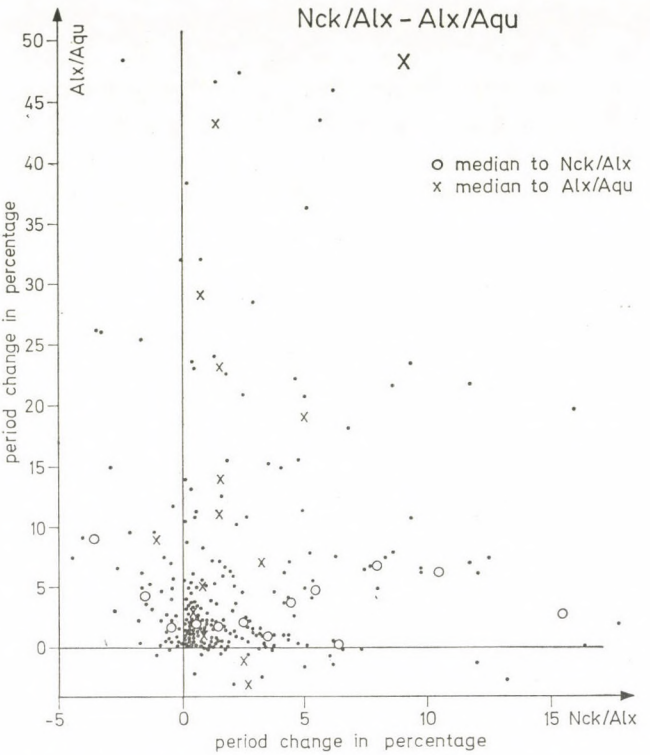

Fig. 5. Correlation of the period changes for the X components of the station pairs Nck/Alx and Alx/Aqu

The rate of period change does depend, however, on local time, it is maximum during local daytime with a maximum around local noon (Fig. 3).

If cross sections of the latitude dependence of periods are constructed, it becomes clear that very different types can occur for both types Pc 3 and Pc 4, the occurrence frequency of these types is rather different. Figure 4 shows some typical examples for the most common types of latitude dependence. Numbers at the curves denote the serial number of the events studied.

There are cases when the period increases more (*e*) or less (*f*, *g*) rapidly, sometimes with a minimum at one intermediate station (*a*), or at two stations (*c*), or with a maximum (*b*). In case *d*, there is a nearly stepwise increase between the two Northern stations.

It is therefore clear that the period increase in function of the latitude takes place on the background of rather big random variations which are uncorrelated at the different stations, thus for their interpretation more or less independent sources, e.g. shell resonances are necessary.

The uncorrelated changes of the periods between different stations can be seen in Fig. 5, where the period changes at the station pairs Nck/Alx and

Alx/Aqu (X components) are shown in function of each other. As the medians shown lie along horizontal and vertical lines, the two kinds of changes are independent. Similar situation is found for the station pairs (Ngk/Nck and Alx/Aqu which are computed from fully different stations (Fig. 6). If, however, station pairs are compared where one section (pair of stations) includes the other, as e.g. in case of Ngk/Alx and Ngk/Nck, the correlation is very strong, the medians lie both along nearly the same oblique line (Fig. 7).

As already mentioned, a minor part of the several hundred events were of Pc4 type. According to the present and other investigations, it seems that the boundary between the two types is by no means a sharp one, and it would be more acceptable to set the boundary at 30 s.

In the majority of the events the period — as mentioned — was shorter even than 30 s. The average change of the periods is stronger if the period is shorter (Fig. 8). This regularity has been illustrated in form of an adjusting family of curves, each of them representing the rate of the period change for a certain period in Nagycenk in form of averages for the different local times. The curves are represented in Fig. 9 for periods 15, 20, 25 . . . 90 s, and show that the rates of period change are greater during local day, and increase with decreasing period. Both the rate of the period change and its daily variation are rather big if the period is shorter than 30 s, for longer period

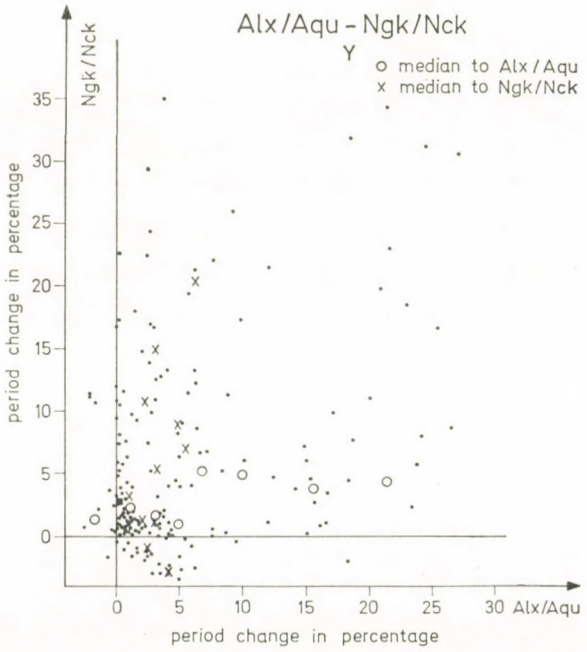

Fig. 6. Correlation of the period changes for the station pairs Alx/Aqu and Ngk/Nck (Y components)

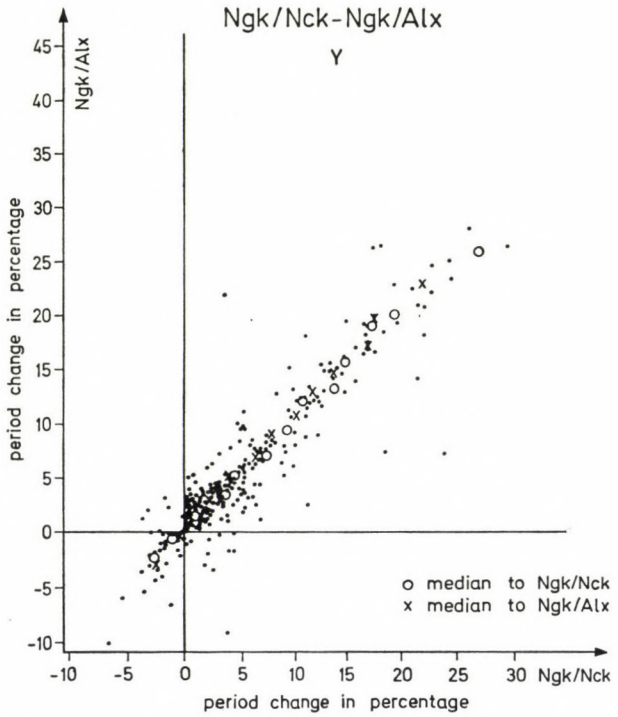

Fig. 7. Correlation of the period changes for the station pairs Ngk/Nck and Ngk/Alx (*Y* components)

both are much smaller. It should be remarked that the daily variation of the occurrence frequencies has a single daily wave for periods less than 30 s, for longer periods it has a double wave (morning and evening maxima). The transition at 30 s is here naturally continuous as the mathematical model does not allow abrupt changes [Cz. MILETITS, 1980a].

From a time-series of the period changes not shown here it is evident that the rate of the period change is at first rather big for a certain time, then gets small, and remains so for some hours, then after it becomes again greater. When the rate changes, the form of the pulsations can remain unaltered.

All these facts show that pulsations with periods less than 30 s and those with longer periods belong to different physical classes. (There is some overlapping, as in a part of the shorter period pulsations, the signals belong to the "longer period" group; the inverse case does not occur.) As it was supposed that in addition to the period difference, the regularity of the two groups differ, too, an immediate comparison of regularity and rate of period changes seemed necessary.

The pulsation events of the Nagycenk observatory are grouped into 4 groups according to their regularity:

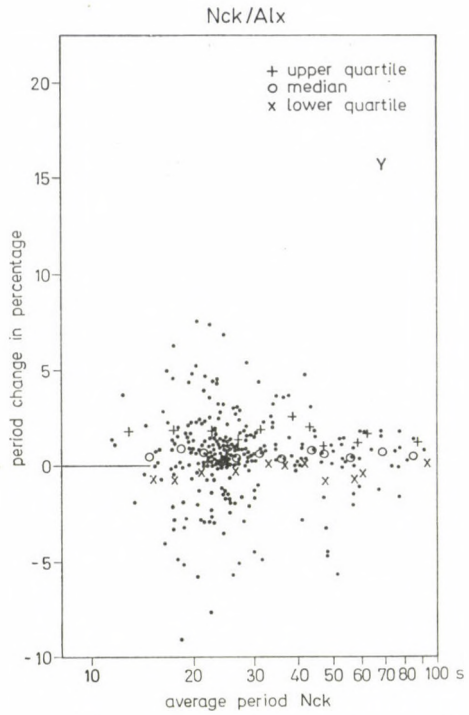

Fig. 8. **The period changes in *Y* components of the station pair Nck/Alx in function of the pulsation period in the observatory Nck**

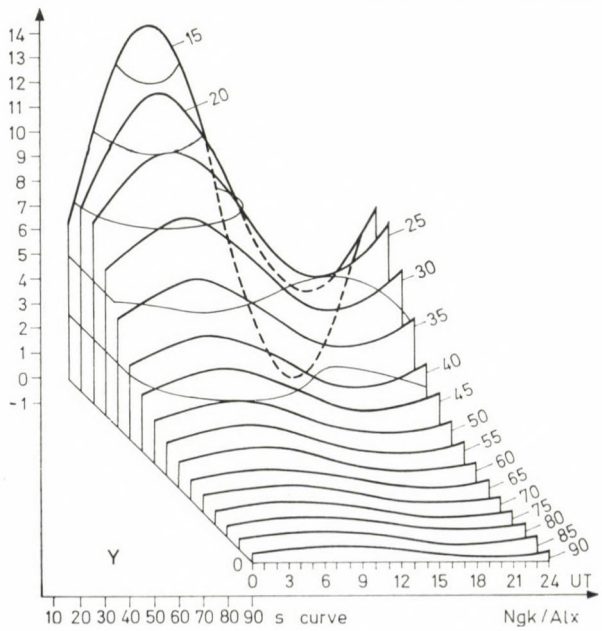

Fig. 9. **The daily variation of the period change in function of local time and period for the observatory Nck**

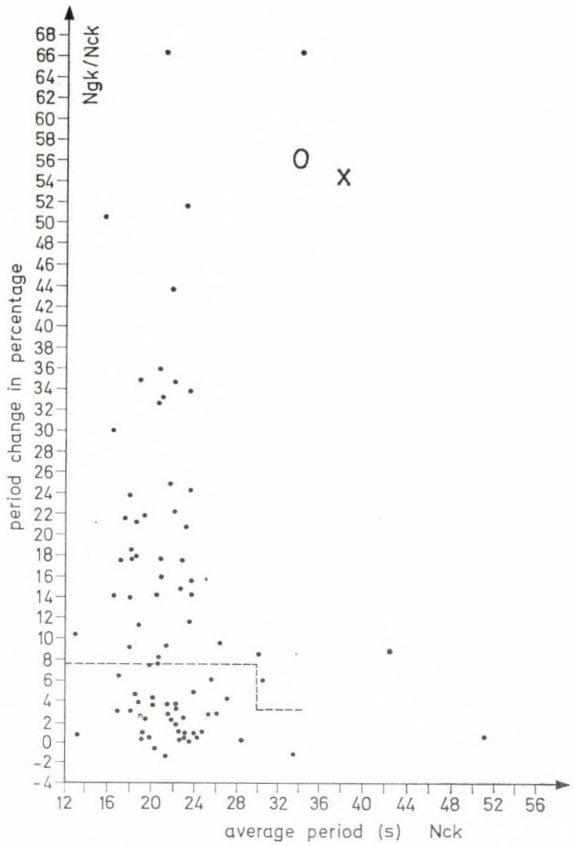

Fig. 10. The period changes for the station pair Ngk/Nck for events of very regular character (O-s) in function of the average period (*X* components)

1. Oscillations (O), if the difference of the periods in the event is less than $\pm 10\%$,

2. Quasi-oscillation (Q): the periods differ by less than $\pm 50\%$;

3. Waves (W): any period is allowed, if the form is sinusoidal;

4. Irregular variations (T): all others (in the present case, less than 5% of all events belong to this group).

Figures 10 and 11 show two typical groups, O and W from the material of the pair Ngk/Nck, in function of the Nagycenk periods. Medians are shown separately for periods less and more than 30 s. It can be seen, that in case of the group W, there are more variations with periods above 30 s, and even the shorter period cases have higher rates of period change.

A physical boundary in the pulsations at periods of 30 s has been already supposed several times (e.g. [RANKIN and KURTZ, 1970; GOKHBERG et al., 1976]), but without greater emphasis. The first mention of a difference in the latitude dependence for periods above and below 30 s is at JACOBS and SINNO

(1960), who found latitude-dependent periods only for shorter period events, similarly to the present results.

A number of other differences have also been found between the two kinds of pulsations: VERŐ (1980) found for the shorter period group a weak influence by the geomagnetic activity, and a strong one by the interplanetary medium, and vice versa. He has also shown that the frequency of occurrence spectra can be supposed to be the sums of two, nearly lognormal distributions: one includes the regular, shorter period cases (between about 10 and 30 s), the other the remaining pulsations (between 10 and 90 s).

It is paradoxical that periods changing with geomagnetic latitude, i.e. from station to station would follow a connection $T = 160/B$ which seems to be valid for both kinds of pulsations. VARGA (1980) carried out computations based on KOVNER's model and found that the primary spectrum is rather wide, being several times 10 s wide. From this the shell-resonance selects the corresponding period. If the resonance is strong, the latitude dependence follows the characteristic shell periods, which can depend on the IMF due to the distortion of the magnetosphere. If the primary spectrum contains the actual shell resonant period, the resonance is active, and regular pulsations appear. If it does not contain the shell resonance, the variations are less regular, but the dependence on the IMF intensity remains. Thus, the extramagnetospheric signals are strongly modified inside of the magnetosphere.

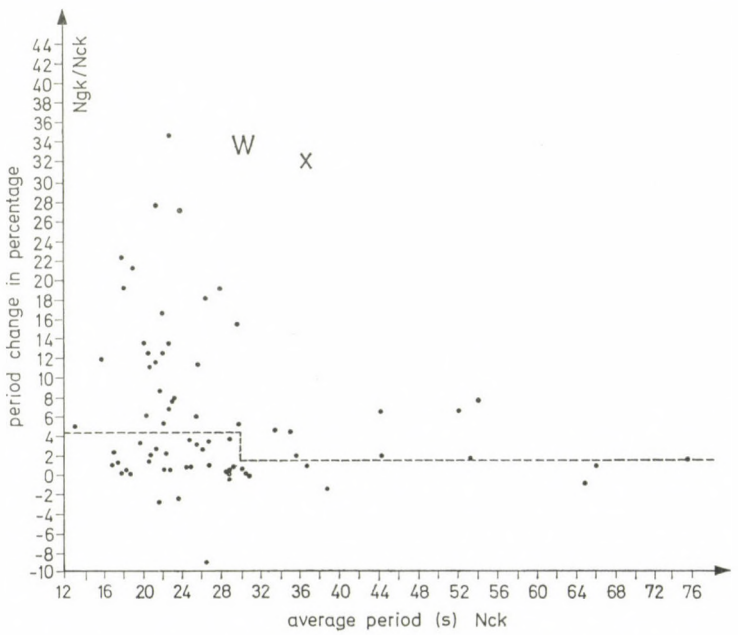

Fig. 11. The period changes for the station pair Ngk/Nck for events of rather irregular character (W-s) in function of the average period (X components)

Our investigations with the meridional chain of 4 stations has shown that the period changes of the pulsations in different sections of the chain are uncorrelated, thus yielded an important proof for the shell resonance idea. The most important point is the separation of the two groups of pulsations, one of them having periods less than 30 s and regular form, a strong latitude dependence of the period and an occurrence maximum at local noon. The other type has periods of 10—60 s, the latitude dependence of the period is small, the waveform is less regular and the occurrence peaks at morning and evening.

We identified the pulsations from shell resonances with those having great latitude dependence and regular wave forms. As the shells are only loosely coupled, they resonate rather independently, thus the high rate of period change can be explained. The shell thickness is a function of momentaneous ionospheric and magnetospheric parameters, thus the uncorrelated latitudinal changes can also be explained. The other group contains variations which reflect more or less directly the primary spectrum, therefore the wave form is irregular and the period does not depend on the latitude.

REFERENCES

ÁDÁM, A.—CZ. MILETITS, J.—VERŐ, J. 1972: Das Mikropulsationsfeld in Osteuropa (Ergebnisse der KAPG-Synchronmessungen vom Jahre 1969). *Acta Geod. Geoph. Mont. Hung.*, 7, 289—304.

ÁDÁM, A.—CZ. MILETITS, J.—VERŐ, J. 1976: Inhomogeneity of the pulsation field and its effect on the MT values. Geoelectric and Geothermal Studies (East-Central Europe, Soviet Asia) KAPG Geophysical Monograph, Akadémiai Kiadó, Budapest, 296—302.

БАРАНСКИЙ, Л. Н.—БОЛЬШАКОВА, О. В.—ГЕЛЛЕР, Л. А.—КАЗАК, Б. Н. 1969: О широтной зависимости периода и амплитуды устойчивых колебаний Pc 3—4. Геомагн. аэрон., 9, 1128—1129.

БОЛЬШАКОВА, О. В.—ЗЫБИН, К. Ю. 1964: Устойчивость и частотный спектр микропульсаций геомагнитного поля. Геомагнитные Исследования № 6. Изд. Наука. Москва, 87—94.

CZ. MILETITS, J. 1971: On the latitude dependence of Pc-type pulsations. *Acta Geod. Geoph. Mont. Hung.*, 6, 141—153.

CZ. MILETITS, J. 1975: New investigation on the latitude-dependence of Pc-type geomagnetic pulsations. To the 75th birthday of Professor Antal Tárczy-Hornoch. Geodetical and Geophysical Research Institute of the Hungarian Academy of Sciences. Sopron, 256—266.

CZ. MILETITS, J. 1977: Pulzációk spektrum vizsgálata (A spectral analysis of pulsations). Ionoszféra és magnetoszféra fizika, IV. 139—143.

CZ. MILETITS, J. 1978: A study of geomagnetic pulsations periods. *Acta Geod. Geoph. Mont. Hung.*, 13, 425—435.

CZ. MILETITS, J. 1979: Pc típusu pulzációk periódusának szélességfüggőségi vizsgálata egy meridionális állomásláncon (A study of the latitude dependence of pulsation periods using a meridional chain of stations). Ionoszféra és magnetoszféra fizika, VII. 63—78.

CZ. MILETITS, J. 1980 a: A szélességfüggő és nem szélességfüggő periodusu Pc típusu pulzációk (30 sec körüli) periódus határáról (On the boundary of pulsations with latitude dependent and independent periods at 30 s). Ionoszféra és magnetoszféra fizika, VIII. 58—66.

CZ. MILETITS, J. 1980 b: Microstructure of the latitude dependence of Pc-type pulsation periods. *J. Atmos. Terr. Phys.*, 42, 563—567.

CZ. MILETITS, J.—VERŐ, J. 1965: A földi elektromágneses tér pulzációinak kapcsolata a hosszabb periódusu variációkkal (On the connection of electromagnetic pulsations with longer period pulsations). *MTA Műsz. Tud. Oszt. Közl.*, 35, 107—117.

CZ. MILETITS, J.—VERŐ, J. 1975: Vergleich simultaner Pulsationsspektra bei grossen Längenunterschieden. *Acta Geod. Geoph. Mont. Hung.*, 10, 147—153.

DUNCAN, R. A. 1961: Some studies of geomagnetic micropulsations. *J. Geoph. Res.*, 66, 2087—2094.
DUNGEY, J. W. 1954: Electrodynamics of the outer atmosphere. Penn. State Univ. Ionosph. Res. Sci. Report No 69, 1—52.
ELEMAN, F. 1967: Studies of giant pulsations, continuous pulsations, and pulsation trains in the geomagnetic field. *Arkiv för Geof.*, 5, 231—282.
ELLIS, G. R. A. 1961: Geomagnetic micropulsations. *Austr. J. Phys.*, 13, 625—632.
FANSELAU, G. 1966: Zur Feinstruktur der geomagnetischen Pulsationen Pc 3. *PAGEOPH*, 65, 73—94.
FANSELAU, G. 1968: Physical aspects of Pc 3 and Pc 4. *Ann. Géoph.*, 24, 241—243.
ГОХБЕРГ, М. В.—ПОХОТЕЛОВ, О. А.—ТРОИЦКАЯ, В. А. 1976: О возможности определения структуры собственных колебаний магнитосферы по наземным данным. Докл. Акад. Наук СССР, 229, 587—589.
GUL'ELMI, A. V. 1974: Diagnostics of the magnetosphere and interplanetary medium by means of pulsations. *Space Sci. Rev.*, 16, 331—345.
ГУЛЬЕЛЬМИ, А. В.—ПОТАПОВ, А. С.—Д'КОСТА, А. 1976: К теории возбуждения геомагнитных пульсаций типа Pc 3. Исследования по геомагнетизму, аэрономии и физике солнца, Вып. 39, 27—32.
HERRON, T. J.—HEIRTZLER, J. R. 1966: Latitude-period dependency of geomagnetic micropulsations. *Nature*, 210, 361—363.
JACOBS, J. A.—SINNO, K. 1960: World-wide characteristics of geomagnetic micropulsations. *Geoph. J. RAS*, 3, 333—353.
КОВНЕР, М. С.—МИШИН, В. В.—ШКЕЛЕВ, Е. И. 1977: О гидромагнитных пульсациях в магнитосфере и неустойчивости Кельвина—Гельмгольца. *Геомаг. аэрон.*, 17, 714—718.
OBAYASHI, T.—JACOBS, J. A. 1958: Geomagnetic pulsations and the earth's outer atmosphere. *Geoph. J. RAS*, 1, 53—63.
ORR, D. 1973: Magnetic pulsations within the magnetosphere: A review. *J. Atmos. Terr. Phys.*, 35, 1—50.
ORR, D.—MATTHEW, J. A. D. 1971: The variation of geomagnetic micropulsation periods with latitude and the plasmapause. *Planet. Space. Sci.*, 19, 897—905.
RANKIN, D.—KURTZ, R. 1970: Statistical study of micropulsation polarization. *J. Geophys. Res.*, 75, 5444—5452.
SAITO, T. 1969: Geomagnetic pulsations. *Space Sci. Rev.*, 10, 319—412.
STUART, W. F.—USHER, M. J. 1966: An investigation of micropulsations at middle latitudes. *Geoph. J. RAS*, 12, 71—86.
VARGA, M. 1980: A numerical study of the excitation of Pc 2—4 type pulsations. *J. Atmos. Terr. Phys.*, 42, 365—369.
VERŐ, J. 1969: On the variability of micropulsationperiods. *Acta Geod. Geoph. Mont. Hung.*, 4, 3—12.
VERŐ, J. 1980: Geomagnetic pulsations and parameters of the interplanetary medium. *J. Atmos. Terr. Phys.*, 42, 371—380.
VOELKER, H. 1962: Zur Breitenabhängigkeit der Perioden erdmagnetischer Pulsationen. *Die Naturwissenschaften*, 49, 8—9.
VOELKER, H. 1963: Zur Breitenabhängigkeit erdmagnetischer Pulsationen. Mitteilungen Max-Planck-Inst. Aeronomie, Nr. 11. 1—55.

ПЕРИОД ГЕОМАГНИТНЫХ ПУЛЬСАЦИЙ ТИПА Пц 3—4 ВДОЛЬ МЕРИДИОНАЛЬНЫЙ ЦЕПИ В СРЕДНЕЙ ЕВРОПЕ

Й. Ц. МИЛЕТИЧ

РЕЗЮМЕ

В статье излагаются результаты исследований проведенных автором в отношении зависимости пульсаций типа Пц 3—4 от широт. Более детально рассматриваются результаты исследований проведенных на геомагнитных обсервационных материалах, регистрированных в течение месяца вдоль меридиональной цепи, состоящейся из 4 станций ($\Phi = 42{,}9°-52{,}2°$ северной широты). Так как зависимость от широты тесно связана с вопросом возникновения пульсаций, автором излагаются и теории, связанные с возникновением пульсаций. Зависимость от широты позволяет проверку некоторых соображений, обнадеживая лучшим познаванием околоземного пространства.

Acta Geodaet., Geophys. et Montanist. Acad. Sci. Hung. Tomus 16 (2—4), pp. 397—403 (1981)

ABOUT THE CONNECTION BETWEEN LONGER PERIOD GEOMAGNETIC VARIATION AND THE INTERPLANETARY MAGNETIC FIELD

L. HOLLÓ

GEODETIC AND GEOPHYSICAL RESEARCH INSTITUTE OF THE HUNGARIAN ACADEMY OF SCIENCES, SOPRON

In this paper investigations are presented on the connection between geomagnetic variations with periods 2—60 min and intensity and direction of the interplanetary magnetic field (IMF). It seems that IMF influences mainly the variations with periods longer than 12 min and this effect is maximum for variations with periods of about 1 hour. In this case the activity is namely increasing — mainly for the night time activity — if the IMF is directed towards south. The variations with periods 2—12 min are primarily connected with the overall geomagnetic activity, and depend on the IMF only indirectly.

In situ space measurements caused a basic change of our ideas on events in the geomagnetic field and their connection with the interplanetary magnetic field.

Geomagnetic pulsations were shown to correlate with certain parameters of the interplanetary magnetic field and solar wind [1]. It was found that the pulsation periods are inversely proportional with the IMF intensity, while the pulsation activity is correlated with the IMF direction and solar wind velocity.

Among a wide range of longer period geomagnetic events, mostly substorms were investigated as they constitute the most remarkable class of phenomena. They mainly occur during geomagnetic storms, but are often met also during quiet times indicating some kind of instability in the magnetospheric tail.

The aim of the present investigation was to look for general connections between longer period geomagnetic variations (periods 2—60 min) and the parameters of the IMF. A statistical study was carried out using the 4 out of the 5 period bands applied for the description of the geomagnetic activity in the Nagycenk ($\Phi = 47.2°$, $\Lambda = 98.3°$) observatory. The activity of these bands is determined in each hour from the telluric current records of the observatory permanently. These values were then grouped according to certain direction groups of the IMF. The period ranges are the following:

K_1 periods of 0— 2 min (pulsations, not discussed here)
K_2 periods of 2— 6 min (long period pulsations)

K_3 periods of 6—12 min
K_4 periods of 12—24 min
K_5 periods of 24—60 min (including substorms).

The average daily activity in each period band is characterized by an index number between 0 and 9, with each index having the same frequency of occurrence in a basic interval. Original records have a scale value 0.18 mV per km for 1 mm.

From the NASA-NSSDC Data Book the intensity [4] (in nT) and the direction (in solar ecliptic coordinates, azimuth and inclination, ϑ, i) of the IMF could be obtained for any time between 1963 and 1974. In the present investigation the data of the year 1972 were used so, that directions of the IMF, pointing towards certain parts of the unit sphere were grouped and the corresponding activity indices computed. Altogether about 40,000 data were averaged.

Since the K_p index characterizing the geomagnetic activity is in connection with the parameters of the solar wind and the IMF (solar wind energy and velocity, respectively, direction of the IMF), the effect of the geomagnetic field must be separated from the effect of the IMF. The grouping of the IMF data has enabled that the situation in case of different IMF intensities, or of different geomagnetic activity levels could be studied. By holding the geomagnetic activity on a certain level, the variations due to changes in the IMF could be obtained and *vice versa*.

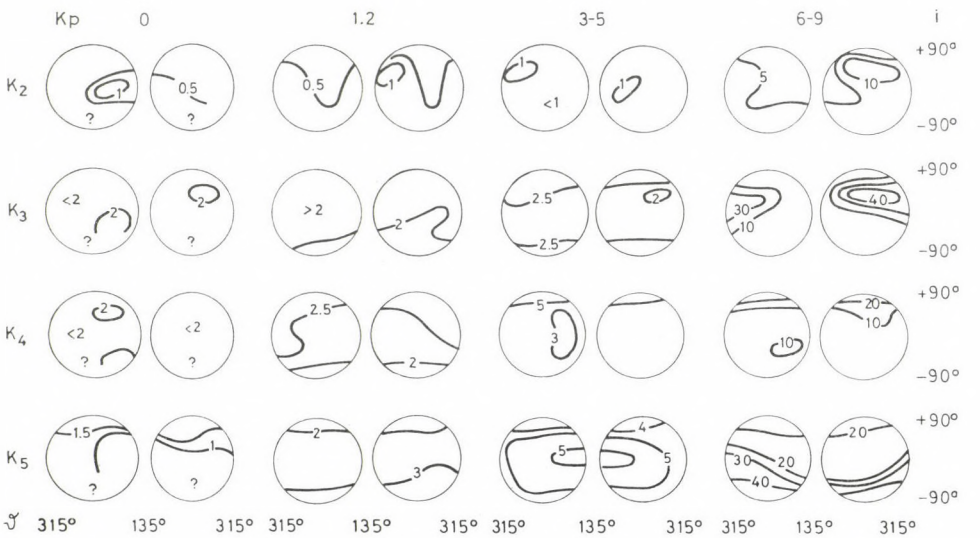

Fig. 1. Average amplitudes in the different period ranges in function of the geomagnetic activity (K_p) and of the direction of the IMF

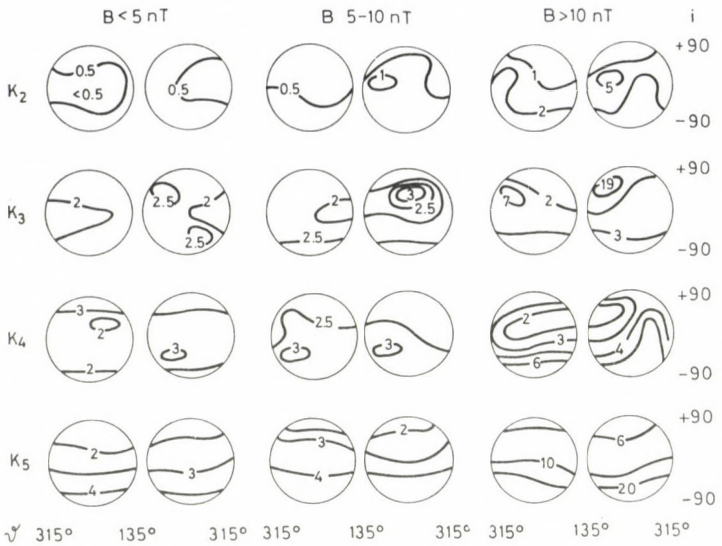

Fig. 2. Average amplitudes in different period ranges in function of the IMF intensity (B) and of the direction of the IMF

The special events observed in Nagycenk during the year 1972 were the following:

Bays	357 cases,	average amplitude	30 nT
ssc-s	19 cases,	average amplitude	49 nT
si-s	41 cases,	average amplitude	13 nT
pi-s	260 cases,	average amplitude	5 nT.

These events have increased the activity in the corresponding period band (bays mainly in K_5, ssc-s and si-s in K_2 or K_3, pi-s in K_1 or K_2).

The amplitudes in function of the geomagnetic activity and of the direction of the IMF show (Fig. 1) that in K_5, the amplitudes are significantly higher in case of southwards directed IMF than in case of northward fields. This effect can be seen most definitely in case of high geomagnetic activities.

If the variable (in addition to the IMF-direction) is the scalar magnitude of the IMF, a similar conclusion can be drawn (Fig. 2). Here the increased activity in case of southwards directed fields can be seen for all intensity levels. At medium or high IMF-intensities, the effect is also visible in K_4 amplitudes, while it is apparent in K_2 and K_3 only at the highest IMF-intensities.

If the effects of the geomagnetic activity and of the IMF area separated (Fig. 3), the following conclusions can be drawn:

1. In the period bands K_2—K_4 a very high geomagnetic activity causes a sharp increase of the amplitudes, while at medium or low activity its effect

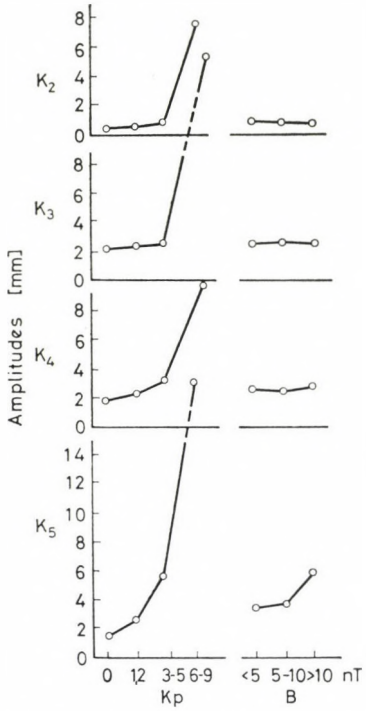

Fig. 3. Results of the separation of the K_p- and B-effects on the activity of different period variations

is rather small. In the longer period range (K_5) the increase is continuous with increasing geomagnetic activity (substorms).

2. The increase of the IMF intensity does not cause any appreciable increase in activity levels in the period ranges K_2—K_4 (2—24 min), while in the period range K_5 (24—60 min) the increase of the IMF intensity causes a significant increase of the activity.

As at middle latitudes, thus in the Nagycenk observatory substorm occur generally only during night, it is of interest to see separately the day and night time activity. In case of the daytime activity, the amplitudes increase in the period range K_4 with increasing southward component of the IMF, similarly in the range K_5, with the exception of the strongest fields (Fig. 4).

In case of the night time activity this correlation can be found only for the K_5 range where a continuous increase was found with the increasing of the southward component of the IMF (Fig. 5). Here no similar effect can be found in the range K_4. In the range K_2, something similar can also be seen, mainly in case of stronger interplanetary fields, perhaps due to an increase of the longer period component of Pi-impulses (Pi 3).

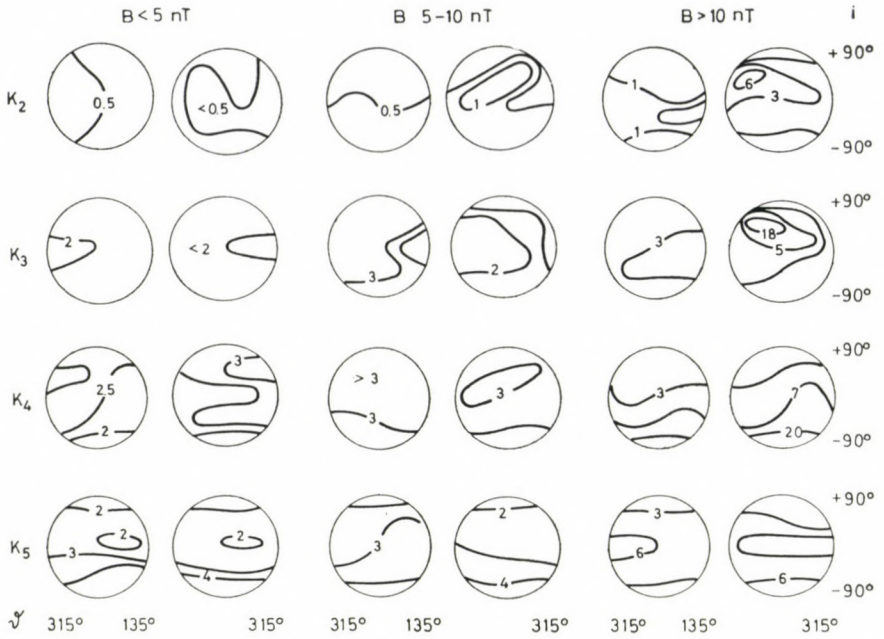

Fig. 4. The day time activity in function of B, and of the direction of the IMF in the different period ranges

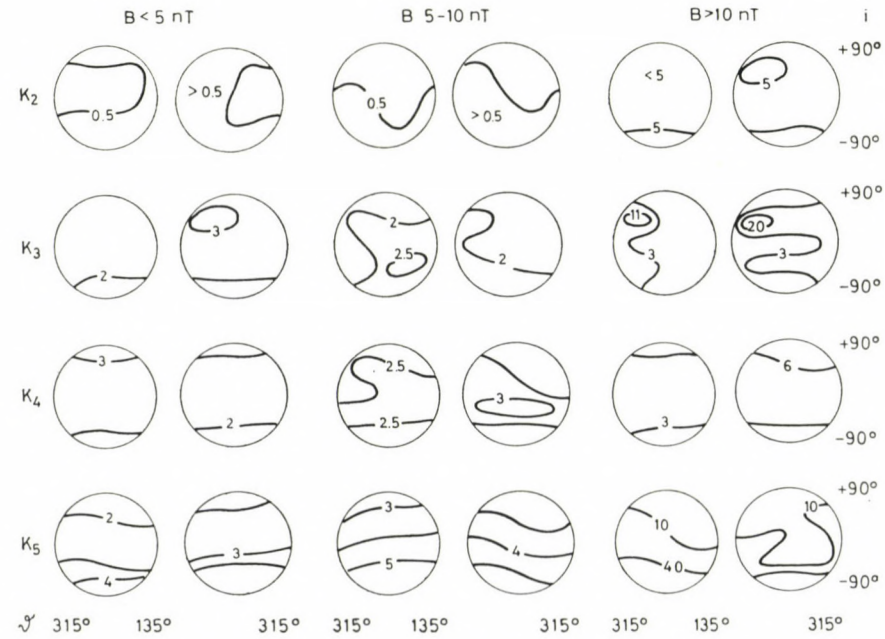

Fig. 5. The night time activity in function of B, and of the direction of the IMF in the different period ranges

Summarizing it can be stated that:

1. The geomagnetic activity changes due to changes in the intensity of the interplanetary magnetic field, but the effect is strongly modulated by the direction of the IMF.

2. The variations in the period ranges K_2-K_3 (2—12 min periods) are mainly connected with the geomagnetic activity, and depend on the interplanetary field indirectly. The outer effect reaches these variation types through an increased geomagnetic activity and magnetospheric convection. The maximum activity during disturbed periods appears 1—2 days earlier in the ranges K_2 and K_5, than in the ranges K_3-K_4 [5]. In present case simultaneous geomagnetic and IMF data were used, therefore this effect could not be studied. Anyway, the connections of the IMF with K_2 and K_5 are somewhat stronger, and there is a minimum between them. This could be an expression of the primary and secondary character of these period ranges.

3. The present investigations have shown that the direction and intensity of IMF influences mainly the variations with periods longer than 12—20 min (in addition to pulsations with periods shorter than 2 min and not discussed here), and their effect is strongest and unambiguous in the substorm period range, i.e. around 1 hour. A study of the periods longer than 1 hour is not possible based on the present material.

The effects in the period range 12—60 min can be well explained by reconnection and following substorm activity. An effect of the substorms can be supposed on the dayside geomagnetic field, too, thus enabling an explanation of the daytime enhancement in this period range. For shorter periods, in addition to substorm-associated events, the propagation of magnetohydrodynamic waves from the interplanetary space through the magnetopause cannot be excluded, as it was discussed by WOLFE and KAUFMANN [6]. It seems probably that at the dayside magnetosphere both effects play a similarly important role.

REFERENCES

1. GOLIKOV, Y. Y.—PLYASOVA-BAKOUNINA, T. A.—TROITSKAYA, V. A.—CHERNIKOV, A. A.—PUSTSTOVALOV, V. V.—HEDGECOCK, P. C.: Where do solar wind-controlled micropulsations originate? *Planet, Space Sci.*, 28 (1980), 535—543.
2. AKASOFU, S.: The interaction between a magnetised plasma flow and a magnetised celestial body: a review of magnetospheric studies. *Space Sci. Rev.*, 21 (1978), 489—526.
3. HEIKKILA, W. J.: Criticism of reconnection models of the magnetosphere. *Planet. Space Sci.*, 26 (1978), 121—135.
4. Interplanetary Magnetic Field Data Book. National Space Data Center, NASA 1975.
5. VERŐ, J.: Earth-current variations of different period in the observatorium near Nagycenk. *J. Atm. Terr. Phys.*, 13 (1958), 375—376.
6. WOLFE, A.—KAUFMANN, R. L.: MHD wave transmission and production near the magnetopause. *J. Geoph. Res.*, 80 (1975), 1764—1775.

О СВЯЗИ ДЛИННО-ПЕРИОДИЧЕСКИХ ЭЛЕКТРОМАГНИТНЫХ ВАРИАЦИЙ И МЕЖПЛАНЕТНОГО МАГНИТНОГО ПОЛЯ

Л. ХОЛЛО

РЕЗЮМЕ

В статье изучается связь между вариациями с периодом 2—60 минуты, интенсивностью ММП и направлением. Выявлено, что влияние ММП в первую очередь происходит при электромагнитных вариациях с периодом длиннее чем 12 минут, которое более значительно при периоде около 1 часа. Здесь же — особенно при ночной активности — в зависимости от интенсивности ММП, при вариациях, происходящих в южном направлении, активность возрастает пропорционально. Вариации с периодом 2—12 минут в первую очередь связаны с геомагнитной активностью, а с межпланетным магнитным полем они связаны только косвенно.

Acta Geodaet., Geophys. et Montanist. Acad. Sci. Hung. Tomus 16 (2—4), pp. 405—414 (1981)

A STUDY OF THE VARIATION OF IONOSPHERIC ABSORPTION AND WIND INDUCED ION-CONVERGENCE AFTER GEOMAGNETIC DISTURBANCES

P. BENCZE
CAND. GEOSCI.
F. MÄRCZ
GEODETIC AND GEOPHYSICAL RESEARCH INSTITUTE OF THE HUNGARIAN ACADEMY OF SCIENCES, SOPRON,

The ion-convergence induced by atmospheric waves at mid-latitudes is used to study the possible role of dynamic processes in the lower ionosphere after geomagnetic disturbances. The after-effect in ionospheric absorption has been investigated in dependence of season. Its amplitude is larger during summer (between April and September) than in winter (between October and March). It has been found that in summer the after-effect is larger, if at the same time the ion-convergence is long-lasting decreased. In winter the after-effect seems to be more pronounced during periods when the ion-convergence is increased. Considering the ion convergence as an indicator of turbulent transport the conclusion might be drawn that transport processes also influence the development of the after-effect.

Introduction

It has been long ago assumed [1] that in the development of ionospheric storms following geomagnetic disturbances dynamic processes play a significant role. Later satellite measurements, enabling in situ determination of different atmospheric parameters, verified this supposition [2]. However, the question needs further investigation. Namely, on the one hand satellite measurements can be carried out for a long time only at altitudes above about 150 km. Thus, for long-lasting observations at altitudes lower than this height indirect and ground based methods are needed. On the other hand a post-storm effect revealed by the ionospheric absorption of radio waves also takes place in the lower ionosphere [3, 4], to the formation of which dynamic processes may also contribute [5, 6]. These conditions prompted the investigation of the problem by means of an ionospheric parameter which is connected with the dynamics of the lower ionosphere and which can be determined on the basis of ground based measurements. From the data obtained by the widely used vertical soundings, at mid-latitudes only the sporadic E parameters are directly related to the dynamical conditions in the lower ionosphere.

Assuming the validity of the wind-shear theory of mid-latitude sporadic E, first the background electron density has been computed on the basis

of the International Reference Ionosphere [7]. In the computation [8] the maximum electron density was calculated from the observed f_0E value. The height of the sporadic E layer for which the background electron density has to be determined was given by the measured parameter $h'Es$. The background electron density has been computed below the valley region by means of a polynomial of third degree and in the valley on the basis of a polynomial of fifth degree. The electron density deduced from the observed blanketing frequency has been considered as maximum electron density of the Es layer. Then following REDDY and MATSUSHITA [9] the ion-convergence was computed by means of a relation derived from the starting equation of the wind-shear theory and giving the ion-convergence as a function of the maximum electron density of the Es layer, the background electron density, as well as the effective recombination coefficient outside of the Es layer. It has been assumed that the effective recombination coefficient inside of the Es layer is equal to that outside of it and the effect of ambipolar diffusion can be neglected. The former supposition may be justified, if only variations of the ion-convergence are studied. For the sake of completeness it should be mentioned that the ion-convergence can be easily converted into wind-shear by multiplying the former with a factor. This factor is a function of the ion-neutral collision frequency and the gyrofrequency of ions. Thus, the time variation of the factor is practically negligible, but the factor itself is decreasing with increasing height. This means that the time variation of the ion-convergence can be considered identical with that of the wind-shear.

Seasonal dependence of the after-effect observed in radio wave absorption

Investigations carried out by LAUTER and KNUTH [3] have revealed a seasonal dependence of the after-effect observed at mid-latitude in case of sunspot maximum conditions ($\bar{R} > 50$). It was found that days with increased ionospheric absorption (at $\chi = 90°$) occurred more frequently in summer than in winter. Such an annual variation was not experienced in case of sunspot minimum conditions. LAUTER and KNUTH [3] attributed the strong summertime maximum in the occurrence of the increased absorption (at $\bar{R} > 50$) to the increase of air density in the mirror point region of the outer radiation belt electrons. The precipitation of these electrons into the lower ionosphere (D-region) following certain geomagnetic storms is generally accepted as the main cause of increased absorption.

We carried out two independent superposed epoch analyses by using the ionospheric absorption of obliquely incident radio waves measured at 245 kHz in Kühlungsborn (reflection point: $\varphi = 54.9°$ N, $\lambda = 11.4°$ E) at sunset ($\chi = 90°$) between 1968 and 1974. One was based on summertime values,

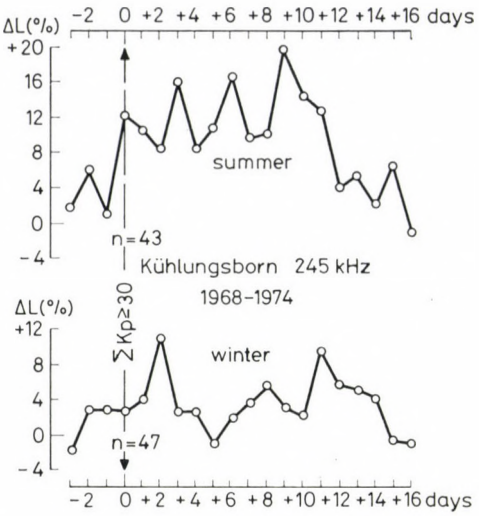

Fig. 1. Variation of mean departures from the corresponding monthly medians of sunset absorption (ΔL) measured at 245 kHz Kühlungsborn between 1968 and 1974 after selected geomagnetic disturbances in summer (upper curve) and in winter (lower curve)

another on wintertime data. Key days were selected on the basis of the daily sum of K_p indices. Those days were accepted as key days, when the criterion $\Sigma K_p \geq 30$ was fulfilled. In addition it was required that on two days out of three preceding the key day the ΣK_p-value must not surpass the mean value of ΣK_p determined for the corresponding year.

The year has been divided into a summer and a winter half on the basis of the change of dynamic conditions in the strato-mesosphere. The zonal circulation at mid-latitudes (e.g. $\sim 50°$ N) is characterized by distinct changes of the wind-system in spring and autumn. The eastward wind (W) predominates during winter, i.e. between autumn and spring. On the contrary, between spring and autumn the westward wind (E) becomes prevailing. Thus, the period between April and September can be regarded as summertime and that between October and March as wintertime by considering only the changes of the general wind direction.

In Fig. 1 the mean departures (ΔL) of sunset absorption from the corresponding monthly medians are presented around the selected key days. The departures given in percentages are separately shown for the summer months (in the upper part) and the winter months (in the lower part). It can be seen that the amplitude of the after-effect is larger in summer than in winter. In summertime the primary storm effect is indicated by a peak occurring immediately on the storm day, however, in winter this peak is shifted to the second day following the geomagnetic disturbance. The more pronounced after-effect shown for summer seems to have a main phase lasting

till day + 11 and it terminates in a declining phase between days + 12 and + 15. In case of the winter months, the primary storm effect and the after-effect are clearly separated. The latter (being quite moderate in comparison to summer) is finished on day +14 without a declining phase.

The results shown in Fig. 1 hint at characteristics of the increased absorption which are rather different in summer and winter. An association of these characteristics with seasonal changes in the dynamics of the lower ionosphere cannot be excluded. In addition, LAUTER and KNUTH [3] reported that strong after-effects are mainly produced in the summer months during sunspot maximum conditions ($\bar{R} > 50$). The data used in the present investigation were partly measured during solar maximum (1968—1970) and partly in an interval (1971—1972) where the $\bar{R} > 50$ criterion applied by LAUTER and KNUTH [3] was also fulfilled.

The dependence of the mean departures of ion-convergence on season during the after-effect in ionospheric absorption

In order to complete the informations on the conditions of the lower ionosphere during after-effects in radio wave absorption the values of ion-convergence were applied. As it has previously been mentioned, the ion-

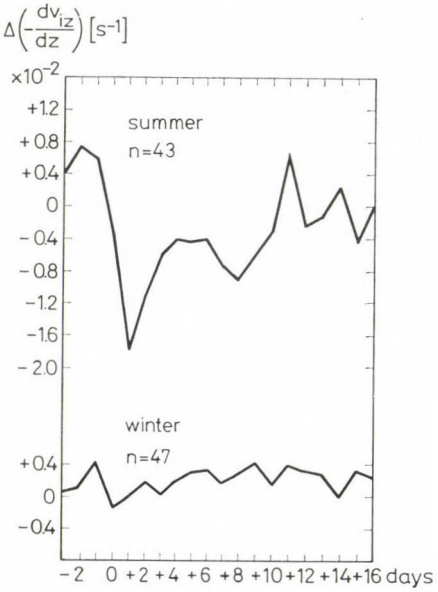

Fig. 2. Variation of the average of departures of ion-convergence $\left[\Delta\left(-\frac{dv_{iz}}{dz}\right)\right]$ from the corresponding monthly mean of day time hourly values after selected geomagnetic disturbances of the period 1968—74 in summer (upper curve) and in winter (lower curve)

convergence is a parameter which is connected with the dynamics of the lower ionosphere. For the computation of ion-convergence we needed data of an ionospheric station situated close to the reflection point of the radio waves used for absorption measurements. Thus, the sporadic E parameters, determined on the basis of the vertical soundings of the ionospheric station Juliusruh (54° 38′ N, 13° 23′ E) have been chosen. The average of departures of ion-convergence $\left[\Delta\left(-\frac{\mathrm{d}v_{iz}}{\mathrm{d}z}\right)\right]$ from the corresponding monthly mean of daytime hourly values was determined for each day of the interval (from day −3 to day +16) around the selected geomagnetic disturbances of the period 1968–74.

In Fig. 2 results of the superposed epoch analyses carried out with the latter values are given separately for summer (in the upper part) and winter (in the lower part). It can be seen that in summer the ion-convergence shows decreased values following the geomagnetic disturbance till day +10. Then, a period of fluctuating values follows. In winter the average departures indicate a characterless variation of the ion-convergence during the whole period covered by the superposed epoch analysis.

Discussion

The foregoing results have revealed that in summer the ion-convergence is generally decreased during the after-effect. Naturally, this does not occur in each individual case, it is valid only on the average. Therefore, the selected 43 geomagnetic disturbances were examined one by one and it was found that during 21 events the ion-convergence showed continuously decreased values. Sometimes the ion-convergence was decreased for several days also in the remaining 22 cases, however, these periods alternated with intervals of increased values. On the basis of the two kinds of events the previously used absorption data were divided into two groups and separately analysed by the superposed epoch method (the number of events was quite equal in both groups).

The results are presented in Fig. 3, where the upper part includes the events with a durable decrease of ion-convergence and the lower part the remaining ones. The illustration reveals that in summer the after-effect is more pronounced in cases, when the ion-convergence is decreased for a longer period. Thus, it can be assumed that during the after-effect interval especial dynamic processes might also contribute to the more effective ionization of the lower ionosphere, as well as to the increase of absorption.

For the comparison of ionospheric absorption and wind induced ion-convergence the superposed epoch method was applied to the average of departures of ion-convergence determined for the two kinds of events. In the

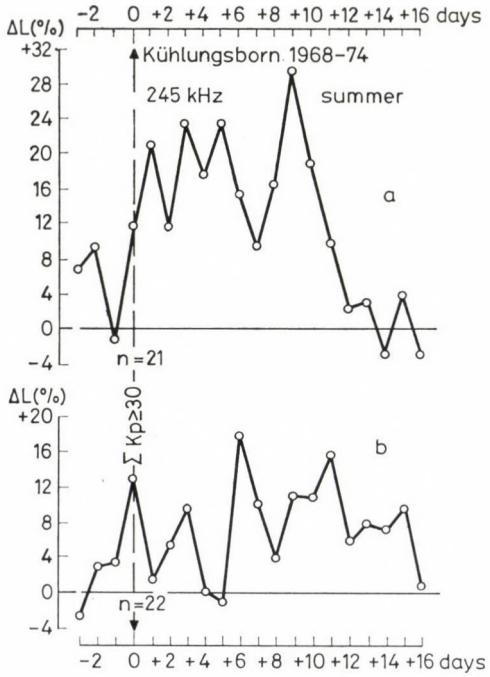

Fig. 3. The results of superposed epoch analyses carried out with mean departures from the corresponding monthly medians of sunset absorption (ΔL) measured at 245 kHz in Kühlungsborn in summer *a)* Key days: Selected geomagnetic disturbances, decreased ion-convergence for a longer period. *b)* Key days: All the other cases of geomagnetic disturbances used in this study (in Fig. 1 upper part)

upper and lower parts of Fig. 4 the mean variation of this parameter for the 21 events, respectively for the remaining 22 cases are plotted. As regards the upper curve, the ion-convergence shows a depressed interval from the beginning of the disturbance to day +10, while the lower curve indicates no systematic changes except the period before day +2. These results justify that the selection of events has been properly performed.

Though in winter the variation of the average departures of ion-convergence did not indicate characteristic changes, the 47 geomagnetic disturbances were separately examined. It has been found that during 16 events the ion-convergence showed continuously increased values. In the remaining 31 cases the ion-convergence could be characterized by alternating increased and decreased periods. The absorption data were divided into two groups corresponding to this classification of events and both groups were processed by means of the superposed epoch method. (It is to be mentioned that the number of events was rather different in the two groups.)

In the upper part of Fig. 5 the variation of the mean departures of absorption is shown in case of events with a durable increase of ion-con-

vergence, while in the lower part the variation of the absorption departures during the remaining events is plotted. It can be seen that the shifted primary storm effect and the after-effect is somewhat more pronounced in cases, when the ion-convergence is increased for a longer period. Notwithstanding the rather small number of this kind of events (a) the variation of increased absorption is quite similar to that shown for all winter cases in Fig. 1. Consequently, the more numerous remaining events (b) without a durable increase of ion-convergence should be less important in point of view of the after-effect observed in winter. Thus, it can be assumed that after geomagnetic disturbances dynamic processes may to a certain extent contribute also in winter to the ionization conditions of the lower ionosphere.

For the control of the above mentioned the superposed epoch method was applied to the average departures of the ion-convergence obtained for the two groups of events. In the upper and lower parts of Fig. 6 the mean variations of this parameter for the 16 events, respectively for the remaining 31 cases are illustrated. The upper curve indicates increased ion-convergence

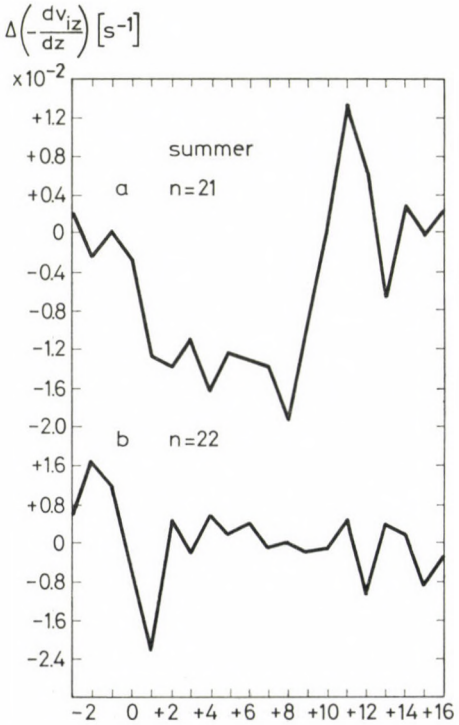

Fig. 4. Illustration showing the effectiveness of the separation of ion-convergence departures $\left[\Delta\left(-\frac{dv_{iz}}{dz}\right)\right]$ in summer into cases of durable decrease (a) and all the other cases used in this study (b)

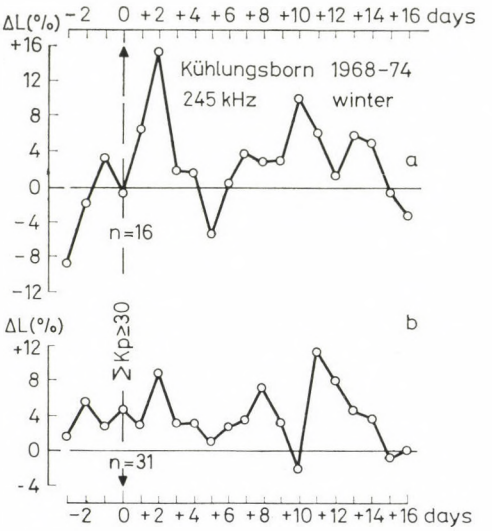

Fig. 5. The results of superposed epoch analyses carried out with mean departures from the corresponding monthly medians of sunset absorption (ΔL) measured at 245 kHz in Kühlungsborn in winter. *a)* Key days: Selected geomagnetic disturbances, increased ion-ionvergence for a longer period. *b)* Key days: All the other cases of geomagnetic disturbances used in this study (in Fig. 1. lower part)

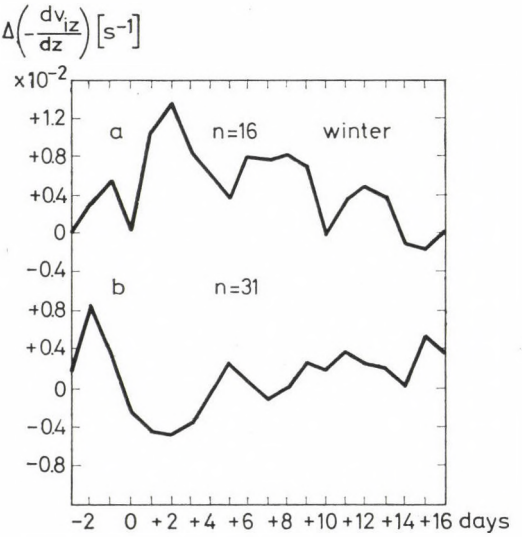

Fig. 6. Illustration showing the effectiveness of the separation of ion-convergence departures $\left[\Delta\left(-\frac{dv_{iz}}{dz}\right)\right]$ in winter into cases of durable increase (a) and all the other cases used in this study (b)

from day +1 to day +10, as it has been expected. The lower curve shows decreased values from the beginning of the disturbance to day +4. Again the Figure gives evidence of the proper selection of events. Thus, the characterless shape of the lower curve in Fig. 2 results from the superposition of portions of the upper and lower curves in Fig. 6 showing positive, respectively negative departures.

On the basis of the investigations described in the present paper the conclusion might be drawn that the increased absorption of radio waves observed at mid-latitudes after geomagnetic disturbances is more pronounced in summer, than in winter. Using wind induced ion-convergence determined for the same periods, it has been found that in summer the after-effect in absorption is more important, if at the same time the ion-convergence is decreased. In winter the shifted primary storm effect and the after-effect seem to be more distinct during periods of increased ion-convergence. Taking into account that wind induced ion-convergence may be considered as an indicator of turbulent transport, the results hint at a possible influence of transport processes in the development of the after-effect. Thus, disregarding the role of the temperature gradient, in summer decreased, while in winter increased turbulence would favour the formation of the after-effect.

REFERENCES

1. SEATON, M. J.: A possible explanation of the drop in F-region critical densities accompanying major ionospheric storms. *J. Atmos. Terr. Phys.*, 8 (1956), 122—123.
2. PRÖLSS, G. W.: Magnetic storm associated perturbations of the upper atmosphere: Recent results obtained by satellite-born gas analyzers. *Rev. Geoph. Space Phys.*, 18 (1980), 183—202.
3. LAUTER, E. A.—KNUTH, R.: Precipitation of high energy particles into the upper atmosphere at medium latitudes after magnetic storms. *J. Atmos. Terr. Phys.*, 29 (1967), 411—417.
4. MÄRCZ, F.: Further studies on ionospheric absorption and geomagnetic activity. *Acta Geod. Geoph. Mont. Hung.*, 8 (1973), 297—311.
5. BELROSE, J. S.: The oblique reflection of CW low frequency radio waves from the ionosphere. In: Propagation of Radio Waves at Frequencies below 300 kc/s (ed. by W. T. Blackband). Agardograph 74, 149—165. Pergamon Press, London, 1964.
6. BENCZE, P.—SZEMERÉDY, P.: Variation of the level of atmospheric radio noise after geomagnetic disturbances-I. *Acta Geod. Geoph. Mont. Hung.*, 8 (1973), 251—257.
7. RAWER, K.—RAMA KRISHNAN, S.: Tentative Tables of Electron Density and Excess Electron Temperature for Temperate Latitude. Arbeitsgruppe f. Physik. Weltraumforschung, Freiburg, 1972.
8. BENCZE, P.: Height variation of wind shear deduced from ionospheric sporadic E during stratospheric warmings. *Acta Geod. Geoph. Mont. Hung.*, 15 (1980), 247—256.
9. REDDY, C. A.—MATSUSHITA, S.: The variation of neutral wind shears in the E region as deduced from blanketing Es. *J. Atmos. Terr. Phys.*, 30 (1968), 747—762.

ИЗУЧЕНИЕ ВАРИАЦИЙ ИОНОСФЕРНОГО ПОГЛОЩЕНИЯ И СХОДИМОСТЬ ИОНОВ ВЕТРОВОГО ПРОИСХОЖДЕНИЯ ПОСЛЕ ГЕОМАГНИТНЫХ ВОЗМУЩЕНИЙ

П. БЕНЦЕ—Ф. МЕРЦ

РЕЗЮМЕ

Сходимость ионов, созданных атмосферными волнами в средних широтах, используется для исследования возможной роли динамических процессов в нижней ионосфере после геомагнитных возмущений. Последействие, наблюдаемое в ионосферном поглощении изучалось как функция времен года. Его амплитуда летом (с апреля до сентября) больше чем зимой (с октября до марта). Установлено, что последействие летом больше, если в то же время сходимость ионов продолжительно уменьшается. Зимой последействие кажется больше в те периоды, когда сходимость ионов увеличивается. Считая сходимость ионов индикатором турбулентного транспорта, можно делать вывод, что процессы транспорта тоже влияют на формирование последействия.

Acta Geodaet., Geophys. et Montanist. Acad. Sci. Hung. Tomus 16 (2—4), pp. 415—422 (1981)

VARIATIONS OF THE ATMOSPHERIC ELECTRIC POTENTIAL GRADIENT AT NAGYCENK OBSERVATORY

F. MÄRCZ

P. BENCZE

CAND. GEOSCI.

GEODETIC AND GEOPHYSICAL RESEARCH INSTITUTE OF THE HUNGARIAN ACADEMY OF SCIENCES, SOPRON

Two kinds of variations of the atmospheric electric potential gradient are reviewed: the long term and the short term variations. Both are presented on the basis of the continuous measurement of the potential gradient at Nagycenk observatory. Three types of the long term variations have been investigated: the diurnal, the seasonal and the 11-year variation. The two former can be regarded as periodicities regularly recurring at Nagycenk, however, the 11-year period have not been found in the investigated characteristics of the potential gradient. Several types of the short term variations are presented. The atmospheric electric noise is shown for different seasons and examples of oscillation type variations are also given.

1. Introduction

The continuous measurement of the atmospheric electric potential gradient at Nagycenk observatory covers a period of almost two decades. Using this rather large observation material, we review three of the long term periodic variations already recognized on the basis of records at other stations [1]. The diurnal and the seasonal (or annual) variations of the potential gradient can be regarded as regularly recurring periodicities. Some uncertainties exist about the third one. Namely, sometimes a correlation between the 11-year period of solar activity and certain atmospheric electric parameters could be revealed [2], but in other cases a connection seemed to be dubious [3]. The use of potential gradient data measured between 1964 and 1976, i.e. during the last 11-year solar cycle, makes possible an analysis of all the three mentioned periodicities in case of Nagycenk observatory.

In addition, variations much shorter than the diurnal one have also been studied. The most common variations occur during periods of minutes up to fractions of an hour and they can be regarded as atmospheric electric noise [1]. Though it is possible to find variations of a periodic character, the unperiodic fluctuations are more frequent. The occurrence of both types is a sign of increased atmospheric electric activity. Its appearance may be associated with the changes of meteorological conditions and seasons, too.

2. Long term variations

2.1 *The diurnal variation*

It is known [1] that three predominant types of the diurnal variation of the potential gradient exist:

a) the single-oscillation continental type, in local time

b) the double-oscillation continental type, in local time

c) the single-oscillation oceanic type, in universal time.

In order to clear what type of them occurs at Nagycenk observatory, hourly means of the potential gradient have been determined. They are shown in universal time (UT) for the interval between 1964 and 1976 in Fig. 1. (There is not large difference between UT and the local time at Nagycenk observatory: LT = UT + 1 hour.) The hourly means were calculated without a greater selection of data, however, those uncertain for some reason have been omitted.

In Fig. 1, the mean diurnal variation of the potential gradient for the period, mentioned above is roughly a single-oscillation. Its continental character is indicated by a steeper increase in the morning and an earlier afternoon maximum than those observed in case of the oceanic type. The minimum appears at 03 00—04 00 LT, the maximum at 14 00 — 15 00 LT. The range of the mean daily variation (i.e. the difference between the maximum and minimum value) is about 40 V/m.

Figure 2 shows the mean diurnal variation of the potential gradient separately for winter (W = November, December, January, February), equinoxes (E = March, April, September, October) and summer (S = May, June, July, August). The curve indicating the variation in the equinoxes (E) scarcely differs from that of Fig. 1. Both have quite similar features, as regards their shape and the positions of their extreme values. A rather different morning increase can be seen in winter (W) and summer (S).

The slower increase of the winter curve during forenoon is comparable to that observed in case of oceanic conditions. On the contrary, the steep increase in the morning and the early afternoon maximum of the summer curve clearly indicates the continental character. This can be attributed to the sudden rise of temperature in the morning which causes a more effective

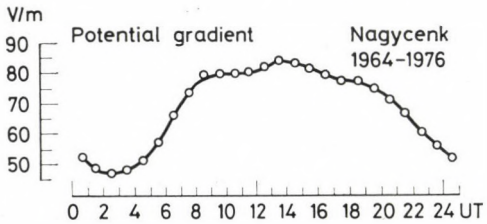

Fig. 1. The diurnal variation of the potential gradient at Nagycenk (between 1964 and 1976)

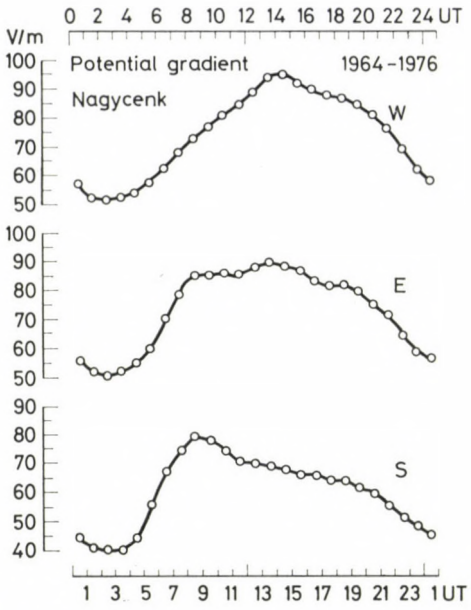

Fig. 2. The same as in Fig. 1 but for different seasons

evaporation in summer than in other seasons. This evaporation yields an enrichment of the suspension content of the air near the ground which results in the early morning maximum of the potential gradient (between 09 00 and 10 00 LT). Nevertheless, with rising temperature the convection and thus the mixing of the air near the ground also becomes more effective. Consequently, a part of the suspensions is lifted from the ground to higher levels and the potential gradient does not increase further. This is shown by the decreasing tendency of the summer curve starting well before noon.

It should be mentioned that in spite of the position change of the maximum, the minimum appears on each curve between 03 00 and 04 00 LT, i.e. it does not depend on season. Also the amplitude of the diurnal variation (the difference between the maximum and minimum value) seems to be unchanged. In all three cases it is $\sim$ 40 V/m on the average.

2.2 *The seasonal variation*

The same data set of the potential gradient which was utilized for the presentation of the diurnal variation, has been used in order to determine the seasonal variation. Averaged monthly means have been calculated for the interval 1964—1976 and they are presented in Fig. 3. Disregarding the fluctuations, a single-oscillation is shown by the averaged monthly means.

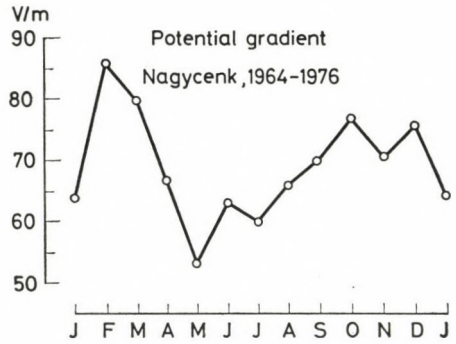

Fig. 3. The seasonal (or annual) variation of the potential gradient at Nagycenk (between 1964 and 1976)

The maximum of the potential gradient appears in the winter months (except January) and the minimum in the summer months.

The rather small average in January seems to be peculiar. According to a detailed analysis (not shown here), in 6 years out of the investigated 13 ones the January mean remained below the 13-year summer average ($\sim$ 60 V/m). This occurred only once in case of February and twice in the two remaining winter months (November and December). In all of the other years in the winter months the mean values of the potential gradient were larger than the above mentioned summer average. For the present, we have no explanation for the peculiarity observed in January. Nevertheless, the winter maximum of the Nagycenk potential gradient cannot be questionable.

It was found that the single-oscillation of the seasonal variation occurs not only in the northern but also in the southern hemisphere and even above the oceans [1]. The maximum value regularly appears in the northern winter (southern summer) months. The amplitude of the seasonal variation, however, is depending on the hemisphere. It is larger in the northern hemisphere ($\sim$ 40%) than in the southern one ($\sim$ 16%). In case of the Nagycenk observatory the annual average calculated from the monthly means of the period 1964—1976 is about 70 V/m. The difference between the highest and the lowest values shown in Fig. 3 amounts to about 30 V/m, i.e. at Nagycenk the amplitude of the seasonal variation corresponds to that usually observed in the northern hemisphere.

2.3 *Study of the 11-year period*

According to an early study of BAUER [2] the annual mean of the potential gradient should change in an 11-year cycle in accordance with solar activity. For the investigation of this periodicity the annual means of the Nagycenk potential gradient have been determined for the years of the last solar cycle,

between 1964 and 1976. They are presented in Fig. 4 (by crosses) together with a parameter indicating (by dots) the changes in solar activity. The potential gradient varies between 1964 and 1967 more or less parallel with solar activity. In years of solar maximum the potential gradient shows a sudden decrease and rather large fluctuations occur after the maximum. A regular 11-year periodicity can hardly be found.

In Fig. 5 the mean values of the potential gradient are given separately for the individual seasons (W = winter, E = equinoxes, S = summer) of the investigated interval (1964—1976). A comparison with Fig. 4 reveals that the changes of the winter means are principally responsible for the run and fluctuations of the potential gradient during the period shown there. Smaller fluctuations and a slow decrease in the declining phase of solar activity can be seen in case of the equinoxes. The summer means show a rather smooth character with a continuous decrease starting in 1966. Thus the presentation

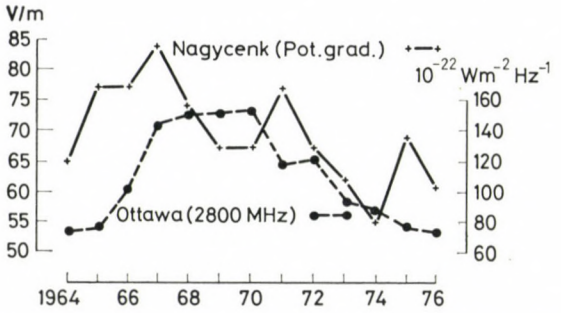

Fig. 4. The annual means of the Nagycenk potential gradient and a solar parameter (radio flux measured at 2800 MHz in Ottawa) for the 1964—1976 interval

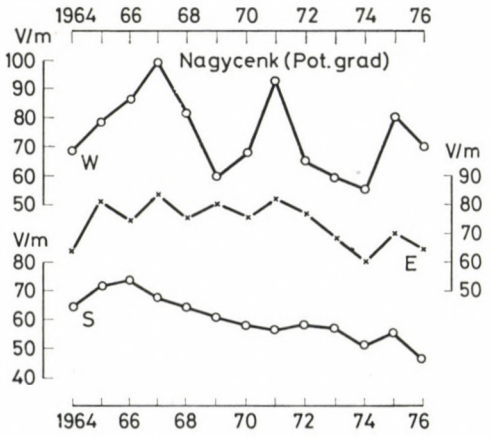

Fig. 5. The mean values of the potential gradient for different seasons in the 1964—1976 interval

based on the seasonal separation of data has also not indicated a regular 11-year periodicity of the Nagycenk potential gradient.

MÜHLEISEN [4] reported an inverse run of the yearly means of the ionosphere potential measured by balloons in comparison with solar activity characterized by relative sunspot number. The measurements were carried out at Weissenau (FRG) between 1959 and 1971. Taking into account the connection between the ionosphere potential and the atmospheric electric field measured at the surface, the long term variation of the potential gradient should also be inverse to that of solar activity. Results shown in Figures 4 and 5 do not indicate even this kind of variation in the Nagycenk potential gradient.

BAUER [2] found that also the amplitudes of the annual and the diurnal variation changed in accordance with the 11-year period of solar activity. Figure 6 shows the variation of the difference between the highest mean during the winter months and the lowest one during the summer months for each year of the interval 1964—1976. The calculated difference can be accepted as an amplitude of the annual variation, but in Fig. 6 there is no indication of a regular 11-year period reported by BAUER [2].

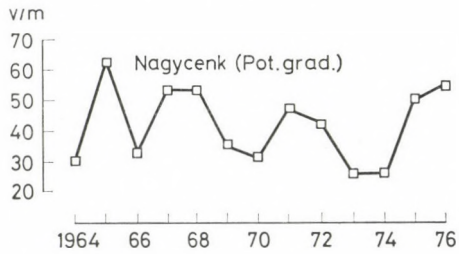

Fig. 6. Changes in the amplitude of the annual variation of the potential gradient for the 1964—1976 interval

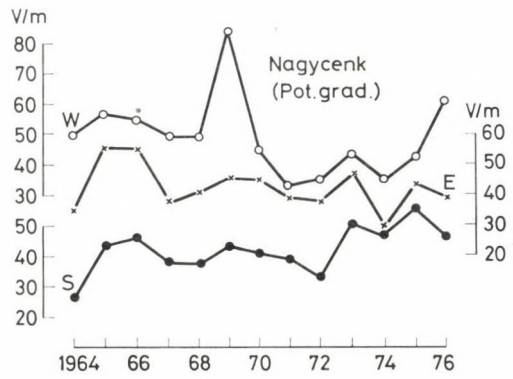

Fig. 7. Changes in the amplitude of the mean daily variation of the potential gradient for different seasons between 1964 and 1976

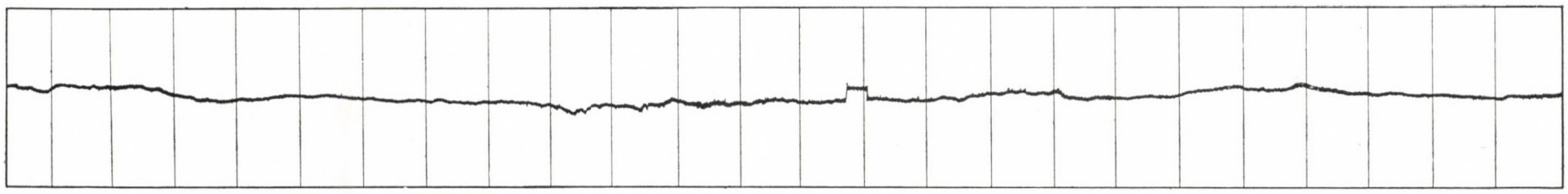

Fig. 8a. The diurnal variation of the potential gradient in spring (14. 03. 1980) showing the atmospheric electric noise around noon

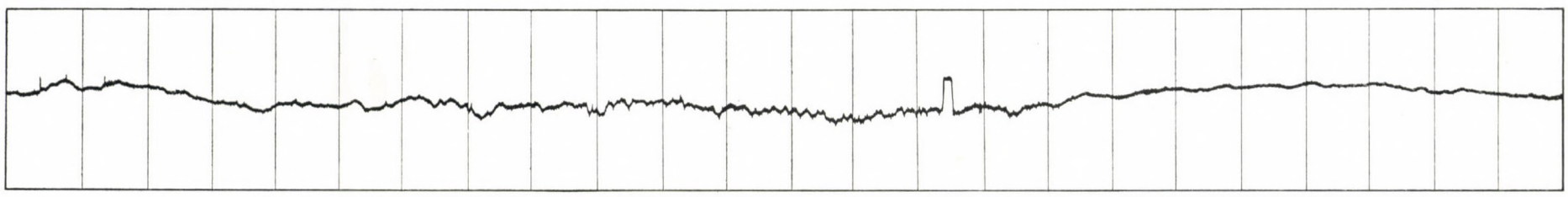

Fig. 8b. The same as in Fig. 8a, but for summer (31. 07. 1980)

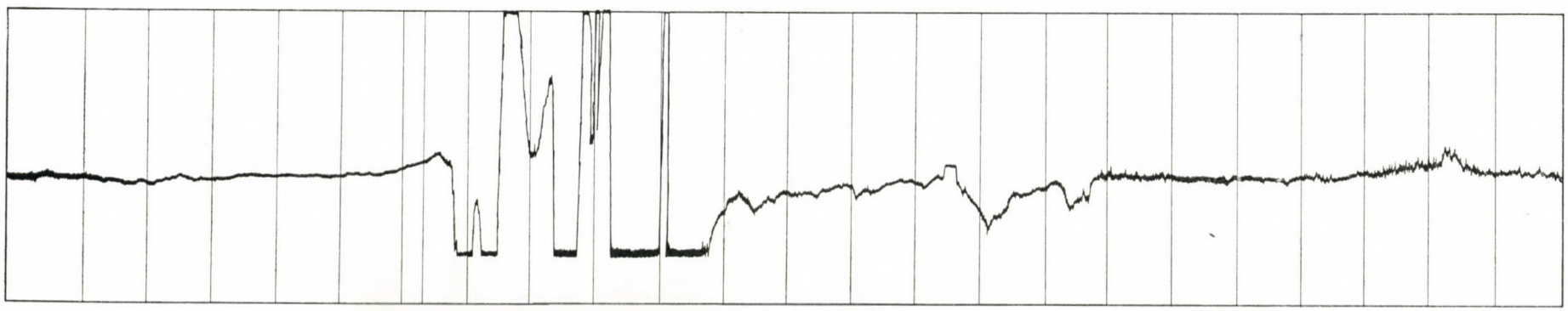

Fig. 8c. Potential gradient record of a summer day (11. 07. 1980) showing thunder-storm conditions in the afternoon

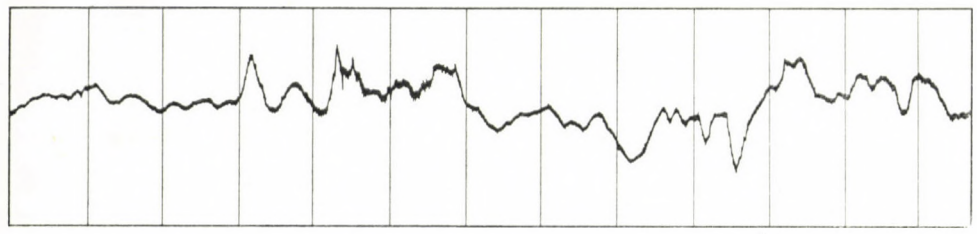

Fig. 8d. Large period (20—60 min) and large amplitude variations of the potential gradient

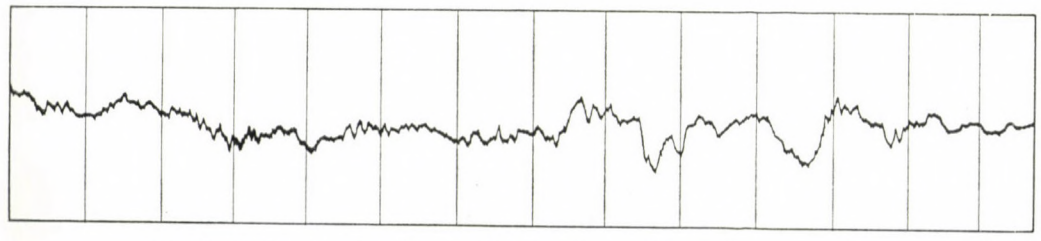

Fig. 8e. Medium period (3—10 min) variations of the potential gradient

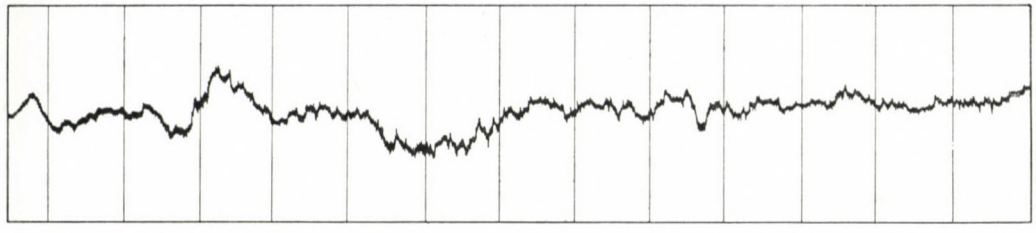

Fig. 8f. Small period (<3 min) fluctuations superposed on large period variations of the potential gradient

Finally, in Fig. 7 the amplitude of the mean daily variation is presented for the individual seasons of the investigated interval. A more or less parallel run of this parameter is seen in the individual seasons, however, the influence of solar activity does not appear.

On the basis of results shown in Figures 4, 5, 6 and 7 a long term variation depending on solar activity cannot be assumed in case of the Nagycenk potential gradient. Nevertheless, previous investigations [5] have revealed a connection between ionospheric absorption and potential gradient on a short er term. An increase of the potential gradient for some days following anomalously high ionospheric absorption hinted at a temporary association of the two parameters due to extraterrestrial influences including geomagnetic and solar ones, too.

3. Short term variations

Some ineteresting features of the short term variations of the atmospheric electric potential gradient recorded in the observatory are shown in Fig. 8. In Fig. 8a a record illustrating the diurnal variation of the atmospheric electric potential gradient in spring is shown. The variation of the potential gradient is quite smooth during the night and in the morning. Fluctuations called the atmospheric electric noise (agitation) appear only around noon, as the exchange in the atmospheric boundary layer becomes more intense (stability decreases). In Fig. 8b a record showing the diurnal variation of the potential gradient in summer is presented. The amplitude of the atmospheric electric noise in daytime is larger than in spring due to the increased exchange in the boundary layer.

Figure 8c shows a record of a summer day, when in the afternoon due to thunder-storm conditions the potential gradient reached values exceeding the range of the equipment (± 250 V). Figs 8d, e and f are illustrations of different periodic variations of the atmospheric electric potential gradient. In Fig. 8d large period (20—60 min) and large amplitude variations can be seen. It is to be noted that there are almost no fluctuations of smaller period. Figure 8e shows a part of a record, where variations of medium period (3—10 min) occurred connected probably with drifting ion clouds. These pulsations have sometimes sinusoidal character. Figure 8f is an example for small period (< 3 min) fluctuations superposed on variations of large period. Such small period fluctuations occur mostly, when the humidity of the air is large.

REFERENCES

1. ISRAËL, H.: Atmosphärische Elektrizität. Leipzig. Teil II. 1961.
2. BAUER, L. A.: Sunspots and Annual Variations of Atmospheric Electricity with Special Reference to the Carnegie-Observations 1915—1921. Res. Dep. Terr. Magn. Carnegie Inst. Wash. Publ. 175. 1926.
3. WATSON, R. A.: Electric Potential Gradient Measurements at Eskdalemuir. 1913—1923. Geophys. Mem. London, 4. No. 38. 1928.
4. MÜHLEISEN, R.: Neue Ergebnisse und Probleme in der Luftelektrizität. *Zeitschrift für Geophys.*, 37 (1971), 759—793.
5. MÄRCZ, F.: Links between atmospheric electricity and ionospheric absorption due to extraterrestrial influences. *J. Geophys. Res.*, 81 (1976), 4566—4570.

ВАРИАЦИИ ГРАДИЕНТА ПОТЕНЦИАЛА АТМОСФЕРНО-ЭЛЕКТРИЧЕСКОГО ПОЛЯ В ОБСЕРВАТОРИИ В НАДЬЦЕНКЕ

Ф. МЕРЦ—П. БЕНЦЕ

РЕЗЮМЕ

Рассмотрены два типа вариаций градиента потенциала атмосферно-электрического поля, длино- и кратковременные вариации. Оба типа представлены на основании непрерывных измерений градиента потенциала в Надьценкской обсерватории. Три типа длинновременных вариаций были исследованы соответственно суточной, сезональной и вариации с периодом 11 лет. Первые два типа регулярно повторяются в Надьценке, но 11-летний период не наблюдался в исследованных характеристиках градиента потенциала. Представлены многие численные типы коротковременных вариаций. Атмосферно-электрический шум показан в различных сезонах и представлены также примеры вариаций осциллационного характера.

Acta Geodaet., Geophys. et Montanist. Acad. Sci. Hung. Tomus 16 (2—4), pp. 423—434 (1981)

75 YEARS OF SEISMOLOGICAL RESEARCH IN HUNGARY

E. BISZTRICSÁNY

DOCTOR OF SCI.

D. CSOMOR

CAND. OF SCI.

GEODETIC AND GEOPHYSICAL RESEARCH INSTITUTE OF THE HUNGARIAN ACADEMY OF SCIENCES, DEPARTMENT OF SEISMOLOGY, BUDAPEST

The rise, development and present situation of seismological research in Hungary is summed up in the paper. The direction of further development is indicated.

Scientific interest for earthquakes has early arisen in Hungary, too, but an organized data collection and interpretation exists only since 1881. Let us look over — without the claim to completeness — the early works dealing with earthquakes in Hungary. They are mainly catalogues, as e.g. GROSSINGER; Dissertatio de terrae montibus Regni Hungariae, a catalogue published in Győr in 1873, further the works by HOLÉCZY (1824), by HUNFALVY (1859), by SALY and JEITTELES (1860) and by KOCH (1880).

Among papers in connection with individual earthquakes, that one issued by P. KITAIBEL and A. TOMTSÁNYI dealing with the earthquake of 1. 14. 1810 is the most important, since the authors introduced in it the concept of isoseismals, thus being ahead of his time by 50 years. Isoseismals are even now an indispensable basis for the processing of earthquakes by macroseismic methods.

INKEY (1876), HANTKEN (1882), SCHAFARZIK (1880, 1901), RÉTHLY (1907, 1908, 1910, 1911, 1912, 1918, 1922), BALLENEGGER (1911), CHOLNOKY (1912), SZILBER (1913, 1914), SCHRÉTER (1925), MORAVETZ (1925), SIMON (1931, 1937) and others dealt with individual earthquakes or investigated the seismological conditions of a smaller area.

On special sessions of the Hungarian Geological Society some authors gave reports on earthquakes burst out or detected in the Hungarian territory or dealt with some strong world-wide quakes.

Questions in connection with earthquakes were considered as important by the Hungarian Geological Society. Already on a committee session of Dec. 1, 1880, F. SCHAFARZIK proposed to establish an institution after the model of the Swiss Erdbeben-Commission, which as the task of observation data-collecting and scientific processing of seismic phenomena all over the country. The committee accepted the proposal and delegated a commission consisting

of K. HOFFMANN, B. INKEY, L. LÓCZY, F. SCHAFARZIK, S. SCHMIDT and M. STAUB to work out a detailed plan in this question.

The committee sessions of Jan. 5, and March 2, 1881 dealt with the question to constitute a Seismological Committee and at the March session a temporary committee of 3 members was nominated (KÁROLY HOFFMANN, BÉLA INKEY, FERENC SCHAFARZIK) taking into account the urgency. In 1881 the Committee of Mathematics and Natural Sciences of the Hungarian Academy of Sciences ensured the requested financial support to the Hungarian Geological Society for the Seismological Committee and the six members of the Seismological Committee were elected at the committee session of Nov. 9, 1881

JÓZSEF SZABÓ, as president
LAJOS LÓCZY, as vice-president
FERENC SCHAFARZIK,
MIKSA HANTKEN,
TAMÁS SZONTÁGH,
MIKLÓS VÁLYA, as members.

According to the proposal of this session, the activity of the Committee has been self-regulated. The activity of the Seismological Committee started with a session on Nov. 25, 1881 on the basis of the plans of the temporary seismological commission. These plans were sent to the Committee of Mathematics and Natural Sciences of the Hungarian Academy of Sciences.

The following resolutions were accepted on the first session of the Seismological Committee:

1. A circular will be sent to the redactions of all newspapers in Hungary.
2. Letters in Hungarian and German will be sent to the provincial cities.
3. A short explanation of earthquakes and a description of their observation will be compiled for correspondents.
4. A questionary will be printed for these correspondents and finally
5. After having done the preparatory work, the Committee will connect the Hungarian Central Meteorological Institute.

The leaflet and the questionary were compiled by the Seismological Committee on the basis of a paper by ALBERT HEIM, professor at the Zürich University.

It should be mentioned here that the Swiss Seismological Committee was the first in Europe.

It was discussed already at the first session of the Committee that it would be necessary to install seismograph stations at several points of the country besides to the collection and interpretation of the macroseismic material of earthquakes.

In the meantime the Committee was increased to 8 members with the new members JÓZSEF BERNÁTH and SÁNDOR KALECSINSZKY.

In 1886 the Committee found it necessary to establish a data collecting centre in Kolozsvár (Cluj-Napoca). As its leader Prof. Dr. ANTAL KOCH was nominated by the Geological Society.

From 1888 on MIHÁLY KISPATICH, professor in Zagreb regularly sent the macroseismic material collected in Croatia to the Seismological Committee and so the activity of the Committee was extended over the whole kingdom.

The Seismological Committee organized within the Hungarian Geological Society was regularly supported by the Hungarian Academy of Sciences.

In 1891 the Seismological Committee purchased 10 Lepsius-type seismometers in order to install them in suitable scientific institutions. S. KALECSINSZKY described the above mentioned seismometer in the "Földtani Közlöny" (1892). Data corresponding to the installation of these instruments are lost. These instruments are fundamentally no seismographs, but seismoscopes.

The personal composition of the Seismological Committee changed in the meantime and the Committee was reorganized on January 20, 1900, by the Geological Society with F. SCHAFARZIK as president. On April 4, 1900 the Seismological Committee asked the Hungarian Academy of Sciences for a scholarship to study foreign seismological stations and took contact with the director of the Meteorological Institute and asked him to support or to take over the seismological service.

The Seismological Committee sent RADÓ KÖVESLIGETHY to study the Strasbourg Institute. KÖVESLIGETHY visited not only the Strasbourg Institute, but also several other seismological stations in Western Europe and Italy. In his report he described the different seismological observatories and instrument types. At the end of his report he summed up his experiences and made a proposal for the organization of a seismological observatory network in Hungary. The 7th International Geographical Congress in Berlin in its resolution of October 4, 1899 — which proposed the establishment of an international seismological network and missed the stations in Hungary — did not declare the necessity of the unification of instruments in contrast with KÖVESLIGETHY. He pointed out the lack of Hungarian stations in the European network and proposed to set up five stations in Hungary. The central station was planed in the cellar of the Geological Institute in Budapest, further the Meteorological Institute should install a seismological station in Ógyalla (Hurbanovo) and for the others he suggested the places in Fiume (Rijeka), Kolozsvár (Cluj-Napoca) and Zagreb.

Kövesligethy gave estimates in this report for the installation and operation of the stations Budapest, Fiume (Rijeka) and Kolozsvár (Cluj-Napoca). He calculated the installation costs in 6500—7000 Korona, their operational cost 1000 Korona/year. To these estimates he completed a research plan, too. At the last session of the Geographic Congress GERLAND's proposal was accepted to call into being an international seismological committee.

The first international seismological meeting was held in Strasbourg between April 11—13, 1901. Hungarian participants were KONKOLY-THEGE, KÖVESLIGETHY and SCHAFARZIK. SCHAFARZIK reported on the work done by the Hungarian Seismological Committee since its establishment. He presented the occurrence of the more important earthquakes on the geological map of Hungary. This was the first seismological map of the territory of Hungary. KÖVESLIGETHY reviewed the First Hungarian Earthquake Catalogue by FERENC LAJOS, which compiled the data of the earthquakes occurred in Hungary from the 11th century.

The participants of the meeting elected KÖVESLIGETHY as one of the seven members of the Committee. KÖVESLIGETHY considered already then the possibility of the practical application of seismology.

On the initiative of the Seismological Committee of the Hungarian Geological Society seismometric instruments were installed and checked in the cellar of the Geological Institute and regular recording started on March 1, 1902. GRABLOVITZ, OMORI and BOSCH installed the so-called Strasbourg pair of horizontal pendulums, which were able to record only rather strong earthquakes. Till 1902 the Seismological Committee got a regular financial support from the Hungarian Academy of Sciences. The costs of purchase and installation of the seismological instruments in the Geological Institute were paid by ANDOR SEMSEY, director h. c. of the Royal Hungarian Geological Institute from his own funds.

As an order of the Minister of Agriculture (February 10, 1903) put the tasks of earthquake observations in Hungary and the establishment of the new seismological station network into the competence of the Meteorological Institute, the Geological Society dissolved its Seismological Committee at the committee session of March 4, 1903 on condition that the Society will further deal from a scientific point of view with earthquakes and its observatory will be sustained. In order to perform these tasks, a new committee was called into being under the name: Seismological Observatory of the Hungarian Geological Society with the members: KÁLMÁN ERNSZT, SÁNDOR KALECSINSZKY, RADÓ KÖVESLIGETHY and FERENC SCHAFARZIK.

The collection and processing of macroseismic data were made till 1911 by the Royal Hungarian Meteorological and Geomagnetic Institute. Here ANTAL RÉTHLY dealt with the collection of earthquake data and compiled the yearly report: Earthquakes in Hungary. The Publishing House of the Hungarian Academy published in 1952 the macroseismic data of earthquakes, which he collected in this life entitled Earthquakes in the Carpathian Basin (455—1918). This book has first of all as a catalogue an immense value. Its interpretations and estimations require in many cases a revision.

Under the influence of the first international seismological meeting in Strasbourg, 1901, the leadership of the Royal Hungarian Meteorological and

Geomagnetic Institute decided to take the observation of earthquakes into its. plans. The Meteorological Institute installed already in 1901 a Strasbourg seismometric pendulum pair, the recording was started on January 1, 1902. In 1901 in Temesvár (Timisoara) a Cacciatore and in 1902 an Agamennone seismoscope have been installed.

The initiatives of the Hungarian Geological Society did not lead to the establishment of a Hungarian seismological observatory network. As in the meantime the Meteorological Institute installed in Ógyalla (Hurbanovo) a horizontal pendulum pair of the Vincentini type, the Institute let 5 pairs of Vincentini—Konkoly pendulums be manufactured from the 5000 Korona paid to the Geological Society. Three pairs of them had been installed in Budapest, Ógyalla (Hurbanovo) and Temesvár (Timisoara), while it was planned to outfit seismological stations with the other two in Kolozsvár (Cluj-Napoca) and Zagreb.

The Imperial and Royal Naval Academy established a seismological station in Fiume (Rijeka) in 1903.

KÖVESLIGETHY became in 1904 member and representant of Hungary in the Permanent Committee of the International Seismological Society and in 1905 he founded with the financial support of the Hungarian Academy of Sciences the Budapest Seismological Observatory and the International Earthquake Calculation Institute in connection with the Institute for Geography of the Royal Hungarian Péter Pázmány University. The Hungarian Geological Institute presented the instruments to the Central Seismological Observatory. The government charged KÖVESLIGETHY with the leadership of the Observatory, as leader of the Calculation Institute KÁROLY JORDÁN, former honorary lecturer at the Geneva University was appointed and one assistant post to each was secured. The new institutes were accommodated by Professor LAJOS LÓCZY. For the Central Observatory IMRE SZALAY, director of the Hungarian National Museum, gave place in the cellar of the Museum. From the financial support of the Department III of the Hungarian Academy of Sciences a Wiechert astatic horizontal seismograph (1000 kg) and other outfit were purchased in 1905. The Wiechert pendulums was installed in July 1906.

The Meteorological Institute installed in January 1903 a Vicentini—Konkoly pendulum pair in Temesvár (Timisoara) and a Konkoly seismoscope in Kalocsa.

In the year following the foundation of the Central Seismological Observatory 4 seismological stations were run in the territory of Hungary and two seismoscopes were installed. Further seismological stations were set up on the territory of our country between 1910 and 1914 in Kalocsa, Kecskemét, Kolozsvár (Cluj-Napoca), Szeged and Ungvár (Uzhgorod).

At the foundation of the Central Seismological Observatory in Budapest, KÖVESLIGETHY considered the location in the cellar of the Hungarian National

Museum only as temporary and in 1911 he made plans and took the necessary steps to secure a proper place for the new central observatory to be built in the capital. For this purpose the capital gave on the southern slope of Istenhegy a proper ground for the new observatory. The WW 1 and its consequences hindered him to realize his plans. After the peace treatment only 4 observatories remained on the territory of Hungary (Budapest, Kalocsa, Kecskemét and Szeged). The observations of Budapest were run from 1905 till 1962 in the Hungarian National Museum.

The two Institutes founded by Kövesligethy were unified in September 1912 under the name of Budapest Seismological Observatory. After the death of KÖVESLIGETHY in 1934 the Institute was removed at first into the Semmelweis Street and in 1937 into the Deák Ferenc Street where BÉLA SIMON at first as deputy director and later as director could secure an accommodation fulfilling modern requirements. All research workers had own rooms with reference library, typewriter, etc. In 1942 the Institute got two researcher posts and two mechanician posts from the Ministry of Culture, thus the number of researchers increased to four. In this way objective conditions for a successful research work and the undisturbed operation of the observatories were created.

Here we should like to sum up briefly the activity in the Institute founded by KÖVESLIGETHY and its development. Four seismological observatories (Budapest, Ógyalla (Hurbanovo), Fiume (Rijeka) and Temesvár (Timisoara) and a seismoscope in Kalocsa operated in Hungary in 1904. During the following ten years five new observatories have been set up (Zagreb, Kalocsa, Ungvár (Uzhgorod), Kolozsvár (Cluj-Napoca) and Kecskemét. KÖVESLIGETHY and his coworkers dealt not only with theoretical problems as e.g. the emerging angle of the initial ray, density distribution, but also called attention to the possibilities of practical application (they gave expertises to the Hungarian State Railway and to private persons in 1913) and emphasized the necessity of special instruments for this purpose. The Seismological Calculation Institute was commissioned by the Association Internationale de Sismologie founded in 1906 — its first secretary general was KÖVESLIGETHY till 1916 — to carry out practical tasks, as e.g. to compile the international scientific catalogues of the macrographic stations. Further calculations were made in connection with the gas-eruption of Kis-Sármás. KÖVESLIGE∝HY dealt with the problems of the possibility of scientific earthquake prediction, too. BÉLA SIMON considered as the task of the Institute besides the seismological service and the scientific research the application of seismology in practice, too.

WW 1 stopped already the well-starting development in almost all respect, worldwar II hit the Hungarian Seismological service and research by an even harder blow.

During WW 2 the rooms of the National Seismological Observatory (since 1937), respectively the Hungarian Seismological Institute (1943) were almost totally destroyed. The Institute suffered irreperable losses, as among others the original macroseismic material collected by the Hungarian Geological Society and the Meteorological Institute were destroyed. During the war only the stations Kalocsa and Ógyalla (Hurbanovo) worked in 1943 and in 1945 for a short time only Kalocsa. Almost the total equipment of the stations Kecskemét and Szeged were destroyed.

Between 1946 and 1950 only the stations Budapest and Kalocsa were operated. Recording in Kecskemét was restarted in 1951 with the 100 kg Krumbach horizontal pendulum pair transferred from Budapest. In the meantime the workshop set up in the National Museum restored tha Mainka-type horizontal pendulum pair of Szeged, thus recording in Szeged could be restarted in February 1952, too. Since the rooms of the Institute in the Deák Ferenc street has been destroyed, the institutes was accommodated in the Kanizsai street where it could work only in very tight rooms. Although BÉLA SIMON, the director of the Institute often asked the Ministry of Culture for an appropriate accommodation, his requests were overdone, they did not correspond to the realistic possibilities. At the end of January 1952, the Institute moved into the rooms of the Loránd Eötvös Geophysical Institute in the Damjanich Street and it became a Department of this Institute.

When the Ministry of Culture (Religion and Education) gave over the non-educational Institutions to other government offices, the seismological institute being an institution founded with the support of the Hungarian Academy of Sciences and dealing with basic research — came under the supervision of the Ministry of Mines and Energy due to ununderstandable and inconceivable reasons, while at the same time the Astronomic Institute was put under the supervision of the Hungarian Academy of Sciences. The Minister of Mines and Energy incorporated it with January 1, 1952 into the Loránd Eötvös Geophysical Institute with the clause that in international relation the old name: Hungarian Seismological Institute can be retained. The Eötvös Institute had then already primarily the task of exploring raw materials.

The observatory remained further on in the cellar of the Hungarian National Museum, a place which became in consequence of the ever increasing traffic quite unsuited for the installation of instruments more sensible than the 1000 kg Wiechert pendulum. It had been possible already during WW 2 to identify with minute exactness the beginning and the end of air alarms, because then the short periode disturbances caused by factories and traffic ceased and the otherwise thick basic line became thin.

In 1953 the Institute received Krumbach type horizontal seismographs with optical recording as well as the electrodynamic vertical seismographs which were ten times more sensitive than the Wiechert pendulum. They

could not be installed in the cellar of the National Museum, therefore the Department got the task to find a suitable place in the environment of Budapest. Experimental recordings with portable pendulums started from Mt. Dobogókő towards Budapest. The instruments worked in 1956 in the district Óbuda, in the Schmiedt manor-house and yielded acceptable seismograms of the earthquake in Dunaharaszti and of its after-shocks. Some vibration measurements required by the industry and public authorities could have been carried out with these instruments.

Following the earthquake of Dunaharaszti a Soviet-made Kirnos-type three-components seismograph with electrodynamic recording was received in 1957 with which only experimental records were made in the National Museum, and which has been later (1963) installed in the new observatory in Sopronbánfalva.

A great development was reached in the fifties worldwide in the level of seismological instruments, 1000 kg seismographs — where great mass was intended to overcome the friction — were transferred slowly from the observatories into museums. Although GALITZIN constructed the electrodynamic seismograph already in 1911, its use, however, spread slow by due to the high costs of photographic paper. In Hungary its use started only at the beginning of the sixties. The development of seismology being still dynamic at the turn of the century slowed down in Hungary, one of the reasons were without doubt the two WW-s. But for a time after the wars it cannot be spoken from any development. If we survey the first fifty years of seismology in our country, we can see how it changed from one supreme authority to the other, and its position was not essentially improved in the fifties when it operated as a Department of the Loránd Eötvös Geophysical Institute. It is of interest to compare the development of the seismology with that of astronomy in Hungary. While the latter developed due to its continuous independence, due to the capacity and diligence of its experts a richly outfitted observatory network and a successful staff, in the meantime the seismology had a network with old instruments, its staff consisted of four scientists and one mechanician with small scientific output. An out-of-date instrumentation can results only in very exceptionally cases in up-to-date scientific results.

The late Professor LÁSZLÓ EGYED turned his attention to this situation in the middle of the fifties. He recognized early that the seismological observatory network of the world will soon get an important role. As head of the Geophysical Institute of the Loránd Eötvös University Budapest, he decided to organize a seismological research group and started to develop an up-to-date observation network as basis to this group.

In the beginning the seismological group consisted only of one scientist one mechanician and two assistants, but the seismological research in Hungary

got without doubt a sudden impulse at the end of the fifties. New stations were built in Budapest, Sopron, Piszkéstető and Jósvafő with considerably better noise levels, thus it was possible to apply seismographs with 1000—100,000 times magnification. Hence, the number of recorded quakes increased from some hundreds to some thousands in a year. This necessitated to increase the staff. On EGYED's initiative, the Seismological Department of the Loránd Eötvös Geophysical Institute was incorporated into the Seismological Research Group of the Hungarian Academy of Sciences at the Loránd Eötvös University. EGYED knew that a research group at the University Institute was not the adequate form for the whole seismological research of a country as well as he recognized the social and political importance of the seismology, therefore he planned to establish an institute where all the geophysical research and observation units of the national observatory service would have got their places, among them the seismology with greatest weight due to its greatest importance. In consequence of his early death this remained only a plan. Since the Seismological Research Group has outgrown the frame of a university institute, it was unified after his death in 1971 with the Geodetic and Geophysical Research Laboratories of the Hungarian Academy of Sciences in Sopron in the form of a new Institute called Geodetic and Geophysical Research Institute of the Hungarian Academy of Sciences.

The development of the seismology was accelerated at that time. This had more reasons. At first the very quick development of mass communication in the last decade widened the interest of people from theis immediate surroundings to events all over the world. Disasters in far continents became topic of conversation, a world-wide public matter. From events in Central America we are informed with a delay of some hours through the television. Attention is paid to the possibility of disasters even in our country, thus seismology came into the centre or social interest all over the world. The other reason is in close connection with the experiments with nuclear bombs and with the threat of nuclear war. We hope that the convention to stop nuclear experiments in the atmosphere, space and sea will be extended to underground explosions in the future, too. The effective control of such a treaty would be one of the tasks of seismology. A total nuclear silence would have a great political effect to the countries, which do not take part in this treaty.

The rapid development of seismology was supported by the immense modernization of electronics and by the improvement of the financial situation.

The speed of development in seismology and the effectiveness of observation can be illustrated by an example.

Between 1940 and 1945 the Hungarian network with instruments of 200 times magnification recorded 200 earthquakes in a year. With the new network described above about 2000—3000 seismological events can be detected in a year. With the most up-to-date arrays where the magnification

is some millions, fifteen thousand tremors can be recorded. By means of up-to-date instruments the amplitude of 10^{-9} m i.e. 10 Å can already be observed.

This development is imperative for us, too. We got the possibility at the beginning of the present five years plan to establish a more up-to-date seismological observatory network as the present one. This includes not only the finances for constructing new instruments, but also the unavoidable increase of staff, too. According to the plans the signals will be transmitted by radio waves to the centre in Budapest, where automatic signal processing is planned. Analoguous transmission of signals has been existing since some years from the station in the Mátra Mts, the final digital data transmission and automatical signal processing will probably start in mid 1981 using three stations. The installation of two further stations is planned for 1982—83.

The number of research workers in the Observatory increased only a little bit in the last 25 years, i.e. from four to five, but the number of papers yearly published has been multiplied. It can be stated today that the change was not only quantitative, but qualitative, too. The results of certain investigations are used world-wide. A method to calculate earthquake magnitudes based on the duration of the surface waves, published at the UGGI Conference in Toronto, 1957 brought the first international success.

A new map of seismic risk has been constructed as well as several isoseismal maps, and all these contribute to the economic and seismically safe planning of housing estates and industrial plants in our country.

Further on, the seismicity maps became part of the seismic risk map of Central Europe constructed with the cooperation of the socialist countries.

A method to calculate the depth of the low velocity layer from seismic data was published and a map of the LVL depths for a great part of Europe constructed.

Investigation of the coda waves resulted in new aspects on the characteristics of the final part of the surface waves.

A method has been developed for the rapid construction of microrayon maps and investigations in this direction are intended to be continued. Investigations of mining security have been also done since some years.

The establishment of the telemetric observatory network is a very complicated task. With except of a few units, the automatical recording, signal-recognizing and source determining system will be developed in our department. We hope that this development will soon lead to an up-to-date seismological network of observatories and together with this further important results can be achieved on the fields of both seismology and of engineering seismology.

REFERENCES

The historical references can be found in the following Hungarian publications:
Földtani Értesítő 1880., 1881., 1882.
Földtani Közlöny 13, 1883; 14, 1889; 21, 1891; 22, 1895; 25, 1900; 30, 1901; 31, 1902; 32, 1906; 36, 1907; 37, 1917; 67, 1918; 68, 1918; 69, 1919.
Math. és Természettudományi Értesítő 23, 1905; 29, 1907; 25, 1910; 28, 1911.
Királyi Magyar Pázmány Péter Tudományegyetem Almanach, 1899/1900., 1901/1902.
A Magyarhoni Földtani Társulat Obszervatóriumának jelentései, 1902—1905.
Magyarország Közoktatásügye 1906—1914. Vallás és Közokt. Min. Atheneneum, Budapest 1907—1916.

* * *

Atlas of isoseismal maps Central and Eastern Europe. 1978. Geophys. Institute Czechosl. Acad. Sci. Prague.

Biszrticsány, E. 1957: On the new method of determining earthquake magnitudes. Travaux Scientifiques, Ser. A. Fasc. 1959. UIGG conference in Toronto.

Bisztricsány, E. 1960: On the problem of magnitude determination. *Zeitschrift f. Geophysik*, 24, 153—160.

Bisztricsány, E. 1970: Analysis of codas of shallow focus earthquakes. *Geofizikai Közlemények*, 19, No. 3—4, 21—49.

Bisztricsány, E. 1974: The depth of the LVL in Europa and in some adjacent regions. *Geofizikai Közlemények*, 22, 65—66.

Bisztricsány, E. 1974: Mérnökszeizmológia (Engineering seismology) Akadémiai Kiadó, Budapest.

Bisztricsány, E.—Csomor, D.—Egyed, L.—Kiss, Z. 1968: New network of seismological stations in Hungary. Proceedings of the eight Assembly of the European Seismological Commission. Budapest.

Bisztricsány, E.—Hetesi, L.—Szabó. I.—Szeidovitz, Gy. 1980: Seismological Telemetry network in Hungary. *Acta Geod. Geoph. Mont. Hung.* (in press).

Broucek, I.—Csomor, D.—Prohackove, D. 1977: First version of the seismic activity map of Czechoslovakia, Hungary and Austria. *Acta Geol. Acad. Sci. Hung.*, 21, 297—300.

Csomor, D. 1975: Seismic mapping of Hungary. *Acta Geod. Geoph. Mont. Hung.*, 10, 155—160.

Egyed, L. 1955: Geofizikai alapismeretek (Elements of geophysics). Tankönyvkiadó. Budapest.

Egyed, L. 1956: A Föld fizikája. Általános geofizika I. (Physics of the Earth. Pure Geophysics Vol. I) Akadémiai Kiadó, Budapest.

Egyed, L. 1957: Механизм возникновения глубоких землетрясении. Seism. Bull., Moscow, No 6, 89—96.

Egyed, L. 1966: A földrengések és a Föld (Korunk Tudománya). (Earthquakes and the Earth (Science of our times)). Budapest.

Egyed, L.—Meskó, A. 1967: Determination of focal depth from macroseismic data. *Pure and Applied Geophysics*, 67, 107—111.

Kiss, Z. 1972a: Die Laufzeitkurven der Raumwellen naher Erdbeben bezogen auf Budapest. (Vorläufige Bearbeitung.) *Acta Geod. Geoph. Mont. Hung.*, 7, 405—409.

Kiss, Z. 1972b: Robbantással keltett rövidperiódusú felületi hullámok vizsgálata. Kandidátusi értekezés összefoglalója (Investigation of short-period surface waves from an explosive source. Abstract from dissertation). *MTA Föld- és Bányászati Tudományok Oszt. Közl.*, 5, 193—194.

Kiss, Z.—Ungváray, J.—Rajczi, P. 1980: The accuracy of the Epicentre Determination from a Network of five seismological Stations. *Acta Geod. Geoph. Mont. Hung.*, 15, 105—110.

Kövesligethy, R. 1907, 1909: Évi jelentés a Magyar Szent Korona országainak földrengési állomásairól (Annual report on the seismological stations of the Hungarian Holy Crown). 1906., 1907., 1908. Budapest.

Kövesligethy, R. 1913: Rapport sur observations faites pendant les années 1909—1912 aux Observatoires Séismologiques de Hongrie. Budapest.

Kövesligethy, R. 1920: Rapport sur les observations séismologiques faites pendant les années 1913—1919 à l'Observatoire de Budapest. Budapest.

Réthly, A. 1906—1909: Magyarországi Földrengések 1900—1907-ig (Earthquakes in Hungary between 1900—07). M. Kir. Orsz. Meteorológiai és Földmágneses Int. Budapest.

Réthly, A. 1952: A Kárpátmedencék földrengései (455—1918). (Earthquakes in the Carpathian Basins (455—1918). Akadémiai Kiadó, Budapest.

SIMON, B. 1935: Radó de Kövesligethy Bolletino della Societá Sismologica Italiana. Tipografia Editrice Sallustiana, Roma.
SIMON, B. 1937a: Földrengési Obszervatórium mint a bánya- és iparvállalatok támogatója (The seismological observatory as supporter of the activity of mining and industrial companies). *Bányászati és Kohászati Lapok*, 70, 187—189.
SIMON, B. 1937b: A földrengési Obszervatórium elhelyezésének kérdéséhez (On the problem of the situation of a seismological observatory). *Bányászati és Kohászati Lapok*, 70, 443—445.
SIMON, B. 1943: A földrengések (Earthquakes). Királyi Magyar Természettudományi Társulat, Budapest.
SIMON, B. 1957: A magyar—földrengéskutatás 50 éve (50 years seismological research in Hungary). *Geofizikai Közlemények*, 6, 69—72.
SIMON, B. 1963: Kövesligethy as a seismologist. *Ann. Univ. Scien. Budapest R. Eötvös nom. Sectio geol.* 6, 11—12.
SIMON, B.—KISS, Z. 1965: On the relationship between seismic amplitudes and charge in quarry blasting. *Ann. Univ. Sci. Budapest R. Eötvös nom. Sectio geol.*, 9, 13—14.
SZEIDOVITZ, GY. 1972: Elméleti összefüggések a robbantások szeizmikus hatására különböző modellek esetében. (Theoretical connections for the seismic effects of explosions for different models). *Magyar Építőipari Tudományos Egyesület Robbantástechnikai Szakosztálya Közleményei*, 1—2.
SZEIDOVITZ, GY. 1973: Study of the effect of underground blastings on their environment. *Acta Geod. Geoph. Mont. Hung.*, 8, 409—426.
SZEIDOVITZ, GY. 1974: The Destructive Effect of Earthquakes as Function Geologic Structure. *M. Áll. ELGI Közlemények*, 22, 69—76.
SZEIDOVITZ, GY. 1977: A földrengésveszélyeztetettségi térképek szerkesztése (On the construction of seismic risk maps). *Magyarhoni Földtani Társulat Mérnökgeológiai Szemle*, 5—14.
SZEIDOVITZ, GY. 1979: Amplitude and velocity of seismic waves excited by weight dropping. *Acta Geod. Geoph. Mont. Hung.*, 14, 149—154.

75 ЛЕТ СЕЙСМОЛОГИЧЕСКИХ ИССЛЕДОВАНИЙ В ВЕНГРИИ

Э. БИСТРИЧАНИ—Д. ЧОМОР

РЕЗЮМЕ

В статье излагаются итоги возникновения, развития и современного состояния сейсмологических исследований в Венгрии. Показаны направления дальнейшего развития.

Acta Geodaet., Geophys. et Montanist. Acad. Sci. Hung. Tomus 16 (2—4), pp. 435—441 (1981)

SEISMOLOGICAL TELEMETRY NETWORK IN HUNGARY

E. BISZTRICSÁNY—L. HETESI—I. SZABÓ—GY. SZEIDOVITZ

GEODETIC AND GEOPHYSICAL RESEARCH INSTITUTE OF THE HUNGARIAN ACADEMY OF SCIENCES, DEPARTMENT OF SEISMOLOGY, BUDAPEST

The Hungarian seismic station network will be reorganized in the next three years. Telemetry stations will be built and this system will work just like an array. The data transmission from the stations to the centre will happen by radio link. At present the data transmission is a one-way link from the first station, but in the future there will be possibility for duplex. Temporarily the first link has worked on analog FM — FM way for three years. In the next future (from the second half of 1980) digital data transmission will be achieved.

On the stations, the amplified and filtered seismic signals will be converted in digital form moreover completed by error correction code. Using digital phase shift keying, the data will be transmitted by VHF radio telephone. The rate of data transmission will be 3.000 bit/s. In the centre the receiver and signal converter decodes the signal train after demodulation, and there will be a simple analysis of the signals for discrimination. Using the arrival times of the first onsets originated from different stations, the time difference $\Delta t_{ik} = t_i - t_k$ will be computed too. t_i and t_k are the arrival times of the first onsets at the i-th and k-th stations. Having a knowledge of the Δt series, the coordinates of the events can be computed automatically.

Hungary lies beyond the northern side of the Alpide and Balkan earthquake belt. This area is poorer in seismic events than the Mediterranean zone, but this does not mean that the damages of the Hungarian earthquakes have not to be taken into consideration. In this century ten earthquakes occurred in the Carpathian Basin, with the intensities $7 \leq I_0 \leq 9$. These earthquakes were followed by several aftershocks with magnitudes of $2 \leq M \leq 4$. Shocks with less than $M = 2$ cannot be observed by our present instrumentation, except if the event occurred in a close neighbourhood of a station. Foreshocks were observed in very few cases, but we may suppose that they occurred more frequently, than they were recorded with relatively low sensitive instruments (highest magnification is 60,000 with galvanometric recording).

If we should like to study microearthquakes which are indispensable in earthquake prediction, the complete seismological network has to be reformed.

For quick and as far as possible accurate information, a telemetry network was planned. In a first step only five stations will be established (Fig. 1). The network centre is in Budapest.

At first, every station will be equipped by short period vertical pendulums. Since the central station is Budapest, where the noise level is rather high, the pendulum will be set up in a 200 meters deep borehole.

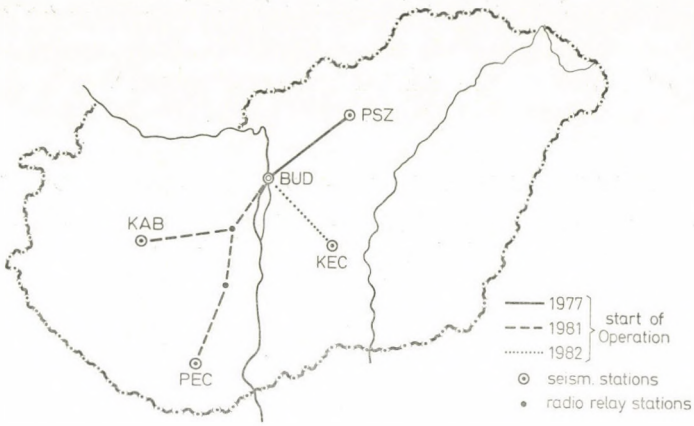

Fig. 1. Telemetry seismic network in Hungary

The data transmission from the stations to the centre occurs via radio link. The first installed station is the Mátra Mountains the distance between the station Piszkéstető (PSZ) and Budapest (BUD) is 90 km. Since the altitude of PSZ is more than 900 m and that of the central observatory 260 m, moreover there are no higher hills between Mátra and Budapest, the data can be transmitted directly. The next station will be established at Pécs (PEC), here seismic data are to be transmitted from 200 km, therefore the radio contact consists of theree radio links. From the middle part of Transdanubia the radio chain consists of two parts, and from the fourth station a direct line will be sufficient again.

At present permitted VHF frequencies are less than 100 MHz but only temporarily, later more than 400 MHz will be used. Now from the first station to the centre, the data transmission is one-way, but in the future there will be possibility for duplex channels.

A requirement for the radio link is that the signal-noise ratio must be better than 26 dB. As far as possible short antenna cables and multielement Yagi antennae are used. The gain of these Yagi antennae are nearly 6 dB. The permitted transmitter power is 10 W for each radio station. Where this relatively high power is not necessary, only 2—5 W will be used. Double modulation has been applied in the experimentals. The frequency of the 2kHz subcarrier has been modulated by the amplified seismic signal and it modulates the carrier frequencies. Phase-locked loop IC-s are used for modulation and demodulation. The subcarrier zero-phases stay unchanged or jump 180° depending on the value of data which can be 0 or 1. The data signal contents an error correcting Haming code to decrease the transmission noise of the carrier.

The facilities of the telemetry network have to possess the features as follows:

— digital recording of the amplified seismic signals
— the signal train has to be supplied by a key system for error detection
— the digitized and coded signal must be suitable for remote transmission
— the signals have to arrive to the central receiver and recording site by means of the data transmission system,
— the signals from the single stations to the centre have to be received independently from each other. The initial phase must be determined in spite of the noise
— using arrival times of the first onsets originated from the different stations the time differences $t_{i0} = t_i - t_0$ for all channels have to be determined. In this formula t_0 is the arrival time of the first onset at the station which first observed an event
— if an event was observed by a station, the centre has to waits 20 s for the other first onsets originated from the rest stations of the network
— the central set must be suitable for monitoring of analog and digital data as well as digital recording, moreover it must be fitted for connection with a separated set which has analyzing tasks.

Short description of the Hungarian telemetry system.

The schematic diagram of the telemetry network can be seen in Fig. 2. The planned Hungarian telemetry network consists of four field stations with the centre in Budapest, as shown in Fig. 1. Naturally the instruments in the centre join by direct digital lines to the processing facilities, while the other four have radio connections.

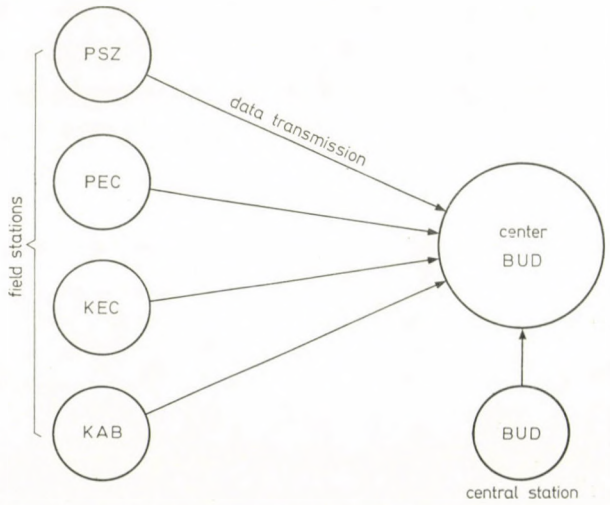

Fig. 2. Schematic diagram of the telemetry network

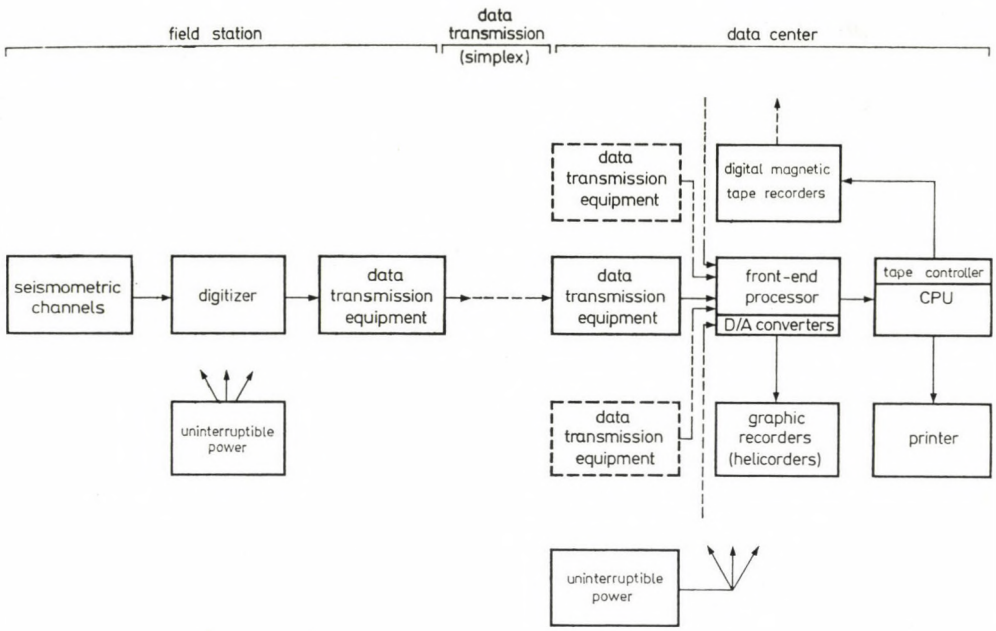

Fig. 3. Data acquisition and handling system

The data acquisition and handling system can be seen in Fig. 3. These systems consist of two parts, namely field station and centre.

The block diagram of the station is shown in Fig. 4. These facilities consist of four main parts. The amplified and filtered seismic signal arrives to a 12 bit A/D converter. The sampling time is 20 ms. A Hamming coder is applied for hindering defective data transmission. This coder gives possibility to correct three errors or to mark six errors. The correction and marking are made in the decoder unit at the centre. The signal can be received by means of a parallel/serial converter. The data signal controlled by the phase shift keying modulator (PSK) is sent to the transmitter.

Digital front-end-processor

The detailed block diagram of the centre can be seen in Fig. 5. From the output of the receiver, the signal is guided after demodulation to the front-end processor's input. This block ensures temporary storage and error correction. If the data are stored without error, they go to the input of the amplitude averager and D/A converter. The D/A converter enables to use a pen recorder and provides opportunity for monitoring the frequency changes of seismic signals. If the amplitude of a seismic event can be identified from the noise so this unit generates an "error signal". In this case the time measuring controller starts and gives a zero time signal for the channel which observed the event first. For the other channels the time difference $-\ t_{i0}$ will be indicated if the seismometers received the event.

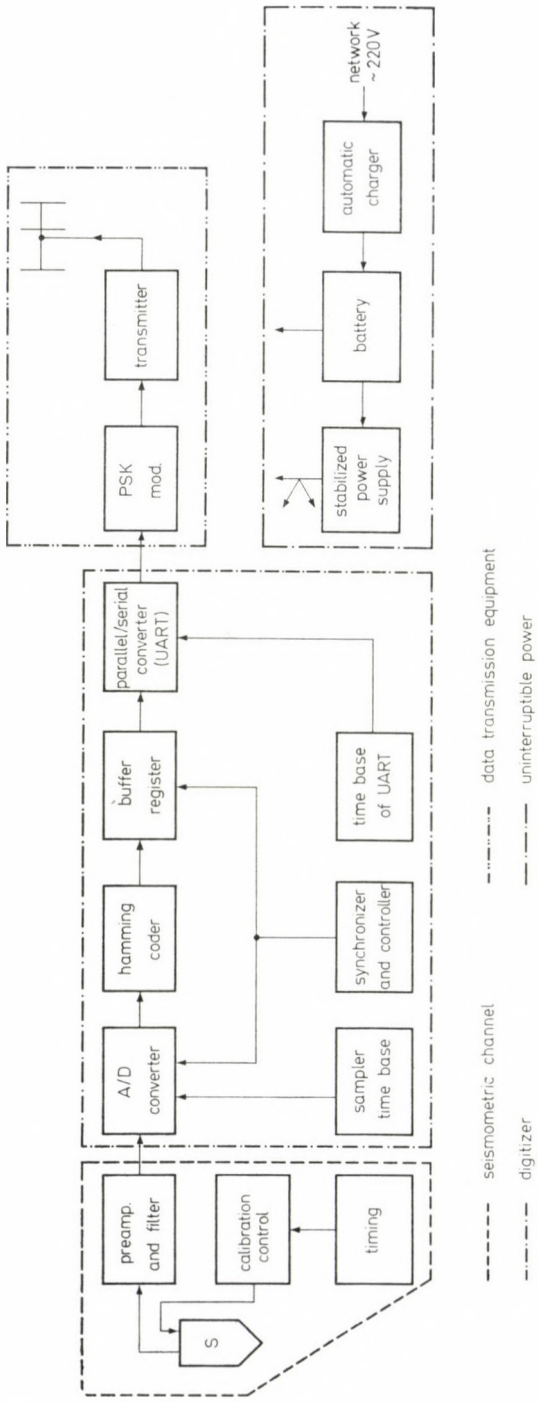

Fig. 4. **Block diagram of a field station**

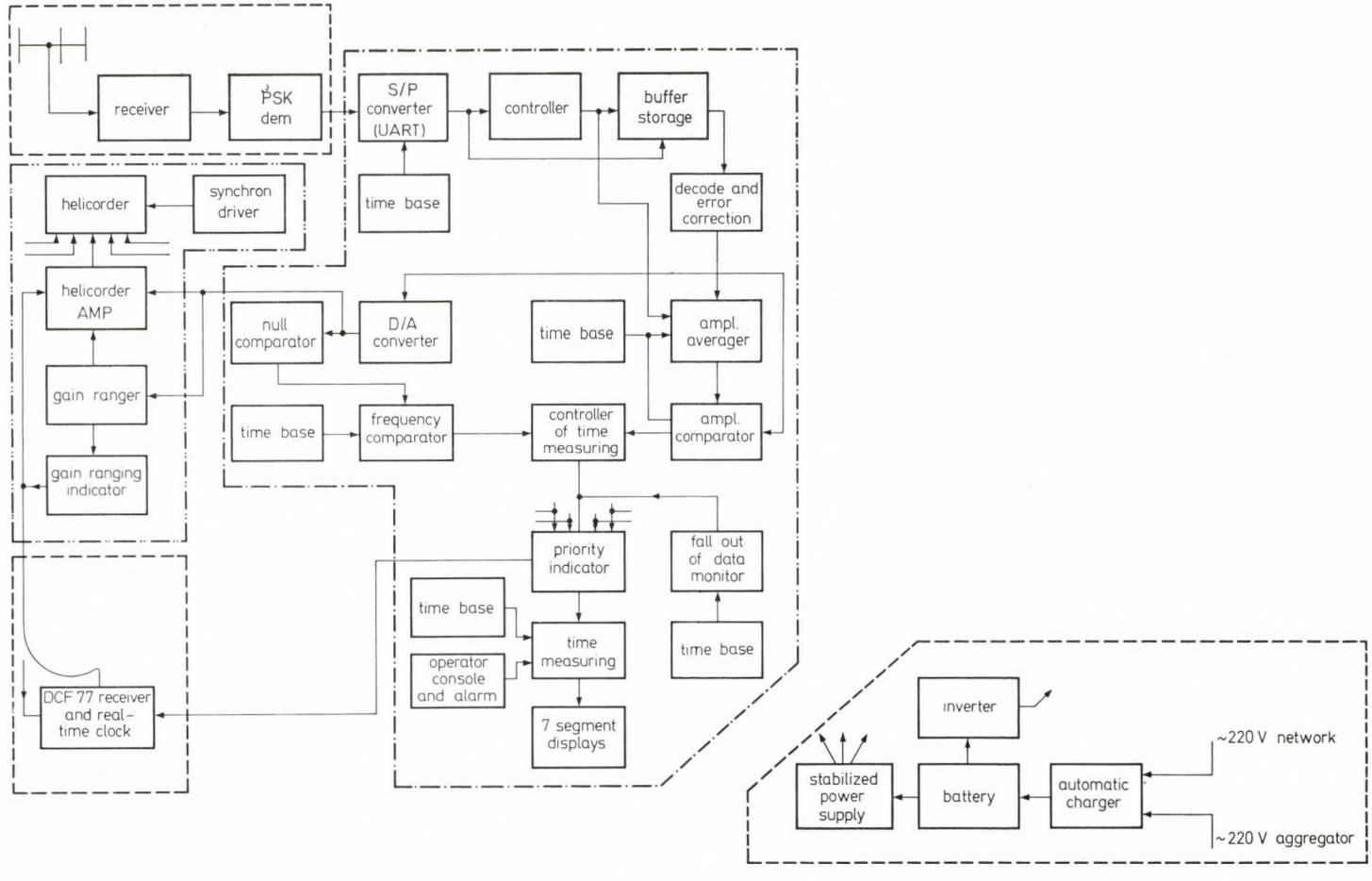

Fig. 5. **Block diagram of the centre**

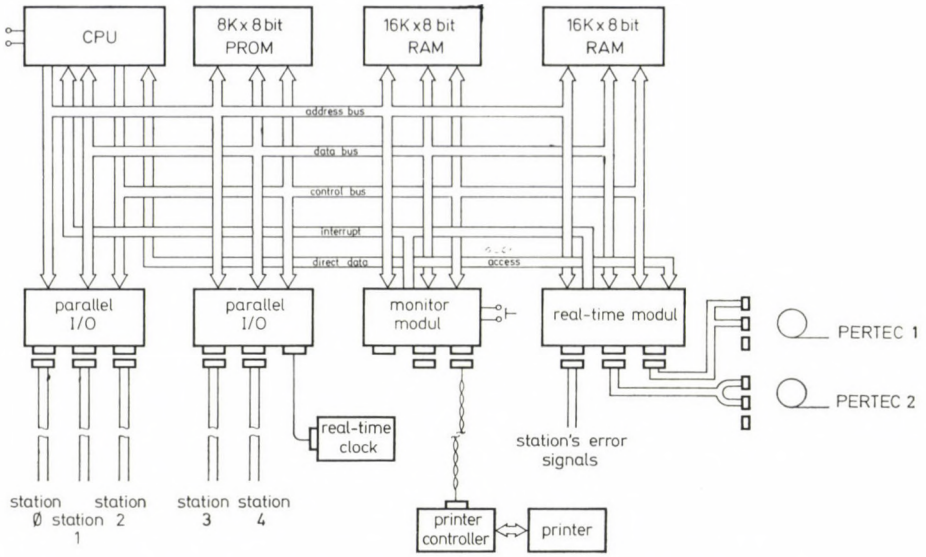

Fig. 6. **Block diagram of data processing and recording system**

The block diagram of data processing and recording system can be seen in Fig. 6.

The automatic phase identification, location and the magnitude determination occur by means of a system controlled by a micro processor. Two random access memory (RAM) units are provided for storage. One of the RAM-s collects the continuously arriving signals, the other gives the possibility for recording on digital tape. The two RAM-s provide these tasks by turn. There is a monitor unit which consists of a serial-parallel (S/P) converter, a universal asynchronous receiver transmitter (UART) and drives the printer controller.

СЕЙСМОЛОГИЧЕСКАЯ ТЕЛЕМЕТРИЧЕСКАЯ СЕТЬ В ВЕНГРИИ

Е. БИСТРИЧАНИ—Л. ХЕТЭШИ—И, САБО—Г. СЕЙДОВИЦ

РЕЗЮМЕ

В следующие три года в Венгрии реорганизуется сеть сейсмологических станций. Будут построены телеметрические станции, и эта система будет работать в режиме ,,аррai,,. Передача данных от станций до центра осуществляется через радио. В настоящее время передача, данный от первой станции проводится однонаправленно, но в будущем станет возможным работа в режиме ,,дуплекс''. В качестве эксперимента первая линия работает уже года три аналоговым методом ФМ—ФМ. В ближайшем будущем (вероятно с первой половины 1980 г.) осуществляется цифровая передача данных. Усиленные и фильтрированные сейсмические сигналы на станциях преобразуются в цифровую форму, потом дополняются кодом с исправлением ошибок. Применяя цифровую манипуляцию фаз, данные передаются при помощи радиотелефона ВХФ· Скорость передачи данных 3000 бит/сек. Находящийся в центре приемник и устройство для преобразования сигналов после демодуляции декодируют последовательность сигналов и производят простой анализ распознавания сигналов.

Используя времена прихода сигналов от разных станций, исчисляется разница $\Delta t_{ik} = t_i - t_k$. Величины t_i и t_k — время прихода начала сигналов. Зная последовательности Δt координаты событий исчисляются автоматически.

Acta Geodaet., Geophys. et Montanist. Acad. Sci. Hung. Tomus 16 (2—4), pp. 443—451 (1981)

MAGNITUDE DETERMINATION AND RELATED PHENOMENA

E. BISZTRICSÁNY
DOCTOR OF SCI.

GEODETIC AND GEOPHYSICAL RESEARCH INSTITUTE OF THE HUNGARIAN ACADEMY OF SCIENCES, DEPARTMENT OF SEISMOLOGY, BUDAPEST

The coda waves are in connection with the earths crust. Since the duration of the surface waves depends mainly on the magnitude of the earthquake and the coefficient of epicentral distance is of a small value, it was assumed that the coda waves are guided waves at greater distances.

The estimation of an earthquake size does not cause a great difficulty if it occurred on populated area. Therefore the first Hungarian isoseismal map was made as long ago as by KITAIBEL and TOMTSÁNYI in 1814 after the earthquake of Mór (Hungary) of January 14, 1810. But in most cases earthquakes occur in unpopulate areas because the surface of the globe is covered predominantly by oceans and moreover many continental faults lie fortunately in unpopulated regions.

But for various reasons we have to determine the size of the earthquakes whether they touched populated or unpopulated areas.

Therefore the method requires instrumental observation. First this size determination was introduced by RICHTER and his method was based on the maximum amplitudes of surface waves registered by Anderson-Wood seismographs. RICHTER's magnitude scale was applied in California and was soon extended by GUTENBERG and RICHTER to remote earthquakes, too.

In Hungary these researches began in 1954 and the first calibration curve was made for the Wiechert seismograph in Budapest. For the first equation was well usable if the epicentral distances are more than ten degrees. The magnitudes of local and near earthquakes were overestimated by this method. An excellent example are the Greek shocks whose epicentral distance related to Prague was about 12°, and to Athens within a few hundreds kilometer. Both stations determined the Richter magnitude of these Greek earthquakes but the magnitudes determined by Athens were some 0.4 units above the values given by Prague (Fig. 1). By investigating several Hungarian earthquakes of small epicentral distance a similar result was obtained. Thus the need arose to seek a different way of magnitude determination.

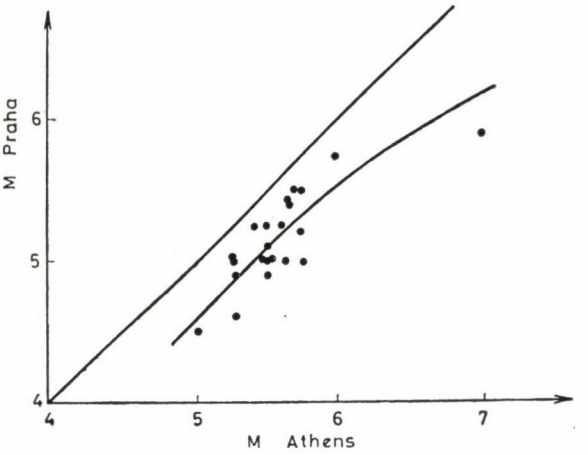

Fig. 1. A comparison of earthquake determined in Athens and Prague

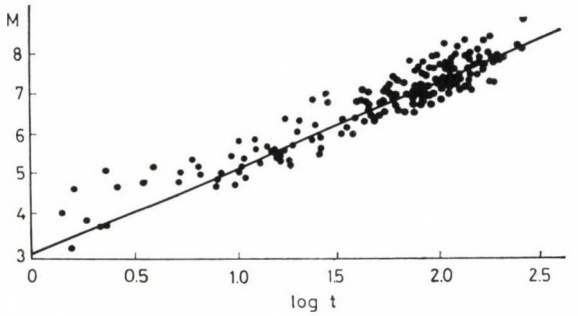

Fig. 2. A plot of magnitudes vs. duration t ($\log t$) of surface waves

It was observed earlier that the duration of surface waves depends mainly on the size of the earthquake. Therefore a mathematical form of this relation was looked for.

It was found that the logarithm of surface wave duration is in a linear relation with the Richter magnitude, namely

$$M = a \log t + b\Delta^\circ + c. \tag{1}$$

The magnitude of 166 shocks were determined by

$$M = \log A_{20} + 1.37 \log \Delta^\circ + 2.63 \tag{2}$$

and plotted against $\log t$. Here t was defined as the time difference between F and L in minutes, as usually given in the literature, L being the first onset and F the end of the surface waves.

Performing a least-squares approximation, a straight line

$$M = 2.12 \log t + 0.005\Delta^\circ + 2.98 \tag{3}$$

was obtained. The epicentral interval used in this study was $3^\circ < \Delta^\circ < 180^\circ$. It can be seen in the Fig. 2, that the values of local earthquakes are above the straight line because the magnitudes are overestimated some half M unit by equation (2). It well agrees with the above mentioned statement shown in Fig. 1.

It is a striking feature of Eq. 3 that the coefficient of Δ° is very small i.e. the duration of surface waves is almost independent on the epicentral distance if the pendulum's natural period is 10 sec.

The slight distance dependence of the duration of surface waves turned the attention among others to investigations of coda waves [AKI, 1969; BISZTRICSÁNY 1970, 1971]. In the first case the seismograms of Kirnos ($V = 600$, $T_p = 12.5$ s, $T_g = 1.25$ s) vertical seismograph were used, since we wanted to investigate the properties of Rayleigh coda waves of shallow focus earthquakes. The epicentral distances were in an interval of $5^\circ \leq \Delta^\circ \leq 50^\circ$.

Before the properties of coda waves would be discussed, the earthquake mechanism has to be summed up shortly. An earthquake is anticipated by accumulation of elastic stresses along a discrete fracture like a geological fault. If the stress and strain are great enough, the fault will be splitted. The duration of this process of tearing is rather short as compared with the total duration of surface waves, as it was shown by Eq. 3. Aki gave an explanation for build up of coda waves of local earthquakes which are responsible for the long duration of surface waves. But the decreasing of duration of surface waves is light if the epicentral distance increases. Therefore the cause of this nearly constant duration was studied in a greater interval of epicentral distance. Since the train form of coda waves are very similar to the form of seismic noise, a connection of coda waves was supposed with the layers of the earth's crust as it was studied by HARDTWIG (1962) for long period noise.

If the coda waves were in connection with the properties of the plates in the earth's crust, the recurrence of the periods of coda waves might not depend on epicentral distance significantly. Investigating this question, the interval of $5^\circ \leq \Delta^\circ \leq 50^\circ$ was divided into four parts (Fig. 3). It can be seen that there is a very significant maximum at 7.5 s between two smaller peaks (at 5 and 9 s). If the recurrence maxima do not depend on epicentral distance in the interval of $5^\circ \leq \Delta^\circ \leq 50^\circ$, it ought to be done so if $\Delta^\circ < 5^\circ$, provided that the magnitudes of the earthquakes are in similar intervals. This value of the magnitude $5 < M < 7$ is very rare in the Carpathian Basin.

The earthquake of May 6, 1976 of North Italy ($M = 7$, $\Delta^\circ = 4^\circ$), provided a suitable seismogram (Fig. 4). The result of the investigation of coda waves

periods is shown in Fig. 5. The similarity is remarkable between Figs 1 and 3 in spite of the fact that in Fig. 3 more earthquake seismograms were used and in Fig. 5 only one. The two curves show similar resonance properties. The dominant period probably exists in consequence of the geometric and geophysical properties of the layers. This effect travels in the different layer of the earth's

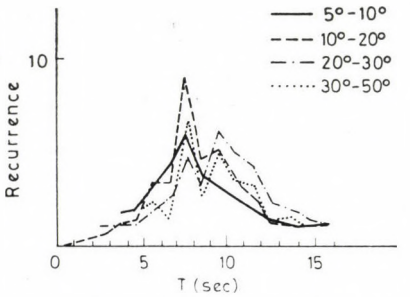

Fig. 3. The recurrence of periods of coda waves in the interval of $5° \leq \Delta° \leq 50°$

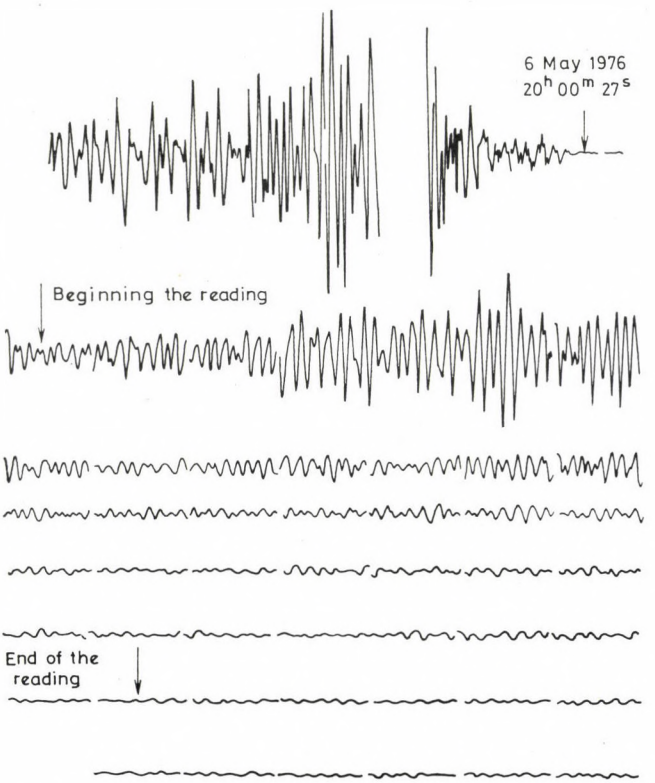

Fig. 4. Seismogram of the analysed Rayleigh-type coda waves

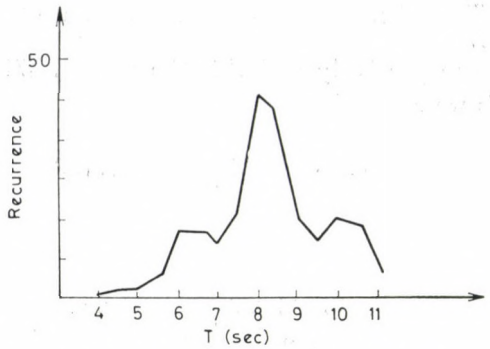

Fig. 5. The results of the investigation of coda wave periods

crust with little damping, therefore the duration of surface waves stays unchanged.

In case of small earthquakes, the energy is insufficient to shake a thick layer. Therefore in case of near, small, shallow focus earthquakes, the frequency maximum reflects the properties of thinner layers, sometimes presumably the properties of the unconsolidated upper layer.

Henceforth we shall investigate the relation between maximum recurrence of periods and layer thickness. We shall follow Hardtwig's method (1962). In accordance with HARDTWIG the microseisms are supposed to be plate vibrations and they may be interpreted as Rayleigh waves, but naturally they are not pure Rayleigh waves.

For Rayleigh waves, the motion can be described by

$$u = c\Gamma_1(k, z) \cos k(x - Vt) \tag{4}$$

$$w = c \frac{1 - \varkappa}{\sqrt{1 - 2\varkappa}} \Gamma_2(k, z) \sin k(x - Vt), \tag{5}$$

where

$$\Gamma_1 = e^{-q_1 z} - (1 - \varkappa)e^{-q_2 z}, \Gamma_2 = -(1 - \varkappa)e^{-q_1 z} + e^{-q_2 z} \tag{6}$$

and

$$\varkappa = 1 - \frac{\sqrt{3}}{3} = 0.42265$$

is the root of the equation

$$3\varkappa^3 - 12\varkappa^2 + 14\varkappa - 4 = 0\,.$$

and c is an arbitrary constant.

The displacement will decrease with depth according to

$$q_1 = k\sqrt{-1\frac{2}{3}\varkappa}\,, \qquad q_2 = k\sqrt{1 - 2\varkappa}\,.$$

Substituting $k = \frac{2\pi}{L}$ and $L = VT$ (where V and L are the velocity and wave length of the waves respectively and T is the period. With the experimental value $V = 3.2$ km/s we can write

$$q_1 = \frac{6.28 \cdot 0.8475}{3.2} \cdot \frac{1}{T} = \frac{0.7723}{T} \tag{7}$$

and

$$q_2 = \frac{6.28 \cdot 0.3933}{3.2} \cdot \frac{1}{T} = \frac{1.6640}{T}. \tag{8}$$

We have to investigate the amplitude η and ζ of u and w namely

$$\eta = c\Gamma_1(k, z), \quad \zeta = c\Gamma_2(k, z) \frac{1 - \varkappa}{\sqrt{1 - 2\varkappa}}.$$

For normalizing of c, let the horizontal displacement be of unit value at $z = 0$. Then

$$c\Gamma_1(k, o) = c\varkappa = 1.$$

The amplitude of the vertical displacement as it is expectable, 1.4679 at $z = 0$.

Let us suppose that the amplitudes decrease continuously and rapidly at the depth $z = z_0$ of boundary layer of less solidity. Moreover we shall suppose that the Z and Z' amplitudes of the Rayleigh waves with periods T and T' will decrease by a factor of n.

Therefore it can be written

$$\zeta = \frac{Z}{n} \quad \text{and} \quad \zeta' = \frac{Z'}{n'}.$$

The depth of the boundary layer can be determined, if $n = n'$, then

$$\frac{Z}{\zeta} = \frac{Z'}{\zeta'}$$

or

$$\zeta = \frac{Z}{Z'} \zeta' \tag{9}$$

(we remark that the value of ζ is 10—20 percent of Z at the boundary layer).

Substituting Eqs (7) and (8) into Γ_2 at Eq. (6) moreover considering that $\Gamma_2 = \zeta = \zeta'$, by putting the values of ζ and ζ' into Eq. (9) we get

$$e^{-0.7723\frac{z_0}{T}} - 0.5774\, e^{-1.6640\frac{z_0}{T}} = \frac{Z}{Z'} e^{-0.7723\frac{z_0}{T}} - 0.5774\, e^{-1.6640\frac{z_0}{T}}. \qquad (10)$$

From (10), z_0 can be determined, but the solution is lengthy.

If we neglect the second part at both sides of Eq. (10), a very simple relation can be obtained:

$$e^{-0.7723\frac{z_0}{T}} = \frac{Z}{Z'} e^{-0,7723\frac{z_0}{T}}$$

and

$$z_0 = \frac{TT' \ln \frac{Z'}{Z}}{(T' - T)\, 0.7723}. \qquad (11)$$

Having determined the $T = a(Z)$ function a series of values T, T' and Z, Z' can be obtained in a close neighbourhood of the period with recurrence maximum; by substituting them into Eq. (11), z_0 can be determined.

Using the least squares method, the first $T = a(Z)$ equation was determined by BISZTRICSÁNY (1970):

$$T = 4.28Z - 0.47Z^2 + 1.83. \qquad (12)$$

Computing the pairs of values from Eq. (12) according to the peaks of the curve seen in Fig. 3, we get

$$\begin{aligned} 5.6 &\leq T \leq 6.6 \quad & z_0 &= 13.2 \text{ km}, \\ 7.48 &\leq T \leq 8.7 \quad & z_0 &= 18.4 \text{ km}, \\ 9.4 &\leq T \leq 10.7 \quad & z_0 &= 29.65 \text{ km}. \end{aligned}$$

These layer thicknesses are in good agreement with the results of deep seismic sounding.

Since the pairs of data (T, Z) have a great scatter [BISZTRICSÁNY, 1971], later that part of the seismograms were measured, where well developed wave groups could be found. In such a way a more favourable data distribution was obtained with less scatter [BISZTRICSÁNY, 1971]. This shows a great similarity with the results on long period noise obtained by WALZER (1969). The $Z = a(T)$ relation was determined by means of 1000 data:

$$Z = 0.035T^2. \qquad (13)$$

Substituting Eq. (13) into Eq. (11):

$$z_0 = \frac{TT' \ln \frac{T'^2}{T}}{(T' - T)\,0.7723}. \tag{14}$$

It can be derived in a simple way from Eq. (14)

$$z_0 = \frac{2T}{0.7723}, \tag{15}$$

where T is the maximum of the recurrence curve [BISZTRICSÁNY, 1975]. The discrepancy between z_0 values computed by means of Eq. (10) and Eq. (15) may be neglected.

On the basis of this study it was assumed that the coda waves are in connection with the thickness of different layers in the earth's crust. Further it is supposed that these waves travel as guided waves (that is perhaps the reason of small energy loss) from the neighbourhood of the epicentral zone where they build up in a way defined by AKI.

REFERENCES

AKI, K. 1969: Analysis of the seismic coda of local earthquakes as scattered waves. *J. Geophys. Res.*, 74. 2.

BISZTRICSÁNY, E. 1959: On a new method of determining earthquake magnitudes. *Trav. Sc. Ser.* A, 20.

BISZTRICSÁNY, E. 1970: Analysis of codas of shallow focus earthquakes. *Geofiz. Közl.*, 19, 3—4.

BISZTRICSÁNY, E. 1971: Computation of strata thickness on the basis of coda waves. XII[6] Assemblée Générale de la Commission Séismologique Européenne, Luxembourg, 21—29 Sept, 1970.

BISZTRICSÁNY, E. 1975: Properties of coda waves. *Acta Geod. Geoph. Mont. Hung.*, 10, 131—135.

HARDTWIG, E. 1962: Theorien zur Mikroseismischen Bodenruhe. Akad. Verlagsgesellschaft, Leipzig.

LEE, W. H. K.—BENNETT, R. E.—MEAGHER, K. L. 1972: A method of estimating magnitude ..., U. S. Geol. Survey, Open file report.

SOLOVIEV, S. L. 1965: Seismicity of Sakhalin. *Bull. Earthq. Res. Inst.*, 43.

TSUMURA, K. 1967: Determination of earthquake magnitude from total duration of oscillation *Bull. Earthq. Res. Inst.*, 45.

WALZER, U. 1969: Untersuchung der Polarisation und anderen Eigenschaften der langperiodischen Mikroseismik. Forschungbereich Kosmische Physik. *Zentralinstitut Physik d. Erde*, No. 1.

ОПРЕДЕЛЕНИЕ ВЕЛИЧИНЫ ЗЕМЛЕТРЯСЕНИЯ И СВЯЗАННЫЕ С НИМ ЯВЛЕНИЯ

Э. БИСТРИЧАНИ

РЕЗЮМЕ

Волны кода связаны с земной корой. Так как продолжительность поверхностных волн главным образом зависит от величины землетрясений и коэффициент расстояния эпицентра в уравнении для определения величин землетрясений является небольшой величиной, предполагается, что волны кода представляют собой направленные волны, носящие характерные геометрические и физические свойства слоев земной коры.

Acta Geodaet., Geophys. et Montanist. Acad. Sci. Hung. Tomus 16 (2—4), pp. 453—467 (1981)

MICROTREMOR MEASUREMENTS IN BUDAPEST

GY. SZEIDOVITZ

GEODETIC AND GEOPHYSICAL RESEARCH INSTITUTE OF THE HUNGARIAN ACADEMY OF SCIENCES, DEPARTMENT OF SEISMOLOGY, BUDAPEST

Microtremors source processes in Budapest are not stationary broad-band phenomena with flat spectrum. In order to obtain informations on the natural ground frequency, one would have to make repeated measurements in the hope that some common spectral peaks can be attributed to site conditions. Thus the study of site conditions by the microtremor technique is a time-consuming process of questionable reliability. The greatest difficulty — even in the case of a one-layer system — associated with the application of the microtremor technique is the fact that it is almost impossible to select from many, often sharp spectral peaks the right one which may be characteristic for the ground properties.

Studies of the distribution of damages caused by earthquakes indicate that large differences in the extent of damage often occur over relatively short distances. Damage to engineering structures caused by earthquakes is known to depend on the nature of the arriving seismic energy as well as on the characteristics of structures. For the purpose of engineering design, the characteristics of ground shaking that are of primary importance are the amplitude, the frequency content and the duration. These characteristics are dependent on various factors such as the earthquake source mechanism, the orientation of the site with respect to the source, the material properties of the earth media along with the waves propagate, the nature and orientation of various geological discontinuities, the local topographic and subsoil conditions.

Microtremors are low-amplitude oscillations ($1—3\mu$) of the ground surface produced by natural sources such as the wind and the sea breaking on nearby shores, and by artificial ones such as vehicular traffic and other cultural noise. The microtremor motions may be modified by local soil and geological conditions and hence the records may contain information on these local conditions.

KANAI and TANAKA (1961) made several studies of microtremors. Their investigations typically made use of 2 min long records from one horizontal component of ground motion and involved measuring the intervals between successive zeros. The periods of ground motion were taken to be twice the time interval. By plotting the number of waves vs. period, they obtained the occurrence frequency curve of periods. From this study the suggested [KANAI,

1962] that for a given site such curves had some correlation with similar plots obtained from those of strong earthquake ground motions.

Before studying the nature of microtremors a short review of its physical characteristics is to be made.

WILSON (1953) studied microtremors of frequenices 4 to 100 Hz and found the main sources to be heavy traffic, machinery, aircraft, other and wind man-made noises. AKI (1957) stated that microtremors at a particular site had a uniform intensity with respect to azimuth. He found that these waves had a definite velocity at a given frequency and identified them as Love waves. AKAMATU (1961) by studying particle orbits arrived at the conclusion that they are mainly combinations of Love and Rayleigh waves. KANAI (1962) has interpreted microtremors as being chiefly multiple reflections of SH waves in parallel subsoil layers. Recordings made at the surface and at different depths by DOUZE (1964) indicated that microtremors may be both *P* and Rayleigh waves, while ALLAM (1969) concluded that microtremors are combinations of body and surface waves.

UDWADIA and TRIFUNAC (1973) found that in El Centro, California microtremor and earthquake processes were widely different in character, being little to no correlation between the ground responses to earthquake and microtremor excitations.

Microtremors were found to be non-stationary within a day or so.

The above brief outline was intended to indicate the diversity of prevalent opinions on the basic nature of microtremors.

This paper attempts to investigate the influence of local conditions on the seismic energy of microtremors. Low-amplitude ground motions of microtremors were measured at ten different locations at which geological condition were investigated.

Field measurement of microtremors

Three VEGIK seismographs with a natural period of about 1 sec and 70 per cent damping were used to measure the three components of microtremors. The output was then recorded by a four channel FM magnetic tape recorder. A direct display of the ground motions was obtained simultaneously by oscilloscope.

A part of the measurements was carried out during night in order to eliminate as far as possible the effects of local disturbances. In order to get an idea about the stationarity of the process, all the sites were revisited during following nights or days when measurements were made once more.

Data analysis

Microtremor ground motions with a recorded length of 300 s were analyzed in the frequency range 0 to 100 Hz by a Real Time Narrow Band Analyser (Brüel & Kjaer, Typ 3348). The spectra produced by the system were linearly averaged according to the equation:

$$A = \frac{1}{K} \sum_{r=1}^{r=K} Tr$$

where A is the final averaged spectrum, K is the number of spectra to be averaged (in our case 32) and Tr is a spectrum making up the average.

Spectral analysis of microtremor motions

At four sites the equipments were placed on "outcrops". In these cases microtremors have been considered by many investigators as a process analogous with white noise. The spectra (Figs 1 to 4 left side) obtained from microtremor-records on these sites are different of white noise spectra and a number of spectral peaks can be seen. In order to see if the stationarity persists over relatively longer periods (a day or so) measurements were reiterated on the following day. The spectra on the right side of Figs 1 to 4 show the nature of ground motion about 24 h after the first measurements were made. A visual comparison of these spectra indicated low similarity between spectral peaks. Some of the peaks observed in these spectra might be the result of a particular excitation which took place at the time the recording was made.

Figures 5 to 10 show the spectra of typical one layer system. At site number five (Fig. 5), the dolomite was covered by a (11 m thick) loose layer. The stationarity of the spectral peaks is rather good. Both horizontal components indicate a spectral peak at about 5 Hz which might be the result of a resonant effect. The velocity of P waves (V_p) in the loose layer was 200 m/s and from the equation

$$T = V_p/4H$$

where T is the period in sec and H is the thickness of the loose layer in m, the predominant frequency can be calculated. The measured (5 Hz) and calculated (4.5 Hz) predominant frequencies are quite similar in this case.

At site No. 6 (Fig. 6), limestone was covered by (5 m thick) loess.

A weak sign of oscillations can be seen on the spectra of the EW-component. A peak at 4 Hz in the vertical component seems to be non-stationary and disappeared in the spectra of the next day indicating that these peaks

were possibly results of forced oscillations of the ground surface caused by local sources.

Limestone was covered by *detritus* limestone (6.2 m thick) at site No. 7 (Fig. 7). In the spectra of all three components of microtremor motions a peak at about 10 Hz can be observed which seems to be stationary and characterizes the ground properties. A similar peak, however, occurs also in the spectra measured at other sites and on other days. Deductions from such spectra must be made with caution.

At site No. 8 (Fig. 8) limestone was covered by loose clay (8.9 m thick). The velocity of P waves is 472 m/s in the upper loose layer. A resonance is expected at 13 Hz. A peak at about 10 Hz can be found in the spectra of all three components. As we mentioned, a spectral peak occurs here almost in every spectrum and it is probably a characteristic of microtremors in Budapest. There is a sharp peak in these spectra at 24.5 cps and one may conclude that probably a resonant ground frequency exists.

However, a correspondence between the geological structure of the site and the spectral peak cannot be found. The two sets of spectra measured in different time have dissimilar appearance (Fig. 8, left and right sides), the prominent spectral peak at 24.5 Hz observed in spectra of June 16 however has appeared in the spectra of June 17, indicating that this peak was possible a forced oscillation of the surface caused by local sources.

Figure 9 shows the spectra of three components measured over geological structures being similar to the previous models. Compact marl was covered here by yellow marl (4.8 m thick). The peak frequency calculated is 24.6 Hz in agreement with a spectral peak of the EW components. The two sets of spectra measured at different times are similar especially below 20 Hz. This similarity can be explained with the relatively short time difference (5 h) between the two measurements.

Figure 10 shows the spectra of all three components measured on clay covered by (1.3 m thick) filling. The calculated frequency is rather high, about 38 Hz. The two sets of records were carried out at 10 a.m. and 15 p.m. on the same day. A sharp spectral peak at 34—35 Hz can be found in the spectra of the NS component only. A visual comparison of the spectra of vertical components measured at different times indicates a high similarity of spectra. These spectra show that the form of peaks has a stationary character within 5 h.

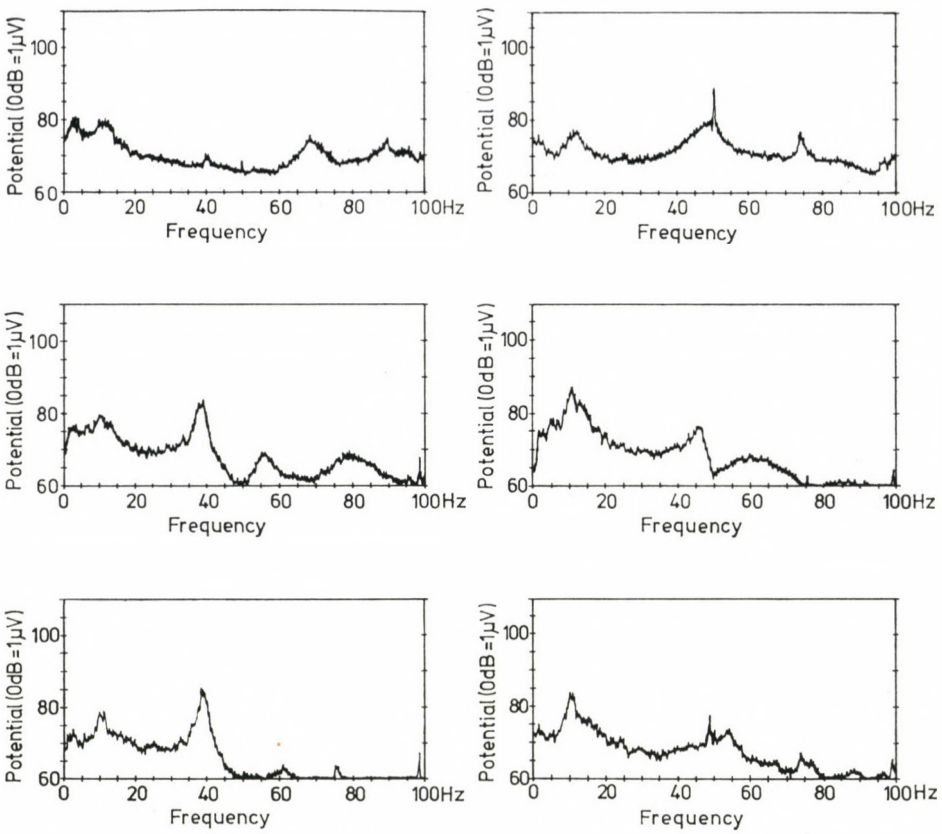

Fig. 1. Two sets of the spectra of three components (from top: V, NS, EWH) measured on June 16, at 15 h (left) and on June 17 at 15 h (right)

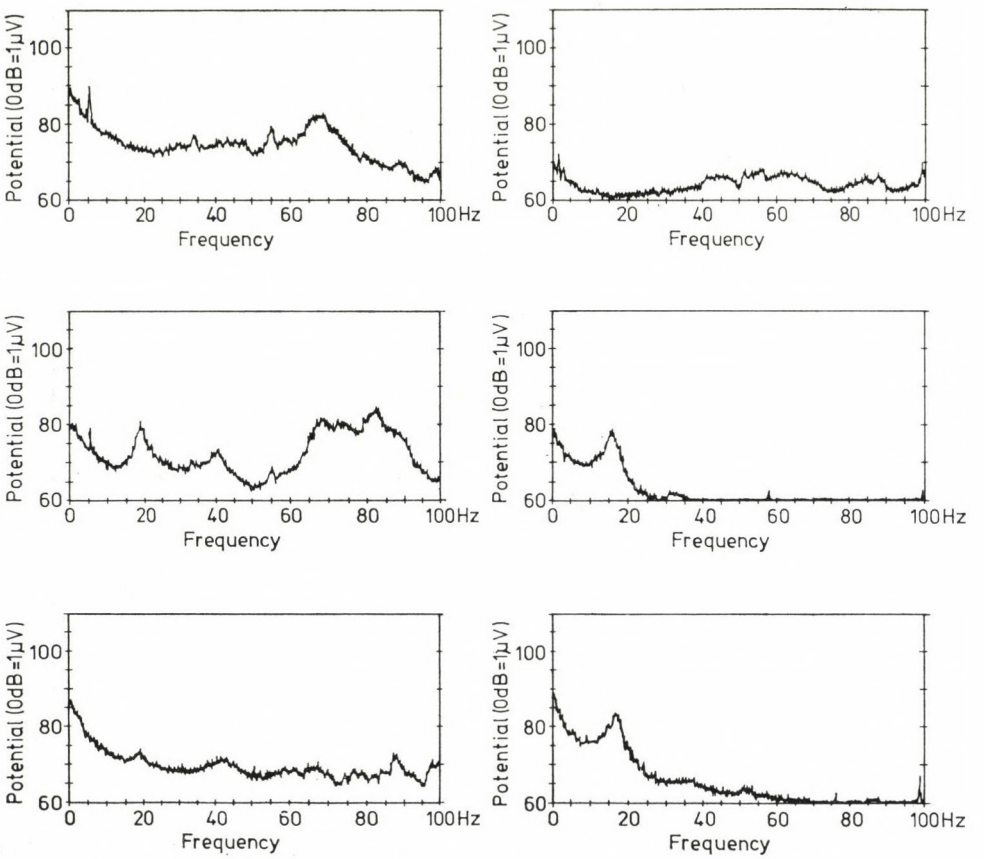

Fig. 2. **Two sets of the spectra of three components (from top: V, NS, EW) measured on June 16 at 10 h (left) and on June 17 at 13 h (right)**

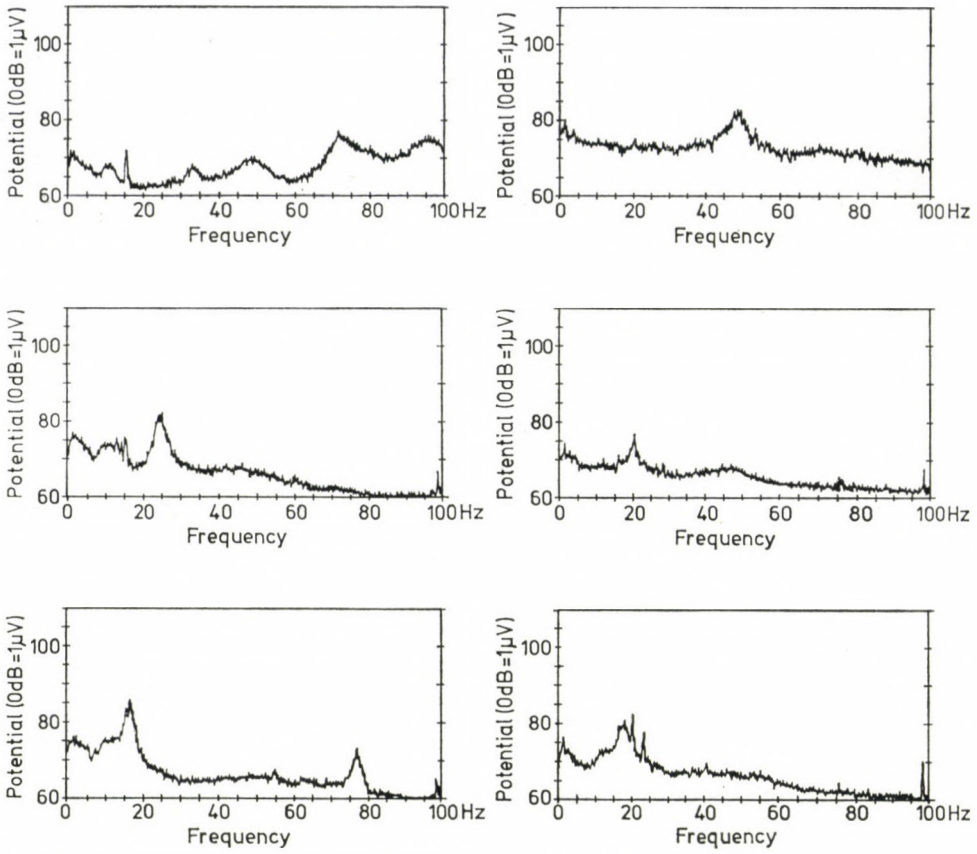

Fig. 3. **Two sets of the spectra of three components (from top: V, NS, EW) measured on June 9 at 17 h (left) and on June 10 et 6 h (right)**

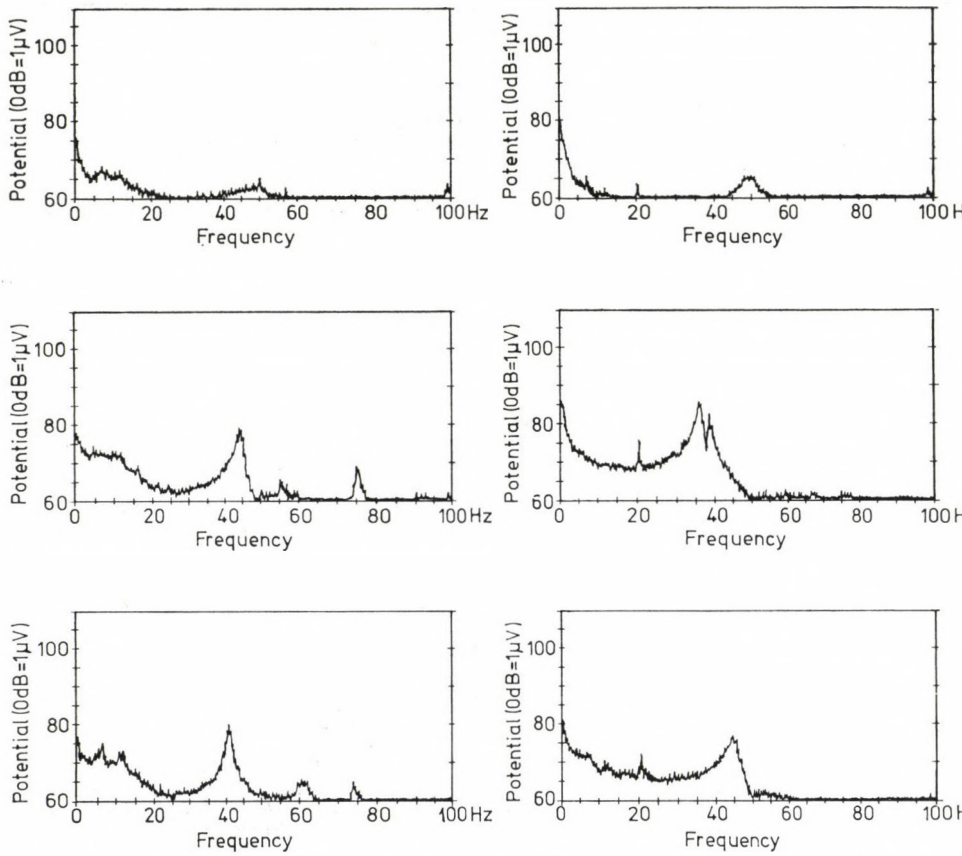

Fig. 4. **Two sets of the spectra of three components (from top: V, NS, EW) measured on June 9 at 13 h (left) and on June 10 at 4 h (right)**

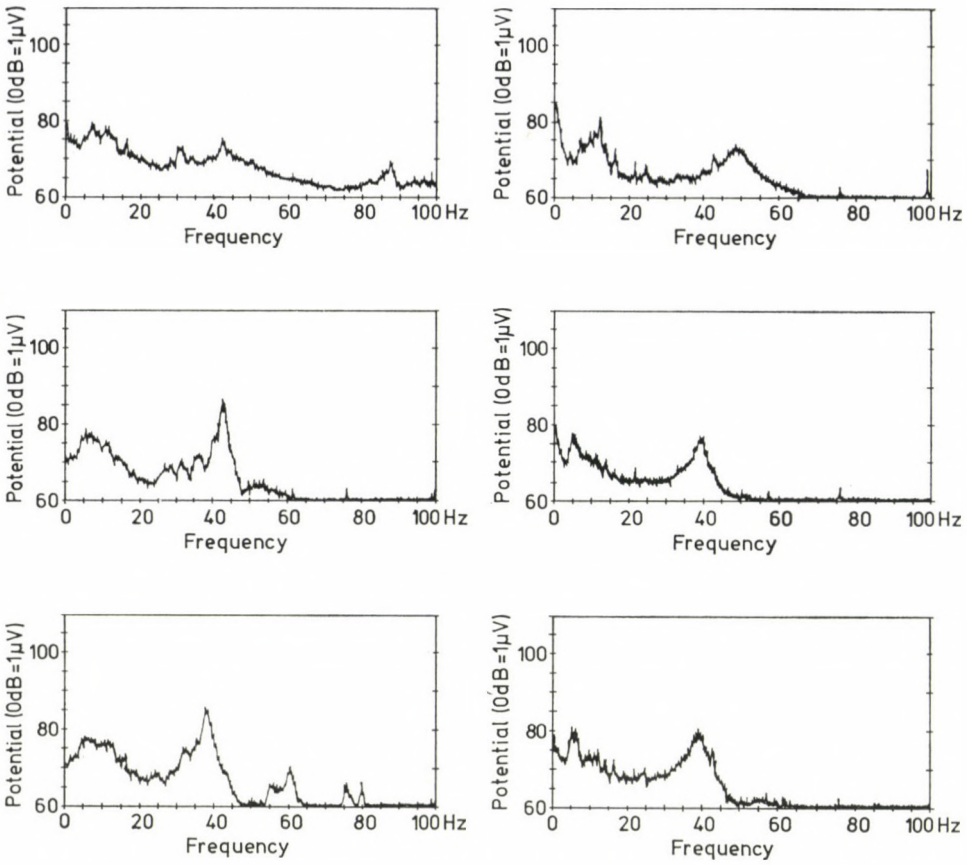

Fig. 5. Two sets of the spectra of three components (from top: V, NS, EW) measured on June 9 at 13 h (left) and on June 10 at 3 h (right)

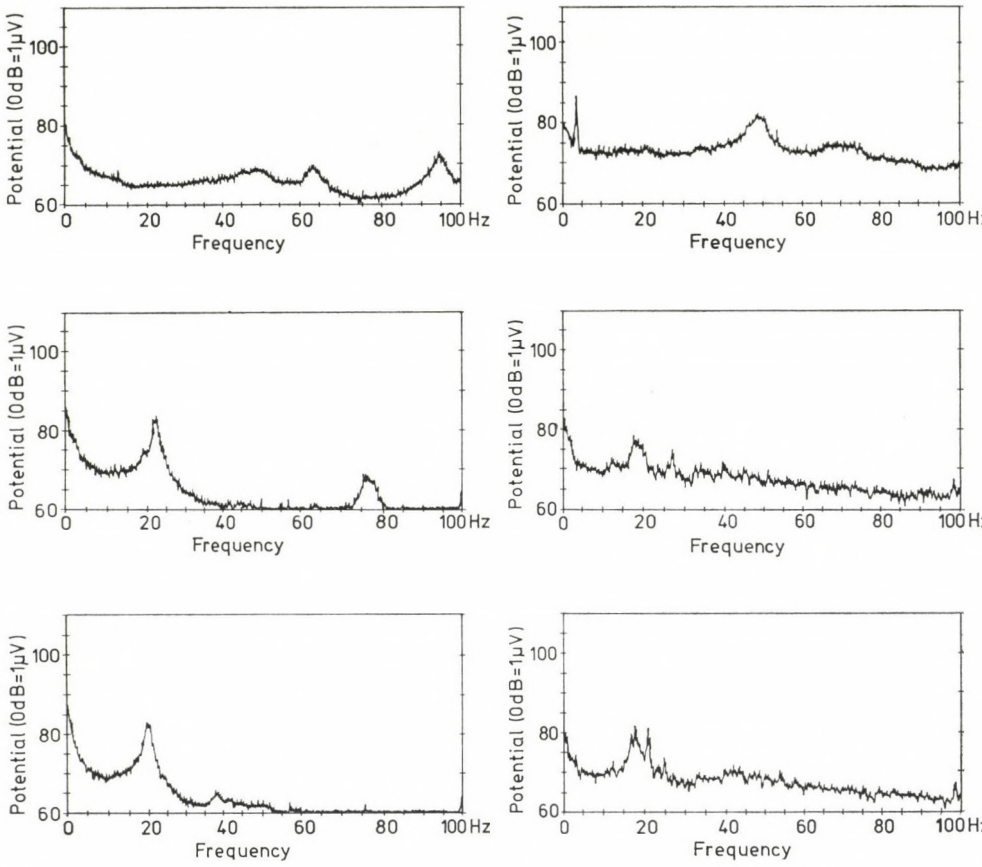

Fig. 6. Two sets of the spectra of three components (from top: V, NS, EW) measured on June 9 at 16 h (left) and on June 10 at 5 h (right)

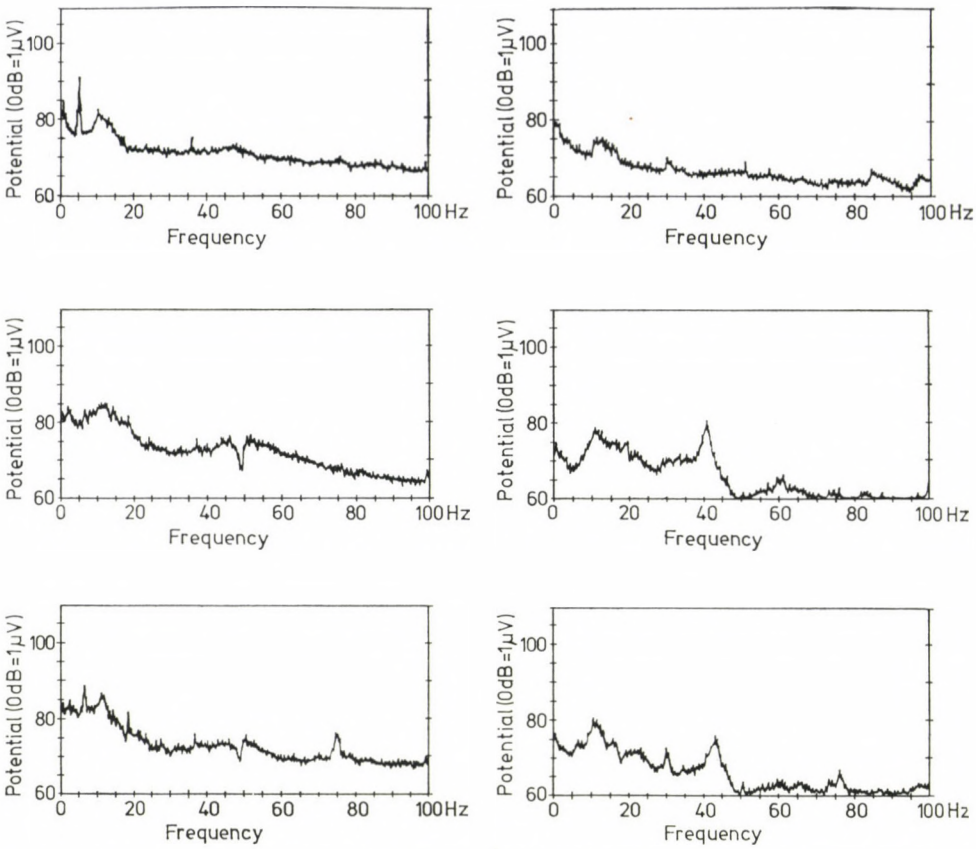

Fig. 7. **Two sets of the spectra of three components (from top: V, NS, EW) measured on June 16 at 11 h (left) and on June 17 at 6 h (right)**

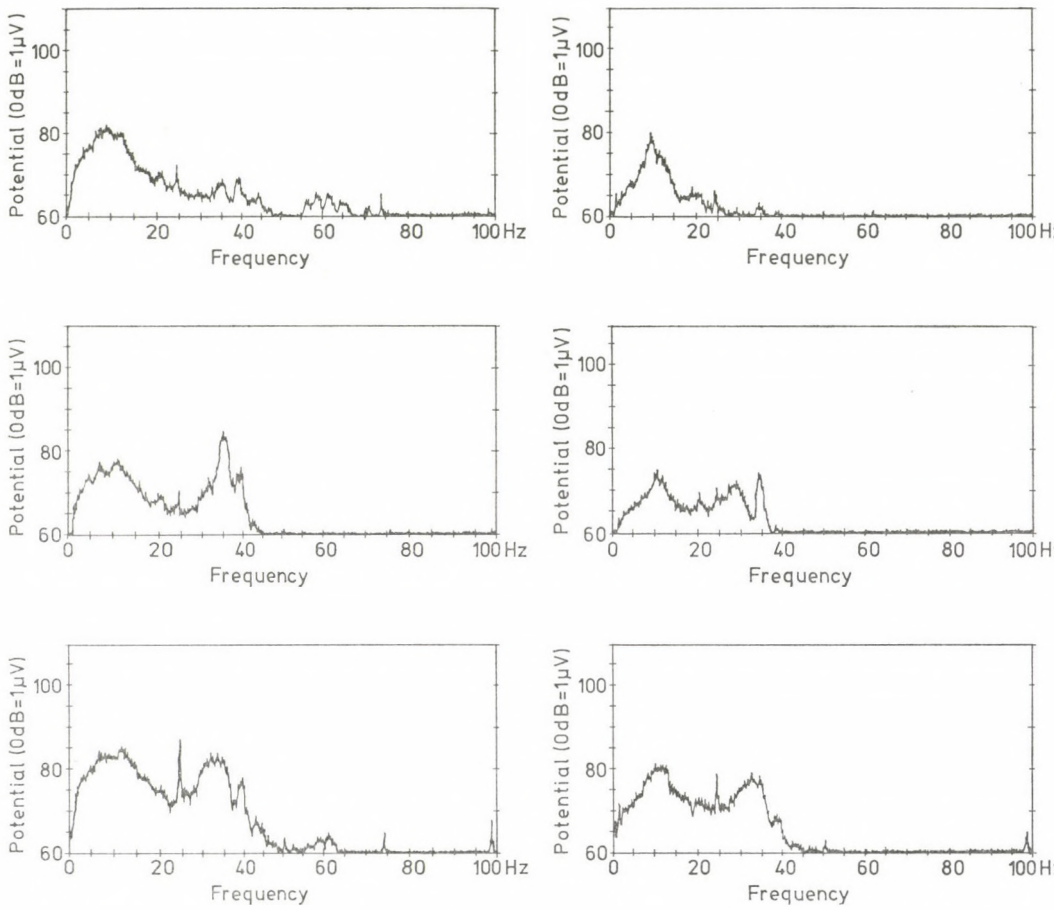

Fig. 8. Two sets of the spectra of three components (from top: V, NS, EW) measured on June 16 at 14 h (left) and on June 17 at 6 h (right)

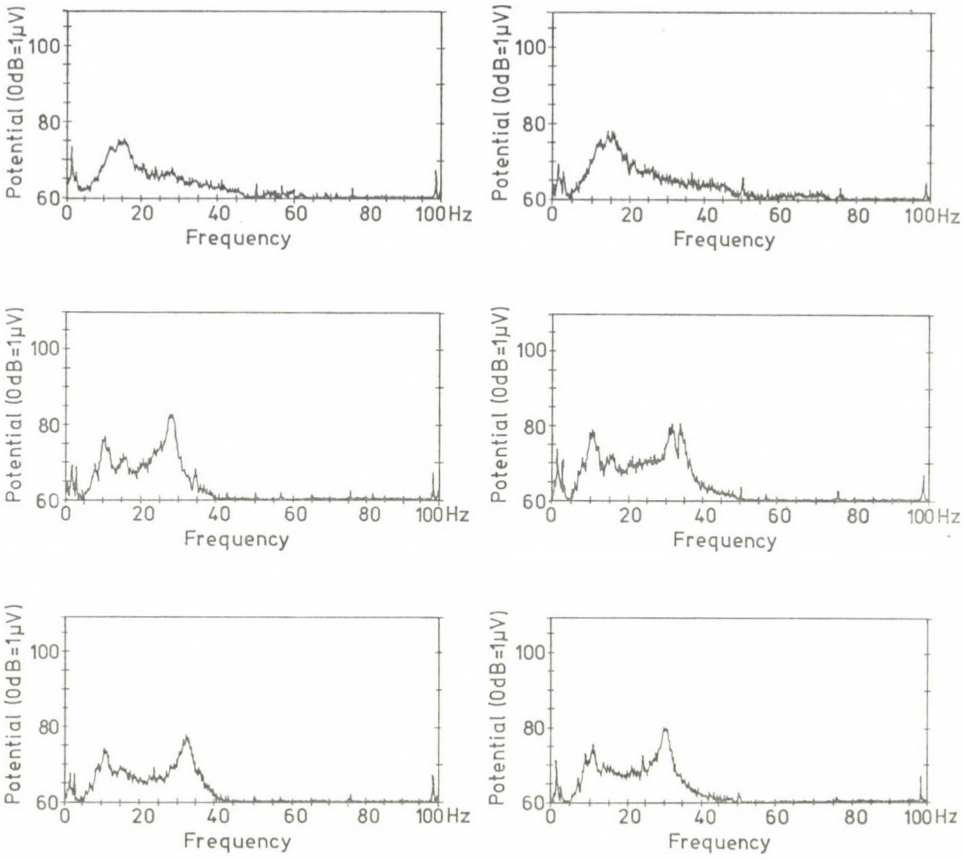

Fig. 9. Two sets of the spectra of three components (from top: V, NS, EW) measured on June 23 at 11 h (left) and on June 23 at 16 h (right)

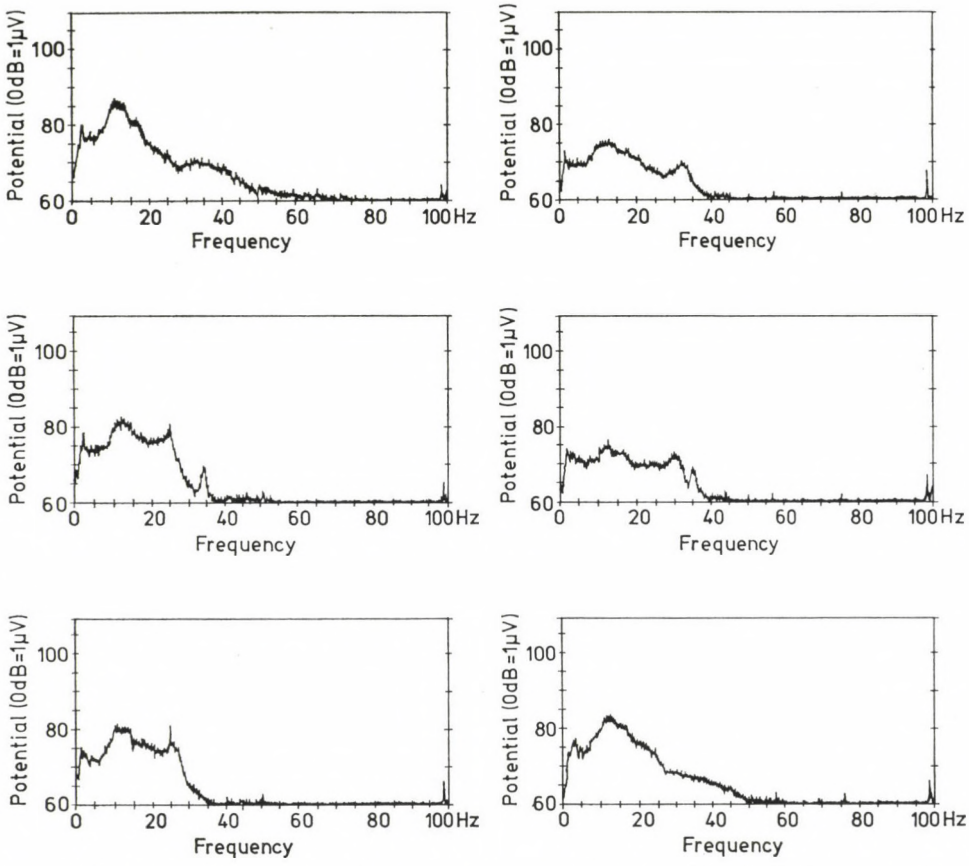

Fig. 10. **Two sets of the spectra of three components (from top: V, NS, EW) measured on June 23 at 10 h (left) and on June 23 at 15 h (right)**

REFERENCES

AKAMATU, K. 1961: On microseisms in frequency range 1 c/s to 200 c/s. *Bull. Earthquake Res. Inst., Tokyo Univ*, 39, 23—76.

AKI, K. 1957: Space and time spectra of stationary stochastic waves, with special reference to microtremors. *Bull. Earthquake Res. Inst. Tokyo Univ.*, 35, 415—456.

ALLAM, A. 1969: An investigation into the nature of microtremors. Ph. D. Thesis, Tokyo University.

Brüel and Kjaer. Instruction Manual Real — Time Narrow Band Analyzer Type 3348.

DOUZE, E. J. 1964: Signal and noise in deep wells. *Geophysics*, 29, 721—732.

KANAI, K. 1962: On the spectrum of strong earthquake motions. *Primeras J. Argentinas Ing. Antisismica* 24. l.

KANAI, K.—TANAKA, T. 1961: On microtremors. VIII., *Bull. Earthquake Res. Inst., Tokyo Univ.*, 39, 97—115.

UDWADIA, F. E.—TRIFUNAC, M. D. 1973: Comparison of Earthquake and Microtremor Ground Motions in El Centro, California. *Bull. the Seism. Soc. of America*, 4, 1227—1253.

WILSON, C. D. V. 1953: The origin and nature of microseisms in the frequency range 4 to 100 cps. *Proc. Roy. Soc.* (London), Ser. A. 217, 176.

ИЗМЕНЕНИЯ МИКРОСЕЙСМОВ В БУДАПЕШТЕ

Д. СЕЙДОВИЦ

РЕЗЮМЕ

Источником наблюдаемых в Будапеште микросейсмов является нестационарное, широкополосное явление с плоским спектром. Для сбора данных об естественной частоте грунта необходимы повторные измерения, надеясь, что некоторые общие пики присваиваются местным условиям. Таким образом, изучение местных условий при помощи техники микросейсмов будет кропотливым процессом, надежность его тоже будет сомнительным. Наибольшим затруднением в связи с использованием техники микросейсмов — даже в случае однослойной системы — тот факт, что почти невозможно из многих — часто острых — пиков спектры тот, который может характеризовать свойства грунта.

Acta Geodaet., Geophys. et Montanist. Acad. Sci. Hung. Tomus 16 (2—4), pp. 469—475 (1981)

ESTIMATION OF SEISMIC DETECTION THRESHOLDS OF SEISMOGRAPH STATIONS IN HUNGARY

L. TÓTH

GEODETIC AND GEOPHYSICAL RESEARCH INSTITUTE OF THE HUNGARIAN ACADEMY OF SCIENCES, DEPARTMENT OF SEISMOLOGY, BUDAPEST

The event detection probability of a seismic station is function of event magnitude and epicentral distance. In order to have a quantitative measure on the relative information contribution from individual stations the detection threshold has been introduced. This is defined as magnitude of an event at a given probability of detecting. Based on one year of data, January 1975—December 1975, the routine event detectability of Hungarian stations has been investigated in terms of 50 and 90 per cent detectability thresholds.

1. Introduction

Several methods have been developed to estimate the detection thresholds of seismic stations [3]. The main methods are as follows:

a) Indirect estimation method. By measuring the seismic noise level and estimating the signal-to-noise ratio required for detection, one can reasonably well predict the actual detection performance of a system.

b) The recurrence curve estimation method is a two-step procedure. First the seismicity of a region is estimated by extrapolating the observed data, using the exponential magnitude — frequency relationship. Then, the observed number of events is compared to the estimated seismicity in order to establish detection thresholds.

c) The direct method based on comparison to a reference system.

The recurrence curve estimation method has been applied in this study to determine the detection thresholds of Hungarian stations.

2. The recurrence curve estimation method

The true $P(m)$ detection probability of the station as a function of magnitude m is [2, 3]

$$P(m) = \Phi\left(\frac{m - \mu_T + b_A}{(\sigma_T^2 + \sigma_A^2)^{1/2}}\right) \tag{1}$$

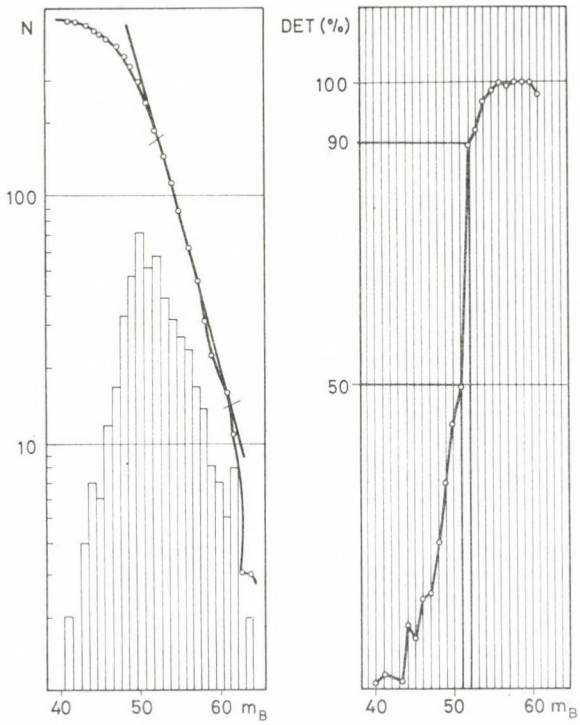

Fig. 1. Frequency — magnitude distributions for all events with epicentral range 30°—90° from JOS (region 14). On the right hand side is the detectability in percentage as a function of body wave magnitude

where μ_T and σ_T are the expectation and variance of the threshold magnitude, $m + b_A$ and σ_A are the expectation and variance of the m_A station magnitude, and Φ denotes the standard cumulative Gaussian distribution function. This is derived by assuming:

a) the magnitude m_A at the station in question is normally distributed $m_A \sim N(m + b_A, \sigma_A^2)$

b) the threshold magnitude m_T is normally distributed

$$m_T \sim N(\mu_T, \sigma_T^2)$$

c) m_A and m_T are independent

d) the event is detected if $m_A > m_T$.

To estimate the frequency curve we assume that

$$\log N = a + bm_b \tag{2}$$

where N is the number of events of magnitude m_b or greater, and a and b are

parameters estimated from the distribution. The observed number of events is compared to the estimated seismicity (Fig. 1).

As shown by RINGDAL [3], this method estimates the curve

$$P_1(m) = \Phi\left(\frac{m - \mu_T}{\sigma_T}\right) \tag{3}$$

(the notations are the same as in (1)) which gives significantly lower thresholds than the true value [1].

3. Data basis and seismic regionalization

The data basis used in this study consists of all events found in [4].

Locations of the Hungarian seismograph stations are shown in Fig. 2 and Table I.

For several reasons the detection capability of a station varies with the source region, therefore some kind of regionalization is to be used. There are

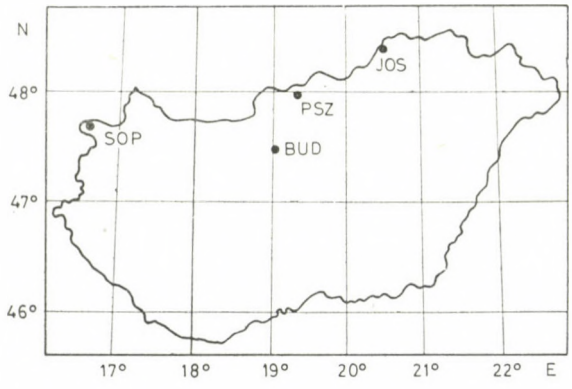

Fig. 2. Hungarian seismograph stations

Table I

Seismic stations in Hungary

Station	Code	lat. (°N)	long. (°E)
Budapest	BUD	47.48	19.02
Jósvafő	JOS	48.50	20.54
Piszkéstető	PSZ	47.92	19.89
Sopron	SOP	47.68	16.56

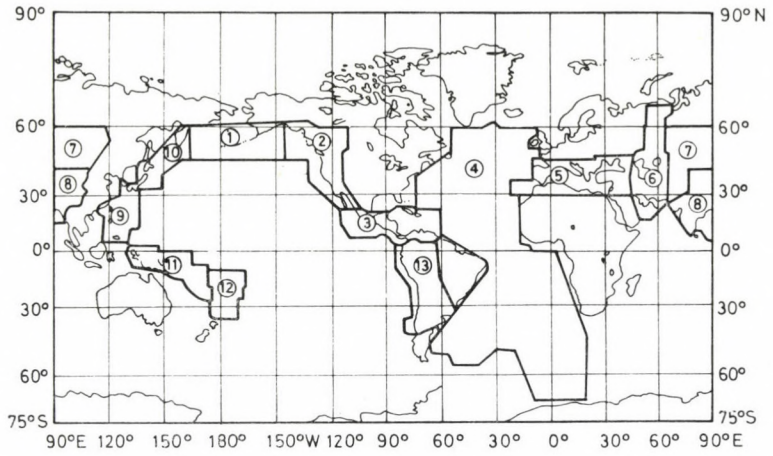

Fig. 3. The geographic regions used in this study

two conflicting arguments which must be considered: on one hand the regions should be small enough to give an adequate representation of regional variations and on the other hand each one should be so large that an acceptable amount of data should be available.

The regions used in this study (Fig. 3, Table II) are the same as widely used, defined by GUTENBERG and RICHTER [5] and FLINN and ENGDAHL [6].

Table II

Definition of the regionalization used in this study

Region	Area of coverage	Region	Area of coverage
1.	Aleutians — Alaska	10.	Japan — Kamchatka
2.	Western North America	11.	New-Guinea — Hebrides
3.	Central America	12.	Fiji — Kermadec
4.	Mid-Atlantic Ridge	13.	South America
5.	Mediterranean — Middle East	14.	distance range 30—90°
6.	Iran — Western Russia	15.	distance range 110—180°
7.	Central Asia	16.	distance range 0—30°
8.	Southern — Eastern Asia	17.	distance range 90—110°
9.	Ryukyu — Philippines	18.	the whole earth

4. Detectability results

The detection thresholds estimated by the method described previously are shown in Table III. A dash indicates that available data were not sufficient.

Table III

The estimated detection thresholds

	Region	BUD	JOS	PSZ	SOP
1.	MB 50	5.62	5.00	5.02	5.43
	MB 90	5.70	5.11	5.13	5.74
2.	MB 50	—	—	—	—
	MB 90	—	—	—	—
3.	MB 50	5.14	5.11	5.12	5.16
	MB 90	5.31	5.22	5.24	5.25
4.	MB 50	5.10	5.02	5.10	5.10
	MB 90	5.21	5.20	5.27	5.23
5.	MB 50	4.72	4.33	4.34	4.42
	MB 90	4.93	4.41	4.51	4.81
6.	MB 50	4.93	4.84	4.90	4.92
	MB 90	5.10	5.02	5.04	5.17
7.	MB 50	—	4.50	4.92	4.73
	MB 90	—	4.92	5.01	5.02
8.	MB 50	5.32	4.92	4.95	5.02
	MB 90	5.61	5.17	5.13	5.14
9.	MB 50	5.54	5.32	5.33	5.31
	MB 90	5.64	5.43	5.42	5.42
10.	MB 50	5.32	5.01	5.12	5.03
	MB 90	5.43	5.22	5.33	5.20
11.	MB 50	5.10	5.00	5.02	5.04
	MB 90	5.72	5.12	5.70	5.12
12.	MB 50	5.02	5.05	5.03	5.17
	MB 90	5.46	5.14	5.11	5.48
13.	MB 50	—	—	—	—
	MB 90	—	—	—	—
14.	MB 50	5.21	5.13	5.15	5.17
	MB 90	5.39	5.21	5.23	5.25
15.	MB 50	5.07	5.01	5.05	5.00
	MB 90	5.29	5.13	5.17	5.33
16.	MB 50	4.36	4.32	4.38	4.32
	MB 90	4.99	4.55	4.51	4.57
17.	MB 50	5.44	5.49	5.42	5.46
	MB 90	5.56	6.52	5.54	5.74
18.	MB 50	5.22	5.21	5.25	5.24
	MB 90	5.41	5.33	5.47	5.48

The limits for a least-squares fit were determined manually (Fig. 1). The difference in percentage between the straight line and the actual data was plotted as a function of magnitude, and a sixth — degree polynomial was then fitted to the data at magnitudes below the 100 per cent point. Finally, the 90 and 50 per cent levels of detectability were computed.

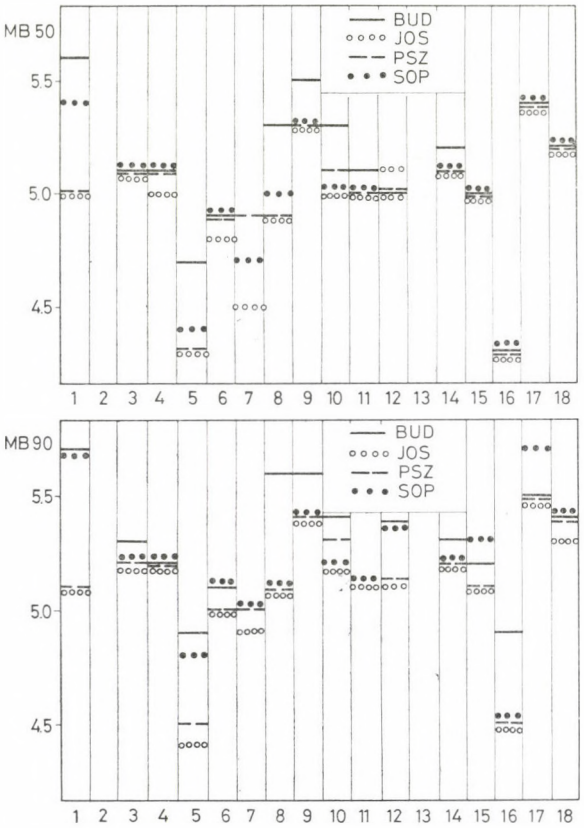

Fig. 4. The estimated detection thresholds in terms of 50 (upper part) and 90 (lower part) per cent

One should notice that all regions (region 5, 6, 7) located on the same tectonic plate as the stations give the best results. On the other side, the regions where the stations have the poorest event detectability are found in the shadow zone (region 2, 13).

The results show that station JOS has the best event detectability, while BUD and SOP have the poorest, corresponding to the magnification of the seismographs operating at these stations. But it should be noted that the detectability can not be increased sufficiently by increasing seismograph magni-

fication. Other conventional single stations also have detection thresholds at about 4.5—5.5m_b value [2]. Only arrays give much better event detectability, below the 4.0m_b value [1].

REFERENCES

1. Bungum, H.—Husebye, E. S.: Analysis of the Operational Capabilities for Detection and Location of Seismic Events at NORSAR. *Bull. Seism. Soc. Amer.* 64. (1974), 637—656.
2. Pirhonen, S. E.—Ringdal, F.—Berteussen, K. A.: Event Detectability of Seismograph Stations in Fennoscandia. *Physics of the Earth and Planetary Interiors*, 12 (1976), 329—342.
3. Ringdal, F.: On the Estimation of Seismic Detection Thresholds. *Bull. Seism. Soc. Amer.*, 65 (1975), 1631—1642.
4. Mikroszeizmikus Jelentés 1975 (Rapport Microseismique de Hongrie). MTA Geod. és Geof. Kut. Int. Szeizm. Obsz. Budapest.
5. Gutenberg, B.—Richter, C. F.: Seismicity of the Earth. *Princeton University Press*, Princeton, N. J. 1949.
6. Flinn, E. A.—Engdahl, E. R.: A Proposed Basis for Geographical and Seismic Regionalization. *Rev. Geophys.* 3 (1965) 123—149.

ОЦЕНКА ПОРОГА СЕЙСМИЧЕСКОЙ ЧУВСТВИТЕЛЬНОСТИ СЕЙСМОГРАФИЧЕСКИХ СТАНЦИЙ В ВЕНГРИИ

Л. ТОТ

РЕЗЮМЕ

Вероятность выявления событий сейсмической станции является функцией величины и расстояния от эпицентра события. Для получения качественной меры об относительном вкладе информации отдельных станций было введено понятие порога сейсмической чувствительности. Этот порог был определен как величина события при данной вероятности выявления. На основе данных одного года (январь—декабрь 1975 г.) была исследована рутинная обнаруживаемость венгерских станций в случаях 50 и 90 процентов порогов выявления.

Acta Geodaet., Geophys. et Montanist. Acad. Sci. Hung. Tomus 16 (2—4), pp. 477—478 (1981)

OBITUARY

FERENC HALMOS
(1931—1980)

Prof. FERENC HALMOS, Doctor of Technical Sciences, deputy director of the Geodetic and Geophysical Research Institute of the Hungarian Academy of Sciences suddenly died after a short but serious illness on 21 October, 1980. His death is a great loss for the Hungarian geodetic science.

FERENC HALMOS, born in Hásságy on 5 September 1931 completed the secondary school in Pécs in 1949 and graduated at the Technical University of Sopron in 1953. Here he became assistant at the Department of Geodesy and Mining Survey. Since the foundation of the Geodetic Research Laboratory of the Hungarian Academy of Sciences in 1955 he had worked there as a scientist, senior scientist, since the reorganization into Geodetic and Geophysical Research Institute in 1971 as head of department and since 1977 as deputy director. He obtained the degree candidate of technical sciences in 1963 and doctor of technical sciences in 1973.

The main fields of his research work were: application of least squares adjustment in geodesy, investigation of gyroscopic theodolites, construction of mathematical models in geodesy and satellite geodesy. The results of his versatile research work were published in about 200 papers, mostly in English or German, several of them in this journal.

He was very efficient in the organization of research too, especially in that of international scientific symposia. He had been secretary of a FIG com-

mittee since 1971 and secretary of IAG Section 4 of IUGG since 1979. Further he was secretary of the Geodetic Committee of the Hungarian Academy of Sciences and chairman of the Sopron local group of the Geodetic and Cartographic Society.

As appreciation of his outstanding scientific work he was awarded with titular professorship in 1979.

FERENC HALMOS's name is internationally well-known among geodesists. His early death ended a successful and promising scientific career.

Acta Geodaet., Geophys. et Montanist. Acad. Sci. Hung. Tomus 16 (2—4), pp. 479—480 (1981)

RECENSIONES

M. Wyss (Ed.)
Earthquake Prediction and Seismicity Patterns
Contributions to Current Research in Geophysics 8
Birkhäuser, Basel—Boston—Stuttgart, 242 p.
Reprinted from Pure and Applied Geophysics, Vol. 117 (1979)

The series of reprints from PAGEOPH has received a new volume being an extremely interesting lecture even for those not being engaged exactly in the same field. Accounts as by T. GARZA and C. LOMNITZ on the recent history of the Caxaca gap in Mexico, or by W. H. K. LEE and D. R. BRILLINGER on an analysis of historical earthquake data in Chine, including an estimation of reliability on the basis of population density and document survival can be nearly read as fiction. The volume is introduced by a review on the seismic gap theory by McCANN, NISHENKO, SYKES and KRAUSE, followed by papers on some more or less prominent gaps, like those in Costal Peru (DEWEY and SPENCE) Kurile Island (WYSS and HABERMANN), the Makran region in Pakistan (QUITTMEYER), North Anatolia (TOKSÖZ, SHAKAL and MICHAEL), and Kanto in Japan (FUJII and NAKANE). MOGI, one of the initiators of the seismic gap theory, describes two distinct classes of seismic gaps whose confusion can result in misinterpretation. DELSEMME and SMITH used the migration method for South American earthquakes, and LI-SHENG HUANG, McRANEY, TA-LIANG TENG and PREBISH found correlation between precipitation in an arid zone (Southern California) and large earthquakes.

The volume offers interesting reading for anybody interested in geophysics or in this new branch of seismology which received impetus by recent research. Its wide scope yields possibilities for future students of this topic.

J. Verő

K. Rinner (Red.)
Festschrift zur Emeritierung von o. Univ.-Prof. Dipl. Ing. Dr. techn. KARL HUBENY
Mitteilungen der geodätischen Institute der Technischen Universität Graz, Folge 35. Graz, 1980 p. 200

K. RINNER: Zur Emeritierung von o. Univ. Prof. Dr. techn. KARL HUBENY
F. ALLMER: Gauß-Krüger Koordinaten oder wer war LOUIS KRÜGER?
W. K. BACHMANN: Die Zuverlässigkeit von Luftaufnahmen (französisch)
T. J. BLACHUT: Gehört die Fernerkundung zur Photogrammetrie, oder die Photogrammetrie zur Fernerkundung? (englisch)
G. BRANDSTÄTTER: Richtungsfehler außerachsialer Strahlengänge in Kompensatorfernrohen
K. BRETTENBAUER: Über Zentralschnitte des Rotationsellipsoides
R. BURKHARD: Untersuchungen zur Kalibrierung eines Elektromikroskopes
H. ETTL: Der Ingenieur für Vermessungstechnik und seine Ausbildung in Österreich
L. HOMORÓDI: Die Anfänge der Vermessungsingenieurausbildung in Ungarn
K. KILLIAN—P. MEISSL: Bestimmung der Lage von gegenseitig nicht sichtbaren Stationen der Erdoberfläche aus Dopplereffekt-Messungen zu bewegten Zielen mit unbekannten Koordinaten

F. KOPPENWALLNER: Das Lichtschnittverfahren nach Prof. HUBENY bei der ÖBB 1958—1980
F. LEBERL: Die Erforschung der Oberfläche des Planeten Venus
H. MORITZ: Das geodätische Bezugssystem 1980
G. SCHELLING: Mobile Schwimmlote als Elemente der Schüttdammbeobachtung
H. SCHMID: Die Chancen und technischen Möglichkeiten eines Kontaktes mit extraterrestrischen Intelligenzen (CETI)
A. SCHÖDLBAUER: Kugeln als Hilfsflächen bei der Lösung der beiden geodätischen Hauptaufgaben

Die Arbeit entstand anläßlich des 70-ten Geburtstages und der Emeritierung von Herrn Prof. HUBENY, dem Vorstand des Institutes für Allgemeine Geodäsie der Technischen Universität Graz. Prof. RINNER befaßt sich in der ersten Studie mit der Bedeutung dieses Ereignisses und bringt Angaben über seinen Lebenslauf, bzw. dessen wichtigere Stationen. Die Liste der wissenschaftlichen Tätigkeit des Jubilars wird auch angeführt. Im weiteren folgen Arbeiten von Mitprofessoren, Kollegen, Freunden und gewesenen Schülern von Prof. HUBENY. Die Themen entsprechen dem Forschungsbereich des Jubilars, oder behandeln angrenzenden Gebiete.

So befassen sich BACHMANN, BURKHARD und KOPPENWALLNER mit der Photogrammetrie, die Fernerkundung wird von BLACHUT und LEBERL behandelt. SCHMID erörtert die Chancen eines Kontaktes mit extraterrestrischen Intelligenzen.

Die Arbeit von ALLMER gehört zum Themenkreis der höheren Geodäsie. Er befaßt sich mit der Entstehungsgeschichte des Gauss-Krügerschen Koordinatensystems und schreibt über das Leben, Wirken bzw. Daten von L. KRÜGER. Die Arbeit von BRETTENBAUER behandelt eine neue Anwendung des Rotationsellipsoids, den sog. Zentralschnitt. SCHÖDELBAUER's Studie gibt eine Lösung der beiden geodätischen Hauptaufgaben mit Hilfsflächen. Die Arbeit von MORITZ bringt Daten über geodätische Bezugssysteme einiger Ellipsoide von nunmehr historischer Bedeutung und gibt Angaben über angenommene Bezugssysteme der IAG (1964), der IAG (1967) Luzern, der IAG (1975) Moskau und der IUGG (1980) Canberra.

BRANDSTÄTTER's Arbeit behandelt ein instrumententechnisches Problem und bringt eine vektoranalytische Lösung für die Richtungsfehler außerachsialer Strahlengänge in Nivellier instrumenten und für den Fall der Durchführung von Almukantorat-Durchgängen. Letztere wird vor allem bei der präziseren Berechnung der mit Vorsatzprismen durchgeführten auf Astrolabium bezogenen Messungen angewendet.

ETTL's Arbeit befaßt sich mit Fragen des österreichischen Hochschulwesens, HOMORÓDI behandelt die Geschichte der Ausbildung von Vermessungsingenieuren in Ungarn.

Gy. Szádeczky-Kardoss

INDEX

Printed in Hungary

A kiadásért felel az Akadémiai Kiadó igazgatója. Műszaki szerkesztő: Zacsik Annamária

A kézirat nyomdába érkezett: 1981. II. 12. — Terjedelem: 28,0 (A/5) ív, 172 ábra (1 melléklet)

81.9297 Akadémiai Nyomda, Budapest — Felelős vezető: Bernát György

Acta Geodaetica, Geophysica et Montanistica, eine Halbjahresschrift der Ungarischen Akademie der Wissenschaften. Sie veröffentlicht Originalbeiträge aus dem Bereich der Geodäsie, Geophysik und des Bergbaus in deutscher, englischer, französischer oder russischer Sprache.

Redaktion: H-9400 Sopron, Múzeum u. 6.

Bestellbar bei »Kultura« Außenhandelsunternehmen (1389 Budapest 62, P.O.B. 149) oder seinen Auslandsvertretungen.

Acta Geodaetica, Geophysica et Montanistica est une revue biannuelle de l'Académie Hongroise des Sciences publiant des essais originaux du domaine de la géodésie, géophysique et des sciences minières en français, anglais, allemand ou russe.

Rédaction: H-9400 Sopron, Múzeum u. 6.

On peut s'abonner à l'Entreprise du Commerce Extérieur « Kultura » (1389 Budapest 62, P.O.B. 149) ou chez représentants à l'étranger.

Acta Geodaetica, Geophysica et Montanistica выходят два раза в год в издании Академии наук Венгрии. В журнале публикуются оригинальные исследования по проблемам геодезии, геофизики и горного дела на русском, английском, немецком и французском языках.

Адрес редакции: H-9400 Sopron, Múzeum u. 6.

Заказать журнал через Внешнеторговое предприятие «Kultura» (1389 Budapest 62, P.O.B. 149) или через его заграничные представительства.

Reviews of the Hungarian Academy of Sciences are obtainable at the following addresses:

AUSTRALIA
C.B.D. LIBRARY AND SUBSCRIPTION SERVICE, Box 4886, G.P.O. *Sydney N.S.W. 2001*
COSMOS BOOKSHOP, 135 Ackland Street, *St. Kilda (Melbourne), Victoria 3182*

AUSTRIA
GLOBUS, Höchstädtplatz 4, *1200 Wien* XX

BELGIUM
OFFICE INTERNATIONAL DE LIBRAIRIE, 30 Avenue Marnix. *1050 Bruxelles*
LIBRAIRIE DU MONDE ENTIER, 162 Rue du Midi, *1000 Bruxelles*

BULGARIA
HEMUS, Bulvar Ruszki 6, *Sofia*

CANADA
PANNONIA BOOKS, P.O. Box 1017, Postal Station "B", *Toronto, Ontario M5T 2T8*

CHINA
CNPICOR, Periodical Department, P.O. Box 50, *Peking*

CZECHOSLOVAKIA
MAD'ARSKÁ KULTURA, Národní třida 22 *115 66 Praha*
PNS DOVOZ TISKU, Vinohradská 46, *Praha 2*
PNS DOVOZ TLAČE, *Bratislava 2*

DENMARK
EJNAR MUNKSGAARD, Norregade 6, *1165 Copenhagen*

FINLAND
AKATEEMINEN KIRJAKAUPPA, P.O. Box 128, *SF-00101 Helsinki 10*

FRANCE
EUROPERIODIQUES S. A., 31 Avenue de Versailles, *78170 La Celle St.-Cloud*
LIBRAIRIE LAVOISIER, 11 rue Lavoisier, *75008 Paris*
OFFICE INTERNATIONAL DE DOCUMENTATION ET LIBRAIRIE, 38 rue Gay-Lussac, *75240 Paris Cedex 05*

GERMAN DEMOCRATIC REPUBLIC
HAUS DER UNGARISCHEN KULTUR, Karl-Liebknecht-Strasse 9, *DDR-102 Berlin*
DEUTSCHE POST ZEITUNGSVERTRIEBSAMT, Strasse der Pariser Kommüne 3—4, *DDR-104 Berlin*

GERMAN FEDERAL REPUBLIC
KUNST UND WISSEN ERICH BIEBER, Postfach 46, *7000 Stuttgart 1*

GREAT BRITAIN
BLACKWELL'S PERIODICALS DIVISION, Hythe Bridge Street, *Oxford OX1 2ET*
BUMPUS, HALDANE AND MAXWELL LTD., Cowe Works, *Olney, Bucks MK46 4BN*
COLLET'S HOLDINGS LTD., Denington Estate, *Wellingborough, Northants NN8 2QT*
W.M. DAWSON AND SONS LTD., Cannon House, *Folkestone, Kent CT19 5EE*
H. K. LEWIS AND CO., 136 Gower Street, *London WC1E 6BS*

GREECE
KOSTARAKIS BROTHERS, International Booksellers, 2 Hippokratous Street, *Athens-143*

HOLLAND
MEULENHOFF-BRUNA B.V., Beulingstraat 2, *Amsterdam*
MARTINUS NIJHOFF B.V., Lange Voorhout 9—11, *Den Haag*
SWETS SUBSCRIPTION SERVICE, 347b Heereweg, *Lisse*

INDIA
ALLIED PUBLISHING PRIVATE LTD., 13/14 Asaf Ali Road, *New Delhi 110001*
150 B-6 Mount Road, *Madras 600002*
INTERNATIONAL BOOK HOUSE PVT. LTD., Madame Cama Road, *Bombay 400039*
THE STATE TRADING CORPORATION OF INDIA LTD., Books Import Division, Chandralok, 36 Janpath, *New Delhi 110001*

ITALY
EUGENIO CARLUCCI, P.O. Box 252, *70100 Bar*
INTERSCIENTIA, Via Mazzé 28, *10149 Torino*
LIBRERIA COMMISSIONARIA SANSONI, Via Lamarmora 45, *50121 Firenze*
SANTO VANASIA, Via M. Macchi 58, *20124 Milano*
D. E. A., Via Lima 28, *00198 Roma*

JAPAN
KINOKUNIYA BOOK-STORE CO. LTD., 17-7 Shinjuku-ku 3 chome, Shinjuku-ku, *Tokyo 160-91*
MARUZEN COMPANY LTD., Book Department, P.O. Box 5056 Tokyo International, *Tokyo 100-31*
NAUKA LTD., IMPORT DEPARTMENT, 2-30-19 Minami Ikebukuro, Toshima-ku, *Tokyo 171*

KOREA
CHULPANMUL, *Phenjan*

NORWAY
TANUM-CAMMERMEYER, Karl Johansgatan 41—43. *1000 Oslo*

POLAND
WĘGIERSKI INSTYTUT KULTURY, Marszałkowska 80, *Warszawa*
CKP I W ul. Towarowa 28 *00-958 Warsaw*

ROMANIA
D. E. P., *Bucureşti*
ROMLIBRI, Str. Biserica Amzei 7. *Bucureşti*

SOVIET UNION
SOJUZPETCHATJ — IMPORT, *Moscow* and the post offices in each town
MEZHDUNARODNAYA KNIGA, *Moscow G-200*

SPAIN
DIAZ DE SANTOS, Lagasca 95, *Madrid 6*

SWEDEN
ALMQVIST AND WIKSELL, Gamla Brogatan 26 *101 20 Stockholm*
GUMPERTS UNIVERSITETSBOKHANDEL AB, Box 346, *401 25 Göteborg 1*

SWITZERLAND
KARGER LIBRI AG, Petersgraben 31, *4011 Basel*

USA
EBSCO SUBSCRIPTION SERVICES, P.O. Box 1943, *Birmingham, Alabama 65201*
F. W. FAXON COMPANY, INC., 15 Southwest Park, *Westwood, Mass, 02090*
THE MOORE-COTTRELL SUBSCRIPTION AGENCIES, *North Cohocton, N. Y. 14838*
READ-MORE PUBLICATIONS, INC., 140 Cedar Street, *New York, N. Y. 10003*
STECHERT-MACMILLAN, INC., 7250 Westfield Avenue, *Pennsauken* N. J. 08110

VIETNAM
XUNHASABA, 32, Hai Ba Trung, *Hanoi*

YUGOSLAVIA
JUGOSLAVENSKA KNJIGA, Terazije 27, *Beograd*
FORUM, Vojvode Mišića 1, *21000 Novi Sad*

10. XII. 1981 HU ISSN 0374—1842 Index: 26.031